Lecture Notes in Operations Research

Robin Qiu · Wai Kin Victor Chan · Weiwei Chen · Youakim Badr · Canrong Zhang *Editors*

City, Society, and Digital Transformation

Proceedings of the 2022 INFORMS International Conference on Service Science

Springer

Lecture Notes in Operations Research

Lecture Notes in Operations Research is an interdisciplinary book series which provides a platform for the cutting-edge research and developments in both operations research and operations management field. The purview of this series is global, encompassing all nations and areas of the world.

It comprises for instance, mathematical optimization, mathematical modeling, statistical analysis, queueing theory and other stochastic-process models, Markov decision processes, econometric methods, data envelopment analysis, decision analysis, supply chain management, transportation logistics, process design, operations strategy, facilities planning, production planning and inventory control.

LNOR publishes edited conference proceedings, contributed volumes that present firsthand information on the latest research results and pioneering innovations as well as new perspectives on classical fields. The target audience of LNOR consists of students, researchers as well as industry professionals.

Robin Qiu · Wai Kin Victor Chan · Weiwei Chen ·
Youakim Badr · Canrong Zhang
Editors

City, Society, and Digital Transformation

Proceedings of the 2022 INFORMS International Conference on Service Science

Springer

Editors
Robin Qiu
Division of Engineering and Information Science
Pennsylvania State University
Malvern, PA, USA

Weiwei Chen
Department of Supply Chain Management
Rutgers, The State University of New Jersey
New Jersey, NJ, USA

Canrong Zhang
Shenzhen International Graduate School
Tsinghua University
Shenzhen, China

Wai Kin Victor Chan
Shenzhen International Graduate School
Tsinghua University
Shenzhen, China

Youakim Badr
Division of Engineering and Information Science
Pennsylvania State University
Malvern, PA, USA

ISSN 2731-040X ISSN 2731-0418 (electronic)
Lecture Notes in Operations Research
ISBN 978-3-031-15643-4 ISBN 978-3-031-15644-1 (eBook)
https://doi.org/10.1007/978-3-031-15644-1

This Springer imprint is published by the registered company Springer Nature Switzerland AG
The registered company address is: Gewerbestrasse 11, 6330 Cham, Switzerland

Contents

Chapter 1
A Penalized Neural Network Model for Predicting Unobserved Scores of Construct Indicators and Reproducing Latent Scores of the Theoretical Constructs by Using Text Information

Toshikuni Sato

Abstract This paper discusses a novel application of construct measurement with a penalized neural network in a text analysis. Conducting a survey with the measures of constructs is a traditional approach to scoring customers' mental states, such as feelings, perceptions, and attitudes. Numerous types of scales are continuously developed for marketing and consumer behavior research. To connect this traditional methodology with machine learning and big data analysis, our proposed neural network model uses two penalty functions, which specify the confirmatory factor model as a measurement equation. In the empirical analysis, the proposed model shows stable parameter estimates compared with a standard unconstrained neural network and supports theoretical interpretations. By applying the learned proposed model, predictive item scores of each questionnaire and alternative scores of theoretical constructs can be obtained through text information. The proposed methodology helps marketers and researchers visualize consumers' representations of perceived theoretical constructs without the survey. To enhance the proposed model's accuracy and validity, limitations and potential works are also discussed for future study.

Keywords Penalized neural network · Construct measurement · Text analysis · Parameter identification

Introduction

The rapid growth of digital technologies promotes machine learning (ML) approaches, such as face detection, image classification, and natural language processing (NLP) in marketing and business applications. These methods remarkably help efficient handling of large-scale and unstructured data, such as movies, images, and text messages [1–3]. Therefore, applying ML techniques or algorithms

T. Sato (✉)
School of Commerce, Meiji University, Chiyoda, Tokyo 101-8301, Japan
e-mail: tsato@meiji.ac.jp

R. Qiu et al. (eds.), *City, Society, and Digital Transformation*, Lecture Notes in Operations Research, https://doi.org/10.1007/978-3-031-15644-1_1

is an essential step in advancing marketing analyses to convert them to tractable formats and obtain business insights.

In addition to acknowledging these situations, the role of the traditional approach is reconsidered to support artificial intelligence (AI) and ML applications; for example, experimental research provides evidence for the advantages of AI coaches [4] and recommendation systems [5], and survey research investigates psychological and behavioral attitudes related to AI [6, 7]. Furthermore, establishing knowledge fusion from both aspects of traditional marketing and Big Data analysis has been noted to succeed in new product development [8, 9]. According to these studies, applying the traditional approach with new technologies and datasets has become increasingly crucial to address variable marketing environments.

As stated in the aforementioned background, we consider a collaborative application of the traditional marketing analysis with ML and unstructured dataset. Specifically, this study aims to explore new means of psychological and marketing scales in text analysis by extending the conventional measurement model. It has been of essential interest for marketers and researchers to measure consumer behavior, feelings, perceptions, and attitudes on the common standard of measurement theory, which still plays an important role in present marketing research [10]. Indeed, the scale developments and their applied research on new hypothetical constructs are ongoing in various contexts [11–15].

In this paper, we propose a penalized neural network that employs the specification of a confirmatory factor analysis (CFA). The CFA is a classical and standard method for analyzing the measured scores of construct indicators. Accordingly, we provide an extension of the CFA for building the neural network model to predict the unobserved scores and measure the theoretical constructs with only text information. Although the interpretability is often a matter in neural networks, this finding also implies that our proposed methodology helps visualize explainable customers' mental states with the neural network, as shown in Sect. "Results and Discussion".

Related Research

The proposed method in this paper is related to consumer sentiment analysis and automated text analysis [3, 16–21]. For example, the *attribute embedding model* [3] extracts hierarchical product attributes from contextual relationships among words in customer reviews. The product attributes can be considered as empirical constructs that describe customers' perceptions of the product usage. In the hotel industry, customer reviews also provide latent topics which represent several aspects of operations and services [16]. Additionally, the *scale-directed analysis* [19] employs an automatically created dictionary based on the theoretical constructs and AFINN sentiment analysis to achieve a purpose similar to that of our study, that is, to measure the latent constructs through the textual data.

Compared with these approaches, our proposed method still requires additional validation. However, we focus on not only the text analysis but also on extending

the model specification in the conventional methodology of construct measurement. Based on our methodology, replacing the CFA with a penalized neural network can extend the applied fields of any psychological and marketing scales with the latest techniques of various neural networks and deep learnings, in line with the same background of the traditional measurement theory. Therefore, our proposed model can easily provide a common understanding of the empirical results as shown in Sect. "Results and Discussion", which helps reevaluate and validate or update the existing knowledge and theories of the hypothetical constructs with new types of datasets and technologies in marketing and consumer behavior research.

Methods and Materials

Proposed Model

Our proposed model contains two types of important parameters and one by-product: (1) item weight, (2) term weight, and (3) latent factor (hidden unit). The item weights indicate the strength of the relationship between latent factors and item scores, whereas the magnitudes of term weights explain the relationship between single words and latent factors. The latent factors are produced by inputs and estimated a term weight matrix and represent the latent scores of theoretical constructs. Therefore, the proposed model visualizes consumers' mental states and properties through text information. In other words, our proposed model requires only text information to predict unseen theoretical constructs. The proposed model and procedure are illustrated in Fig. 1.1.

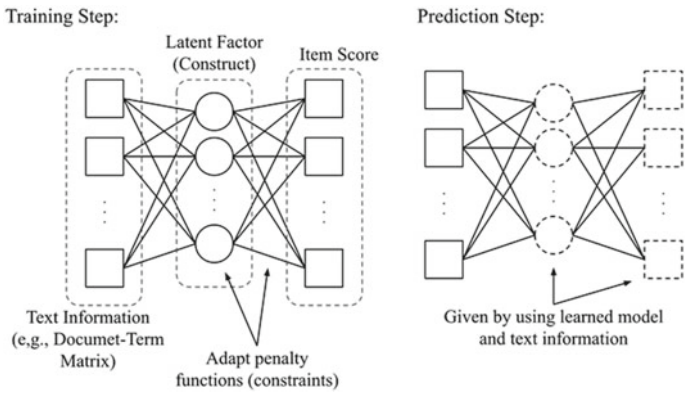

Fig. 1.1 The proposed model and analytics framework

To achieve our purpose, the proposed neural network model adopts a penalty method introduced by [22]. We use the following penalty function to obtain standardized (zero mean and unit variance) latent factors (hidden units) and their correlation matrix.

$$\underset{(U:Standardization)}{Loss(\mathbf{U})} = \frac{1}{2}\left[\left\|\mathrm{diag}\left\{\frac{1}{N^*}\mathbf{U}'\mathbf{U}\right\} - I_q\right\|_2^2 + \left\|\overline{\mathbf{U}}\right\|_2^2\right], \tag{1.1}$$

where $\mathbf{U}$ is the $N^* \times q$ matrix of latent factors, N^* is an input sample size or batch size, q is the number of latent factors, $N^{*-1}\mathbf{U}'\mathbf{U}$ is the covariance matrix of latent factors, $\mathrm{diag}\left\{N^{*-1}\mathbf{U}'\mathbf{U}\right\}$ is the diagonal matrix whose diagonal elements equals to the diagonal elements of $N^{*-1}\mathbf{U}'\mathbf{U}$, I_q is the $q \times q$ identity matrix, and $\overline{\mathbf{U}}$ is the mean vector of latent factors.

For the item weight matrix, we also propose the following block diagonal penalty function:

$$\underset{(W:Block-diag.)}{Loss\left(\mathbf{W}^{(Item)}\right)} = \frac{1}{2}\left\|\mathbf{W}^{(Item)} - B \odot \mathbf{W}^{(Item)}\right\|_2^2, \tag{1.2}$$

where $\mathbf{W}^{(Item)}$ is the $p \times q$ item weight matrix, p is the number of questionnaire items, $\odot$ indicates the element-wise product, and B is a block diagonal matrix whose elements take 1 based on the relationships between theoretical constructs and their indicators; $\mathbf{W}^{(Item)}$ and B have the same dimension. An example of the block diagonal matrix B is given as follows:

$$B' = \begin{bmatrix} I^{(1)} & 0 \\ 0 & I^{(2)} \end{bmatrix} = \begin{bmatrix} 1\,1\,1\,0\,0\,0 \\ 0\,0\,0\,1\,1\,1 \end{bmatrix}. \tag{1.3}$$

This implies that the 1st to 3rd and 4th to 6th questionnaire items reflect the 1st and 2nd theoretical constructs because of the parameter identification, respectively. Therefore, we find that the decoder stage of the proposed neural network model indicates the CFA-based measurement equation.

Data Collection and Preprocessing

The research survey was conducted in support of a Japanese marketing research company, and the data were collected on December 15–20, 2021. The sample comprises 800 Japanese customers who stayed at a hotel within the last three months. The gender is almost even (49.6% female; 50.4% male). For the sample age, the average age is 45.8 years old, and the range is between 20 (min) to 69 (max) years old.

Construct measurement. The hotel brand experience scale included a questionnaire of 17 items [23] to measure five latent constructs (Hotel location; Hotel stay and ambiance; Hotel staff competence; Hotel website and social media experience; Guest-to-guest experience) as shown in Table 1.1. The original questionnaires ask about "hotel brand" experience; however, we did not limit our investigation to "brand" experience and asked about "hotel" experience. All of the 17 items for these latent constructs are measured by a seven-point Likert scale that ranges between 1 = strongly disagree and 7 = strongly agree. Table 1.1 summarizes the details of items and corresponding latent constructs.

Open-ended questions and text preprocessing. The textual data that represent customer reviews of the hotel experience were gathered and paired with the item scores. We prepared an open-ended question and asked: "Write a review of the hotel supposing that you post it on the hotel review website (e.g., Google Map, TripAdvisor, Rakuten Travel)." The textual answers are converted to a set of single terms and counted the frequency of each term per customer review sentences (documents). The

Table 1.1 Measurement of latent constructs

Hotel location (HL)		**Hotel website and social media experience (HSE)**	
HL1	Location of this hotel stimulates my senses	HSE1	Website of this hotel provides accurate results
HL2	I find location of this hotel appealing	HSE2	I find online reviews of this hotel informative
HL3	Location of this hotel is convenient that makes me feel relaxed	HSE3	Presence of this hotel on social media appeals to my visuals
Hotel stay and ambiance (HSA)		**Guest-to-guest experience (GGE)**	
HSA1	Stay at this hotel is memorable to me	GGE1	Conduct of guests at this hotel is gentle
HSA2	This hotel has attractive architectural design	GGE2	Guests at this hotel make me feel comfortable
HSA3	Ambience of this hotel is very relaxing to me	GGE3	Guests at this hotel value the privacy of other guests
HSA4	The cleanliness and décor of this hotel is pleasing		
Hotel staff competence (HSC)			
HSC1	Staff of this hotel is helpful and friendly that brings out emotions		
HSC2	Appearance of this hotel staff is impressive		
HSC3	The way in which the staff of this hotel serves is admirable		
HSC4	I feel good at this hotel because of the staff personnel's attentiveness		

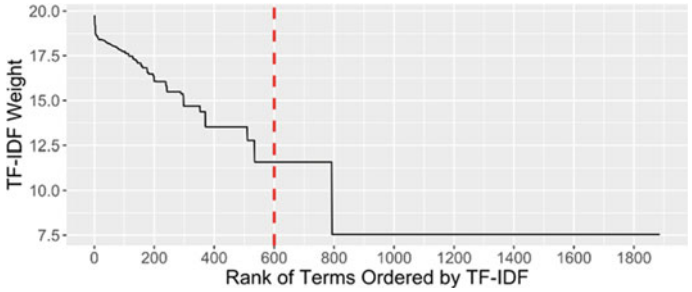

Fig. 1.2 TF-IDF weights and rank of terms

matrix of this count data is known as the "document-term matrix (DTM)" or "bag of words." The details of preprocessing are explained as follows.

First, we identified the single words from all of the text sentences; adapted a part of speech tagging; and extracted the terms corresponding to "noun," "verb," "adjective," and "adverb." Second, we removed numbers, symbols, and common stop words, for example, "is" and "do," which frequently appear in many documents. Third, we ranked the remaining words based on the term frequency-inverse document frequency (TF-IDF) according to [24, 25]. Figure 1.2 shows the TF-IDF weights for every remaining word, and we selected the terms ranked 600 or over (see also the dotted line in Fig. 1.2). Therefore, we use 600 terms out of a total of 2,196.

Model Estimation and Validation

We estimate and compare our proposed model with a standard unconstrained neural network model (i.e., a standard feedforward neural network, noted as a benchmark model). To simplify, both models employ the following common settings: (1) two layers (input, one hidden, and output layers), (2) 5 hidden units (latent constructs), and (3) the hyperbolic tangent (tanh) activation function. Moreover, the proposed model is constrained by two penalty functions explained in Sect. "Methods and Materials". For the estimation, Adam optimizer [26] is applied to minimize each total loss function with learning rate $\alpha = 0.1$. The DTM data is normalized, which divides each frequency by a maximum frequency in each document, whereas we use item score data without standardization.

To compare the models, the sample is divided into three parts; (1) training sample (N = 400), (2) validation sample (N = 240), (3) test sample (N = 160). Moreover, each root mean squared error (RMSE) is calculated. First, we shuffle individual data randomly, use the training sample to learn the model, and calculate the training RMSE. We further check the RMSE with the validation sample to avoid overfitting. Finally, we use the test sample for the prediction step and obtain the test RMSE.

For the model validation and comparison of model stability, we repeat estimating each model 300 times with every different initial value generated from the standard normal distribution. Therefore, all estimation results are reported as the average of 300 estimations, and we use the standard deviation (SD) to check the stability of each estimated value (i.e., estimates for item weight, the covariance matrix of hidden units, and term weight).

Results and Discussion

Model comparison. Table 1.2 shows the means and SDs of RMSE in each trial. The smaller SD indicates that the RMSE does not depend on initial values. Both models show almost equivalent stable prediction performances in each subsample. Although the RMSEs between the benchmark and proposed models are not significantly different, this implies that the constraints of penalty functions did not interrupt the prediction performance of the proposed model.

Item weights. The upper and bottom sides in Fig. 1.3 show the means and SDs of estimates for item weights in the benchmark model, respectively. Similarly, Fig. 1.4 shows the results for the proposed model. The deeper color indicates the larger value. Although the label switching probably occurs in the benchmark model, the 4th factor shows a clear relationship between several item scores (e.g., HSA3, HSA4, HSC1, HCS2, and GGE3). However, this result implies that the theoretical pattern was not reproduced, and thus, it is very difficult to explain each latent factor. In the bottom plot of Fig. 1.3, the SDs of item weights also indicate the difficulty of stable interpretations for the item weight matrix and the corresponding latent factor because almost all of the estimated item weights in around 32% of 300 estimation trials differ over ± 1.0 from the averaged item weights. Compared with these results, our proposed model provides more stable and explainable results as shown in Fig. 1.4, and this figure also indicates that the penalty function (Eq. 1.2) performed well. Therefore, each factor is interpretable consistent with the background theories and definitions of constructs.

Factor covariance. For the stability of latent factors, we also calculated the means and SDs of the factor covariance matrix. These are reported on the left and right sides of Figs. 1.5 and 1.6 for the benchmark and proposed models, respectively. In Fig. 1.5, the latent factors estimated from the benchmark model are almost uncorrelated and look stable enough. However, the coefficients of variation between the means and SDs are slightly large, particularly in the diagonal elements (i.e., factor variance). By

Table 1.2 Root mean squared error of competitive models

	Benchmark model			Proposed model		
	Training	Validation	Test	Training	Validation	Test
Mean	1.037	1.443	1.403	0.972	1.432	1.385
SD	0.061	0.064	0.090	0.024	0.042	0.057

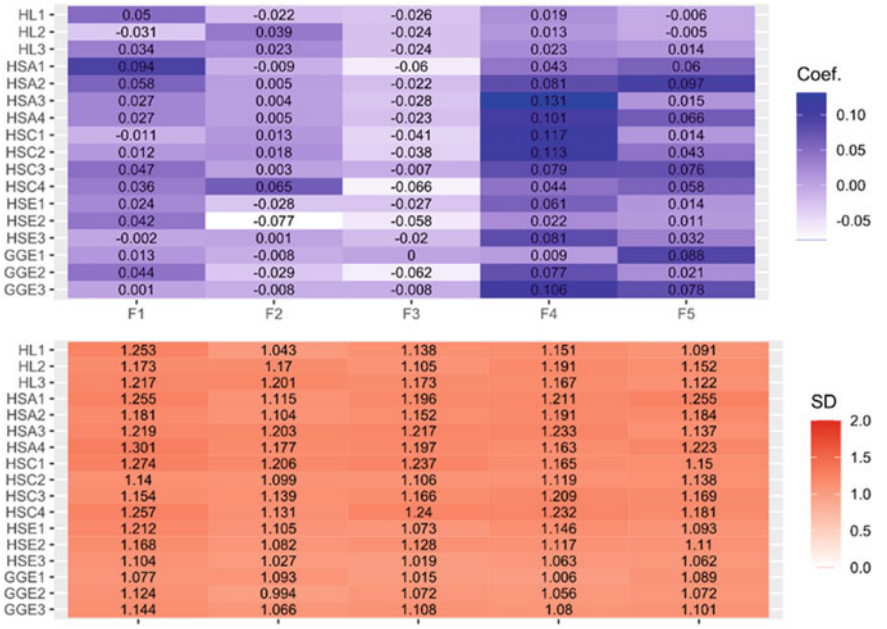

Fig. 1.3 Means (upper) and SDs (bottom) of estimates for item weights in the benchmark model

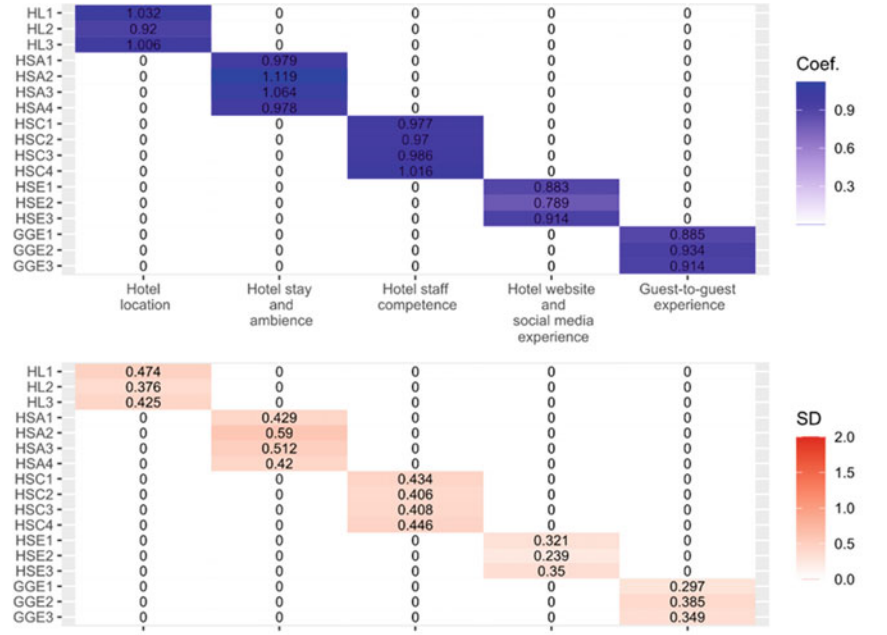

Fig. 1.4 Means (upper) and SDs (bottom) of estimates for item weights in the proposed model

contrast, the latent factors produced by the proposed model show quite stable results. The left side of Fig. 1.6 shows the factor covariance matrix close to the correlation matrix. Therefore, the penalty function (Eq. 1.1) worked well to constrain the factor covariance matrix, and we can easily understand the correlated relationship among latent factors.

Term weights. As same as item weights, we report the means and SDs of estimates for term weights in Figs. 1.7 and 1.8 with selected top 20 TF-IDF words. For the benchmark model, the upper plot of Fig. 1.7 shows the relationship between each term and latent factors; however, the estimates will be easily changed with different initial values as seen in the bottom plot of Fig. 1.7. By contrast, we find that the SDs of term weights produced by the proposed model are much smaller when comparing the bottom plots of Figs. 1.7 and 1.8. The upper plot of Fig. 1.8 shows the estimated term weight matrix of the proposed model, which illustrates the relationship between each term and latent constructs. For example, the word "time" contributes positively to the latent score of "Hotel location" but negatively to the latent scores of "Hotel staff competence" and "Guest-to-guest experience."

Prediction results. Further, we report the prediction results of item scores. Because the predictive item score is given by a continuous value, it is transformed

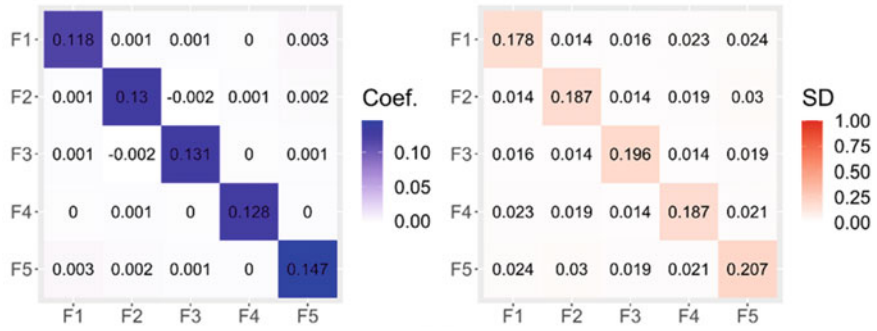

Fig. 1.5 Means (left) and SDs (right) of estimates for factor covariance in the benchmark model

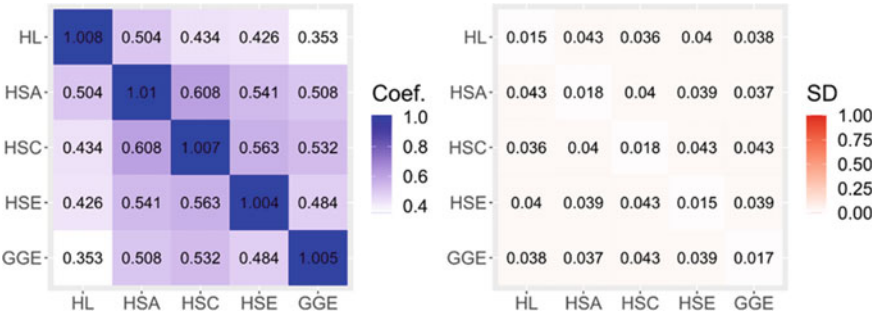

Fig. 1.6 Means (left) and SDs (right) of estimates for factor covariance in the proposed model

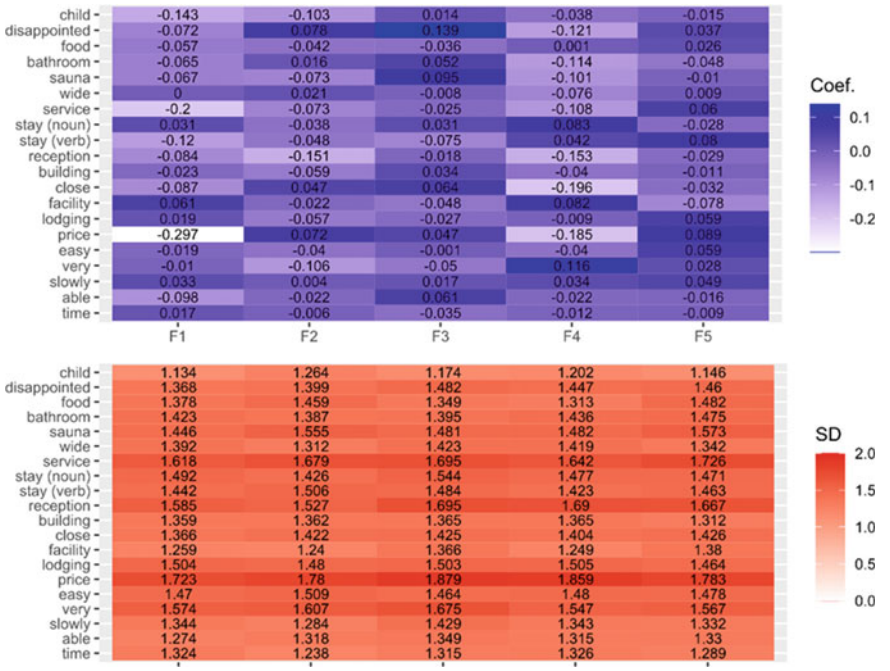

Fig. 1.7 Means (upper) and SDs (bottom) of estimates for term weights in benchmark model (Top 20 TF-IDF words)

into an integer value with rounding. Table 1.3 shows the accuracy rates for each item score prediction in the training and test samples. The range of accuracies is 38% (HSA2) to 54.8% (HSC3 and GGE2) in the training sample, whereas it is 22.5% (HSA2) to 39.4% (GGE3) in the test sample. However, these accuracies might be not special results and should be improved in future research.

Figure 1.9 shows an example result of a comparison between true and predictive scores for an individual customer. The left and right bar charts in each item questionnaire indicate the true and predictive scores, respectively. Evidently, the perfect prediction cannot be produced; however, we find that the predictive scores are not significantly different from the true scores. In fact, the averaged test RMSE of the proposed model is 1.385 (see also Table 1.2), which is not so large against the seven-point scale.

Finally, Fig. 1.10 shows the predictive latent scores given by the learned proposed model for selected 20 example customers in the test sample. We emphasize that these latent scores represent alternative scores of the theoretical constructs produced by only text information. Although a marketing scale of construct measurement is traditionally applied to obtain these scores in survey research, the learned model with our proposed method does not require a survey. This finding implies that the various applications can be developed with our proposed method. For example, many services like review websites, Twitter, and Facebook provide the posted text information but

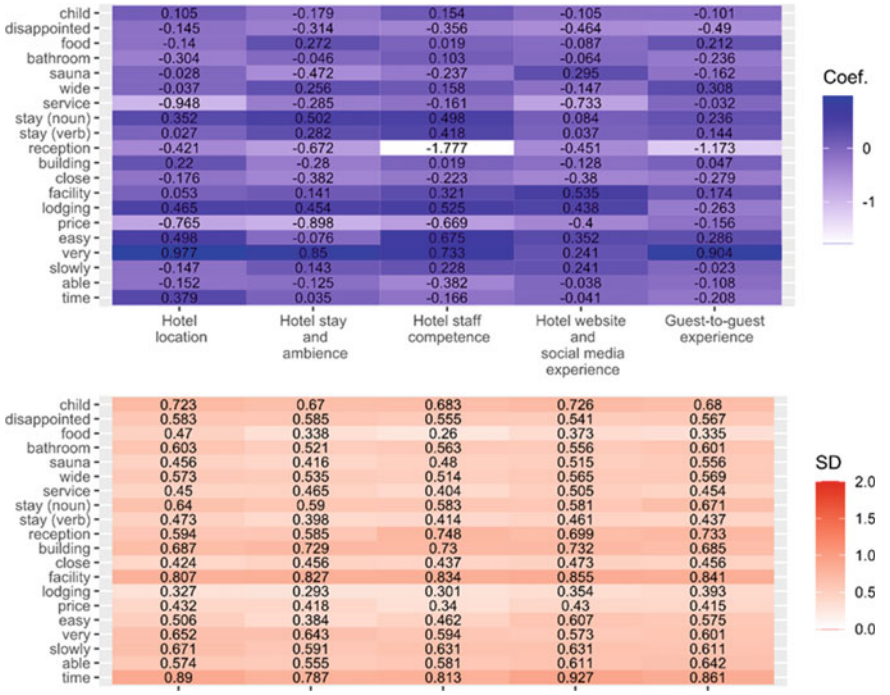

Fig. 1.8 Means (upper) and SDs (bottom) of estimates for term weights in the proposed model (Top 20 TF-IDF words)

Table 1.3 Accuracy rates of predictive scores on actual item scores

	HL1	**HL2**	**HL3**	**HSA1**	**HSA2**	**HSA3**	**HSA4**	**HSC1**	**HSC2**	**HSC3**	**HSC4**
Train	0.460	0.438	0.430	0.393	0.380	0.470	0.458	0.490	0.415	0.548	0.510
Test	0.269	0.306	0.269	0.306	0.225	0.338	0.306	0.338	0.275	0.313	0.319
(Cont.)	**HSE1**	**HSE2**	**HSE3**	**GGE1**	**GGE2**	**GGE3**					
Train	0.495	0.465	0.455	0.535	0.548	0.523					
Test	0.288	0.300	0.294	0.331	0.344	0.394					

not with the scores of construct measurement. In these cases, the alternative scores of the theoretical constructs can be obtained with the textual data, thereby adapting the leaned model results in past research. It is possible for researchers not only to summarize the customer reviews based on the theoretical constructs but also to use the alternative scores for additional analysis or decision-making to approach the customers. Our methodology will help and enhance the investigation of consumer psychologies and behaviors by using any text information.

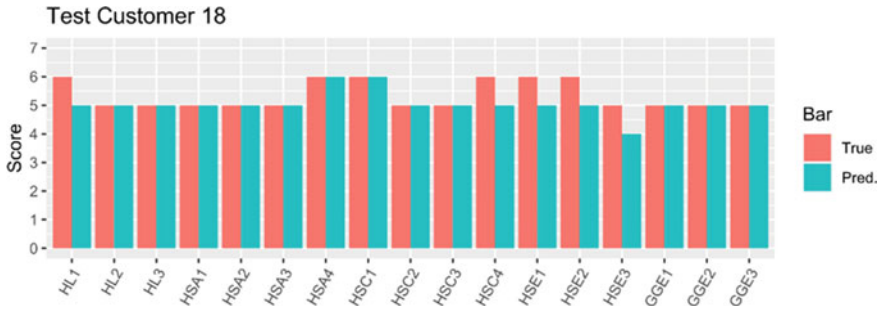

Fig. 1.9 Estimates of item score predicted with only text information in the test sample (An example customer)

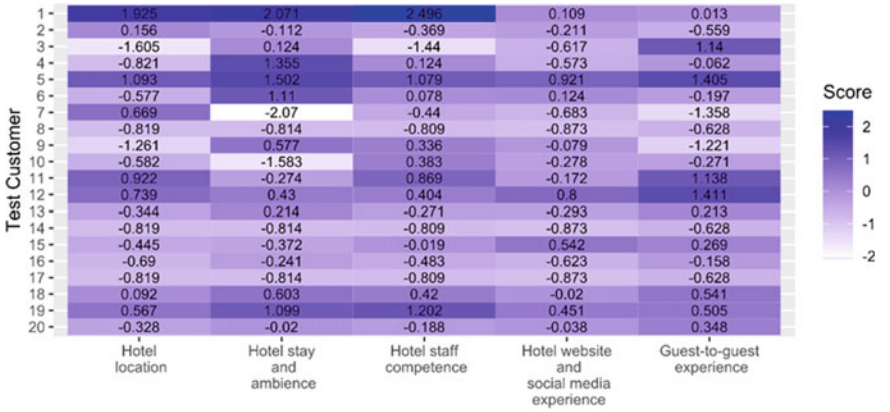

Fig. 1.10 Estimates of factor scores reproduced with only text information in the test sample (20 example customers)

Concluding Remarks

In this paper, we introduced and demonstrated a penalized neural network for the construct measurement with text information. Our proposed model provides stable and explainable results compared with a standard type of unconstrained neural network. Furthermore, we can predict unobserved item scores and obtain alternative scores of theoretical constructs from only textual data via the learned model. This alternative score will support marketers and researchers to measure theoretical constructs without marketing scales. We believe that this methodology potentially contributes to creating various applications and analyzing different combinations of datasets. However, we could not find a significantly large difference in model fitting performance between the benchmark and proposed models. To improve the accuracy, it might be possible to increase the number of hidden units and layers. Although tuning the overcomplete and deep neural network is technical and not easy, it should

be considered in future investigations, including the comparisons with other machine learning methods.

For limitations and remaining tasks, there are three possible discussions. First, the open-ended question should be improved to lead to various words and sentence expressions from respondents. The dimension of effective terms was only 600, and the total of the single words (2,196 words) was also not large. When obtaining the new types of words that were not contained in the training dataset, we must drop these new words or count them as zero to conduct a prediction for unseen latent and item scores in practical applications. This situation probably reduces the prediction performance. Second, validation with different data sources is required. Because we tested only with the survey dataset, it will be possible to adapt our results to other textual data such as actual hotel reviews on the internet. Third, it is also necessary to consider how to improve the validity of our methodology. For example, we showed the estimated term weight matrix in Fig. 1.9; however, this result does not imply a causal relationship. It may be an important topic for marketing and consumer behavior research to find reasonable causes between single words and constructs and to specify them manually in the model.

Acknowledgements The author gratefully acknowledges the partial supports of JSPS KAKENHI Grant Numbers 20K22125 and 22K13496. The author would also like to thank Enago (www.enago.jp) for the English language review.

References

1. Bharadwaj, N., et al. (2022). A new livestream retail analytics framework to assess the sales impact of emotional displays. *Journal of Marketing, 86*(1), 27–47.
2. Hartmann, J., et al. (2021). The power of brand selfies. *Journal of Marketing Research, 58*(6), 1159–1177.
3. Wang, X. (Shane), et al. (2021). Attribute embedding: Learning hierarchical representations of product attributes from consumer reviews. *Journal of Marketing,* 1–21.
4. Luo, X., et al. (2021). Artificial intelligence coaches for sales agents: Caveats and solutions. *Journal of Marketing, 85*(2), 14–32.
5. Gai, P. J., & Klesse, A.-K. (2019). Making recommendations more effective through framings: Impacts of user-versus item-based framings on recommendation click-throughs. *Journal of Marketing, 83*(6), 61–75.
6. Braganza, A., et al. (2021). Productive employment and decent work: The impact of AI adoption on psychological contracts, job engagement and employee trust. *Journal of Business Research, 131*, 485–494.
7. Wang, W., et al. (2021). Accelerating AI adoption with responsible AI signals and employee engagement mechanisms in health care. *Information Systems Frontiers,* 1–18.
8. Aljumah, A. I., et al. (2021). Traditional marketing analytics, big data analytics and big data system quality and the success of new product development. *Business Process Management Journal, 27*(4), 1108–1125.
9. Xu, Z., et al. (2016). Effects of big data analytics and traditional marketing analytics on new product success: A knowledge fusion perspective. *Journal of Business Research, 69*(5), 1562–1566.

10. Hair, J. F., & Sarstedt, M. (2021). Data, measurement, and causal inferences in machine learning: Opportunities and challenges for marketing. *J. Mark. Theory Pract., 29*(1), 65–77.
11. Gäthke, J., et al. (2021). A cross-national service strategy to manage product returns: E-Tailers' return policies and the legitimating role of the institutional environment. *Journal of Service Research,* 1–12.
12. Padmavathy, C., et al. (2019). Online second-hand shopping motivation—Conceptualization, scale development, and validation. *Journal of Retailing and Consumer Services, 51*, 19–32.
13. Panagopoulos, N. G., et al. (2020). Firm actions to develop an ambidextrous sales force. *Journal of Service Research, 23*(1), 87–104.
14. Teng, H.-Y., & Tsaur, S.-H. (2021). Charismatic tour-guiding: Scale development and validation. *Journal of Travel Research,* 1–13.
15. Wittkowski, K., et al. (2020). What gets measured gets done: can self-tracking technologies enhance advice compliance? *Journal of Service Research, 23*(3), 281–298.
16. Mankad, S., et al. (2016). Understanding online hotel reviews through automated text analysis. *Service Science, 8*(2), 124–138.
17. Humphreys, A., & Wang, R.J.-H. (2018). Automated text analysis for consumer research. *The Journal of Consumer Research, 44*(6), 1274–1306.
18. Pandey, S., & Pandey, S. K. (2019). Applying natural language processing capabilities in computerized textual analysis to measure organizational culture. *Organizational Research Methods, 22*(3), 765–797.
19. Tsao, H.-Y. (Jody), et al. (2020). A machine-learning based approach to measuring constructs through text analysis. *European Journal of Marketing, 54*(3), 511–524
20. Jain, P. K., et al. (2021). A systematic literature review on machine learning applications for consumer sentiment analysis using online reviews. *Computer Science Review, 41*, 100413.
21. Onan, A. (2021). Sentiment analysis on product reviews based on weighted word embeddings and deep neural networks. *Concurrency and Computation: Practice and Experience, 33*(23), 1–13.
22. Sato, T. (2021). Penalizing neural network and autoencoder for the analysis of marketing measurement scales in service marketing applications. In R. Qiu, K. Lyons, & W. Chen (Eds.), *AI and analytics for smart cities and service systems* (pp. 31–42). Springer International Publishing.
23. Khan, I., & Rahman, Z. (2017). Development of a scale to measure hotel brand experiences. *International Journal of Contemporary Hospitality Management, 29*(1), 268–287.
24. Blei, D. M., et al. (2003). Latent dirichlet allocation. *Journal of Machine Learning Research, 3*, 993–1022.
25. Hansen, S., et al. (2018). Transparency and deliberation within the FOMC: a computational linguistics approach. *The Quarterly Journal of Economics, 133*(2), 801–870.
26. Kingma, D.P., & Ba, J. (2017). Adam: A method for stochastic optimization. ArXiv14126980 Cs.

Chapter 2
Deep Learning-Based Prediction of Mechanical Ventilation Reintubation in Intensive Care Units

Hangtian Li and Xiaolei Xie

Abstract Mechanical ventilation is widely used in intensive care units, especially for the treatment of acute respiratory distress syndrome and acute lung injury. Physiological parameters of critically ill patients change rapidly, which poses a challenge to the strategy development of mechanical ventilation. Despite the existence of multiple clinical guidelines, a personalized ventilation strategy is still lacking. With the rapid development of machine learning, many studies have applied machine learning methods to ventilator strategy optimization, but there is currently a lack of research on predicting the situation of reintubation after weaning. This study proposes a deep learning algorithm including an attention mechanism to predict the situation of reintubation after weaning, and achieved better performance than the basic algorithm.

Keywords Mechanical ventilation · Deep learning · Attention mechanism · Reintubation

Introduction

The use of mechanical ventilation in the intensive care unit (ICU) is quite common, with approximately 33% of patients in the ICU requiring mechanical ventilation and incurring very high costs [1]. One survey showed that patients ventilated in the ICU cost 59% more than those who did not [2]. Mechanical ventilation is an important component in the treatment of acute respiratory distress syndrome (ARDS) [3] and also plays a key role in the treatment of acute lung injury [4].

Although there are several clinical guidelines and basic studies on mechanical ventilation, there is still a lack of individualized ventilation strategies for individual

H. Li · X. Xie (✉)
Department of Industrial Engineering, Tsinghua University, Beijing 100084, China
e-mail: xxie@tsinghua.edu.cn

H. Li
e-mail: liht19@mails.tsinghua.edu.cn

R. Qiu et al. (eds.), *City, Society, and Digital Transformation*, Lecture Notes in Operations Research, https://doi.org/10.1007/978-3-031-15644-1_2

patients [5]. With the development of machine learning techniques and the construction of medical databases, some researchers have applied machine learning methods for the prediction and optimization of mechanical ventilation strategies. Chang et al. used a variety of machine learning algorithms-logistic regression, random forest, SVM, light GBM, MLP, XGBoost, and Naïve Bayes Classifier-to predict whether a patient who has completed lung resection can be taken off the ventilator immediately [6]. Jia et al. proposed a convolutional neural network algorithm to predict whether a patient would be off the ventilator within one hour based on the MIMIC-iii dataset [7]. Prasad et al. used a reinforcement learning algorithm to calculate the timing of patient withdrawal based on the patient's physiological monitoring data and achieved results that exceeded clinical practice [8]. Peine et al. proposed a reinforcement learning algorithm to optimize ventilator settings for patients undergoing mechanical ventilation: Vtset, PEEP, and FiO_2, and the algorithm yielded more agile ventilator operations compared to clinical practice [5].

The timing of ventilator withdrawal is a critical decision in ventilator use. 20–30% of patients are considered difficult to detach from the ventilator [9], and patients are reintubated within 48 h of extubation, defined as extubation failure [10]. Ventilator extubation failure is considered to be associated with high mortality and increases the risk of patients contracting pneumonia [11]. Therefore, predicting whether a patient will be reintubated after weaning is critical to ventilator use.

In this study, a deep learning approach was used to predict the occurrence of patient reintubation, based on more than 10,000 ventilator usage data. The major contributions of this study are as follows:

(1) We use the Long Short Term Memory (LSTM) neural network algorithm to predict ventilator reintubation. To the best of our knowledge, there are no studies using deep learning for reintubation prediction so far.
(2) An attention mechanism is introduced between patient physiological monitoring data and patient physiological characteristics, which allows LSTM to focus on key information of the monitoring data in conjunction with patient's individual characteristics (e.g., diagnosis) to enhance model prediction.

Data Set

The MIMIC-iii dataset is a large, freely available intensive care dataset that contains medically informative data on 53,423 adult patients and 7870 pediatric patients treated in the ICU at Beth Israel Deaconess Medical Center between 2001 and 2012 [12]. The MIMIC-iii database recorded physiological indicators related to mechanical ventilation such as: heart rate, respiratory rate, pH, Oxygen saturation (SPO_2), Partial pressure of oxygen in arterial blood (PAO_2), Partial pressure of carbon dioxide ($PACO_2$), Fraction of Inspired Oxygen (FIO_2), and other operations related to mechanical ventilation (Table 2.1).

We extracted more than 20,000 patients who had used ventilators from the total number of MIMIC-iii patients. Of these, children, patients who used the ventilator

Table 2.1 Distribution of patient types

	ARDS	Others (Non-ARDS)	Sum
Non-reintubation	2624	5236	7860
Reintubation	1445	2426	3871
Sum	4069	7662	11,731

for less than 12 h [7], and patients with missing key information were subsequently excluded. This resulted in 11,731 records of ventilator use, each including eight physiological monitoring data during patient use (hr, rr, pH, SPO_2, PAO_2, $PACO_2$, FIO_2, PAO_2/FIO_2), as well as the patient's age, gender and primary diagnosis. Among the extracted data, 4069 patients with ARDS were included. Of the total number of patients, 7860 were not reintubated within 24 h of weaning and 3871 patients were reintubated.

Each physiological monitoring data of the patient was discretized at 10-min intervals, and time points for which no data were recorded were imputed in using linear interpolation. We pooled the monitoring data for each patient for the 8 h prior to their extubation, i.e., the length of each time series was $8 * 6 = 48$. The pre-processed time series data of one patient is shown in Fig. 2.1, containing eight series of hr, rr, pH, SPO_2, PAO_2, $PACO_2$, FIO_2, PAO_2/FIO_2.

Methods

First, we use the Long Short Term Memory (LSTM) algorithm, which feeds the preprocessed time series directly into the neural network, using the labels (whether the patient is reintubated or not) for training. This method is commonly used to deal with time series prediction, but suffers from two major shortcomings. The first is that LSTM has a weak ability to capture data correlation in long series, another is LSTM is unable to adequately capture the correlation between static variables and time series. Figure 2.2 is the flow chart of our baseline method.

The attention mechanism can enhance the model's ability to focus on essential information and discover correlations, which in turn can compensate for these deficiencies of the LSTM approach [13]. Therefore, this study added an additive attention mechanism to the prediction model. The additive attention mechanism can assign a weight α_i to the output of step i of the LSTM, and the final output of the model is the output of each step multiplied by its corresponding weight and summed [14]. The weight α_i is calculated as:

$$\alpha_i = \exp[s(h_i, q)] / \sum_{k=1}^{T_h} \exp[s(h_k, q)] \tag{2.1}$$

$$s(h_i, q) = v^T \tanh(Wh_i + Uq) \tag{2.2}$$

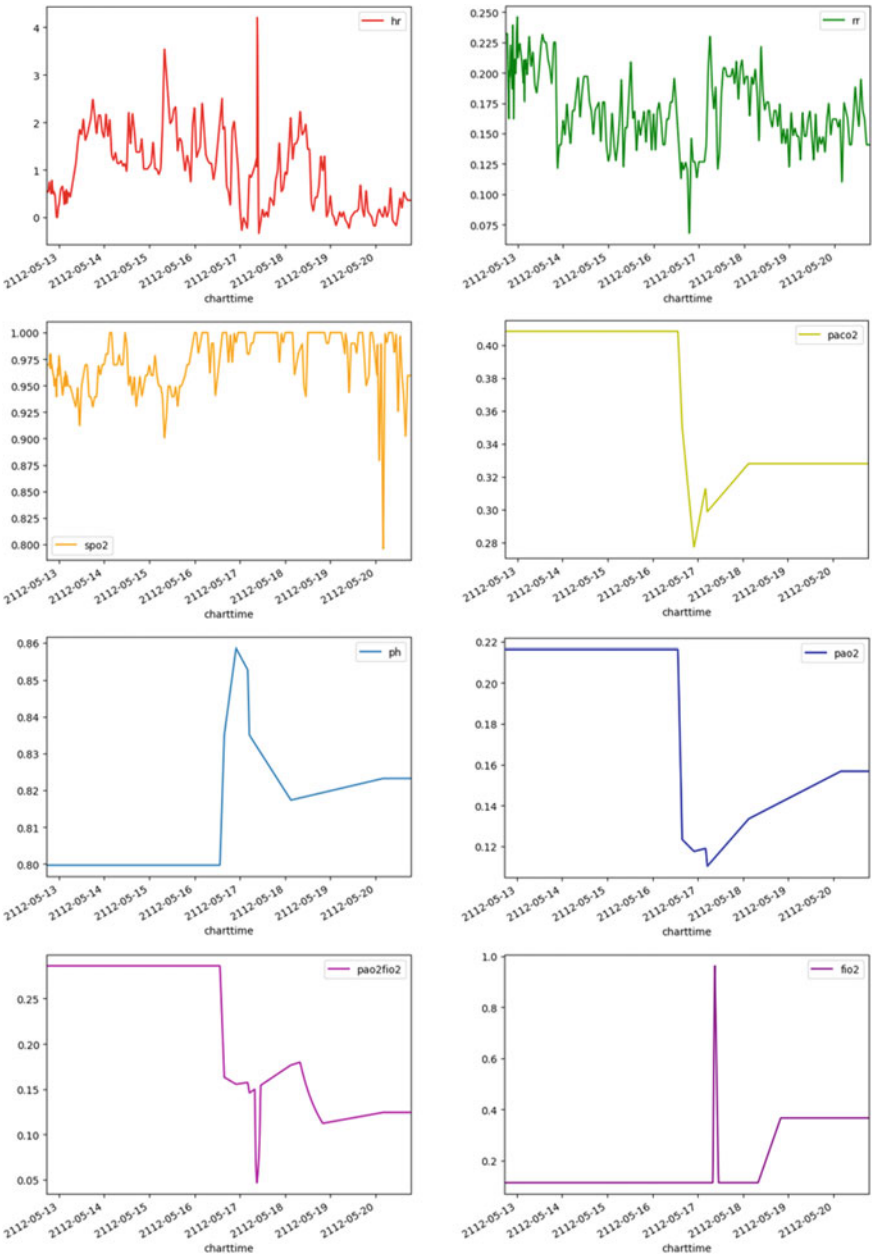

Fig. 2.1 Pre-processed physiological monitoring data from a patient

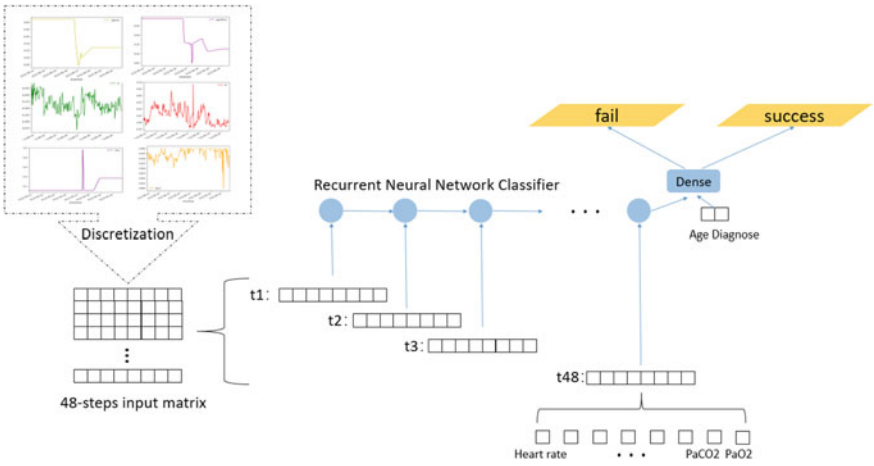

Fig. 2.2 Flow chart of LSTM algorithm

where h_i = the output of step i of the LSTM and q = the query vector. The s is computed equivalent to a fully continuous neural network using the tangent function as the activation function, where W, v and U are the parameters in the neural network.

The full computational flow chart for LSTM + attention is as Fig. 2.3. First, the patient's primary diagnosis is coded as one-hot and inputted to a fully connected neural network for coding, after which it is combined with the patient's age and gender to form the patient's physiological characteristics (i.e., the vector q in the attention calculation formula). Second, the eight physiological monitoring data of the patient for eight hours before ventilator weaning are sliced into 48 8-dim vectors (i.e., sampled every 10 min) and input to the LSTM network. Then we input the output vectors (i.e., hi in the attention calculation formula) of LSTM together with the physiological characteristics of the patient into the additive attention network and calculate the attention weights. Last, based on the computed attention weights, the 48 steps data are weighted and summed, and the results are input to the fully connected neural network together with the patient's physiological characteristics for classification prediction.

Experiments and Results

The data were divided into training and test sets according to 7:3. The LSTM and LSTM + attention algorithms were tested for different prediction ranges and patient populations, i.e., for reintubation within 12 h, reintubation within 24 h, and for reintubation in the ARDS group, all patients, respectively. Due to the unbalanced distribution of data, we used Area under the ROC Curve (AUC) to measure the

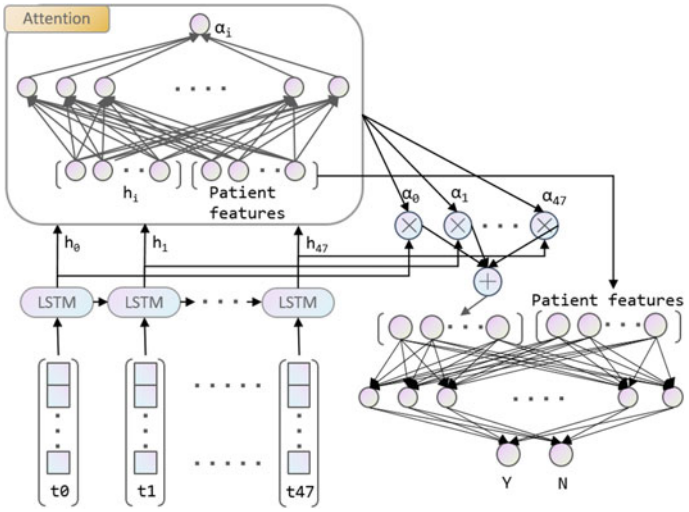

Fig. 2.3 Flow chart of LSTM + attention algorithm

predictive ability. Each algorithm test was repeated 10 times, and the results of the 10 times were averaged.

Tested separately for different prediction horizons (i.e., predicting reintubation at 12 and 24 h) and different patient groups (i.e., all patients and ARDS patients), the results show that LSTM + attention outperforms the LSTM method in all cases. And the most significant improvement was observed in the ARDS patient group. In predicting reintubation within 24 h, both methods were tested 20 times. The pair t-test shows that the LSTM + attention method has better performance ($p < 0.01$) (Tables 2.2 and 2.3), the bold numbers denote better performance.

Table 2.2 Performance of LSTM and LSTM + attention in different prediction horizons

Method	AUC	Improve
LSTM (within 12 h)	0.597	–
LSTM + attention (within 12 h)	**0.606**	**1.51**%
LSTM (within 24 h)	0.607	–
LSTM + attention (within 24 h)	**0.616**	**1.48**%

Table 2.3 Performance of LSTM and LSTM + Attention in different patient group

Method	AUC	Improve
LSTM (ARDS)	0.584	–
LSTM + attention (ARDS)	**0.605**	**3.60**%
LSTM (ALL)	0.607	–
LSTM + attention (ALL)	**0.616**	**1.48**%

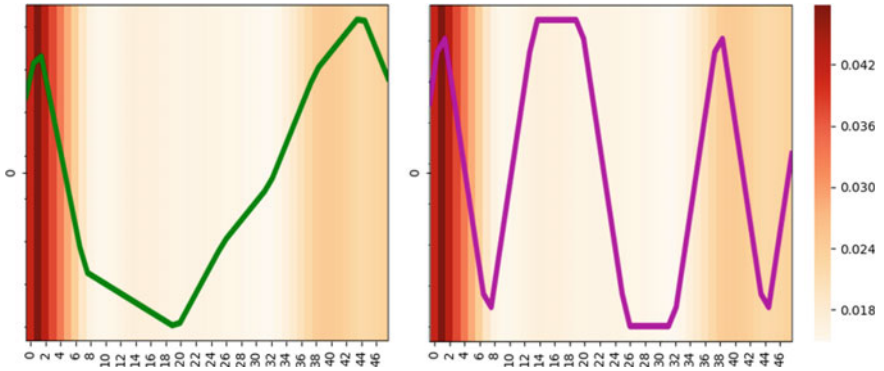

Fig. 2.4 Heatmap of attention weights of a randomly sampled patient. Visualized attention weights aligned with respiration rate (left) and blood oxygen saturation (right), respectively

The AUC of our algorithm is around 0.6, which is not high for a two-class problem. This may be caused by insufficient data volume and low data quality. And it also illustrates that predicting reintubation is a challenging task. The introduction of the attention mechanism improves the prediction performance by 1.48–3.60%, and the inherent property of the attention mechanism can directly quantify the attention weight of the algorithm. We visualized the attention weights of physiological monitoring data of a sample patient using a heat map, as shown in Fig. 2.4. This mechanism and visualization provide the possibility and convenience for clinicians to summarize relevant guideline information in the future.

Summary

This study proposed a deep learning approach to build an algorithm for predicting patient reintubation after ventilator withdrawal using patient physiological monitoring data recorded in the MIMIC-iii database. The prediction of reintubation helps patients avoid additional pain and prognostic risk due to failed weaning. The prediction algorithm uses not only the time series data recorded by the device in the ICU, but also incorporates static data such as the patient.s diagnosis and age, and employs an attention mechanism, which allows the algorithm to determine the focus of attention on the time series based on both static and dynamic information about the patient. Experiments show that introducing an attention mechanism can steadily improve the method prediction performance. Furthermore, the introduction of the attention mechanism can enhance the interpretability of the model, and valuable clinical guidance information can be summarized in the future based on the information that the model focuses on.

Acknowledgements This study is sponsored by Tsinghua-Toyota Joint Research Institute Interdisciplinary Program.

References

1. Dasta, J. F., McLaughlin, T. P., Mody, S. H., & Piech, C. T. (2005). Daily cost of an intensive care unit day: The contribution of mechanical ventilation. *Critical Care Medicine, 33*(6), 1266–1271.
2. Kaier, K., Heister, T., Wolff, J., & Wolkewitz, M. (2020). Mechanical ventilation and the daily cost of ICU care. *BMC Health Services Research, 20*(1), 1–5.
3. Girard, T. D., & Bernard, G. R. (2007). Mechanical ventilation in ARDS: A state-of-the-art review. *Chest, 131*(3), 921–929.
4. Krishnan, J. A., & Brower, R. G. (2000). High-frequency ventilation for acute lung injury and ARDS. *Chest, 118*(3), 795–807.
5. Peine, A., Hallawa, A., Bickenbach, J., Dartmann, G., Fazlic, L. B., Schmeink, A., Ascheid, G., Thiemermann, C., Schuppert, A., Kindle, R., & Celi, L. (2021). Development and validation of a reinforcement learning algorithm to dynamically optimize mechanical ventilation in critical care. *NPJ Digital Medicine, 4*(1), 1–12.
6. Chang, Y.-J., Hung, K.-C., Wang, L.-K., Yu, C.-H., Chen, C.-K., & Tay, H.-T. (2021). A real-time artificial intelligence-assisted system to predict weaning from ventilator immediately after lung resection surgery. *International Journal of Environmental Research, 18*(5), 2713.
7. Jia, Y., Kaul, C., Lawton, T., Murray-Smith, R., & Habli, I. (2021). Prediction of weaning from mechanical ventilation using convolutional neural networks. *Artificial Intelligence in Medicine, 117*, 102087.
8. Prasad, N., Cheng, L.-F., Chivers, C., Draugelis, M., & Engelhardt, B.E. (2017). A reinforcement learning approach to weaning of mechanical ventilation in intensive care units. arXiv preprint arXiv:.06300.
9. Heunks, L. M., & Van Der Hoeven, J. G. (2010). Clinical review: The ABC of weaning failure-a structured approach. *Critical care, 14*(6), 1–9.
10. Boles, J. M., Bion, J., Connors, A., Herridge, M., Marsh, B., Melot, C., Pearl, R., Silverman, H., Stanchina, M., Vieillard-Baron, A., & Welte, T. (2007). Weaning from mechanical ventilation. *European Respiratory Journal, 29*(5), 1033–1056.
11. Torres, A., Gatell, J.M., Aznar, E., El-Ebiary, M., Puig de la Bellacasa, J., González, J., Ferrer, M., & Rodriguez-Roisin, R. (19950.) Re-intubation increases the risk of nosocomial pneumonia in patients needing mechanical ventilation. *American Journal of Respiratory Critical Care Medicine, 152*(1), 137–141.
12. Johnson, A.E., Pollard, T.J., Shen, L., Lehman, L.W.H., Feng, M., Ghassemi, M., Moody, B., Szolovits, P., Anthony Celi, L., & Mark, R.G. (2016). MIMIC-III, a freely accessible critical care database. *Scientific Data, 3*(1), 1–9.
13. Vaswani, A., Shazeer, N., Parmar, N., Uszkoreit, J., Jones, L., Gomez, A.N., Kaiser, Ł., & Polosukhin, I. (2017). Attention is all you need. *Advances in Neural Information Processing Systems, 30*
14. Bahdanau, D., Cho, K., & Bengio, Y. (2014). Neural machine translation by jointly learning to align and translate. arXiv preprint arXiv:1409.0473

Chapter 3
Mitigating Braess's Paradox with Information Design

Zhenxiao Chen, Yonghui Chen, and Qiao-Chu He

Abstract Building a new route for public transportation suffers Braess's paradox in which introducing a cost-efficient link ends up with congestion and efficiency loss. To curb this paradox, this paper incorporates information design in a congestion network model to demonstrate that an optimal information design rule can be leveraged to nudge commuters' overcrowding behaviors and eliminate Braess's paradox. This finding highlights that smart communications are critical for improving urban transportation efficiency.

Keywords Information design · Braess's paradox · Public transportation

Introduction

To ease urban traffic congestion, governments invest billions of dollars in developing public transportation, such as new metro or bus lines, to encourage commuters to reduce private car dependency. With more public transportation routes available, it is believed that more traffic efficiency will be generated. However, the reverse can be true due to the well-known Braess's paradox where introducing a new cost-efficient link to a network ends up with congestion and efficiency loss due to users overcrowding the new link. This paper studies how a transportation authority can leverage information design to eliminate Braess's paradox and improve urban traffic efficiency when introducing public transportation links.

Z. Chen · Y. Chen · Q.-C. He (✉)
No. 1088 Xueyuan Avenue, Nanshan District, Shenzhen, China
e-mail: heqc@sustech.edu.cn

Z. Chen
e-mail: 12131290@mail.sustech.edu.cn

Y. Chen
e-mail: chenyh3@sustech.edu.cn

R. Qiu et al. (eds.), *City, Society, and Digital Transformation*, Lecture Notes in Operations Research, https://doi.org/10.1007/978-3-031-15644-1_3

Literature Review

[1] extend the study of Braess's paradox to an asymmetric information environment where some users have more information than others. Based on the Wardrop equilibrium where users choose the shortest route, they show that Braess's paradox persists even when users are provided with more information. In experimental tests, [5] find behavioral evidence for the persistence of Braess's paradox in networks with both negative and positive externalities.

There are studies on how to improve traffic efficiency by means of information provision. [4] show that whether more information provision improves traffic efficiency depends on the population size of informed travelers. Incorporating uncertainty of traffic state into a routing model, [7] study the value of information for informed travelers when there is information asymmetry among them.

Information design is based on Bayesian persuasion proposed by [3] where the sender's signaling rule is characterized by receivers' posterior belief under a credibility constraint. Information design has been applied to persuade voters in elections [2], and customers in online review platforms [6].

Model

Consider an urban traffic network as shown in Fig. 3.1 where commuters travel from the origin O to the destination D via vertexes A and B. There are two routes OAD and OBD, denoted by r_1 and r_2, respectively, available for private transportation. OAD represents a route where a commuter drives a private car through the first-mile link OA and then the highway link AD to the destination; OBD describes the route that a commuter drives through the highway link OB followed by the last-mile link BD. We assume that traffic cost via the highway link OB/AD is sufficiently large and fixed at b while congestion cost of the first/last-mile link OA/BD is αf, where f is the traffic flow it carries and α measures the marginal congestion cost.

Public transportation and uncertainty. The government introduces a new route for public transportation which connects the first and last-mile links OA and BD.

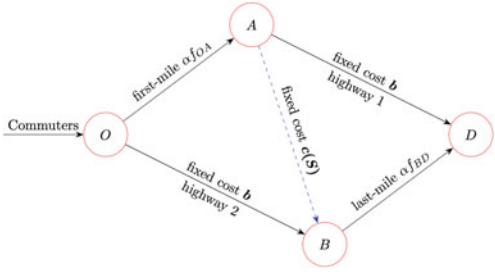

Fig. 3.1 The traffic network with both private and public transportation

Thus, a third route $OABD$, denoted by r_3, is a mix of private and public transportation. The state of public transportation s follows a two-type distribution with probability θ for a "bad" state $s = H$, and the other probability $1 - \theta$ for a "good" state $s = L$. Consider the "bad" state as public transportation disruptions, such as bus breakdowns or metro system failures. The new public transportation link AB has a fixed and state-dependent traffic cost c^s where $0 < c^L < c^H < b$.

Travel flows. There is a mass of λ commuters traveling from O to D, each of whom can choose one of the three routes in the network. Denote f_k as the number of commuters (traffic flow) on the link k, where $k \in \{OA, AD, AB, OB, BD\}$. Then the following equations hold:

$$f_{AB} + f_{AD} = f_{OA} \tag{1}$$

$$f_{OB} + f_{AB} = f_{BD} \tag{2}$$

$$f_{OA} + f_{OB} = f_{AD} + f_{BD} = \lambda \tag{3}$$

Denote F_1, F_2, and F_3 as the traffic flows on routes $r_1(OAD)$, $r_2(OBD)$ and $r_3(OABD)$, respectively. Then it can be derived that $F_1 = f_{AD}$, $F_2 = f_{OB}$, and $F_3 = f_{AB}$. As r_1 and r_2 are symmetric, traffic flows on these two routes are the same, i.e., $f_{AD} = f_{OB} \in [0, \frac{\lambda}{2}]$ such that $f_{OA} = f_{BD} = \lambda - f_{AD} \in [\frac{\lambda}{2}, \lambda]$ according to Eq. (3). Thus, the traffic flows on routes r_1 and r_2 can be written as $F_1 = F_2 = f_{OB} = \lambda - f_{OA}$ and the traffic flow on route r_3 is $F_3 = 1 - 2F_1 = 2f_{OA} - \lambda$. As traffic flows on the three routes depend on f_{OA} only, we regard f_{OA} as the traffic equilibrium throughout this paper.

Preliminary analysis In the basic network with private transportation routes r_1 and r_2 available, it is easy to see that half of the commuters choose route r_1 and the other half of them choose route r_2, resulting total congestion cost $TC_0 = (\frac{\alpha\lambda}{2} + b)\lambda$. This allocation is consistent with the social optimal outcome.

Full Information

We first investigate commuters' routing behaviors under full information to show the overcrowding problem on public transportation and its coexistence with Braess's paradox.

Commuters' self-selected decisions. Each commuter makes a self-selected routing decision by choosing a route with lower cost (between r_1/r_2 and r_3), and incurs an individual congestion cost

$$IC = \min\{\alpha f_{OA} + b, 2\alpha f_{OA} + c^s\}, \forall s \in \{H, L\} \tag{4}$$

Each commuter's goal is to minimize the individual congestion cost, leading to a Wardrop equilibrium, where any chosen routes have the same expected congestion cost and any unchosen routes have strictly higher congestion cost than chosen

ones. As routes r_1 and r_2 are symmetric, there are three possible traffic allocations among the three routes. If congestion cost on the public link AB is significantly high, i.e., $c^s > b - \frac{\alpha\lambda}{2}$, then route r_3 generates a greater cost than r_1 and r_2 even when no commuter chooses public transportation (i.e., $\alpha\lambda + c^s > \frac{\alpha\lambda}{2} + b$). In this case, public transportation is not used and all the commuters choose private transportation with equal traffic flows on routes r_1 and r_2, i.e., $f_{OA} = \frac{\lambda}{2}$. In contrast, if the congestion cost on the public link is sufficiently low, i.e., $c^s < b - \alpha\lambda$, then public transportation always has a lower cost than private transportation, leading all the commuters to public transportation, i.e., $f_{OA} = \lambda$. If the congestion cost of the public link is intermediate, i.e., $b - \alpha\lambda \le c^s \le b - \frac{\alpha\lambda}{2}$, then the equilibrium traffic assignment is such that all the three routes have the same expected congestion cost, i.e., $\alpha f_{OA} + b = 2\alpha f_{OA} + c^s$, implying the equilibrium $f_{OA} = \frac{b-c^s}{\alpha}$. We summarize the equilibrium results under self-selected routing in the following equation.

$$f_{OA}^{SR} = \begin{cases} \frac{\lambda}{2} & \text{if } c^s > b - \frac{\alpha\lambda}{2} \\ \frac{b-c^s}{\alpha} & \text{if } b - \alpha\lambda \le c^s \le b - \frac{\alpha\lambda}{2} \\ \lambda & \text{if } c^s < b - \alpha\lambda \end{cases} \tag{5}$$

Based on the equilibrium allocation f_{OA}^{SR}, the traffic flow on each route is $F_1^{SR} = F_2^{SR} = \lambda - f_{OA}^{SR}$ and $F_3^{SR} = 2f_{OA}^{SR} - \lambda$, and the congestion cost on each route is $C_1^{SR} = C_2^{SR} = \alpha f_{OA}^{SR} + b$ and $C_3^{SR} = 2\alpha f_{OA}^{SR} + c^s$. Thus, the total congestion cost $TC_{SR}^s = 2F_1^{SR}C_1^{SR} + F_3^{SR}C_3^{SR}$ in state s can be derived as follows:

$$TC_{SR}^s = \begin{cases} (\frac{\alpha\lambda}{2} + b)\lambda & \text{if } c^s > b - \frac{\alpha\lambda}{2} \\ (2b - c^s)\lambda & \text{if } b - \alpha\lambda \le c^s \le b - \frac{\alpha\lambda}{2} \\ (2\alpha\lambda + c^s)\lambda & \text{if } c^s < b - \alpha\lambda \end{cases} \tag{6}$$

Proposition 1 *Introducing the new public transportation link results in Braess's paradox (i.e., $TC_{SR}^s \ge TC_0$) when the congestion cost of the new link is intermediate (i.e., $c^s \in [b - \frac{3}{2}\alpha\lambda, b - \frac{1}{2}\alpha\lambda]$.)*

Proposition 1 shows that whether introducing a public link helps ease congestion depends on the congestion cost of the public link. If the congestion cost is so high that no commuters choose public transportation, introducing the link has no impact on traffic congestion. In contrast, if the congestion cost is so low that all commuters benefit from using public transportation, introducing the new link mitigates traffic congestion. If the congestion cost is intermediate, traffic congestion deteriorates as public transportation is overused–the well-known Braess's paradox.

The first-best The total traffic cost of the traffic system in state s is

$$\min_{f_{OA} \in [\frac{\lambda}{2}, \lambda]} \quad TC^s = 2F_1(\alpha f_{OA} + b) - F_3(2\alpha f_{OA} + c^s), \forall s \in \{H, L\} \tag{7}$$

Solving the optimization problem yields

$$f_{OA}^{FB} = \begin{cases} \frac{\lambda}{2} & \text{if } c^s > b - \alpha\lambda \\ \frac{b-c^s}{2\alpha} & \text{if } b - 2\alpha\lambda \le c^s \le b - \alpha\lambda \\ \lambda & \text{if } c^s < b - 2\alpha\lambda \end{cases}, \tag{8}$$

such that the traffic flow on public transportation is $F_3^{FB} = 2f_{OA}^{FB} - \lambda$.

Proposition 2 *1. For intermediate cost (i.e., $c^s \in [b - 2\alpha\lambda, b - \frac{\alpha\lambda}{2}]$) commuters overcrowd the new route (i.e., $F_{3,SR}^s \ge F_{3,FB}^s$.)*

2. For high or low cost (i.e., $c^s > b - \frac{\alpha\lambda}{2}$ or $c^s < b - 2\alpha\lambda$) commuters' self-select decisions coincide with the first-best (i.e., $F_{3,SR}^s = F_{3,FB}^s$.)

Proof As $f_{OA}^{SR} > f_{OA}^{FB}$ for $c^s \in [b - 2\alpha\lambda, b - \frac{\alpha\lambda}{2}]$, $F_3^{SR} = 2f_{OA}^{SR} - \lambda > 2f_{OA}^{FB} - \lambda = F_3^{FB}$ holds.

Given that the public link has been introduced, Proposition 2 shows that commuters' self-selected decisions deviate from the first-best and cause an overcrowding problem on public transportation if the congestion cost is intermediate. Otherwise, it is socially optimal that all/no commuters choose public transportation if the congestion cost is sufficiently low/high.

We depict the results of Propositions 1 and 2 in Fig. 3.2 to show the coexistence of public transportation overcrowding and Braess's paradox as the public link's congestion cost changes: (1) Given an extremely high/low congestion cost of the public link ($c^s > b - 0.5\alpha\lambda$ or $c^s < b - 2\alpha\lambda$,) public transportation is fully utilized/abandoned by all commuters whose self-selected decisions are socially optimal. In this case, both

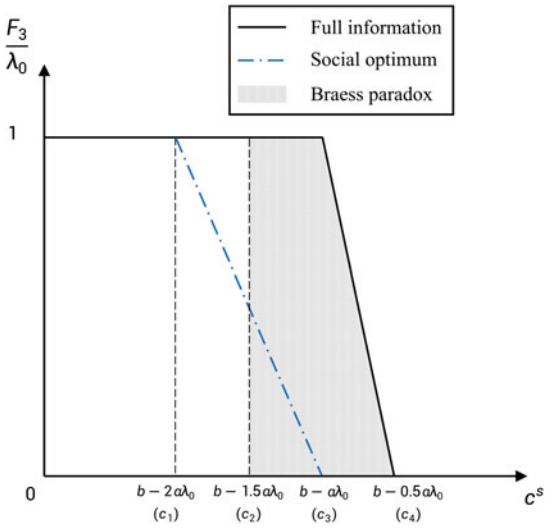

Fig. 3.2 Effect of the public link's cost on traffic assignment

Table 3.1 Coexistence of overcrowding and Braess's paradox under full information

c^s	Overcrowding	Paradox	Optimality of full information
$[0, b-2\alpha\lambda)$	No	No	Yes
$[b-2\alpha\lambda, b-1.5\alpha\lambda)$	Yes	No	No
$[b-1.5\alpha\lambda, b-0.5\alpha\lambda)$	Yes	Yes	No
$[b-0.5\alpha\lambda, +\infty)$	No	No	Irrelevant

the overcrowding problem and Braess's paradox are absent. (2) Given an intermediately high congestion cost of the public link ($b-1.5\alpha\lambda < c^s \leq b-0.5\alpha\lambda$,) both the overcrowding problem and Braess's paradox occur due to commuters' self-selected decisions. However, (3) commuters' self-selected decisions can cause public transportation overcrowding but keep Braess's paradox silent given an intermediately low congestion cost ($b-2\alpha\lambda < c^s \leq b-1.5\alpha\lambda$). Thus, commuters' overcrowding public transportation (deviating from the first-best) does not necessarily imply Braess's paradox.

Under full information, we have so far identified conditions for the coexistence of public transportation overcrowding and Braess's paradox which hinders the positive impacts of introducing public transportation on improving traffic efficiency. To address this issue, the transportation authority may need to leverage information design to nudge commuters' self-selected behaviors. We summarize conditions for full information disclosure to be optimal in Table 3.1: Full information leads to both public transportation overcrowding and Braess's paradox (overcrowding only) when the public link's congestion cost is intermediately high (low). Otherwise, either full information is optimal or information has no influence on commuters' behaviors.

Information Design

We analyze the optimal information design under Bayesian persuasion which allows us to focus on the posterior belief of commuters. Denote the system's information design is such that the commuters' posterior expectation of c^s is (Ec^H, Ec^L) in states H and L, respectively. Each commuter's posterior expected congestion cost is as follows

$$EIC = \min\{\alpha f_{OA} + b, 2\alpha f_{OA} + Ec^s\}, \forall s \in \{H, L\} \tag{9}$$

Similar to the case of full information, commuters choose a route with a lower expected congestion cost and we can derive the Wardrop equilibrium under the posterior expectation Ec^s as follows.

$$f_{OA}^{ID} = \begin{cases} \frac{\lambda}{2} & \text{if } Ec^s > b - \frac{\alpha\lambda}{2} \\ \frac{b - Ec^s}{\alpha} & \text{if } b - \alpha\lambda \le Ec^s \le b - \frac{\alpha\lambda}{2} \\ \lambda & \text{if } Ec^s < b - \alpha\lambda \end{cases} \tag{10}$$

Based on the equilibrium traffic assignment f_{OA}^{ID} in state s, the traffic flow on each route can be derived as $F_1^{ID} = F_2^{ID} = \lambda - f_{OA}^{ID}$ and $F_3^{ID} = 2f_{OA}^{ID} - \lambda$.

Assumption 1 $c^H > b - \frac{\alpha\lambda}{2} > \bar{c} > c^L$, *where* $\bar{c} \triangleq \theta c^H + (1-\theta)c^L$.

To demonstrate the role of information design in restoring traffic efficiency, we focus on the case in which commuters overcrowd the public link when it is in the "good" state L while their self-selected behaviors are consistent with the first-best is the "bad" state H, i.e., $c^H > b - \frac{\alpha\lambda}{2} > c^L$, such that $f_{OA}^{ID} = f_{OA}^{FB}$. In this case, full information disclosure is optimal in state H as shown in Table 3.1, and information design is needed to restore efficiency in state L. Under Assumption 1, information design improves traffic efficiency in state L by upward distorting commuters' posterior beliefs on the public link's cost ($Ec^L \ge c^L$), leading fewer commuters to public transportation. In comparison to the network without the public link, information design can also be leveraged to eliminate Braess's paradox.

Conclusions

When introducing a public transportation link with an intermediate congestion cost into a traffic network, Braess's paradox prevails as it ends up with efficiency loss. The underlying reason for this paradox is commuters overcrowding public transportation under full information. Thus, careful information design is needed to nudge commuters' overcrowding behaviors. We derive the optimal information design rule for the government to mitigate the overcrowding problem and show that information design eliminates Braess's paradox such that introducing public transportation improves urban traffic efficiency along with strategic communications.

References

1. Acemoglu, D., Makhdoumi, A., Malekian, A., & Ozdaglar, A. (2018). Informational Braess' paradox: The effect of information on traffic congestion. *Operations Research, 66*(4), 893–917.
2. Alonso, R., & Câmara, O. (2016). Persuading voters. *American Economic Review, 106*(11), 3590–3605.
3. Kamenica, E., & Gentzkow, M. (2011). Bayesian persuasion. *American Economic Review, 101*(6), 2590–2615.
4. Liu, J., Amin, S., & Schwartz, G. (2016). Effects of information heterogeneity in Bayesian routing games. arXiv:1603.08853
5. Mak, V., Seale, D. A., Gisches, E. J., Yang, R., Cheng, M., Moon, M., & Rapoport, A. (2018). The Braess paradox and coordination failure in directed networks with mixed externalities. *Production and Operations Management, 27*(4), 717–733.

6. Papanastasiou, Y., Bimpikis, K., & Savva, N. (2018). Crowdsourcing exploration. *Management Science, 64*(4), 1727–1746.
7. Wu, M., Amin, S., & Ozdaglar, A. E. (2021). Value of information in Bayesian routing games. *Operations Research, 69*(1), 148–163.

Chapter 4
The Impact of Electronic Shelf Label on Customer Well-Being in the Omnichannel Smart Retail

Darren Jonathan Ovani and Nila Armelia Windasari

Abstract While the number of online retail transactions shows a significant upward trend, most people still shop offline with the higher preferences on contactless encounters. The future technologies in omnichannel retail are enabled through in-store technology (IST) and one of the applications is Electronic Shelf Label (ESL). While a lot of studies have developed IST little is known about the impact of IST on customers well-being and their behavior. This study aims to assess the impact of ESL as an emerging and prospective IST on customer well-being. Data were collected through an online survey embedded with a video of ESL features stimuli. A total of 305 valid responses from people living in Indonesia were collected and analyzed using partial least square structural equation modeling (PLS-SEM). This study provides empirical evidence of how smart retails affect customers' subjective well-being (SWB) and psychological well-being (PWB). Practically, it also helps retail managers in considering ESL implementation in the next-normal era.

Keywords Customer well-being · Electronic shelf label · Omnichannel retail · Smart retail

Introduction

The emergence of the COVID-19 pandemic has transformed the retail industry more rapidly. The implementation of social distancing and governments order to stay at home has accelerated the adoption of e-commerce usage at a significant level [1]. Retail and wholesale companies are disrupted and forced to implement significant amendments in running their business and further planning to adapt [2]. A global consumer survey in 2020 unveiled that 63% of respondents are buying more groceries

D. J. Ovani (✉) · N. A. Windasari
School of Business and Management, Institut Teknologi Bandung, Bandung, West Java 40132, Indonesia
e-mail: darren_jonathan@sbm-itb.ac.id

N. A. Windasari
e-mail: nila.armelia@sbm-itb.ac.id

R. Qiu et al. (eds.), *City, Society, and Digital Transformation*, Lecture Notes in Operations Research, https://doi.org/10.1007/978-3-031-15644-1_4

online than before social distancing and 86% are going to continue this behavior [3]. However, despite the pandemic condition, traditional trade and modern trade channels have still become the major preferences for several product categories [4].

New technologies like the internet of things (IoT), the communication between machine to machine [5], are suggested to be the initial phase of the development of omnichannel commerce [6]. Smart retail is projected to develop significantly in the near future. 80% of customers use smartphones as in-store shopping assistants and 78% of customers' mark integrating e-commerce with in-store experience as critical [7]. A study among Generation Z consumers suggests that smart retail experience is important for meeting or even exceeding consumer expectations (price and customer service) [6, 8]. Furthermore, smart retail is affirmed to enhance customer experience and build consumer loyalty [9].

A product of smart retail that is growing and predicted to have an even more significant growth at a CAGR of 21.8% between 2021 and 2028 is Electronic Shelf Label (ESL) [10]. ESL is a substitute for traditional paper labels to display product information through a digital screen and is connected through a network to enable rapid and automatic updates [10, 11]. However, there is a lack of study of how ESL will affect customer behavior. Meanwhile at the customer level, there is an arguable impact of digitalization on human well-being [12].

Well-being is the combination of feeling good and functioning well [13]. It is a preferable measure in the service context due to its focus on promoting consumer and societal welfare [14]. A unique retail experience and well-being-focused retail are argued to be the ones that can bring back the brick and mortar retail industry after the massive loss caused by the COVID-19 pandemic [15]. This is due to the increased attention to health and wellness, as well as the transforming customer expectation of gaining leisure, social, and wellness value from shopping as a result of the sophistication of the retail environment [15]. The use of well-being measures in today's retail services is important. This study aims to study how ESL features and attributes will affect customer well-being.

Literature Review

Electronic Shelf Label (ESl)

ESL is equivalent to price tags in retail stores, product ID labels in warehouses, and instruction sheets in manufacturing assembly lines [16]. It is a device that enables product price to be displayed digitally [11], using an electronic paper, liquid crystal display, or thin-film transistor in various dimensions [17]. It offers a quick synchronization between background database, cash register, and price inquiry through various network technology, for instance, Near Field Communication (NFC), Zigbee, RFID, Bluetooth Low Energy (BLE), and so forth [10, 17].

Table 4.1 ESL features available on market

Feature	Description	Source/Company
Always updated information	Quick synchronization through several network technology allowing always updated information	Ref. [10]
Digital display	Offering visualization of products on the label, able to display up to 3 different colors, and able to create a personalized label design template	High Bright Enterprise Limited, Opticon Sensors Europe
Detailed product information	Through QR code, NFC, and barcode, customer is able to get detailed product information on their smartphone	Tronitag, Solum ESL [11]
Product wayfinding	Locate product through external applications and blinking LED light on ESL	LabelNest
Buttons on ESL	Buttons on ESL body to change ESL page, call service help, report low stock, and send system report	Solum ESL
Unmanned shopping experience	Digital shopping cart and payment through customer card, credit card, debit card, and NFC	Opticon Sensors Europe

The ESL provides several advantages both for retailers and customers. It elevates store operational efficiency [18], enabling the retailers to change the price quickly and accurately while cutting back on the number of labor needed [11]. While for customers, ESL as a product of IoT will enhance the customer experience and satisfaction [9, 19]. Technology companies are developing ESL, increasing ESL features and functionality. Several identifications of ESL features that may affect customer experience are listed in Table 4.1.

An example of ESL implementation is the partnership between Kroger and Microsoft in creating Enhanced Display for Grocery Environment (EDGE) [20]. EDGE gain positive feedback from 90% of customers [21]. It is also preferred by 7 out of 8 mystery shoppers and influences customer decisions [22]. Personalization, in-the-moment marketing, and interactive wayfinding are EDGE features favored by customers [20]. On the retailer's side, EDGE has helped to increase offline retail value [20, 21].

Customer Wellbeing

Despite the preference of using well-being as a measure in the service context [14], the definition and concept of well-being vary in the literature [23]. Three well-being concepts are indicated to have a relationship with the retail context are presented in Table 4.2.

The CWB measures well-being on all of the consumption processes, acquisition, possession, consumption, maintenance, and disposition [27]. Thus, since this study measures the impact of ESL on well-being only on the in-store experience, the CWB is inapposite. The different approaches of SWB and PWB complement each other and are the dimension of well-being [24]. Reference [28] also reviews the usage of both SWB and PWB on measuring UK national well-being. As for this research, SWB and PWB will both be used in the context of smart retail.

Reference [29] recognizes three dimensions of SWB: life satisfaction, positive feeling, and negative feeling. Life satisfaction and positive feeling have a positive effect on well-being while negative feeling has a negative effect on well-being. Ryff mentioned 6 dimensions of PWB: self-acceptance, good social relations, autonomy, environmental control, life purpose, and personal growth [30]. Used dimensions from the two concepts used for each hypothesis are listed in Table 4.3.

Reference [31] discussed how the physical and informative aspect of a promotion display can increase customer attraction to promote customer positive attitudes. Sales promotion is the encouragement of customer action through the offering of additional benefits, commonly on a specific period, place, and target [32]. The rapid information update on ESL and its ability to provide a more sophisticated visualization as well

Table 4.2 Wellbeing concepts and definitions

No.	Concept	Description	Reference
1	Subjective well-being (SWB)	Hedonic approach of well-being, focusing on attainment of pleasure and avoidance of pain	[24, 25]
2	Psychological well-being (PWB)	Eudaimonic approach of well-being, focusing on meaning and self-realization	[24, 26]
3	Consumer well-being (CWB)	Individual well-being as a consumer on the consumption-related aspects	[23, 27]

Table 4.3 Wellbeing dimensions

Hypothesis	Concept	Dimension used
1	SWB	Positive feeling
2	SWB	Life satisfaction
3	PWB	Life purpose
4	SWB	Life satisfaction
5	PWB	Environmental mastery

as information compared to traditional paper labels should elevate customer positive feeling.

H1: Customer attraction has a significant positive effect on SWB.

ESL offers to provide more product information. Limitations on consumer capability in processing information may cause unsatisfactory decisions [33]. A study reveals that satisfaction in the acquisition, possession, and consumption process has a significant contribution to overall life satisfaction [27]. Thus, the abundance of information offered by ESL can be detrimental to a person's overall life satisfaction.

H2: Enhanced product information has a significant negative effect on SWB.

On the other hand, omnichannel consumers are identified to purchase consumption based on needs, financial rationality, and personal characteristic-and-individual value [34], demanding product information. Thus, enhanced product information should help and convince customers on determining their purchase decision better for their needs and value.

H3: Enhanced product information has a significant positive effect on PWB.

ESL can realize the unmanned shopping experience through digital payment and virtual shopping cart [35]. The unmanned shopping experience will provide time savings as a result of automation. The automated product wayfinding and quicker payment or even a check-out free feature are the examples. Time savings is suggested to elevate customer satisfaction [36]. Referring to the above-mentioned study, hypothesis 4 is made.

H4: Unmanned shopping experience has a significant positive effect on SWB.

Furthermore, features such as automated product wayfinding and check-out free will enable customers to have more control over their surroundings. Thus, hypothesis 5 is made.

H5: Unmanned shopping experience has a significant positive effect on PWB.

Method

Samples and Data Collection Procedure

Data were collected through an online survey distributed by agencies. Participants were restricted to those who are living in Indonesia and born between 1965 and 2012 (Gen X − Gen Z age cohort). Total valid responses collected was 305 respondents, far above the minimum sample of 125 respondents calculated using G Power 3.1 [37] (F test, linear multiple regression, fixed model, R2 deviation from zero, a priori type for 95% confidence interval using the least R square value from SWB of 0.167).

All variable indicators were measured using a fully labelled 5-point Likert scale. The measurement items are shown on Table 4.4. All indicators were presented in Bahasa Indonesia as an everyday language in Indonesia to let the respondents have a better understanding. To ensure participant fully immersed to the ESL usage and environment, a 93-s video explaining ESL in general and ESL features was made and embedded into the online questionnaire. The video begins with ESL definition and system overview. ESL features of

(1) always updated information;
(2) advanced label visualization;
(3) product information access through smartphones;
(4) access to information of product availability-and-in-store location, and
(5) the full unmanned store experience.

were visualized and narrated in Bahasa Indonesia. Several real case examples were also mentioned. The video was complemented with auto-generated subtitles for various languages provided by YouTube. Respondents should watch the video and tick the statement 'I have watched the video' prior to continuing to fill out the survey. A summary list of ESL features is also attached to ease respondents in reviewing the ESL features. A pilot study was conducted to ensure the survey was well-understood by the respondents and to select the final valid indicators. The snapshot of the video can be seen on Fig. 4.1.

Data Analysis

Employing the final indicator list, all factor loadings are proved to be statistically significant ($\lambda > 0.5$), showing that each indicator is a good measure for the latent variable [41]. The composite reliability score for all variables is above 0.7 [42] showing good internal consistency. Furthermore, all AVE score is above 0.5, showing a good discriminant validity [43, 44]. In addition, the heterotrait-monotrait (HTMT) ratio is also assessed to further ensure the discriminant validity. Although several variable HTMT values are close to 1, all of the values are still below 0.9 and acceptable [45].

Results and Discussions

Hypothesis were analyzed using 5000 resample complete bootstrapping with Smart PLS 3 [46]. Bias-Corrected and Accelerated Bootstrap for two-tailed test with significance level of 0.05 is employed. The results of hypothesis testing are shown on Table 4.5, as well as Fig. 4.2. Post-hoc analysis was conducted by split the samples based on respondents' demographic profile of age cohort, Gen X and Millennials for those

Table 4.4 Measurement items

Variables	Measurements	Source	Loadings	AVE	CR
Customer attraction	ESL makes a pleasing color scheme	[38]	0.790	0.584	0.849
	ESL makes an attractive physical facility		0.759		
	ESL makes impressive in-store display		0.766		
	ESL is able to display adequate in-store information		0.742		
Enhanced product information	ESL provides easy access to various product information	Self-developed	0.848	0.644	0.878
	ESL can provide easy access to detailed product information		0.811		
	ESL can provide easy access to product availability information		0.826		
	ESL can provide easy access to in-store product location information		0.719		
Unmanned shopping experience	ESL can realize the unmanned shopping experience	Self-developed	0.800	0.612	0.863
	Self-payment features as well as virtual shopping lists can realize an unmanned shopping experience		0.778		
	The product availability information feature can realize an unmanned shopping experience		0.816		
	In-store product location information feature can realize unmanned shopping experience		0.732		
Subjective wellbeing	In most ways my life is close to my ideal	[39]	0.824	0.650	0.903

(continued)

Table 4.4 (continued)

Variables	Measurements	Source	Loadings	AVE	CR
	The conditions of my life are excellent		0.809		
	I am satisfied with my life		0.820		
	So far I have gotten the important things I want in life		0.810		
	If I could live my life over, I would change almost nothing		0.765		
Psychological wellbeing	Generally, I feel confident and positive about myself	[30, 40]	0.705	0.542	0.876
	I am quite able to manage the many responsibilities about myself in my life		0.756		
	My daily life is full of busy activities, but I get a satisfaction feeling for I can do/follow it all		0.725		
	I have goals in my life		0.752		
	I live my life from day to day and just think about the future		0.738		
	In my final analysis, I am sure that my life means a lot		0.739		

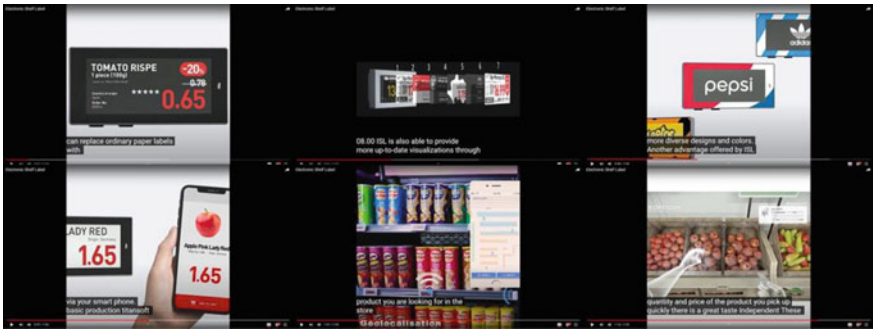

Fig. 4.1 ESL stimuli for survey

who were born between 1965 and 1996 and Gen Z for those who were born between 1997 and 2012.

Hypothesis 1, customer attraction has a significant positive effect on SWB is accepted. The visual enhancement is promoting customer convenience, excitement, and decreases complexity to ease information processing which results in customer positive emotion [31, 47, 48]. ESL's ability to provide various colors and personalized template designs on the electronic labels should ease customers in processing label information. Thus, ESL increases customer positive feelings.

However, hypothesis 1 is rejected by Gen X and Millennials on the split population test. The reason underlying this difference is technology exposure. Gen X are people who were born between baby boomers, which are considered a totally traditional generation, and Millennials, a more tech-savvy generation [49]. On the other hand, Gen Z has been exposed to technology from an early age [50]. Generation X is more comfortable to combine both traditional and technology-applied communication [51]. Gen X uses technology for utilitarian needs, unlike Gen Z which truly favored technology [52]. ESL changes the store environment to be very technologically applied. Thus, it is not very comforting and favored for Gen X and Millennials when compared to Gen Zers.

Hypothesis 2, enhanced product information has a significant negative effect on SWB is rejected. While the hypothesis is rejected, the relation of enhanced product information to SWB is still negative. The previous study shows how information overload may cause dissatisfaction and create irrational decision making due to customer inability to process the information and unknown information sources and quality

Table 4.5 Hypothesis results

Relationship	General				Gen X and Millennials		Gen Z	
	Std Beta	Std Error	t-value	*p*-value	t-value	*p*-value	t-value	*p*-value
H1. Customer attraction > SWB	0.408	0.094	4.232	0.000***	1.506	0.132	5.559	0.000***
H2. Enhanced product information > SWB	−0.133	0.098	1.313	0.189	0.146	0.884	2.822	0.005**
H3. Enhanced product information > PWB	0.236	0.067	3.518	0.000***	2.545	0.011*	2.46	0.014*
H4. Unmanned store experience > SWB	0.127	0.075	1.694	0.09	1.176	0.24	1.46	0.144
H5. Unmanned store experience > PWB	0.381	0.064	5.901	0.000***	3.288	0.001**	5.338	0.000***

Note *$p < 0.05$; **$p < 0.01$; ***$p < 0.001$

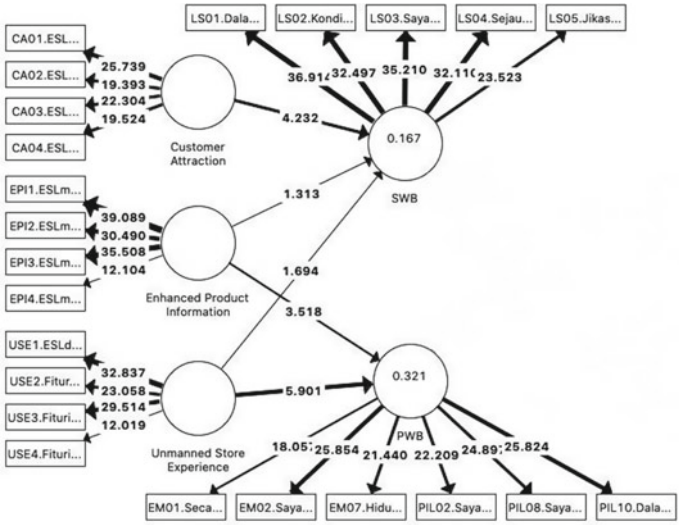

Fig. 4.2 Variable loadings

[33, 53, 54]. The enhanced product information provided by ESL may still cause information overload and causes dissatisfaction. However, the source of the information is clear and should be able to give customers a hint of information quality. Furthermore, information on product availability and in-store product location should not confuse customers.

However, on the split sample hypothesis testing, hypothesis 2 is accepted for Gen Z. The reason is because Gen Z has a higher demand for frictionless purchases than other cohorts [55, 56]. Gen Z likes to have the convenience and individualized experience [56, 57]. The process of gaining product information through QR code, NFC, and barcode that is provided by ESL may cause customer friction. Gen Z would prefer to be presented with information that suits them rather than being given a lot of information and letting them find what works for them. It is in contrast with Gen X who do product research prior to buying [58]. Thus, the significance of hypothesis 2 differs between the age cohorts.

Hypothesis 3, enhanced product information has a significant positive effect on PWB is accepted. Omnichannel consumers are said to respect their values on choosing products [34]. Self-identity is also moderating the positive effect of product information on purchase intention [59]. ESL's ability to provide various detailed information of a product through smartphones helps customers in choosing products that align with their values and identity. Information such as product material used, product supplier, and nearly anything is able to be presented.

Hypothesis 4, unmanned shopping experience has a significant positive effect on SWB is rejected. It was suggested that time savings should have a positive significant effect on customer satisfaction [36]. Satisfaction on the acquisition, possession, and consumption stage of consumption is also elucidated to influence satisfaction

[27]. Conversely, a study also suggests the negative effect of in-store technology if shopping is seen as a sociable event [8]. Kargal and Suresh also mention roadblocks of in-store IoT adoption, namely customer privacy issues, information misuse, and so forth [9]. The time savings provided by ESL might increase satisfaction, however, several factors such as the leisure factor of shopping and customer privacy concerns might also contribute significantly to the shopping satisfaction and other dimensions of SWB.

Hypothesis 5, unmanned shopping experience has a significant positive effect on PWB is accepted. ESL is able to provide customers with a high degree of customer independence, resulting in the realization of unmanned store experience at its best. Product availability information, automated product wayfinding, as well as virtual shopping cart-and-self check-out are ESL features that contribute to promoting customer independence. This high degree of independence gives a sense of positive functioning by enabling customers in creating the desired environment by themselves.

The proven effects of ESL features on customer well-being will help retail businesses to consider investing in ESL in the next normal era. Several studies have elucidated the connection of SWB and PWB that promotes customer behavioral outcomes to be beneficial for the retail businesses. For instance, promoting customer willingness to pay more and positive word of mouth that has a direct positive effect on product price and sales volume, the two variables that affect retail business revenue.

For willingness to pay, customer satisfaction and positive emotion (SWB) have been explained to have a positive significant effect on customers' willingness to pay more [36, 60]. Premium price is an important financial outcome, showing the price premium customers are willing to spend for the same goods at different providers [61]. This is an indication for retailers that they might be able to increase their product prices with ESL implementation through SWB promotion.

For positive word of mouth, a study discovers that positive emotion (SWB) is the best predictor of positive word of mouth among cognitive components and negative emotion [60]. Another study proves a significant effect of quality of life well-being (SWB) on positive word of mouth [62]. From PWB, service use self-efficacy is approved to have a significant positive effect on positive word of mouth [63]. A study found that word of mouth and product sales is known to have a reciprocal effect that creates a snowball effect [64]. In addition, word of mouth is said to determine 20–50% of purchasing decisions [65]. The promotion of SWB and PWB through ESL implementation should increase positive word of mouth that is able to generate more sales volume.

Furthermore, retailers should put consideration in realizing the enhanced product information feature if the customer is in the Gen Z age cohort. Retailers should consider offering enhanced product information through personalization rather than providing information to avoid friction that causes negative feeling.

Conclusions and Implications

This study responds to the current-future trend of omnichannel smart retail. While most papers discuss the development of IST and the managerial implications [66], little is known about its influence on customer well-being. This study evaluates the impact of ESL implementation as an emerging and prospective IST on customer well-being in Indonesia. The use of the customer well-being construct aligns with the transformative service research paradigm in responding to the transforming customer expectation of gaining leisure, social, and wellness value from shopping as a result of the sophistication of the retail environment [15].

Theoretically, this study provides empirical evidence of how smart retails affect SWB and PWB in a retail context. The concept is able to mediate the effect of ESL features on customer post purchase behavior. Practically, the study provides an initial picture of how ESL technology may impact retail businesses by discussing how customer well-being may be affected by the ESL features to choose which features should or should not be utilized in actual retail settings.

Several limitations are identified in this study. First, this study only restricts the respondents to those who are living in Indonesia and provides a general result. A future study might use a more specific segmentation by determining a more specific population beforehand. For instance, control variables based on rural and urban areas, as well as different technology adoption levels are able to be used.

Second, this study uses video-stimuli of ESL features. Respondents are required to individually imagine their ESL shopping experience based on the explanation video embedded in the survey. Future studies may replicate the framework using an actual ESL shopping environment. Several improvements are also able to be made on the conceptual framework adapting to the improvement of ESL features and relevant customer post-transaction behavior. For example, customer willingness to pay more and positive word of mouth. Relevant moderating variables with the well-being concept as the dependent variable are also able to be added. For instance, perceived risk of use, risk of privacy, information misuse, and so forth. These will increase the understanding of ESL's impact on the retail context. Future studies should focus on developing shorter and more reliable indicators for well-being concepts. Study of the impact of ESL on customer post transaction behavior is important as well, mainly for practical purposes.

Acknowledgements The authors report there are no competing interests to declare. This work was supported by the P2MI Research Grant 2022 from Institut Teknologi Bandung.

References

1. O'Hara, T., et al. (2020). *Are you ready for e-commerce acceleration?* https://www.oliverwyman.com/our-expertise/insights/2021/jan/boardroom-volume-6/e-commerce/are-you-ready-for-e-commerce-acceleration1.html (While many retailers are still, the pivotal point of change).
2. Haller, K., Lee, J., Cheung, J. (2021). *Resetting the rules for consumer companies.* https://www.ibm.com/thought-leadership/institute-business-value/report/retail-wholesale-disruption
3. An, L., et al. (2020). *The consumer transformed: Changing behaviours are accelerating trends along a reinvented customer purchase journey.* https://www.pwc.com/id/en/industry-sectors/consumer-industrial-products-services/consumer-insights-survey.html
4. Nurhayati-Wolff, H. (2021). *Preferred retail channels among households in Indonesia as of September 2020, by product category.* https://www.statista.com/statistics/1239085/indonesia-preferred-purchase-channels-by-category/ (According to a consumer survey, online channels among Indonesian households).
5. Petrescu, M., Krishen, A., & Bui, M. (2020). The internet of everything: Implications of marketing analytics from a consumer policy perspective. *Journal of Consumer Marketing, 37*(6), 675–686. https://doi.org/10.1108/JCM-02-2019-3080
6. Kaczorowska-Spychalska, D. (2017). Consumer perspective of omnichannel commerce. *Management, 21*(2), 95–108. https://doi.org/10.1515/manment-2017-0007
7. Dobreva, K. (2018). Global e-commerce trends and statistics. https://amasty.com/blog/wp-content/uploads/2021/02/Global-E-Commerce-Trends-And-Statistics.pdf
8. Priporas, C. V., Stylos, N., & Fotiadis, A. K. (2017). Generation Z consumers' expectations of interactions in smart retailing: A future agenda. *Computers in Human Behavior, 77*, 374–381. https://doi.org/10.1016/j.chb.2017.01.058
9. Kargal, R.G., Suresh, R. (2020). Internet-of-Things (IoT) in the retail industry: Consumer perceptions and key considerations for retail adoption. *AAYAM, 10*(2), 9–14.
10. Khan, M. A. A., Lian, X., Mirani, I. K., & Tan, L. (2021). Research on key technologies of electronic shelf labels based on LoRa. *Journal on Big Data, 3*(2), 49–63. https://doi.org/10.32604/jbd.2021.016213
11. McKenzie, B., & Taylor, V. (2016). The use of electronic shelf labels in the retail food sector. *International Journal of Economic and Management Engineering, 10*(2), 627–630. https://doi.org/10.5281/zenodo.1111981
12. Anderson, J., & Rainie, L. (2018). The future of well-being in a tech-saturated world. *Pew Research Center*, April 2018. https://www.pewresearch.org/internet/2018/04/17/the-future-of-well-being-in-a-tech-saturated-world/
13. Ruggeri, K., Garcia-Garzon, E., Maguire, Á., Matz, S., & Huppert, F. A. (2020). Well-being is more than happiness and life satisfaction: A multidimensional analysis of 21 countries. *Health and Quality of Life Outcomes, 18*(192), 1–17. https://doi.org/10.1186/s12955-020-01423-y
14. Rosenbaum, A.S.M.S., et al. (2011). Conceptualisation and aspirations of transformative service research. *19*, 1–6.
15. Maggioni, I. (2021). The science of well-being in retail. *The Choice*, January 2021. https://thechoice.escp.eu/tomorrow-choices/the-science-of-well-being-in-retail/
16. Banakar, K., & Shetty, S. (2019). RapidNet IP: A synchronized, high throughput , low power wireless networking solution for ESL. *5*(15). https://doi.org/10.4108/eai.16-7-2019.162213
17. Meticulous Market Research. Electronic shelf label market worth $2.57 billion by 2028. *Meticulous Research.* https://www.meticulousresearch.com/pressrelease/434/electronic-shelf-label-market-2028
18. Devanesan, M. D., & Venkatesh, R. (2021). Impact of in-store retail technologies on enhancing retail footfall among physical retail formats in India. *Academy of Marketing Studies Journal, 25*(6), 1–13.
19. Abdel-Basset, M., Mohamed, M., Chang, V., & Smarandache, F. (2019). IoT and its impact on the electronics market: A powerful decision support system for helping customers in choosing the best product. *Symmetry (Basel), 11*. https://doi.org/10.3390/sym11050611

20. Walton, C. (2019). Retailers should pay extra special attention to Kroger's shelf labeling plans with Microsoft. *Forbes*, February 2019. https://www.forbes.com/sites/christopherwalton/2019/02/11/retailers-should-pay-extra-special-attention-to-krogers-shelf-labeling-plans-with-microsoft/?sh=64fa3bed25a8
21. Briggs, B. (2018). Kroger's smart shelves ditch the paper, drop the lights and delight the shoppers. *Microsoft*, June, 2018. https://news.microsoft.com/transform/kroger-smart-shelves-ditch-paper-drop-lights-delight-shoppers/
22. Hofbauer, R. (2019). Test shoppers find Kroger's new digital shelves 'influential' on purchase decisions," progressive grocer, Feb-2019. https://progressivegrocer.com/test-shoppers-find-krogers-new-digital-shelves-influential-purchase-decisions
23. Zhao, C., & Wei, H. (2019). The highest hierarchy of consumption: A literature review of consumer well-being. *Open Journal of Social Sciences, 07*(04), 135–149. https://doi.org/10.4236/jss.2019.74012
24. Ryan, R. M., & Deci, E. L. (2001). On happiness and human potentials: A review of research on Hedonic and Eudaimonic well-being. *Annual Review of Psychology, 52*(1), 141–166. https://doi.org/10.1146/annurev.psych.52.1.141
25. Diener, E. (1984). Subjective well-being. *Psychological Bulletin, 95*(3), 542–575.
26. Ryff, C. D. (1989). Beyond Ponce de Leon and life satisfaction: New directions in quest of successful ageing. *International Journal of Behavioral Development, 12*, 35–55. https://doi.org/10.1177/016502548901200102
27. Lee, D. J., Sirgy, M. J., Larsen, V., & Wright, N. D. (2002). Developing a subjective measure of consumer well-being. *Journal of Macromarketing, 22*(2), 158–169. https://doi.org/10.1177/0276146702238219
28. Allin, P., & Hand, D. J. (2017). New statistics for old?— Measuring the wellbeing of the UK. *Journal of the Royal Statistical Society, Series A, 180*(1), 3–43. https://doi.org/10.1111/rssa.12188
29. Burroughs, J.E., & Rindfleisch, A. (2002). Materialism and well-being: A conflicting values perspective. *Journal of Consumer Research, 29*. https://doi.org/10.1086/344429
30. Ryff, C. D. (1989). Happiness is everything, or is it? Explorations on the meaning of psychological well-being. *American Psychological Association, 57*(6), 1069–1081.
31. Gorji, M., & Siami, S. (2020). How sales promotion display affects customer shopping intentions in retails. *48*(12), 1337–1355. https://doi.org/10.1108/IJRDM-12-2019-0407
32. Peattie, S., & Peattie, K.J. (1994) Sales promotion. In M. J. Baker (Ed.), *The marketing book* (3rd ed.). London.
33. Houdek, P., Koblovský, P., Šťastný, D., & Vranka, M. (2018). Consumer decision making in the information age. *Social Science and Public Policy, 55*(5), 422–429. https://doi.org/10.1007/s12115-018-0283-5
34. Hsieh, M.Y. (2020). Interdisciplinarily exploring the most potential IoT technology determinants in the omnichannel e-commerce purchasing decision-making processes. *Applied Sciences, 10*(2). https://doi.org/10.3390/app10020603
35. Opticon. *Opticon electronic shelf labels*. https://opticon.com/product-category/display-solutions/electronic-shelf-labels/. Accessed October 15, 2021.
36. Savastano, M., Bellini, F., D'Ascenzo, F., & De Marco, M. (2019). Technology adoption for the integration of online–offline purchasing: Omnichannel strategies in the retail environment. *International Journal of Retail and Distribution Management, 47*(5), 474–492. https://doi.org/10.1108/IJRDM-12-2018-0270
37. Faul, F., Erdfelder, E., Lang, A.-G., & Buchner, A. (2007). G*Power 3: A flexible statistical power analysis program for the social, behavioral, and biomedical sciences. 175–191.
38. Kumar, A., & Kim, Y. (2014). The store-as-a-brand strategy: The effect of store environment on customer responses. *Journal of Retailing and Consumer Services, 21*(5), 685–695. https://doi.org/10.1016/j.jretconser.2014.04.008
39. Diener, E., Emmons, R.A., Larsen, R.J., Griffin, S. (1985). The satisfaction with life scale. *Journal of Personality Assessment*. https://eddiener.com/scales/7

40. Engger. (2015). Adaptation of the RYFF psychological well-being scale in the Indonesian context.
41. Hulland, J. (1999). Use of partial least squares (PLS) in strategic management research: A review of four recent studies. *Strategic Management Journal, 20*(2), 195–204.
42. Gefen, D., Straub, D., & Boudreau, M.-C. (2000). Structural equation modeling and regression: Guidelines for research practice. *4*(7). https://doi.org/10.17705/1CAIS.00407
43. Bagozzi, R.P., & Yi, Y. (1988). On the evaluation of structural equation models. *Journal of the Academy of Marketing Science, 16*(74). https://doi.org/10.1177/009207038801600107.
44. Fornell, C., & Larcker, D.F. (1981). Evaluating structural equation models with unobservable variables and measurement error. *XVIII*, 39–50.
45. Gold, A. H., Malhotra, A., & Segars, A. H. (2001). Knowledge management: An organizational capabilities perspective. *Journal of Management Information Systems, 18*(1), 185–214.
46. Hair, J.F., Hult, G.T.M., Ringle, C.M., & Sage, M.S. (2017). *A primer on partial least squares structural equation modeling* (2nd Editio). Sage.
47. Murnawati, & Khairani, Z. (2018). Store environmental atmosphere on giant hypermarket Pekanbaru: Do effect on consumers positive emotion and impulse ? *175*. https://doi.org/10.1088/1755-1315/175/1/012046
48. Nilsson, E., & Ballantyne, D. (2014). Reexamining the place of servicescape in marketing: A service-dominant logic perspective. *Journal of Services Marketing, 28*(5), 374–379. https://doi.org/10.1108/JSM-01-2013-0004
49. Kowalewicz, R. (2021). *Three tips for marketing to generation X*. https://www.forbes.com/sites/forbesagencycouncil/2021/05/12/three-tips-for-marketing-to-generation-x/?sh=ee6a8d57cf9e.
50. Francis, T., & Hoefel, F. (2018). *True Gen: Generation Z and its implications for companies*. https://www.mckinsey.com/industries/consumer-packaged-goods/our-insights/true-gen-generation-z-and-its-implications-for-companies
51. Sponaugle, S. (2019). Communicating across generation. 18(1), 16–23.
52. Calvo-Porral, C., & Pesqueira-Sanchez, R. (2019). Generational differences in technology behaviour: Comparing millennials and generation X. *Kybernetes, 49*(11), 2755–2772. https://doi.org/10.1108/K-09-2019-0598
53. Gottschalk, S. A., & Mafael, A. (2017). Cutting through the online review jungle—Investigating selective eWOM processing. *Journal of Interactive Marketing, 37*, 89–104. https://doi.org/10.1016/j.intmar.2016.06.001
54. Hu, H., & Krishen, A. S. (2019). When is enough, enough? Investigating product reviews and information overload from a consumer empowerment perspective. *Journal of Business Research, 100*, 27–37. https://doi.org/10.1016/j.jbusres.2019.03.011
55. Kleber & Associates. (2020). *Gen Z: Reaching the next generation of building product customers*.
56. Kastenholz, C. (2021). *Gen Z and the rise of social commerce*. https://www.forbes.com/sites/forbesagencycouncil/2021/05/17/gen-z-and-the-rise-of-social-commerce/?sh=56843f0c251d
57. IBM. (2018). *What do Gen Z shoppers really want?* https://www.ibm.com/thought-leadership/institute-business-value/report/genzshoppers
58. Hillel, S. (2020). *Getting product discovery right for every generation*. https://www.syte.ai/blog/product-discovery/product-discovery-for-each-generation/
59. Osburg, V., Yoganathan, V., Brueckner, S., & Toporowski, W. (2020). How detailed product information strengthens eco-friendly consumption. *Management Decision, 58*(6), 1084–1099. https://doi.org/10.1108/MD-10-2017-1012
60. Yu, Y.-T., & Dean, A. (2001). The contribution of emotional satisfaction to consumer loyalty. *International Journal of Service Industry Management, 12*(3/4), 234.
61. Evanschitzky, H., Ramaseshan, B. (2011). Consequences of customer loyalty to the loyalty program and to the company. *Journal of the Academy of Marketing Science, 40*(5). https://doi.org/10.1007/s11747-011-0272-3
62. Hedhli, K. L., Chebat, J., & Sirgy, M. J. (2013). Shopping well-being at the mall: Construct, antecedents, and consequences. *Journal of Business Research, 66*(7), 856–863. https://doi.org/10.1016/j.jbusres.2011.06.011

63. McKee, D., Simmers, C. S., & Licata, J. (2006). Customer Self-Efficacy and Response to Service. *Journal of Service Research, 8*(3), 207–220. https://doi.org/10.1177/1094670505282167
64. Mayzlin, D., & Godes, D. (2002). Using online conversations to study word of mouth communication. *Marketing Science, 23*(4), 545–560. https://doi.org/10.2139/ssrn.327841
65. Bughin, J., Doogan, J., & Vetvik, O.J. (2020). A new way to measure word-of-mouth marketing. McKinsey, Apr-2020
66. Rosenbaum, M.S. (2015). Transformative service research: Focus on well-being. *The Service Industries Journal,* 363–367. https://doi.org/10.1080/02642069.2015.1025061

Chapter 5
Targeted Bayesian Persuasion in a Basic Selfish Routing Game

Yinlian Zeng, Qiao-Chu He, and Xiaoqiang Cai

Abstract Travellers are selfish and make routing choices maximizing their own utility, which inevitably leads to congestion and inefficiency in the traffic network. However, travellers' route choices are affected by the availability and accuracy of travel information. This raises the question: *How can the central planner reduce the congestion of the traffic network by designing the information environment for travellers?* We approach this question in the framework of Bayesian persuasion. We consider a basic selfish routing game with one risky route and one safe route, wherein the central planner conducts Bayesian persuasion (by sending noisy signals) to a fraction of travellers and no information to the rest of travellers. We first identify travellers' equilibrium route choice given a certain persuasion strategy. Then, with the objective of minimizing total congestion cost, we decide the optimal persuasion policy, which includes the optimal percentage of travellers that should be targeted by Bayesian persuasion (persuasion coverage) and the optimal information accuracy. We find that first-best outcome can be restored under certain situations by leveraging both the instruments of persuasion coverage and information accuracy.

Supplementary Information The online version contains supplementary material available at https://doi.org/10.1007/978-3-031-15644-1_5.

Y. Zeng
College of Urban Transportation and Logistics, Shenzhen Technology University, Shenzhen 518118, Guangdong, China
e-mail: zengyinlian@sztu.edu.cn

Ordinary University Rail Transit Smart Maintenance Engineering Technology Development Center, Shenzhen 518118, Guangdong, China

Q.-C. He (✉)
Department of Information Systems and Management Engineering, Southern University of Science and Technology, Shenzhen 518055, Guangdong, China
e-mail: heqc@sustech.edu.cn

X. Cai
School of Data Science, The Chinese University of Hong Kong, Shenzhen 518172, Guangdong, China
e-mail: xqcai@cuhk.edu.cn

The Shenzhen Research Institute of Big Data, Shenzhen 518172, Guangdong, China

R. Qiu et al. (eds.), *City, Society, and Digital Transformation*, Lecture Notes in Operations Research, https://doi.org/10.1007/978-3-031-15644-1_5

Keywords Information design · Routing game · Uncertainty · Bayesian persuasion

Introduction

Traffic network has inherent uncertainties due to unpredictable events like car accidents, extreme whether, emergencies, and etc. Travellers often acquire traffic information and update their routing decisions based on the information they have so as to reduce travel time. In general, travellers are selfish and make routing choices maximizing their own utility. Hence, even when full information regarding the state of the traffic network is provided to all vehicles on the road, congestion and inefficiency in the traffic network is inevitable because of travellers' selfish routing behaviour. A few theoretical studies have identified instances wherein providing information to drivers result in social welfare loss and an increase in the overall traffic congestion [1, 2, 6, 7, 12]. These results have also been supported by observations in reality. For example, there are reports stating that with the wide-spread use of navigation apps which facilitate drivers finding short-cuts, the road across quiet residential area is overcrowded and complaints arise from residents [3, 10, 11]. Indeed, travellers' route choices are affected by the availability and accuracy of travel information. This raises the question: *How can the central planner reduce the congestion of the traffic network by designing the information environment for travellers?*

The main goal of this paper is to apply information design in the framework of Bayesian persuasion to improve the efficiency of a self-routing network from the perspective of a central planner. In particular, we consider a two-route traffic network with one safe route and one risky route wherein the central planner conducts Bayesian persuasion (by sending noisy signals) to a fraction of travellers and no information to the rest of travellers. We need to decide the optimal persuasion policy for the central planner. Specifically, the research questions we want to answer in this paper include: *what is the optimal percentage of travellers should be targeted by Bayesian persuasion and what is the corresponding optimal information design scheme*?

There has been a growing number of literature examining how to leverage the instrument of information design to reduce congestion in the traffic network. Das et al. [5] investigate how optimal information design can reduce congestion in a traffic network wherein some paths have uncertain states. The authors consider the setting where a continuum of users simultaneously decide on the path they wish to take to minimize their own cost. They assume that the informational signals provided are public and intended for all users. Liu and Whinston [8] apply the idea of Bayesian persuasion and the unified information design framework to improve the efficiency of real-time routing for autonomous vehicles. The feasible information structures they consider satisfy the obedience condition, that is, if the designer privately communicates information as stochastic action recommendations, the vehicles will want to follow the recommendations. Chen et al. [4] consider the interaction of connected autonomous vehicle platoons and human-driven vehicles and design information structure for the human-driven vehicles. Liu and Yang [9] examine how

information provision and congestion pricing jointly affect travellers' travel strategies and route choices in a road network with a risky route and a safe route. In particular, they consider heterogeneity of travellers in value of time (VOT) and examine the distributional effects of information provision across travellers with different VOTs. However, they focus only on three special information provision policies: no information, free full information or full information with a fee.

Our paper is closely related to Wu and Amin [13]. Wu and Amin [13] consider a similar routing network to ours. They consider the case that the authority sends a noisy signal of the state to a given fraction of travellers, and the rest of travellers receive no information. They design an information structure to minimize the average traffic spillover—the amount of equilibrium route flow exceeding a certain threshold—on one of the routes. We divert from their paper from the following aspects: (i) Our objective is to minimize the total congestion cost in the network instead of the traffic spillover; (ii) we not only leverage the instrument of information accuracy, but also the instrument of persuasion coverage (i.e., the percentage of travellers targeted by Bayesian persuasion); (iii) we work on the posterior belief of the travellers while they work directly on the signals of the senders.

The rest of this paper is organized as follows. Section "Model Setup" presents the model setup. Section "Travellers' Equilibrium Route Choice" derives travellers' equilibrium route choice and Sect. "Optimal Persuasion Policy" presents the optimal persuasion policy. Section "Conclusion" concludes this paper.

Model Setup

Our model considers a basic two-route network with one risky route r_1 and one safe route r_2 as illustrated by Fig. 5.1. The risky route represents those routes in practice that are more likely to be subject to unexpected events, for example, those routes that are more likely to have car accidents because of confluence of another route.

Specifically, there is congestion cost on both routes, which is dependent on the load on that route. The risky route r_2 has an uncertain state which follows a two-type distribution from the set $\mathrm{S} = \{\mathrm{H}, \mathrm{L}\}$. For a given load on r_1, the congestion cost on r_1 is higher in the "bad" state H than in the "good" state L. The state $i \in S$ is decided by "Nature" according to a fixed and exogenous distribution such that the probability of state H is θ and that the probability of state L is $1 - \theta$. We also assume that the congestion cost is linear to the load on the route. The intercept of the congestion cost function for r_1 is state-dependent, denoted by β^H (β^L) in state H(L) and we assume $\beta^H > 0 > \beta^L$. Hence, the cost for a traveller on each route is characterized as follows:

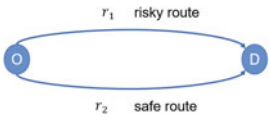

Fig. 5.1 A two-route network

$$c_1(l_1) = \alpha_1 l_1 + \beta^i, i = L, H$$
$$c_1(l_2) = \alpha_2 l_2$$

where l_1 and l_2 are the load on routes r_1 and r_2, respectively, and we assume $l_1 + l_2 = 1$. Moreover, we assume that $\alpha_2 > \beta^H$ and $\alpha_1 + \beta^L > 0$ to ensure that there will be travellers on both routes in both state H and L. These two assumptions are reasonable in the sense that $\alpha_2 > \beta^H$ means that when all travellers use r_2, the congestion cost on r_2 is larger than that on r_1, whereas $\alpha_1 + \beta^L > 0$ means that when all travellers use r_1, the congestion cost on r_2 is larger than that on r_2. To facilitate our discussion, throughout this paper we refer to r_1 as the "good" route and r_2 as the "bad" route in state L, while in state H r_1 becomes the "bad" route and r_2 the "good" route. We use "bad" and "good" route to denote the route that is less crowded and more crowded in the practice, respectively.

We apply the framework of Bayesian persuasion to design the information environment faced by the travellers. This framework allows us to abstract away from the actual persuasion process via the sender's signaling strategy and the receivers' information updating process, and it suffices to focus on the travellers' posterior beliefs about the state of the traffic network. Moreover, we refer to the travellers who receive the information sent from the central planner as the targeted travellers and those who do not as uninformed travellers. We denote the posterior belief of the targeted travellers by t defined over the state set {H, L}. The distribution of the travellers' posterior belief is measured by the probability

$$\rho^i = \Pr(t = i|i), \forall i \in \{H, L\},$$

which indicates the accuracy that travellers' posterior belief is the same as the true state, i.e., $t = i$. Therefore, the central planner's problem is reformulated as to manipulate the travellers' posterior beliefs for a certain objective, e.g., congestion minimization. For uninformed travellers, their beliefs are untouched such that they believe that the state is H with probability θ (and L with probability $1 - \theta$). However, the central planner cannot design the information scheme freely but conform to a *credibility constraint*, which requires that the expectation of the targeted travellers' posterior belief equals to the prior. The credibility constraint can be written as

$$\rho^H \theta + \left(1 - \rho^L\right)(1 - \theta) = \theta,$$

where the left-hand side is the expected posterior belief for state H and the right-hand side item is the prior belief for state H. The credibility constraint also guarantees the expected posterior belief equals to the prior for state L, i.e., $\left(1 - \rho^H\right)\theta + \rho^L(1 - \theta) = 1 - \theta$. Furthermore, ρ^H and ρ^L should satisfy $\rho^H \geq \theta$ and $\rho^L \geq 1 - \theta$, which means that the targeted travellers' posterior belief is always not weaker than their prior belief. This is because the information the targeted travellers receive to update their

posterior belief should always be somehow meaningful; otherwise, they can just ignore the information and withhold their prior belief.

Travellers' Equilibrium Route Choice

In this section, we focus on deriving travellers' equilibrium route choice. Let λ_t denote the part of travelers that are targeted by Bayesian persuasion and λ_u denote the part of travelers that are not, where $\lambda_t + \lambda_u = 1$. Let γ_t^i denote the load of targeted travelers on r_2 in state $i \in \{L, H\}$ and γ_u denote the load of uninformed travelers on r_2, where $\gamma_t^i \in [0, \lambda_t]$ and $\gamma_u \in [0, \lambda_u]$. Then the load of targeted travelers and uninformed travelers on r_1 is $\lambda_t - \gamma_t^i$ and $\lambda_u - \gamma_u$. Therefore, the aggregate load on r_2 and r_1 is $l_2^i = \gamma_t^i + \gamma_u$ and $l_1^i = 1 - \gamma_t^i - \gamma_u$, respectively.

Targeted travellers' posterior expectation on β is $E\beta^i = \rho^i \beta^i + \left(1 - \rho^i\right)\beta^{-i}$ in state i, where $i = H, L$, and $-i = L, H$, respectively. The targeted travellers make their self-interested decisions based on their posterior belief. By choosing the route with a lower congestion cost, each targeted traveller's utility is as follows:

$$U_t^i = V - \min\left\{\alpha_2\left(\gamma_t^i + \gamma_u\right), \alpha_1\left(1 - \gamma_t^i - \gamma_u\right) + E\beta^i\right\}$$

where $E\beta^i$ denotes the expectation on β^i in state i, given the environmental information revealed by the central planner. Each targeted traveller makes self-interested route choice such that the expected congestion cost of the two routes are equal. Given uninformed travellers' strategy γ_u, the best response of targeted travelers on r_2 is as follows:

$$\gamma_t^i = \begin{cases} \lambda_t, \gamma_u < \frac{\alpha_1 + E\beta^i}{\alpha_1 + \alpha_2} - \lambda_t, \\ \frac{\alpha_1 + E\beta^i}{\alpha_1 + \alpha_2} - \gamma_u, \frac{\alpha_1 + E\beta^i}{\alpha_1 + \alpha_2} - \lambda_t \le \gamma_u \le \frac{\alpha_1 + E\beta^i}{\alpha_1 + \alpha_2}, \\ 0, \gamma_u > \frac{\alpha_1 + E\beta^i}{\alpha_1 + \alpha_2}. \end{cases} \tag{5.1}$$

The uninformed travellers make their decisions based on the prior of the state and has no knowledge about the information that the targeted travellers receive. By choosing the route with a lower congestion cost, each uninformed traveller's utility is as follows:

$$U_u = V - \min\left\{\alpha_1\left(\frac{\lambda_u - \gamma_u}{\lambda_u}\right) + E\beta, \alpha_2 \frac{\gamma_u}{\lambda_u}\right\},$$

where $E\beta = \theta\beta^H + (1 - \theta)\beta^L$. Lemma 5.1 describes the equilibrium strategy of the uninformed travellers, which follows directly from the Wardrop equilibrium and the assumption that $\alpha_1 + \beta^L > 0$ and $\alpha_2 > \beta^H$.

Lemma 5.1 *The equilibrium strategy of uninformed travellers in both state H and L is as below:*

$$\gamma_u^e = \frac{\alpha_1 + E\beta}{\alpha_1 + \alpha_2}(1 - \lambda_t). \tag{5.2}$$

From Lemma 5.1 we can see that the equilibrium strategy of uninformed travellers is independent of the state. This is because the uninformed travellers have no additional information regarding the state and the only information available for them to make decision is the prior probability of the states. We then present the results regarding the equilibrium strategy of the targeted travellers. The proofs of propositions and theorems in this paper are provided in the electronic supplementary material due to page limit.

Proposition 5.1 *Suppose the persuasion strategy* (ρ^H, ρ^L) *is given. In state L, the equilibrium targeted traveller population on route* r_2 *is as follows:*

a. *If* $0 \le \lambda_t \le \left(E\beta - E\beta^L\right)/(\alpha_1 + E\beta)$, *then* $\gamma_t^{eL} = 0$. *The aggregate load on* r_2 *is* $l_2^L = (\alpha_1 + E\beta)(1 - \lambda_t)/(\alpha_1 + \alpha_2)$.
b. *If* $\lambda_t \ge \left(E\beta - E\beta^L\right)/(\alpha_1 + E\beta)$, *then* $\gamma_t^{eL} = \left[(\alpha_1 + E\beta)\lambda_t + E\beta^L - E\beta\right]/(\alpha_1 + \alpha_2)$. *The aggregate load on* r_2 *is* $l_2^L = \left(\alpha_1 + E\beta^L\right)/(\alpha_1 + \alpha_2)$.

In state H, the equilibrium traveller population on route r_2 *is as follows:*

a. *If* $0 \le \lambda_t \le \left(E\beta^H - E\beta\right)/(\alpha_2 - E\beta)$, *then* $\gamma_t^{eH} = \lambda_t$. *The aggregate load on* r_2 *is* $l_2^H = [(\alpha_1 + E\beta) + (\alpha_2 - E\beta)\lambda_t]/(\alpha_1 + \alpha_2)$.
b. *If* $\lambda_t \ge \left(E\beta^H - E\beta\right)/(\alpha_2 - E\beta)$, *then* $\gamma_t^{eH} = \left[(\alpha_1 + E\beta)\lambda_t + E\beta^H - E\beta\right]/(\alpha_1 + \alpha_2)$. *The aggregate load on* r_2 *is* $l_2^H = \left(\alpha_1 + E\beta^H\right)/(\alpha_1 + \alpha_2)$.

Proposition 5.1 indicates that either in state H or L, given a persuasion strategy (ρ^H, ρ^L) provided by the central planner, the equilibrium behavior of the targeted travellers varies with the persuasion coverage λ_t. For example, in state L, when percentage of targeted travellers is low enough, the percentage of targeted travellers who are persuaded to switch from the "bad" route r_2 to the "good" route r_1 is increasing with and exactly equals to the persuasion coverage. However, when the percentage of targeted travellers reaches some threshold, the percentage of targeted travellers who are persuaded to switch from the "bad" route r_2 to the "good" route r_1 remains constant and does not increase with the persuasion coverage. That is, for any persuasion strategy, there exists a threshold beyond which the aggregate cost is independent of the percentage of targeted travellers.

Optimal Persuasion Policy

Now that we understand the relationship between the persuasion coverage and the percentage of persuaded travellers for a given persuasion strategy (information accuracy), in this section we are interested in investigating how the central planner can leverage both instruments of information accuracy and persuasion coverage to mitigate congestion. Based on the equilibrium route load in both states, the central planner decides its optimal persuasion policy (persuasion coverage λ_t and information accuracy (ρ^H, ρ^L) by solving the following optimization problem:

$$
\begin{aligned}
(OPT)\, TC^* = \min_{\lambda_t, \rho^H, \rho^L} \; & \theta TC^H(l_2^H) + (1-\theta) TC^L(l_2^L) \\
\text{s.t.} \;\; & \rho^H \theta + (1-\rho^L)(1-\theta) = \theta, \\
& 0 \le \lambda_t \le 1, \\
& \rho^H \ge \theta, \rho^L \ge 1-\theta.
\end{aligned}
$$

where $TC^i = (\alpha_1+\alpha_2)(l_2^i)^2 - \big(2\alpha_1+\beta^i\big)l_2^i + \beta^i$. Note that for the special cases wherein $\theta = 1$ or 0, it can be easily verified that the optimal solution is $\lambda_t^* = 0$, that is, there is no need for persuasion when there is no uncertainty of the state. Hence, in the rest of this paper we will only focus on the interesting case with $0 < \theta < 1$. To describe the optimal persuasion policy, we first categorize the persuasion policies into three classes:

(i) Full information targeting part of travellers (λF);
(ii) Bayesian persuasion targeting all travellers ($A\rho$);
(iii) Bayesian persuasion targeting part of travellers ($\lambda\rho$).

Note that λF and $A\rho$ are special cases of the general policy $\lambda\rho$. Moreover, we refer to those $\lambda\rho$ policies that are equivalent to the $A\rho$ policy as $\lambda_A\rho$ policy, and those $\lambda\rho$ policies that are equivalent to the λF policy as $\lambda\rho_F$ policy. Before we present the result on optimal persuasion policy, for notational convenience, we define $P_0 = -\beta^L/\big(\beta^H-\beta^L\big)$, $P_{\alpha\beta} = (\alpha_1+\beta^L)/\big(\alpha_2-\beta^H+\alpha_1+\beta^L\big)$, $P_{\alpha\beta/2} = (\alpha_1\beta^H/2 + \alpha_2\beta^L/2)/\big[\big(\alpha_1-\beta^H/2+\alpha_2+\beta^L/2\big)\big(\beta^H-\beta^L\big)\big] - \beta^L/\big(\beta^H-\beta^L\big)$. It can be easily verified that either $P_0 \le P_{\alpha\beta/2} \le P_{\alpha\beta}$ or $P_{\alpha\beta} \le P_{\alpha\beta/2} \le P_0$. Now we present the theorem regarding the optimal persuasion policy.

Theorem 5.1 *Let $(\lambda_t^*, \rho^{*H}, \rho^{*L})$ be an optimal solution to OPT.*

1. *Suppose $\alpha_1\beta^H + \alpha_2\beta^L \ge 0$, that is, $P_0 \le P_{\alpha\beta/2} \le P_{\alpha\beta}$.*

a. *When $0 < \theta < P_0$, the optimal persuasion policy is $\lambda_A\rho$ policy with $\rho^{*H} = (1+\theta)/2$, $\rho^{*L} = 1-\theta/2$, and $\lambda_t^* \ge \big(\beta^H - E\beta\big)/2(\alpha_2 - E\beta)$.*

b. *When $P_0 \le \theta \le P_{\alpha\beta/2}$, the optimal persuasion policy is $\lambda\rho$ policy with $\lambda_t^* = \big(\beta^H - 2E\beta\big)/2(\alpha_2 - E\beta)$, $\rho^{*L} = \big(2\beta^H - \beta^L\big)/2\big(\beta^H-\beta^L\big)$, $\rho^{*H} = 1 + (1-\theta)\beta^L/2\theta\big(\beta^H-\beta^L\big)$, and the first-best is achieved.*

c. *When* $P_{\alpha\beta/2} \leq \theta \leq P_{\alpha\beta}$, *the optimal persuasion policy is* $\lambda\rho_F$ *policy with* $\rho^{*L} \geq (\alpha_1 + E\beta)\lambda_t^*/\left(\beta^H - \beta^L\right) + 1 - \theta$ *and*

$$\lambda_t^* = \frac{(1-\theta)(\alpha_1 + E\beta)(E\beta - \beta^L/2) + \theta(\alpha_2 - E\beta)(\beta^H/2 - E\beta)}{\theta(\alpha_2 - E\beta)^2 + (1-\theta)(\alpha_1 + E\beta)^2}$$

d. *When* $\theta > P_{\alpha\beta}$, *the optimal persuasion policy is* $\lambda_A\rho$ *policy with* $\rho^{*H} = (1+\theta)/2$, $\rho^{*L} = 1 - \theta/2$, *and* $\lambda_t^* \geq \left(E\beta - \beta^L\right)/2(\alpha_1 + E\beta)$.

2. *Suppose* $\alpha_1\beta^H + \alpha_2\beta^L < 0$, *that is,* $P_{\alpha\beta} \leq P_{\alpha\beta/2} \leq P_0$.

a. *When* $0 < \theta < P_{\alpha\beta}$, *the optimal persuasion policy is* $\lambda_A\rho$ *policy with* $\rho^{*H} = (1+\theta)/2$, $\rho^{*L} = 1 - \theta/2$, *and* $\lambda_t^* \geq \left(\beta^H - E\beta\right)/2(\alpha_2 - E\beta)$.

b. *When* $P_{\alpha\beta} \leq \theta \leq P_{\alpha\beta/2}$, *the optimal persuasion policy is* $\lambda\rho_F$ *policy with* $\rho^{*H} \geq (\alpha_2 - E\beta)\lambda_t^*/\left(\beta^H - \beta^L\right) + \theta$ *and*

$$\lambda_t^* = \frac{(1-\theta)(\alpha_1 + E\beta)(E\beta - \beta^L/2) + \theta(\alpha_2 - E\beta)(\beta^H/2 - E\beta)}{\theta(\alpha_2 - E\beta)^2 + (1-\theta)(\alpha_1 + E\beta)^2}$$

c. *When* $P_{\alpha\beta/2} \leq \theta \leq P_0$, *the optimal persuasion policy is* $\lambda\rho$ *with* $\lambda_t^* = \left(2E\beta - \beta^L\right)/2(\alpha_1 + E\beta)$, $\rho^{*H} = \left(2\beta^H - \beta^L\right)/2\left(\beta^H - \beta^L\right)$, $\rho^{*L} = 1 - \theta\beta^H/2(1-\theta)\left(\beta^H - \beta^L\right)$, *and the first-best is achieved.*

d. *When* $\theta > P_0$, *the optimal persuasion policy is* $\lambda_A\rho$ *policy with* $\rho^{*H} = (1+\theta)/2$, $\rho^{*L} = 1 - \theta/2$, *and* $\lambda_t^* \geq \left(E\beta - \beta^L\right)/2(\alpha_1 + E\beta)$.

From Theorem 5.1 we can see that when the prior uncertainty is low, that is, θ is very small or very large, the $\lambda_A\rho$ policy is the optimal policy, while when θ is in the intermediate range, $\lambda\rho$ or $\lambda\rho_F$ is the optimal policy. Basically, in this model the central planner leverages both instruments of information accuracy (ρ^{*H} and ρ^{*L}) and persuasion coverage (λ_t^*) to reduce the aggregate congestion cost. These two instruments have interactions and they reduce the total congestion cost together. In the cases wherein the $\lambda_A\rho$ policy is optimal, the central planner should focus on the information accuracy when the persuasion coverage reaches a threshold. In the cases wherein $\lambda\rho_F$ policy is optimal, the central planner should focus on persuasion coverage while the information accuracy is irrelevant. Specifically, in the case wherein $\alpha_1\beta^H + \alpha_2\beta^L \geq 0$, when $0 < \theta < P_0$ or $\theta > P_{\alpha\beta}$, the information accuracy plays a more significant role; When $P_0 \leq \theta \leq P_{\alpha\beta/2}$, information accuracy is more relevant in the state L and persuasion coverage is more relevant in state H, which results in the first-best outcome; When $P_{\alpha\beta/2} \leq \theta \leq P_{\alpha\beta}$, the persuasion coverage is more relevant in both states. When $\alpha_1\beta^H + \alpha_2\beta^L < 0$, $0 < \theta < P_{\alpha\beta}$ or $\theta > P_0$, the information accuracy is more relevant in both states; When $P_{\alpha\beta} \leq \theta \leq P_{\alpha\beta/2}$, the persuasion coverage is more relevant in both states. Similarly, when $P_{\alpha\beta/2} \leq \theta \leq P_0$, information accuracy becomes more relevant in the state H and persuasion coverage is more relevant in state L, which results in the first-best outcome.

Intuitively, when θ is extreme (either low or high), the prior belief is already informative, and thus there is limited room for the instrument of information accuracy to

play a role. Hence, in this case, the $\lambda_A \rho$ policy is optimal. When θ is in an intermediate range, the prior uncertainty is high, the instrument of information accuracy plays a more significant role and the targeted travellers can be easily persuaded. However, persuasion coverage is insufficient to guarantee the first-best outcome. In this case, the $\lambda \rho_F$ policy is optimal, i.e., the persuasion power should be fully exhausted such that Bayesian persuasion targeting part of travellers degenerates to full information targeting part of travellers. When the central planner is not constrained by credibility, the first-best outcome can be restored when the $\lambda \rho$ policy is optimal.

Conclusion

In this paper, we show that for any persuasion strategy, there exists a threshold beyond which the aggregate cost is independent of the percentage of targeted travellers. It is somewhat interesting that the maximum persuasion power can be exhausted when too many travellers are targeted. In practice, the central planner needs to do a careful trade-off between persuasion coverage and information accuracy. When the prior belief is optimistic (i.e., θ is small) and the expected traffic congestion is mild, targeting all travellers can be optimal. When the prior belief becomes less optimistic, targeting part of travellers becomes optimal and the information accuracy increases to become perfect. Notably, when the prior belief is intermediately optimistic, the first-best outcome can be achieved with Bayesian persuasion targeting part of travellers. The converse is true when the prior belief becomes pessimistic. We find out that when prior belief is extreme (either over-pessimistic or over-optimistic), the prior belief is already informative, the instrument of persuasion coverage plays a more significant role. In contrast, when prior uncertainty is high, the instrument of information accuracy plays a more significant role. The central planner should carefully spend his credibility leveraging on both instruments so that the first-best outcome can be restored before the persuasion power is exhausted.

Acknowledgements This research was supported, in part by National Natural Science Foundation of China (Grant No. 72201175), Ordinary University Engineering Technology Development Center Project of Guangdong Province (Grant No. 2019GCZX006), the Leading Talent Program of Guangdong Province (Grant No. 2016LJ06D703), Shenzhen Science and Technology Innovation Comsmission (Grant No. JCYJ20210324115604012).

References

1. Acemoglu, D., Makhdoumi, A., Malekian, A., & Ozdaglar, A. (2018). Informational Braess paradox: The effect of information on traffic congestion. *Operations Research, 66*(4), 893–917.
2. Arnott, R., De Palma, A., & Lindsey, R. (1991). Does providing information to drivers reduce traffic congestion? *Transportation Research Part A: General, 25*(5), 309–318.

3. Brunhuber, K. (NBC Miami). (2016). Shortcut-finding app Waze creating residential traffic headaches. www.cbc.ca/news/technology/shortcut-app-waze-1.3463004, February 29, 2016.
4. Chen, Y. H., Xu, A., He, Q., & Chen, Y. J. (2020). Smart navigation via strategic communications in a mixed autonomous paradigm. Working Paper, https://papers.ssrn.com/sol3/papers.cfm?abstractid=3752727
5. Das, S., Kamenica, E., & Mirka, R. (2017). Reducing congestion through information design. In *55th annual Allerton conference on communication, control, and computing (Allerton)*, pp. 1279–1284, IEEE.
6. De Palma, A., Lindsey, R., & Picard, N. (2012). Risk aversion, the value of information, and traffic equilibrium. *Transportation Science, 46*(1), 1–26.
7. Lindsey, R., Daniel, T., Gisches, E., & Rapoport, A. (2014). Pre-trip information and route-choice decisions with stochastic travel conditions: Theory. *Transportation Research Part B: Methodological, 68*, 154–172.
8. Liu, Y., & Whinston, A. B. (2019). Efficient real-time routing for autonomous vehicles through correlated equilibrium: An information design framework. *Information Economics and Policy, 47*, 14–26.
9. Liu, Y., & Yang, Z. (2021). Information provision and congestion pricing in a risky two-route network with heterogeneous travelers. *Transportation Research Part C, 128*, 103083.
10. Nelson, L. (Los Angeles Times). (2015). New traffic apps may be pushing cars into residential areas. www.latimes.com/local/california/la-me-california-commute-20150106-story.html, January 5, 2015.
11. Richards, G. (The Mercury News). (2016). Is Googles Waze app making traffic worse? www.mercurynews.com/2016/01/21/is-googles-waze-app-making-traffic-worse/, January 21, 2016.
12. Thai, J., Laurent-Brouty, N., & Bayen, A. M. (2016). Negative externalities of GPS-enabled routing applications: A game theoretical approach. In *19th International conference on intelligent transportation systems (ITSC)*, pp. 595–601. IEEE.
13. Wu, M., & Amin, S. (2019). Information design for regulating traffic flows under uncertain network state. In *57th annual Allerton conference on communication, control, and computing (Allerton)*, pp. 671–678, IEEE.

Chapter 6
Stochastic Churn Modeling with Dynamic Attribution and Bayesian Estimation

Ping Chou and Howard Hao-Chun Chuang

Abstract Parametric probability models, such as Beta-Geometric, are workhorse models for contractual customer churn prediction. Due to their simplicity, robustness to missing and censored data, and managerially relevant statistics, those models are applied to different business sectors such as healthcare and finance. Nonetheless, the existent models tend to assume a stationary churn process or an identical distribution of latent churn rate. The Beta-Logistic model by Hubbard et al. (Survival prediction-algorithms, challenges and applications. PMLR, pp 22–39 [17]) allows for time-invariant covariates and captures non-identically distributed individual churn. To further accommodate time-varying determinants of churn rate, we apply a Grassia(II)-Geometric (G2G) model by Fader and Hardie (Incorporating time-varying covariates in a simple mixture model for discrete-time duration data [9]). Grounded on the flexible model structure, we propose Bayesian estimation and inference of G2G and empirically assess its prediction performance. Using a workforce dataset from an electronic manufacturing service company, we show that G2G with greater flexibilities outperform extant models in terms of model fitness and employee churn prediction. Additionally, we identify major determinants of churn processes in manufacturing plants and generate cohort-wised survival curves. With built-in interpretability and posterior inference, our Bayesian G2G modeling approach can be useful for churn prediction in marketing and operations management.

Keywords Stochastic modeling · Employee churn modeling · Bayesian estimation

P. Chou (✉)
Department of Management Information Systems, National Chengchi University, Taipei 11605, Taiwan
e-mail: 108356508@nccu.edu.tw

H. H.-C. Chuang
College of Commerce, National Chengchi University, Taipei 11605, Taiwan
e-mail: chuang@nccu.edu.tw

R. Qiu et al. (eds.), *City, Society, and Digital Transformation*, Lecture Notes in Operations Research, https://doi.org/10.1007/978-3-031-15644-1_6

Introduction

Probability models for churn prediction in contractual settings, e.g., Beta-Geometric (BG) [8] and Beta-Weibull [13], have been used in customer retention across business sectors, e.g., online platforms [19], video/music streaming [17], and insurance [27]. The use of such models goes beyond churn prediction and extends to predicting time to purchase [14], patient revisit [20], conversion rate of online advertising [17], and customer-based valuation of business [5, 21]. The models are robust to incomplete information [7], able to leverage interval-censored and non-censored data [10], and provides managerially relevant statistics, e.g., residual lifetime, lifetime value, and their distributions [5, 6, 12]. Despite the proven efficacy, some criticize those models for being covariate-free and hence unable to fully capture group-level and individual-level heterogeneity [22, 23]. Hubbard et al. [17] introduce the Beta-Logistic (BL) model—an extended BG with time-invariant covariates—and empirically improve churn prediction performance in streaming subscribers. While relaxing the restrictive assumption that all individuals share an identical distribution of latent churn rate, BL assumes the heterogeneous distributions to be time-invariant (stationary). That is, BL does not allow for time-varying covariates such as seasonality and tactical marketing activities that are common in many business sectors and result in nonstationary distributions of latent attrition/churn rate [1, 21, 26].

To fill the gap, Fader and Hardie [9] propose a Grassia(II)-Geometric (G2G) model with time-varying covariates, which captures heterogeneous and non-stationary latent churn process. Notwithstanding the theoretical flexibility, G2G's efficacy has not been empirically examined, and it remains unclear whether G2G effectively improves the less generic BG (assuming a common churn rate distribution) and BL (assuming heterogeneous yet stationary churn rate distributions). We collaborate with a leading electronic manufacturing services (EMS) company and assess the G2G for predicting employee churn in its production plants. Due to high turnover rates, individual heterogeneities, and seasonal variations in employee churn risks (e.g., there are more competing offers in peak seasons), the focal EMS requires a flexible yet interpretable model for predicting churn proportion and remaining lifetime for labor planning and hiring in advance. Motivated by the conceptual similarity between customer and employee churn [24, 25], our analysis shows that stochastic churn modeling can be useful in not only consumer services but also workforce operations.

The contribution of this paper is multi-facet. First, we apply Bayesian estimation to BL and G2G, going beyond prior studies' focal interest in churn prediction and instill posterior inference in such models. Second, we empirically show that the more generic and flexible G2G significantly outperforms both BG and BL models. Third, we find that covariate-free BG precisely projects the global survival curves and job durations, whereas G2G effectively captures individual heterogeneity and satisfactorily projects local curves that BG cannot capture. Last, unlike some machine learning approaches that are short of rationales and difficult to obtain test statistics, the proposed Bayesian G2G is highly interpretable with readily available credible regions

of model estimates, such that managers can gauge the significance of predictors and their impact on the metrics of managerial relevance.

General Problem and Models

Contractual Churn and Probability Modeling

Per [11], the problem of churn modeling in general can be categorized into four quadrants by two dimensions: transaction opportunity (continuous/discrete) and relationship type (noncontractual/contractual). This paper focuses on contractual and discrete-time setting that matches the EMS operations, in which employees have an opportunity to decide on whether quitting from production plants at the end of each period. An employee is considered "survival" if he/she stays on-job in the beginning of the next period. Otherwise, he/she is considered "churn".

Throughout the paper, we use index i to represent individuals, and $T_i \in Z^+$, $C_i \in \{0, 1\}$, and $X_i \in R^d$ refer to one's duration of survival subject to right-censoring, censor indicator ("1" censored survival, "0" observed churn instance), and d-dimensional covariates. For notational brevity, we use $D = \{T_i, C_i, X_i\}_{i=1}^N$ to denote data with N individuals and $\{\cdot\}$ to represent all model parameters. Mathematically, the objective of stochastic churn modeling is to optimize $\{\cdot\}$, including the coefficients on covariate effects and distributional parameters, such that the overall likelihood function is maximized,

$$P(D|\cdot) = \left\{ \prod_{i:C_i=0} P(T_i|\cdot) \right\} \cdot \left\{ \prod_{i:C_i=1} S(T_i|\cdot) \right\} \tag{6.1}$$

where the first part is the probability mass function $P(T|\cdot)$ for employee churned ($C_i = 0$) and the second part is the survival function $S(T|\cdot)$ for employee survival ($C_i = 1$). Given the estimated model parameters, one can easily apply the survival function $S(T_i|\cdot)$ to infer an individual's discounted expected residual lifetime (*DERL*) [5]:

$$DERL(d|\cdot, n) = \sum_{t=n}^{\infty} \frac{S(t|\cdot)}{S(n-1|\cdot)} \cdot \left(\frac{1}{1+d} \right)^{t-n} \tag{6.2}$$

where n stands for the number of periods an individual has survived and d denotes a discount rate. The DERL can be adapted to predict an unseen individual's expected lifetime (*EL*) by setting $n = 1$. That is,

$$EL(d|\cdot) = \sum_{t=1}^{\infty} S(t|\cdot) \cdot \left(\frac{1}{1+d}\right)^{t-1} \tag{6.3}$$

Probability Churn Models from Marketing

Beta-Geometric (BG)

Beta-Geometric (BG) is built on a simple idea assuming that at each period, an individual determines whether to stay active by flipping a two-sided coin with a latent attrition parameter θ (i.e., "head" one ends the contract, "tail" one renews it). The number of trials before showing up of the first head follows a geometric distribution, whereas the probability of attrition θ is heterogeneous across individuals and static over time. Assuming heterogeneous θ follows a beta distribution, the geometric churn process results in the BG model, i.e.,

$$P(T_i|\theta) = \theta(1-\theta)^{T_i-1},\ S(T_i|\theta) = (1-\theta)^{T_i},\ f(\theta|\alpha,\beta) = \frac{\theta^{\alpha-1}(1-\theta)^{\beta-1}}{\mathrm{B}(\alpha,\beta)} \tag{6.4}$$

Integrating out the latent (θ), the probability mass and survival functions can be re-written as:

$$P(T_i|\alpha,\beta) = \frac{\mathrm{B}(\alpha+1,\beta+T_i-1)}{\mathrm{B}(\alpha,\beta)},\ S(T_i|\alpha,\beta) = \frac{\mathrm{B}(\alpha,\beta+T_i)}{\mathrm{B}(\alpha,\beta)} \tag{6.5}$$

where α and β are model parameters to be estimated such that the overall likelihood $P(D|\cdot)$ is maximized.

Beta-Logistic (BL)

Unlike BG that assumes a stationary and common beta distribution of latent churn rate θ, BL extends BG by leveraging covariate information and results in stationary yet heterogeneous beta distributions. More specifically, BL makes μ_i (mean) and σ_i^2 (variance) of the latent attrition rate θ functions of individual-specific and time-invariant covariates ($\boldsymbol{X_i} = \left[x_{i,1}, \ldots, x_{i,d}\right]$), i.e.,

$$\begin{aligned} \mu_i &= \mathrm{logit}\left(\gamma_{\mu,0} + \gamma_{\mu,1}x_{i,1} + \ldots + \gamma_{\mu,d}x_{i,d}\right), \\ \sigma_i^2 &= \exp\left(\gamma_{\sigma,0} + \gamma_{\sigma,1}x_{i,1} + \ldots + \gamma_{\sigma,d}x_{i,d}\right) \end{aligned} \tag{6.6}$$

Our parameterization (μ, σ^2) differs from (α, β) in [17] for ease of interpretation. Technically, the formulas below allow one to transform (μ_i, σ_i^2) back into (α_i, β_i), and compute the likelihood using $P(T_i|\alpha_i, \beta_i)$ and $S(T_i|\alpha_i, \beta_i)$.

$$\alpha_i = \left(\frac{1-\mu_i}{\sigma_i^2} - \frac{1}{\mu_i}\right)\mu_i^2, \;\; \beta_i = \alpha_i\left(\frac{1}{\mu_i} - 1\right) \tag{6.7}$$

Since the covariates in combination with the coefficients ($\left[\gamma_{\mu,0}, \ldots, \gamma_{\mu,d}\right]$ and $\left[\gamma_{\sigma,0}, \ldots, \gamma_{\sigma,d}\right]$) fully determine the parameters μ_i and σ_i^2 of latent churn rate distributions, the overall likelihood of BL is conditioned on the coefficients, which leaves them the only parameters to be optimized.

Grassia(II)-Geometric (G2G)

Previous studies have acknowledged that the parametric formulation of BG may fit data poorly sometimes owing to ignoring time-varying factors and duration dependence, e.g., long-living individuals tend to live longer [8, 13]. For such contexts, we need to consider a geometric process with dynamic attrition/churn rate that is generic and flexible. That is,

$$P\left(T_i|\theta_{i,1}, \ldots, \theta_{i,T_i}\right) = \theta_{i,T_i}\prod_{t=1}^{T_i-1}\left(1-\theta_{i,t}\right), \;\; S\left(T_i|\theta_{i,1}, \ldots, \theta_{i,T_i}\right) = \prod_{t=1}^{T_i}\left(1-\theta_{i,t}\right) \tag{6.8}$$

However, it is impractical to apply separate prior for each $\theta_{i,t}$ and integrate over all the priors. Alternatively, Fader and Hardie [9] propose a Grassia(II)-Geometric (G2G) model that replaces the Beta prior in BG with a Grassia(II) distribution. Their formulations based on the clog-log link and gamma heterogeneity are[1]:

$$\theta_{i,t} = 1 - \exp\left(-\eta\phi_{i,t}\right), P(\eta) \sim Gamma(a, b) \tag{6.9}$$

where $\phi_{i,t}$ captures observable heterogeneity and subsumes effects of time-invariant and time-varying covariates over time. Let $\boldsymbol{X_i^c} = \left[x_{i,1}^c, \ldots, x_{i,d}^c\right]$ be d-dimensional time-invariant covariates (with effect $\boldsymbol{\gamma^c}$) and $\boldsymbol{X_i^{v,t}} = \left[x_{i,1}^{v,t}, \ldots, x_{i,d'}^{v,t}\right]$ be d'-dimensional time-varying covariate at timing t (with effect $\boldsymbol{\gamma^v}$), $\phi_{i,t}$ brings together the stationary component ($\boldsymbol{\gamma^c x^c}$) and non-stationary component ($\boldsymbol{\gamma^v x^{v,t}}$):

$$\phi_{i,t} = \exp\left(\boldsymbol{\gamma^c X_i^c} + \boldsymbol{\gamma^v X_i^{v,t}}\right) = \exp\left(\gamma_1^c x_{i,1}^c + \ldots + \gamma_d^c x_{i,d}^c + \gamma_1^v x_{i,1}^{v,t} + \ldots + \gamma_{d'}^v x_{i,d'}^{v,t}\right) \tag{6.10}$$

[1] a and b denote the shape and rate parameter of *Gamma*.

The above formulation breaks the limitation of stationarity and exclusively time-invariant covariates in BL. Integrating $P\left(T_i|\theta_{i,1},\ldots,\theta_{i,T_i}\right)$ and $S\left(T_i|\theta_{i,1},\ldots,\theta_{i,T_i}\right)$ with respect to the latent η, we can derive churn rate ($P(T|\cdot)$) and survival rate ($S(T|\cdot)$), which constitute the likelihood function and are directly conditioned on *Gamma* parameters (a, b) and coefficients ($\boldsymbol{\gamma}^{\boldsymbol{c}}$ and $\boldsymbol{\gamma}^{\boldsymbol{v}}$),[2]

$$\begin{aligned} P(T_i|a,b,\gamma) &= \left\{\frac{b}{b+\sum_{t=1}^{T_i-1}\phi_{i,t}}\right\}^a - \left\{\frac{b}{b+\sum_{t=1}^{T_i}\phi_{i,t}}\right\}^a, \\ S(T_i|a,b,\gamma) &= \left\{\frac{b}{b+\sum_{t=1}^{T_i}\phi_{i,t}}\right\}^a \end{aligned} \tag{6.11}$$

Empirical Methods and Data

EMS Workforce Data

Aimed at examining the model's efficacy and eliciting insights potentially valuable to workforce management practice, we co-work with an anonymous EMS company, Alpha, who provides us with a dataset on 20,000 employees over 145 weeks. In the dataset, in addition to T_i (duration of survival) and C_i (censor status), each employee is characterized by 28 time-invariant covariates, including gender, age, hometown, onboard month, category of recruit/contract, mean salary bonus, ratios working on rest day and working on daytime, and mean working hour. In addition, 16 time-varying covariates such as cumulative weeks of survival and season/month indicators for each period are included for capturing time dynamics in distributions of $\theta_{i,t}$. In Table 6.1, we summarize and explain our operationalization of time-invariant (x_1 to x_{28}) and time-varying covariates (x_{29} to x_{44}).

In Fig. 6.1, we show the distribution of employee's on-job duration (with density rescaled). Employees onboarding in Year 1 (during weeks 1–52) are on the left panel, whereas employees onboarding in Year 2 (during weeks 53–104) are on the right panel. As can be seen, both distributions are right-skewed and have a majority of employees having duration less than 20 weeks. Moreover, both panels exhibit bimodal curves for duration between 0 and 10 weeks and multi-modals for duration longer than 20. The shape implies mixtures of heterogeneous employee cohorts, echoing the proposal of BL/G2G to bring in covariates to explicitly account for cross-sectional heterogeneity which covariate-free BG cannot capture.

[2] It should be reminded particularly that the coefficient vector does not involve an intercept.

Table 6.1 Summary of covariates

	Covariate	Definition		Covariate	Definition
x_1	Male	1 if male	x_{23}	C-Category (F)	1 if contract category = 'full-time'
x_2	Age (≤20)	1 if age ≤ 20	x_{24}	C-Category (D)	1 if contract category = 'dispatch'
x_3	Age (21–30)	1 if 20 < age ≤ 30	x_{25}	Salary bonus	Mean salary bonus
x_4	Age (31–40)	1 if 30 < age ≤ 40	x_{26}	Rest day work	Ratio working on rest day
x_5	Area (E)	1 if hometown = 'East'	x_{27}	Shift ratio	Ratio working on daytime
x_6	Area (N)	1 if hometown = 'North'	x_{28}	Work hour	Mean working hour
x_7	Area (NE)	1 if hometown = 'North-East'	x_{29}	Cum. Survival	Cumulative weeks of survival
x_8	Area (NW)	1 if hometown = 'North-West'	x_{30}	Cum. Survival2	Squared term of Cum. Survival
x_9	Area (SC)	1 if hometown = 'South-Central'	x_{31}	Is Spring	1 if next period is in Spring
x_{10}	Onboard (1)	1 if onboard month = '1'	x_{32}	Is Summer	1 if next period is in Summer
x_{11}	Onboard (2)	1 if onboard month = '2'	x_{33}	Is Autumn	1 if next period is in Autumn
x_{12}	Onboard (3)	1 if onboard month = '3'	x_{34}	Is January	1 if next period is in January
x_{13}	Onboard (4)	1 if onboard month = '4'	x_{35}	Is February	1 if next period is in February
x_{14}	Onboard (5)	1 if onboard month = '5'	x_{36}	Is March	1 if next period is in March
x_{15}	Onboard (6)	1 if onboard month = '6'	x_{37}	Is April	1 if next period is in April
x_{16}	Onboard (7)	1 if onboard month = '7'	x_{38}	Is May	1 if next period is in May
x_{17}	Onboard (8)	1 if onboard month = '8'	x_{39}	Is June	1 if next period is in June
x_{18}	Onboard (9)	1 if onboard month = '9'	x_{40}	Is July	1 if next period is in July
x_{19}	Onboard (10)	1 if onboard month = '10'	x_{41}	Is August	1 if next period is in August
x_{20}	Onboard (11)	1 if onboard month = '11'	x_{42}	Is September	1 if next period is in September
x_{21}	R-Category (F)	1 if recruit category = 'full-time'	x_{43}	Is October	1 if next period is in October

(continued)

Table 6.1 (continued)

	Covariate	Definition		Covariate	Definition
x_{22}	R-Category (D)	1 if recruit category = 'dispatch'	x_{44}	Is November	1 if next period is in November

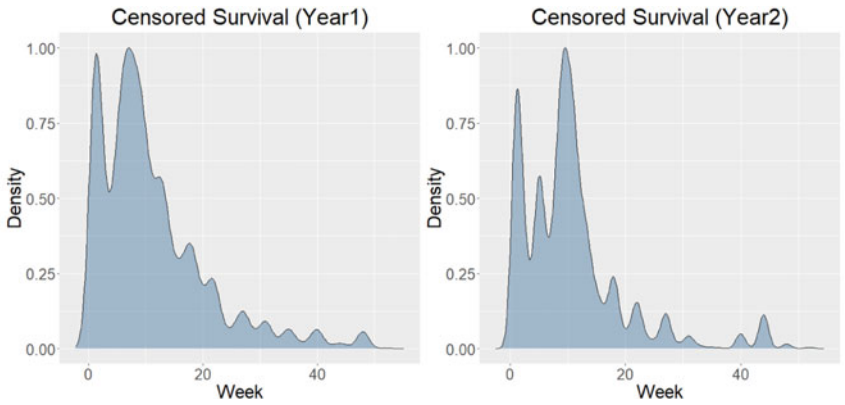

Fig. 6.1 Density plots of survival (on-job) duration

Bayesian Estimation and Inference

For BL and G2G with covariates, to construct the posterior distributions of covariate effects $\boldsymbol{\gamma}$ from Bayesian inference, we adopt Gibbs sampling—a Markov Chain Monte Carlo (MCMC) method for model calibration (see [4] for an extensive review). Based on a preliminary test on convergence and distribution of covariate effects, we adopt independent normal priors [15][3] with identical parameters. Specifically, we set $N(0, 0.2)$ for G2G and $N(0, 0.5)$ for BL. Based on the simulated posterior distributions, we estimate posterior modes (i.e., *maximum a posterior*, MAP) and the credible regions of covariate effects. Let $N(\cdot)$ be the normal density function, and define collection $\{\cdot\} = \{\gamma_j, \gamma_{-j}\}$, where γ_j denotes the jth coefficient being updated and γ_{-j} be all the other coefficients, the full conditional distribution $P(\gamma_j|\gamma_{-j}, D)$ can be simply written as:

$$P\left(\gamma_j|\gamma_{-j}, D\right) \propto P(D|\cdot) \times N\left(\gamma_j\right) \tag{6.12}$$

We calibrate the models on 2000 randomly sampled employees who start their jobs in Year 1, whose survival (employment) durations are censored at week 52. For the models, we run 2000 MCMC iterations and discard the first 1000 draws

[3] In the preliminary analysis, we found that improper prior such as uniform may lead to unstableness in optimization.

as burn-in samples. On the other hand, we select employees who join in Year 2 as test samples for the sake of assessing out-of-sample prediction performance. Survival durations for those in test set who survive after week 104 are censored. We apply log-likelihood (LL), Bayesian Information Criterion (BIC), Akaike Information Criterion (AIC) to assess the models' fitness, and use C-statistics [16] to evaluate the models' performance on projecting hold-out employees' job duration:

$$C = \frac{\sum_{i \neq j} \left\{ I(T_i > T_j) \cdot I(EL_i > EL_j) \right\} \cdot I\left(C_j = 0\right)}{\sum_{i \neq j} I(T_i > T_j) \cdot I\left(C_j = 0\right)} \tag{6.13}$$

of which EL denotes the expected lifetime assuming no discount (i.e., $d = 0$).

Data Analysis

We first assess the computational efficiency that is critical for model adoption and application. In Table 6.2, we report the CPU time it takes to calibrate the foregoing models. We implement the code in R, and execute the programs on a platform with a Win10 operating system, an Intel i7-1165G7 processor, and a 16 GB RAM. Compared with the 2-parameter BG with gradient-based optimization, which takes 35.67 s for calibration, MCMC-based BL (with 30 parameters) and G2G (with 44 parameters) take 701.31 and 10,009.55 s (equivalently, 19.66 and 280.62 times of BG's execution time). Not surprisingly, the most sophisticated G2G—with time-varying and individual-specific latent churn rate—comes at higher computing cost. Nonetheless, given its unique flexibility in modelling heterogeneous and nonstationary churn distributions, we posit the estimation cost induced by generic formulations is acceptable and affordable in modern computing. We then formally assess the performance gains of G2G.

Table 6.3 reports the fitness and performance of the foregoing models (i.e., LL, AIC, BIC based on training samples as well as LL and C-index on hold-out samples). Taking BG as our benchmark, we find that modeling time-invariant covariates makes BL rather flexible and able to capture cohort-level stationary heterogeneity, leading to better fitness on in- and hold-out samples. G2G with time-invariant and time-varying covariates enhances performance further and outperforms BL. The improvement of G2G over BL is more salient than that of BL over BG, evidencing the non-trivial

Table 6.2 Computational cost

	# of parameters	Method	CPU time (s)	Normalized time
BG	2	Gradient	35.67	1
BL	30	MCMC	701.31	19.66
G2G	44	MCMC	10,009.55	280.62

Table 6.3 Performance evaluation

	Year 1: in-sample (N = 2000)			Year 2: out-of-sample (N = 11,673)	
	LL	AIC	BIC	LL	C-Statistic
BG	−6360.33	12,724.66	12,735.86	−34,875.05	0.500
BL	−5741.50	11,542.99	11,711.02	−33,179.62	0.826
G2G	−5031.14	10,150.28	10,396.72	−31,235.94	0.832

value of accounting for time-varying covariates and nonstationary heterogeneity distributions of latent churn.

As for projecting employees' survival, BL and G2G achieve C-statistics of 0.826 and 0.832, respectively. These are high values considering the high uncertainty of employee churn data and simplicity of the models' parametric formulations [28]. Because the expected lifetimes that BG produces are not differentiable between individuals, leading to a C-statistic of 0.500, we apply the same protocol to train a survival forest [18]. The survival forest achieves a C-statistic of 0.835. This finding implies that simple parametric yet interpretable formulations do not necessarily undermine prediction accuracy.

Given the significantly better model fitness and prediction performance of G2G, in Table 6.4, we report the MAP effect estimates and 90% credible regions of covariates [2]. For brevity, we report only the top-10 covariates based on their absolute effect size in descending order.

As expected, *Salary Bonus* as a motivating factor outranks other covariates and reduces employee churn. The ratio working on daytime (*Shift Ratio*) tells if one often works on normal shift hours, thus reducing employee churn. Full-time (*R-Category (F)*) and dispatch job categories (*R-Category (D)*), compared to part-time job (the baseline category), are positions seeking regular and long-term workers. Therefore, employees who have full-time and dispatch jobs are less likely to churn. Negative

Table 6.4 Effect estimates and credible regions of G2G estimates

	Covariate	Estimates (MAP)	Credible region
1	Salary bonus	−3.995	(−4.24, −3.52)
2	Work hour	−2.526	(−2.64, −2.35)
3	Rest day work	−1.775	(−2.30, −1.41)
4	Shift ratio	−1.620	(−1.84, −1.37)
5	R-category (F)	−1.063	(−1.31, −0.70)
6	R-category (D)	−1.048	(−1.23, −0.83)
7	Age (≤20)	−0.806	(−0.95, −0.55)
8	Age (21–30)	−0.727	(−0.87, −0.55)
9	Age (31–40)	−0.607	(−0.77, −0.37)
10	Is Summer	−0.518	(−0.69, −0.36)

relationship between age and churn rate (*Age* (≤20), *Age* (21–30), *Age* (31–40)) makes sense in that physically fit younger workers are generally better suited for labor-intensive tasks.

Some of the estimated effects are counterintuitive: (a) Why are employees having longer mean working hour (*Work Hour*) and having higher ratio working on rest day (*Rest Day Work*) less likely to churn? (b) Additionally, why is the latent churn rate of an employee lower, when the upcoming period is in Summer (*Is Summer*)? An unpublished interview by the authors' colleague reveals that the majority of Alpha's employees are job-hoppers that seek over-time working for extra bonus, thus making (a) reasonable. For (b), it reveals that salary level for the industry is lower during May to June, explaining why employees are unlikely to churn in Summer.

The above discussion focuses specifically on the model fitness and the covariate effects. Below we examine if the estimated effects consistently reflect survival curve at aggregate-level. In Fig. 6.2, we project survival curves using the calibrated BG and G2G models. In addition to the global curve (on the left panel), we take *Salary Bonus* with the strongest effect as an illustrative example to divide the sample into two sub-groups. We project two local curves, i.e., one with bonus below-median (on the middle) and another with bonus above-median (on the right).

For the full sample, except for a few shocks uncaptured, overall both BG and G2G fit the global curve fairly well (with mean discrepancy less than 4%). The result is surprising given the simplicity of BG as we introduced in Sect. 2.2.1. As for the two groups, despite the larger discrepancy between data and model projections, G2G does a decent job at characterizing the two local curves. Arguably, BG will be useful and robust if a decision-maker is only interested in inferring the curve reflecting global survival rate. Nonetheless, the proposed Bayesian G2G will be a more effective and appropriate technique for one to predict the survival rate/remaining job duration of an individual or a specific cohort over time.

To offer managers practical insights in workforce planning, we project survival curves for each individual employee, and by pairwise CORT dissimilarity [3] and hierarchical clustering we cluster the curves. In Fig. 6.3, we show the aggregated

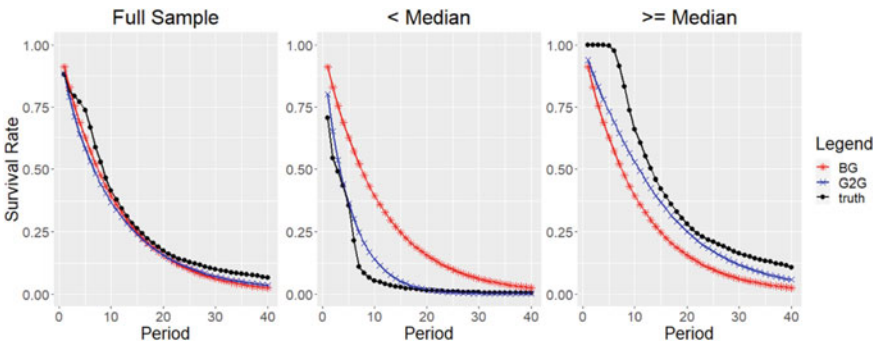

Fig. 6.2 The survival curves

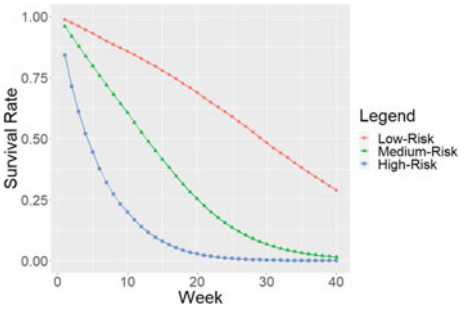

Fig. 6.3 Survival curves clustering

Table 6.5 Averages of features in all clusters

	High-risk	Medium-risk	Low-risk
Salary bonus	0.043	0.244	0.591
Work hour	0.768	0.798	0.807
Rest day work	0.440	0.474	0.469
Shift ratio	0.289	0.526	0.512
R-category (F)	0.110	0.185	0.282
R-category (N)[5]	0.890	0.815	0.718
Age (≤20)	0.100	0.129	0.148
Age (21–30)	0.725	0.723	0.657
Age (>30)	0.175	0.148	0.195

survival curves,[4] and summarize their mean characteristics in Table 6.5. We identify three clusters: *High-Risk*, *Medium-Risk*, and *Low-Risk*. *High-Risk* has more of 20s and dispatch workers, who seldom work overtime and in irregular hour for extra bonus. *Medium-Risk* is younger, while having more full-time workers and extra working hours and bonus. The *Low-Risk*, while being the oldest and having fewer shifts on daytime and rest day, has the highest proportion of full-time workers and the most working hours and bonus. Clearly, the clusters are high in some drivers of survival tendencies but low in the others. For churn anticipation and retention, we suggest one to focus on the factors strictly increasing or decreasing survival risk (e.g., *Salary Bonus*), or to focus on the combination of drivers (e.g., high *Salary Bonus* and low *Shift Ratio*) for the sake of developing countermeasures against employee churn.

[4] For each of the clusters, we produce the aggregated survival curve by taking average over all member curves in the cluster.

[5] For ease of interpretation, we denote dispatch and part-time jobs by *R-Category (N)*.

Conclusion

Marketing modelers have invented a lasting stream of contractual churn models and exerted their influences over applications outside the realm of marketing in the past two decades. However, numerous models ignore time-varying covariates by assuming stationary and identical distributions of latent attrition. Such models are thus restrictive and not flexible enough for tenure duration predictions in many business sectors and problem settings. Fader and Hardie [9] propose G2G that offers a generic structure for incorporating time-varying covariates. Instilling Bayesian inference and estimation into G2G, this paper empirically assess the model's efficacy and the value of time-varying covariates in predicting employee churn, which shares a great similarity with customer churn.

Our analysis of workforce data from manufacturing plants shows that stochastic churn modeling from marketing can be useful for operations management. We find that G2G allowing for nonstationary heterogeneity distributions and time-varying covariates has the best performance in model fitness and survival rate projection. Furthermore, we identify the drivers of employee churn, including factors that are immediately comprehensible (e.g., upcoming seasonality, recruitment category, and age) and counterintuitive ones (mean working hour and working on rest day). When project survival curves globally and locally, the consistently decent performance of G2G suggests that managers can apply G2G to predict churn proportion and remaining lifetime for labor planning and hiring in practice.

Notwithstanding the promising result, our modeling effort is not without limitations and leaves several directions for continual explorations. First, we encourage subsequent studies to triangulate our findings using datasets from different firms and industries. Such efforts will enhance the validity of our Bayesian G2G modeling approach. Second, the fine-tuning of Gamma prior and the MCMC calibration of covariate effects is computationally intensive. Hence, computationally efficient optimization method of G2G deserves more investigations. Third, in this paper, we assume homogeneous employee value and calibrate the models accordingly. Models aimed at delivering maximum workforce performance (e.g., working output and return-on-investment ratio) should take heterogeneous employee value into account. In sum, the probability models provide unique value on prediction and inference front, and G2G having more realistic assumptions is a promising framework in theory and practice of stochastic churn modeling.

References

1. Bachmann, P., Meierer, M., & Näf, J. (2021). The role of time-varying contextual factors in latent attrition models for customer base analysis. *Marketing Science, 40*(4), 783–809.
2. Besag, J., Green, P., Higdon, D., & Mengersen, K. (1995). Bayesian computation and stochastic systems. *Statistical Science*, 3–41.

3. Chouakria, A. D., & Nagabhushan, P. N. (2007). Adaptive dissimilarity index for measuring time series proximity. *Advances in Data Analysis and Classification, 1*(1), 5–21.
4. Dunson, D. B., & Johndrow, J. E. (2020). The Hastings algorithm at fifty. *Biometrika, 107*(1), 1–23.
5. Fader, P. S., & Hardie, B. G. (2010). Customer-base valuation in a contractual setting: The perils of ignoring heterogeneity. *Marketing Science, 29*(1), 85–93.
6. Fader, P. S., & Hardie, B. G. (2017). Exploring the distribution of customer lifetime value (in contractual settings). http://www.brucehardie.com/notes/035/distribution_of_CLV__contractual.pdf
7. Fader, P. S., & Hardie, B. G. (2009). Fitting the sBG model to multi-cohort data. http://www.brucehardie.com/notes/017/sBG_estimation.pdf
8. Fader, P. S., & Hardie, B. G. (2007). How to project customer retention. *Journal of Interactive Marketing, 21*(1), 76–90.
9. Fader, P. S., & Hardie, B. G.: Incorporating time-varying covariates in a simple mixture model for discrete-time duration data. http://www.brucehardie.com/notes/037/time-varying_covariates_in_BG.pdf
10. Fader, P. S., & Hardie, B. G. (2020). Musings on fitting the P(II) distribution to single-event timing data. http://www.brucehardie.com/notes/038/musings_on_pareto-ii_parameter_estimation.pdf
11. Fader, P. S., & Hardie, B. G. (2009). Probability models for customer-base analysis. *Journal of Interactive Marketing, 23*(1), 61–69.
12. Fader, P. S., & Hardie, B. G. (2018). The mean and variance of customer lifetime value in contractual settings. http://www.brucehardie.com/notes/036/mean_and_var_of_CLV_in_contractual_settings.pdf
13. Fader, P. S., Hardie, B. G., Liu, Y., Davin, J., & Steenburgh, T. (2018). "How to project customer retention" revisited: the role of duration dependence. *Journal of Interactive Marketing, 43*, 1–16.
14. Fader, P. S., Hardie, B. G., McCarthy, D., & Vaidyanathan, R. (2019). Exploring the equivalence of two common mixture models for duration data. *The American Statistician., 73*(3), 288–295.
15. Ghosh, J., Li, Y., & Mitra, R. (2018). On the use of Cauchy prior distributions for Bayesian logistic regression. *Bayesian Analysis, 13*(2), 359–383.
16. Harrell, F. E., Califf, R. M., Pryor, D. B., Lee, K. L., & Rosati, R. A. (1982). Evaluating the yield of medical tests. *JAMA, 247*(18), 2543–2546.
17. Hubbard, D., Rostykus, B., Raimond, Y., & Jebara, T. (2021). Beta survival models. In *Survival prediction-algorithms, challenges and applications* (pp. 22–39). PMLR.
18. Ishwaran, H., Kogalur, U. B., Blackstone, E. H., & Lauer, M. S. (2008). Random survival forests. *The Annals of Applied Atatistics., 2*(3), 841–860.
19. Kumar, S. (2018). Long Wix.com: Sohn investment idea contest entry (NASDAQ:Wix). https://seekingalpha.com/article/3976965-long-wix-com-sohn-investment-idea-contest-entry
20. Lee, K. L., Fader, P., & Hardie, B. (2007). How to project patient persistency. *Foresight: The International Journal of Applied Forecasting, 8*, 31–35.
21. McCarthy, D. M., Fader, P. S., & Hardie, B. G. (2017). Valuing subscription-based businesses using publicly disclosed customer data. *Journal of Marketing, 81*(1), 17–35.
22. Park, C. H. (2012). Essays on shopping dynamics in customer base analysis. https://ecommons.cornell.edu/bitstream/handle/1813/30999/cp247.pdf
23. Pfeifer, P. E. (2011). On estimating current-customer equity using company summary data. *Journal of Interactive Marketing, 25*(1), 1–14.
24. Ribes, E., Touahri, K., & Perthame, B. (2017). Employee turnover prediction and retention policies design: A case study. arXiv preprint arXiv:1707.01377
25. Saradhi, V. V., & Palshikar, G. K. (2011). Employee churn prediction. *Expert Systems with Applications., 38*(3), 1999–2006.
26. Schweidel, D. A., Fader, P. S., & Bradlow, E. T. (2008). Understanding service retention within and across cohorts using limited information. *Journal of Marketing, 72*(1), 82–94.

27. Soleymanian, M., Weinberg, C., & Zhu, T. (2021). 'Privacy concerns, economic benefits, and consumer decisions: a multi-period panel study of consumer choices in the automobile insurance industry'. https://papers.ssrn.com/sol3/papers.cfm?abstract_id=3905034
28. Wang, L., Li, Y., & Chignell, M. (2021). Combining ranking and point-wise losses for training deep survival analysis models. In *2021 IEEE international conference on data mining (ICDM)*, pp. 689–698. IEEE.

Chapter 7
Trade Credit Pricing with Retailer's Capital Heterogeneity

Mingyu Zheng, Yonghui Chen, and Qiao-Chu He

Abstract This paper studies a supplier's optimal trade credit provision and pricing decisions when there is capital heterogeneity among its retailers. To this end, we start with a baseline model where there is a capital-constrained retailer requiring trade credit financing from the supplier. We identify a capital threshold at which providing trade credit or not is indifferent to the supplier. The identification allows us to extend our analysis to a supply chain including various retailers. We find that the supplier should provide trade credit to retailers whose capital level is lower than the threshold. Those retailers who need trade credit but have relatively high capital will be excluded. Thus, our results provide managerial insights for the supplier to decide which retailers should be provided with trade credit.

Keywords Trade credit · Wholesale pricing · Retailer heterogeneity

Introduction

Trade credit is commonly used by suppliers to provide short-term financing for retailers, which allows retailers to defer payments after goods are delivered. For example, the trade credit term "net 30" indicates that retailers are allowed to make payment for purchased products 30 days after delivery. It is critical to offer trade credit by suppliers to their retailers, especially small and medium-sized ones who have difficulty in obtaining bank financing due to the lack of collateral. As internal supply chain financing, trade credit has been proven to be more effective than bank financing. However, there is little research on how the supplier selects which retailers should be provided with trade credit among others.

M. Zheng · Y. Chen · Q.-C. He (✉)
Southern University of Science and Technology, Shenzhen 518055, Guangdong Province, China
e-mail: heqc@sustech.edu.cn

M. Zheng
e-mail: aaron_tseng@outlook.com

Y. Chen
e-mail: yonghui.c@yahoo.com

R. Qiu et al. (eds.), *City, Society, and Digital Transformation*, Lecture Notes in Operations Research, https://doi.org/10.1007/978-3-031-15644-1_7

This paper analyzes the supplier's optimal trade credit provision and wholesale pricing decisions in a supply chain including one supplier and multiple retailers who have heterogeneous capital levels. We show that trade credit is provided by the supplier to retailers whose capital levels are under a threshold. But for those with capital levels above that threshold, the supplier should never provide trade credit to them.

Literature Review

Based on the newsvendor model, our paper focuses on wholesale pricing. Lariviere and Porteus [1] study the optimal wholesale pricing without trade credit provision in a supply chain. Dada and Hu [2] examine the supplier's optimal wholesale pricing when capital-constrained retailers have access to bank credit. Gupta and Wang [3] characterize the supplier's optimal wholesale pricing under market demand uncertainty.

This paper contributes to studies on trade credit provision with capital constrained retailers in a supply chain . Cachon [4] argues that trade credit affects the allocation of inventory risk between suppliers and retailers and thus trade credit provision can be used to achieve supply chain coordination. Kouvelis and Zhao [5] propose a wholesale pricing and trade credit provision model where they formulate the supplier's optimal pricing decisions given that retailers need trade credit. Yang and Birge [6] further incorporate bankruptcy cost into the model and derive the optimal trade credit decisions of the supplier. Our paper extends this strand of research and addresses the optimal trade credit provision of the supplier among heterogeneous retailers.

Model

Consisting of one deep-pocket supplier and one constrained-capital retailer, a supply chain produces and sells a product to the market. The market-clearing price is normalized to $p = 1$. Market demand D is a random variable whose distribution is characterized by the cumulative distribution function $F(D)$ and the probability density function $f(D)$. We denote $\bar{F}(D) \triangleq 1 - F(D)$ as the probability that market demand is higher than D. The distribution satisfies the property of increasing failure rate (IFR): the failure rate $h(D) \triangleq \frac{f(D)}{\bar{F}(D)}$ is increasing in D. We assume that market demand is limited by $\bar{D}$ such that $F(D) = 1$ and $f(D) = 0$ for any $D \geq \bar{D}$. Thus, we can focus on the demand interval $D \in [0,\ \bar{D}]$.

Timeline We consider a single cycle of production and sales as shown in Fig. 7.1: (1) At the beginning of the cycle, the supplier makes trade credit provision and wholesale pricing decisions with a cash price of w_c and a trade credit price of w_t (if trade credit is offered.) (2) Based on the wholesale price(s), the retailer settles

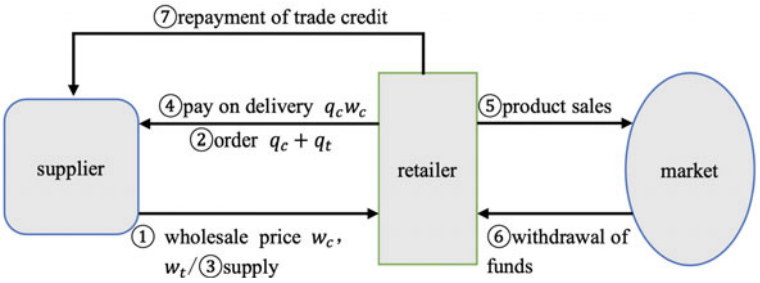

Fig. 7.1 Time sequence

the ordering quantity $Q = q_c + q_t$, where q_c is the quantity paid in cash and q_t is the quantity paid in trade credit. (3) The products are produced at a unit cost of $c \in (0, 1)$ and delivered to the retailer following receipt of the retailer's order. (4) On delivery, the retailer uses its owned capital B to make the cash payment $q_c w_c$. (5) The retailer sells as many products as possible and market demand is met. (6) The retailer's revenues are generated from sales. Any unmet demand disappears and any unsold product has zero salvage value. (7) At the ending of the cycle, if the revenue of the retailer is sufficient to pay off trade credit $L \triangleq q_t w_t$, it will keep the residual. Otherwise, the retailer will go bankrupt under limited liability after paying all of the revenue to the supplier.

Payoffs The expected profit of the retailer is written as:

$$\begin{aligned} \pi &= \int_{Q}^{+\infty} (Q - L) dF(D) + \int_{L}^{Q} (D - L) dF(D) - B \\ &= \int_{L}^{Q} \bar{F}(D) dD - B, \end{aligned} \tag{1}$$

where $Q - L$ and $D - L$ are the remaining revenues retained by the retailer after paying off trade credit when the demand realization is higher than inventory Q and trade credit L, respectively. Similarly, the expected profit of the supplier is evaluated as:

$$\begin{aligned} \Pi &= \int_{L}^{+\infty} L dF(D) + \int_{0}^{L} D dF(D) + B - cQ \\ &= \int_{0}^{L} \bar{F}(D) dD + B - cQ, \end{aligned} \tag{2}$$

where L is the full payment made by the retailer when the demand realization is higher than L. Otherwise, the supplier obtains the entire revenue D.

Preliminary analysis Given the wholesale pricing (w_c, w_t), the retailer determines the order quantities $q_c \in [0, \frac{B}{w_c}]$ and $q_t \in [0, \bar{D}]$, to get the expected profit maximized in Eq. (1). If it uses trade credit, the optimal order quantity can be derived as in Proposition 1.

Proposition 1 *If the retailer has a capital level $B < \bar{B}$ and uses trade credit, its optimal order response to wholesale prices is $q_c = \frac{B}{w_c}$ and $q_t > 0$ implied by $\bar{F}(\frac{B}{w_c} + q_t) = w_t \bar{F}(q_t w_t)$, where $\bar{B} \triangleq c\bar{F}^{-1}(c)$.*

In the following, we focus on the supplier's optimal wholesale pricing (w_c, w_t). By comparing the supplier's expected profit under trade credit provision with that under cash order only, conditions in which trade credit provision improves the supplier's profitability are identified.

Optimal Wholesale Pricing

Based on the optimal order decision by the retailer in Proposition 1, the supplier sets wholesale prices (w_c, w_t) to maximize its expected profit Π in Eq. (2). Denote the optimal solution as (w_c^*, w_t^*). The optimal trade credit pricing is presented in Proposition 2.

Proposition 2 *Given $B \in [0, \bar{B}]$, the optimal wholesale pricing by the supplier is as follows:*

1. *Without trade credit provision, the optimal pricing of the supplier is $w_c^* = \hat{w}$ for $B \in [\hat{B}, \bar{B}]$, and $w_c^* > \hat{w}$ for $B \in [0, \hat{B})$;*
2. *With trade credit provision, the optimal pricing of the supplier is $w_c^* = w_t^*$;*

where $\hat{B} = \hat{w}\hat{Q}$ and $\hat{w} = \bar{F}(\hat{Q})$ with $\hat{Q}$ implied by $\bar{F}(\hat{Q})[1 - h(\hat{Q})\hat{Q}] = c$.

Given that the supplier adopts a high-pricing strategy such that trade credit is not used by the retailer, its capital level influences the supplier's optimal wholesale pricing. If the retailer has a capital level higher than $\hat{B}$, the supplier sets the wholesale price at $\hat{w}$ which is also the optimal pricing when facing a retailer without capital constraint [1]. However, if the capital level of the retailer is lower than the threshold, the supplier will set the price higher than $\hat{w}$. In this case, even though the retailer with constrained capital has demand for trade credit, the supplier will upward distort wholesale pricing such that trade credit is not provided. This pricing difference implies that the supplier's pricing power results in supply chain efficiency loss when the capital level of the retailer is lower than $\hat{B}$.

However, given that the supplier adopts a low-pricing strategy, its optimal decision is to offer net term trade credit, i.e., $w_c^* = w_t^*$. That is because the increase in the cash price decreases the cash order quantity but also increases the order quantity paid in trade credit. As the retailer exhausts its capital to order, the supplier's revenue from cash orders is fixed. Thus, the supplier will increase the cash price as much as possible

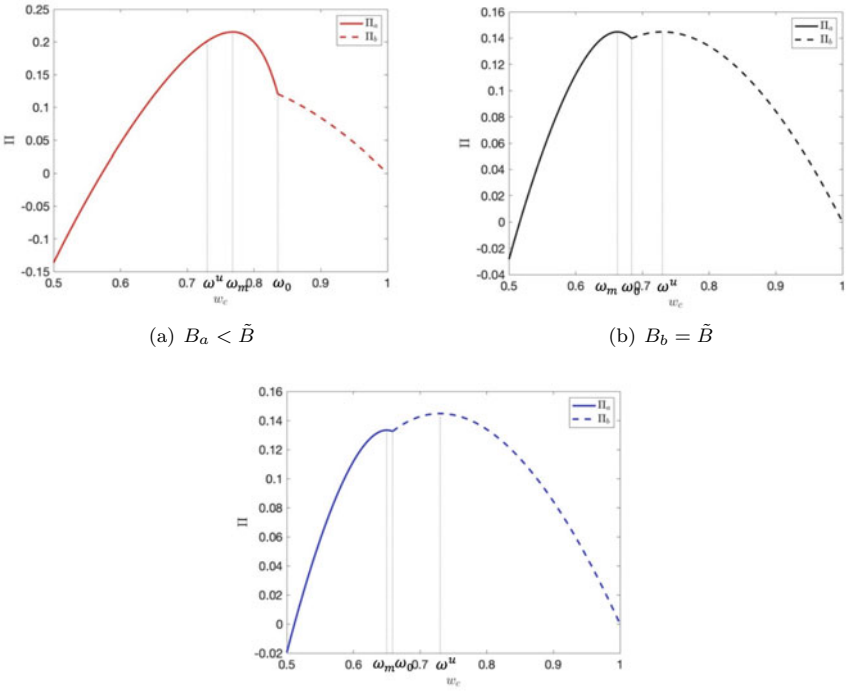

(a) $B_a < \tilde{B}$

(b) $B_b = \tilde{B}$

(c) $B_c > \tilde{B}$

Fig. 7.2 Capital level B and the optimal trade credit provision by the supplier *Notes* Parameters in the simulation include an exponential distribution with $\lambda = 0.5$ for market demand D, $c = 0.5$ for the marginal production cost. In panels (**a**), (**b**), and (**c**), the capital level of the retailer is given by $B_a = 0.300$, $B_b = \tilde{B} = 0.520$, and $B_c = 0.550$, respectively. As the wholesale price w_c increases, each panel shows how the expected profit of the supplier changes, where the solid line represents trade credit provision and the dotted line represents cash order only.

to reduce the production cost cq_c. Furthermore, the supplier will decrease the trade credit price as much as possible to increase sales on trade credit. Note here that the trade credit price is always provided to be greater than or equal to the cash price. Therefore, the same wholesale price is set for both cash and trade credit orders.

Proposition 3 *There exists a* $\tilde{B} \in (\hat{B}, \bar{B})$ *beneath which trade credit is granted to retailers.*

Proposition 3 shows that whether the supplier should provide trade credit is affected by the capital level of the retailer. A capital threshold $\tilde{B}$ is identified at which for the supplier it is indifferent to provide trade credit or not . If the retailer has a capital level lower than the threshold, trade credit is granted to retailers. In contrast, if the retailer has a capital level above the threshold, the supplier should not grant trade credit.

We depict these results in Fig. 7.2 which shows how the expected profit of the supplier changes as the wholesale price w_c increases given the different capital levels of the retailer. The expected profit of the supplier under trade credit provision is represented by the solid line while the dotted line represents the expected profit without trade credit provision. In Fig. 7.2b where the capital level of the retailer is at the threshold $\tilde{B}$, the optimal expected profit of the supplier under trade credit is the same as that under no trade credit provision. When the retailer has a lower/higher capital level as shown in Fig. 7.2a/c, trade credit provision leads to a larger/smaller expected profit than that under no trade credit provision.

Our findings on the optimal trade credit decision by the supplier supplement Kouvelis and Zhao [5] who leave a capital interval of the retailer unstudied. Whether the supplier should offer trade credit to retailers within this interval is unidentified. In a supply chain with multiple retailers and one of them has a capital level located within the interval, the optimal trade credit decisions by the supplier cannot be specifically characterized. As a result, the existence of an unidentified interval makes it difficult to adapt the basic model to a more extensive supply chain network. Fortunately, as we identify the capital threshold $\tilde{B}$, our analysis can be easily extended to a more general supply chain with multiple heterogeneously-capitalized retailers. Our results suggest that the supplier will offer trade credit to those retailers whose capital levels are less than the threshold.

Conclusions

This paper first studies a baseline trade credit model with a single retailer and shows how the optimal wholesale pricing and trade credit provision decisions by the supplier depend on the capital level of the retailer. We then further identify a capital threshold beneath which trade credit is granted to retailers. The specific capital threshold has not been found in the existing literature, which makes it impossible to derive the optimized trade credit decision of the supplier in a supply chain with multiple retailers. Our identification of the threshold fills this gap such that we can extend the baseline model to models with more complex supply chain structures.

References

1. Lariviere, M. A., & Porteus, E. L. (2001). Selling to the newsvendor: An analysis of price-only contracts. *Manufacturing & Service Operations Management, 34*, 293–305.
2. Dada, M., & Qiaohai, H. (2008). Financing newsvendor inventory. *Operations Research Letters, 36*(5), 569–573.
3. Gupta, D., & Wang, L. (2009). A stochastic inventory model with trade credit. *Manufacturing & Service Operations Management, 11*(1), 4–18.

4. Cachon, G. P. (2004). The allocation of inventory risk in a supply chain: Push, pull, and advance-purchase discount contracts. *Management Science, 50*(2), 222–238.
5. Kouvelis, P., & Zhao, W. (2012). Financing the newsvendor: Supplier vs. bank, and the structure of optimal trade credit contracts. *Operations Research, 60*(3), 566–580
6. Yang, S. A., & Birge, J. R. (2018). Trade credit, risk sharing, and inventory financing portfolios. *Management Science, 64*(8), 3667–3689.

Chapter 8
Systemic Risk Spillover Analysis of China's Banking Industry Based on Generalized Variance Decomposition Network

Xuejing Ji and Chuanmin Mi

Abstract The spillover effect of systemic risk is the key driver for the outbreak of financial crises. To study the systemic risk spillover effect of China's bank industry, the generalized variance decomposition method is used to calculate spillover index and build risk spillover network of Chinese listed banks. By quantifying the risk spillover strength from static and dynamic dimensions, and investigating the dynamic evolution process of the spillover network, it is found that: (1) In general, the systemic risk spillover of China's banking industry has asymmetric characteristics and amplification effect, and the spillover effect will enhance significantly when crises occur. (2) From the perspective of institutions, large state-owned banks such as Bank of China are risk receivers in risk transmission, play a vital role in maintaining system stability. Hua Xia Bank, Shanghai Pudong Development Bank, Bank of Communications are risk senders, and they are core nodes in the spillover network.

Keywords Bank · Systemic risk · Generalized variance decomposition · Spillover network

Introduction

Taking the 2008 financial crisis as the turning point, financial supervision changed from micro-prudential to macro-prudential, and the research focus also shifted from the measurement of individual institution risks to the generation, measurement and spillover of systemic risk. High correlation is a primary feature of the modern financial system. The complex and diverse connections between financial institutions tend to cause the spread of risk, and the risk spillover effect becomes more and more significant. The risk spillover increases the complexity of risk research.

X. Ji · C. Mi (✉)
College of Economics and Management, Nanjing University of Aeronautics and Astronautics, Nanjing 211100, Jiangsu, China
e-mail: cmmi@nuaa.edu.cn

X. Ji
e-mail: jxj123@nuaa.edu.cn

R. Qiu et al. (eds.), *City, Society, and Digital Transformation*, Lecture Notes in Operations Research, https://doi.org/10.1007/978-3-031-15644-1_8

At present, Chinese economy is in a critical period of transforming the development model, optimizing the economic structure and changing the growth drivers. The current financial situation of China is complex, and it is in the period of high incidence of financial risk. It is necessary to pay attention to the prevention of systemic financial risk. The banking system is a crucial component of Chinese financial system. According to data released by the People's Bank of China, by the end of 2021, the total assets of China's banking industry accounted for more than 90% of the total assets of financial industry. Maintaining the stability of the banking system is essential for the soundness of China's financial system. Bank institutions are highly related due to their own business characteristics. The inter-bank lending relationship, overlap of investment assets and asset price correlation between banks constitute the direct and indirect channels of risk transmission, boosting the spillover of systemic risk. The initial crisis of individual banks is more easily transmitted to other banks, which may eventually cause a whole system crisis. Studying the systemic risk spillover of the banking industry meets the requirements of developing modern banking industry, which is also of great significance for preventing banking systemic risk, ensuring the healthy operation of the banking system.

The remainder of this paper is organized as follows. Section "Literature Review" reviews the relevant literature. Section "Model Construction and Description" introduces the main models and methods, including volatility model, generalized variance decomposition model. An empirical study is conducted to analyze the risk spillover strength and spillover network characteristics in Sect. "Empirical Analysis of the Systemic Risk Spillover Effect". And research conclusions are summarized in Sect. "Conclusion".

Literature Review

Scholars mainly use network analysis methods to study systemic risk spillover. The network model can capture the complex relationships between financial institutions. There are three main types of networks: physical networks, correlation networks, and information spillover networks [1].

Physical networks are usually constructed using business data between institutions directly, such as inter-bank lending data and common asset data. Allen and Gale [2] earlier applied the network model to study the risk contagion among financial institutions, using the risk exposure data between institutions to build a network model. Fricke and Lux [3] constructed an inter-bank loan network based on bank overnight transaction data on the e-MID trading platform, and studied the network structure of the banking system. Greenwood et al. [4] constructed a network of common asset risk exposures to study bank risk contagion. Huang et al. [5] explored the risk contagion path and strength of banks based on the overall lending data of China's interbank market. Lu and Wang [6], Ma and He [7] established a risk contagion network based on the balance sheet data of Chinese listed banks to study risk contagion. However, due to the fact that the debt and asset data between institutions are not required to

be disclosed to the public, the business data is difficult to obtain and can only be estimated through some methods.

The correlation networks are mainly constructed by using the correlation between market data such as stock prices. Mantegna [8] first proposed a correlation network based on Pearson correlation to analyze the similarity behavior among Dow Jones Industrial Average (DJIA) stocks. Coelho et al. [9], Brida and Risso [10] also began to study the connectedness between financial institutions using correlation networks. Li et al. [11] built multilayer networks to analyze the impact of network structure on bank spillover based on the correlation of stock returns. The disadvantage of the correlation network is that it can only reflect the degree of the correlation between institutions, but cannot reveal the direction of risk spillovers.

The construction of the information spillover networks is mainly through the variance decomposition method or the conditional value at risk (CoVaR) method. Diebold and Yilmaz [12] constructed an information spillover network through variance decomposition method to reflect the connectedness between variables. Liu et al. [13], Gong et al. [14] drew on the research of Diebold and Yilmaz [12] to construct a directed weighted information spillover network to study the risk spillover among financial markets. The CoVaR method proposed by Adrian and Brunnermeier [15] on the basis of value at risk (VaR), can measure the risk contribution of an institution to other institutions when it is in trouble. It has been widely used in the study of systemic risk spillover. Drakos and Kouretas [16] used quantile regression to estimate CoVaR to study the systemic risk contribution of foreign banks when they are in distress. Girardi and Ergünb [17] considered risk dependencies and used the DCC-GARCH model to estimate the CoVaR of different financial institutions. Weng and Yan [18] used the GARCH-Copula-CoVaR model to measure the systemic risk spillover of Internet finance on commercial banks.

The information spillover network method has been wildly used in recent years. Compared with other network construction approaches, it can reveal the strength and direction of risk spillover both and does not focus on the specific reasons why the risk occurs. Therefore, this paper applies the generalized variance decomposition method to construct the risk spillover network.

Model Construction and Description

Volatility Model

The calculation of the risk spillover index is based on the volatility of stock prices, which can only be estimated. We use stock price range to estimate volatility [19–21]:

$$V_{it} = 0.511(H_{it} - L_{it})^2 - 0.019[(C_{it} - O_{it})(H_{it} + L_{it} - 2O_{it}) - 2(H_{it} - O_{it})(L_{it} - O_{it})] - 0.383(C_{it} - O_{it})^2 \quad (8.1)$$

H_{it}, L_{it}, O_{it} and C_{it} represent the natural logarithms of the highest, lowest, opening and closing stock price of institution i in t day.

Risk Spillover Network Model

We apply the generalized variance decomposition method proposed by Diebold and Yilmaz [12] to construct risk spillover network. The risk spillover index can be obtained by calculating the variance contribution between variables. Considering a N-dimensional covariance-stationary VAR(p) model:

$$Y_t = \sum_{i=1}^{P} \phi_i Y_{t-i} + \varepsilon_t \tag{8.2}$$

Its moving average representation:

$$X_t = \sum_{i=0}^{\infty} A_i \varepsilon_{t-i} \tag{8.3}$$

ε is the N-dimensional error term whose components are independently and identically distributed, $\varepsilon \sim (0, \sum)$, $\sum$ represents the covariance matrix. The coefficient matrix of the N × N moving average formula obeys the following recursive process:

$$A_i = \phi_1 A_{i-1} + \phi_2 A_{i-2} + \cdots + \phi_p A_{i-p} \tag{8.4}$$

A_0 is a N × N identity matrix, when $i < 0$, $A_i = 0$.

The key to calculating the risk spillover index based on the generalized variance decomposition method is to get the variance contribution between variables. The variance contribution θ_{ij}^H of variable j to variable i represents the proportion of the H-step forecast error variance explained by y_j when y_i is shocked by external factors. Variance contribution can reflect how the variable is affected by itself or other variables in the system. The calculation formula is as follows:

$$\theta_{ij}^H = \frac{\sigma_{jj}^{-1} \sum_{h=0}^{H-1} (e_i' A_h \sum e_j)^2}{\sum_{h=0}^{H-1} (e_i' A_h \sum A_h' e_i)} \tag{8.5}$$

$\sum$ is the covariance matrix of the shock vector ε_t, σ_{jj} is the jth diagonal element of the matrix $\sum$, e_j is a selection vector with the jth element is 1 and the rest are 0. H represents the forecast step, and h is the lag order of the shock vector. The variance decomposition matrix can be obtained by calculating the prediction error variance contributions between variables. Since the sum of each row in the

matrix is unnecessarily unity, for better explanation, standardization is required. Let $d_{ij}^H = \frac{\theta_{ij}^H}{\sum_{j=1}^N \theta_{ij}^H}$, then we have $\sum_{j=1}^N d_{ij}^H = 1$, $\sum_{i,j=1}^N d_{ij}^H = N$.

The standardized variance decomposition matrix $D^H = [d_{ij}^H]$ can be formulated as:

$$D^H = \begin{pmatrix} d_{11}^H & d_{12}^H & \cdots & d_{1N}^H \\ d_{21}^H & d_{22}^H & \cdots & d_{2N}^H \\ \vdots & \vdots & \ddots & \vdots \\ d_{N1}^H & d_{N2}^H & \cdots & d_{NN}^H \end{pmatrix} \tag{8.6}$$

The elements in the variance decomposition matrix D^H can represent the risk spillovers among institutions. We construct a risk spillover network $G = (V, E)$ based on the matrix, the nodes set V represents all the institutions and the edges set E represents all the spillover relationships between institutions. Since the matrix is asymmetric, we can get a directed weighted network. To remove the redundant or noise information, we use the threshold approach to filter the fully connected spillover network. Given a threshold a_{thr}, a_{ij} represents whether the edge exists:

$$a_{ij} = \begin{cases} 1, \, if \; i \neq j \; and \; d_{ij}^H > a_{thr} \\ 0, \, other \end{cases} \tag{8.7}$$

Empirical Analysis of the Systemic Risk Spillover Effect

Data Sources and Basic Statistical Analysis

Chinese listed banks are taken as research objects. To ensure that the data covers as many financial events as possible, we choose banks listed before 2008, a total of 14 banks, and collect their stock price data. The data comes from the Oriental Fortune platform. The time span of the data is from September 25, 2007 to December 31, 2020, with a total of 3228 samples. Table 8.1 shows the abbreviations and numerical codes of each bank.

The stock price volatility of the 14 Chinese listed banks is shown in Fig. 8.1.

According to Fig. 8.1, it can be seen that the volatility of 14 banks is clustered, especially around 2008, 2013 and 2015, showing obvious volatility clustering, mainly causing by the global financial crisis in 2008, the money shortage in 2013 and the stock market crash in 2015 respectively. These phenomena also prove that volatility data can effectively reflect the risk situation.

As presented in Table 8.2, the mean and standard deviation of Bank of China, Industrial and Commercial Bank of China, and China Construction Bank are smaller

Table 8.1 Bank codes and abbreviations

Code	Abbreviation	Bank
0	BCM	Bank of Communications
1	BOB	Bank of Beijing
2	BOC	Bank of China
3	BONB	Bank of Ningbo
4	BONJ	Bank of Nanjing
5	CCB	China Construction Bank
6	CIB	Industrial Bank
7	CMB	China Merchants Bank
8	CMSB	China Minsheng Bank
9	CNCB	China CITIC Bank
10	HB	Hua Xia bank
11	ICBC	Industrial and Commercial Bank of China
12	PAB	Ping An Bank
13	SPDB	Shanghai Pudong Development Bank

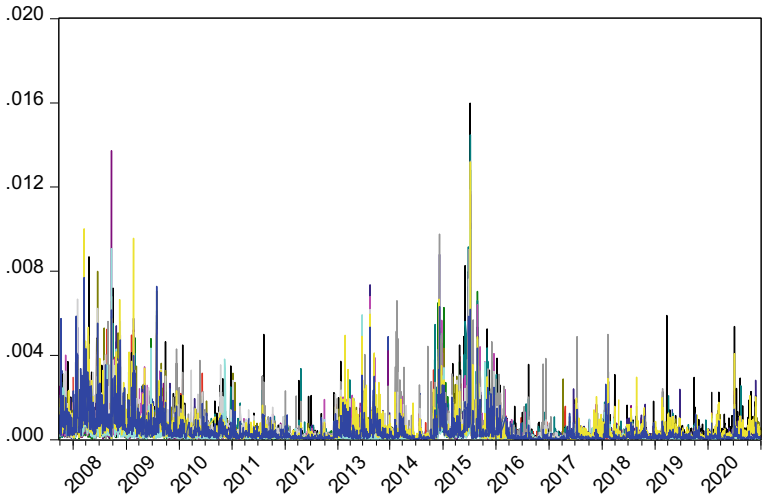

Fig. 8.1 Daily volatility of 14 banks

than those of other banks, indicating that their share price is more stable. These three banks occupy an important position in Chinese banking system, their large scale, decentralized operations, and implicit government guarantees make them doing better in risk taking and risk diversification.

Table 8.2 Basic statistical description of volatility

Bank	Mean	Median	Std. Dev	Skewness	Kurtosis
BCM	3.26E−04	1.14E−04	6.33E−04	5.99E+00	5.79E+01
BOB	3.74E−04	1.55E−04	6.25E−04	4.79E+00	3.84E+01
BOC	2.38E−04	8.43E−05	5.84E−04	8.81E+00	1.20E+02
BONB	5.35E−04	2.84E−04	8.24E−04	5.74E+00	6.25E+01
BONJ	4.28E−04	2.09E−04	7.26E−04	6.10E+00	6.97E+01
CCB	2.79E−04	1.17E−04	5.77E−04	9.68E+00	1.66E+02
CIB	4.24E−04	1.96E−04	6.53E−04	4.19E+00	2.87E+01
CMB	4.21E−04	2.27E−04	6.68E−04	6.14E+00	6.38E+01
CMSB	3.57E−04	1.48E−04	6.39E−04	5.73E+00	5.53E+01
CNCB	4.50E−04	1.96E−04	7.73E−04	5.48E+00	5.27E+01
HB	4.45E−04	1.77E−04	7.68E−04	4.88E+00	4.13E+01
ICBC	2.44E−04	9.63E−05	5.20E−04	7.90E+00	9.94E+01
PAB	5.02E−04	2.73E−04	7.41E−04	5.43E+00	5.63E+01
SPDB	4.08E−04	1.77E−04	6.49E−04	4.37E+00	3.13E+01

Static Risk Spillover Analysis

The ADF unit root test is performed on all volatility series, and the results show that at the 1% significance level, all series are stationary. According to the SC criterion, the optimal lag order of the volatility series is 3. The constructed VAR model passed the stability test, with the characteristic roots all fall within the unit circle. Then we establish the corresponding generalized forecast error variance decomposition model, set the predictive horizon to 10 days, about two weeks of trading time.

Based on the samples from September 25, 2007 to December 31, 2020, a full-sample static analysis is conducted. Table 8.3 is the risk spillover table, the diagonal elements represent the risk spillovers of the institutions to themselves, which is often the maximum value in the row and column, the off-diagonal elements measure pairwise directional spillovers. The rightmost column indicates the total risk that each institution accepts from other institutions, the penultimate row represents the total risk that each institution emits to others, and the last row represents the net risk spillover of each institution (risk emitted minus the risk received). The bold figures in Table 8.3 represent the overall directional risk spillover and average risk spillover of the entire banking system after removing the impact of institutions on themselves. Due to standardization, the total risk spillovers in the "To" direction and the "From" direction within the system are equal, both are 1200.98.

The average spillover level among banking institutions reaches 85.78%, indicating that the overall connectedness is in a high level. The "From" column suggests that there is little difference in risk acceptance among institutions. From the "To" row, it can be seen that Bank of Communications, Hua Xia Bank and China Merchants

Table 8.3 Static risk spillovers of 14 banks

	BCM	BOB	BOC	BONB	BONJ	CCB	CIB	CMB	CMSB	CNCB	HB	ICBC	PAB	SPDB	From
BCM	12.83	7.21	6.75	6.33	7.00	5.89	6.76	7.69	7.26	4.99	7.88	6.35	5.60	7.48	87.17
BOB	7.67	13.80	5.60	6.97	7.19	5.56	7.06	7.22	6.56	5.26	8.15	5.59	5.93	7.44	86.20
BOC	8.68	6.63	14.04	6.78	7.03	7.19	5.18	7.04	6.96	5.86	6.71	7.82	4.63	5.46	85.96
BONB	6.79	7.86	5.32	15.69	8.92	5.32	6.31	6.76	6.47	5.89	7.61	5.12	5.84	6.11	84.31
BONJ	6.97	7.91	5.78	8.93	16.66	4.99	6.46	6.95	5.80	5.49	7.27	4.57	6.03	6.18	83.34
CCB	8.45	6.84	7.78	6.44	5.92	13.79	5.34	7.02	6.20	5.27	6.91	8.90	5.22	5.91	86.21
CIB	7.59	7.37	4.97	5.78	6.48	4.60	13.23	8.06	7.67	3.95	8.28	5.04	7.65	9.34	86.77
CMB	7.48	7.25	5.41	6.12	6.34	5.53	7.20	12.76	7.48	4.31	8.55	6.20	7.11	8.24	87.24
CMSB	8.07	6.83	5.95	6.32	5.95	5.01	7.15	7.92	13.70	4.99	8.14	5.76	6.40	7.81	86.30
CNCB	7.82	7.31	7.35	7.56	7.34	5.47	5.21	6.26	7.14	15.27	6.98	5.61	5.29	5.40	84.73
HB	7.61	7.67	5.17	6.44	6.16	5.27	7.16	7.90	7.48	4.46	13.71	5.61	6.52	8.85	86.29
ICBC	8.23	6.51	7.88	6.13	5.17	8.34	5.47	7.52	6.68	4.45	7.23	14.97	4.98	6.44	85.03
PAB	7.17	6.55	5.01	5.98	6.51	4.90	8.02	8.00	7.49	4.42	8.07	5.32	14.44	8.13	85.56
SPDB	7.74	7.35	4.77	5.33	6.07	4.84	8.49	8.13	7.77	3.84	9.18	5.35	7.01	14.14	85.86
To	100.26	93.29	77.72	85.10	86.08	72.91	85.81	96.46	90.97	63.17	100.97	77.23	78.21	92.79	**1200.98**
Net	13.09	7.09	−8.24	0.79	2.74	−13.29	−0.96	9.22	4.67	−21.55	14.67	−7.80	−7.35	6.93	**85.78**

Bank have larger risk spillovers than other banks, and the corresponding risk net spillovers are also larger, they are important risk senders. In terms of the net directional spillovers, Bank of China, China Construction Bank, Industrial and Commercial Bank of China, these three large state-owned commercial banks and China CITIC Bank have negative net spillovers, which means that they are important risk receivers and play an important role in maintaining the stability of the banking system.

Dynamic Risk Spillover Analysis

In the previous subsection, the total risk spillover of full-sample period is reflected by analyzing the unconditional static inter-bank spillovers. In this subsection, the dynamic risk spillovers are explored based on the rolling estimation window method. We set 250 days as a window, about one year of trading time. Through the rolling estimation window, the dynamic characteristics of the spillover index can be revealed.

Total Spillover Analysis

Figure 8.2 reflects the dynamic risk spillover level (excluding spillovers to themselves).

Figure 8.2 illustrates that Chinese banking system has high internal connectedness, with the average spillover level exceeds 80%, and the inter-bank risk spillovers are time-varying. It can be found that each large fluctuation is related to a certain financial event.

From 2008 to the first half of 2010, the risk spillover among banking institutions was at a high level and showed an upward trend, mainly causing by the shock of the

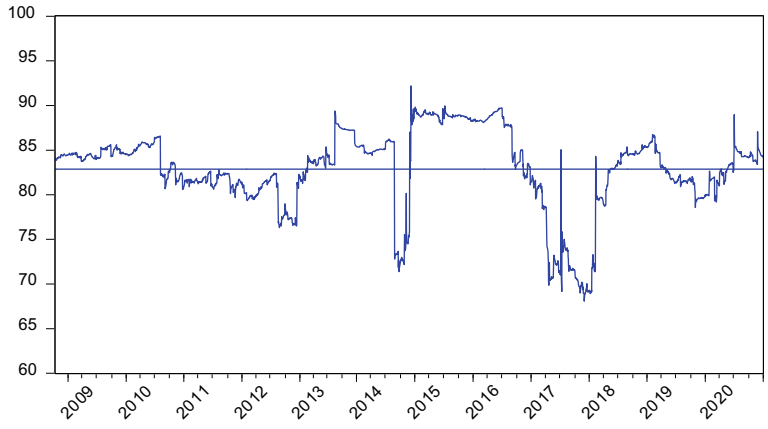

Fig. 8.2 Dynamic risk spillover of 14 banks

2008 global financial crisis and the European debt crisis, which had a certain impact on China's financial sector, resulting in operating losses and the decline in asset quality, banking systemic risk have risen, and risk spillover effect has increased. Since the financial crisis in 2008, Chinese government has introduced a series of policy measures to promote economic growth, such as reducing bank interest and launching a four trillion economic stimulus plan, which has laid the foundation for economic recovery and systemic risk reduction in the later period. As shown in Fig. 8.2, after the second half of 2010, risk spillover showed a downward trend. In 2013, the structural shortage of funds caused by the misallocation of funds led to the outbreak of the "money shortage", various potential risks were increased. It can be seen from the Fig. 8.2 that the spillover has peaked in 2013. After 2014, China's economy has entered a "new normal" stage, when opportunities and risks coexist, the growth of banks size has slowed down, and credit risks have increased. As a result, the inter-bank risk spillovers have been at a high level, and it did not begin to decline until the second half of 2016. After 2017, with the slowdown of economic growth and structural adjustment, the risks accumulated in the banking industry in the early stage have gradually been exposed, the risk has risen sharply. In 2020, affected by the epidemic, the spillover rose again, but is generally controllable.

Directional Spillover Analysis

The previous subsection considers the average level of risk spillovers in the banking system. Now we focus on the directional spillovers between banking institutions. Figure 8.3 reflects the dynamic changes of the risks that each bank accepts from others and sends to others respectively.

In Fig. 8.3, the same scale is used for drawing, it can be seen that there are significant differences in risk sending and risk receiving. The fluctuation in the "From" graph are much smoother than those in the "To" graph, which is consistent with the findings of Diebol and Yilmaz [12]. This difference also reveals the fact that risks have a magnifying effect in the process of contagion. When an institution is subject to external shocks, resulting stock fluctuates, such fluctuations will be transmitted to other institutions which it has business or capital transactions with. Due to the existing potential risk factors of the infected institutions, they tend to transmit greater volatility than they have received. On the other hand, since the institutions in the banking system are interconnected, the risk transmitted by one institution may be very large, but when shared with other institutions, the risk received by each institution may be small.

Table 8.4 shows the top five banks in risk transmission, risk acceptance and net spillover. In terms of the mean value of spillover, Hua Xia Bank, Shanghai Pudong Development Bank, Bank of Communications, Bank of Beijing and Bank of Nanjing have larger risk spillovers than other banks. From the perspective of spillover variance, China Merchants Bank and Bank of Ningbo appear more frequently, indicating that these two banks are more prone to instability under external shocks. Except for Bank of Communications and Shanghai Pudong Development Bank, the assets of

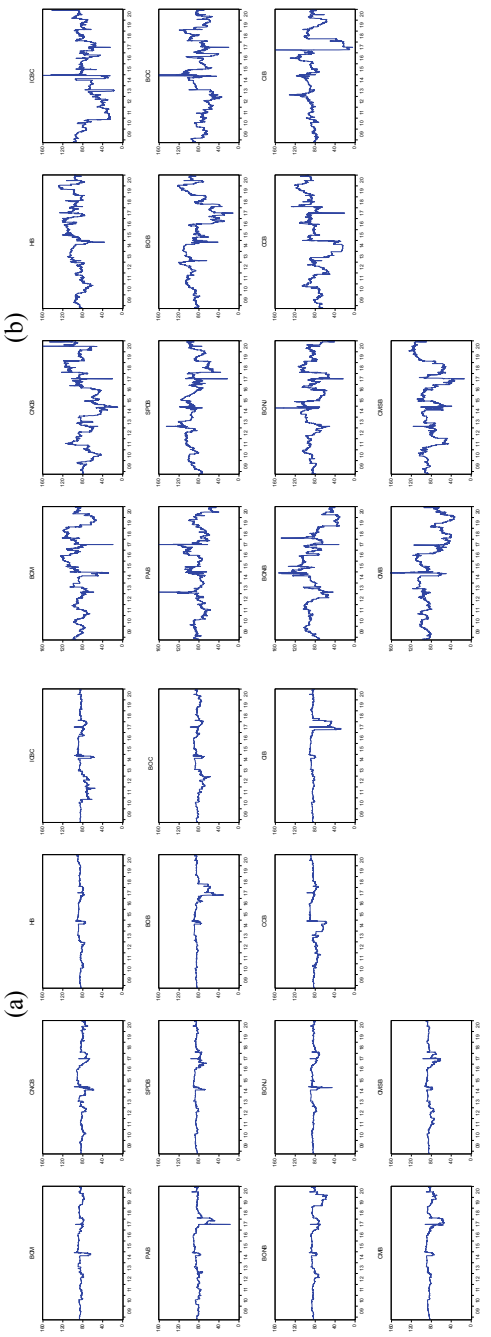

Fig. 8.3 Risks "from" others (**a**) and risks "to" others (**b**)

Table 8.4 Top 5 banks by risk spillover

Rank	To		From		Net	
	Mean	Std. Dev	Mean	Std. Dev	Mean	Std. Dev
1	HB	CMB	HB	CIB	HB	CNCB
2	SPDB	BONB	SPDB	BOB	SPDB	PAB
3	BCM	ICBC	BCM	CMB	BCM	CMB
4	BOB	CIB	CMSB	BONB	BOB	BONB
5	BONJ	BOB	BONJ	CCB	BONJ	CMSB

other institutions are at the back end of the 14 banks, which shows that banks with smaller assets may also play an important role in risk spreading.

Risk Spillover Network Analysis

Referring to the research of Gong et al. [14], the 0.25 quantile of the full-sample spillover index is taken as the threshold to obtain the static network. The node numbers correspond to different banks, which can be known from Table 8.1. Based on rolling window method, the dynamic characteristics of spillover network can be captured. And the network edges, average clustering coefficient and average shortest path are calculated to describe the global network structure, as shown in Fig. 8.4.

The network topology indicators reveal that the network structure of the banking system has been in dynamic changes over time, especially the clustering coefficient and number of edges increase significantly when financial events occur such as money shortages in 2013 and stock market crash in 2015. The occurrence of financial events will lead to closer connections among institutions in the banking system.

In order to clarify the network structure changes during the crisis period, we compare the full-sample period and the money shortage period, raise the threshold to 0.5, the networks are shown in Fig. 8.5. Nodes represent different banks, and edges represent spillover relationships.

Figure 8.6 shows the in-degree centrality (IDC), out-degree centrality (ODC), closeness centrality (CC) and eigenvector centrality (EC) of each bank node in different periods.

Comparing the networks in Fig. 8.5 and the histograms in Fig. 8.6, obviously, the network connectedness has enhanced and the network indicators of each bank node have increased as well when crisis strikes.

Table 8.5 reveals the top five banks of each indicator during the full-sample period and money shortage period.

Table 8.5 suggests that the node importance of Hua Xia Bank and Shanghai Pudong Development Bank has increased significantly during the crisis period. Apart from this, Bank of Beijing, China Minsheng Bank, and Industrial Bank also belong to core nodes in spillover network, playing an important role in risk contagion.

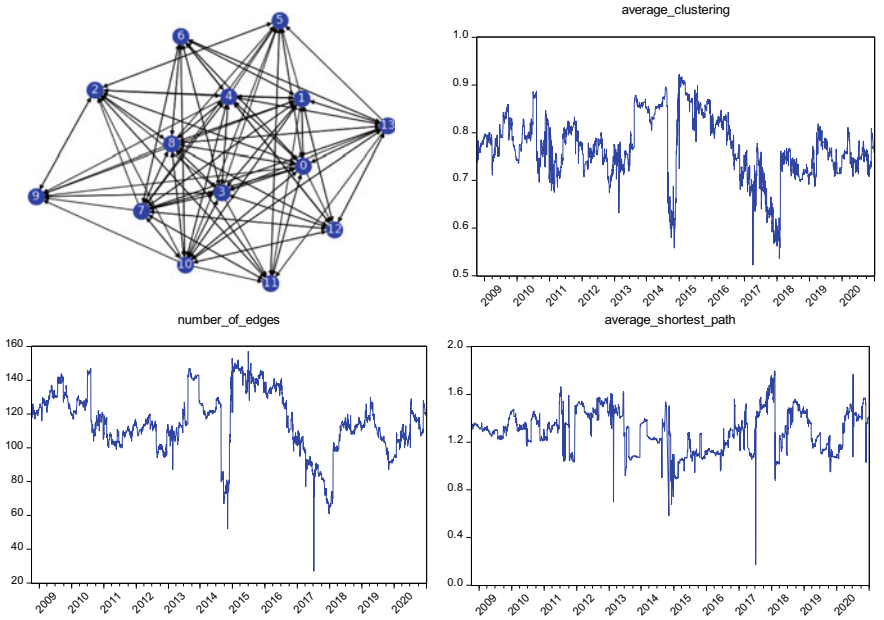

Fig. 8.4 Static network and dynamic network characteristics

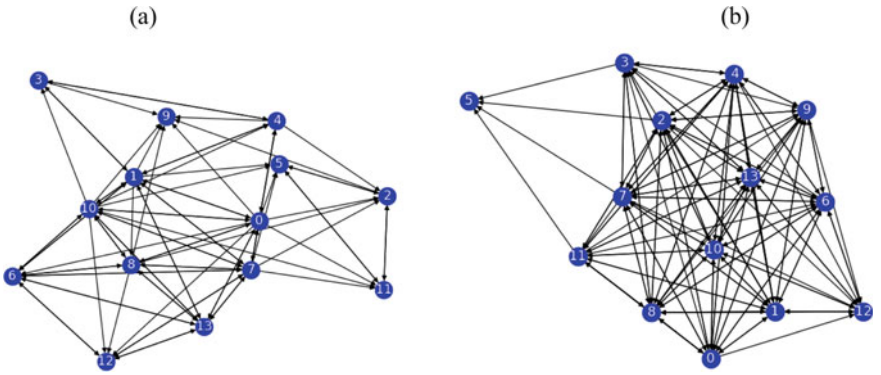

Fig. 8.5 Networks of full-sample period (a) and money shortage period (b)

Conclusion

Based on generalized variance decomposition method, the risk spillover networks are constructed to investigate the risk spillover effect of China's banking industry. We explore the risk spillover strength and network structure characteristics of the banking system from dynamic and static dimensions. The research conclusions are as follows.

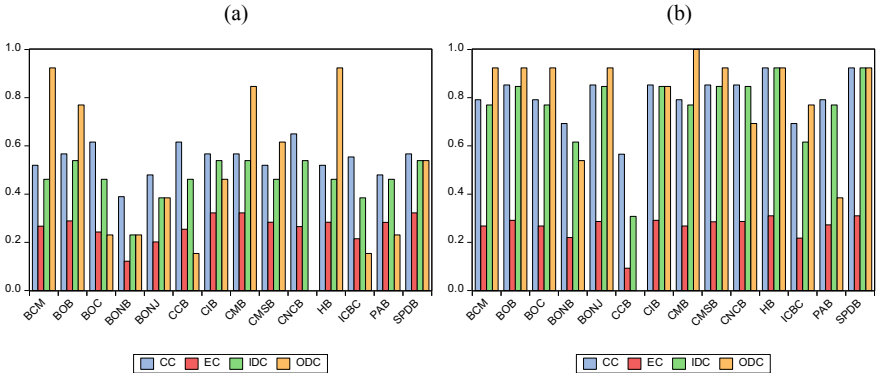

Fig. 8.6 Network indicators of 14 banks during full-sample period (a) and money shortage period (b)

Table 8.5 Top 5 banks in each network indicator

Rank	Full-sample period				Money shortage period			
	IDC	ODC	CC	EC	IDC	ODC	CC	EC
1	BOB	BCM	CNCB	CMB	SPDB	CMB	SPDB	SPDB
2	CIB	HB	BOC	SPDB	HB	SPDB	HB	HB
3	CMB	CMB	CCB	CIB	CIB	HB	BOB	BOB
4	CNCB	BOB	CMB	BOB	BOB	BOB	CMSB	CIB
5	SPDB	CMSB	BOB	HB	CMSB	CMSB	BONJ	CNCB

(1) The risk spillover effect presents asymmetric and time-varying characteristics, and the spillover strength and spillover network connectedness will enhance significantly when crises occur.
(2) Large state-owned banks such as Bank of China, China Construction Bank, and Industrial and Commercial Bank of China usually play the role of risk receivers in risk transmission, and help maintain the stability of banking system.
(3) Hua Xia Bank, Shanghai Pudong Development Bank, Bank of Communications, Bank of Beijing, and Bank of Nanjing are higher than other banks in risk spillover strength and node importance, they are systemically important banks.

For bank risk regulation, the early warning of risks should be strengthened to avoid systemic crises caused by the risk spillover effect among institutions. On the other hand, it is necessary to give priority to the supervision of systemically important banks, and pay attention to the phenomenon of "too big to fail" as well as "too connected to fail".

Acknowledgements This work was supported by "the Fundamental Research Funds for the Central Universities" (NO. NJ2022031).

References

1. Wang, G. J., Chen, Y. Y., Si, H. B., et al. (2021). Multilayer information spillover networks analysis of China's financial institutions based on variance decompositions. *International Review of Economics & Finance, 73*, 325–347.
2. Allen, F., & Gale, D. M. (2000). Financial contagion. *Journal of Political Economy, 108*(1), 1–33.
3. Fricke, D., & Lux, T. (2015). Core-periphery structure in the overnight money market: Evidence from the e-MID trading platform. *Computational Economics, 45*(3), 359–395.
4. Greenwood, R., Landier, A., & Thesmar, D. (2015). Vulnerable banks. *Journal of Financial Economics, 115*(3), 471–485.
5. Huang, W. Q., Fan, M. J., & Zhuang, X. T. (2019). Risk contagion in my country's interbank market based on lending association network. *Journal of System Management, 28*(05), 899–906.
6. Lu, J. G., & Wang, C. (2019). Research on bank risk contagion based on interbank lending and co-loan. *Modern Economic Research, 12*, 41–48.
7. Ma, J., & He, X. B. (2021). Research on financial risk contagion mechanism: Simulation based on China's listed bank data. *Financial Research, 09*, 12–29.
8. Mantegna, R. N. (1999). Hierarchical structure in financial markets. *European Physical Journal B, 11*(1), 193–197.
9. Coelho, R., Gilmore, C. G., Lucey, B., et al. (2007). The evolution of interdependence in world equity markets–evidence from minimum spanning trees. *Physica A: Statistical Mechanics and its Applications, 376*(15), 455–466.
10. Brida, J. G., & Risso, W. A. (2010). Dynamics and structure of the 30 largest North American companies. *Computational Economics, 35*(1), 85–99.
11. Li, S. W., Xie, Y. W., Yang, K., et al. (2019). Research on the impact of multi-layer network structure of commercial banks on systemic risk. *Journal of Southeast University: Philosophy and Social Sciences, 021*(004), 77–84.
12. Diebold, F. X., & Yilmaz, K. (2014). On the network topology of variance decompositions: Measuring the connectedness of financial firms. *Journal of Econometrics, 182*(1), 119–134.
13. Liu, C., Xu, J. H., & Zhou, W. W. (2017). Research on the risk spillover effect of China's financial market–based on spillover index and complex network method. *System Engineering Theory and Practice, 37*(04), 831–842.
14. Gong, X. L., Xiong, X., Zhang, W. (2020). Research on systemic risk measurement and spillover effects of financial institutions in China. *Management World , 8*, 65–82
15. Adrian, T., Brunnermeier, M. K. (2014). CoVaR. *Social Science Electronic Publishing, 106*(7), 1705–1741
16. Drakos, A. A., & Kouretas, G. P. (2015). Bank ownership, financial segments and the measurement of systemic risk: An application of CoVaR. *International Review of Economics and Finance, 40*, 127–140.
17. Girardi, G., & Ergünb, A. T. (2013). Systemic risk measurement: Multivariate GARCH estimation of CoVaR. *Journal of Banking & Finance, 37*(8), 3169–3180.
18. Weng, Z. C., & Yan, M. L. (2019). Measuring the systemic risk spillover effect of internet finance on commercial banks. *Statistics and Decision, 35*(22), 159–163.
19. Diebold, F. X., & Yilmaz, K. (2009). Measuring financial asset return and volatility spillovers, with application to global equity markets. *The Economic Journal, 119*(534), 158–171.
20. Demirer, M., Diebold, F. X., Liu, L., et al. (2018). Estimating global bank network connectedness. *Journal of Applied Econometerics., 33*(1), 1–15.
21. Garman, M. B., & Klass, M. J. (1980). On the estimation of security price volatilities from historical data. *Journal of Business, 53*(1), 67–78.

Chapter 9
Can We Apply Traditional Forecasting Models to Predicting Bitcoin?

Matthew Bobea and Wesley Szuway Shu

Abstract As cryptocurrency becomes more accepted as a valid investment tool within financial markets, and as more financial instruments move on to a decentralized finance platform, demand for more advance methods of modeling cryptocurrency have increased. Having a reliable model will improve investor's confidence in an otherwise high-risk and highly volatized market. Many researchers attempt to create new models and find new variables to forecasting cryptocurrency, however, developing a model that is consistent, accurate, and nondeterministic is still challenging. Nevertheless, traditional models have been proven over time when used for financial market analysis. In this paper, logistic regression and ARIMA will be the key statistical models investigated for use in forecasting Bitcoin. Each model will be tweaked to optimize performance based on current standing research. Furthermore, each model's result will be scored and compared based on their ability to predict Bitcoin's performance.

Keywords ARIMA · Logistic regression · Cryptocurrency · Bitcoin · Financial market prediction · Machine learning

Abbreviations

ADF	Augmented Dickey Fuller Test
AIC	Akaike's Information Criteria score
ANN	Artificial Neural Networks
ARIMA	AutoRegressive Integrated Moving Average
BIC	Bayesian Information Criteria

M. Bobea
Department of Management Information Systems, National Chengchi University, No. 64, Section 2, Zhinan Rd, Wenshan District, Taipei City 116, Taiwan

W. S. Shu (✉)
International Business School Suzhou, Xi'an Jiaotong-Liverpool University, Chongwen Road, Suzhou Industrial Park, Suzhou, Jiangsu, China
e-mail: shuwesley@gmail.com

R. Qiu et al. (eds.), *City, Society, and Digital Transformation*, Lecture Notes in Operations Research, https://doi.org/10.1007/978-3-031-15644-1_9

BTC Bitcoin
KNN K-Nearest Neighbor

Introduction

Since the price of Bitcoin first hit 1$ in February 2011 [1], cryptocurrency has become increasingly sought after as an investment option. This is due to benefits such as: little to no transaction costs, faster international transactions, 24/7 access to funds, no limits to the funds you can transfer, and more [2–4]. Today, cryptocurrency is worth roughly $653 billion USD or just less than 5% of the world's money [5]. However, the cryptocurrency market is well known be volatile which defers many investors [6]. Having a consistent and accurate model is highly in demand as it provides the advantage of improved understanding of the crypto market, reduced investment risk, and ultimately, more significant profits.

Researchers today have already proven that financial instruments such as stocks can be forecasted using models with high levels of accuracy [7–11]. However, cryptocurrency differs from stock market predictions as cryptocurrency tokens lack the independent variables that are typically used in stock models (e.g., company earnings and general financial rations). Chen et al. compared traditional models such as logistic regression and discriminant analysis with machine learning algorithms. They concluded that traditional models show better performance in forecasting Bitcoin prices [12]. Makridakis et al. suggests "Literally hundreds of papers propose new machine learning algorithms, suggesting methodological advances and accuracy improvements. Yet, limited objective evidence is available regarding their relative performance as a standard forecasting tool." [13]. Brownlee proved the effectiveness of classical models such as ARIMA, (AutoRegressive Integrated Moving Average) suggesting that these classical models be used as a baseline when testing more advance and modern forecasting techniques [14]. Knowing this, it is easy to understand why answering the question of "whether or not traditional models can be applied to cryptocurrency" can be a stepping stone to future research involving more advance models.

Numerous studies have tried to predict cryptocurrency using traditional methods such a ARIMA, KNN Random Forest, and more [15–17]. However, many of these models are not being evaluated using well recognized variables and methodologies which have been tested over time in the same manner that modernly used financial investment algorithms are. Instead, many models are based on hypothesized theories and new techniques which makes the models dependent on further testing for consistency. The ARIMA and logistic regression models developed in this study are based on published models which are designed for financial investments and have been tested over time.

To determine if traditional forecasting models are effective cryptocurrency forecasters, the following steps took place. First, we identify the most successful models

and methodologies used in financial market forecasts today. Second, we run these models on a cryptocurrency dataset and then score their effectiveness. Lastly, we fine tune each model so as to determine the most accurate methodology for predicting price surges and dips. In the 'Data Analysis' section, Bitcoin [4] was selected as the dataset to be used in this experiment. Bitcoin's historical trading data was chosen to represent the cryptocurrency market because it encompasses over 79% of the cryptocurrency market and make up the majority of cryptocurrency transactions conducted today [18]. Accordingly, obtaining a model which is applicable to Bitcoin will mean that the model is also applicable to 79% of the cryptocurrency market.

The structure of this paper is broken out into four parts: First, the 'Methods' section covers research used to developing our model. Next, the 'Data Analysis' section uses models and methodologies taken from the literature review section and applies them to a Bitcoin dataset. Adjustments made to each model are based on the settings of the models researched in the literature review section. Lastly, the 'Summary' section summarizes our findings and concludes the research.

Methods

Researchers have suggested that Bitcoin performance correlates with stock market performance [19–21]. In order to test if traditional models used on stock market data can be adapted to Bitcoin, our first step was to identify which stock forecasting models are optimal for testing on Bitcoin data. Ideally, the models should perform well with large datasets while maintaining a high forecast accuracy rating and remains unbiased. We will also consider model selection metrics when choosing a model. Examples include each model's Akaike's Information Criteria (AIC) [22] score, Bayesian Information Criteria (BIC) [23] score and adjusted-R2 scores.

Simultaneously, it is just as important to eliminate any identified models which are hypothesized to be poor Bitcoin forecasters. Three rules were established as to when to rejected a model. First, we will reject models if they have an accuracy rating lower than any existing model of the same type. For example, a regression model scoring 60% will be disregarded if a similar alternative model scoring 80% is already accounted for. Second, models which score less than 55% accuracy will also be rejected. By using a logistic regression model as a baseline, a model that scores purely on chance will score 50%. This is because the outcome of a logistic regression model is binary and thus each outcome has a 1 in 2 chance of occurring. Additionally, each model's data analysis will be conducted using a 95% confidence interval which gives us a 5% margin of error. Taking into account both of these figures (50% + 5%), the lowest acceptable accuracy rating of a model is 55%. Third, models which are not recommended by the researcher will be disregarded. Reasons why a model may not be recommended by a researcher may be attributable to problems such as heteroskedasticity, endogeneity, model misspecification, high AIC or BIC scores, etc.

Once a model is selected, the final step is to optimize each model's methodology for accurate forecasting. For example, should we use short term or long-term moving average when forecasting with a logistic regression model and how do these changes affect our model's accuracy? In our research we hypothesize if we can identify the configurations and methodologies used in models that performed well when forecasting stocks, then these same methodologies can be tested by adapting them into our models using Bitcoin dataset and observing how these changes affect the results. For example, if a logistic regression model predicting stocks performs better by adapting machine learning concepts like using training and testing data, then can these mythologies can be applied to the models concerning Bitcoin. Following the model selection criteria listed above, forecasting models considered were narrowed down to include the follows: ARIMA, artificial neural networks (ANN), K-Nearest Neighbor (KNN), and logistic regression. Additional details on how and why each model was selected for consideration is listed below.

Rejected Models

One option is to use an artificial neural network algorithm to forecast token prices. ANNs were considered because they are good function approximators, as relationships can be examined by them even if the data set is very complex [24]. So, ANN has the potential to tell apart unknown and hidden patterns in information which may be effective for share market prediction [25]. Some researchers have had concerns when using neural networks as, "neural networks are a black box method for providing accurate predictions, but contain little or no explanatory power" [11]. Because the purpose of this research is to understand how to adapt commonly used models for analyzing token performances, we need to fully understand how the model makes its prediction. This black box problem will be an issue if neural networks are selected. A paper published in 2018 stated "predicting the market is very risky and a realistic investment system should be implemented by taking into account the active environment where it is evolving" [26]. He went on to explain that neural networks alone were not sufficient forecasters considering the level of risk investors took when making their investments. Lastly, Shih et al. compared the effectiveness of ANN and logistic regression in making stock forecasts. Here, the logistic regression models produced consistently higher accuracy scores than ANN [27].

Another possible alternative to ANN is using KNN to forecast cryptocurrency. KNN employs unsupervised learning which is advantageous to a cryptocurrency data set where all of the predicting factors may not be available. In contrast to statistical methods that try to identify a model from the available data, the KNN method uses the training set as the model [28]. KNN's main advantage is the effectiveness in situations where the training dataset is large and contains deterministic structures [29]. Nevertheless, there are situations where non-deterministic operations occur on the Blockchain. This includes but is not limited to: (1) using a timestamp inside the smart contract and storing the timestamp on the ledger, and (2) Calling an external

API (running outside the Blockchain) from the smart contract [30]. Ballings et al. compared multiple models for stock price forecasting using data from '5767 publicly listed European companies' [7]. They concluded that models such as Neural network and, KNN were some of the lowest performing models for forecasting stock on the European market. Additionally, Selcuk Disci analyzed futures on the BIST index on the Istanbul Stock Exchange using KNN and ARIMA. This paper concluded that "the ARIMA model is much better than the KNN model for our non-seasonal time series data" as it produced more accurate results [8]. For the mentioned reasons, ANN and KNN were not selected for use in this study.

Selected Models

The overall goal is to predict whether a Bitcoin token (BTC) will rise or fall. Since the possibility of results are binary, (predicting a price increase vs a price decrease) logistic regression will be an ideal choice as it is tailored towards binary classification. Logistic regression is less inclined to over-fitting which is necessary as Bitcoin's historical pricing it is limited to only a few features. The limited number of features in Bitcoin's data set also works well with a logistic regression model because logistic regression models only needs to estimate only a small number of coefficients [17].

Bahtiar et al. analyzed eight months of historical data involving more than eight hundred companies listed under Bursa Malaysia from the Kuala Lumpur Stock Exchange (KLSE) using logistic regression [9]. Their final model stated that logistic regression was successful in predicting stock performance with 89.77% accuracy. Other researchers have also reached their own positive conclusions conducting forecasts on stock exchanges using logistic regression [10, 27, 31]. Consequently, logistic regression was chosen as a model for this research.

Another option to logistic regression is ARIMA which is tailored for times series data such as stock data. Studies have shown many advantages to using ARIMA to forecast financial performance [16, 32, 33]. For example, it is easier to combine ARIMA models with other methods aiming at specific characteristics of the analyzed data (e.g.: targeting volatility clustering with ARIMA and GARCH) [34]. There are many overlapping variables between stock data historical pricing and Bitcoin in these ARIMA models and thus many variables can easily transition to the new model with minimal manipulation. Many researchers have successfully modeled stock prices using ARIMA today [7, 11, 15, 27, 35, 36]. Meanwhile, others have produced positive results used ARIMA to forecast cryptocurrency directly [16, 37]. Since we can build on previous groundwork, ARIMA was selected as a model for this research.

Variable Selection and Model Optimization

Multiple Researchers have used logistic Regression models to predict stock performance using financial ratios as independent variables [10, 27, 31]. Examples include: Earnings per share (EPS), Price to Book Value (PB), Return of Equity (ROE), Current Ratio (CR), Debt to Equity (DE), and others. Nevertheless, cryptocurrencies are not corporations and therefore do not have the same financial ratios to evaluate their performance or be used as a predictor variable. To apply logistic regression to Bitcoin data, these variables must be replaced. Instead, the public Bitcoin data set provides variables which include: 'Close', 'Open', 'High', 'Low'. Additionally, we will need create a dependent variable which tracks whether the stock has risen or fallen. It is necessary to create this variable because one assumption of binary logistic regression is that it requires the dependent variable to be binary [38, 39]. Jamili Zaini et al. was able to make accurate predictions on the stock market using time series data and a logistic regression model by incorporating a moving average methodology [9]. Because of this, we chose to incorporate a moving average methodology into our model. Lastly, a moving average technique can help us understand an overall idea of the trends in a data set [40].

Variable Selection and Model Optimization for ARIMA

Ariyo et al. was successful in using an ARIMA model using the stock's '**close price**' as their independent variable [32]. For these reasons, our ARIMA model will use the 'close price' variable as the independent variable in the data analysis section. Other research has shown that using moving average as a predictor variable was significant when predicting of stock market data [9]. It was specified that, "… MA ranges are between 5 and 25 days" [9]. Since using a moving average of this range produced positive outcomes, a moving average methodology will be tested for better results in the data analysis section below.

Data Analysis

The raw Bitcoin data set has, 4,572,257 observations and 8 variables extending from January 1st, 2015 to March 10, 2021. These include: Timestamp (the time of the transaction), Open (opening price), High (day's high price), Low (day's low price), Close (day's closing price), Volume (of BTC), Volume (currency), and Price (averaged by day). The API that collected data for this exercise extracts all Bitcoin transactions grouped by minute. "If a timestamp is missing, or if there are jumps, this may be because the exchange (or its API) was down, the exchange (or its API) did not exist, or some other unforeseen technical error in data reporting or gathering" [41].

For this reason, the data is populated with NAs which were removed. Removing observations where data was not recorded leaves us with 3,330,541 observations. Next, lagged variables were added to work as the predictors in the linear regression model. Additionally, the volume of transactions which were broken out by minute are aggregate by day. This is saved in a variable called 'agg' (short for aggregate data) and is merge with the main data frame. Since the original data set also contains the 'original volume by minute' data, this information is removed. The next step in the data preparation phase is to create additional independent variables to be used in assessing the model. To do this, lag variables are used so historical data can take part in the model's prediction.

Data Analysis—Logistic Regression

The overall goal of the model is to determine whether the market will rise or fall. Thus, we need a dependent variable which represents this. This is resolved by creating a new factor variable called "direction". If the closing price for an observation is higher than the previous day's closing price, it is tag it as "up". Alternatively, a day to day drop in the closing price will be tagged as "down". In the logistic regression equation, Y is defined as follows:

$$Y = \begin{cases} 1, \ Direction = up \\ 0, \ Direction = down \end{cases}$$

After developing our variable, the new data structure is as follows (Fig. 9.1).

After developing our variable, the new data structure is as follows:

Name	Type	Row 1	Row 2	Row 3	Row 4	Row 5	Row 6
Volume_BTC:	Num	94.802	94.802	33.883	0.296	5	...
Open:	Num	6.65	6.65	6.8	6.8	7	...
High:	Num	6.65	6.65	6.9	6.8	7	...
Low:	Num	6.65	6.65	6.8	6.8	7	...
Close:	Num	6.65	6.65	6.9	6.8	7	...
Volume_ (Currency):	Num	9.75	3.32	63.61	2.01	7	...
Price:	Num	6.65	6.65	6.83	6.8	7	...
Lag1:	Num	6.65	6.65	6.65	6.9	6.8	...
Lag2:	Num	5.57	6.65	6.65	6.65	6.9	...
Lag3:	Num	5.32	5.57	6.65	6.65	6.65	...
Lag4:	Num	5	5.32	5.57	6.65	6.65	...
Lag5:	Num	5	5	5.32	5.57	6.65	...
Direction:	Factor w/ 2 levels "down", "up"*:	2	2	2	1	2	…

Fig. 9.1 Data structure

Fig. 9.2 Confusion matrix

Prediction	Down	Up
Down	728	937
Up	937	3376

Model 1—Logistic Regression

In the following section we will describe the logistic regression model that was created using R programming. We start by specifying "Direction" as our dependent variable. Each lag (Lags 1–5), "volume", "High", "Low", and "Close" will be our independent variables. These are analyzed using R's glm function and then stored in a variable called "fit". Specifying 'binomial' in the syntax tells the glm function to use a logistic regression. Running the model leaves us with the following results (Fig. 9.2):

This model received a 68% accuracy rating. As a baseline, a model with random prediction will result in a 50% accuracy ratio. This means that our model is an 18% improvement overall.

Model 2: Logistic Regression with Training/Testing Data

In the paper "Prediction of stock performance by using logistic regression model" author An Nguyen was able to make improvements on his model when forecasting stocks by incorporating training data [10]. This modification can be adapted to the current model to see how splitting the date affects its accuracy when forecasting Bitcoin. The data is split between training and testing data where approximately 5000 observations are used for training data and approximately 1000 observations are used for testing data. After running the model, the resulting output is as follows (Fig. 9.3):

In the statistics section above, the model's results score an improved accuracy rating of 91%. The next step is to compare these results against a logistic regression model with a moving average variable.

Fig. 9.3 Confusion matrix

Prediction	Down	Up
Down	477	31
Up	63	457

Fig. 9.4 Confusion matrix

Prediction	Down	Up
Down	843	92
Up	347	1289

Model 3: Logistic Regression with Moving Average

The paper "Classify Stock Market Movement Based on Technical Analysis Indicators Using Logistic Regression" the authors are able to make accurate predictions by means of a logistic regression model with moving average. Additionally, it adapts the model for time series data. Consequently, we create an additional new variable called "Movavg" and rerun the model with the additional feature. After rerunning the model, we conclude with the following (Fig. 9.4).

When these results are compared to model 1, using a moving average methodology improves our accuracy from ~69% to ~83%.

Concerns of Correlation

The variables are tested for correlation. More precisely, the variable for "Movavg" is tested against the "Close", "Open" "High", and "Low", variables respectively. This results in the following plot (Fig. 9.5).

The four plots above imply that all four variables have a high degree of correlation, but this can be misleading. According to a paper by San José State University "If both variables have a linear trend this would lead to the appearance of a correlation even if no causal relationship exists."[42]. The variables for "Close", "Open" "High", and "Low" are all priced within one trading day of one another and therefore have very similar values. Consequently, a 10 day moving average would show little change graphically considering that the BTC dataset spans multiple years. In this scenario, the variable "Movavg" will have a nearly identical linear trend as "Close", "Open" "High", and "Low" and consequently give the appearance of correlation. It is safe to state that the approximate coincidence of the plotted pattern of these variable is simply a consequence of scaling and is of no empirical significance.

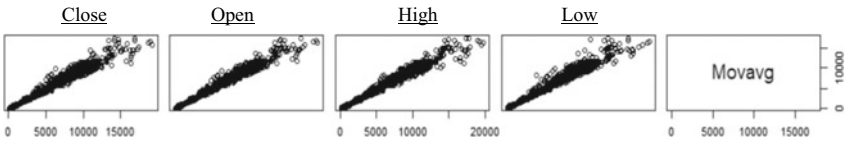

Fig. 9.5 Correlation

Data Analysis—ARIMA

ARIMA is selected as it is most advantageous when using time series data, such as this Bitcoin data set. Unlike the logistic regression models above, this ARIMA model will focus on using the models own lagged variables as its predictor variable. In the equation $Yt = \alpha + \beta 1\ldots$ our dependent variable Yt is predicted using a lagged variable $\beta 1$. In a logistic regression model, our predictions are based on variables that are observable—such as 'Volume_BTC', 'Open', 'High', 'Low', and 'Close'. Nevertheless, there are many other factors that affect cryptocurrency pricing. Some examples include: the news, social media, and public outlook. By moving to an ARIMA model with lagged variables, these additional influences are taken into consideration unlike the logistic regression model. Consequently, it is hypothesized that using an ARIMA model will produce better results.

Model #4: ARIMA Model

When using an Arima model it is necessary to confirm that the model is stationary to ensure "statistical properties such as mean, variance, autocorrelation, etc. are all constant over time" [43]. This is critical because when using ARIMA, seasonality must be resolved prior to running the data through the ARIMA model.

To test for seasonality in our data, the data is tested using an ACF (Autocorrelation function) and PCF (Partial Autocorrelation function) test. In R, the ACF function plots autocorrelation at different lags. The first value (R0) in an ACF chart is always 1. This is calculated by means of ACF (K) = ρ_k = Cov (y_t, y_{t-k})/Var (y_t). Figure 9.6 displays the ACF plot for our data. The dashed lines show the significance level while the downward trend shows that there are no concerns of autocorrelation. Partial autocorrelation is also probed in R and outputted to Fig. 9.7. Here the low levels that trend towards 0 show that stationarity is not an issue in this test.

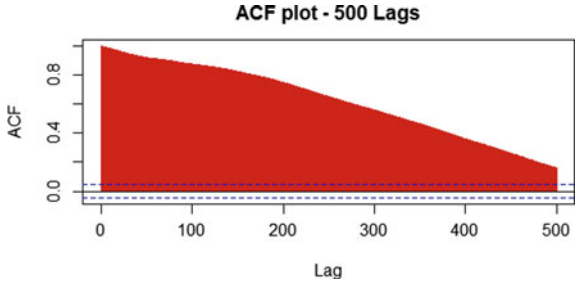

Fig. 9.6 ACF plot

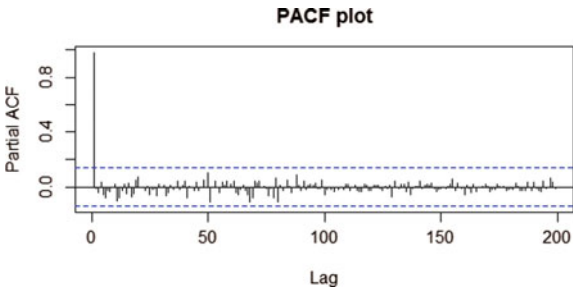

Fig. 9.7 PACF plot

Dickey-Fuller Test

In the Dickey-Fuller Test we continue to ensure that stationarity is not present in the model. The test results show that the original set of data has a p value of 0.7168. This P value would be a concern if this was not conducted for comparison purposes. However, the model's concern is the DF test on the difference. Therefore, the difference is taken and the test is recalculated. The resulting P value is set to 0.01. This means that the null hypothesis is rejected at a 5% significance level on non-stationarity.

ARIMA Analysis

In this model the 'auto.arima' function in R will be used because it "returns best ARIMA model according to either AIC, AIC or BIC value:" [44] and will be used to forecast the next 582 time periods of data. In the plot below, forecasted data points are highlighted in blue while the green line represents the first 2000 observations of bitcoin from our test sample set. The blue line has an upward trend which represents a positive outlook over the next 258 time periods. Additionally, this plot lists a 0 number after the word ARIMA. This value represents the number of auto-regressors if the model. This means that the is the number times the closing price is regressed upon its past values is equal to 0 (Fig. 9.8).

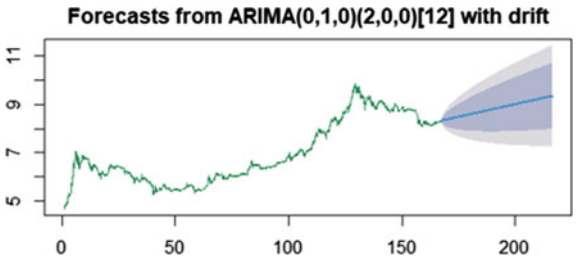

Fig. 9.8 ACF plot

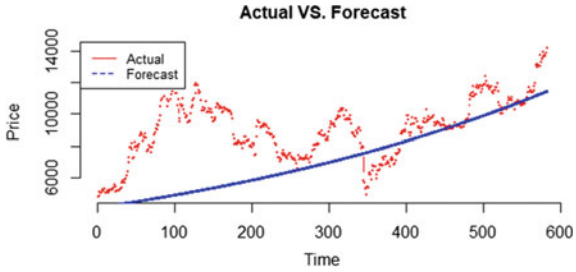

Fig. 9.9 Model 4—actual versus forecast plot

Now that the forecasted data has been generated, it can be compared against 'actuals' to see how well the predictions score. The new data frame comparing the actual results from our training data set and our predicted values is stored in the variable "test". This data frame is then used to create the plot below.

It is shown in the Fig. 9.9 that as the price of BTC stabilizes over time, the predictions become more accurate and vice versa. The final step in this model is to tangibly asses the accuracy of our findings. Unlike the logistic regression model, a confusion matrix is an inaccurate method to assess the model's performance. This is because, the resulting predictions are numeric and not factorial. Instead, the performance of the model was determined by calculating its percent error. The final value is 0.195438 which means that our model is accurate in predicting BTC token pricing within a 19.54% margin of error based solely on its historical value. Alternatively, it can be stated that the model's accuracy at **80.46**%.

Model 5: ARIMA with Moving Average

To improve ARIMA's performance a moving average methodology was chosen based on other successful ARIMA models mentioned previously in the 'methods' section. In this model, instead of taking each day's price as is, each observation's stock price will be priced as an average of the last 5 days. This will create a five-day moving average for Bitcoin pricing. The new variable is ran through the same autocorrelation tests as displayed in model 4. Its results were that the model has no autocorrelation problems. The Fig. 9.10 shows the model's final results.

These results show a 20.65% percent error meaning that the model is approximately 79% accurate. Since this is approximately, 1% less accurate than model 4, it is safe to conclude that using a moving average ARIMA model was not a significant improvement on model 4.

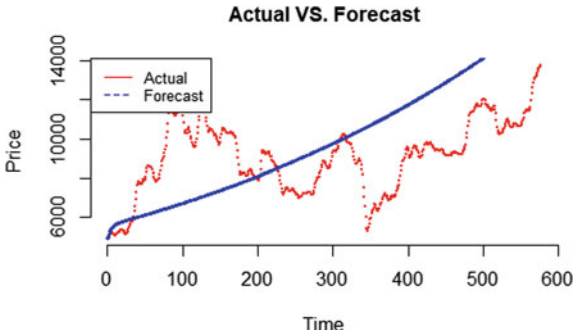

Fig. 9.10 Model 5—actual versus forecast plot

Summary

The results of all 5 models are summarized as follows (Fig. 9.11).

We hypothesized if traditional models and methodologies used in financial market prediction could be adapted to forecast BTC. After researching successful models formerly used in financial market predictions, logistic regression and ARIMA were selected. The moving average methodologies and the use of training and testing data were adapted to optimize the model's accuracy when forecasting BTC. Each model was tested for its robustness in handling Bitcoin's historical data and no concerns were found. Our results show that these models were able to forecast Bitcoin prices with accuracy levels as high as 90.86% and 80.46% respectively. By developing a stable and consistent model we can assist future researchers interested in forecasting Bitcoin by providing them with a baseline model to test against when experimenting with new methodologies and variables.

Generally speaking, when selecting between a logistic regression and an ARIMA model, there are more aspects to consider besides accuracy percentage. For example, when conducting data analysis with logistic regression in this experiment, there were risks of multicollinearity in the logistic regression model. Additionally, when conducting a traditional regression analysis on bitcoin data, there are always omitted variable bias concerns as many variables are difficult to quantify. Author Sinan Inan states that "The price (of cryptocurrency) is not just related to supply and demand" [45]. Examples of these external variable that may affect bitcoin's price include: regulations overseeing its sales, media coverage, internal governance, etc. This is

Model #	Model type	Accuracy percentage
Model 1	Logistic regression	68.65
Model 2	Logistic regression + Training/Test validation	90.86
Model 3	Logistic regression + Moving average	82.92
Model 4	ARIMA	80.46
Model 5	ARIMA + Moving average	79.35

Fig. 9.11 Final results

less of an issue when using ARIMA as it regresses upon itself instead of multiple external variables. Simultaneously, it accounts for unobserved variables in a time series data.

Overall, whether or not a model's accuracy rating is considered acceptable is based on the investors risk tolerance. Additionally, a common issue with these forecasting models is that they fail to inform the investors the quantity of funds they should invest for optimal profits [26]. Rather, further research should be conducted on the topic. Ultimately, it is the investor that decides the optimal model for his or her investment goals. In terms of next steps, now that an accurate model is established, it opens the opportunity for generalization by means of testing it against additional alt coins as well.

Acknowledgements I would like to acknowledge my advisor, Professor Szu-way Shu, whom helped guide me through the strategic aspects of this research. Additionally, I would like to acknowledge the contributions of Di He, Ph.D. and Songquan Pang for their support in this paper.

References

1. Hicks, C. (2020). The history of bitcoin | Investing | US News. *US News & World Report*. https://money.usnews.com/investing/articles/the-history-of-bitcoin. Accessed July 09, 2021.
2. Tredinnick, L. (2019). Cryptocurrencies and the blockchain. *Business Information Review, 36*(1), 39–44. https://doi.org/10.1177/0266382119836314
3. Arora, S. (2021). Understanding cryptocurrency and its benefits. *Simplilearn.com*. https://www.simplilearn.com/tutorials/blockchain-tutorial/what-is-cryptocurrency. Accessed June 27, 2021.
4. Nakamoto, S. (2008). Bitcoin: A peer-to-peer electronic cash system (p. 9).
5. Reiff, N. (2021). How much of all money is in bitcoin? *Investopedia*, May 31, 2021. https://www.investopedia.com/tech/how-much-worlds-money-bitcoin/. Accessed June 27, 2021.
6. Jay, P., Kalariya, V., Parmar, P., Tanwar, S., Kumar, N., & Alazab, M. (2020). Stochastic neural networks for cryptocurrency price prediction. *IEEE Access, 8*, 82804–82818. https://doi.org/10.1109/ACCESS.2020.2990659
7. Ballings, M., Van den Poel, D., Hespeels, N., & Gryp, R. (2015). Evaluating multiple classifiers for stock price direction prediction. *Expert Systems with Applications, 42*(20), 7046–7056. https://doi.org/10.1016/j.eswa.2015.05.013
8. Disci, S. (2020) Time series forecasting: KNN vs. ARIMA. *R-bloggers*, September 29, 2020. https://www.r-bloggers.com/2020/09/time-series-forecasting-knn-vs-arima/. Accessed February 20, 2021.
9. Jamili Zaini, B., Mansor, R., Yusof, N., & Hui Sang, B. (2019). Classify stock market movement based on technical analysis indicators using logistic regression. *Journal of Advanced Research in Business and Management Studies, 1*. http://www.akademiabaru.com/doc/ARBMSV14_N1_P35_41.pdf
10. Syed, S., Mubeen, M., Hussain, A., & Lal, I. (2018). Prediction of stock performance by using logistic regression model: Evidence from Pakistan Stock Exchange (PSX). *Asian Journal Empirical Research*, *8*, July 2018. https://doi.org/10.18488/journal.1007/2018.8.7/1007.7.247.258
11. Jarrett, J., & Kyper, E. (2011). ARIMA modeling with intervention to forecast and analyze Chinese stock prices. *International Journal of Engineering Business Management*. https://doi.org/10.5772/50938

12. Chen, S., Liu, Z., Wang, L., & Hu, J. (2020). Stability of a delayed competitive model with saturation effect and interval biological parameters. *Journal of Applied Mathematics and Computing, 64*(1), 1–15. https://doi.org/10.1007/s12190-020-01341-8
13. Makridakis, S., Spiliotis, E., & Assimakopoulos, V. (2018). Statistical and machine learning forecasting methods: Concerns and ways forward. *PLoS ONE, 13*(3), e0194889. https://doi.org/10.1371/journal.pone.0194889
14. Brownlee, J. (2018) Comparing classical and machine learning algorithms for time series forecasting. *Machine Learning Mastery*, October 30, 2018. https://machinelearningmastery.com/findings-comparing-classical-and-machine-learning-methods-for-time-series-forecasting/. Accessed July 09, 2021.
15. Abraham, J., Higdon, D., Nelson, J., & Ibarra, J. (2018). Cryptocurrency price prediction using tweet volumes and sentiment analysis. *1*(3), 22.
16. Yenidoğan, I., Çayir, A., Kozan, O., Dağ, T., & Arslan, Ç. (2018). Bitcoin forecasting using ARIMA and PROPHET. in *2018 3rd International conference on computer science and engineering (UBMK)*, September 2018, pp. 621–624. https://doi.org/10.1109/UBMK.2018.8566476
17. Chevallier, J., Guégan, D., & Goutte, S. (2021). Is it possible to forecast the price of bitcoin? *Forecasting*, *3*(2), Art. no. 2, June 2021. https://doi.org/10.3390/forecast3020024
18. Bambrough, B. (2020). As the bitcoin price soars, bitcoin's 'real' crypto market dominance is revealed. *Forbes*. https://www.forbes.com/sites/billybambrough/2020/07/30/as-the-bitcoin-price-soars-bitcoins-real-crypto-market-dominance-is-revealed/. Accessed June 27, 2021.
19. Chambers, C. (2020). 'Bitcoin and stocks' correlation reveal a secret. *Forbes*. https://www.forbes.com/sites/investor/2020/05/13/bitcoin-and-stocks-correlation-reveal-a-secret/. Accessed July 23, 2021.
20. Kim, J.-M., Kim, S.-T., & Kim, S. (2020). On the relationship of cryptocurrency price with US stock and gold price using copula models. *Mathematics*, *8*(11), Art. no. 11, November 2020. https://doi.org/10.3390/math8111859
21. Thaker, H.M.T., & Mand, A.A. (2021) Bitcoin and stock markets: A revisit of relationship. *Journal of Derivatives and Quantitative Studies:* 선물연구, *29*(3), 234–256, January 2021. https://doi.org/10.1108/JDQS-07-2020-0016
22. Akaike, H. (1998) Information theory and an extension of the maximum likelihood principle. In E. Parzen, K. Tanabe, & G. Kitagawa, (Eds.) ,*Selected papers of Hirotugu Akaike* (pp. 199–213). Springer. https://doi.org/10.1007/978-1-4612-1694-0_15
23. Schwarz, G. (1978). Estimating the dimension of a model. *Annals of Statistics, 6*(2), 461–464. https://doi.org/10.1214/aos/1176344136
24. Hiransha, M., Gopalakrishnan, E.A., Menon, V.K., & Soman, K.P. (2018). NSE stock market prediction using deep-learning models. *Procedia Computer Science, 132*, pp1351–1362, January 2018. https://doi.org/10.1016/j.procs.2018.05.050
25. Varghese, A., Tarhen, H., Shaikh, A., Banik, P., & Ramdasi, A. (2016) Stock market prediction using time series. *International Journal on Recent and Innovation Trends in Computing and Communication*, *4*, 427–430, May 2016. ISSN 2321-8169
26. Spilak, B. (2018). Deep neural networks for cryptocurrencies price prediction, p. 73.
27. Shih, K.-H., Cheng, C.-C., & Wang, Y.-H. (2011). Financial information fraud risk warning for manufacturing industry—using logistic regression and neural network. *Romanian Journal of Economic Forecasting* , 18.
28. Troncoso Lora, A., Riquelme, J.C., Martínez Ramos, J.L., Riquelme Santos, J.M., & Gómez Expósito, A. (2003) Influence of kNN-based load forecasting errors on optimal energy production. In *Progress in artificial intelligence*, Berlin, Heidelberg, pp. 189–203. https://doi.org/10.1007/978-3-540-24580-3_26
29. Vega, E., Flores, J., & Graff, M. (2014) k-nearest-neighbor by differential evolution for time series forecasting, November 2014, pp. 50–60. https://doi.org/10.1007/978-3-319-13650-9_5
30. Sarfarz, A. (2017). Why smart contracts in blockchain need to avoid non-deterministic functions—DZone security. *dzone.com*. https://dzone.com/articles/why-smart-contracts-in-blockchain-needs-to-avoid-n. Accessed July 22, 2021.

31. Mironiuc, M., & Robu, M.-A. (2013). Obtaining a practical model for estimating stock performance on an emerging market using logistic regression analysis. *Procedia—Social and Behavioral Sciences, 81*, 422–427. https://doi.org/10.1016/j.sbspro.2013.06.454
32. Ariyo, A.A., Adewumi, A.O., & Ayo, C.K. (2014) Stock price prediction using the ARIMA model. In *2014 UKSim-AMSS 16th international conference on computer modelling and simulation*, Cambridge, United Kingdom, March 2014, pp. 106–112. https://doi.org/10.1109/UKSim.2014.67
33. Alahmari, S. (2019) Using machine learning ARIMA to predict the price of cryptocurrencies, July 2019.
34. Desev, K., Kabaivanov, S., & Desevn, D. (2019) Forecasting cryptocurrency markets through the use of time series models. *The Business and Economic Horizons (BEH)*, *15*(2). Accessed: July 22, 2021. https://ideas.repec.org/a/ags/pdcbeh/301145.html
35. Umadevi, B., Sundar, D., & Alli, P. (2013) An effective time series analysis for stock trend prediction using ARIMA model for nifty midcap-50. *Undefined*. Accessed: May 28, 2021. [Online]. Available: /paper/An-Effective-Time-Series-Analysis-for-Stock-Trend-Umadevi-Sundar/356879c2fc72465f5885315a16102975c6716226
36. Christy Jackson, J., Prassanna, J., Quadir, M.A., & Sivakumar, V. (2021). Stock market analysis and prediction using time series analysis. *Material Today Proceedings*, January 2021. https://doi.org/10.1016/j.matpr.2020.11.364
37. Ayaz, Z., Fiaidhi, J., Sabah, A., & Ansari, M. (2020). Bitcoin price prediction using ARIMA model. https://doi.org/10.36227/techrxiv.12098067
38. Peng, J., Lee, K., & Ingersoll, G. (2002). An introduction to logistic regression analysis and reporting. *The Journal of Educational Research, 96*, 3–14. https://doi.org/10.1080/00220670209598786
39. Kabria. Logistic regression for machine learning and classification. *Kambria*, July 09, 2019. https://kambria.io/blog/logistic-regression-for-machine-learning/. Accessed October 12, 2021.
40. M'ng, J.C.P., & Zainudin, R. (2016) Assessing the efficacy of adjustable moving averages using ASEAN-5 currencies. *PLOS ONE, 11*(8), e0160931, August 2016. https://doi.org/10.1371/journal.pone.0160931
41. Zielak. Bitcoin historical data, March 2021. https://kaggle.com/mczielinski/bitcoin-historical-data. Accessed October 17, 2020.
42. Watkins, T. (2021). How the use of moving averages can create the appearance of confirmation of theories where none exists. https://www.sjsu.edu/faculty/watkins/movingaveraging.htm. Accessed February 24, 2021.
43. Nau, R. (2020). Stationarity and differencing of time series data. https://people.duke.edu/~rnau/411diff.htm. Accessed November 7, 2020.
44. Hyndman, R. J., & Khandakar, Y. (2008). Automatic time series forecasting: The forecast package for R. *Journal of Statistical Software, 27*, 1–22. https://doi.org/10.18637/jss.v027.i03
45. Inan, S. (2018). Are cryptocurrency price changes predictable. *Northeastern University*. https://doi.org/10.17760/D20289522

Chapter 10
Research on the Integration of Market Supervision Big Data from the Perspective of Life Cycle—Take the Jiangsu Provincial Market Supervision Bureau as an Example

Ying Liu, Shan Li, and Wendi Pang

Abstract In order to meet the reform and development of state market regulation, it is of great significance that market regulation data must be deeply integrated to create the underlying data support of 'Internet + Regulation', which is supposed to make full use of modern information technologies such as big data, artificial intelligence for supervision. This paper sorts out the current situation of market supervision data management in Jiangsu Province, China, and clarifies the challenges it faces. Based on the perspective of the whole life cycle, the paper puts forward five interrelated and continuous iterative stages of data collection, data processing, data storage, data integration, and data sharing, at the same time, based on the knowledge graph technology, all the information related to the enterprise is mined and the knowledge graph of the food industry is drawn.

Keywords Market regulation · Data · Life cycle perspective · Integration

Introduction

Currently, with the explosive growth of social information, the number of market players and the activity of the market environment is growing rapidly and explosively. The huge amount of big data with scattered sources and various formats poses new challenges to the government's service and supervision capabilities, and at the same time, it also brings new challenges [1]. Premier Li Keqiang especially emphasized that it is necessary to strengthen the construction of market supervision informatization and promote the application of supervision big data, which to effectively realize 'Internet + supervision', improve innovative services for market supervision

Y. Liu (✉) · S. Li
School of Economics and Management, Nanjing University of Aeronautics and Astronautics, Nanjing, Jiangsu, China
e-mail: Liuying66@nuaa.edu.cn

W. Pang
Administration for Industry and Commerce Information Center, Nanjing, Jiangsu, China

R. Qiu et al. (eds.), *City, Society, and Digital Transformation*, Lecture Notes in Operations Research, https://doi.org/10.1007/978-3-031-15644-1_10

and reduce government costs, when he inspected the State Administration of Market Supervision. All requirements are inseparable from the integration of high-quality market supervision data [2]. The Jiangsu Provincial Market Supervision Bureau has many businesses and various data sources, forming a multi-source and heterogeneous market supervision big data, which cannot meet the 'Internet + supervision' service innovation requirements proposed by the national and provincial governments for market supervision. Therefore, it is necessary to carry out exploratory research on the key technologies of big data sharing and integration, so as to better provide data support for service innovation. However, there are few empirical studies on the integration of big data in market supervision, especially the lack of empirical studies based on a holistic perspective. Based on the perspective of the whole life cycle, this paper takes the integration of market supervision data in Jiangsu Province as an example, which analyzes the general situation and challenges of market supervision data management in Jiangsu Province, and tries to explore the path on the integration of market supervision data.

Current Situation and Challenges of Market Supervision Data Management in Jiangsu Province

The Current Situation of Data Management

With the help of Jiangsu Market Supervision Bureau, this paper conducted a survey on the status quo of data management in Jiangsu Market Supervision Bureau, including 38 units in total, including 26 departments of business department, five major institutes (textile inspection Institute, Special inspection Institute, Quality Inspection Institute, Quality standards Institute, Metrology Institute), intellectual Property Office, Drug Administration bureau and local Municipal Bureau. Through investigation, this paper found that the business systems currently used by various departments of Jiangsu market supervision bureau are shown in Fig. 10.1.

The impact and challenges brought by the digital time to government data governance are all-round [3]. Through the investigation, this paper found that there are thirty-eight units in the Market Supervision Bureau of Jiangsu Provincial, including twenty-six departments, five major institutes (Textile Inspection Institute, Special Inspection Institute, Quality Inspection Institute, Quality Standard Institute, Metrology Institute), Intellectual Property Office, Drug Administration. Among this, there are a total of forty-two business systems in use, which are divided into 10 business type system categories. The classification is shown in Fig. 10.1. According to the source of data, the data is roughly divided into that of the former Administration for Industry and Commerce, the former Drug Administration and the former Intellectual Property Office. What is found that: (1) The former Administration for Industry and Commerce has built an integrated data warehouse, which includes seven categories:

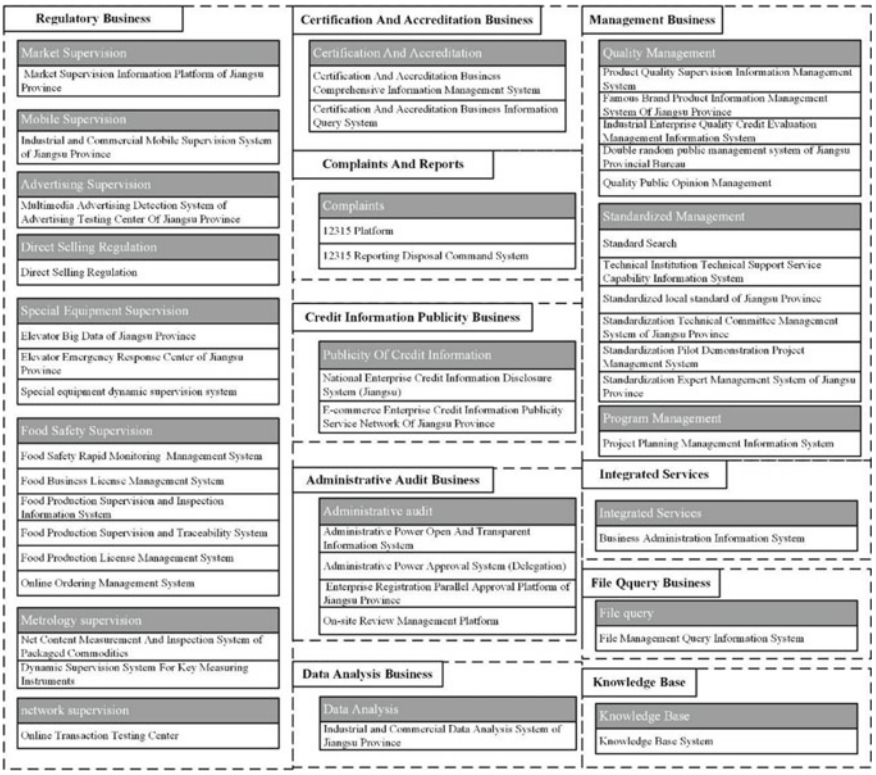

Fig. 10.1 The classification of business system

comprehensive business, market supervision, complaints, credit information, enterprise registration and approval, food production and operation licenses, and chattel mortgages. The storage capacity is about 3.79 T, and a total of 723 kinds of data are generated by 7 systems, whose update cycle is one day. (2) The former Drug Administration has built a unified integrated platform for food and drug administration and a big data center for food and drug supervision. It includes 7 categories, in which is public information, administrative licensing, supervision and inspection, inspection and testing, risk analysis, electronic traceability, and credit management. There are enterprise information, product information, food, medicine, health food, etc., and the data storage capacity is about 470 G. (4) The data resources of the former Intellectual Property Office include two categories of patents and trademarks. The patent data comes from 103 countries around the world, with a total of more than 140 million pieces, which includes case types, applicants and other data. The storage capacity is about 50 TB, and the update cycle is one day.

The Challenges of Data Management

In accordance with the general requirements of the State Council to improve the new market supervision mechanism, in the process of realizing the data integration of the market supervision, the province's market supervision work has the following problems: (1) The data resources involved in various regulatory departments are complex. Firstly, the total amount of data is huge, which is 60 TB and update extremely fast. Secondly, the sources are diverse, which comes from 38 units, and involved in various regulatory departments. Thirdly, there are various formats of data, including structured data, semi-structured data and unstructured data. Therefore, it is difficult to collect data, which makes it impossible to promote data governance in an orderly manner. (2) The original independent operation information platform of each regulatory department has problems such as complicated handling system, different item standards, overlapping system functions, poor data sharing, and insufficient business coordination, which can no longer satisfy the requirements of actively promote the 'Internet + market supervision'. (3) Various real-time data are generated by supervision department in the process of market supervision and provision of services. This type of data comes from a wide range of sources and is constantly updated. There is a lack of a good mechanism of the data integration, resulting in the inability of cross-departmental and cross-regional data sharing and exchange means. It is impossible to provide the support services of data integration for market supervision departments at all levels, so as not to realize data-driven business innovation.

Based on the above problems, this paper attempts to explore the path of data integration of market supervision in Jiangsu Province from the perspective of the whole life cycle.

The Integration of Market Supervision Big Data from the Perspective of Life Cycle

The data management of the big data integration and sharing [4] of market supervision from the perspective of life cycle is divided into five interrelated and continuous iterative stages, what is data collection [5], data processing, data storage, data integration [6] and data sharing [7, 8], as shown in Fig. 10.2.

First of all, data collection is the initial stage of market supervision data integration and sharing. Market supervision departments generate a large amount of data in their daily business, and the quality, content and accuracy of these data need to be strictly screened, that as a reserve resource for market supervision data opening. Secondly, in the data processing stage, according to certain standards, the data categories, metadata elements, data formats, etc. are standardized and organized, after that it enter the data storage stage. Thirdly, what is called data storage is to store the governed data into the basic database, thematic database or thematic database. Meanwhile, data integration is the core link of data life cycle governance. Through

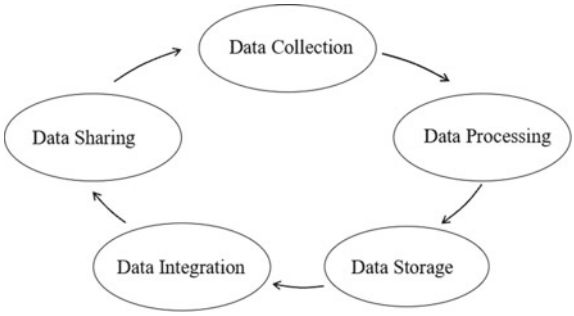

Fig. 10.2 The cycle of data lifecycle governance

the integration of market supervision structured data and unstructured data, the data resource system can achieve less redundancy, high data independence and multi-service adaptability. Last but not least, data sharing is the most critical step in the integration and sharing of market supervision data. Through a specific technical platform, the data resources are released on the market supervision integrated information platform, enabling various market supervision departments, social groups, enterprises, scientific research institutions, stakeholders such as the public can make full use of the sharing platform to obtain household resources, and generate political, economic and cultural value in public participation, scientific decision-making, product innovation, social cooperation and other aspects. In this process, new data resources will be collected, after that it enter the next full life cycle governance cycle of market supervision data.

Data Collection

The collection of massive data is the basic work of data processing [9], and a large amount of data resources are generated in the daily affairs of relevant departments of market supervision, including a large amount of business data, department data, and internet data. Among them, business data refers to the established and new business system databases, which mainly include 10 categories such as market supervision, certification and accreditation, complaints and reports, and criminal investigation and inspection. Departmental data refers to the market supervision departments at all levels in Jiangsu Province, such as the Provincial Food and Drug Administration, the Provincial Intellectual Property Office, the five major academies and other directly affiliated units, as well as the data of relevant provincial government departments. Internet data refers to data sources including website and network data, such as WeChat data, and Weibo data.

How to collect multi-source heterogeneous data is the basic work of market supervision big data integration and sharing. The systems of the former Administration for Industry and Commerce, the former Drug Administration and the former Intellectual Property Office have many and scattered data resources, and the total amount of data

is about 20 TB, including structured data and unstructured data, as well as that do not have corresponding business systems to process such data., which makes the data unable to share fusion processing.

What is used to research the collection and integration technology of multi-source heterogeneous market supervision data is data merger, which is to realize the integration of structured and unstructured data to ensure high data concentration. At the same time, multi-source data merger also supports the collection of data from provincial bureau systems, provincial departmental systems and the Internet into the merger database of the big data center; the data in the merger database is cleaned, converted, standardized, and desensitized before being stored into the basic database and subject database to facilitate application analysis and processing. The methods of data merger supported that structured data collection, unstructured data collection, streaming data collection, real-time data collection and crawler collection.

Data Processing

For the processing of big data in market supervision, it is necessary to proceed from a specific business perspective on the basis of careful research on the data. This link takes the preprocessing of health-care food data and the corresponding enterprise data of health-care food as an example, as shown in Fig. 10.3.

(1) General Data Standardization: What we are supposed to define what data will be used, how it will be formatted and stored, and d basic considerations for each subsequent step. The key fields required are defined according to business requirements, all of which are meaningful data fields; formatting and storage need to meet the requirements of various quality rules, scripts, and business code standard libraries in the data governance system. It mainly standardizes unstructured data, including ordinary text files, JavaScript files, CSS files, and non-text binary text such as pictures, music, and videos.

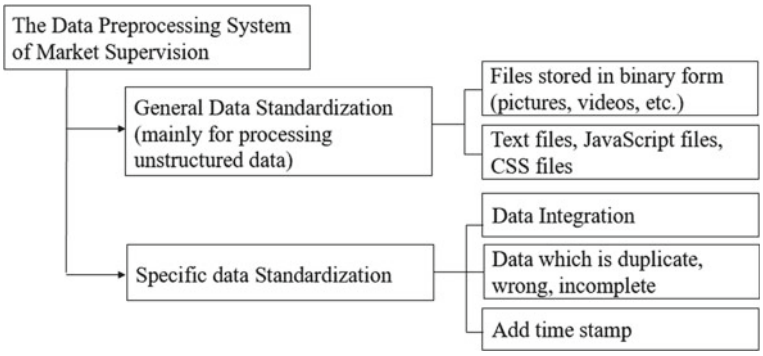

Fig. 10.3 The core process of data preprocessing

(2) Duplicate and redundant data handling: Report duplicate data to data stewards, and remove or discard redundant data. For example, there are currently 8729 pieces of data in the new table of food production license-variety details-new table, with no duplicate ID data, but there are many missing data, such as the lack of 'contractor name WTSMC' and 'contractor address WTSDZ'. At the same time, there are data with meaningless characters in the data table. For example, a data item with a question mark appears in the "Variety Details PZMX" field, which is similar to 'Ailewei?', 'Multivitamin and Mineral Tablets', on account of that meaningless characters are generally replaced by blank characters.
(3) Validation: Run automated checks to compare similar information, such as event time and access records (usually a timestamp field, which is automatically added in every form), further modify unavailable data, and as far as possible in the system, Anomalies are flagged in the application or data.

Data Storage

The integration and sharing of big data in market supervision involves multi-party business, and it needs enough space to support the storage of massive data, on which basis, it is as well as supposed to support a large number of terminal servers to access online at the same time. Meanwhile, it is necessary to solve the calculation and processing of massive data under large number of users and multiple servers. After that is to ensure that the temporary problems of a single link or a single interface will not affect the development of other business processes.

In view of the complex business scope in the market supervision field and the rapidly growing of the big data volume, this paper proposes the distributed big data technology, which is to realize distributed data storage and computing. The framework is shown in Fig. 10.4, which is constructed for complex market supervision data analysis. It has multiple distributed data computing nodes, which is more suitable for multi-dimensional expression of data in the field of market supervision. Hadoop [10], the mainstream distributed system architecture developed by the Apache Foundation, has two core sub-frameworks-HDFS and MapReduce [11], which can be used to solve the difficulties of market supervision of big data mass storage and high-speed computing respectively. The ETL distributed processing framework based on the Hadoop big data processing platform uses the scalable characteristics of the underlying HDFS of the framework to dynamically adjust the performance of the ETL. Its design concept is based on the parallel processing model of the MapReduce framework, and through the distributed advantages of Hadoop in batch processing, which can greatly improve the processing speed.

In the integration and sharing of big data in market supervision, various methods of data exchange and extraction are usually realized by means of traditional data extraction and mapping methods, that is, two isomorphic data tables are created to realize the mapping between the target table and the original table without affecting the to

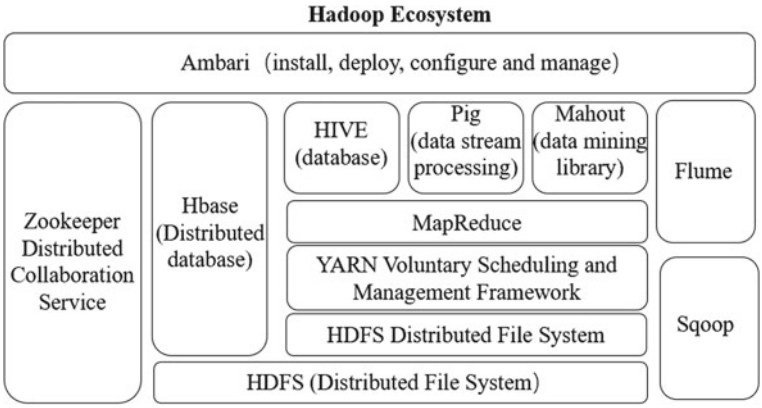

Fig. 10.4 Big data storage and computing Hadoop framework

the table structure. However, for a system with a larger amount of data, data collection usually comes from different business departments and different data collection standards. Market supervision involves 42 business systems and nearly a thousand data resource sheets, which can be understood as a distribution in a sense. The data mapping and reduction (MapReduce) function table can effectively summarize a lot of messy data (tables) according to a certain characteristic, and use the storage data mart data model to replace the storage data mart data. After the MapReduce summary processing for resource data, the specific processing of each structural element in the data table is completed, and the associated mapping of related data forms is realized. For the maintenance and future expansion of the relevant data in the system, it is only need to record the newly added data, and at the same time import the metadata information of the corresponding data record into the data name table to achieve expansion, protect the original data content and the efficiency of system data service has been greatly improved.

Data Integration

The integration of market supervision big data faces challenges such as heterogeneity, semantic transformation, integration performance, integrity, etc. The relationship between different subjects and objects in the market is complex and the needs are changeable, and it is difficult to carefully describe and dig it in the traditional structured data organization model. In view of the above problems, as an emerging form of data transformation and massive knowledge representation, knowledge graph can express higher entity and concept coverage, richer semantic relationship between data, and higher degree of automatic construction. There are significant advantages in terms of high data quality and faster instant response.

Since the entire market supervision system is relatively large and the knowledge system has a huge amount of work to sort out the knowledge system, this paper focuses on health-care food. By analyzing the business data related to health-care food and the relationship between businesses, it explores key technologies for market supervision data integration. Based on the metadata integration of the former Administration for Industry and Commerce, the former Drug Administration and the former Intellectual Property Office, the E-R diagram of the underlying data integration example of market supervision as shown in Fig. 10.5 is constructed. The ER diagram is centered on the 'Enterprise Master Table', and each table is integrated through metadata. The metadata is the attribute of the table, such as 'Unified Social Credit Code\Registration Number', 'Enterprise Name' in the 'Enterprise Owner Table', 'Enterprise domicile', 'Enterprise type', 'Business scope', etc. The first is to screen the health-care food enterprises by the category name in the 'Food Production License, Variety List', and associate it with the 'Food Production License Information Table' through the 'SPSPTJJLB' field, which is as well as associated with the 'Enterprise Owner Form' through the 'Unified Social Credit Code', and at the same time, it can be associated with the 'Main Form for Daily Supervision and Inspection of Food Production and Operation' through the 'License Number'. Moreover, the 'Main Form for Daily Supervision and Inspection of Food Production and Operation' can be associated with the 'Enterprise Owner Form' through the 'Unified Social Credit Code'. Similarly, the 'Inspection Announcement', 'Double Random Spot Check Results', 'Administrative Licensing Information Form', and 'Administrative Punishment Information Form' can all be associated with the 'Enterprise Owner Form' through the 'Unified Social Credit Code'. The 'Measurement and Sampling Inspection Information Form', 'Product Quality State Supervision and Sampling Inspection Result Form', and 'Patent Information Form' are all related to the 'Enterprise Owner Form' through the 'enterprise name'.

This paper extracts five entities, 'enterprise', 'food category', 'registration agency', 'patent' and 'license document', the attributes of each entity and the relationship between entities, and constructs a knowledge graph related to health-care food, such as shown in Fig. 10.6, in that the entity in purple is 'Enterprise', the entity in blue is 'Food Category', the entity in yellow is 'Registration Agency', the entity in pink is 'License Document', and the entity in green is 'Patent'. Afterwards, arrows indicate the relationship between entities, for example, 'Administrative Examination and Approval Bureau of Nanjing Jiangbei New Area Management Committee' is the registration agency of 'Nanjing Taoyuan Applied Biotechnology Co., LTD'.

Data Sharing

It is difficult to share data between provinces, cities and departments, mainly because data is voluntarily and scattered in various market supervision departments, and it is impossible to realize the interconnection and interoperability of data, thus forming 'data islands' and hindering the realization of data sharing [12]. According to the

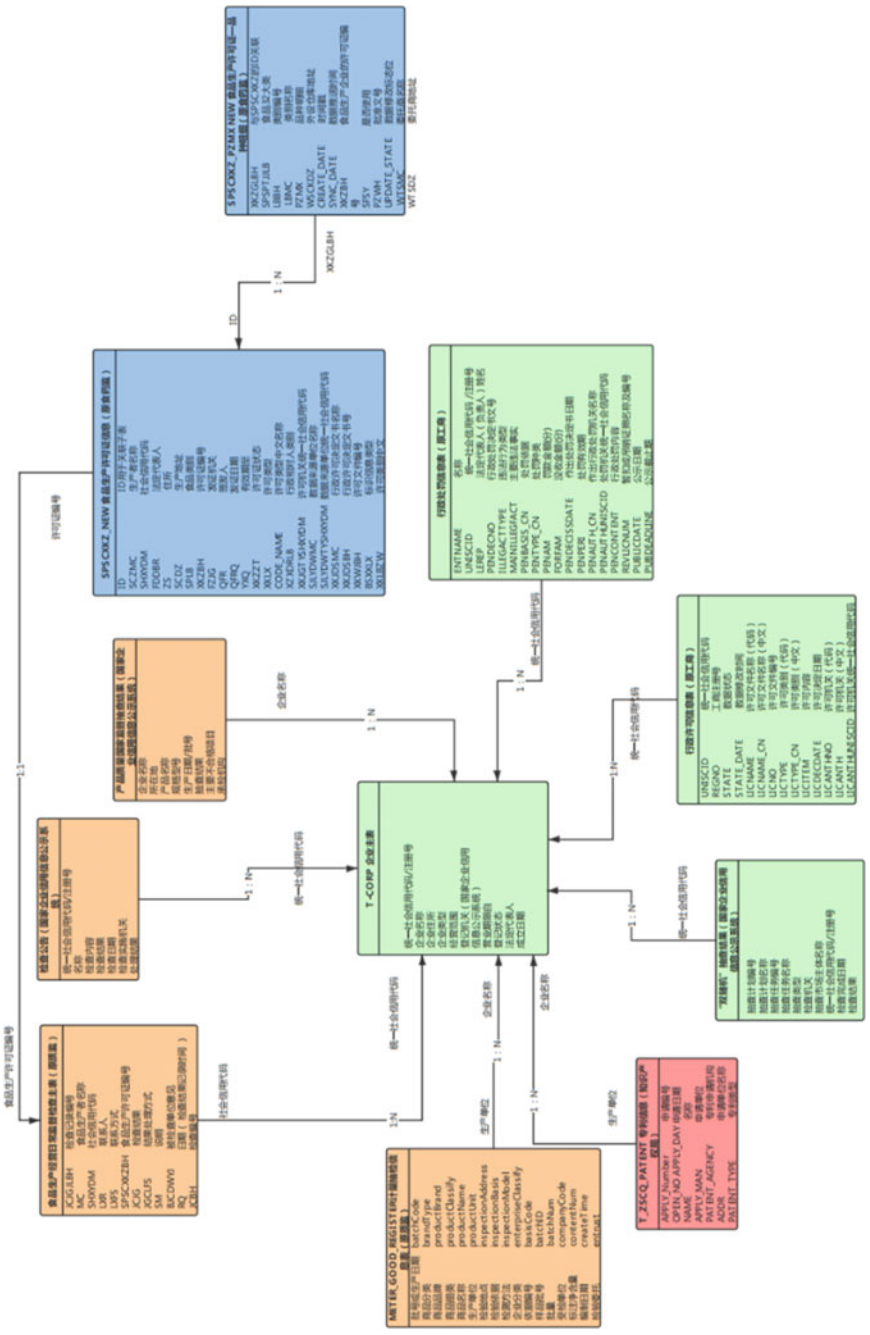

Fig. 10.5 E–R diagram of an example of market supervision underlying data fusion

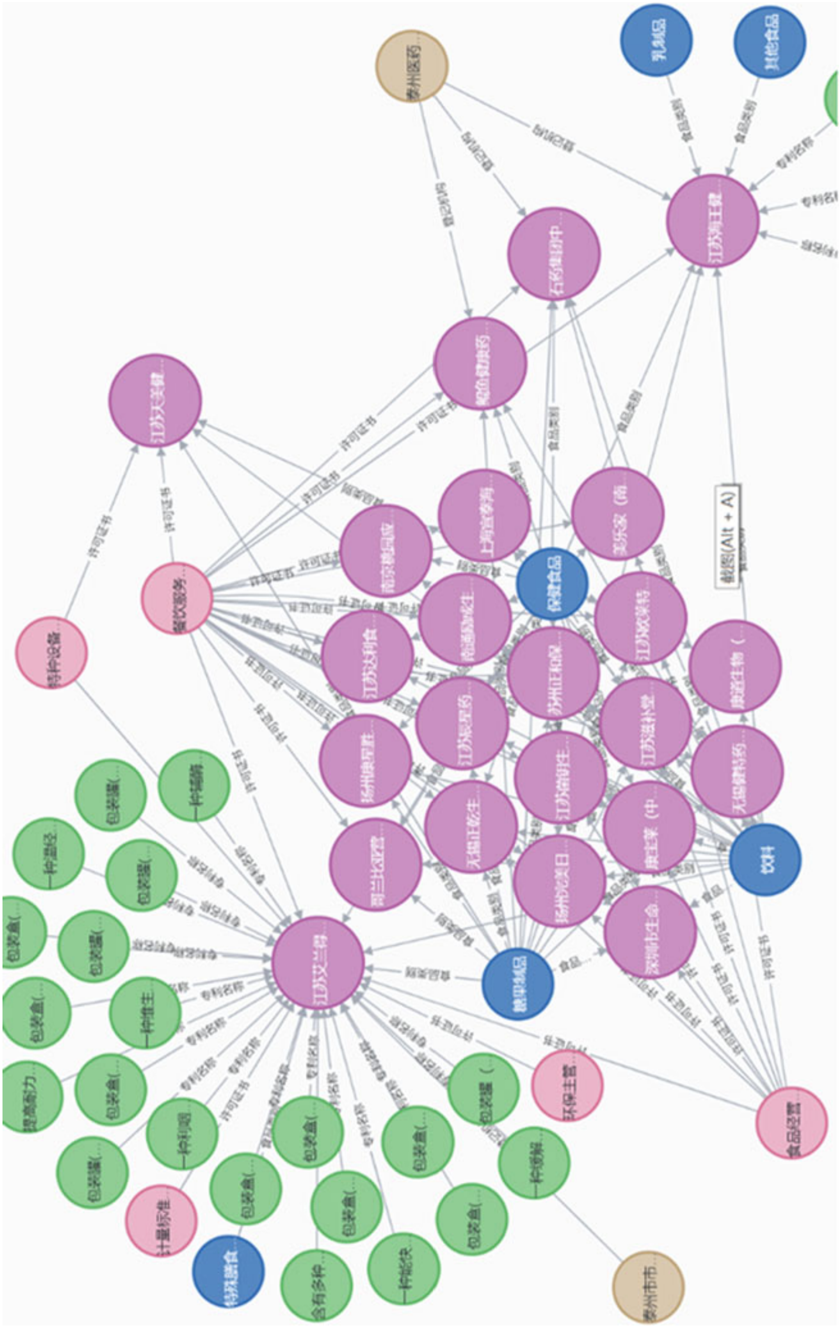

Fig. 10.6 Partial knowledge map of market supervision

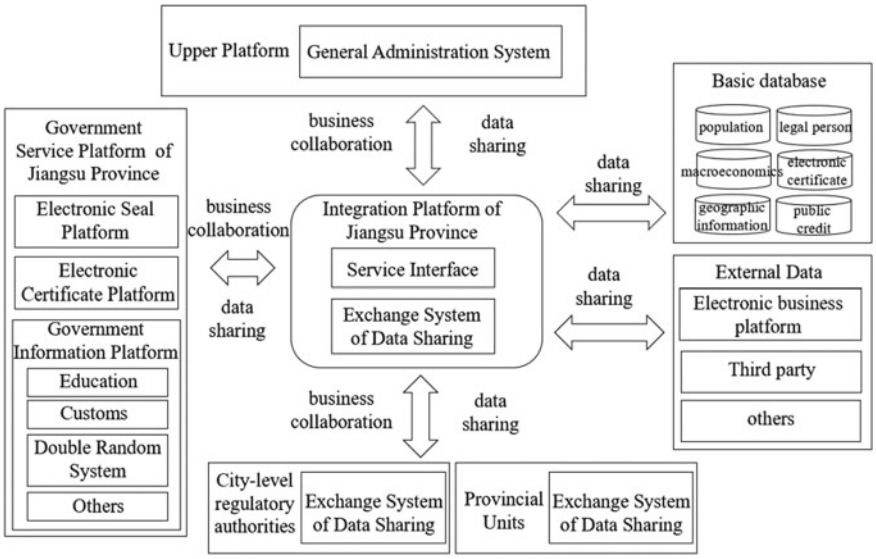

Fig. 10.7 Schematic diagram of the exchange process of market supervision data

problems of data transmission, data storage, data security and multi-source heterogeneity of data involved in the process of data sharing and exchange, streaming data technology can be used to solve the problem of real-time data's acquisition and calculation, which be able to improve the efficiency of data transmission.

The data exchange process of Jiangsu Provincial Market Supervision Bureau is complex, so it needs to use the Jiangsu Provincial Parallel Approval Platform to realize the data sharing with the superior platform, the provincial government service platform, the basic database of the provincial big data center, the prefectural and municipal supervision departments, external data, the provincial directly affiliated units and other departments, as shown in Fig. 10.7.

(1) Data sharing with market supervision business lines: Jiangsu Provincial Market Supervision Bureau has its own business characteristics and development characteristics, which must plan and construct core business and related technical standards, data standards and security standards in a unified manner. According to the list of data catalogues, it should complete real-time business information exchange and regular data aggregation and distribution with the credit platform of the State Administration for Market Regulation, double publicity, and members of the Food Safety Committee. The bureau and the five major academies are interconnected by dedicated lines to realize two-way interaction of various data, and that should realize real-time business information exchange and timed data aggregation and distribution between prefecture and provincial bureaus, though that it provide basic data queries for cities, districts and counties.

(2) Data sharing with provincial departments: It is of great significance to realize the connection with the Jiangsu Provincial Government Service Network, the business system of public services, the unified user platform, and the electronic seal system. Using the government service APP, WeChat applet, Alipay applet, WeChat official account and other mobile terminals, what is connected with the mobile terminal of the government service network, which is to realize the Internet application and information release of the Provincial Market Supervision Bureau. According connecting with the provincial electronic license system, it is workable to share the electronic business license (public version) and face-to-face information with the provincial electronic license library, obtain the corresponding electronic license data and documents of other departments, and the electronic license data in the enterprise information display, and push the electronic license data. Docking with social security, public security and other departmental systems, is to realize the comparison and verification of personnel social security, face identity and other information.
(3) Data sharing with the provincial big data center: Using the infrastructure and public support services of the provincial big data center, which as the disaster recovery center of the provincial bureau market supervision data integration sharing verification system, what is to realize the connection with the provincial big data center, and realize data sharing with the basic database of the provincial big data center, including Population, legal person, electronic certificate, macro economy, etc.
(4) Data sharing with enterprises, technical institutions and third-party platforms: It is important to realize the connection with external systems such as enterprises, third-party testing agencies, and e-commerce platforms, and obtain data related to quality and safety, complaints and reports.

Summary and Outlook

This paper summarizes the data management overview and challenges faced by the Jiangsu Provincial Market Supervision Bureau, mainly due to the huge amount of data resources involved in various regulatory departments, scattered sources and diverse formats, different information platform standards, and lack of good data integration and sharing mechanism. Therefore, from the perspective of the whole life cycle, this paper proposes five interrelated and continuous iterative stages of data collection, data processing, data storage, data integration, and data sharing, forming a closed-loop data governance of the whole life cycle. Due to time constraints, this paper can only conduct data integration research on small fields such as health-care food production as an example. In the future, the scope of the field will be expanded, and more in-depth research will be done in the field of market supervision big data integration and sharing.

References

1. General Office of the State Council. Several opinions on using big data to strengthen the service and supervision of market players (EB/OL) (2015–07–01).
2. Chen, Z., Xuzhou, C., Li, Q., Weifeng, L.V., & Zhang, X. (2014). A new smart city data sharing and fusion framework——SCLDF. *Computer Research and Development, 51*(2), 290–301.
3. Zhou, L., & Lin, T. (2021). Research on Optimization of government data governance system based on file continuum theory. (4), 114–124.
4. Zhang, S., Pan, R., & Zong, Y. (2016). *Big data governance and services.* Shanghai Science and Technology Press.
5. Di Hongyang, R.S. (2017). Research on data management and utilization of government data disclosure network platform. *Library Magazine, 36*(1), 88–96.
6. Gao, X., & Wang, Y. (2002). Overview of data fusion technology. *Computer Measurement and Control, 10*(11), 706–709.
7. China Academy of information and communication Big data white paper (2018) (EB/OL) (2018–06–10).
8. Huang, J., & Zhou, R. (2019) Research on the construction of government data governance framework based on information lifecycle management theory. *E-government,* (09), 85–95.
9. Ma, G., & An, X., Song, Y. (2018). Business driven government big data platform data governance. *Intelligence Data Work,* (01), 21–27.
10. Barroso, L.A., & Holzle, U. (2007) The case for energy-proportional computing. *Computer, 40*(12), 33–37.
11. Dean, J., & Ghemawat, S. (2008). MapReduce: Simplified data processing on large clusters. *Communications of the ACM*, *51*(1), 107–113.
12. Liu, X., Huang, H., Zhang, X., et al. (2016). Data opening, sharing and utilization in smart city construction. E-government (3), 35–42.

Chapter 11
Group-Level Human Affect Recognition with Multiple Graph Kernel Fusion

Xiaohua Huang

Abstract Research on group-level affect recognition has become emerging for predicting human behavior in a group. Due to the variability in group size, a critical issue should be addressed. That is, how to efficiently and effectively describe the affect similarity of two group-level images. To tackle this problem, this paper makes two-fold contributions: (1) similarity measurement of group affect based on graph kernel; (2) incorporation of multiple kernels and deep learning architecture to contribute to recognizing group-level affect. In this paper, we view a group as a graph. Thus, we first formulated the graph of the group, and then build the kernel between any two graphs. Its advantage is to efficiently use any kernel classifier. To further exploit the advantages of multiple kernels, we used two feature descriptors to extract the face features. Subsequently, we proposed straightforwardly using deep multiple kernel learning with three-layer. To resolve non-differential problem, we presented the graph kernel as the input of four kinds of base kernels and learned their corresponding weights. Intensive experiments are performed on a challenging group-level affective database. Performance comparisons considerably demonstrate the advantages of graph kernel and deep multiple kernel learning. Additionally, our proposed approach obtains promising performance for group-level affect recognition compared with the recent state-of-the-art methods.

Keywords Group affect · Graph · Multiple kernel learning · Deep learning · Feature fusion

Introduction

With more pictures being posted every day on social media sites such as Wechat and Instagram, large-scale images enable us to study human behavior through different

X. Huang (✉)
School of Computer Engineering, Nanjing Institute of Technology, Nanjing 211167, Jiangsu, China
e-mail: Xiaohua.huang@njit.edu.cn

Jiangsu Province Engineering Research Center, Nanjing 211167, Jiangsu, China

R. Qiu et al. (eds.), *City, Society, and Digital Transformation*, Lecture Notes in Operations Research, https://doi.org/10.1007/978-3-031-15644-1_11

techniques, such as facial expression recognition [1]. Early studies were conducted for analysing the affect of an individual person. With the success of affect/emotion recognition, several techniques have been spread to other fields including cognitive science, such as computer-assisted social skills training systems [2]. In the last decade, understanding the behavior of groups in an image has recently garnered increasing attention. It focuses on estimating the emotion of a group of people. In contrast to affect recognition of an individual person, group-level affect/emotion recognition becomes more difficult, because one needs to address several challenging problems. For example, in our real-life scenarios, how can we analyze children's affect from a photo when they play in a park? How can we predict the emotions of friends from a photo that was taken while they were drinking in the bar? The backgrounds of the two images might be starkly different from each other. In addition, analyzing the affect of a group may promote the work environment in a work team or a company. During the past century, researchers in social science have studied the structure and performance of small groups [3–5] according to the notable theorem 'group emotion'. They found that affects influence team processes and outcomes [6]. For instance, the study in [7] found that an increase in positive mood results in greater cooperativeness and less group conflict. Therefore, this paper focuses on analyzing the basic affects exhibited by a group of people in an image, namely, group-level affect.

According to group emotion theory proposed by Barsade and Gibson [4], the designed methods are generally separated into bottom-up and top-down categories. The bottom-up methods utilize the individual's attributes to infer group affect, while the top-down approach describes group affect by using some context information including the affect of the scene and the position of the people. For example, for the bottom-up category, in [8], the smile of each person is used to infer the affect of the crowd. For the top-down approach, in [9], contextual features are designed based on the group structure to compute the age and gender of individuals. In [10], a computer vison system using social context was designed for photo albums to select the best photos for a family.

In addition to the abovementioned sole approach, previous methods have investigated hybrid models to effectively fuse bottom-up and top-down approaches. For example, in [11], Huang et al. proposed using global attributes as the top-down component and local attributes such as an individual's feature as the bottom-up component. It concerns the method of modeling global and local social attributes, such as facial attributes. An alternative method, i.e., a multimodal framework, aimed at combining the bottom-up and top-down context features of images. In [1], for the bottom-up component, the facial action unit and facial features are considered, while for the top-down component, scene features are used. To use multiple features, a feature encoding method was proposed to construct the vocabulary and represent each image as a frequency histogram of vocabulary. In [12], the Xception architecture is used to fuse image context and facial features to predict group-level affect. In [13], face and body information are fused to predict the valence and arousal of a group of people. However, previous works lacked adaptation to varied tasks. For

example, in [11], limited by continuous conditional random fields, a group expression model cannot classify emotion categories since it was originally designed to address the problem of group-level happiness intensity. In [14], the multimodal framework proposed by Huang et al. has three adjustable parameters, including the dimensionality of PCA, the number of kernels, and the number of face blocks. This results in the parameters not being adaptive to different applications because for each database, their parameters are different. Although recent methods have focused on deep learning architectures, such as [12, 15, 16], one needs to carefully design a suitable end-to-end framework.

To alleviate the abovementioned issue, Huang et al. [17] considered formulating the distance metric for calculating the distance between images. Motivated by Cuturi et al. [18], they proposed a global alignment kernel-based method to directly measure the distance between two images. They first regarded the faces in an image as a set. Next, they used the global alignment kernel to measure the distance between two sets. In contrast to group expression models and feature encoding, they primarily focused on how to formulate the kernel function such that it would be generalized to the application of any classifier, such as a support vector machine.

The **key contributions** of this paper are described as follows: (1) a graph kernel is presented to formulate the similarity between two images, and it is easily embedded into a support vector machine for group-level affect prediction; (2) a multiple kernel learning approach is used to learn the optimal weights for two graph kernels; (3) deep multiple kernel learning is exploited to further enhance the discrimination of kernels; and (4) comprehensive experiments on 'in-the-wild' databases demonstrate the superiority of the proposed methods over most state-of-the-art methods in group-level affect prediction.

To explain the concepts in our approach, the paper is organized as follows: In Sect. Related Work, we present a review of the related literature. In Sect. Methodology, we provide the details of the proposed method to predict the group affect. In Sect. Experiment, we present the results of examining our proposed approach. Finally, we draw our conclusions in Sect. Conclusion.

Related Work

Kernel learning has successed to machine learning. For example, support vector machine is the most popular learning algorithm based on kernel learning. Currently, kernel methods have been successfully applied to various real-world applications, including group-level affect recognition [17]. Its core is to project the data onto a high-dimensional reproducing kernel Hilbert space and learn an optimal decision boundary. It is known that for kernel learning, the important step is to choose the right kernel function. Thus, multiple kernel learning (**MKL**) has been proposed to address the limitations of choosing the kernel function. The first MKL formulation was first introduced by Bach et al. [19], which aims at learning the optimal kernel sets weighted by the learnable weights. Through the optimization process, the best

target kernel is achieved. Its advantage is that we do not need to manually adjust values for free parameters of kernel functions.

With the success of deep learning, over the last few years, MKL has been further injected by incorporating deep learning architecture. Cho et al. described the first approach by optimizing an arc-cosine kernel, a function that mimics the massive random projections of an infinite neural network, and successfully integrated the kernel in a deep architecture [20]. The kernel admits a normalized kernel and can thus be stacked in multiple layers. Successively combining these kernels can lead to increased performance in some databases. The drawback of this method is that it cannot allow easily tuneable parameters beyond the first layer. Subsequently, Zhuang et al. proposed tuning a combination of kernels but had trouble optimizing the network beyond two layers [21]. Moreover, the second layer only consisted of a single Gaussian radial basis function kernel. However, they had problems when optimizing the network beyond two layers.

Methodology

Problem Formulation

In Fig. 11.1, given a group image X (*for the sake of simplification, we name 'group image' 'image'*), faces are detected, and their corresponding features are extracted. We aim to recognize group-level affect using this face-based information. For simplification, the widely used classifier, i.e., support vector machine (**SVM**), is used as the base classifier. According to the theorem of SVM [22], with the specific kernel function K, its basic formulation is generally depicted as follows:

$$g(X) = \sum_{i=1}^{N} \alpha_i y_i K(X_i, X) + b = \sum_{i=1}^{N} \alpha_i y_i \phi(X_i) \cdot \phi(X) + b, \tag{11.1}$$

where X_i, y_i, and α_i are the ith training image, the corresponding class label, and its Lagrange multiplier, respectively. N is the number of images in the training set, and b is the bias of the SVM. Figure 11.1 illustrates the architecture for mapping two group images into a Hilbert space ϕ.

In Eq. 11.1, the kernel function K can be seen as a measurement to describe the similarity of affect. Intrinsically, as shown in Fig. 11.1, an image often consists of more than two people. X_i is mapped into a high-dimensional Hibert space, denoted as $\phi(X_i)$. Here, $\phi(X_i)$ implicitly represents the properties of the group. Therefore, the kernel function K can be used to bridge the similarity of two images. According to the aforementioned analysis, the kernel function should be carefully considered for group-level affect recognition. As seen from Fig. 11.1, the building kernel function easily suffers from the variability of faces in images. In [17], Huang et al.

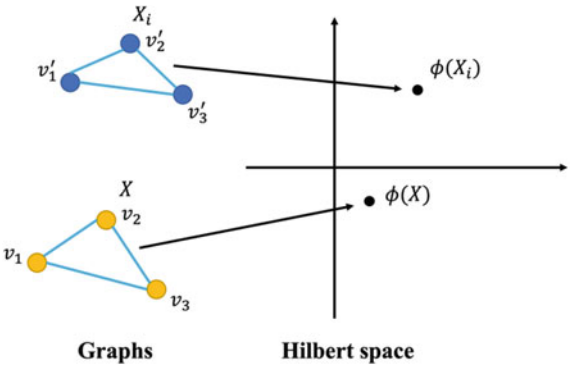

Fig. 11.1 An illustration of the graph and kernel map in group-level affect recognition. Its core is to formualte a right kernel for two images, in which an image contains more than two faces. Note that the number of faces in images may be different

proposed using a global alignment kernel to resolve the variability problem. Its key is to exploit dynamic programming to calculate the minimum distance between two images. However, this method has an inefficient computation method in calculating the distance.

Over the last two decades, graph-structured data have been an integral part of many application domains, including social network analysis. The research on graphs has received much attention to explore the intrinsic structure of graphs. Thus, faces in an image, such as X in Fig. 11.1, can be seen as a social graph. Motivated by Huang et al. [17], we investigate the graph structure to formulate the kernel function K.

Graph Kernel Construction

The graph kernel has widely become a popular approach for learning on graph-structured data. An image at the group level can be considered simple graph-structured data. We want to investigate several attractive statistical properties at the group level. Thus, this part aims to construct the graph kernel based on vertices. It can combine the representative power of graphs and the discrimination power of kernel-based methods.

A face in an image X is viewed as a vertex v, such that all faces formulate a graph. Mathematically, a graph G consists of an ordered set of n vertices $V = \{v_1, v_2, \cdots, v_n\}$ and a set of directed edges $E \subset V \times V$. A vertex v_i is a neighbor of another vertex v_j if $(v_i, v_j) \in E$. This means that v_i and v_j are connected by an edge. In the same way, another image X' is denoted as G' with n' vertices and a set of directed edges $E' \subset V' \times V'$. Therefore, measuring the distance between X and X' is equivalent to defining a graph kernel that computes the similarity between G and G'. Although there are many ways to calculate the graph kernel, such as random walk and iterative label refinement, our natural idea is to use a simple but efficient method to calculate the graph kernel. That is, all node-pair kernels [23]. It belongs to the bag of structures, which considers more complex structures within a graph.

Definition 1 (**All node-pairs kernel**) [23]: Assuming there exist two graphs with node attributes, denoted as $G = (V, E)$ and $G' = \left(V', E'\right)$, the all node-pairs kernel is defined as

$$k\left(G, G'\right) := \sum_{v \in V} \sum_{v' \in V'} k_{node}\left(v, v'\right), \tag{11.2}$$

where $k_{node}\left(v, v'\right)$ is any positive define kernel defined on the node attributes v and v'.

For Eq. 11.2, it is critical to obtain $k_{node}\left(v, v'\right)$. Suppose for each node v, its feature is f. A Gaussian RBF function is used to obtain k_{node}, which is defined as follows:

$$k_{node}\left(v, v'\right) = e^{\|f - f'\|}, \tag{11.3}$$

where $\boldsymbol{f}'$ is the feature of $\boldsymbol{v}'$.

From SVM to Deep Multiple Kernel Learning

According to Eq. 11.3, the discriminant of $k_{node}\left(v, v'\right)$ depends on face features. Group-level affect recognition may suffer from poor illumination, head pose, and poor image quality. It requires a face descriptor robust to these challenges. Additionally, in [24], using multiple features can obtain better performance than using only features. Thus, we propose an effective way to combine multiple features in graph kernels. It consists of feature extraction and deep multiple kernel learning.

For feature extraction, we used a deep convolutional neural network (CNN) based on VGG-face [25] as the high-level feature and the Riesz-based volume local binary pattern (RVLBP) [11] as the low-level feature. Specifically, RVLBP is built on the Reisz transform and local binary pattern. For deep features, VGG-face is fine-tuned on the FER2013 dataset, and features obtained from the FC6-layer of VGG-face are used. Both features are fed into Eq. 11.1 to form two graph kernels $k(G_{RVLBP}, G'_{RVLBP})$ and $k(G_{CNN}, G'_{CNN})$. Next, we will consider the approach to fuse two graph kernels.

As we know, if two kernels of different types are stacked, a representation that is different from either alone could be developed. Given a training set of N images $\{ X_i, y_i)|i = 1, \cdots, N\}$, X_i and y_i are the ith image and its class label, respectively. With the kernel function $k\left(G, G'\right)$ defined in Sect. Graph Kernel Construction, X_i and X_j are mapped to a high-dimensional reproducing kernel Hilbert space. Subsequently, SVM learns the large margin hyperplane that has the small error on the training set. That is, it aims at searching the appropriate α_i in Eq. 11.1. Considering the graph kernel, Eq. 11.1 can be rewritten:

$$f(X) = \sum_{i=1}^{N} \alpha_i y_i k\left(G, G'\right) + b, \tag{11.4}$$

which is optimized by convex optimization according to [22].

To exploit the different roles of multiple kernels, Bach et al. [19] introduced the first formulation of MKL by using a set of M base kernels. With M base kernels, Eq. 11.4 can be rewritten as:

$$f(X) = \sum_{i=1}^{N} \alpha_i y_i \sum_{m=1}^{M} \beta_m k_m\left(G, G'\right) + b, \tag{11.5}$$

where β_m is the learnable weights for M base kernels.

With the success of the deep learning concept, the multilayer idea has been introduced in MKL to improve its performance. It tries to learn deep kernel machines by exploring the combinations of multiple kernels in a multilayer structure. In this paper, we implement a deep multiple kernel learning (DMKL) [26] framework. According to [26], all base kernels in antecedent layers are combined to form new inputs to the base kernels in subsequent layers. Thus, the backpropagation algorithm requires the base kernel function to be differential. However, the graph kernel $k\left(G, G'\right)$ is nondifferential. Instead, we used the differential base kernels behind the graph kernel layer. That is, we use $k\left(G, G'\right)$ as an input for deep architecture. Figure 11.2 shows the structure of the deep multiple kernel learning framework to fuse graph kernels. Here, we use a linear kernel, two polynomial kernels of higher order, and a Gaussian RBF kernel. The resultant kernel of the multilayer is defined as follows:

$$K^{(l)} = \left\{ K^{(l-1)}\left(K^{(l-1)}; \beta_m^{(l)}\right) = \sum_{m=1}^{M} \beta_m^{(l)} k_m^{(l)}\left(K^{(l-1)}\right) \right\}, \tag{11.6}$$

where $k_m^{(l)}$ is the kth base kernel at layer l and $\beta_m^{(l)}$ denotes the weight of the kth kernel at layer l.

The final decision function of the proposed framework is defined as:

$$f(X) = \sum_{i=1}^{N} \alpha_i y_i \sum_{m=1}^{M} \beta_m^{(l)} k_m^{(l)}\left(K^{(l-1)}\right) + b. \tag{11.7}$$

With a differential kernel, Eq. 11.7 can be efficiently solved by the span bound algorithm [26].

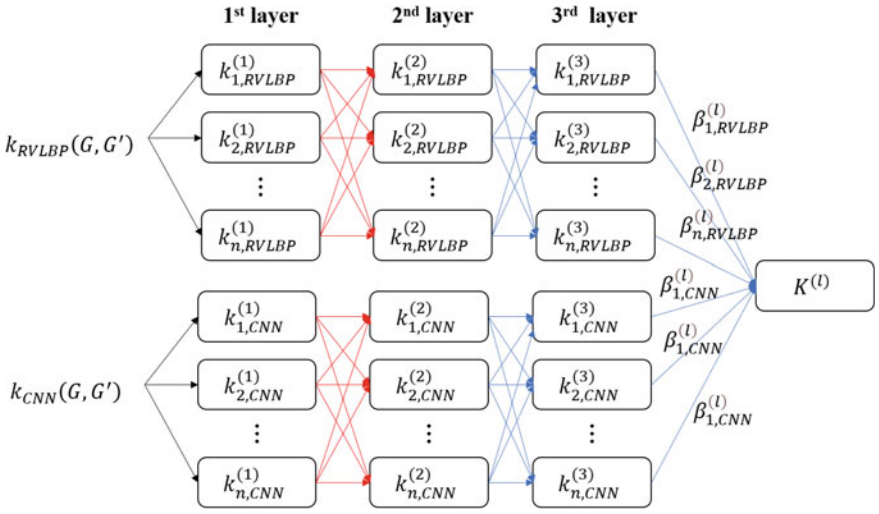

Fig. 11.2 Structure of DMKL with graph kernels, where n is the number of base kernels for RVLBP or CNN, here $n = 4$

Experiment

In this paper, we will perform algorithm analysis and ablate our proposed methods for group-level affect recognition on the Group Affective Database [27]. The corresponding group truth used in the experiments is provided by the authors of the database.

Database Description

The first version of the Group Affective Database [1] contains 504 images, which were created from Flickr and Google images according to the keyword search, such as festival, silent protest, and violence. Two experts annotated them to positive, neutral, and negative. In an open emotion challenge competition [27], the Group Affective Database has been expanded, in which the number of images is greatly increased to 5698. To evaluate the algorithm of participants, this database includes two subsets, including training and validation sets for competition. The training set has 3630 images annotated as positive, neutral, and negative. The validation set contains 2068 images. The examples about group-level images can be referred to [27].

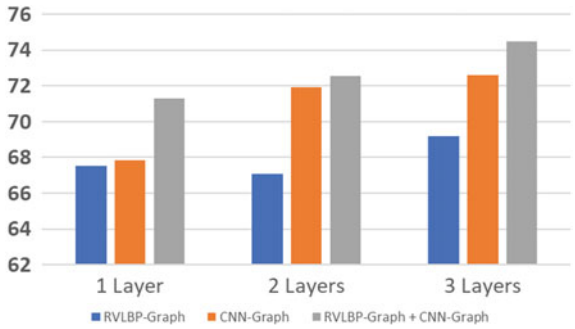

Fig. 11.3 Performance evaluation of the number of layers and graph kernel, where the x axis represents the number of layers and the y axis represents the recognition rate (%)

Ablation Study

In Sect. Related Work, it is noted that for DMKL, the number of layers and various graph kernels are closely related to the performance. To observe their influence, we conducted the performance evaluation of DMKL on the GAFF database, where DMKL is trained up to the three layers.

Figure 11.3 shows the detailed results of affect recognition under different parameters. For RVLBP-Graph, it is seen that the recognition rate is decreased when we use 2 layers compared with 1 layer. The decreased rate is 0.43%. However, when 3 layers are used, DMKL obtained a recognition rate of 69.19%. For CNN-Graph, as the number of layers increases, the recognition rate improves from 67.85% to 72.61%. The same applies to the fusion of RVLBP-Graph and CNN-Graph. According to this analysis, the recognition rate increases with the addition of each successive layer. There was a larger increase in accuracy with the addition of the first layer than with the addition of the third layer. However, the second layer did result in a small decrease for RVLBP-Graph in recognition rate.

The proposed method increases accuracy when the graph kernel is added. Using the graph kernel alone, when we use 1 layer, the recognition rate is obtained at 67.51% and 67.85% for RVLBP and CNN, respectively. Based on CNN, it would obtain better performance than RVLBP. Using both graph kernels, the recognition rate is increased by 3.79% and 3.45% compared with RVLBP and CNN, respectively. This indicates that appending more graph kernels may directly result in good performance.

Comparison with SVM and MKL

This part aims to evaluate the performance of the SVM and MKL algorithms with our algorithm based on DMKL. Here, we evaluated the following algorithms: SVM, SUM-Kernel, SM1MKL [28], and L2MKL [29]. In SUM-Kernel, we use the same weight for two graph kernels and then feed them into the SVM. The LibSVM [30] package is used to solve the SVM optimization problem. SM1MKL was proposed by

Table 11.1 Algorithm comparison of our proposed methods with SVM and MKL algorithms on the GAFF database. The best result is in bold

Component	Context feature	Recognition rate (%)
SVM	RVLBP-Graph	68.82
SVM	CNN-Graph	71.54
SUM-Kernel	RVLBP-Graph, CNN-Graph	72.56
SM1MKL [28]	RVLBP-Graph, CNN-Graph	72.61
L2MKL [29]	RVLBP-Graph, CNN-Graph	72.07
DMKL	RVLBP-Graph, CNN-Graph	**74.49**

Xu et al. [28], who developed a soft margin MKL framework. L2MKL was proposed by Kloft et al. [29]. All algorithms are implemented in MATLAB. Table 11.1 shows the detailed results of the classification of the different algorithms.

By comparing the results between SVM and the two existing MKL methods (L2MKL and SM1MKL), we found that these algorithms do not guarantee much higher performance over SVM with CNN-Graph. For instance, the L2MKL algorithm just surpassed SVM with CNN-Graph by 0.53%. Simply sum two graph kernels (SUM-Kernel) outperforms L2MKL. This indicates that L2MKL cannot obtain the optimal weights for these two kernels. Among all algorithms, DMKL achieves the best performance, followed by SM1MKL. Thus, these results show that DMKL with RVLBP-Graph and CNN-Graph outperforms the SVM and MKL methods. The comparison results demonstrate that using a deep architecture increases the recognition rate of MKL.

Algorithm Comparison

To see the superiority of our proposed method, we compare our method with several comparative algorithms [1, 12, 17], 15, 16, 31–33]. In [1], Dhall et al. implemented a census transform histogram descriptor to extract features from 4×4 nonoverlapping blocks of images and then used an SVM with a nonlinear chi-square kernel to train the classification model. In [12], individual facial emotion CNN and global image-based CNN were proposed. Huang et al. [17] proposed a global alignment kernel based on two face features and multiple kernel learning, namely, SVM-GAK and SVM-CGAK. In [31], face information is combined with scene information for group-level affect recognition. In [15], Abbas et al. combined image context and facial information for group-level affect recognition. Three solo models and two multimodals were proposed. In [16], Rassadin et al. extracted feature vectors of detected faces using a CNN trained for face identification tasks. In the final pipeline, an ensemble of random forest classifiers on four features from VGG-face, VGG-16,

ResNet-50, and Xception on the detected faces was learnt to predict emotion scores using the available training set. In [32], Fujii et al. proposed a hierarchical classification approach, which differentiates between 'Positive' images that include specific facial expressions and those that do not. Additionally, they incorporated visual attention and objectwise semantic information to reduce the effects of background faces. In [33], Shamsi et al. proposed a CNN on an emotion heatmap extracted from an image.

Table 11.2 reports the comparison between our method and several comparative algorithms [1, 12, 15–17, 31–33]. It is noted that the results were straightforwardly comparable due to the same experimental setups. In Table 11.2, Line 1 is the baseline algorithm when this database was published. Lines 2 to 14 indicate that researchers used one context feature, such as face or scene. Lines 15 to 18 represent that the fused feature is used. The algorithm in Line 19 is to exploit hierarchical classification to polish the face image according to several deep learning architectures.

First, as seen from Table 11.2, the baseline algorithm that used the census transform histogram descriptor and SVM reported an initial recognition rate of 52.97%. Compared with the baseline algorithm, our proposed method significantly increases the recognition rate to 74.49%. Among the algorithms in Lines 2 to 14, the best result is obtained by Huang et al. (SVM-CGAK) [17], which is 72.17%. Although the methods of Huang et al. and ours used the same features, our proposed method outperformed SVM-CGAK by 2.32%. Additionally, our proposed method has less computational time than SVM-CGAK.

Second, in [15, 16, 31], they proposed several methods to fuse multiple features, including face information and social context. In [15], it is seen that fusing scene and face, such as "Face-pretrained CNN + Inception V3-FC on scene", increases the recognition rate of sole features. This indicates that fusing different contextual information is a promising way to improve the performance of group-level affect recognition. It also motivates us to use different context features in our model in the future. Among [15, 16, 31], "Face-pretrained CNN + Inception V3-FC on scene" obtained a recognition rate of 72.38%, while our proposed approach achieved an accuracy of 74.49%.

Third, in [32], Fujii et al. studied nonhierarchical and hierarchical approaches. In the nonhierarchical approach, the deep features, including faces with attention mechanisms, objects with attention mechanisms and global features, were concatenated and fed into an FC layer. The recognition rate is 72.82%. Compared with, our proposed method is still competitive with the nonhierarchical approach. The hierarchical approach consists of two classification steps. In the first step, a binary classification is performed to differentiate positive labels, including specific facial expressions, from others. In the second step, a three-class classification is performed on outcomes from the first classification. They also use objectwise semantic information to represent scene features along local and global streams. With the strongly enriched representation and polishing process, the hierarchical approach obtained the highest recognition rate of 80.19%. Although our approach works worse than the hierarchical method, it is believed that adding more information and increasing the number of layers in the future will result in amazing performance.

Table 11.2 Algorithm comparison of our proposed methods with several state-of-the-art methods on the GAFF database. The comparison results are derived from [1, 12, 15–17, 31–33]. The best result is in bold, and the second-best result is in italic

Reference	Method	Recognition rate (%)
Dhall et al. [1]	Census transform histogram descriptor, SVM	52.97
Huang et al. [17]	SVM with global alignment kernel, RVLBP feature	67.32
Huang et al. [17]	SVM with global alignment kernel, CNN feature	70.67
Huang et al. [17]	SVM with combined global alignment kernel, RVLBP and CNN features	72.17
Rassadin et al. [16]	VGG Face feature, SVM	65.41
Rassadin et al. [16]	VGG-16 finetuned on detected face	64.11
Rassadin et al. [16]	ResNet50 finetuned on detected face	62.65
Rassadin et al. [16]	Xception finetuned on detected face	60.18
Lan et al. [12]	Facial emotion CNN	69.97
Abbas et al. [15]	Face-pretrained CNN	60
Abbas et al. [15]	Inception V3-FC on scene	63.19
Abbas et al. [15]	VGG16-FC on scene	66.30
Shamsi et al. [33]	AlexNet on Gaussian Heatmap	55.23
Balaji et al. [31]	Fusion of scene and VGG-face	65.0
Rassadin et al. [16]	Ensemble of classifiers [55]	66.51
Abbas et al. [15]	Face-pretrained CNN + Inception V3-FC on scene	70.09
Abbas et al. [15]	Face-pretrained CNN + VGG16 + FC on scene	72.38
Fujii et al. [32]	Hierarchical classification approach	**80.19**
Fujii et al. [32]	Non-hierarchical approach	72.82
Ours	DMKL	*74.49*

Conclusion

To advance the research in affective computing, it is important to understand the affect exhibited by a group of people in images. In this paper, we propose deep multilayer kernel learning with graph kernels for analyzing group-level affect prediction. First, we propose establishing a graph kernel based on two kinds of features, which can explicitly measure the similarity between two images. Furthermore, based on the graph kernel, we proposed using deep multilayer kernel learning to exploit the superiority of graph kernels, namely, DMKL, for group-level affect prediction. The fused graph kernel exploited the low-level and high-level features and several base kernels. Additionally, it borrowed the benefit of multiple kernel learning and deep learning techniques, which can obtain the optimal weights for combining graph kernel and basic kernels. The optimal learnt weights and multiple feature descriptors

can make DMKL better at group-level affect prediction. Although this paper focused on graph kernel and face features and obtained considerable results, several existing works in [28] demonstrated that adding scene information can significantly improve the performance in group-level affect recognition. It is believed that adding more information from multiple modalities would make more benefits and improvements to DMKL. Additionally, this paper lacked consideration of the data structure. In our future work, we will consider more context information and graph structure to promote the performance of our system. Additionally, we will consider the difference in workflow between social science and computer science for deeply analyzing group-level affect, not only focusing on the technical level.

Acknowledgements This research was in part supported by National Natural Science Foundation of China (Grant No. 62076122), the Jiangsu Specially-Appointed Professor Program, the Talent Startup project of NJIT (No. YKJ201982), the Opening Project of Jiangsu Province Engineering Research Center of IntelliSense Technology and System (No. ITS202102), and the Opening Project of Advanced Industrial Technology Research Institute, Nanjing Institute of Technology (No. XJY202102).

References

1. Dhall, A., Joshi, J., Sikka, K., Goecke, R., & Sebe, N. (2015). The more the merrier: Analysing the affect of a group of people in images. In *International conference automation face gesture recognition*, pp. 1–6.
2. Rice, L., Wall, C., Fogel, A., & Shic, F. (2015). Computer-assisted face processing instruction improves emotion recognition, mentalizing, and social skills in students with ASD. *Journal of Autism and Development Disorders, 45*(7), 2176–2186.
3. Levine, J., & Moreland, R. (1990). Progress in small group research. *Annual Review of Psychology, 41*, 585–634.
4. Barsade, S., & Gibson, D. (1998). Group emotion: A view from top and bottom. *Research on Managing Group and Teams, 1*, 81–102.
5. Kelly, J., & Barsade, S. (2001). Mood and emotions in small groups and work teams. *Organizational Behavior and Human Decision Process, 86*(1), 99–130.
6. Yang, J., & Moossholder, M. (2004). Decoupling task and relationship conflict: The role of intragroup emotional processing. *Journal of Organizational Behavior, 25*(5), 589–605.
7. Penalver, J., Salanova, M., Martinez, I., & Schaufeli, W. (2019). Happy-productive groups: How positive affect links to performance through social resources. *The Journal of Positive Psychology, 14*(3), 377–392.
8. Hernandez, J., Hoque, M., Drevo, W., & Picard, R. (2012). Mood meter: Counting smiles in the wild. In *ACM conference on ubiquitous computing*, pp. 301–310.
9. Gallagher, A., & Chen, T. (2009). Understanding images of groups of people. In *International conference on computer vision*, pp. 256–263.
10. = Dhall, A., Joshi, J., Radwan, I., & Goecke, R. (2013). Finding happiness moments in a social context. In *Asian conference computer vision*, pp. 613–626.
11. Huang, X., Dhall, A., Zhao, G., Goecke, R., & Pietikainen, M. (2015). Riesz-based volume local binary pattern and a novel group expression model for group happiness intensity analysis. In *British machine vision conference*, pp. 1–13.
12. Tan, L., Zhang, K,. Wang, K., Zeng, X., Peng, X., & Qiao, Y. (2017). Group-level emotion recognition with individual facial emotion CNNs and global images based CNNs. In *International conference on multimodal interaction*, pp. 549–552.

13. Mou, W., Celiktutan, O., & Gunes, H. (2015). Group-level arousal and valence recognition from static images: Face, body and context. In *International conference automation face gesture recognition*, pp. 1–6.
14. Huang, X., Dhall, A., Goecke, R., Pietikainen, M., & Zhao, G. (2018). Multimodal framework for analyzing the affect of a group of people. *IEEE Transactions on Multimedia, 20*(10), 2706–2721.
15. Abbas, A., & Chalup, S. (2017). Group emotion recognition in the wild by combining deep neural networks for facial expression classification and scene-context analysis. In *International conference on multimodal interaction*, pp. 561–568.
16. Rassadin, A., Gruzdev, A., & Savchenko, A. (2017). Group-level emotion recognition using transfer learning from face identification. In *International conference on multimodal interaction*, pp. 544–548.
17. Huang, X., Dhall, A., Goecke, R., Pietikainen, M., & Zhao, G. (2022). Analyzing group-level emotion with global alignment kernel based approach. *IEEE Transactions on Affective Computing, 13*(2), 713–728.
18. Cuturi, M., Vert, J., Birkenes, O., & Matusi, T. (2007). A kernel for time series based on global alignments. In *International conference on acoustics, speech, and signal processing*, pp. 413–416.
19. Bach, F., Lanckriet, G., & Jordan, M. (2004). Multiple kernel learning, conic duality, and the SMO algorithm. In *International conference on machine learning*, pp. 1–9.
20. Cho, Y., & Saul, S. (2009). Kernel methods for deep learning. *Advance in Neural Information Processing System, 22*, 342–350.
21. Zhuang, J., Tsang, I., & Choi, S. (2011). Two-layer multiple kernel learning. In *International conference on artificial intelligence and statistics*, pp. 909–917.
22. Vapnik, V. (1998). Statistical learning theory. Chapter 10-11, pp. 401–492.
23. Nikolentzos, G., Siglidis, I., & Vazirgiannis, M. (2021). Graph kernels: A survey. arXiv:1904.12218v2, pp. 1–85.
24. Chen, J., Chen, Z., Chi, Z., & Fu, H. (2018). Facial expression recognition in video with multiple feature fusion. *IEEE Transaction on Affective Computing, 9*(1), 38–50.
25. Parkhi, O., Vedaldi, A., & Zisserman, A. (2015). Deep face recognition. In *British machine vision conference*, pp. 1–9.
26. Strobl, E., & Visweswaran, S. (2013). Deep multiple kernel learning. In *International conference on machine learning and applications*, pp. 414–417.
27. Dhall, A., Goecke, R., Ghosh, S., Joshi, J., Hoey, J., & Gedon, T. (2017). From individual to group-level emotion recognition: Emotiw 5.0. In *International conference on multimodal interaction*, pp. 524–528.
28. Xu, X., Tsang, I., & Xu, D. (2013). Soft margin multiple kernel learning. *IEEE Transaction on Neural Network and Learning System, 24*, 749–761.
29. Kloft, M., Brefeld, U., Sonnenburg, S., & Zien, A. (2011). Lp-norm multiple kernel learning. *Journal of Machine Learning Research, 12*(5), 953–997.
30. Chang, C., & Lin, C. (2011). LIBSVM: A library for support vector machines. *ACM Transactions on Intelligent System and Technology, 2*(3), 27.
31. Balaji, B., & Oruganti, V. (2017). Multi-level feature fusion for group-level emotion recognition. In *International conference on multimodal interaction*, pp. 583–586.
32. Fujii, K., Sugimura, D., & Hamamoto, T. (2021). Hierarchical group-level emotion recognition. *IEEE Transactions on Multimedia, 23*, 3892–3906.
33. Shamsi, S., Singh, B., & Wadhwa, M. (2018). Group affect prediction using multimodal distributions. In *IEEE winter conference on applications of computer vision workshops*, pp. 77–83.

Chapter 12
An Anticipative Order Reservation and Online Order Batching Algorithm Based on Machine Learning

Zhiqiang Qu and Peng Yang

Abstract For e-commerce warehouses, on-time delivery and less order picking cost are of great importance. Order batching is the critical operation issue both in manual picking system and robotic warehousing system. Few studies have considered the effect of future arrival orders on on-line order batching, however there may be potential benefits. In this paper, we propose a novel on-line order batching solution based on machine learning by considering the potential benefit of reserving some promising orders. In this new anticipative order reservation mechanism, when order arrives, we don't batch all arrival orders and consciously reserve some orders to be batched in the following period which may obtain extra efficient improvement. We design a reserving algorithm to decide whether an order should be reserved in order pool or immediately released to next order batching stage. A regression model trained by AutoGluon is used to predict the similarity between a current order and future coming orders. Based on the mechanism, a complete algorithm was developed to solve on-line order batching problem, including batching, sequencing and all necessary process. Finally, we test the algorithm on the real data from an e-commerce warehouse and compare with fixed and variable time-window batching in the previous literature. The result shows using the reservation mechanism has higher performance in reducing order turnover time and picking cost.

Keywords Order picking · On-line order batching · Machine learning · Reservation mechanism

Z. Qu · P. Yang (✉)
Reasearch Center for Modern Logistics, Shenzhen International Graduate School, Tsinghua University, Shenzhen 518055, China
e-mail: yang.peng@sz.tsinghua.edu.cn

Z. Qu
e-mail: qzq20@mails.tsinghua.edu.cn

R. Qiu et al. (eds.), *City, Society, and Digital Transformation*, Lecture Notes in Operations Research, https://doi.org/10.1007/978-3-031-15644-1_12

Introduction

Low operation cost and rapidly delivery are the most concern in e-commerce fulfilment. Warehouse as the logistics facility node has significant impact on improvement of the e-commerce fulfillment efficiency. Order picking, the process of retrieving items form their storage locations in order to satisfy the demand of customer orders, is a critical and time-consuming operation, accounting for more than 55% of total operating cost of a warehouse. Therefore, improvement in order picking will lead to a decrease in operating cost as well as an increase in service level [1].

Order batching is one of the most prominent strategies to improve the performance of order picking [2]. In order batching, the demand from multiple orders is used to form pick batches and a batch will be collected in a single tour, which are constructed to minimize the total travel distance or other performance objective. With respect to the availability of customer orders, two situations for batching customer orders can occur: in off-line batching, all orders are known at the beginning of the planning period. In on-line batching, orders become available dynamically over time [3]. Due to the on-time delivery requirements of e-commerce, the arrival of orders occurs continuously (24 h a day/7 days a week) [4], it belongs to on-line order batching problem (OOBP) in the real e-commerce warehouse. To solve this dynamic optimization problem, some on-line algorithms are designed to keep running while order arrive continuously and batches are formulated every period or upon a triggering event [1, 3, 4]. A drawback of this approach is that batch generation takes time [5]. The waiting time may result in a longer turnover time for orders. Therefore, others focus on dynamic order picking, where batches and routes that have already started can be updated based on new orders arrival or other triggering events [5–7]. However, this dynamic system needs the support of modern order-picking aids and is relatively difficult to achieve in reality. All in all, none of the above studies considered the impact of upcoming orders and information on future orders is not absolutely unavailable. E-commerce warehouses receive tens of thousands of orders in one day, machine learning may help us mining some rules in data to 'predict' the future orders.

In this paper we study on-line order batching problem (OOBP), considering an e-commerce warehouse with picker-to-parts manual order picking system. There are multiple pickers to pick batches. Orders become available dynamically over time. Order batching occurs based on the arrived orders. We propose a novel order reservation mechanism by considering the potential benefit of reserving some promising orders before order batching stage. In the reserving mechanism, when order arrives, we don't batch all arrival orders and consciously reserve some orders to be batched in the following period which may obtain extra efficient improvement (Fig. 12.1). We use machine learning to discover the rules of order data to set order reservation mechanism to approximate global optimization.

The OOBP consider three objectives: minimizing the completion time, minimizing the order turnover time and minimizing the picking time. We propose an algorithm framework and a series related algorithms to solve OOBP based on the

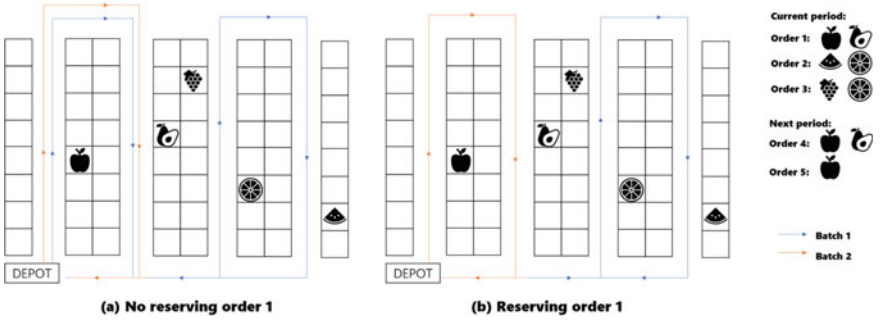

Fig. 12.1 The different between reserving mechanism and no reserving mechanism. In the former, order 1 is reserved, so batch 1 includes order 2\3, batch 2 includes order 1\4\5. In the latter, batch 1 includes order 1/2/3, batch 2 is 4/5

reservation mechanism. Different from algorithms in the literature, we designed a reserving algorithm before batching stage. The current order pool will be split into two parts based on the predict of each order and other system information, one is released to next batching stage and the other reserve in order pool waiting for future orders. We use the similarity between current order and future orders to describe the predictive potential of orders. AutoGluon [8], an Auto-ML framework, is used to predict potential of orders. However, this reserving algorithm can only be considered as one of the subproblems that need to be handled within the OOBP. In order to solve OOBP, other necessary operations include: transfer orders to picking batch (batching), establishing a sequence of the constructed batches (sequencing), assigning each batch to a picker, determining the moment in the time for starting the picking (time window), or designing the route to follow by the picker [4]. Our algorithm framework includes the reserving algorithm and the algorithm for all the necessary operations above. We compare the algorithm with the fixed and variable time-window batching algorithm in literature to validate the proposed reservation mechanism.

Our main contributions are: (i) We are the first to propose the order reservation mechanism and algorithm to obtain the extra benefit from order batching; (ii) We develop a regression predict model trained by AutoGluon to decide which order deserves reservation. This is a novel exploration of machine learning to be used in the order batching area; (iii) We design a new algorithmic based on order reserving mechanism to solve OOBP. The performance is evaluated by comparing with the fixed and variable time-window batching algorithm based the numerical experiments on real e-commerce warehouse order data.

Literature Review

Static Order Batching Problem

As the special case of on-line version, the static order batching problem (OBP), whose objective is to minimize the travel distance, has been proved to be NP-hard in the general case [9]. Therefore, most studies on the exact algorithm of OBP problem can only solve the problem of small instances. The main exact algorithm of OBP is branch and price proposed by Gademann and van de Velde [9], which can solve the optimal solution of up to 32 order sizes. Muter and Oncan [10] propose an exact algorithm of column generation to solve OBP with a heuristic routing strategy, and 100 orders at most can be solved in their experiments. For large instances, heuristic receive wide attention. Seed and saving (C&W) algorithm are famous batch construction heuristic, which is low computational cost but results in shorter travel distance. Aaya et al. [11] proposes an aisled-based heuristic to minimize the number of aisles in one batch [11]. Most meta-heuristic, like Genetic algorithm (GA), Tabu search (TS), Variable neighborhood search (VNS) and Adaptive large neighborhood search (ALNS), are designed to OBP [12–14].

Considering the due date of orders and pickers schedule, other version of OBP with different objective are wildly concerned. The objective of minimizing the total tardy orders, related to the sequence of batches, is model as order batching and sequencing problem (OBPS), and different meta-heuristic are designed to solve OBPS [15, 16]. Based the exact algorithm of OBP, Muter and Oncan [17] extended the column generation to the multi-pickers case to solve order batching and picker scheduling with the makespan objective [17]. Matusiak [18] consider the pickers capability by modelling the characteristics of picker and found that the optimal result could be improved by 10% with makespan objective [18]. The research progress of OBP and OBPS can be seen in the review articles of Cergibozan et al. [19].

On-Line Order Batching Problem

Since static OBP is difficult to deal with improvement of order processing time requirement of e-commerce warehouse, more practical on-line order batching problem (OOBP) are wildly concerned. Henn [3] firstly described the OOBP with singe picker to minimize the maximum the complete time. And three off-line algorithm is redesigned to suit for on-line version. Alipuor et al. [20] extend Henn's model and algorithm to the multi-picker situation. To solve OOBP, Zhang et al. [1] propose two type method, fixed time window batching (FTWB) and variable time window batching (VTWB). A rule-based FTWB algorithm designed by them, considering three types of decision points. Gil et al. study three different objective: minimizing the completion time, the picking time and the differences in the workload of OOBP

with muti-pickers, a multi-start procedure hybridized with a Variable Neighborhood Descent metaheuristic to handle the problem [4].

Using modern order-picking aids, dynamic batching is another effective method to solve order batching order arrival on-line. Different to on-line order batching, batches and routes can be updated based on new orders arrival or other triggering events even when they already started a pick tour. Lu et al. [6], Giannikas et al. [7] propose intervention policies to calculate the updated routes once new orders are received. Gasst et al. [5] develop a mathematical model for dynamic batching that minimizes the order throughput time of incoming customer orders and design a column generation algorithm to solve the model. Husam and Daehan [21] proposes a dynamic-order picking framework where batches and picker routes are continuously modified in response to urgent orders arrival and disruption events, considering conflicts between pickers in narrow aisles. Dynamic batching is more dynamic but presents greater operational challenges.

Machine Learning Method on Order Batching

With the development of machine learning methods and attention to data mining, some researches use machine learning methods based on data to provide novel idea of solving order batching problems. Chen and Wu [22] first proposed a data mining method in OBP problem. They used A-priori algorithm to obtain the support between orders, and then established a 0–1 integer programming model based on this metric in order to maximize the sum of support between orders. Perez et al. [23] pioneered the use of a distributed estimation algorithm (EDA) to solve OOBP problems, a data-driven algorithm that can estimate relationships between different orders from data. Humberto [24] presented a machine learning framework based on decision tree to learn batching rules form historical order batches data generated by heuristic algorithm. These learned batching rules can directly solve OOBP. Bram et al. [25] uses a deep reinforcement learning approach to solve OOBP problems with the objective of minimizing the number of tardy orders, which it describes as a semi-Markov decision process to determine whether orders should pick by order or pick by batch.

In conclusion, for on-line order batching, the current solutions in the literature are heuristics and machine learning which are mainly used in specific situation or static problem. In this paper, a reservation mechanism based on machine learning method is designed to consider the future arrival of orders while approximating global optimization can be obtained in the planning horizon.

Problem Description

In this paper, we use reservation mechanism to solve OOBP, which is a dynamic optimization problem because the arrival of orders is online (24/7) to warehouse. An important issue of the OOBP is that the orders are not fully available at the beginning of the process, but they become available over time. There are multiple available pickers, so the sequence of batches and batches assignment to pickers need to be considered. The reservation mechanism is defined as follows: there is an order pool where newly arrived orders are stored and there is a batching pool, where orders will be batching. In the reservation mechanism, when orders arrived, we don't batch all arrival orders and consciously reserve some orders to be batched in the following period. That means not the entire orders in orders pool are sent to batch pool, some promising orders will be reserved in orders pool based a reserving algorithm. This is the most difference from the traditional problem, where entire orders in orders pool will be released to the batching pool at some time point (like time window end or order arrival time). We define the problem in this paper as the OOBP with reserving mechanism (OOBPRM).

The process of OOBP with reserving mechanism as Fig. 12.2. The main processes of OOBPRM are: (i) releasing/reserving, determines which orders are reserved in the order pool and which are released to the batching pool; (ii) batching, to determine how the orders are grouped into batches; (iii) sequencing, determine the sequence of batch execution; (iv) waiting, decide when the batches delivered to pickers; (vi) assigning, to match batches to the pickers; (vii) servicing, pickers travel in the warehouse to collect batches as the routing method. Besides, there is a waiting process, which to decide when the batches delivered to pickers, between sequencing and assigning.

Refer to Henn [3] for definitions of time periods and points in OOBPRM. The time period necessary to complete a batch is called (batch) *service time*. The batch service time is composed of the *travel time*, the *pick time,* and the *setup time*. The point in time when a customer order becomes available is called *arrival time*. The *start time* of a batch is the point in time when an order picker starts to process this batch. The *start time* of an order is identical to the start time of the batch the orders

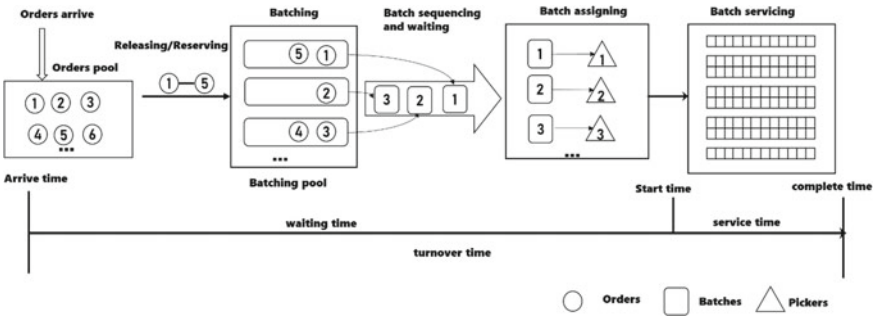

Fig. 12.2 The process of OOBP with reserving mechanism

assigned to. The point in time when the order picker returns to the depot after having collected all items is called *completion time* of a batch or of an order, respectively. The order *waiting time* can be determined as the length of the time period between the arrival time and the start time of a customer order. The *turnover time* is the time period for which a customer order stays in the system, i.e. the time period between the arrival and the completion time of a customer order.

Warehouse and Data Description

The warehouse setting and order data is from an e-commerce warehouse in China. The warehouse is a rectangular single block parallel-aisle layout where storage locations are located on both sides of the pick aisles as shown in Fig. 12.1. There are 16 aisles in total. The patten of picking is sort-while-pick. The batch size (the capacity of picking container) is 24 orders. The order integrity condition (the splitting of a customer order into two or more batches is prohibited) need to be met. The picker routing strategy is S-shape, which is the most common way in reality. Aisles in the warehouse are wild enough to allow several pickers crossing their route.

The real order data form an e-commerce warehouse is taken as the training data of machine learning model of reserving mechanism and the instance of simulation experiments in this paper. There are 7 days of order data, 345,762 lines in total. The SKUs requirements in orders have a distinct ABC classification, i.e. SKUs in the aisle near depot have higher demand frequency while the demand of those away from depot are less. The order arrival rate varies with time in one day, is 34.3 order per minute on average. The number of items in one order ranges from 1 to 16.

Model

Refer to Gils et al. [4], Zhang et al. [1], Alipour et al. [20], the model of on-line order batching is (12.1)–(12.11). Parameters and variables are in Tables 12.1 and 12.2.

Table 12.1 Parameters of model

Parameters	
n	Number of orders in the system
m	Upper bound of the number of batches, $m \leq n$
q_i	Number of items in order i
Q	Batch size
$t_j^{service}$	The service time of batch j
t_i^{arrive}	Arrival time of order i

Table 12.2 Variables of model

Variables	
x_{ij}	0–1 variable, 1 means that order i is assigned to batch j, and vice versa
y_{jk}	0–1 variable, 1 means that batch j is assigned to picker k, and vice versa
t_j^{start}	start time of batch j

$$\min \max_{j\in\{1,\ldots,m\}} \left\{ t_j^{service} + \sum_{k\in K} y_{jk} t_j^{start} \right\} \tag{12.1}$$

$$\min \sum_{i\in I} t_i^{turnover} \tag{12.2}$$

$$\min \sum_{j\in J} t_j^{service} \tag{12.3}$$

$$\sum_{j\in J} x_{ij} = 1, \quad \forall i \in \{1,\ldots,n\} \tag{12.4}$$

$$\sum_{k\in K} y_{jk} = 1, \quad \forall j \in \{1,\ldots,m\} \tag{12.5}$$

$$\sum_{i\in I} q_i x_{ij} \le Q, \quad \forall j \in \{1,\ldots,m\} \tag{12.6}$$

$$t_j^{start} \ge \max_{i\in\{1,\ldots,n\}} \left\{ t_i^{arrive} x_{ij} \right\}, \quad \forall j \in \{1,\ldots,m\},\ k \in \{1,\ldots,l\} \tag{12.7}$$

$$t_j^{start} \ge t_{j-1}^{start}, \quad \forall j \in \{2,\ldots,m\} \tag{12.8}$$

$$t_j^{start} \ge \min_{k\in\{1,\ldots,l\}} \max_{s\in\{1,\ldots,j-1\}} y_{sk} \left(t_s^{start} + t_j^{service} \right), \quad \forall j \in \{1,\ldots,m\} \tag{12.9}$$

$$t_{jk}^{start} \ge 0, \quad \forall j \in \{1,\ldots,m\},\ k \in \{1,\ldots,l\} \tag{12.10}$$

$$x_{ij}, y_{jk} \in \{0,1\},\ \forall i \in \{1,\ldots,n\}, \quad \forall j \in \{1,\ldots,m\},\ k \in \{1,\ldots,l\} \tag{12.11}$$

There are three objectives of this OOBP model, the objective function (12.1) minimizes the maximum completion time, i.e. the makespan, which is determined by the time of pickers complete last batch. The objective (12.2) minimizes the turnover time of orders, which represent the on-time delivery demand. The minimum of the service time of batches is the objective (12.3), which represent the picking cost. Constrain (12.4) guarantee that each order is assigned only to one batch. Constrain (12.5) guarantee that each batch is assigned only to one picker. Constrain (12.6) is the capacity limit of one batch. Constrain (12.7) guarantee the batch j cannot be started

until all orders assigned to the batch have arrived. Constrain (12.8) guarantee the sequence of batches. Constrain (12.9) guarantee that the batch starts to be collected only if there is at least one picker available. Constrain (12.10) guarantee the start time is non-negative. Constrain (12.11) state that x_{ij}, y_{jk} is binary.

Methodology

An Anticipative Order Reservation Mechanism

Different from other solution about OOBP, we propose an anticipative order reservation mechanism to consider the benefit of the arrival of future orders. The basic idea of this mechanism is that we don't batch all arrival orders and consciously reserve some promising orders to be batched in the following period which may obtain extra efficient improvement (Fig. 12.1). Due to the large number of SKUs and the in-time delivery requirement in e-commerce warehouse, it is a great challenge to predict specific orders in a short time. Therefore, instead of predicting actual orders, we use a predictive metric that represents the potential of orders. The metric we chose was the similarity in physical location between orders. Aisles of orders are only considered, because the method of traveling is S-shape. The definition of similarity can be seen (12.12), where | Aisle $i \cap$ Aisle j | represents the number of identical picking aisles between orders i and j, | Aisle $i \cup$ Aisle j | is the total number of picking aisles that the picker needs to visit if combining orders i and j. The predictive metric of an order is the sum of similarity of the future orders over a fixed period of time. We call the metric the *predictive score* of orders, which can be get form a machine learning model trained by AutoGluon.

$$simi_{ij} = \left|Aisle_i \cap Aisle_j\right| / \left|Aisle_i \cup Aisle_j\right| \tag{12.12}$$

AutoGluon is a robust and accurate automated machine learning (AutoML) tool for structured data [25]. It is developed by Amazon and released in late 2020. In this paper, AutoGlon is used to train an order *predictive score* prediction model. The order data consists of 17 features, including 16 0–1 variables representing 16 aisles and a continuous variable representing time. We label the data by the calculation of *predictive score*, and the prediction span is 30 min. There are 7 days of order data, 345,762 lines in total. Among them, six days of data as a training set (297,350) and one day as a test set (48,412).

Reserving Algorithm

Based on the reservation mechanism, an order reserving algorithm is designed to determine orders reserving in orders pool or releasing to batching pool at any time. The purpose of reserving orders is looking forward to get better batches in the future, so when similar orders of batch size are collected, they can be released. Similar orders must have similar *predictive score* according to the calculation rules of it, then orders with similar scores are mostly similar orders. Therefore, orders can be released by determining whether the number of similar *predictive score* orders has reached the batch size. The reserving algorithm flow is described as follows:

- step 1: Predict the *predictive score* of all orders in order pool from AutoGluon model at the current time;
- step 2: Sort orders in the order pool by *predictive score*, index = 0;
- step 3: If index + batch size > length of order pool, end the algorithm; else go to step 4;
- step 4: Calculate the different of *predictive score* between the order of index and the order of index + batch size. if the difference < the set threshold, go to step 5; else index = index + 1, go to step 3;
- step 5: Release the orders from index to index + batch size to batching pool, index = 0, go to step 3;

The procedure starts from the arrival of new orders. The predict model will give a *predictive score* to each order in the order pool based on current time. Then, orders will be sorted by score to make it easier to find similar orders. Orders with the number of batch size, whose difference of *predictive score* lower than threshold, release to batching pool, the process is repeated until no orders meet the condition. The threshold is a parameter that we need to adjust in experiment.

The releasing algorithm can realize the reservation of potential orders and the release when reach batch size to optimize the batches and to decrease the *service time* of batches and orders. However, there may be a problem with possibly long waiting time. If the conditions for release are not met, there should be no long wait, as this would lead to unacceptable *waiting time, turnover time.* Therefore, after the reserving algorithm, we add a setting: when the number of batches that can be formed by released orders is less than the number of idle pickers, orders with lower scores will be released so that there are enough batches to assign to idle pickers. By the above setting and reserving algorithm, the optimization of order *turnover time* and *service time* could be balanced.

Algorithm of OOBPRM

Besides the reserving algorithm, other necessary processes are needed to solve OOBPRM, including batching, sequencing, waiting, assigning and routing. Therefore, a complete algorithm is designed to give the entire solution of OOBPRM.

Reserving: detail in the last section.

Batching: Since aisles similarity is used in this paper to evaluate orders similarity, an aisle-based heuristic proposed by Aaya et al. [11] is considered as batching algorithm. The basic idea of the heuristic is that find the aisles with the most visits in the orders as the star aisles, add the order nearest to the star aisles to the batch, update the star aisles, continue to find the next nearest order until the batch size reached. Detailed algorithm steps and numerical examples are available in the original paper.

Waiting: The algorithm in this paper adopts the idea of variable-time window batching, that is, the waiting is finished when pickers become idle. In other words, the batches are generated and assigned to pickers only when the pickers are idle. Thus, the waiting time of batches is 0 in variable-time window batching.

Sequencing: Refer to the research of Henn [4], the LONG rule is the best performing. Thus, the LONG rule, which sequence batches by the *service time* on descending order, is used as the sequencing algorithm.

Assigning: we use the method proposed by Zhang et al. [5] which assigns the next available batch to the picker that has travel less until that moment.

Routing: S-shape.

Benchmark Algorithm

No Reservation: This is the same as the complete algorithm except no reserving sub-algorithm. When pickers become idle, generate the number of the idles batches by the same aisle-based batching algorithm, sequenced and assigned to idle pickers.

VTWB: The idea of first come and first service, the basic algorithm to solve OOBP. The batch algorithm is that one batch is generated when the number of orders in the order pool accumulates to the batch size. There is no waiting in FCFS, so the batches will be sequenced and assigned to pickers by same algorithm above.

FTWB: There a particular time interval in fixed-time window batching algorithm, all processes occur within the time window. When the time window ends, orders arrived in the time window are collected and assigned to batches by the same aisle-based algorithm, then the batches are sequenced and assigned to pickers by same algorithm. The FTWB can be as a special form of reservation mechanism, i.e. all order must be reserved for a time window. This reservation is also for the optimization of the *service time* of batches and orders.

Result

Instances and Parameters

The experiment instances come from the real order data of an e-commerce warehouse. The warehouse setting and describe of order data see the above section. The parameters of experiment refer to Henn [4]. The depot is in the lower left corner. There are 16 aisles and each aisle has 90 pick location. There is total 1440 pick locations. The length of aisle is 45 and the width is 5. The size of pick location is 1×1. The *setup time* of the batch is 3 min. The travel speed of pickers is 48 length unit/min. The picking speed is 6 items/min. The batch size is 24 orders. The predict span used in AutoGluon model is 30 min. The time interval of FTWB is also 30 min to be compared. The instance of numerical experiments is the orders data of testing set. We use the orders of the first half day considering the calculation time limit, there is 14446 orders in total, average order arrival rate is 20 per min. The *predictive score* range 0 to 1348, average 430. About the AutoGluon model, the R2_score of the model on the valid set is 0.97 and the Pearson rate is 0.99. Thus, the regression model can accurately predict the *predictive score* of orders. The feature importance could be obtained from the SHAP value. The aisles of A class have greater SHAP value, which means orders with A class aisles have greater *predictive score.* This accord with the calculation of *predictive score.* Orders with class A aisles arrive more frequently, so they are easier to optimize in the future and thus get better scores. The arrive time is also an important feature, which reflects the temporal characteristics of the model. That means the same order will get different *predictive scores* at different times because the time distribution of the order arrival is different.

Sensitivity Analysis of Threshold

The threshold in the reserving algorithm controls the intensity of order release. Appropriate threshold makes orders easier to release and vice versa. It is similar to a hyper-parameter of the algorithm and influence the effect of the algorithm. Thus, we tested the optimal released threshold for different numbers of pickers on the algorithm. As Fig. 12.3, the heatmap reflects the influence of threshold change on order turnover time under different picker quantity (has been standardized). The darker the colour, the closer it is to the optimal value. There is a significant positive correlation between the number of picker and the *predictive score* threshold. That is, the higher the number of pickers, the higher the threshold should be set.

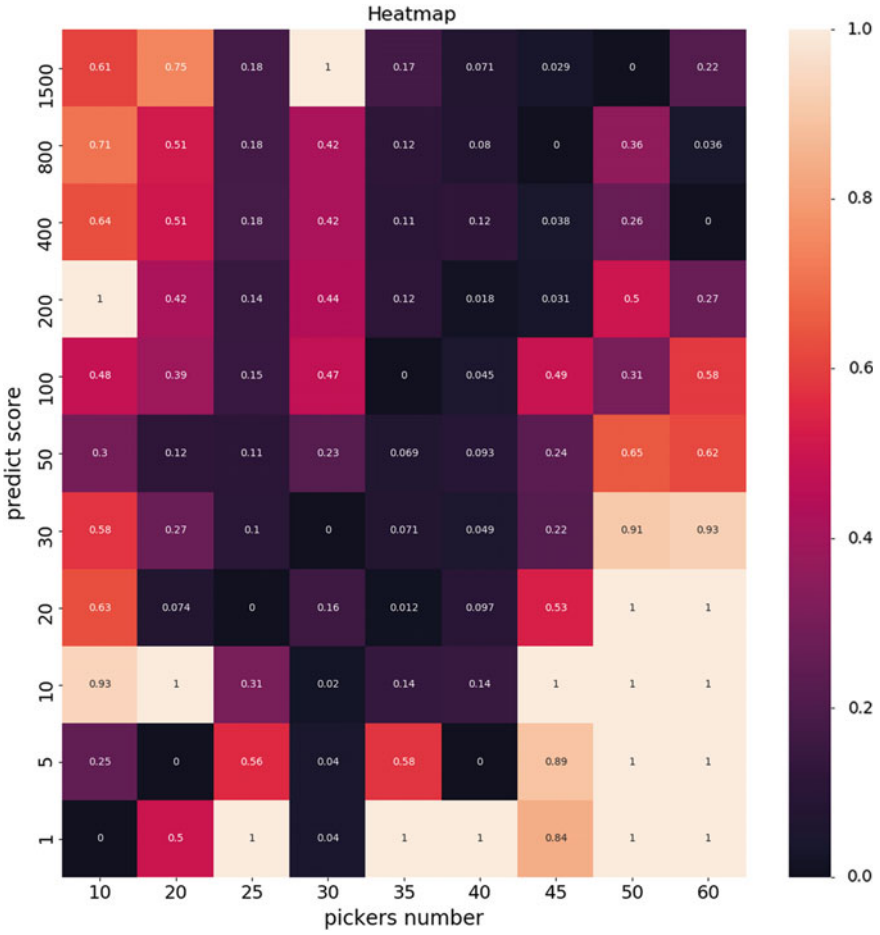

Fig. 12.3 The heatmap of pickers number and predictive score

Numerical Experiments

In Table 12.3, the results for different algorithm are presented. The bold type represents the optimal value under the corresponding column. First, as the number of pickers increases (the more idle the system becomes), the order turnover time, complete time decreases and pickers idle time increase. On the whole, the algorithm has an advantage in the performance of turnover time, especially when the number of pickers is small (less than 40). When the number of pickers is large, the influence of reservation is small and the algorithm with reservation is similar to the algorithm without it. Thus, the performance of the two algorithms is relatively closer. About FTWB and VTWB, they have poor performance on turnover time. When pickers are less, the FTWB is better than the VTWB, and vice versa. On service time, our

algorithm performs best when number of pickers is 10. In the rest of the scenario, FTWB always performs best. The service time and batch volume of our algorithm increases as the number of pickers increases. In FTWB and VTWB, they are fixed value. This shows strong robustness of our algorithm. About the complete time, our algorithm also performed significantly better.

Table 12.3 Result of numerical experiment

Pickers	Algorithm	Turnover time	Service time	Complete time	Pikers idle time	Batch volume
10	Reservation	**242.56**	**13,939.90**	**1401.02**	**2.00**	23.88
	No reservation	244.62	13,965.31	1401.42	**2.00**	23.88
	VTWB	465.53	18,035.48	1828.50	3.10	24.00
	FTWB	312.09	14,242.71	1454.88	24.81	23.49
20	Reservation	**68.52**	16,642.75	**943.75**	102.89	17.24
	No reservation	134.70	16,739.33	948.08	**102.39**	17.26
	VTWB	70.97	18,035.48	1085.31	166.70	24.00
	FTWB	106.98	**14,242.71**	959.37	245.04	23.49
30	Reservation	**34.44**	18,027.98	**817.69**	205.44	16.02
	No reservation	35.44	18,154.08	818.17	**205.26**	15.98
	VTWB	69.85	18,035.48	899.33	279.40	24.00
	FTWB	59.82	**14,242.71**	835.08	345.87	23.49
40	Reservation	**25.82**	19,183.73	785.77	273.99	15.27
	No reservation	25.97	19,263.60	786.04	**273.92**	15.25
	VTWB	44.84	18,035.48	813.96	344.92	24.00
	FTWB	44.04	**14,242.71**	**784.42**	409.20	23.49
50	Reservation	23.59	20,199.23	772.00	331.07	14.64
	No reservation	**23.32**	20,199.75	**763.04**	330.99	14.56
	VTWB	34.12	18,035.48	768.50	391.36	24.00
	FTWB	39.16	14,242.71	778.19	462.06	23.49
60	Reservation	**22.84**	20,769.17	753.94	385.52	14.16
	No reservation	22.86	20,777.40	753.94	**385.40**	14.16
	VTWB	30.64	18,035.48	**753.38**	433.26	24.00
	FTWB	37.92	**14,242.71**	778.19	504.95	23.49

Summary

In this paper we studied on-line order batching with reservation mechanism. We developed a reserving algorithm based on machine learning model. A complete algorithm with reservation was designed to minimize the order turnover time. Compared to VTWB and FTWB, our algorithm has better performance on decreasing turnover time. By predicting future orders, this reservation mechanism could to improve the performance to approximate global optimization, although, this improvement is limited. The further research can focus on increasing the improvement by accurately sketching data distribution of orders, order similarity. A customized model of on-line order batching problem with reservation mechanism is also worth investigating.

Acknowledgements This work was supported by the National Natural Science Foundation of China (Grant No. 71572090), the Shenzhen Basic Research Programs, China (Grant Nos. JCYJ20180306174223343 and JCYJ20190813172201684), a grant from the Institute for Guo Qiang, Tsinghua University, China and supported by Graduate Education Innovation Grants, Tsinghua University.

References

1. Zhang, J., Wang, X., Chan, F. T. S., & Ruan, J. (2017). On-line order batching and sequencing problem with multiple pickers: A hybrid rule-based algorithm. *Applied Mathematical Modelling, 45*(Suppl. C), 271–284.
2. De Koster, R., Le-Duc, T., & Roodbergen, K. J. (2007). Design and control of warehouse order picking: A literature review. *European Journal of Operational Research, 182*(2), 481–501.
3. Henn, S. (2012). Algorithms for on-line order batching in an order picking warehouse. *Computers and Operations Research, 39*(11), 2549–2563.
4. Gil-Borrás, S, Pardo, E. G., Alonso-Ayuso, A., & Duarte, A. (2021). A heuristic approach for the online order batching problem with multiple pickers. *Computer and Industrial Engineering, 160*(May), 107517. https://doi.org/10.1016/j.cie.2021.107517
5. Van Der Gaast, J. P., Jargalsaikhan, B., & Roodbergen, K. J. (2018). *Dynamic batching for order picking in warehouses*. p. 2018.
6. Lu, W., McFarlane, D., Giannikas, V., & Zhang, Q. (2016). An algorithm for dynamic order-picking in warehouse operations. *European Journal of Operational Research, 248*(1), 107–122. https://doi.org/10.1016/j.ejor.2015.06.074
7. Giannikas, V., Lu, W., Robertson, B., & McFarlane, D. (2017). An interventionist strategy for warehouse order picking: Evidence from two case studies. *International Journal of Production Economics, 189*(April 2016), 63–76. https://doi.org/10.1016/j.ijpe.2017.04.002
8. Erickson, N., Mueller, J., Shirkov, A., Zhang, H., Larroy, P., Li, M., & Smola, A. (2020). AutoGluon-tabular: Robust and accurate AutoML for structured data, [Online]. Available: http://arxiv.org/abs/2003.06505
9. Gademann, N., & van de Velde, S. (2005). Order batching to minimize total travel time in a parallel-aisle warehouse. *IIE Transactions (Institute Industrial Engineering), 37*(1), 63–75. https://doi.org/10.1080/07408170590516917
10. Muter, I., & Öncan, T. (2015). An exact solution approach for the order batching problem. *IIE Transactions (Institute Industrial Engineering), 47*(7), 728–738. https://doi.org/10.1080/0740817X.2014.991478

11. Aboelfotoh, A., Singh, M., & Suer, G. (2019). Order batching optimization for warehouses with cluster-picking. *Procedia Manufacturing, 39*(2019), 1464–1473. https://doi.org/10.1016/j.promfg.2020.01.302
12. Albareda-Sambola, M., Alonso-Ayuso, A., Molina, E., & De Blas, C. S. (2009). Variable neighborhood search for order batching in a warehouse. *Asia-Pacific Journal of Operational Research, 26*(5), 655–683. https://doi.org/10.1142/S0217595909002390
13. Henn, S., Koch, S., Doerner, K. F., Strauss, C., & Wäscher, G. (2010). Tabu search heuristics for the order batching problem in manual order picking systems. *Business Research, 3*(1), 82–105. https://doi.org/10.1007/BF03342717
14. Žulj, I., Kramer, S., & Schneider, M. (2018). A hybrid of adaptive large neighborhood search and tabu search for the order-batching problem. *European Journal of Operational Research, 264*(2), 653–664. https://doi.org/10.1016/j.ejor.2017.06.056
15. Henn, S. (2015). Order batching and sequencing for the minimization of the total tardiness in picker-to-part warehouses. *Flexible Services and Manufacturing Journal, 27*(1), 86–114. https://doi.org/10.1007/s10696-012-9164-1
16. Menéndez, B., Bustillo, M., Pardo, E. G., & Duarte, A. (2017). General variable neighborhood search for the order batching and sequencing problem. *European Journal of Operational Research, 263*(1), 82–93. https://doi.org/10.1016/j.ejor.2017.05.001
17. Muter, İ., & Öncan, T. (2021). Order batching and picker scheduling in warehouse order picking. *IISE Transactions* 1–13. https://doi.org/10.1080/24725854.2021.1925178
18. Matusiak, M., de Koster, R., & Saarinen, J. (2017). Utilizing individual picker skills to improve order batching in a warehouse. *European Journal of Operational Research, 263*(3), 888–899. https://doi.org/10.1016/j.ejor.2017.05.002
19. Cergibozan, Ç., & Tasan, A. S. (2019). Order batching operations: An overview of classification, solution techniques, and future research. *Journal of Intelligent Manufacturing, 30*(1), 335–349. https://doi.org/10.1007/s10845-016-1248-4
20. Alipour, M., Zare Mehrjedrdi, Y., & Mostafaeipour, A. (2020). A rule-based heuristic algorithm for on-line order batching and scheduling in an order picking warehouse with multiple pickers. *RAIRO—Operational Research, 54*(1), 101–117. https://doi.org/10.1051/ro/2018069
21. Dauod, H., & Won, D. (2021). Real-time order picking planning framework for warehouses and distribution centres. *International Journal of Production Research*. https://doi.org/10.1080/00207543.2021.1961037
22. Chen, M. C., & Wu, H. P. (2005). An association-based clustering approach to order batching considering customer demand patterns. *Omega, 33*(4), 333–343. https://doi.org/10.1016/j.omega.2004.05.003
23. Pérez-Rodríguez, R., Hernández-Aguirre, A., & Jöns, S. (2015). A continuous estimation of distribution algorithm for the online order-batching problem. *International Journal of Advanced Manufacturing Technology, 79*(1–4), 569–588. https://doi.org/10.1007/s00170-015-6835-6
24. Fuentes Saenz, H. (2011). Data mining framework for batching orders in real-time warehouse operations. *ProQuest Dissertation Theses*, 60, [Online].
25. Cals, B., Zhang, Y., Dijkman, R., & van Dorst, C. (2021). Solving the online batching problem using deep reinforcement learning. *Computers and Industrial Engineering, 156*(March), 107221. https://doi.org/10.1016/j.cie.2021.107221

Chapter 13
Human-Robotic Collaborative Mode Analysis in Human-Robotic Collaborative Order Picking Systems

Shanshan Song, Peng Yang, Zixin Shao, and Yeming Gong

Abstract Human-robotic collaborative order picking system is a flexible and high-efficient warehouse picking system, which integrates the advantages of manual picking system and robotic warehousing system. We are first to propose three collaborative modes, namely **Couple**, **Robot-in-lead**, **Picker-in-lead**, and discuss the resource allocation and zoning strategies in these modes. To investigate the system performance under these modes, we formulate fork-join queueing network models in which an arrive batch orders will be split into robot tasks and picker tasks. We develop an approximation method to estimate the system performance and validate the analytical models by simulation. Numerical experiments are carried out to compare the system throughout time of collaborative modes under different resource allocation and zoning strategies. The results show that, to achieve resource allocation balance, **Couple** should make the number of robots equal with pickers, **Robot-in-lead** should make the number of pickers more than robots, and Picker-in-lead only need to make the number of pickers sufficient. **Robot-in-lead** can benefit from zoning strategy. More zones and pickers will lead to the decrease of the minimal system throughout time, but it does not work in **Picker-in-lead**. If company does not pursue lowest system throughput time, **Picker-in-lead** is the best choice. If company is well-capitalized, **Robot-in-lead** will decrease the system throughout time.

Keywords Human-robotic collaborative order picking system · Fork-join queuing network · Collaborative modes · Warehouse

S. Song · P. Yang (✉) · Z. Shao
Research Center for Modern Logistics, Shenzhen International Graduate School, Tsinghua University, Shenzhen 518055, China
e-mail: yang.peng@sz.tsinghua.edu.cn

S. Song
e-mail: sss20@mails.tsinghua.edu.cn

Z. Shao
e-mail: shao-zx19@mails.tsinghua.edu.cn

Y. Gong
EMLYON Business School, Ecully, France
e-mail: GONG@em-lyon.com

R. Qiu et al. (eds.), *City, Society, and Digital Transformation*, Lecture Notes in Operations Research, https://doi.org/10.1007/978-3-031-15644-1_13

Introduction

Order picking is the most laborious and expensive process, accounts for up to 55% of operation costs in distribution centres, therefore it is not surprising that this process is focused by the academia and enterprises [1]. In traditional manual picking system, although it has high operational flexibility, it is hard to avoid facing the serious challenges such as increasing cost of labour, shortage of land resources and diversification of consumer demand. In addition, from the perspective of human factor, order picking is repetitive, high intensity and poor ergonomic which may affect job satisfaction and health. Automatic picking system which can replace human work gives a feasible solution for enterprises to handle these problems, but it also has some disadvantages such as high capital investment and low system flexibility. In order to strike a balance between manual picking system and automatic picking system, human-robotic collaborative order picking system, also known as AGVs-assisted order picking system, came into being, which can improve efficiency but not loss feasibility.

In this system, batch orders arrive and then are assigned to idle pickers or robots. During the period of collaboration, pickers only need to complete the picking action, robots equipped with a picking cart with multiple bins and transport them to the depot, which greatly reduces the unproductive walking time of pickers and enables order picking process more efficiently and ergonomically. On the other hand, the human-robotic collaborative order picking system has good extensibility and can quickly adapt to different workload. Enterprises can gradually realize the transition from manual picking system to this system, therefor the investment cost and risk brought by automation are significantly reduced. Up to now, although few work has studies the human-robotic collaboration system, several companies have applied it into practice, such as Fetch Robotics, Locus Robotics, 6 River Systems and Toyota, etc., and ABI Research figures out that human-robotic collaborative order picking system has good prospects and will be implemented in over 50,000 warehoused by 2025 [2].

The close collaboration of pickers and robots makes it different from manual picking system and automatic picking system, almost all studies so far are focus on the operation policies, such as order batching, zoning and routing. However, the research about modes how pickers collaborated with robots is neglected, which may significantly influence the system performance. The dimension of research will also be expanded by exploring novel collaborative modes. Since the studies, discussing the collaborative modes and based on it to evaluate the effect of system design and operation policy, are lacking.

This paper focused on the modes innovation and system analysis. We propose three collaborative modes according to whether pickers and robots are dedicated to each other in single batch order process tour, including (1) **Couple**, pickers and robots are both dedicated, (2) **Robot-in-lead** robot collaborate with pickers in sequential zones, (3) **Picker-in-lead**, picker collaborate with robots in sequential zones. We develop a

fork-join queuing network (FJQN) to model the operation process of collaboration modes and evaluate the performance of these modes effectively.

The prime contributions of this paper are as follows: (1) we are first to explore the collaborative modes from the perspective of order batch process method for a human-robotic collaborative order picking system, (2) we develop a fork-join queuing network to capture the parallel movement of the pickers and the robots, (3) we evaluate the resource allocation for all modes and discuss the zoning strategy in modes of **Robot-in-lead** and **Picker-in-lead**.

The remainder of this paper is organized as follows: Sect. Literature Review presents related literature. Section Collaborative Modes and Modelling describes three collaborative modes, and we model these modes by the fork-join queueing network. Section Solution Method for Queueing Network introduce the approximation methods applied for performance estimation. Section Analytical Model Validation and Numerical Experiments contains the simulation validation and numerical experiments. Section Summary presents conclusion.

Literature Review

In this section, we mainly review the literature on human-robotic collaborative order picking systems, automatic picking system and manual picking system, which contributes to system analysis, design optimization, operations planning and control.

Collaborative picking systems: Azadeh et al. [3] and Boysen et al. [4] both pointed out that human-robotic collaborative order picking system has broad prospect in future research and practice application, and the models to analyse the system require to be re-established since the characteristics of this system are different from the perspective of development of robotized and automated warehouse system and warehouse in e-commerce era respectively. In addition, the latter status *fixed-assignment* policy and *free-floating* policy according to whether robot are fixedly assigned to a specific picker. Loffler et al. [5] proposed the important decision problems in different stages of system operation, such as resource allocation in start-up stage. For the fixed-assignment policy, Loffler et al. [6] developed a polynomial time route algorithm and heuristic algorithm to order scheduling, then pointed out that when the approximate optimal sequence is adopted, the walking time of pickers is reduced by 20% compared with the manual picking. Azadeh et al. [7] focused on dynamic zoning and develop a novel closed queuing network model using the technique of two-phase queuing servers, showed that the dynamic zoning can reduce the operating cost by up to 7%. For the free-floating policy, Savannah et al. [8] developed analytical model of zonal picking and verified it by simulation. Under the current pricing system and speed limit, this system is suitable for the warehouse with low picking density and throughput. Loffler et al. [5] proposed that sharing robots can have a pooling effect and reduce the number of robots. Lee and Murray [9] defined a new routing problem that seeks to minimize the total time transporting all items from pick station to depot. They established mixed integer linear programming model

and carried out a large number of numerical analyses, the results showed that when there are more aisles or fewer cross aisles in the warehouse, the system improves significantly compared with the manual picking system. Zulj et al. [10] proposed a new collaborative mode, the picker and robot delivery goods at a fixed location, robots transport goods to depot, and they developed mixed integer programming and heuristic method to evaluate the influence of robot scale and human–robot speed ratio.

Automatic picking system: The review of automatic picking system focuses on AVS/RS and RMFS. In system analysis, Cai et al. [11] developed a multi-class SOQN model for tier-to-tier AVS/RS by modelling the storage and retrieval requests as different classes of customers. Zou et al. [12] developed FJQN model to simulate the parallel movement of vehicle and lift in AVS/RS, and the accuracy of analytical model is verified by simulation. For RMFS, Nigam et al. [13] developed a travel time model and a closed queuing network (CQN) in the situation of single-line order and classified storage, and the system performance was evaluated by robot utilization, system throughput and expected order processing time. Lamballais [14] developed four SOQN models according to single-line or multi-line orders and whether classified storage was used. In design optimization, For AVS/RS, Roy et al. [15] found that the optimal position of cross aisle was set at the end of aisle. For RMFS, Lamballais et al. [6] showed that the maximum throughput was not sensitive to the length ratio of the storage area, but was directly affected by the location of the workstation. In order to achieve higher system throughput, workstations should be located west and east of the storage area if classified storage is used, and vice versa. Yuan and Gong [16] found the optimal number of robots with the goal of minimizing system throughput time. In operation planning and control, For AVS/RS, Cai et al. [11] analysed and compared two kinds of vehicle dwell point strategy, namely point of service completion (POSC) and return I/O point strategy, they found that the former is more suitable. Zou et al. [12] showed that the parallel processing strategy is better than the sequential processing strategy with the height of more than 10 layers and the length-height ratio of more than 7. For RMFS, Nigam et al. [13] discussed pods assignment, the results showed that though closest-open location pod storage policy do not allow to efficiently use the storage spaces in comparison to random location pod storage policy in an aisle, it increases the system throughput for all item classes. Roy et al. [17] studied the robot allocation between the replenishment and picking processes, analysed the situations in which the robots performed replenishment and picking process respectively or jointly. The results show that robots shared between picking and replenishment process significantly reduces the expected order picking time, but also increases the expected replenishment time.

Manual picking system: Due to the high investment of automated equipment, manual picking is still the first choice for many warehouses. In system analysis, Altarazi and Am-mouri [18] proposed a simultaneous simulation-based approach, which can investigate all possible warehousing design combinations with their stochastic nature and interactions. The results show that horizontal layout was preferable over all other types of layouts and small size warehouses perform better than other large sizes. Cheng et al. [19] developed a hybrid approach to solve a joint

order batching and picker routing problem, the core of it is the particle swarm optimization (PSO) and the ant colony optimization (ACO) algorithms. In design optimization, Roodbergen and Vis [20] focused on a layout of single block, and an optimization model was established to find the optimal number of aisles. Roodbergen et al. [21] further extended the study and proposed an optimization model that could consider the layout of any number of blocks and aisles. Taking the minimum average walking distance as the goal, the layout obtained was basically similar to the simulation results, and the distance error difference was 0.3% on average and 2.3% at most. In operation planning, Henn et al. [22] pointed out that the storage location of goods in the warehouse has a specific structure, which makes it different from the general TSP problem. It takes this special property into consideration and establishes a mathematical programming model to better solve the single-person routing problem under a single block. Yang et al. [23] proposed a novel continuous order picking strategy, namely flow-picking strategy, showed that it required fewer pickers and shorter walking distance compared with batch picking.

According to the mentioned literature, we are the first to discuss the collaborative modes in human-robotic collaborative picking system, and queuing network is the important ways to analyse and evaluate the system performance. In addition, SOQN has the characteristics of both CQN and OQN, can simulate the waiting time of resources or jobs, and FJQN can better simulate the parallel process of tasks.

Collaborative Modes and Modelling

We present the operation process of human-robotic collaborative order picking systems under three collaborative modes in this section. Human-robotic collaborative order picking system are mainly supported by Warehouse Management System (WMS), RFID reader and robots. WMS assigns tasks to the scheduling system to generate batch orders and plan optimal routes, then sends to the robots and pickers, RFID reader can help pickers to get demand. The biggest feature of this system is the collaborative process of pickers and robots. Batch orders arrive and are assigned to an idle robot and picker, then they bend and walk through all the aisles together to pick the required items. Once finishing the picklist, they will unbind and robot transport the items back to the depot. Based on this, we proposed basic mode **Couple** which one robot and one picker bound to complete a batch order. The extension to this mode is to include match modes and storage zones. In **Robot-in-lead**, robots are bound with batch order, pickers are dedicated to multiple zones, robot need collaborative with pickers to in each zone. However, the character of robots and pickers will be switched in **Picker-in-lead**.

Table 13.1 Main notation

Notation	Description	Notation	Description
N	The number of zones in storage area	u_{rf}, u_{pf}	The service rate of robots/pickers travel from the depot/the point of service completion to the first picking point
k, p	The number of robots/pickers	u_{rl}, u_{pl}	The service rate of robots/pickers complete the left picking list
u_{lr}, u_{lf}	The service rate of robots travelling from the begin aisle/ the buffer before the conveyor to the aisle pickers in	u_d	The service rate of robots going back to the depot
p_l	The probability that robots in the edge aisle far from the pickers	p_r	The probability that pickers in the rightmost aisle within a zone

Assumptions and Notation

We make the following assumptions for the queueing network models:

(1) We use the random storage policy, items required by a batch order are evenly distributed in aisles, and the picking location in each aisle are sequential statistic;
(2) The number of aisles is even to ensure that the operation process of batch orders always begin and finish at the bottom of the area or the zones;
(3) Next batch order always begin at the picking location near the dwell point of pickers, and pickers *walk back* after completing last batch order to reduce the walk distance of traversing the area or zone.
(4) The way pickers and robots tour the areas or zones for operation process of batch orders is S-shape route.
(5) The robots and pickers follow a Point-of-Service-Completion (POSC) dwell point policy.
(6) The items stored in shelves can always satisfied the demand, the replenishment process will not be considered (Table 13.1).

Mode1: Couple

Figure 13.1 shows the layout of **Couple**, it is composed of depot, shelves, collaborative robots and pickers, and depot is located in middle below the picking area. When batch orders arrive the system, warehouse management system (WMS) will assign them to an idle robot and picker. Then, robot and picker travel from their dwell point to the first picking point, namely depot and the point of service completion respectively. After meeting and binding with each other, they tour the area with S-shape to pick the items required by the batch order. Once completing, picker do not need back to depot but return and start processing next batch order directly. Return ensure

that each process starts at the aisle picker in, it can reduce the travel time of picker. We model this mode as a semi-open queueing network, shows in Fig. 13.2.

In this semi-open queueing network, the batch orders arrive at the fork node with arrival rate λ, robots are modelled as mobile resources, and batch orders need to be matched with robots in the synchronization station which includes a batch order queue Q_o and a robot queue Q_R, before they can be served. Hence, batch orders wait for idle robots in queue Q_o, and the idle robot wait for the arrival of batch orders in Q_R.

The collaborative process is modelled by fork-join queuing network, the batch order is split into robot tasks and pickers tasks in the fork node. For robot tasks, the batch order goes to stations u_{rf} where the robot travels from the depot to the first picking point, and u_{rl} where the robot completes the remaining picklist, and once finished it wait in the join queue of robot tasks, denoted by Q_r. The process of picker

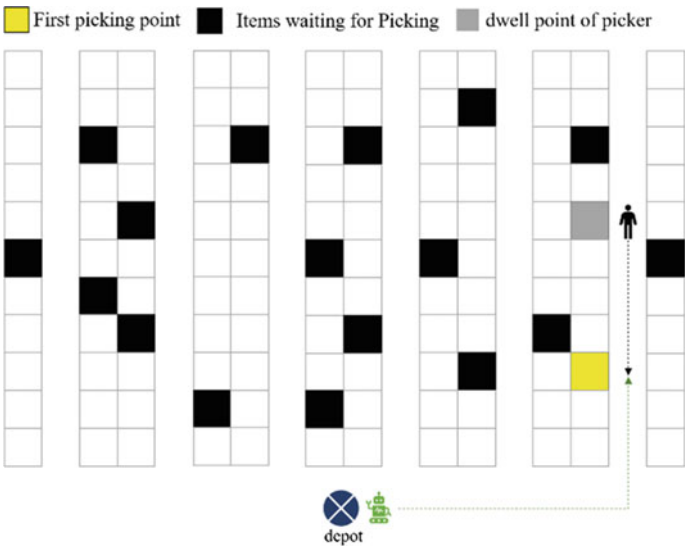

Fig. 13.1 The layout of **Couple**

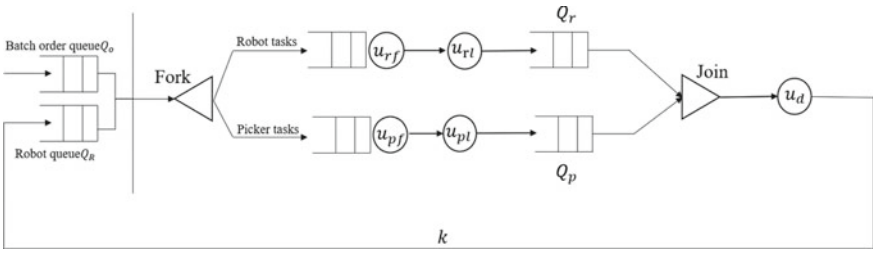

Fig. 13.2 The queueing network of **Couple**

tasks is same as the robot tasks. After the completion of two tasks, they depart their join queues and join at the join node. Then, the batch order goes to the station u_d where the robot transport the loads to the depot.

Mode2: Robot-In-Lead

Figure 13.3 shows the layout of **Robot-in-lead**, the area is split into several zones. In this mode, WMS assigns the batch order to an idle robot, then robot from the leftmost zone enter the area and match with an idle picker in each zone repeatedly. Within the zone, the collaborative process likes **Couple**. Because robots and pickers tour the zone with S-shape, pickers must stop at the edge aisle after the completion of operation process, they have the possibility $\boldsymbol{p_r}$ in the rightmost aisle, so batch order has the possibility $\boldsymbol{p_r}$ to go to the station $\boldsymbol{u_{lr}}$ where robot go from the leftmost aisle to the rightmost aisle. Exceptionally, For the leftmost and rightmost zone in the area, robot enter the zone from which edge aisles doesn't matter. The queueing network of this mode shows in Fig. 13.4.

In the fork-join queueing network, the times of collaborative process of robots and pickers are equal with the number of zones, so the robot and picker tasks are different from **Couple**. For robot tasks, the batch order should choose whether goes to the edge aisle far from them ***N-2*** times. For picker tasks, in each zone, the batch order goes to the stations $\boldsymbol{u_{lr}}$ where the picker traveling from the point of service completion to the first picking point, and $\boldsymbol{u_{pl}}$ where the picker completes the remaining picklist, this process need repeat $\boldsymbol{N}$ times.

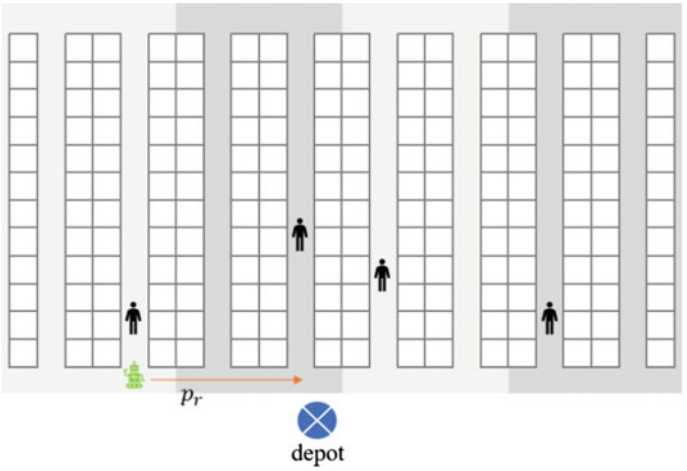

Fig. 13.3 The layout of **Robot-in-lead**

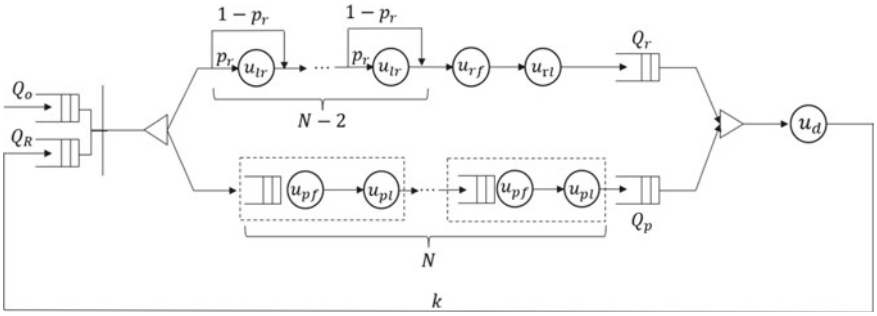

Fig. 13.4 The queueing network of **Robot-in-lead**

Mode3: Picker-In-Lead

Figure 13.5 shows the layout of **Picker-in-lead**, the area is split into several zones, and depot is replaced by a conveyor. In this mode, WMS assigns the batch order to an idle picker, then picker begin the operation process in the point of service completion and match with an idle robot in each zone repeatedly. Within the zone, an idle robots must be in the edge aisle, so it has the possibility p_l from the leftmost aisle and $1 - p_l$ from the rightmost aisle to the first picking point. The queueing network of this mode shows in Fig. 13.6.

In this queueing network, pickers are modeled as mobile resource, and batch order need to be matched with them in the synchronization station which includes a batch order queue Q_o and a picker queue Q_H. For robot tasks, in each zone, the batch order has the possibility p_l to go to the station u_{lf} where the robot travels from the

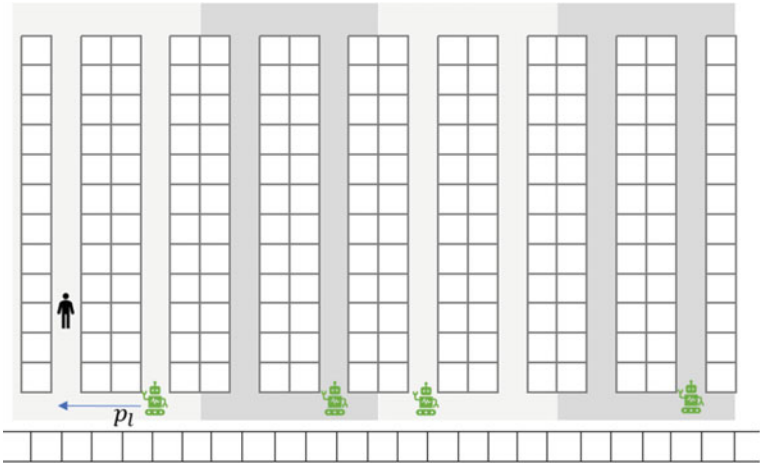

Fig. 13.5 The layout of **Picker-in-lead**

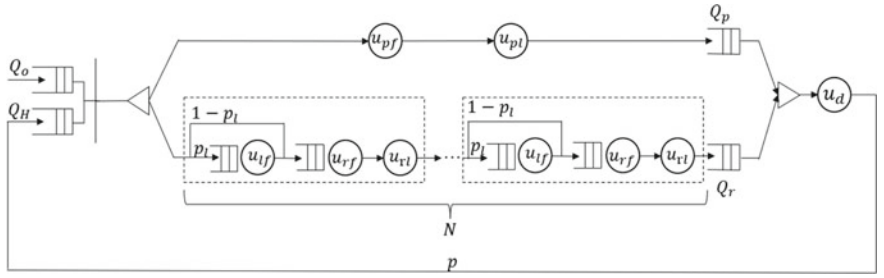

Fig. 13.6 The queueing network of **Picker-in-lead**

buffer before conveyor in edge aisle far from pickers, then goes to the station u_{rf} where the robot travels from the depot to the first picking point, and u_{rl} where the robot completes the remaining picklist. This process needs repeat $\boldsymbol{N}$ times. Picker tasks are same as **Couple**.

Solution Method for Queueing Network

In this section, we develop an approximation method of the queueing network mentioned in Sect. Collaborative Modes and Modelling to estimate the performance measures of the system, since semi-open queueing network doesn't have product-form solution since it has generally distributed service time stations. We use aggregation method to replace the fork-join queueing subnetwork by a load-dependent node, and then use matrix-geometric method (MGM) to solve the composite network (Bolch et al. [24]). The approximation method includes the following steps:

(1) The first step is the estimation of the load-dependent service rate of the fork-join queuing network, including three sub-steps.

   (a) We build a closed queuing network CQN_1 by short-circuiting FJQN, and define the number of states $\boldsymbol{Z_{FJ}(k)}$ in CQN_1 with $\boldsymbol{k}$ robots.
   (b) We establish a new product-form closed queuing network CQN_2 with $\boldsymbol{K}$ robots whose states are approximately equal to the CQN_1 by eliminating the queuing queues, and the throughput $\boldsymbol{\lambda_{PF}(K)}$ of this product-form network is calculated by Approximate Mean Value Analysis (AMVA) algorithm which is regarded as the $\boldsymbol{\lambda_{FJ}(K)}$ of the CQN_1.
   (c) We aggregated the FJQN into a load-dependent node with the service rate $\boldsymbol{\mu(k) = \lambda_{FJ}(k)}$.

(2) The second step is performance evaluation of SOQN, we use the matrix-geometric method (MGM) to derive the steady the state probabilities of the SOQN.

Estimation of Load-Dependent Service Rate of FJQN

We estimate the load-dependent service rate of FJQN in three steps. Firstly, we build a closed queueing network CQN_l by short-circuiting FJQN. If $\boldsymbol{n}$ denotes the number of parallel branches, the ith branch has n_i nodes and k tasks, then the number of states in the CQN_l is given by:

$$Z_{FJ}(k) = \prod_{i=1}^{N} z_i(k) - \prod_{i=1}^{N} z_i(k-1)$$

Secondly, we establish a new product-form CQN_2 with exactly the same $M = \sum_{i=1}^{N} n_i$ number of nodes as the subnetwork. The number of jobs $\boldsymbol{K}$ is chosen to make the number of states in CQN_2 is approximately equal to the number of states in the CQN_1. Since the state-space structures of both networks are almost identical, the throughput of the product-form network $\boldsymbol{\lambda_{PF}(K)}$ will be approximatively equal to the throughput of the fork-join network $\lambda_{FJ}(k)$. The $\boldsymbol{K}$ is determined by:

$$K : |Z_{FJ}(k) - Z_{PF}(K)| = \min_{l} |Z_{FJ}(k) - Z_{PF}(l)|$$

where $Z_{PF}(K) = z_{M-1}(K)$.

Then, we solve the product-form network use AVMA algorithm to determine the throughput as a function of $\boldsymbol{K}$. Finally, we replace the subnetwork in the given system by an aggregated node whose load-dependent service $\mu(k) = \lambda_{FJ}(k)$.

Estimation of the Performance Measures of SOQN

The states of the SOQN are denoted by ($\boldsymbol{a}$, $\boldsymbol{b}$, $\boldsymbol{c}$), where $\boldsymbol{a}$ is the number of batch orders in external queue, $\boldsymbol{b}$ is the number of jobs at the first aggregation station and $\boldsymbol{c}$ is the number of jobs at the second station. We denote the steady-state probability is $\boldsymbol{\Pi_i}$, the vector of steady-state probability is given by

$$\Pi_0 = \left(\pi_0, \pi_1 \ldots, \pi_{\frac{(N_m+1)(N_m+2)}{2}}\right)$$

$$\Pi_i = \left(\pi_{\frac{(N_m+1)(N_m+2)}{2}+(i-1)(N_m+1)+1}, \pi_{\frac{(N_m+1)(N_m+2)}{2}+i(N_m+1)}\right),\ i \geq 1$$

where i is the number of batch orders in external queue and $\boldsymbol{N_m}$ is the mobile resource in the queuing network.

According to the MGM, the generator matrix $\mathbf{Q}$ of SOQN is given by (1). In (1) the repetitive structure starts from the row including $\mathbf{A}$, $\mathbf{B}$, and $\mathbf{C}$ matrixes.

$$\boldsymbol{Q} = \begin{bmatrix} \boldsymbol{B}_{00} & \boldsymbol{B}_{01} & 0 & 0 & \dots \\ \boldsymbol{B}_{10} & \boldsymbol{B} & \boldsymbol{C} & 0 & \dots \\ 0 & \boldsymbol{A} & \boldsymbol{B} & \boldsymbol{C} & \dots \\ 0 & 0 & \boldsymbol{A} & \boldsymbol{B} & \dots \\ \vdots & \vdots & \vdots & \vdots & \ddots \end{bmatrix}$$

$$B_{00} = \begin{array}{c} (0,0,0) \\ (0,1,0) \\ (0,0,1) \\ (0,2,0) \\ (0,1,1) \\ (0,0,2) \\ \vdots \\ 0, N_m, 0 \\ 0, N-1, 1 \\ 0, N-2, 2 \\ \vdots \\ 0, 1, N_m - 1 \\ 0, 0, N_m \end{array} \begin{bmatrix} -\lambda & \lambda & & & & & & & & \\ 0 & -\mu_1(1)-\lambda & \mu_1(1) & \lambda & 0 & & & & & \\ \mu_2(1) & 0 & -\mu_2(1)-\lambda & 0 & \lambda & & & & & \\ 0 & 0 & 0 & -\mu_2(2)-\lambda & \mu_1(2) & 0 & \lambda & 0 & 0 & \\ 0 & \mu_2(1) & 0 & 0 & -\mu_1(1)-\mu_2(1)-\lambda & \mu_1(1) & 0 & \lambda & 0 & \\ 0 & 0 & \mu_2(2) & 0 & 0 & \mu_2(2)-\lambda & 0 & 0 & \lambda & \\ & & & \ddots & \ddots & \ddots & \ddots & \ddots & \ddots & \\ & & & 0 & & & & -\lambda-\mu_1(N) & \mu_1(N_m) & \\ & & & \mu_2(1) & 0 & & & -\lambda-\mu_2(1)-\mu_1(N-1) & \mu_1(N_m-1) & \\ & & & \ddots & & & & & & \\ & & & & \mu_2(2) & & & & -\lambda-\mu_2(2)-\mu_1(N_m-2) & \mu_2(N_m-2) \\ & & & & \ddots & & & & \ddots & \ddots \\ & & & & & 0 & & & & -\lambda-\mu_2(N_m-1)-\mu_1(1) \\ & & & & & \mu_2(N_m-1) & 0 & & & \\ & & & & & & \mu_2(N_m) & & & -\lambda-\mu_2(N_m) \end{bmatrix}$$

$$B_{01} = \begin{array}{c} (0,0,0) \\ (0,1,0) \\ (0,0,1) \\ (0,2,0) \\ (0,1,1) \\ (0,0,2) \\ \vdots \\ 0, N_m, 0 \\ 0, N-1, 1 \\ 0, N-2, 2 \\ \vdots \\ 0, 1, N_m - 1 \\ 0, 0, N_m \end{array} \begin{bmatrix} \lambda & & & & & \\ & \lambda & & & & \\ & & \lambda & & & \\ & & & \ddots & & \\ & & & & \lambda & \\ & & & & & \lambda \end{bmatrix}$$

$$B_{10} = \begin{matrix} (1, N_m, 0) \\ (1, N_m - 1, 1) \\ (1, N_m - 2, 2) \\ \vdots \\ (1, 1, N_m - 1) \\ (1, 0, N_m) \end{matrix} \begin{bmatrix} 0 & & & & & \\ \mu_2(1) & 0 & & & & \\ & \mu_2(2) & 0 & & & \\ & & \ddots & 0 & & \\ & & & \mu_2(N_m - 1) & 0 & \\ & & & & \mu_2(N_m) & 0 \end{bmatrix}$$

$$C = \begin{matrix} (i, N_m, 0) \\ (i, N_m - 1, 1) \\ (i, N_m - 2, 2) \\ \vdots \\ (i, 1, N_m - 1) \\ (i, 0, N_m) \end{matrix} \begin{bmatrix} 0 & & & & & \\ \mu_2(1) & 0 & & & & \\ & \mu_2(2) & 0 & & & \\ & & \ddots & \ddots & & \\ & & & \mu_2(N_m - 1) & 0 & \\ & & & & \mu_2(N_m) & 0 \end{bmatrix}$$

$$B = \begin{matrix} (i, N_m, 0) \\ (i, N_m) - 1, 1) \\ (i, N_m - 2, 2) \\ \vdots \\ (i, 0, N_m - 1) \\ (i, 0, N_m) \end{matrix} \begin{bmatrix} -\lambda - \mu_1(N_m) & \mu_1(N_m) & & & & \\ & -\lambda - \mu_2(1) - \mu_1(N_m - 1) & \mu_1(N_m - 1) & & & \\ & & -\lambda - \mu_2(2) - \mu_1(N_m - 2) & \mu_1(N_m - 2) & & \\ & & & \ddots & & \\ & & & & -\lambda - \mu_2(N_m - 1) - \mu_1(1) & \mu_1(1) \\ & & & & & -\lambda - \mu_2(N_m) \end{bmatrix}$$

$$A = \begin{matrix} (i, N_m, 0) \\ (i, N_m) - 1, 1) \\ (i, N_m - 2, 2) \\ \vdots \\ (i, 1, N_m - 1) \\ (i, 0, N_m) \end{matrix} \begin{bmatrix} \lambda & & & & & \\ & \lambda & & & & \\ & & \lambda & & & \\ & & & \lambda & & \\ & & & & \lambda & \\ & & & & & \lambda \end{bmatrix}$$

After obtaining the generator matrix $\mathbf{Q}$, we can calculate the rate matrix $\mathbf{R}$ by

$$\boldsymbol{R} = -(\boldsymbol{C} + \boldsymbol{R}^2\boldsymbol{A})\boldsymbol{B}^{-1}$$

The states probability vector $\boldsymbol{\Pi}_0$ and $\boldsymbol{\Pi}_1$ are calculated by,

$$[\Pi_0\ \Pi_1]\begin{bmatrix} e' & B_{00} & B_{01} \\ (I - R)^{-1} & B_{10} & B_{11} + RA \end{bmatrix} = [1\ 0]$$

From the matrix-geometric property, other vector of states probability can be calculated by $\boldsymbol{\pi}_{i+1} = \boldsymbol{\pi}_i\boldsymbol{R}$, $i \geq 1$.

The expected external queue length $\boldsymbol{L_{eq}}$ can be calculated by

$$L_{eq} = \Pi_1 (I - R)^{-2} e$$

The expected number of jobs being processed $\boldsymbol{L_{DC}}$ can be calculated by

$$L_{DC} = \sum_{i+j \leq K} (i + j)\pi(0, i, j) + \sum_{\mathrm{i}=1}^{+\infty} R|\Pi_i|$$

Based on the Little's law, the expected waiting time of resource and system throughout time, the utilization rate of resource can be calculated by

$$W_{N_m} = \frac{L_{eq}}{\lambda}$$
$$THT_{DC} = \frac{L_{eq} + L_{DC}}{\lambda}$$
$$\rho_{N_m} = \frac{L_{DC}}{N_m} \cdot 100\%$$

Analytical Model Validation and Numerical Experiments

In this section, the queueing network formulated in this study is validated by simulation. Then, we carry out a series of numerical experiments to compare the performance of resource allocation in all three collaborative modes, and discuss the zoning strategy in **Robot-in-lead** and **Picker-in-lead**.

Validation with Simulation

We develop three simulation models for three collaborative modes based on MATLAB R2019a. We consider a human-robotic collaborative order picking systems has 16 aisles and 30 location in each aisle, and each batch order has 64 items. To validate the analytical models under different modes and zoning strategy, the arrival rate takes 4 levels in each mode, $\boldsymbol{\lambda} = 10, 20, 40, 60$ per hour, and the number of zones takes 2,4 in **Robot-in-lead** and **Picker-in-lead**, 60 scenarios are examined based on the variation of resource allocation in total.

For each examined case, the simulation model runs 200 h to eliminate the initial bias. We take three performance metrics to validate the analytical models: The expected external queue length $\boldsymbol{L_{eq}}$, system throughout time $\boldsymbol{THT_{DC}}$, the utilization of resource $\boldsymbol{\rho_R}$, respectively. The accuracy of analytical models is measured by

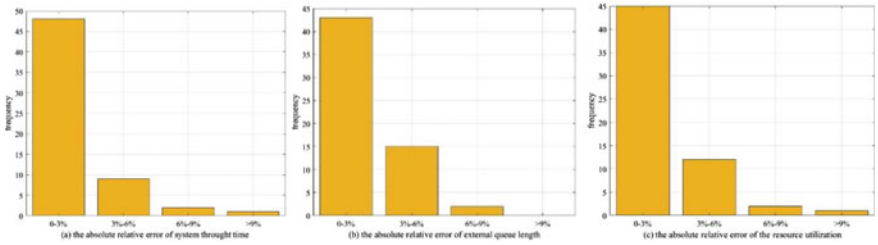

Fig. 13.7 Relative errors of the analytical results to the simulation results

absolute relative error $\boldsymbol{\varepsilon}$.

$$\boldsymbol{\varepsilon} = \frac{|\boldsymbol{R_a} - \boldsymbol{R_s}|}{\boldsymbol{R_s}} \times 100\%$$

The average relative error of analytical results to simulation results is $\boldsymbol{\varepsilon_{THD_{DC}}} = 1.94\%$, $\boldsymbol{\varepsilon_{L_{eq}}} = 2.27\%$, $\boldsymbol{\varepsilon_{\rho_R}} = 2.22\%$. The frequency of the relative error is presented in Fig. 13.7.

The simulation validation results show that the analytical models can accurately estimate the system response time for batch orders, the expected waiting time in the external queue and the utilizations of the resource.

Resource Allocation and Zoning Strategy

In human-robotic collaborative picking system, it is important to optimize resource allocation for avoiding resource slack. We carry out numerical experiments to compare the performance of different number allocation of robots and pickers in each collaborative mode, and the arrive rate of batch orders tasks $\boldsymbol{\lambda} = 10, 30, 60$ per hour.

In **Couple**, the contour line of system throughput time with the variation of resource allocation is almost axially symmetric with the line $y = x$, it means that when the number of robots is equal with the pickers, namely resource allocation balance, the system has reached the optimal resource allocation under the certain throughput time. At this time, increasing the number of robots or pickers may not improve the performance. When resource allocation keeps balance, we find that with the increasing number of resources, the system throughput time decreases exponentially and tends to be stable. When the number of resources is **0.4** times the arrival rate, the system efficiency has been significantly optimized. The minimal system throughout time is reached firstly in a certain resource allocation threshold. Meanwhile, the utilization rate of robots and pickers are close. While resource allocation is unbalanced, more or fewer pickers will lead to the increasement of utilization rate of robots (Fig. 13.8).

In **Robot-in-lead** and **Picker-in-lead**, the contour line of system throughout time is not symmetric with the line $y = x$, resource allocation balance is not realized by the equal number of robots and pickers. For **Robot-in-lead**, the resource allocation balance is more likely to happen when the number of pickers is more than robots. For **Picker-in-lead**, the system gets balance when the number of pickers is efficient (Figs. 13.9 and 13.10).

Meanwhile, we focus on the zoning strategy in **Robot-in-lead** and **Picker-in-lead**, we take the number of zones $N = 2, 4, 8$ to examine the zoning effect for system performance. For **Robot-in-lead**, when the number of pickers reach the threshold in **Couple** with same arrive rate, increasing the number of zones or pickers can decrease

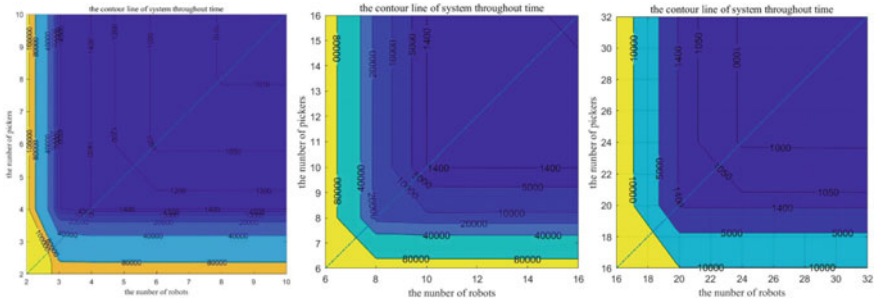

Fig. 13.8 The contour line of system throughout time in **Couple** for $\lambda = 10, 30, 60$

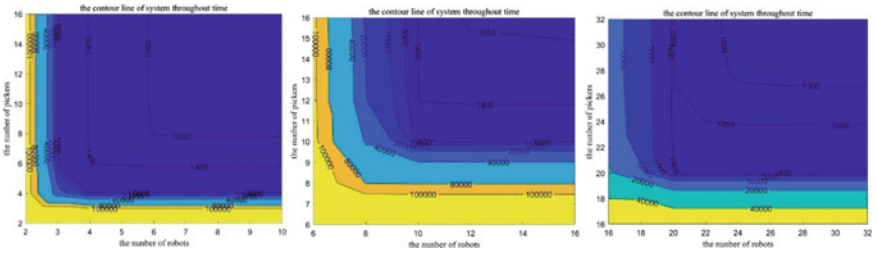

Fig. 13.9 The contour line of system throughout time in **Robot-in-lead** for $\lambda = 10, 30, 60$

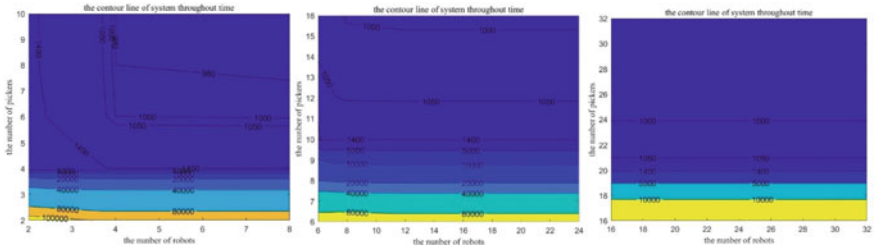

Fig. 13.10 The contour line of system throughout time in **Picker-in-lead** for $\lambda = 10, 30, 60$

the minimal system throughout time achieved by **Couple** up to 10%. However, if the number of pickers less than the threshold, more zones cause greater system imbalances. For **Picker-in-lead**, zoning strategy does not work because it is limited by the travel time of pickers. The comparison of three collaborative is shown in Table 13.2 (Figs. 13.11 and 13.12).

Table 13.2 The comparison of three collaborative modes

Collaborative modes	Characteristics
Couple	1. The optimal system throughout time is bigger than **Robot-in-lead** 2. The optimal system requires the maximum number of robots 3. The optimal system requires the minimum number of pickers
Robot-in-lead	1. The optimal system throughout time is less than other modes 2. The optimal system requires the maximum number of pickers 3. The optimal system requires the number of pickers less than **Couple**
Picker-in-lead	1. The optimal system throughout time ±3% compared to **Couple,** but bigger than **Robot-in-lead** 2. The optimal system requires the minimum number of robots 3. The optimal system requires the number of pickers same as **Couple**

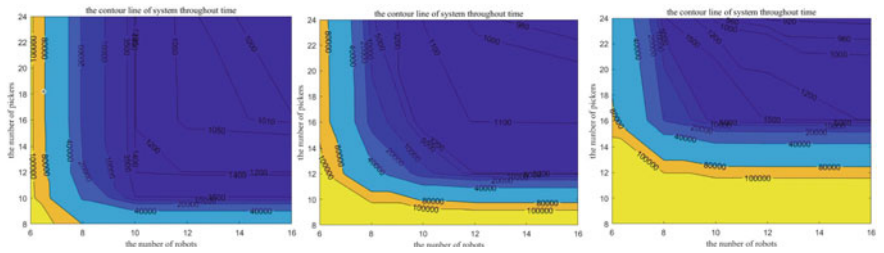

Fig. 13.11 The contour line of system throughout time in **Robot-in-lead** for N = 2, 4, 8

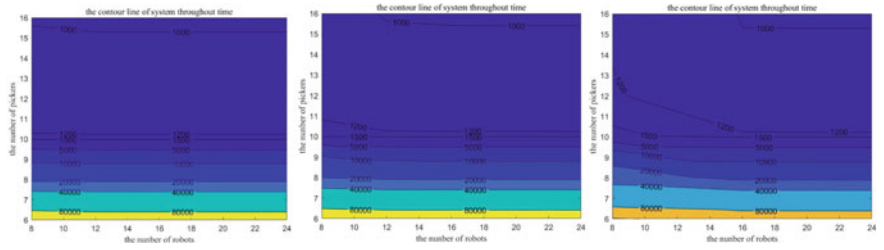

Fig. 13.12 The contour line of system throughout time in **Picker-in-lead** for N = 2, 4, 8

Summary

This study focuses on the collaborative modes of robots and pickers in human-robotic collaborative order picking system. We propose three collaborative modes based on the different batch orders process methods, namely **Couple**, **Robot-in-lead** and **Picker-in-lead**, and discuss the resource allocation in all three modes and zoning strategy in **Robot-in-lead** and **Picker-in-lead**. To investigate the performance of these modes, we formulate a fork-join queueing network in which a batch order will be split into robot tasks branch and picker tasks branch. Then, we develop an approximate method to estimate the system performance, including the system throughout time, expected number of batch orders in external queue, the utilization rate of resource.

We build simulation models to validate the analytical model. The results show that the analytical model can accurately estimate the performance of three collaborative modes. We carry out numerical experiments to compare the system throughout time of resource allocation in all three modes and zoning strategy in **Robot-in-lead** and **Picker-in-lead**. The results show that to achieve resource allocation balance, **Couple** should make the number of robots equal with pickers, **Robot-in-lead** should make the number of pickers more than robots, and **Picker-in-lead** only need make the number of pickers sufficient. Zoning strategy work for **Robot-in-lead**, more zoning and pickers will decrease the minimal system throughout time up to 10% compared to **Couple**, but it does not work in **Picker-in-lead** because of the limit of picker's travel time.

We compare the three collaborative modes, the minimal system throughout time achieved by **Robot-in-lead** is smaller than the other two modes, but it need more pickers than **Couple**. The minimal system throughout time achieved by **Picker-in-lead** $\pm 3\%$ compared to **Couple**, but it only need fewest robots and the number of pickers equals to **Couple**. **Couple** need most robots than the other two modes to achieve the minimal system throughout time. This result shows that if company does not pursue system throughput speed, **Picker-in-lead** is the best choice, but if throughput speed will be a bottleneck of the supply chain and company is well-capitalized, **Robot-in-lead** will decrease the system throughout time.

In future work, it is interesting to investigate the cost comparison for three collaborative modes in a certain service rate. Moreover, we can also examine the different improvement of human factors by these three collaborative modes, it will testify the ergonomics of human-robotic collaborative order picking system.

Acknowledgements This work was supported by the National Natural Science Foundation of China (Grant No. 71572090), the Shenzhen Basic Research Programs, China (Grant Nos. JCYJ20180306174223343 and JCYJ20190813172201684), a grant from the Institute for Guo Qiang, Tsinghua University, China and supported by Graduate Education Innovation Grants, Tsinghua University.

References

1. De Koster, R., Le-Duc, T., & Roodbergen, K. J. (2007). Design and control of warehouse order picking: A literature review. *European Journal of Operational Research, 182*(2), 481–501.
2. ABI Research.: Robotics in e-commerce fulfillment. Accessed May 3, 2019 https://bit.ly/2YwQg3J (2019).
3. Azadeh, K., De Koster, R., & Roy, D. (2019). Robotized and automated warehouse systems: Review and recent developments. *Transportation Science, 53*(4), 917–945.
4. Boysen, N., de Koster, R., & Weidinger, F. (2019). Warehousing in the e-commerce era: A survey. *European Journal of Operational Research, 277*(2), 396–411.
5. Loffler, M., Boysen, N., & Schneider, M. (2021). Picker routing in AGV-assisted order picking systems. *INFORMS Journal on Computing, 01*.
6. Lamballais, T., Roy, D., & De Koster, M. B. (2017b). Estimating performance in a robotic mobile fulfillment system. *European Journal of Operational Research, 256*(3), 976–990.
7. Azadeh, K., Roy, D., & de Koster, M. R. (2020). Dynamic human-robot collaborative picking strategies. *SSRN Electronic Journal*, 1–54.
8. Savannah, I. P., Meller, R. D., Thomas, L. M., & Meller, R. D. (2018). Digital Commons@ Georgia Southern Collaborative Bots in Distribution Centers Collaborative Bots in Distribution Centers..
9. Lee, H. Y., & Murray, C. C. (2019). Robotics in order picking: Evaluating warehouse layouts for pick, place, and transport vehicle routing systems. *International Journal of Production Research, 57*(18), 5821–5841.
10. Zulj, I., Salewski, H., Goeke, D., & Schneider, M. (2021). Order batching and batch sequencing in an AMR-assisted picker-to-parts system. *European Journal of Operational Research.*
11. Cai, X., Heragu, S. S., & Liu, Y. (2014). Modeling and evaluating the AVS/RS with tier-to-tier vehicles using a semi-open queueing network. *IIE Transactions (Institute of Industrial Engineers), 46*(9), 905–927.
12. Zou, B., Xu, X., Gong, Y., & De Koster, R. (2016). Modeling parallel movement of lifts and vehicles in tier-captive vehicle-based warehousing systems. *European Journal of Operational Research, 254*(1), 51–67.
13. Nigam, S., Roy, D., de Koster, R., & Adan, I. (2014). Analysis of class-based storage strategies for the mobile shelf-based order pick system. *Progress in Material Handling Research*, 1–9.
14. Lamballais, T. (2017a). Inventory allocation in robotic mobile fulfillment systems. *SSRN Electronic Journal*, 1–43.
15. Roy, D., Krishnamurthy, A., Heragu, S., & Malmborg, C. (2015). Queuing models to analyze dwell-point and cross-aisle location in autonomous vehicle-based warehouse systems. *European Journal of Operational Research, 242*(1), 72–87.
16. Yuan, Z., & Gong, Y. Y. (2017). Bot-in-time delivery for robotic mobile fulfillment systems. *IEEE Transactions on Engineering Management, 64*(1), 83–93.
17. Roy, D., Nigam, S., de Koster, R., Adan, I., & Resing, J. (2019). Robot-storage zone assignment strategies in mobile fulfillment systems. *Transportation Research Part E: Logistics and Transportation Review, 122*(December 2018), 119–142.
18. Altarazi, S. A., & Ammouri, M. M. (2018). Concurrent manual-order-picking warehouse design: A simulation-based design of experiments approach. *International Journal of Production Research, 56*(23), 7103–7121.
19. Cheng, C. Y., Chen, Y. Y., Chen, T. L., & Jung-Woon Yoo, J. (2015). Using a hybrid approach based on the particle swarm optimization and ant colony optimization to solve a joint order batching and picker routing problem. *International Journal of Production Economics, 170*, 805–814.
20. Roodbergen, K., & Vis, I. (2006). A model for warehouse layout. *IIE Transactions (Institute of Industrial Engineers), 38*(10), 799–811.
21. Roodbergen, K. J., Sharp, G. P., & Vis, I. F. (2008). Designing the layout structure of manual order picking areas in warehouses. *IIE Transactions (Institute of Industrial Engineers), 40*(11), 1032–1045.

22. Henn, S., Scholz, A., Stuhlmann, M., & Wascher, G. (2015). Working paper series a new mathematical programming formulation for the single-picker routing problem in a single-block layout, (5).
23. Yang, P., Zhao, Z., & Shen, Z. J. M. (2021). A flow picking system for order fulfillment in e-commerce warehouses. *IISE Transactions, 53*(5), 541–551.
24. Bolch, G., Greiner, S., de Meer, H., & Trivedi, K. S. (2006). Queueing networks and Markov chains. *Queueing Networks and Markov Chains.*

Chapter 14
Electric Power Personal Accident Evolution Analysis Based on Event Evolutionary Graph

Fang Jing and Mi Chuanmin

Abstract At present, electric power personal accidents happen suddenly followed with serious consequences and the accident evolution process is complex and uncertain, which have put forward high requirements for accident emergency response. Therefore, the discovery of accident evolutionary patterns among events is of great value for accident prevention. This article firstly collects and pre-processes the massive accident raw texts, then concludes several syntax patterns to recognize the causal and sequential relation between events; secondly, the event triples are extracted through dependency parsing analysis. Finally, the electric power personal casualty accidents event graph generates and the abstract event evolutionary graph is constructed based on event generalization. The study indicates that the constructed event evolutionary graph can clearly describe the events evolution path and reveal the accident evolution patterns.

Keywords Event evolutionary graph · Electric power personal accident · Accident evolution

Introduction

In recent years, the overall situation of power safety production in China has improved, however, various power accidents have occurred from time to time and power enterprises need to further improve the level of safety management. According to statistics from the National Energy Administration, from 2014 to 2020, a total of 398 power accidents and power safety incidents occurred nationwide, of which 305 were electric power personal casualty accidents, mainly including the fields of power production and power construction. The power casualty accidents happened

F. Jing · M. Chuanmin (✉)
College of Economics and Management, Nanjing University of Aeronautics and Astronautics, Nanjing 211100, State, China
e-mail: cmmi@nuaa.edu.cn

F. Jing
e-mail: fangjing1127@nuaa.edu.cn

R. Qiu et al. (eds.), *City, Society, and Digital Transformation*, Lecture Notes in Operations Research, https://doi.org/10.1007/978-3-031-15644-1_14

suddenly and grew with complexity and uncertainty, which have brought adverse effects on human life, health and economic development and raised higher standards for accident pre-control and emergency response.

The research on the accident evolution mechanism mainly focuses on two aspects, one is the accident causation theory and the other is the accident evolution path analysis. The accident causation theory reveals the internal mechanism of the accident to a certain extent, which is the foundation of the qualitative or quantitative analysis in the field of accidents. Typical accident causation models emphasize the causal relationship and, including Domino Model [1], Trajectory Intersection Model, SCM (Swiss Cheese Model) [2], HFACS (Human Factors Analysis and Classification System) [3], which describe the accident in the form of a chain, a series of discrete events according to a specific time sequence. Actually, the accident evolution process is a complex and interrelated event network, rather than a simple causal chain [4]. From the perspective of system science, safety is regarded as the interaction of system elements in a certain environment and some accident causation models based on system theory emerged, including AcciMap, STAMP (Systems Theoretic Accident Model and Processes) [5], CREAM (Cognitive reliability and error analysis method) [6]. As for the study of accident evolution path, many scholars have made efforts and many methods were adopted, including Event Tree Analysis [7], System Dynamics [8], Bayesian network [9], and Complex network [10].

However, in the above research methods, the recognition of risk factors and the relations mainly depend on qualitative analysis methods [8, 10, 11], including existing the accident causation theory and expert experience, which are subjective and cannot make full use of the potential knowledge contained in massive accident texts and the new knowledge management technology is needed. Knowledge Graph (KG) is proposed by Google in 2012, which is a knowledge base and used to enhance its search engine capabilities. Li [12] proposed the concept of Event Evolutionary Graph (EEG) in 2017, from the perspective of cognitive intelligence [13], the EEG is an event logic knowledge base used to describe the evolution patterns between events and can be formally expressed as a directed cyclic graph, where the nodes represent events and directed edges represent the relationship between events, including sequential relation, causality, conditional relation, etc. Events in the event graph have a specific relationship and are associated with a certain probability. According to the event sequence and causal relationship contained in the domain event graph, the evolution process of events can be analyzed, the rules can be summarized, and future events can be further predicted. From the perspective of the construction process of the management graph, including a series of information extraction tasks such as event extraction, relationship extraction, and event generalization, the deep mining of knowledge contained in large-scale domain data through artificial intelligence technology can not only improve efficiency but also avoid defects of traditional methods, the subjectivity brought about by manual analysis. The EEG has been widely used in network public opinion [14–16], finance [17], major emergencies [18], security situational awareness [19] and other fields. There is still room for research in the field of accident evolution analysis.

This paper will take accident report texts as the data source, recognize the relationship between events, including causal and sequential relation by matching syntactic patterns, and then use dependency parsing analysis to extract event triples in clauses. The abstract EEG will be constructed based on event generalization. Through the analysis of event evolution path, we can catch the accident evolution patterns and provide useful suggestions for power enterprises.

Proposed Framework

In this study, we propose a construction framework to construct EEG from the electric power accident reports, as illustrated in Fig. 14.1, including data pre-processing, relationship recognition, event extraction and event generalization. Details about the main construction steps are described below.

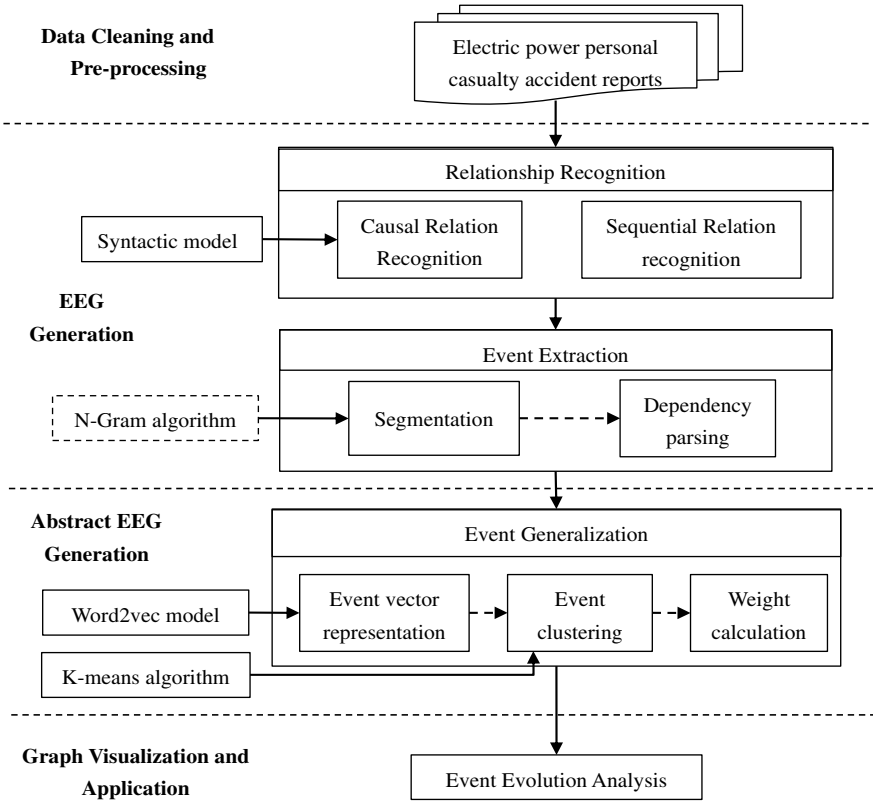

Fig. 14.1 Framework for constructing electric power personal casualty accident event evolutionary graph

Relationship Recognition

The relationship between events can clarify the association between events and reveal the pattern of event evolution. The relationships between events are various, mainly including causal, temporal and conditional relation. Considering conditional relationships are difficult to obtain and contribute little to the analysis of accident evolution, this paper mainly focuses on causality and sequential relation extraction.

Event causality is the correlation between the cause event and the effect event. In order to extract the causal relation, this paper summarizes the following 5 syntactic patterns, according to the different positions of the causal prompts. The causal syntactic models are illustrated in Table 14.1.

To Accurately identify the causal and effect clauses, for each syntactic model, the corresponding rules are show in Table 14.2, where s_i represents the whole sentence in the text, after segmentation, the word list can be formally expressed $wordList = \{w_1, w_2, ..., w_n\}$. In the expression of rules, the mark represents the punctuation of a sentence, Cause and Effect represents the cause clause and the effect clause accordingly.

Sequential relation refers to the partial order relation in which two events occur successively in time, which is also called temporal relation. Similar to causality, temporal connectives such as "after" and "before" appear in text. But the accident description texts restate the facts in chronological order, most of which do not contain the prompt word of time sequence. Therefore, when sequential relation extraction is carried out, the sentences without sequential relation connectives are extracted directly according to the sequence of events.

Event Extraction

Event extraction is the process of extracting event information from the description texts and presenting the information in the form of structured data. The current event semantic representation models mainly include the elements of the event itself, event participants, the characteristics of space and time, relationships between events and other elements, other ancillary information elements and so on. The current event semantic representation models mainly include narrative representation, core vocabulary expression mode, event component element expression and event ontology [20]. In this study, we use core vocabulary expression mode to represent the event. In this way, event can be presented as event tuples ET = (Sub, Pred, Obj), where Pred is the event trigger, Sub is the trigger-agent and Obj refers to the trigger-patient. Pred is mostly verbs, which indicates the types of the event. Sub and Obj are mostly nouns.

Event triples are extracted from raw texts through word segmentation and dependency parsing. For a given sentence, we use the segmentation tool to segment the sentence, and then parse the sentence with LTP [21] to extract the event tuples.

Table 14.1 Causal syntactic models

Number	Causal syntactic model	Cue	Example sentences
p1	<cue1> [cause], [effect]	Cue1{in consequence of, because of, as a result of}	As a result of the epidemic situation, according to the company management regulations, the construction site is not allowed to live during the epidemic situation
p2	[cause], <cue2> [effect]	Cue2{lead to, bring about, so that, result in, give rise to, cause, therefore, as a result}	The waste soil is not cleaned and transported in time, which leads to the excessive accumulation of the waste soil in the inner cylinder
p3	[cause], <cue3> [effect]	Cue3{be due to, the proximate cause of, the possible cause of, the main reason of, the indirect cause of}	The proximate cause of the accident was that the operator took the risk of cleaning
p4	<cue4> [cause], <cue5> [effect]	Cue4{by the reason of, because}, Cue5{cause, lead to}	Because the operation scope is big, causes the safety rope not to be able to be in the tense condition, the safety rope does not have the protection function
p5	<cue6> [cause], <cue7> [effect]	Cue6{cause}, Cue7{the reason is, the immediate cause is, is because, is due to}	The immediate cause of the accident is that the larger concrete blocks which were removed from the chimney inner cylinder were broken and cut again by the construction workers, and the concrete blocks which were interlaced and piled up on the working surface collapsed

Table 14.2 Causality extraction rules

Rule	Expressions
Rule 1	if w_i in Cue1 and w_j in mark then $s_i \in p_1$ $Cause = \{w_{i+1}, w_{i+2}, ..., w_{j-1}\}$ and $Effect = \{w_{j+1}, w_{j+2}, ..., w_n\}$
Rule 2	If w_i in Cue2 then $s_i \in p_2$ $Cause = \{w_1, w_2, ..., w_{i-1}\}$ and $Effect = \{w_{i+1}, w_{i+2}, ..., w_n\}$
Rule 3	If w_i in Cue3 then $s_i \in p_3$ $Cause = \{w_1, w_2, ..., w_{i-1}\}$ and $Effect = \{w_{i+1}, w_{i+2}, ..., w_n\}$
Rule 4	If w_i in Cue4 and w_j in Cue5 then $s_i \in p_4$ $Cause = \{w_{i+1}, w_{i+2}, ..., w_j\}$ and $Effect = \{w_{j+1}, w_{j+2}, ..., w_n\}$
Rule 5	If w_i in Cue6 and w_j in Cue7 then $s_i \in p_5$ $Cause = \{w_{j+1}, w_{j+2}, ..., w_n\}$ and $Effect = \{w_{i+1}, w_{i+2}, ..., w_{j-1}\}$

Text segmentation is the first step in text processing. In order to understand and analyze the domain knowledge contained in the text, we first need to extract the technical terms and domain vocabulary from the sentences. In this paper, we identify and extract terms from the text through the N-gram algorithm mentioned in [22]. With the weight value of GF/GL (Formula 14.1) calculated, we set the threshold to filter words with low weight, and then remove repetitive and redundant words to generate the field dictionary.

$$GF/GL = \log_2(FREQ) * \log_2(LEN + 1) \tag{14.1}$$

where, FREQ is the frequency with which the string S appears in text, and LEN is the length of the string S.

Dependency Parsing (DP) is one of the key techniques in natural language processing. Its basic task is to determine the syntactic structure of a sentence or the dependency of words in a sentence. This paper analyzes the dependency syntax of the sentences, analyzes the grammatical modificatory relations among the elements in the sentences, reveals the syntactic structure of the sentences, and further extracts the elements of the event triple.

For an event triple ET (Sub, Pred, Obj), Pred is the most accurate keyword to identify the occurrence of a particular type of event, usually a verb or a verb phrase. Therefore, in order to describe the event semantics accurately, the modifiers of the predicate verb must be extracted when extracting predicate of the event. Three kinds of Chinese verb-predicate sentences are summarized in [23], including verb, verb phrase and complex verb phrase.

An illustration of sentence dependency parsing analysis is shown in Fig. 14.2. The sentence is “The safety officer was not in the work place, failed to promptly

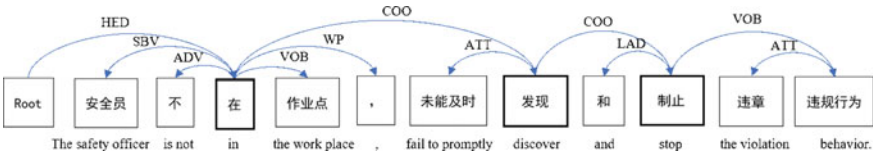

Fig. 14.2 Dependency parsing example

Table 14.3 Dependency relation

Dependency relation	Relation type
SBV	Subject-predicate
ADV	Adverbial
HED	Head
VOB	Verb-object
COO	Coordinate
LAD	Left adjunct
ATT	Attribute

discover and stop the violation behavior". The dependency relations are illustrated in Table 14.3.

After relationship recognition and event extraction, an event evolutionary graph can be generated, which is a directed cyclic graph, whose nodes are events, and edges stand for relations between events. EEG can be formally denoted as G = {E, R}, where $E = \{e_1, e_2, ..., e_n\}$ is the node set and $R = \{r_1, r_2, ..., r_p\}$ is the edge set. Each node $e_i \in E$ represents event tuples and each edge $r_j \in R$ denotes semantic relation, including causality and sequential relation.

Event Generalization

In order to capture the evolutionary patterns and logics of events, we need to merge event pairs to obtain abstract event by generalizing each specific event and finally construct an abstract event evolutionary graph. The Word2vec model was put forward by Mikolov and other [23], which is a tool of word embedding. By using word2vec model to train the text, we can get the word vector. Based on word vector representation, the vector of event triple $ET_{\mathrm{i}} = (sub_i, pre_i, obj_i)$ can be obtained (Formula 14.2).

$$vec(ET_i) = \frac{1}{3} * (vec(sub_i) + vec(pre_i) + vec(obj_i)) \tag{14.2}$$

The K-means algorithm is applied to the event generalization, which merges the event triples with high semantic similarity by computing Euclidean distance of event

vectors. According to the number of clustering centers, the corresponding abstract event nodes are obtained. For each clustering center, we count the word frequency of its containing event triples and get the general description of the abstract event node.

In the abstract EEG, the node represents the abstract event, the directed edge $e_i \rightarrow e_j$ and weight w of a directed edge can be computed by Formula (14.3).

$$w(e_i|e_j) = \frac{count(e_i, e_j)}{\sum_k count(e_i, e_k)} \tag{14.3}$$

where, $count(e_i, e_k)$ means the frequency of the directed edge $e_i \rightarrow e_k$ appears in the whole event chains.

Experiment

Data Pre-Process

The data come from the book compiled by the National Energy Administration whose name is National Electricity Accident and Electricity Safety Incident Compilation. According to the Statistics, a total of 305 electric power personal injury accidents occurred from 2014 to 2020, 285 of which have full reports.

A complete accident report includes accident brief, accident history, accident cause, and preventive and corrective measures. And the accident cause is a detailed description of the causes and consequences of the accident, which has important reference value. In this paper, we collect and process the description text of the causes, including denoising and removing special characters, and then use the LTP to perform sentence and word segmentation and make preparation for subsequent steps.

Electric Power Personal Casualty Accident EEG Generation

After pre-processing 285 texts of electric power personal accident reports, pattern matching was performed on the text content using the syntactic models above, and the clauses were extracted. Finally, a total of 2164 sentences with causality or succession relationship were obtained.

According to the steps of event extraction, the first step is building a dictionary in the field of power security. We filter Chinese words with GF/GL weight lower than 5 and remove repeated and redundant words, and finally obtain a dictionary of 781 words. Then sequentially perform word segmentation and dependency parsing on sentences and a total of 6426 event triples are extracted. The extracted event pairs

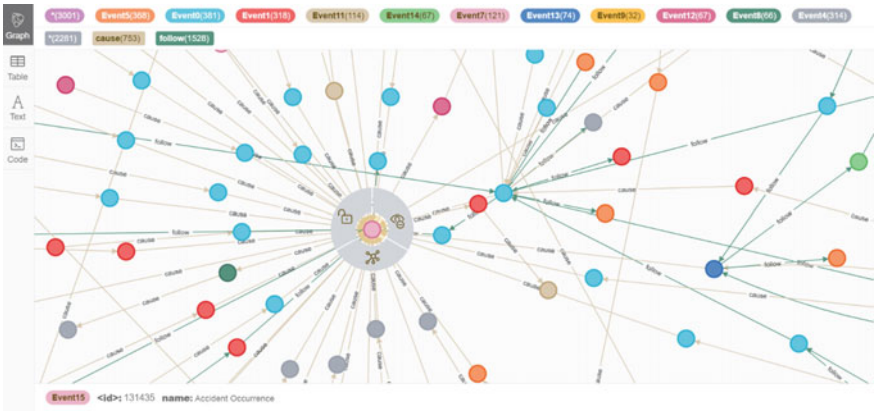

Fig. 14.3 Electric power personal casualty accident EEG

are imported into the neo4j graph database and event nodes with the same name are merged. Finally, there are a total of 5477 event nodes and 4345 associated edges in the electric power personal casualty accident EEG, and the part subgraph is shown in the Fig. 14.3.

Electric Power Personal Casualty Accident Abstract EEG Generation

With specific event nodes generalized, we obtain a total of 18 abstract event nodes whose content are illustrated in Table 14.4 and calculate the weights of the associated edges of the abstract event. Import the abstract event node and their associated edges into Gephi, and get the abstract EEG of electric power personal injury accident as shown in Figs. 14.4 and 14.5.

Electric Power Personal Casualty Accident Evolution Analysis

The event evolutionary graph reveals that evolutionary path of events in multi-directional. Part of the evolution paths of electric power personal injury accident is shown in Table 14.5, where the event chains numbered 1 to 3 represent the causal relation, and event chains numbered 4 and 5 represent a sequential relationship.

The causal event chain indicates that there is a direct impact relationship between events. By analysing these causal event chains, the antecedents and consequences of the accident can be clarified. For example, the causal event chain numbered 1 shows that the company's lack of education for employees will may lead to their weak safety

Table 14.4 Abstract event nodes

Node number	Description
E0	Personnel work without a license
E1	Poor safety awareness of workers
E2	Insufficient implementation of the main responsibility for safety production
E3	Operators work privately and blindly
E4	Poor company management
E5	Insufficient safety education and training
E6	Poor construction environment
E7	Misoperation of workers
E8	Insufficient implementation of safety management responsibilities
E9	Damaged equipment quality
E10	Insufficient performance of regulatory responsibilities
E11	Personnel adventure
E12	Violations not detected and corrected
E13	Insufficient risk assessment
E14	Insufficient awareness of security risks
E15	Accident occurrence
E16	The company failed to review the situation
E17	Absence of supervisors

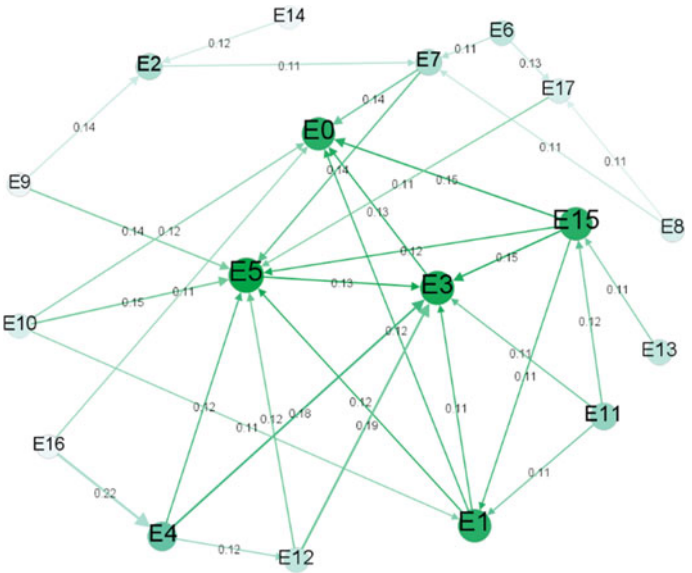

Fig. 14.4 Electric power personal casualty accident abstract EEG with causal relation

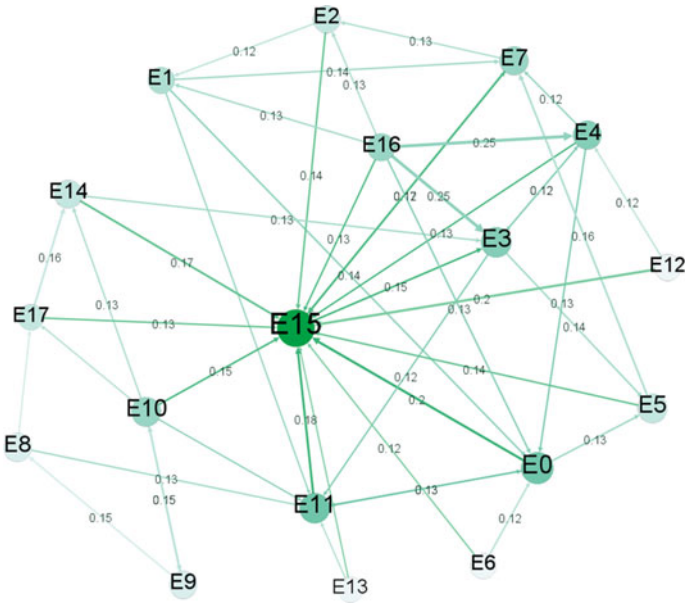

Fig. 14.5 Electric power personal casualty accident abstract EEG with sequential relation

Table 14.5 Event evolution paths

Number	Event evolution path
1	Insufficient safety education and training → Poor safety awareness of the worker → The worker did not wear protective equipment. → Worker Violations → Accident occurrence
2	There were hidden dangers in the lighting of the scene. → Dark light- Staff inspection was insufficient. → The staff did not find the problem
3	The guardian did not fulfill the responsibilities. → The guardian left the job site. → The guardian did not inform staff. → Staff worked privately. → Staff violation → Accident occurrence
4	The victim accidentally slipped. → The victim did not grasp the railing. → The victim fell off platform. → Accident occurrence
5	An Employee operated the machine. → The employee did not cut off the power. → The employee violated regulations

awareness. These workers are probably not wearing protective equipment during the work, which is a violation and may causes an accident eventually. We can figure out the direct cause of the accident is the violation of personnel without equipment, but through in-depth excavation and analysis, the fundamental or indirect cause of the accident is the company's lack of personnel safety education.

In the same way, the sequential event chain represents the ordering relationship of events according to the time of occurrence, which contributes to clarify the time

context of the accident. Take the sequential event chain numbered 5 as an example, which contains four event nodes and reveals a series of events of the drop accident. From the analysis, we can understand the whole process of the incident and learn more details.

Through the analysis of the accident cases, we find that the events of a specific accident present a chain structure. By collecting lots of event chains extracted from massive accidents reports, it can be found that the whole evolution process of all the accidents presents a complex network structure. The causal and sequential relationship between events can be analysed intuitively and effectively through the event network.

As Fig. 14.4 shows, there are multiple nodes with high degree values in the causal abstract EEG, including E15, E5, E3, E1, and E0. E5 and E3 are mostly pointed by the head of arrows and are mostly consequence events, which shows that the unsafe human behavior such as "Inadequate safety education and training" and "Operators work privately and blindly" are easily affected by other events. We can reduce the probability of such unsafe events and the risk through controlling their antecedent events. The causal weight value between events E16 and E4 is highest, which means that "The company failed to review the situation" is likely to lead to "The company's management was poor". Therefore, the company needs to strengthen the review of the on-site operating environment and fully investigate potential safety hazards and formulate targeted safety measures, which is the key to improve the level of safety management.

Analysing the causation path "E16 → E4 → E3 → E0", it is indicated that the company's negligence in personnel qualification review and inadequate personnel management resulted in operators working privately and ultimately, so the root cause of personnel violations was the company's management level. Therefore, in order to reduce the probability of employee violations, the company needs to improve its own management level and strengthen safety education for operators and supervisors.

As illustrated in Fig. 14.5, there is an obvious unique abstract event node center in the sequential abstract EEG, that is, the abstract event E15 with high in-degree. In electric power personal casualty accidents, the sequential event chains mostly evolved to accident occurrence. The weight between E15 and E0, E12 is highest associated edge weight, which is 0.2, which indicates that the event evolution paths of the electric power personal accident are diversified, but eventually evolved to "accident occurrence". Workers' violation behaviors, such as "Personnel work without a license", " Violations not detected and corrected " are more likely directly evolve into accident.

Analysis of the sequential event path "E16 → E4 → E0 → E15", it can be seen the operator without the license is directly related to the occurrence of the accident. From the perspective of the time sequence, the company did not review the qualifications of personnel is the source event, which is indirectly related to the evolution of the accident. Therefore, to avoid the occurrence of such violations, the company should strengthen the qualification review of operators and strengthen the management of the operation, including undocumented employment.

Conclusion

Aiming at the deficiency of traditional accident evolution analysis methods that do not deeply absorb the massive and multi-dimensional risk event information in electric power accident texts, the analysis process is highly subjective and time-consuming, this study introduces the event evolutionary graph into the field of accident analysis. Through the analysis of real cases of personal accidents in power industry, the following conclusions are drawn.

1. This paper proposes a framework for constructing an EEG, which uses automated methods to extract relevant knowledge of risk events contained in accident texts and fully taps the potential knowledge in accident reports. It reduces manual participation, improves the efficiency of knowledge extraction, and makes up for the shortcomings of traditional accident qualitative analysis methods.
2. This study reveals the evolution paths and patterns of electric power personal accidents through EEG model, which indicate the method we developed are effective. The sequential relation shows the development context and timing evolution path of the accident, and the causal relation explains the cause and effect of the accident, which can provide decision-making support for accident prevention of power enterprises.

The construction process of the EEG is a relatively complex process, which involves a series of information extraction tasks. The event extraction method proposed in the text is not effective for long sentences. Therefore, our future research will further study how to extract events based on deep learning to improve the accuracy of event recognition and the quality of EEG. In addition, it is very meaningful and worthwhile to consider how to make prediction about accident consequences based on the constructed EEG.

Acknowledgements This work was supported by "The Fundamental Research Funds for the Central Universities", NO.NJ2022031.

References

1. Heinrich, W. H., Petersen, D. C., & Roos, N. R. (1980). *Industrial accident prevention: A safety management approach.* McGraw-Hill Companies.
2. Reason, J. (1990). *Human error*. Cambridge University Press.
3. Shappell, S. A., & Wiegmann, D. A. (2012). *A human error approach to aviation accident analysis: The human factors analysis and classification system.* Ashgate Publishing Ltd.
4. Hollnagel, E., & Woods, D. D. (2005). *Joint cognitive systems: Foundations of cognitive systems engineering.* CRC Press.
5. Levenson, N. (2011). *Engineering a safer world: Systems thinking applied to safety.* Mit Press.
6. Hollnagele. (1998). *Cognitive reliability and error analysis method (CREAM).* Elsevier.
7. Du, Z. G., Luo, P. C., Li, H. T., et al. (2011). A security risk analysis method based on dynamic ETA. *Science Technology and Engineering, 11*(22), 5264–5269.

8. Chen, G. H., & Wang, Y. X. (2018). Simulation of accident evolution in chemical industry park based on system dynamics. *Science Technology and Engineering, 18*(19), 347–352.
9. Song, H. Y., Liu, H. X., Jiang, X. Y., et al. (2018). Research on food safety accident scenario deduction based on knowledge element and Bayesian network. *Information Science, 37*(7), 712–720.
10. Xiong, X. X., Chen, L., & Chen, Y. X. (2018). Research on generation and evolution of road traffic accident chain based on Bayesian network model. *Journal of Highway and Transportation Research and Development, 35*(05), 99–107.
11. Guo, Z. H., Jiang, H., & Gong, C. (2022). Research on identification of risk factors and network evolution mechanism of chemical explosion accidents. *Industrial Engineering and Management* 1–13.
12. Li, Z., Ding, X., & Liu, T. (2018). Constructing narrative event evolutionary graph for script event extraction. In *Proceedings of the 27th international joint conference on artificial intelligence*, pp. 4201–4207.
13. Wang, J. P., Zhang, W. S., Wang, Y. F., et al. (2020). Constructing and inferring event logic cognitive graph in the field of big data (in Chinese). *Scientia Sinica Information, 50*(7), 988–1002.
14. Tian, Y. L., & Li, X. (2021). Analysis of the evolution path of network public opinion on the new crown pneumonia epidemic based on the event evolutionary graph. *Information Studies: Theory & Application, 44*(3), 76–83.
15. Xia, L. X., Chen, J. Y., & Yu, H. J. (2020). Research on the visualization summary generation of multi-dimensional feature network public opinion events based on event evolutionary graph. *Information Studies: Theory & Application, 43*(10), 157–164.
16. Shan, X. H., Pang, S. H., Liu, X. Y., et al., (2019). Analysis of the evolution path of network public opinion based on evolution evolutionary graph—Taking medical public opinion as an example, 42(9), 99–103,85.
17. Liao, K. (2020). Research on the key technologies for the construction of event evolutionary graphs in the financial field. *Harbin Institute of Technology.*
18. Zhang, H. T., Li, J. W., Liu, W. L., et al. (2021). Research on the construction of the event evolutionary of major emergencies. *Library and Information Service, 65*(18), 133–140.
19. Li, G., Wang, S. Y., Mao, J., et al. (2021). Research on the construction of national security event graph for situational awareness. *Journal of the China Society for Scientific and Technical Information, 40*(11), 1164–1175.
20. Xu, L., & Pan, J. (2019). Research on event representation and its semantic representation model. *Journal of Intelligence, 38*(06), 159–167.
21. Che, W. X., Li, Z. H., & Liu, T. (2010). Ltp: A Chinese language technology platform. In *ICCL, Association for Computational Linguistics*, pp. 13–16.
22. Lv, M. X., He, L., Li, Y., et al., (2010). Research on construction of keyword dictionary in news domain based on N-Gram text expression. 28(04), 571–574+615.
23. Mikolov, T., Sutskever, I., Chen, K., et al., (2013). Distributed representations of words and phrases and their compositionality. In Proceedings of the 26th international conference on neural information processing systems, pp. 3111–3119.

Chapter 15
Research on Suicide Risk Spectrum of Prisoners Based on Fourier Transform

Sainan Gao and Yang Shen

Abstract Prisoner suicide risk prevention and control cannot be ignored, yet there is a lack of relevant quantitative studies to support risk management. We quantify the risk of prisoner suicide based on the Fourier transform, establish a relevant data model, and examine the impact of different frequencies of influencing factors on the overall risk of prisoner suicide through simulation. At the same time, we innovatively use Fourier transform to obtain the frequency spectrum of prisoner suicide risk data, and conduct frequency domain analysis. The simulation results show that negative events are the most influential factor on the overall prisoner suicide risk, and the frequency domain analysis provides the cyclical characteristics of suicide risk for different types of prisoners. We emphasize the importance of fairness in prison enforcement to reduce the occurrence of negative events and the need for periodic suicide screening and prevention based on the behavioral characteristics of prisoners.

Keywords Prison suicide · Fourier transform · Simulation · Prison management

Introduction

The first global report on suicide published by World Health Organization in 2014, pointed out that at least 800,000 people die by suicide worldwide every year, and this number is most likely to be underestimated [1], suggesting that suicide has become a global public health problem that cannot be ignored, and its prevention has become a global priority. Prisoners are at high risk of suicide than the general population [2]. In recent years, suicide has become the main risk factor threatening prison security, and the prevention of suicide has become one of the key points of prison work.

S. Gao (✉) · Y. Shen (✉)
College of Economics and Management, Nanjing University of Aeronautics and Astronautics, Nanjing 211106, Jiangsu, China
e-mail: sainang@nuaa.edu.cn

Y. Shen
e-mail: shen.y@nuaa.edu.cn

R. Qiu et al. (eds.), *City, Society, and Digital Transformation*, Lecture Notes in Operations Research, https://doi.org/10.1007/978-3-031-15644-1_15

At present, interviews, questionnaires, scales and other survey methods such as logistic regression are mostly used in the research on suicidal behavior, the method is relatively simple. The essence of Fourier transform is that "arbitrary" periodic function can be expressed as the combination and superposition of sinusoidal functions with different frequency and intensity. Inspired by the Thought of Fourier transform, suicide can be regarded as a complex phenomenon, which is composed of several factors acting repeatedly (i.e. frequencies) at different intensities. Our research focus on the impact of the frequency of influencing factors on the suicide risk of prisoners. At the same time, Fourier transform maps data from time domain to frequency domain, providing a new perspective to observe the characteristics of suicide risk of prisoners. The idea of Fourier transform is generally used in traditional mathematics and physics, but fundamentally it is suitable for explaining the generation of complex phenomena, which also provides a quantitative method for the study of suicide. Opposite to one-way determinism, Bandura put forward the ternary interactive determinism, believing that personal factors, environmental factors and behavioral factors are interconnected and mutually determined. The occurrence of suicide is also determined by the prisoner's personal, environmental and corresponding behavioral factors.

Therefore, we will integrate the existing research on suicide behavior of general population and prisoners, evaluate and screen the sociological and psychological factors affecting suicide, combined with the ternary interactive determinism build prisoners' suicide influencing factors, then analyze and model the mechanism of suicide based on Fourier transform, establish basic model for a single factor, according to the current prison management mode and expert evaluation, the reasonable frequency and intensity of each factor are set up to establish a suicide model suitable for prison. Finally, through the simulation of the model and the Fourier transform from time domain to frequency domain, a conclusion is drawn and reasonable suicide prevention strategies are proposed to provide suggestions for prison management and decision making.

The main contributions of this paper include:

(1) Quantifying and modelling data on the factors influencing suicide;
(2) Transferring the idea of the Fourier transform to management to examine the impact of factors on suicide at different frequencies, and shifting the analytical perspective to the frequency domain

Related Work

Suicide is a complex pathological phenomenon with various influencing factors. Existing researches divide the influencing factors into the following five categories: biological factors, psychological factors, environmental factors, mental disorders and negative life events [3–10].

With the deepening of people's understanding of suicidal behavior, researchers have turned to the mechanism of suicide, thus establishing a number of theoretical

models of suicide: Stress-Diathesis Model [11], Interpersonal Theory of Suicide [12], and Integrated Motivational-Volitional Model of Suicidal Behavior [13] and so on. IMV is framed by the Theory of Planned Behavior, which posits that there are three stages of suicide: a pre-motivational stage that includes background factors and trigger events for suicide, a motivational stage that forms suicidal ideation and intention, and a volitional stage that implements a suicidal programme. IMV integrates the etiology of suicidal behavior with biological and psychological factors in the developmental process. It is a more comprehensive and in-depth theoretical model of suicide.

Prisoners serving prison sentences and social isolation have always been regarded as high-risk groups for suicide [2], it is difficult for them to attack others in prison and they can only choose self-attack. Violent prisoners have a greater risk of suicide due to their strong aggression. Some researchers used cross-sectional surveys to find that factors affecting suicide include life experience, demographic characteristics, mental health status, mental illness and so on [14, 15]. Fang Yangsong investigated the suicide risk of prisoners, found that prisoners with a history of suicide, long sentences, age of 26–50, violent crimes and physical disease tend to have more obvious tendency to commit suicide, he also analyzed the causes of prisoners' suicide from the aspect of prisoners' special identity, imprisonment and social environment [16]. Kong Yi conducted an empirical analysis of the suicide cases of prisoners and found that long prison term and low education level were the most influential factors for prisoners who committed suicide or attempted suicide [17]. Chen penglan analyzed the influencing factors of suicide tendency from the perspectives of social culture, family, and mental health [18].

In a word, existing studies have found that social and psychological factors have a great impact on suicide, and the established suicide theoretical models attempt to explain the mechanism of suicide from the psychological level, but researchers have different perspectives, and the models are one-sided. As for prison suicide, domestic researches started slowly, mostly focusing on the influencing factors, and the understanding of the mechanism of the factors and the compound influence of various factors seems to be not deep enough.

Methods

Influencing Factors

American psychologist Bandura put forward a theoretical framework for analyzing people's motivation, thought and action based on the social cognition view, namely the famous "ternary interactive determinism [19]. He pointed out that "behavioral, personal and environmental factors actually act as interconnected and interacting determinants".

The personal factors include the individual's cognition, emotion, self, etc., while the environment refers to the external environment where the individual is lived in, and the behavior is the actual behavior that the individual implements.

We divide the influencing factors of prison suicide into three categories: basic factors, management factors and behavioral factors. The basic factors are static factors, the influence on suicide is definite, and it reflects the initial suicidal tendency of individuals. The frequency and intensity of management factors are different due to the different management modes of prison, which affect the suicidal ideation of the individuals. Behavioral factors are the external performance and behavioral characteristics of the individual, and the general suicide high-risk group will have obvious behavioral characteristics.

Basic factors and management factors are modelled to obtain a data model of suicide risk, in which the modelling of management factors is the focus. On the basis of this model, the management of prisoners is adjusted in combination with behavioral factors.

The research data was obtained from relevant research literature and field research in prisons (supported by the Foundation project) and was subjected to some screening and pre-processing before final use.

Basic Model

The **basic factors** are the prisoner's personal factor, which is a constant in the model, including education level, offense type, sentence and time served. We directly use the suicide rate in prison data [17] to approximate the suicide tendencies of prisoners, the suicide risk is $y_{el}(y_{ot}, y_s) = C$, Table 15.1 shows the value of C.

As for time served. We set the term of imprisonment for more than 15 years as "long-term prisoners" (whose suicide risk is denoted as y_{lt}). Such prisoners are at high risk of suicide before at the beginning of their sentence, while short-term prisoners (whose suicide risk is denoted as y_s) do not consider the impact of the already served sentence. The suicide rate [16] of prisoners who have served different sentences is a typical anti-S type, so equations can be obtained, where x represents

Table 15.1 Suicide rates of different types of prisoner

Education level	Suicide rates/%	Offense type	Suicide rates/%	Sentence	Suicide rates/%
University/college	0	Homicide	54.087	<5 years	4.678
High school	2.404	Assult	5.269	5 ~ 10 years	7.637
Junior high school	3.239	Rape	11.773	10 ~ 15 years	1.039
Primary school	9.280	Rob	2.364	15 ~ 20 years	7.692
illiteracy	28.490	Theft	5.731	>= 20 years	20.604
		Other	5.769		

characteristics of prisoners:

$$k_{ts} = 1 - \left(\frac{1.17}{1 + 5.46e^{0.19x}} \right) \tag{15.1}$$

$$y_{lt} = (k_{ts} + 1) y_s \tag{15.2}$$

The **management factors** include visitation, mental disorders, personality defects and negative events. We follow the conclusion in [11, 20–22] to obtain the equation below. Equations (15.4), (15.5) are segmented functions, with each segment having a different coefficient (a, b, c, m_1, d_1, m_2, d_2). MAX denote Maximum suicidal ideation for normal prisoners. Specially, according to Pressure-quality model [11], people with personality defects have a higher risk of suicide when they encounter negative events. Therefore, this factor should be considered together with negative events, and taken this factor as the coefficient of suicide risk calculation, and we set $k_{pd} = 4$ [22].

$$y_v = 225.56x^3 + 32.30x^2 + 1.07x + 0.29 \tag{15.3}$$

$$y_{md} = a(x - t)^2 + b \tag{15.4}$$

$$y'_{ne} = m_1 x + d_1 (y'_{ne} \leq MAX),\ cx^{-m_2} + d_2 (else) \tag{15.5}$$

$$y_{ne} = k_{pd} y'_{ne} \tag{15.6}$$

People at high risk of suicide have obvious psychological characteristics and external manifestations, which is the **behavioral factors** including the following three stages:

(1) Obvious changes in behaviors and emotions, including but not limited to: large changes in behavior, confrontation with various people and events, mood swings with depressive tendencies, difficulty in handling relationships, difficulty in digesting negative emotions, etc.
(2) Reveal suicidal thoughts, talk about the topic of suicide in daily conversation, and ask about suicide methods from time to time.
(3) Attempted suicide. The first stage is the basic feature, and prisoners with these behavioral features should be properly paid attention to. If the second and third stage features appear, they are at high risk of suicide, and suicide intervention should be carried out in a timely manner.

Integrated model

Initial suicidal tendency model. The basic factors reflect the initial suicidal tendency of the prisoners, which cannot be adjusted by prison, but determined by the characteristics of the prisoners themselves. The models of the basic factors were summed to obtain the individual suicidal tendency model, and then multiplied by the corresponding coefficients and distributions to obtain the overall initial suicidal tendency model of the prisoners. We calculate the value using the data, which is 0.06731 (while long-term prisoners should multiply $k_{ts} + 1$). The coefficients (i.e. intensity) and distributions set for each factor are shown in Table 15.2.

$$y_{overall\_tendency} = K_{el} y_{el} T_{el} + K_{ot} y_{ot} T_{ot} + K_s y_s T_s (sentences < 15), \\ K_{el} y_{el} T_{el} + K_{ot} y_{ot} T_{ot} + K_s y_{lt} T_s (sentences \geq 15) \quad (15.7)$$

Suicidal ideation model. The effect of a prison management activity on the suicide risk of all prisoners was described by the suicide ideation model. The various basic models of the suicidal ideation model need to set factor intensity (i.e., coefficient) and frequency (i.e., the actual frequency of prison management activities).

$$y_{overall\_ideation} = K_v y(F_v)_v + K_{md} T_{md} y(F_{md})_{md} + K_{ne}(1 - T_{ne}) y(F_{ne})'_{ne} + K_{ne} T_{ne} y(F_{ne})_{ne} \quad (15.8)$$

According to the ternary interactive determinism, suicide tendency and suicidal ideation account for half of prisoners' suicide risk. In summary, the data model of prisoners' overall suicide risk is as follows:

$$y_{overall\_risk} = 0.5 y_{overall\_tendency} + 0.5 y_{overall\_ideation} \quad (15.9)$$

Table 15.2 Coefficient and distribution and frequency for each factor

Factors	Coefficient (K)		Distribution (T)		Frequency (f)	
Education level	K_{el}	0.4	T_{el}		/	/
Offense types	K_{ot}	0.2	T_{ot}		/	/
Sentence	K_s	0.4	T_s		/	/
Visitation	K_v	0.2	/	/	F_v	12
Mental disorders	K_{md}	0.5	T_{md}	0.1299 [23]	F_{md}	1/2
Negative event	K_{ne}	0.3	T_{ne}	0.3146 [23]	F_{ne}	4

Experiments

Simulation of Overall Prisoner Suicide Risk

The model was established in Simulink and then conducted simulation experiments. The simulation time (Sentence) was set to 10 and 20. In order to understand the influence of each factor on suicide risk, the control variable method was used to conduct 6 simulations for each simulation time, a total of 12 simulations. Through the preliminary analysis of the simulation results, it is found that modifying the frequency of the management factors has a similar effect on the results under different sentences, and modifying the frequency of three factors at the same time is not significantly different from two factors. Therefore, we show the curve (Fig. 15.1) of the most typical experiments 7 and 11. In the figure, the change of the maximum value and the minimum value of each cycle is also plotted. Table 15.3 shows partial results (* indicates a significant increase in value, # indicates a significant decrease). The time when the maximum/minimum value is reached is in parentheses.

We can conclude that:

(1) Changing the simulation time, that is, the length of the prison sentence, will significantly increase the overall suicide risk of prisoners. The risk of long-term prisoners increases significantly in the early stage and the maximum risk increases by 3%, but the rate of decline in the later period is faster than that of

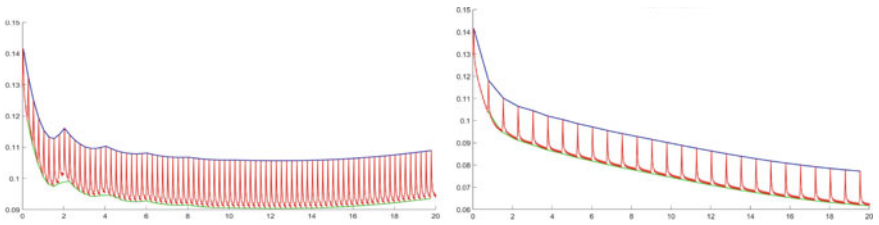

Fig. 15.1 Simulation results (*L* experiments 7; *R* experiments 11)

Table 15.3 Simulation results of some experiments

No	Time	F_v	F_{md}	F_{ne}	Initial	Max	Min	Final
1	10	12	1/2	4	0.10167	0.1141 (0.0417)	0.070599 (3.25)	0.078279
7	20	–	–	–	0.12924	0.1416 (0.0417)	0.090336 (12.5)	0.093815
8	–	–	1/1.5	–	0.12924	0.1416 (0.0417)	0.090304 (12.5)	0.093752
9	–	–	–	4/3	0.12924	0.1416 (0.0417)	0.061654 (20)$^{\#}$	0.061654$^{\#}$
10	–	24	-	-	0.12924	0.1571 (0.0417)*	0.090685 (12.483)	0.094397
11	–	–	1/1.5	4/3	0.12924	0.1416 (0.0417)	0.061591 (20)$^{\#}$	0.061591$^{\#}$
12	–	24	1/1.5	4/3	0.12924	0.1571 (0.0417)*	0.061836 (19.982)$^{\#}$	0.062174$^{\#}$

short-term prisoners, and The upward trend is small. This is because the suicidal tendency of long-term prisoners is affected by the already served sentence, while the suicidal tendency of prisoners tends to stabilize in the later period of sentence.

(2) Only changing the frequency of mental disorder screening will reduce the overall risk to a minimum value more quickly, but the decline is not obvious in the later period; and reducing the frequency of negative events has a better effect, which significantly reduces the fluctuation of the suicide risk of prisoners. Because of the higher initial frequency of negative events and their greater impact on suicidal ideation.

(3) Changing the frequency of negative events has a greater impact on long-term prisoners, because too long sentences make negative events occur too many times, and the accumulation of negative stimuli for prisoners is greater.

(4) Simultaneously changing the frequency of mental disorder screening and the frequency of negative events has the most significant effect on the overall suicide risk of prisoners. But changing the frequency of three factors at the same time makes little difference compared to changing only two factors.

(5) Regardless of whether it is a long-term prisoner or a short-term prisoner, only changing the frequency of current visits will even increase the maximum risk at the initial stage, but it has little effect on the risk at the later stage. This special case will be explained in the latter experiment.

Simulation of Specific Prisoner Groups

The model we proposed can also be used to simulate specific prison groups, which can provide more reasonable and targeted management suggestions for prison. This experiment found that the most common prisoners, namely, the prisoners with the education level of junior high school, offense type of rape and 5–10 years sentence, had particular changes in the risk of suicide when they suffered from personality disorders. The comparison of simulation results is shown in Fig. 15.2.

Different from the overall suicide risk, the maximum risk for the entire sentence occurred in the later part of the sentence, because the negative stimulus had a more pronounced effect on such prisoners. However, when the frequency of visits

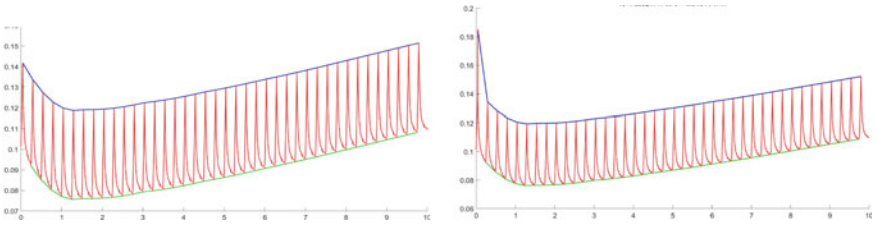

Fig. 15.2 Simulation for specific prisoner groups (*L:* initial frequency; *R:* increased frequency of visitation)

was increased, the risk of initial suicide increased sharply, which explains why the overall suicide risk increased slightly after increasing the frequency of visits in the previous simulation. Increased visits reduced suicidal ideation in general prisoners, but increased the overall suicide risk by triggering suicidal ideation in such prisoners.

Frequency Domain Analysis

By sampling the overall suicide risk simulation results in Sect. Simulation of Overall Prisoner Suicide Risk, Fourier transform was performed to transform the time domain into a frequency spectrum. In Fig. 15.3, the horizontal axis represents the frequency (reciprocal period, unit: year) of suicide risk, and the vertical axis represents the intensity of suicide risk. Each peak represents the frequency and intensity of suicide risk for a group of prisoners (the Y-axis represents the initial suicidal tendency of prisoners, while the remaining peaks represent the suicidal ideation of prisoners). The dashed line in the figure represents the suicide risk of 0.0006. Since the initial suicidal tendency of the prisoners is calculated as 0.06731, the suicide risk (ideation) of the prisoners can be ignored when it is less than 1% of the initial suicidal tendency. Also, the data was noted in the figure with the corresponding cycle (T).

We can figure out that:

(1) The spectrogram of prisoner suicide risk in Fig. 15.3 (L) (that is, at the initial frequency) has 5 peaks (>0.0006), the distribution is relatively scattered, and the frequency and intensity are large; while in Fig. 15.3 (R) (optimized the frequency of management factors) the risk spectrogram has 7 peaks (drop the first peak which cycle is longer than 20 years), the distribution tends to be concentrated, and the frequency and intensity are both reduced.

(2) Reason for the increase of peaks: It can be seen from the previous simulation experiments that negative events have the greatest impact on the suicide risk of prisoners, so it will blur the influence of other factors. When the frequency of negative events is high, the suicide risk of prisoners will be relatively high, while the influence of other factors on the suicide risk of prisoners is difficult to show, which leads to the clustering of characteristics of various prisoners and it is difficult to distinguish them. After reducing the frequency of negative events, the suicide risk of prisoners was more affected by other factors, resulting in

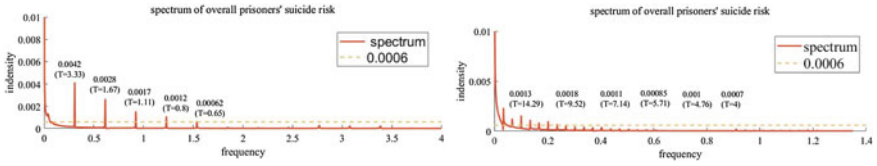

Fig. 15.3 Spectrum of overall prisoners' suicide risk with data (*L:* experiments 7; *R:* experiments 11)

a higher degree of discrimination and more complex classification, but at the same time the peak value was greatly reduced.

(3) The data also shows that the cycle of suicidal ideation among different types of prisoners is basically stable at 10 months at the initial frequency, but increases to 57 months after modifying the management frequency, indicating that different groups of prisoners have a periodical suicidal risk ideation.

Results

Through the above experiments and results analysis, it can be concluded that long sentence and the frequency of negative events are the factors that have the greatest impact on suicide. The impact of visitation is different from types of prisoners. The new prison stage has the greatest suicide risk. Different types of prisoners have cyclical characteristics, although the frequency and magnitude of suicide risk vary. In order to reduce the overall suicide risk of prisoners by adjusting management methods, prisons should start from reducing negative events in prisons and eliminating negative stimuli in prisoners.

Specific suggestions for prison management are as follows:

(1) Pay attention to the fairness of law enforcement and strengthen the education of prisoners. But at the same time, it will make the distinction between different types of prisoners higher, which requires more precise classification management.

(2) According to the periodicity of the suicide risk of prisoners, the prison can arrange periodic suicide prevention and investigation to stabilize the suicide risk of most prisoners in the prison.

(3) To better reduce the overall suicide risk, it is necessary to increase the frequency of screening of prisoners with mental disorders (once every 1.5 years) and reduce the occurrence of negative events in prison (the less the better). At the same time, different visiting strategies are adopted for prisoners in different situations.

(4) When the overall suicide risk of prisoners is high, that is, the prisoners are newly entering prisons, prison should pay close attention to prisoners with obvious behavioral characteristics, especially those who meet the second and third stages of behavioral factors, and take corresponding preventive actions.

Conclusion

We first described the influence mechanism of each factor on suicidal tendency and suicidal ideation, established the corresponding basic model, and then based on the Fourier transform idea, set the intensity and frequency of the influencing factors according to the actual situation, and considered the distribution of prisoners to obtain overall suicide risk model.

The effects of different frequencies of management factors on the overall suicide risk were investigated through simulation, and it was found that the management factors that had the greatest impact on prisoner suicide were negative events. Notably, our model can also simulate suicide risk for specific prison populations and find that visitation is counterproductive for prisoners with personality disorders. Then the simulation results were analyzed in frequency domain by Fourier transform, and found that the suicidal ideation of different types of prisoners is periodic. It is initially believed that adjusting the frequency of screening for mental disorders and negative events is an effective method to reduce the suicide rate in prisons, but it should be combined with more refined classification management, and suicide prevention should be carried out in combination with the behavioral characteristics of prisoners and the cycle of suicide risk.

In the future, we can also consider more comprehensive influencing factors (i.e. prison reform), explore the impact of visiting deeper (i.e. different visitors and conversations), and design models for prisoner mobility.

Acknowledgements Our research was supported by funding and data from the National Key Research and Development Program "Digital twin-based virtual practice for emergency response in prisons" (2020YFC0833104).

References

1. WHO. (2014). Preventing suicide: a global imperative.
2. Zhai, S. T. (2002). Interventions for suicide in China. *Shanghai Archives of Psychiatry, 14*, 4.
3. Mckay, W. L. (2007). *Hope and suicide resilience in the prediction and explanation of suicidality experiences in university students*. University of Wyoming.
4. Fei, L. P. (2004). The current situation of suicide in China and future directions of work. *Chinese Journal of Epidemiology, 25*(4).
5. Xu, H. L. (2009). *A psychosocial autopsy study of 15–35 year olds who died by suicide in rural Hunan*. Central South University.
6. Wang, K. T., Wong, Y. J., & Fu, C. C. (2013). Moderation effects of perfectionism and discrimination on interpersonal factors and suicide ideation. *Journal of Counseling Psychology, 60*(3).
7. Zhao, L. C. (2016). Relationship between depression level, quality of life and suicide risk in patients with depression. *Chinese Journal of Health Psychology, 24*(07).
8. Xu, H. L., Xiao, S. H., Chen, J. P., et al. (2000). A study on the epidemiology of suicide among some elderly people in rural and urban areas of Hunan Province. *Chinese Journal of Mental Health, 02*, 121–124.
9. Hor, K., & Taylor, M. (2010). Review: Suicide and schizophrenia: a systematic review of rates and risk factors. *Journal of Psychopharmacology, 24*(4 Suppl).
10. Vivian, K., Ella, A., & Philip, S. (2002). Negative life events and depression in elderly persons. *Journals of Gerontology* (1), 1.
11. Mann, J. J., & Waternaux, C. (1999). Toward a clinical model of suicidal behavior in psychiatric patients. *American Journal of Psychiatry, 156*(2), 181–181.
12. Joiner, T. E. (2007). *Why people die by suicide*. Harvard University Press.
13. O'Connor, R. (2011). Towards an integrated motivational-volitional of suicidal behavior. In *International handbook of suicide prevention: research, policy and practice*. John Wiley & Sons, Ltd.

14. Chapman, A. L., Specht, M. W., & Cellucci, T. (2005). Factors associated with suicide attempts in female inmates: The hegemony of hopelessness. *Suicide & Life-Threatening Behavior, 35*(5).
15. Smith, P. N., Selwyn, C. N., Wolford-Clevenger, C., et al. (2014) Psychopathic personality traits, suicide ideation, and suicide attempts in male prison inmates. *Criminal Justice and Behavior, 41*(3).
16. Fang, Y. S. (2019). Investigation and prevention countermeasures of prisoner suicide: An example from a prison in Zhejiang Province. *Crime and Rehabilitation Research, 09*, 61–65.
17. Kong, Y. (2005). Research on prisoner suicide: An empirical analysis of prisoner suicide cases in Zhejiang Province. *Journal of People's Public Security University of China (Social Sciences Edition), 01*, 40–43.
18. Chen, P. L. (2010). Prevention and control of prisoner suicide from a psychological perspective. *The Guide of Science & Education, 10*, 138–139.
19. Albert, B. (1986). Social foundations of thought and action: a social cognitive theory. *Journal of Applied Psychology, 12*(1).
20. Siennick, S. E., Mears, D. P., & Bales, W. D. (2013) Here and gone: Anticipation and separation effects of prison visits on inmate infractions. *Journal of Research in Crime & Delinquency*, *50*(3), 417–444.
21. Tang, H. Y., Fang, Y. R., & Li, Z. J. (2014). *Psychiatry*. People's Health Press.
22. Hu, M. H. (2018) *A study on the factors influencing suicidal ideation among male antisocial personality inmates*. Nanjing Normal University.
23. Lv, C. R., Huang, Y. Q., Zhao, S., et al. (2020). A survey on the current situation of mental disorders among offenders in a provincial prison. *Chinese Journal of Mental Health, 34*(05), 403–407.

Chapter 16
A Deep Learning Model for Mining Behavioral Preference of Home Care Demanders to Suppliers

Hongying Fei and Mingzhu Xu

Abstract This study aims at developing a deep learning prediction model for the preference of home care service demanders to suppliers available in a health care management platform. Firstly, a Node2vec-based algorithm enhanced by minimizing patients' preference difference, is developed for capturing behavioural pattern of demanders; then an advanced deep learning GRU model, combing attention mechanism for service categories, is constructed to predict the visiting preference to various service suppliers by taking into account not only the constraints of technical requirement but also personal behavioural preference. Experimental results show that the proposed deep learning model, compared to the traditional deep learning GRU model, can significantly improve the quality of behavioural preference prediction, which can help improve the recommendation success rate of service suppliers to demanders.

Keywords Home care service · Deep learning · Attention mechanism · Preference prediction

Introduction

With an aging population, increasing prevalence of chronic diseases and patients' desire for home care, the demand for home care services is increasing rapidly [1]. Home care services can not only help reduce the pressure of medical resources and improve the utilization rate of medical services, but also provide patients with affordable, cost-effective [2], more convenient and professional medical care services, and significantly reduce the readmission rate and risk of death [3, 4]. As indicated in Healthy China strategy, home care service (HCS) is becoming an important part of national health system in China. Since the patients who need to reserve home care services prefer high-level hospitals or public home care sectors rather than private

H. Fei · M. Xu (✉)
School of Management, Shanghai University, Shanghai 200444, China
e-mail: Xumingzhu97@shu.edu.cn

H. Fei
e-mail: Feihy@shu.edu.cn

R. Qiu et al. (eds.), *City, Society, and Digital Transformation*, Lecture Notes in Operations Research, https://doi.org/10.1007/978-3-031-15644-1_16

institute even when the latter can offer high quality service as well, it can be observed that high level public healthcare sectors are always overcrowded while the health care service resources of community hospitals or private institutions are under-utilized. Therefore, it is necessary to take efficient measures to help balance the utilization of home care service resources from various sectors to improve overall service efficiency in field of home care service.

In recent years, with the development of *Internet* + technologies, especially the advancement of *Smart City* projects, various health care management platforms have been constructed. Considering that historical data relevant with home care services can be extracted from the database of health care management platform, machine learning technologies can help improve the understanding of platform users' behavioral patterns, making it possible to balance resource utilization by impacting the selection of home care patients with dedicated recommendation system.

This study focuses on mining behavioral patterns of users registered on a home care management platform. The purpose is to develop an efficient recommending model for home care services, wth an objective to not only improve the response to home care service demanders but also balance the utilization of various home care resources.

Literature Review

Health Care Industry (HCI) has become one of the largest economic sectors in the world [5]. As an important part of HCI in many countries, Home Health Care (HHC), providing service to patients at their home, attracts more and more attention from researchers [6]. In China, numerous HHC service platforms were constructed in recent years though the majority of such platforms are used as bulletins rather than coordinators [6].

Traditional methodologies for learning behavioral preference of users on e-commerce platforms are mainly based on analyzing the characteristics of users or objects/projects, and the purpose of the recommendation system based on such behavioral learing technoques is mainly to maximize the profit. However, the recommendation system dedicated to home care services should consider ethical issues rather than commercial purpose, and the continuity of services should also be considered when recommending home care service suppliers to demanders [7].

According to the literature, machine learning techniques have been widely applied in predicting user behavioral preference. As an important part of machine learning, Deep Learning (DL),such as Deep Neural Network (DNN), can be applied to mine high-order interactive features, and the Recurrent Neural Network (RNN), like Gated Recurrent Unit (GRU), has been successfully applied to mining user behavioral features based on time series data [8]. Furthermore, some researchers combined RNN with attention mechanism model to reduce feature sparsity and improve solution quality.

In this study, a deep learning GRU model, combined with attention mechanism, is developed to extract the behavioural preference of home care demanders to service suppliers, based on historical data collected from an HHC platform.

Problem Formulation

Assumptions are as follows:

(1) Necessary information of available home care service resources is recorded in the targeted HHC platform, and this platform is accessible to all residents in the corresponding area.
(2) Historical information of services offered by suppliers to demanders are recorded in the HHC platform and can be used for assessing the performance of users when necessary.
(3) Each user, service supplier or demander, has a unique account in the HHC platform.
(4) There is no significant difference between the suppliers that can offer the same type of home care services, in other words, service quality of available suppliers is equivalent.
(5) Home care service suppliers can just provide the types of services pre-registered on the HHC platform, i.e., the types of services required by home care demanders must be considered (Table 16.1).

General Framework of the User Behavioral Preference Mining

As shown in Fig. 16.1, the User Behavioral Preference Mining (UBPM) model dedicated to HHC platform mainly consists of four layers:

Table 16.1 Parameter setting of patient access behavior preference prediction model based on attention mechanism

Notation	Description
$T \in [t_{\min}, t_{\max}]$	The time range of data used on the HHC platform
$U = \{u_1, u_2, u_3, ..., u_n\}$	n users on the HHC platform, i.e., n home health care demanders
$V = \{v_1, v_2, v_3, .., v_m\}$	m me health care service organizations on the HHC platform
$S = \{s_1, s_2, s_3, ..., s_i\}$	i home health care service categories on the HHC platform
$L = \{(u_1, v_1, t_{\min}, s_1), ..., (u_n, v_m, t_{\max}, s_i)\}$	Visiting and service information recorded in this time range on the HHC platform

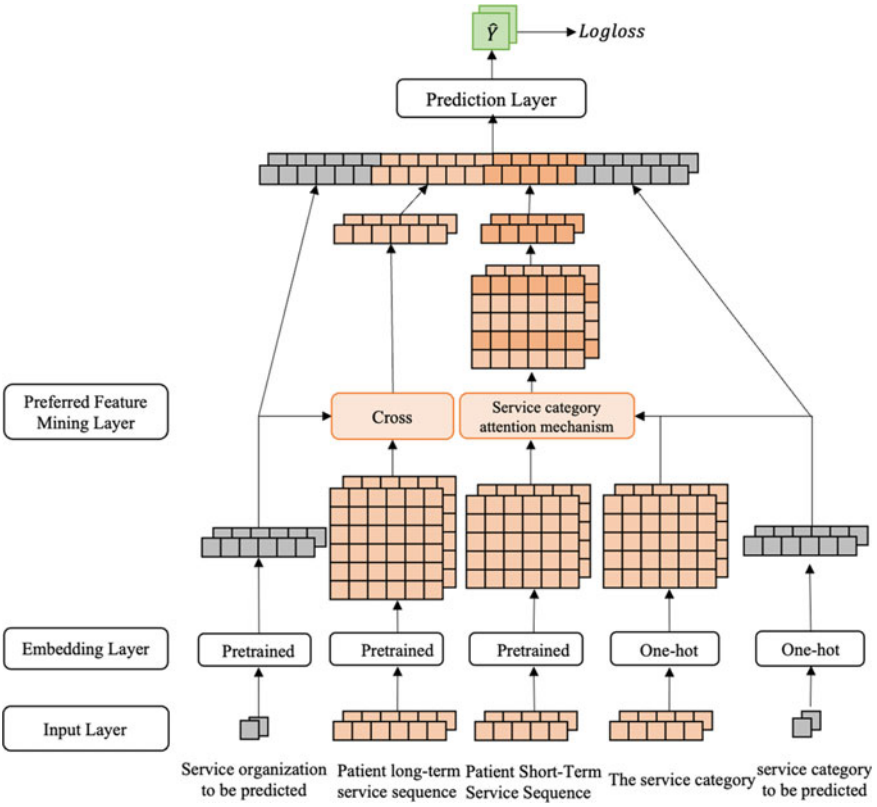

Fig. 16.1 General framework of UBPM model

(1) Input layer: behavior-related data and service-related data are put into the UBPM model.
(2) Embedding layer: one-hot and node2vec considering minimizing patients' preference difference are respectively used to different data from input layer.
(3) Preferred feature mining layer: short-Term visiting preference mining (STVPM) considering service category attention mechanism and long-term visiting preference mining (LTVPM) based on feature intersection are introduced in this layer.
(4) Prediction layer: the preference of home care demanders to organizations are predicted.

Input Layer

At the input layer, the UBPM model receives both historical data and online data extracted from HHC platform. The historical data consists of the information of home

care service organizations and possible service records. The online data are relevant with the patient's requirement, such as the patient's ID, type of the desired service etc. Accordingly, the data can be classified into two parts: behavior-related data and service-related data.

(1) Behavior-related data.

The behavioral data considered in this study are: (1) Type of service offered by home care organizations to patients; (2) Date when the home care service took place, which can be used to identify the service sequence offered by HHC organizations to patients.

Considering that the recent behavior may have greater impact on the decision, the UBPM model is enhanced by combining shot-term and long-term records from the targeted HHC platform in this study. Here below are the definition of these two categories of data: Short-Term Service Sequence (STSS), and Long-Term Service Sequence (LTSS).

Definition 1: **Short-Term Service Sequence**

For any patient $u \in U$, all the service records extracted from the HHC platform are sorted in descending order of timestamps. Set t as the cut-off time threshold, all the records observed within the period $(t - t_{short}, t]$ is classified to short-term service sequence, noted as $L_{short} = \{(u, v_1, t - t_{short} + 1, s_1), ..., (u, v_m, t, s_i)\}$.

Definition 2: **Long-Term Servicing Sequence.**

For any patient $u \in U$, all the records observed within the period $\left(t - t_{short} - t_{long}, t - t_{short}\right]$ are classified as long-term records, and the corresponding long-term service sequence is noted as $L_{long} = \left\{\left(u, v_1, t - t_{short} - t_{long} + 1, s_1\right), ..., \left(u, v_m, t - t_{short}, s_i\right)\right\}$.

(2) Service-related data

The service-related data, so called "prediction target" in the input layer, consists of two kinds of data:

(1) "Service category to be predicted": refers to the type of service required by patients.
(2) List of HHC service organizations with available resources to provide the service desired by the patient.

Embedding Layer

Receiving data from the input layer, two embedding functions are processed at the embedding layer, service category embedding and service organization embedding. Service categories are embedded using one-hot. For example, E_s^o is the embedding vector of service category s using one-hot. And service organizations are embedded as follows.

Step 1. **Construct patient behavioral preference matrix**

In this study, the patient behavioral preference matrix is constructed based on Term Frequency-Inverse Document Frequency (TF-IDF). Considering that the patient's behavioral preference may change over time, a hyperbolic function is applied here to fit Ebbinghaus's nonlinear forgetting curve [9], formulated as (16.1)–(16.4).

$$P_{u,v} = TF_{u,v} \times IDF(v) \times h(u) \tag{16.1}$$

$$T = \frac{\sum_{l'=1}^{l} I_{u,v,l'}}{\sum_{v'=1}^{m} \sum_{l'=1}^{l} I_{u,v',l'}} \tag{16.2}$$

$$IDF(v) = \log\left(\frac{\sum_{u'=1}^{n} \sum_{v'=1}^{m} \sum_{l'=1}^{l} I_{u',v',l'}}{\sum_{u'=1}^{n} \sum_{l'=1}^{l} I_{u',v,l'}}\right) \tag{16.3}$$

$$h(u) = (1-\theta) + \theta\left(\frac{t_{v\max} - t_{\min} + 1}{t_{\max} - t_{\min} + 1}\right)^2 \tag{16.4}$$

where $P_{u,v}$ represents the preference of patient u. to HHC service organization v; $TF_{u,v}$ represents the proportion of the services provided by the organization v for patient u; $IDF(v)$ represents the proportion of institution v in all service records L; $I_{u,v,l}$ indicates the proportion of occurrences in L. $I_{u,v,l}$ is equal to 1 if the organization v served patient u in record l, and 0 otherwise; t_{vmax} represents the time corresponding to the latest service provided by HHC service institution v to the patient u(time unit: one day); t_{min} and t_{max} represent the earliest and latest times that the patient u received home care service from the organizations registered in the HHC platform respectively; θ represents the forgetting coefficient.

Step 2. **Evaluate behavioral preference of HHC demander to supplier**

A network graph can be obtained based on patient behavioral preference matrix from step 1, which has patients and institutions nodes and service records' edges. Node2vec is a graph embedding method that considers both deep sample and breadth sample. In this paper, the goal of minimizing user preference differences is integrated into Node2vec to improve the effectiveness of feature embedding.

First, every node will be the starting point of ρ paths, whose length is q. If the starting point is t, the sampling probability $a_{t,x}$ of the neighbor node x of node t is the preference constructed from step 1, formulated as (16.5).

$$a_{t,x} = P_{t,x} \tag{16.5}$$

Second, the sample probability $\alpha_{t,x}$ of the rest nodes in the paths is considering minimizing user preference differences, formulated as (16.6). In particular, the network node in this paper is different from the general Node2vec, there is no patient- patient or institution- institution edge, so there is no $d_{tx} = 1$ case.

$$\alpha_{t,x} = \begin{cases} \frac{1}{\lambda} & if\, d_{t,x} = 0 \\ \frac{max(p_{t,v}, p_{v,x})}{|p_{t,v} - p_{v,x}|} & if\, d_{t,x} = 2 \end{cases} \tag{16.6}$$

where t is the last node in the sampled path; v is the penultimate node in the sampled path. x is one of the neighbor nodes of t. $p_{t,v}$ is the patient behavioral preference between node t and v;$p_{v,x}$ is similar. λ controls the probability of sampling duplicate node v.

Finally, to get embedding vectors of demanders and suppliers, we use Skip-gram to maximum likelihood optimization, formulated as (16.7).

$$max_f \sum_{t \in U,V} log\, Pr(N_w(t)|E_t^n) \tag{16.7}$$

where t is node in the network graph; $N_w(t)$ are neighbor nodes of t in the window w;E_t^n is the embedding vector of node t using node2vec.

Now we can embed all the service sequences by embedding the organizations and service categories. The short-term service sequence $L_{short} = \{(u, v_1, t - t_{short} + 1, s_1), ..., (u, v_m, t, s_i)\}$ can be embedded as $E_{L_{short}} = \left\{\left(u, E^n_{v_{t-t_{short}+1}}, t - t_{short} + 1, E^o_{s_{t-t_{short}+1}}\right), ..., \left(u, E^n_{v_t}, t, E^o_{s_t}\right)\right\}$. And the long-term service sequence $L_{long} = \left\{\left(u, v_{t-t_{short}-t_{long}+1}, t - t_{short} - t_{long} + 1, s_{t-t_{short}-t_{long}+1}\right)\right\}$, …, $\left(u, v_{t-t_{short}}, t - t_{short}, s_{t-t_{short}}\right)$ can be embedded as $E_{L_{long}} = \left\{\left(u, E^n_{v_{t-t_{short}-t_{long}+1}}, t - t_{short} - t_{long} + 1, E^o_{s_{t-t_{short}-t_{long}+1}}\right)\right\}$,..., $\left(u, E^n_{v_{t-t_{short}}}, t - t_{short},\right) E^o_{s_{t-t_{short}}}$.

Preferred Feature Mining Layer

Receiving short-term and long-term embedded sequences data from the embedding layer, the preference feature mining layer considers different feature mining functions: Short-Term Visiting Preference Mining (STVPM) considering the target service category and Long-Term Visiting Preference Mining (LTVPM) considering the target organization.

1 **STVPM Module**

First, the short-term embedded sequence $E_{L_{short}} = \left\{\left(u, E^n_{v_{t-t_{short}+1}}, t - t_{short} + 1, E^o_{s_{t-t_{short}+1}}\right), ..., \left(u, E^n_{v_t}, t, E^o_{s_t}\right)\right\}$ is put into GRU module to learn time series feature $E^{GRU}_{L_{short}} = \left\{\left(u, E^{GRU}_{v_{t-t_{short}+1}}, t - t_{short} + 1, E^o_{s_{t-t_{short}+1}}\right), ..., \left(u, E^{GRU}_{v_t}, t, E^o_{s_t}\right)\right\}$. Second, considering the similarity between the service category at each time step and the target

service category, the attention mechanism is used. This paper adopts the inner product method to measure the attention similarity, formulated as (16.8) and (16.9).

$$short_u = \sum_{T=t-t_{short}+1}^{t} \alpha\left(E_s^o \odot E_{s_T}^o\right) E_{v_T}^{GRU} \tag{16.8}$$

$$\alpha_T = \frac{e^{E_{v_T}^n}}{\sum_{i=0}^{t} E_{v_i}^n} \tag{16.9}$$

where $E_{v_T}^{GRU}$ is the deep feature get from GRU model; E_s^o is the one-hot embedding of the target service category; $E_{s_T}^o$ is the one-hot embedding of user's service category at time T; $\odot$ is the dot product operation, which is used to calculate the similarity between the target service category and the sequence behavior service category; α_T is the attention weight obtained by normalizing the similarity; $short_u$ is the user's short-term visiting preference.

(2) **LTVPM module**

First, considering the target organization, the long-term embedded sequence $E_{L_{long}} = \left\{\left(u, E_{v_{t-t_{short}-t_{long}+1}}^n, t - t_{short} - t_{long}\right)\right\} + 1, E_{s_{t-t_{short}-t_{long}+1}}^o$,..., $\left(u, E_{v_{t-t_{short}}}^n, t - t_{short}, E_{s_{t-t_{short}}}^o\right)$ is put into long cross module to learn interactive feature $E_{L_{long}}^{cross} = \left\{\left(u, E_{v_{t-t_{short}-t_{long}+1}}^{cross}, t - t_{short} - t_{long} + 1, E_{s_{t-t_{short}-t_{long}+1}}^o\right)\right\}$,..., $\left(u, E_{v_{t-t_{short}}}^{cross}, t - t_{short}, E_{s_{t-t_{short}}}^o\right)$, and then we concatenate all interactive features, formulated as (16.10). Second, we can get deep long-term visiting preference $long_u$ by put $long_u^{cross}$ into DNN.

$$\begin{aligned} long_u^{cross} &= \sigma\left(E_{v_{t-t_{short}-t_{long}+1}}^n \odot E_v^n\right) \oplus \ldots \oplus \sigma\left(E_{v_{t-t_{short}}}^n \odot E_v^n\right) \\ &= E_{v_{t-t_{short}-t_{long}+1}}^{cross} \oplus \ldots \oplus E_{v_{t-t_{short}}}^{cross} \end{aligned} \tag{16.10}$$

where E_v^n is the embedding vector using node2vec of target organization; $E_{v_{t-t_{short}}}^n$ is the embedding vector of the service organization in user's long-term sequence at time $t - t_{short}$; $E_{v_{t-t_{short}}}^{cross}$ is the cross feature of the service organization in user's long-term sequence at time $t - t_{short}$.

Prediction Layer

In the Prediction layer, we consider the all behavior-related feature and service-related data, so called "prediction target". We concatenate target service category embedding vector using one-hot, target organization embedding vector using

node2vec from embedding layer, the short-term visiting preference $short_u$ and long-term visiting preference $long_u$ from preferred feature mining layer. And we put them into DNN module to predict the probability y_{uvs} of visiting organization v when a user u with service sequence L under the demand of service category s.

Training Layer

The learning layer in this paper uses Logloss as the loss function, formulated as (16.11).

$$Logloss = -\frac{1}{|Y|}\sum_{y_{uvs}\in Y}\left[y_{uvs}log\widehat{y_{uvs}} + (1 - y_{uvs})log\left(1 - \widehat{y_{uvs}}\right)\right] \tag{16.11}$$

where $y_{uvs} \in \{0, 1\}$ is the real label value of whether user u with service sequence L visits organization v under the demand of service category s; Y is the set of real labels, $\widehat{y_{uvs}}$ is the predicted probability of visiting organization v when a user u with service sequence L under the demand of service category s.

Experiments and Results

Data Preparation

The data used in the experiment in this paper is a simulation data set generated based on the home service data table of fengxian District Civil Affairs Comprehensive service for the elderly obtained from Shanghai Public Data Open Platform [10] and combined with the characteristics of home care service demand referring to the definition of service categories in "Shanghai Regulations on Nursing Services of Long-term Care Insurance Community Home and Elderly Care Institutions (Trial)" [142] of Shanghai municipality. Without loss generality, the number of service categories considered in this study is set as 20. And the patient data was anonymized.

As shown in Table 16.2, when generating experimental data, we divided patients into six grades [11]. Considering the long-term sustainability of home care services and the periodicity of user needs, the corresponding frequency of visits should be set for each service category according to the evaluation and grading standards of user care needs in "Shanghai Long-term Care Insurance Policy 108 questions" [11]. At present, users with assessment grade 1 do not meet the user requirements of Shanghai long-term care insurance, and the service frequency is defined as one visit per week in this paper. The proportion of Patients of each grade and the corresponding proportion of demand service categories are in columns 4 and 5. The service records

Table 16.2 Proportion of patients with different levels of care in the experimental dataset

Patient grade	Nb. visits per week	Proportion of patients	Demand category proportion
CL 1	1	35%	5%
CL 2	3	20%	10%
CL 3	3	20%	10%
CL 4	5	10%	15%
CL 5	7	10%	30%
CL 6	7	5%	30%

Table 16.3 Parameter setting of patient access behavior preference prediction model based on attention mechanism

Patient grade	Value
Number of sampling paths per node ρ	80
Path length q	10
The probability of sampling repeated nodes λ	0.25
Time window in path w	5
Feature vector embedding dimension	128
Number of Iterations	3000
The number of GRU network layers	3
Learning rate	0.001

of the experimental data set covered a time span of six months and about 26 weeks and contained 274,300 service records from 1000 users to 100 home care providers.

Parameter Setting and Operating Environment

All the algorithms are coded with Python on the Jupyterlab platform with an Apple laptop (M1 Pro CPU, 16 GB memory). As proposed, 80% of the samples are used for training and the rest is reserved for validation. The details of parameter setting are shown in Table 16.3.

Experimental Results

According to the experimental results, it is observed that the AUCs for the training set, verification set, and test set are 0.881, 0.865 and 0.858 respectively, which are all greater than 0.85. As shown in Fig. 16.2, when the number of iterations increases, the logloss decreases gradually to 0.3, and the accuracy rate of the top 10 most favorable suppliers is near to 0.8. Furthermore, it is observed that when learning rate is 0.001,

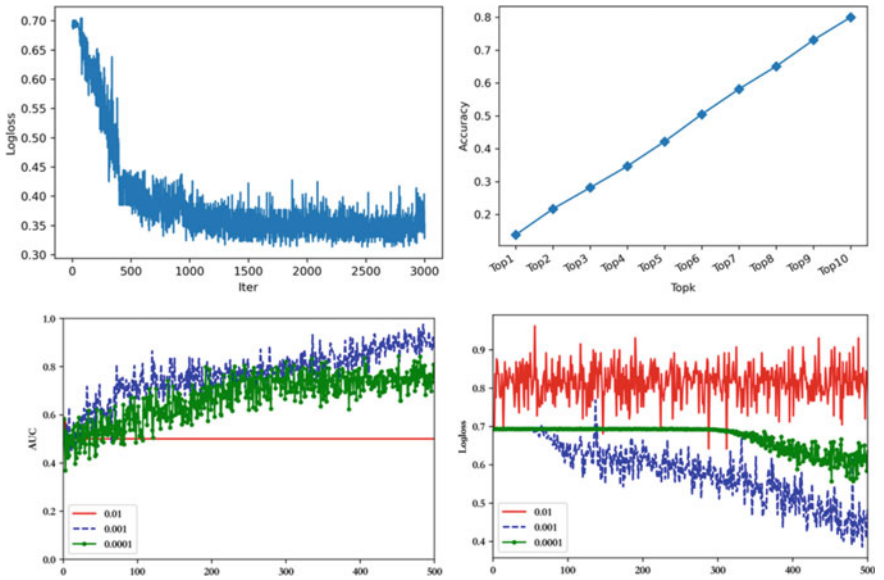

Fig. 16.2 Experimental results

the model preform the best. In consequence, it is reasonable to verify that the proposed DL model can effectively extract the preferences of home care demanders to service suppliers. The results of our study can help improve the quality of recommending service suppliers to home care demanders since it is reasonable that the higher the accuracy of the model in predicting the patient's behavior preference, the greater the probability of prediction accuracy will be.

To analyze the impact of short-term historial results on the prediction results, the attention mechanism is applied to improve the learning model in this study. In addition, both long-term and short-term historical data that may reveal different behavior features are combined as well to enhance the quality of prediction results. In order to verify the performance of the advanced model, the model not only using attention mechanisom to mine short-term behavior characeristics but also implementing cross embedding of long-term behavior characteristics (Model DL-SA-L-C), three benchmarks are constructed as follows:

Model DL-NS-L-NC: do not use short-term behavior data; use long-term sequence data but do not mine long-term behavior features, i.e. use directly the traditional depth neural network to predict the behavioral preference of home care demanders.

Model DL-SM-L-NC: mine short-term behavior features with deep cyclic neural network without attention mechanism; use deep neural network to learn long-term behavior features, but do not crossover long-term behavior features with short-term features.

Model DL-NS-L-C: do not mine short-term behavior feature; Implement cross embedding of long-term behavior characteristics.

Table 16.4 AUC of different models

Model	AUC in test dataset	AUC in train dataset	AUC in valid dataset
DL-NS-L-NC	0.697	0.699	0.701
DL-SM-L-NC	0.825	0.781	0.817
DL-NS-L-C	0.812	0.790	0.829
DL-SA-L-C	0.881	0.865	0.858
Wide&Deep	0.502	0.503	0.500
DeepFM	0.586	0.616	0.608
DCN	0.586	0.631	0.622

And we compare our model with Wide&Deep, DeepFM, DCN. As shown in Table 16.4, it can be observed that (1) the AUC of model DL-SM-L-NC is better than that of model DL-NS-L-NC, indicating that patients' preferences are affected by short-term behavior, and the short-term behavior mining model based on deep GRU is effective in predicting patients' preferred behavior; (2) the AUC of model DL-NS-L-C is better than that of the model DL-SM-L-NC, indicating that the model using feature crossover can help improve the prediction of long-term behavior features; (3) the model DL-SA-L-C always outperforms the model DL-NS-L-C, indicating that both the attention mecanishm and the crossover of short-term and long-term behavioral preference can help improve the accuracy of prediction accuracy. At this problem, our model is best among the compared models.

Furthermore, it is observed that about 50% of the demanders' actual selection can be observed within list of HHC suppliers ranked as the top 5 most preferred service suppliers, and the rate increases to 80% when the list of suppliers extended to the top 10, indicating that the proposed prediction model can be applied to provide good quality solution for predicting the preference of HHC demanders to various suppliers available in HHC platform, which can be applied further in the recommendation system to balance the utilization of valuable HHC service resources and patients' satisfaction.

Summary

In this study, an advanced deep learning model, combined with attention mechanism for mining the short-term preference demanders to service suppliers and crossover of short-term features with long-term features relevant with specified service type, is constructed for predicting the visting preference of a user to home care service suppliers on an HHC platform. Experimental results show that the proposed model can effectively mine HHC demanders' behavioral preference and give valuable recommendation information to home care demanders.

References

1. Casebeer, A. W., et al. (2022). A comparison of home health utilization, outcomes, and cost between Medicare advantage and traditional Medicare. *Medical Care, 60*(1), 66–74.
2. Rest, K. D., & Hirsch, P. (2022). Insights and decision support for home health care services in times of disasters. *Central European Journal of Operational Research, 30*, 133–157.
3. Xiao, R., Miller, J. A., Zafirau, W. J., et al. (2018). Impact of home health care on health care resource utilization following hospital discharge: A cohort study. *American Journal of Medicine, 131*(4), 395-407.e35.
4. Deo, S. V., Sharma, V., Altarabsheh, S. E., Raza, S., et al. (2021). Home health care visits may reduce the need for early readmission after coronary artery bypass grafting. *The Journal of Thoracic and Cardiovascular Surgery, 162*(6), 1732-1739.e4.
5. Liu, W., Dridi, M., Fei, H., & El Hassani, A. H. (2021). Solving a multi-period home health care routing and scheduling problem using an efficient matheuristic. *Computers & Industrial Engineering., 162*, 107721.
6. Wang, Q., Liu, F., Zhao, X., et al. (2022). Session interest model for CTR prediction based on self-attention mechanism. *Science and Reports, 12*(7), 252.
7. Yalcindag, S., & Lanzarone, E. (2021). Merging short-term and long-term planning problems in home health care under continuity of care and patterns for visits. *Journal of Industrial & Management Optimization, 18*(2), 1487–1504.
8. Liu, Y. W., Pei, A. X., Wang, F., et al. (2021). An attention-based category-aware gru model for the next POI recommendation. *International Journal of Intelligent Systems, 36*(7), 3174–3189.
9. Liu, C., Liang, G. L., & Tan, G. P. (2013). Fusion of personalized recommendation model based on user's interest drifting. *Computer Engineering and Design, 34*(08), 2944–2950.
10. People's Government of Fengxian District, Shanghai, China: 'Home service data sheet of Fengxian District civil affairs comprehensive service for the elderly'. (2021). https://data.sh.gov.cn/view/data-resource/index.html#:~:text=%E6%9C%8D%E5%8A%A1%E5%B1%85%E5%AE%B6%E6%9C%8D%E5%8A%A1-,%E6%95%B0%E6%8D%AE,-%E8%A1%A8
11. Shanghai Civil Affairs Bureau, China: 'Shanghai long-term care insurance policy 108 questions'. (2021). http://ylgw.shweilao.cn/cms/cms/Detail?uuid=a44bfbea-6edb-4c90-b76b-7e6515181f85

Chapter 17
Dynamic Ranking of Physicians in Online Healthcare Platforms with Multiple Service Types

Ziwei Wang, Jie Song, and Jingtong Zhao

Abstract Online healthcare services are developing rapidly in recent years. They provide a convenient way for patients to consult with physicians across the country. However, they also bring new challenges to online healthcare platforms. Physicians' resources are usually limited. What's more, patients are heterogeneous, and vary in their severity of illness, choice behaviors and preferences for different service types. In this work, we consider a multiple service type setting, where we characterize the choice behaviors of patients, and formulate the problem of the platforms using dynamic programming. With the huge number of choices usually displayed on online healthcare platforms and great uncertainty in patient behaviors, our goal is to design personalized physician ranking methods to maximize the total pairing reward. We propose two types of methods based on improving the inventory balancing methods and the value function approximation methods to better fit our setting. Through numerical experiments, we show that our methods generally outperform the existing methods. Our findings can help online healthcare platforms adopt the most suitable ranking method in different situations to improve service quality.

Keywords Ranking · Dynamic programming · Heuristic algorithms · Simulations

Supplementary Information The online version contains supplementary material available at https://doi.org/10.1007/978-3-031-15644-1_17.

Z. Wang · J. Song
Department of Industrial Engineering and Management, College of Engineering, Peking University, Beijing, China
e-mail: wangzwdl@pku.edu.cn

J. Song
e-mail: songjie@coe.pku.edu.cn

J. Zhao (✉)
School of Economics, Renmin University of China, Beijing, China
e-mail: zhaojingtong@ruc.edu.cn

R. Qiu et al. (eds.), *City, Society, and Digital Transformation*, Lecture Notes in Operations Research, https://doi.org/10.1007/978-3-031-15644-1_17

Introduction

Internet technologies have boosted the development of online healthcare services in recent years. Over the past two years, more than 600 Internet hospitals have been launched in China. Different from traditional healthcare systems, where patients go to a real hospital with limited choices of physicians, online healthcare platforms hire physicians from hospitals across the country and patients can get professional medical advice while staying at home. Many online healthcare platforms offer multiple service types to meet the needs of different patients. For example, HaoDF and WeDoctor in China offer consultations via texts, graphs, phone calls as well as online scheduling for offline visits. Offering multiple service types has many benefits. Usually, text services are cheaper, and less time consuming than phone calls. This provides patients with minor deceases a more efficient way of treatment than going to hospital and can save resources in offline hospitals for more urgent needs. For patients with deceases that require instant medical attention such as cuts and wounds, they can get immediate advice via graph consultations.

Although online healthcare services have many advantages, they also bring new challenges to management. The number of physicians and patients is growing explosively for many online platforms recently, so a main problem is how to match patients with physicians efficiently in real time. This is especially important when each physician can only devote a limited amount of time to online consultation, and patients tend to flock to experts with high reputations. Since online healthcare platforms usually have fixed prices for physicians, the main method to influence patients' choices is the way physicians are displayed. According to the study [1], the click-through rate of an item is greatly influenced by its position in the list. HaoDF platform currently shows to each patient a ranking list computed by a hidden rule called the "hot index". However, it might show a physician whose capacity is used up, and the recommendations are not personalized. As a result, patients have to spend more time to search for a physician that meet their needs. Thus, in our paper, we focus on designing methods to better rank the physicians so that the resources are allocated in an optimal way.

Specifically, upon a patient's arrival, the platform offers a list of physicians, containing information about their areas of expertise. The patient browses the list, then either chooses a physician or leaves the platform. The browsing behaviors of patients can be captured by a discrete choice model. If the patient chooses one physician, he will then choose a specific type of service, e.g. text consultation or phone consultation. Different types of services consume different units of a physician's capacity and provide different pairing rewards.

In practice, online healthcare platforms usually have access to information about patients' requirements and preferences, because it saves a profile for each patient once they register and records whether they've been to first class hospital, their past medical history, patients' condition descriptions, etc. Hence, the platforms can categorize patients according to their profiles. Patients of the same type often have similar behaviors, so in this way, the platforms can better predict patients' needs and offer personalized ranking lists. Physicians are also specialized in different areas,

and being served by the same physician may cause different pairing rewards due to a patient's disease type. Our goal is to maximize the total pairing rewards over a finite horizon with limited physician capacities.

Our main contributions are as follows. First, we are one of the first to model the multiple service types offered by online healthcare platforms. Previous studies assume each physician only offers one service type, whereas considering multiple service types brings new challenges. In our setting, the platform cannot just assign a physician to a patient, because the units of capacity the patient will consume is uncertain, and ignoring this effect may lead to inefficiency of service. For instance, if a patient chooses a physician whose remaining capacity is less than the units required by the service he chooses, the patient will leave. Thus, the number of service types a physician can offer now should also be taken into account during recommendation. Besides, although a patient who consumes larger units of capacity achieves a higher reward at the moment, it may make the physician unavailable to subsequent patients. Hence, we need more delicate allocation of physician resources. In order to deal with the new challenges, we propose two methods for the problem based on inventory balancing methods and value function approximation methods, and compare the performances of different algorithms. Different from the original methods, we add capacity consumption of different services into consideration to better allocate physicians' resources. We find that our methods generally perform better than the other ones, and we summarize the most applicable scenarios for each of our two methods. Third, we give a theoretical bound of the linear approximation function under certain conditions, which explains why the linear approximation method performs robustly to some extent. We believe our findings can be implemented in practice and help online medical platforms improve service quality.

Our paper is organized as follows. In section "Literature Review", we give a literature review of choice models and dynamic resource allocation. In section "Problem Formulation", we build our model including patients' choice behavior and platform's service mechanisms, and formulate a dynamic program. In section "Dynamic Ranking Methods", we propose our main algorithm as well as introducing some benchmark algorithms. In section "Numerical Experiment", we use numerical experiment to testify the advantage of our proposed method.

Literature Review

Choice Models

Choice models concern how people make decisions, and can help platforms predict the behaviors of future customers using historical data. For example, Multinomial Logit (MNL) model [2, 3] to model customers' choice behaviors in retailing and revenue management respectively. Since the MNL model cannot model multiple customer segments, the mixed multinomial logit (MMNL) model is proposed [4].

The MNL model has a strong assumption called Independence from Irrelevant Alternatives. The Nested logit (NL) model weakens this assumption, and allows it to be satisfied only within a nest [5]. Another stream of choice models originates from web search problems, and is also referred to as click models. Joachims et al. [6] find that the click through rate (CTR) at the first position is much larger than that at the tenth position, and formulate the rank based CTR model. Craswell et al. [7] estimate the CTR of each query-document pair and propose a cascade model. Their model assumes a user will scan from the top to the bottom until he find a document that meets his need. In practice, users are usually impatient, so Guo et al. [8] build a click chain model (CCM) to handle the situation where a user may abandon the search and leave in the middle.

In practice, click data can be easily collected, while MNL type of models requires modeling user utility and further estimation of the parameters. The utility function might include many factors such as price, physicians' ratings, locations, etc., and the effects are usually hard to measure. Thus, the choice model in our paper is mainly based on the click models [7] and [8].

Dynamic Resource Allocation

How to selectively satisfy customers' demands for resources to achieve the optimal allocation policy is an important topic in revenue management. To deal with such an online resource allocation problem, one natural way is to assign an index to each resource. The indices are required to take both the pairing rewards and the remaining capacities into account. This can be achieved by multiplying the reward by a penalty function with respect to the remaining capacity. Mehta et al. [9] are among the first to apply this method. Their goal is to maximize the total revenue earned from displaying ads for a search engine while respecting the budget constraints of the bidders. The fraction of bidder i's budget that has been spent is represented by $f(i)$. And the penalty function is in the form of $1 - e^{f(i)}$. Golrezaei et al. [10] apply this idea to a resource allocation problem similar to ours, and their method is referred to as the Inventory Balancing Algorithm (IB). They define a discount function $\Phi(x) = \left(1 - e^{-x}\right)$. This is a concave function that decreases rapidly near 0. They assume customers have the same pairing reward r_j with a certain product j. The IB method ranks products in decreasing order of $r_j * \Phi\left(c_{tj}/c_j\right)$, where c_{tj} is the inventory level of resource j at time t, and c_j is the initial capacity of resource j. Later, Wen et al. [11] adjust the index function to the case where a type i patient's pairing reward with physician j depends on his types, namely r_{ij}. They propose the Adjusted Exponential Inventory Balancing Algorithm (AEIB). Denote $\overline{r}_i = \sum_j r_{ij}/N$ as the average pairing reward, where N is the total number of physicians. They include the relative pairing term $r_{ij}/\overline{r}_i$ in the index function, which then has the form $r_{ij}\Phi\left(c_{tj}r_{ij}/\overline{r}_i c_j\right)$. We will extend these index based methods in our problem.

One shortcoming of this index-based type of methods is that it completely ignores the underlying dynamic programming (DP) structure in the problem. Another stream

of research focuses on approximating the value functions in DP. Bernstein et al. [12] approximate the marginal value in DP with marginal value in the news vendor function, and propose two heuristic methods. Gallego et al. [13] solve an offline choice based linear program (CDLP) to get the optimal probability of showing each ranking list, and use it in the value approximation method called First Come First Serve (FCFS). However, when the number of ranking lists is large, there might be an exponentially large number of columns in the LP, and is hard to solve. Gallego et al. [14] propose another looser offline upper bound called sales based linear program (SBLP) that is easier to solve. Pan et al. [15] and Wen et al. [16] use this offline value to form an approximation of the value functions for online healthcare platforms. Another way is to use approximate dynamic programming (ADP). For example, linear approximation is used in Refs. [17, 18]. They compute the parameters via iterations and the policy can obtain at least 50% of the optimal revenue in Ref. [18]. Our work is mainly based on Ref. [18] and we extend this method to allow more than one unit of resources to be consumed at a time. This stream of methods also has disadvantages, caused by assumptions for the form of value functions. It's hard to directly analyse which type of method is better, and we will evaluate their performances with numerical experiment in section "Numerical Experiment".

Problem Formulation

We consider the problem faced by an online healthcare platform with a discrete planning horizon of length T. Note that this is equivalent to assuming patients arrive sequentially according to a Poisson process, because we can split time into small enough intervals so that the case of more than one person arriving during the same time interval can be ignored. This assumption is commonly used, for example in Refs. [11, 16, 20]. Hence, we assume that the patients arrive at discrete time $t = 1, 2, \ldots, T$. The platform has a total of M types of patients, indexed by $i = \{1, 2, \ldots, M\}$, and N physicians, indexed by $j = \{1, 2, \ldots, N\}$. Physician j has a limited capacity c_j at the beginning of the planning horizon. Each physician provides K types of services, indexed by $k = \{1, 2, \ldots K\}$. Each type of service consumes different units of a physician's capacity. For example, phone consultations usually take more time than text consultations. We use the vector $\boldsymbol{D}$ to characterize it, where d_k denotes the units consumed if service type k is chosen. For a patient that arrives at time t, the platform can identify the patient's type i_t based on his uploaded information. After observing the patient's type, the platform chooses a subset of physicians S and shows an ordered list of physicians $\boldsymbol{\sigma}(S)$ to him. The order function $\boldsymbol{\sigma}(S)$ can be viewed as a mapping from S to $\mathbb{Z}^+$. Let $\sigma(m)$ represent the physician at position m that is in the subset S. Then the patient browses the list and either chooses a physician or leaves.

We use a cascade click model to capture the browse behaviors of patients. After the platform shows a list of physicians to the patient, he will view it from the top, examine the detailed disease type each physician specializes on, and click on the

service page of the first physician that meets his need. Due to limited patience, the patient will leave the platform after browsing a certain number of physicians on the list if none of them meets his need. The probability of viewing the information of m number of physicians is represented by f_m. We assume that all type i patients have similar preferences, and similar probabilities of clicking on physicians after viewing them, represented by $\boldsymbol{v_i}$, where v_{ij} denotes a type i patient's probability of clicking on physician j. It can be viewed as the click probability when physician j is placed at the top. Let $m_j = \sigma^{-1}(j)$ denote the position of physician j on the list. Then his probability of choosing physician j can be represented by

$$p_{ij}(\boldsymbol{\sigma}(S)) = v_{ij}\left[\prod_{m=1}^{m_j-1}\left(1 - v_{i\sigma(m)}\right)\right]\left(1 - \sum_{m=1}^{m_j-1} f_m\right) \tag{17.1}$$

where we use p_{ij} to denote the probability that physician j is chosen by a type i patient, given that the list shown is function $\boldsymbol{\sigma}(S)$. The Eq. (17.1) consists of three parts. The first part v_{ij} denotes the click probability when he sees physician j. The second part $\prod_{m=1}^{m_j-1}\left(1 - v_{i\sigma(m)}\right)$ is the probability that he does not choose any physician before j, i.e. he continues browsing until he sees physician j. The third part $\left(1 - \sum_{m=1}^{m_j-1} f_m\right)$ denotes the probability he does not leave the platform before viewing at least m_j physicians. The final probability of choosing physician j is then the multiplication of these three parts. If physician j is not in the list, then he cannot be chosen, the probability is therefore 0. Adding more physicians to the browsing list will always increase the probability of a physician being chosen. However, usually there are limited positions on the web page, and the marginal increase in revenue of adding a physician decreases. Thus, we assume the length of the ranking list $|S|$ is not larger than a constant L.

If a patient chooses a physician, he will then choose a type of service that is available. We use $\boldsymbol{q_i}$ to denote the probability of choosing each type of service, where q_{ik} represents the probability of choosing service type k. If none of the physicians shown can provide the service the patient wants, he will leave the platform.

The pairing reward is related to the chosen physician and the service type. Suppose a type i patient chooses physician j and type k service, then the reward will be r_{ijk}. The platform's goal is to maximize the total pairing reward in a finite horizon where patients arrive randomly. Since the platform does not know the number of each type of patients in advance, this is an online dynamic resource allocation problem. We want to develop methods with relatively high rewards in expectation comparing to an optimal offline method that knows all the demands in advance.

Static Ranking Problem

First, we will discuss a recommendation problem in the static setting because the policies in the dynamic ranking problem is composed of static ranking problems each time a patient arrives. The static ranking problem for type i patients can be written as

$$\begin{aligned} &\max_{\boldsymbol{\sigma}(S)} \sum_{j\in S} p_{ij}(\boldsymbol{\sigma}(S))\tilde{r}_{ijt} \\ &\text{s.t.} \quad |S| \le L \end{aligned} \tag{17.2}$$

$\tilde{r}_{ijt}$ here can be regarded as a ranking index for type i patient, and is related to both the pairing reward and the remaining capacity of physician j at the moment t. This index can be computed by the inventory balancing methods or the value function approximation methods in the next section. Note that $\tilde{r}_{ijt}$ can be negative. As it is hard to find the optimal solution, we will use a greedy ranking policy here. To be specific, we first neglect physicians with negative index, and then we rank the remaining set of physicians denoted by $J_t^+(i)$ in decreasing order of $v_{ij}\tilde{r}_{ijt}$, i.e. we pick the largest $\min\left\{\left|J_t^+(i)\right|, L\right\}$ ones to recommend. The greedy method is efficient, as shown in Theorem 1, and the proof can be found in our appendix:

Theorem 1 The objective function of the static ranking problem is submodular, so that the greedy algorithm can achieve a performance ratio of at least $1 - \frac{1}{e}$.

Dynamic Programming Formulation

The platform's problem can be formulated using dynamic programming, so we will first describe the states and the transitions of the system. The state at time t can be represented by a vector $\boldsymbol{c_t} = (c_{1t}, c_{2t}, \ldots, c_{Nt})^\top$. The component c_{jt} represents the remaining capacity of physician j at time t. Note that the set of all possible states is finite. If a type i patient arrives at time t and chooses physician j and service type k, and the physician has enough capacity to accept the patient, then

$$c_{t+1l} = \begin{cases} c_{tl} - d_k & l = j \\ c_{tl} & \text{otherwise} \end{cases}. \tag{17.3}$$

If the patient leaves without choosing a physician, or the chosen physician does not have enough capacity, then

$$\boldsymbol{c_{t+1}} = \boldsymbol{c_t}. \tag{17.4}$$

Let λ_i denote the probability of having a type i patient at each time step, which could also be understood as the arrival rate of each type of patients in a Poisson arrival process. We are now at the point to introduce the DP equations. Let $V_t(\boldsymbol{c_t})$ denote the maximum total expected revenue from the rest of planning horizon at time t when the current capacity vector is $\boldsymbol{c_t}$. Then the recursion formula is

$$\begin{aligned} V_t(\boldsymbol{c_t}) = \sum_i \lambda_i \max_{\boldsymbol{\sigma}(S)} \{ & p_{i0}(\boldsymbol{\sigma}(S)) V_{t+1}(\boldsymbol{c_t}) \\ & + \sum_j p_{ij}(\boldsymbol{\sigma}(S)) \sum_k q_{ik} \Big[1_{\{c_{tj} \geq d_k\}} \big(r_{ijk} + V_{t+1}(\boldsymbol{c_t} - d_k \boldsymbol{e}_j) \big) \Big] \\ & + \Big(1 - 1_{\{c_{tj} \geq d_k\}} \Big) V_{t+1}(\boldsymbol{c_t}) \Big] \Big\} \\ & + \left(1 - \sum \lambda_i \sum_i \right) V_{t+1}(\boldsymbol{c_t}), \end{aligned} \tag{17.5}$$

The first line in the summation represents the case where the patient leaves without choosing a physician, which happens with probability $p_{i0}(\boldsymbol{\sigma}(S))$. The second line represents the case where patient i chooses physician j and service k. We use the indicator function $1_{\{c_{tj} \geq d_k\}}$ to represent whether there is enough capacity. If the capacity is enough, then we allocate the patient to the physician and receive a reward of r_{ijk}. In this case, the state transforms into $V_{t+1}\big(\boldsymbol{c_t} - d_k \boldsymbol{e}_j\big)$. The notation $\boldsymbol{e}_i$ here stands for a size N unit vector whose jth component is 1, and 0 elsewhere. Otherwise, the patient leaves without consuming any capacity, and the value of this is included in the third line. The last line represents the case where no patient arrives at time t. This happens with probability $\big(1 - \sum_i \lambda_i\big)$.

Dynamic Ranking Methods

Usually, the number of physicians on a healthcare platform is much larger than that in a real hospital. Hence, the number of states in Eq. (17.5) will grow explosively in our problem. Due to the curse of dimensionality, it is time consuming to directly calculate the value function in every state. Instead, heuristic methods and value approximation methods are often used to deal with such problems. We will propose a heuristic inventory balancing method called Multiple Service Exponential Inventory Balancing Method (MSEIB) and a linear approximation method called Multiple Service Linear Approximation Algorithm (MSLAA). We will also compare these algorithms with another benchmark methods.

Both the inventory balancing methods and the approximation methods aim to reduce the dynamic programming problem to a static ranking problem. Since a static ranking problem has a time complexity of at most $O(N \log N)$, it can be used to

compute a ranking quickly in response to each arriving demand. The main difference between these two types of method is that inventory balancing methods are heuristic methods, and do not use any kind of value functions of the states. In contrast, approximation methods focus on how to approximate the value functions efficiently based on the structure of the DP equation. Intuitively, when resources are scarce, i.e. the average available resources for each demand is small, we need to allocate the resources more carefully, and the second type of methods may perform better if the error of approximation does not exceed the error of completely ignoring the dynamic programming structure. However, when capacity is sufficient, the error caused by linear assumption in approximation methods may be larger. The details of each method will be explained below, and we will use numerical experiment to verify our intuition in the next section.

Inventory Balancing Methods

In our setting, different service types consume different units of capacity. The penalties for service types consuming more units should be larger. We use the function Φ to penalize the pairing reward when the remaining capacity is low. Assume that at time t a type i patient arrives and chooses physician j and type k service. The platform's initial reward is r_{ijk}. Let $r_{ij} = \sum_k q_{ik} r_{ijk}$ denote the general pairing reward between a type i patient and physician j, and similarly, let $\bar{r}_i = \sum_j r_{ij}$ denote the average pairing reward. In order to distinguish between different service types, a naive approach is to penalize r_{ijk} with $c_{tj} - d_k + 1$, the remaining capacity after the service is provided plus one. We call this the Strict Exponential Inventory Balancing Method (SEIB). Its penalty form is

$$\tilde{r}_{ijt} = \sum_k q_{ik} 1_{\{c_{tj} \geq d_k\}} r_{ijk} \Phi\left(\frac{c_{tj} - d_k + 1}{c_j} \frac{r_{ij}}{\bar{r}_i} \right) \tag{17.6}$$

However, such a policy might be too conservative about the remaining capacity. As a result, physicians with lower pairing rewards are often recommended solely because of their higher remaining capacities. An intermediate policy might work better. Thus, we propose the Multiple Service Exponential Inventory Balancing Method (MSEIB) that extends the current method by taking different capacity consumption into consideration. When the remaining capacity is $\boldsymbol{c_t}$, we set the inventory balancing reward of matching a type i patient to physician j as

$$\tilde{r}_{ijt} = \sum_k q_{ik} 1_{\{c_{tj} \geq d_k\}} r_{ijk} \left(\frac{1}{d_k} \sum_{m=0}^{d_k - 1} \Phi\left(\frac{c_{tj} - m}{c_j} \frac{r_{ij}}{\bar{r}_i} \right) \right) \tag{17.7}$$

We can see from Eq. (17.7) that if $d_k = 1$, the penalty part reduces to $\Phi\left(c_{tj} r_{ij} / c_j \bar{r}_i\right)$, which is exactly the form proposed by Wen et al. [11], namely, the

AEIB method. However, that function penalizes each type of service using the same term. For the pairing reward r_{ijk}, MSEIB method takes an average over penalty functions whose remaining capacity terms vary from $c_{tj} - d_k + 1$ to c_{tj}. In the next section, we will use numerical experiments to compare MSEIB with the original inventory balancing method AEIB and the stricter version SEIB. Recall that our choice model is (17.1), and our decision at time t when a type i patient arrives is formulated as (17.2). Since $\tilde{r}_{ijt}$ is non-negative, a larger size of S will always increase the total revenue in (17.2). Hence, the optimal ranking is obtained when $|S| = L$. Then, we will use the greedy algorithm in section "Static Ranking Problem" to find a ranking of length L. To be specific, we rank the physicians in decreasing order of $v_{ij}\tilde{r}_{ijt}$, and select the top L physicians to show to the customer.

Linear Approximation Methods

Before introducing this type of methods, we will first adjust Eq. (17.5) a little bit in order to let it contain an expression of the marginal value. Equation (17.5) can be rewritten equivalently as:

$$V_t(\boldsymbol{c_t}) = \sum_i \lambda_i \max_{\sigma(S)} \Bigg\{ \sum_j p_{ij}(\sigma(S)) \sum_k q_{ik} 1_{\{c_{ij} \geq d_k\}} \\ \left[r_{ijk} + V_{t+1}\left(\boldsymbol{c_t} - d_k \boldsymbol{e}_j\right) - V_{t+1}(\boldsymbol{c_t}) \right] \Bigg\} + V_{t+1}(\boldsymbol{c_t}) \tag{17.8}$$

By replacing p_{i0} with $1 - \sum_j p_{ij}$ in Eq. (17.5), and combining the terms multiplied by p_{ij}, we can get the form of Eq. (17.8). Intuitively, if a type i patient chooses physician j and type k service, then we will get a reward of r_{ijk}, but physician j's capacity will also decrease by d_k, so the net benefit of the platform is $r_{ijk} + V_{t+1}\left(\boldsymbol{c_t} - d_k \boldsymbol{e}_j\right) - V_{t+1}(\boldsymbol{c_t})$. In all the other cases, there will be no match between the patient and any physician, so the capacities will remain the same, and the value of that in the next period is $V_{t+1}(\boldsymbol{c_t})$.

Linear approximation method is applied in Ref. [18] to estimate the value function in a reusable resource allocation problem. They presented a tractable approach to compute a policy such that the size of the total capacity no longer influences the computational efficiency. They also prove that their method can obtain at least 50% of the optimal expected revenue. We adopt this approximation method and extend it to an algorithm called the Multiple Service Linear Approximation Algorithm (MSLAA) for our multiple service type setting. We will explain the details below. Consider the linear approximation of the value function given by

$$\widehat{V}_t(\boldsymbol{c_t}) = \sum_j \beta_{jt} c_{jt} \tag{17.9}$$

where the parameter β_{jt} represents the marginal value of each unit of physician j's capacity at time t. We can compute the value $\widehat{V_t}(\boldsymbol{c_t})$ recursively, and the method is given in Algorithm 1.

Algorithm 1 Multiple Service Linear Approximation Algorithm (MSLAA)

Input: Initial capacity $\boldsymbol{c}_0 = (c_1, c_2, \ldots, c_N)^\top$, total horizon T, pairing reward r_{ijk}, units of consumption d_k, arrival rate λ_i and choice parameters q_{ik}, v_{ij}.

Output: β_{jt} of all $0 < j \leq N$ and $0 \leq t \leq T$.

1: **Initialize**: Set $\beta_{jT} = 0$,∀j, and $\alpha_{ijt} = 0$,∀i,j,t

2: **for** $t = T-1, T-2, \ldots, 0$ **do**

3: **for** $i = 1, 2, \ldots, M$ **do**

4: **For** $j = 1, 2, \ldots N$ **do**

$$\alpha_{ijt} = \sum_k q_{ik}\left(r_{ijk} - \beta_{j(t+1)}d_k\right) \tag{17.10}$$

5: **end for**

$$A_t(i) = \underset{\boldsymbol{\sigma}(S)}{\operatorname{argmax}} \sum_j p_{ij}(\boldsymbol{\sigma}(S))\alpha_{ijt} \tag{17.11}$$

6: **end for**

7: **For** $j = 1, 2, \ldots N$ **do**

$$\beta_{jt} = \frac{1}{c_j}\left[\sum_i \lambda_i p_{ij}(A_t(i))\alpha_{ijt}\right] + \beta_{j(t+1)} \tag{17.12}$$

8: **end for**

9: **end for**

In the above algorithm, α_{ijt} represents the expected immediate reward of matching a type i patient with physician j minus the value of the capacity consumed at time t. β_{jt} represents the value of each unit of capacity of physician j at time t. If a patient of type i arrives at time t, and the current state is $\boldsymbol{c_t}$, the platform will offer the ranking given by:

$$\begin{aligned}\boldsymbol{\sigma}_t(S) = \underset{\boldsymbol{\sigma}(S)}{\operatorname{argmax}} \sum_j p_{ij}(\boldsymbol{\sigma}(S)) \sum_k q_{ik} \\ 1_{\{c_{ij} \geq d_k\}}\left(r_{ijk} - d_k\beta_{j(t+1)}\right)\end{aligned} \tag{17.13}$$

We will again use the greedy ranking method mentioned before and rank the physicians in decreasing order of $v_{ij}\sum_k q_{ik}1_{\{c_{tj}\geq d_k\}}\left(r_{ijk}-d_k\beta_{j(t+1)}\right)$. Unlike in the cases of the inventory balancing methods, the term $r_{ijk}-d_k\beta_{i(t+1)}$ might not be positive. Denote $S^+=\left\{j\leq N:\sum_k q_{ik}1_{\{c_{tj}\geq d_k\}}\left(r_{ijk}-d_k\beta_{i(t+1)}\right)\geq 0\right\}$. If the total number of positive terms $\left|S^+\right|$ is less than L, then we will only display the first $\left|S^+\right|$ physicians with positive rewards. Note that in practice, it is time consuming to solve problem (17.11) directly, so we will also use the greedy algorithm in MSLAA.

Benchmark Methods

In this section, we discuss some benchmark methods to evaluate the performance of the algorithms.

One commonly used benchmark is the greedy method. Upon a patient's arrival, the platform greedily recommends a list of physicians who have the highest expected pairing rewards, regardless of the potential influence of this action on future patients. To be specific, when a type i patient arrives, the ranking is given in decreasing order of $v_{ij}\sum_k q_{ik}1_{\{c_{tj}\geq d_k\}}r_{ijk}$.

Another type of benchmarks we use are from relaxation methods. Relaxation methods first formulate the offline problem, and relax it to acquire a looser upper bound of the problem. The solution of the relaxed offline problem gives us the probability a certain physician will be shown. We then approximate the value function of each state using this upper bound. We will explain the methods in detail below.

The choice-based deterministic linear programming (CDLP) model in Ref. [19] provides an upper bound for the expectation of the dynamic assortment optimization problem. However, as N grows, the sigma field of the ranking decisions is too large. In order to deal with this problem, relaxation methods are usually applied here. For example, Pan et al. [15] apply this relaxation method and use real data experiments to show that this method performs well in their setting. Instead of assigning a probability to each ranking decision, this method assigns a probability to each physician. Note that this is equivalent to reducing $p_{ij}(\boldsymbol{\sigma}(S))$ to p_{ij}, which means the choice probability is no longer relevant to the rankings. This simplified optimization method is called Simplified Linear Programming (SLP), and it is defined below.

$$\begin{aligned}\max_{p_{ij}}\ & \textstyle\sum_i \lambda_i \sum_j p_{ij}\sum_k q_{ik}r_{ijk}\\ \text{s.t.}\ & \textstyle\sum_i \lambda_i p_{ij}\sum_k q_{ik}d_k \leq \frac{c_j}{T}\ \forall j=1,\ldots,N\\ & \textstyle\sum_j p_{ij}\leq 1\ \forall i=1,\ldots,M\\ & p_{ij}\geq 0\end{aligned}\tag{17.14}$$

After solving the above linear programming problem, the value function is approximated as

$$\widehat{V}_t(\boldsymbol{c_t}) = (T-t)\sum_i \lambda_i \sum_j \frac{c_{jt}}{c_j} p_{ij} \sum_k q_{ik} r_{ijk}. \tag{17.15}$$

We then approximate $V_{t+1}(\boldsymbol{c_t}) - V_{t+1}\left(\boldsymbol{c_t} - d_k \boldsymbol{e_j}\right)$ in Eq. (17.8) as $\hat{V}_{t+1}(\boldsymbol{c_t}) - \hat{V}_{t+1}\left(\boldsymbol{c_t} - d_k \boldsymbol{e_j}\right)$. Then like in the case of the linear approximation method, Eq. (17.5) reduces to a static ranking problem. We can apply the greedy ranking method similarly. This method is named as RELAX in our numerical experiment for brevity.

Besides comparing with the existing methods, we also need to know the gap between the optimal solution and the methods we proposed. Since it is time consuming to directly compute the optimal solution via DP, we use offline problems to compute upper bounds instead. Since in reality, the number of physicians on a platform is often very large, we will use SLP to compute an upper bound, and denote the optimal value obtained this way as ***OFFLINE***.

Numerical Experiment

In this section, we conduct numerical experiments to compare the methods we propose with a number of benchmark methods in different scenarios. We then give suggestions on how to make recommendations in different situations to provide better services to patients.

Before showing the results, we briefly comment on the computational efficiency of the methods we use in the numerical experiments. The main difference between inventory balancing methods and approximation methods is that the second type requires prior computation before the arrival of patients. The time complexity of MSLAA is $O(TMN\max\{\log N, K\})$. For the benchmark methods, the time complexity of RELAX is about $O\left(\max\left\{(MN)^{2.5}, MNK\right\}\right)$, where $O(MN)^{2.5}$ is an approximation of the time of solving the LP in problem (17.14).

Numerical Experiment Design

For each specific problem setting, we generate a random sequence of patients and make recommendations to them using different algorithms. We repeat the simulation for the same set of parameters 1000 times and take the average reward as an approximation to the expected reward of each method. Next, we introduce our parameter settings for the numerical experiments.

In our experiments, we set the number of patient types to be $M = 5$ and the number of service types to be $K = 3$. The number of physicians N ranges from 10 to 100. The pairing reward r_{ijk} is generated from a uniform distribution that lies in the interval [10, 100]. The initial capacity c_j of each physician is an integer generated uniformly at random from the range [5, 20]. And the capacity consumption

of each type of service d_k is an integer generated uniformly from the range [1, 10]. For a specific pair of patient i and physician j, we require the service type with a higher pairing reward consumes more units of capacity. The probability of choosing a service q_{ik} is first generated uniformly in [0, 1] and then normalized to $q_{ik}/\sum_k q_{ik}$, so that $\sum_k q_{ik} = 1$.

For the click model, the maximum length of the recommendation list is set to be $L = 20$. We assume the number of physicians a patient reads follows a Poisson distribution with parameter $\Lambda = 10$. The click probability v_{ij} is generated from a uniform distribution in [0, 1]. In order to test the robustness of these methods, besides offering different numbers of physicians, we consider different congestion level as well. Let $C = \sum_j c_j$ denote the total capacity at the beginning. In our experiments, we set $C/T = 10, 5, 2/3, 1/2$. C/T can be understood as the available capacity for each patient on average. A patient's expected demand of resources is $E[d] = \sum_i \lambda_i \sum_k q_{ik} d_k$, and in our settings, $E[d] = 2.38$. When $E[d] < C/T$, the platform might be able to satisfy the demands of most patients. But when $E[d]$ is much larger than C/T, resources are rather scare, so the platform has to decide more carefully which patients to serve.

Numerical Results

In this section, we will display part of the results of different algorithms. The rest is in our appendix. The first column shows the name of the different algorithms, and the other columns represent the performances of each algorithm under scenarios with different number of physicians. In the numerical experiments, we test a total of seven methods, and also compute the offline benchmark from problem (17.14) (Table 17.1).

When the capacity is sufficient relative to the demand, inventory balancing methods such as AEIB and MSEIB generally perform better than approximation methods. Besides, MSEIB generally performs better than AEIB, while SEIB performs worse. The reason is that the penalty for SEIB is too large, and as a result physicians with small pairing rewards but large capacities are often ranked high. MSEIB can distinguish between service types using a relatively loose penalty function, so that it generally outperforms the other two methods. All of the three methods perform better than the IB method. This shows that it is necessary to add the pairing rewards into the penalty functions to address patients' compatibility with the physicians. When the resources are relatively scarce, methods based on approximations perform better. When $C/T = 2/3$ and $C/T = 1/2$, MSLAA performs the best in most cases. Considering that when C/T is relatively large, the gap between these two methods are relatively small, and that in reality, the platform usually cannot predict the total capacity very precisely, MSLAA is preferred for its robustness in different situations.

We now provide some possible explanations for our findings. First, we observe that when C/T is large, approximation methods, especially the relax method, do not

Table 17.1 Total pairing reward of different algorithms

ALGs	C/T = 5					C/T = 1/2				
	N = 10	N = 30	N = 50	N = 70	N = 100	N = 10	N = 30	N = 50	N = 70	N = 100
IB	774.8	1325.2	3606.4	7301.5	7452.7	1307.2	1754	4710.3	8075.9	8502.3
AEIB	789.4	1365.5	3717.1	7470.4	7708	1364.2	1847.2	5077	8602.7	8888.4
SEIB	774.1	1340.8	3699	7299.3	7511.3	1333.4	1774	4878.3	8400.9	8635.1
MSEIB	798.8	1371.7	3721.2	7485.1	7723.6	1366.6	1856.6	5090.7	8628	8913.1
MSLAA	795.8	1349.9	3653.4	7362.2	7608.1	1635.6	2101.4	5961.8	9692.9	10,480.9
RELAX	731.2	1326	3508.8	7132.3	7820.6	1606.8	2161.6	5851.8	9562.3	10,264.1
GREEDY	773.4	1328.4	3568.1	7292.3	7487.4	1322.6	1795.8	4843.2	8403.9	8619.9
OFFLINE	1239	2033.9	4803.9	8737.9	10,659.8	1643.2	2537.6	6425.3	11,141.2	11,525.4

perform well. The reason for this phenomenon is that both MSLAA and RELAX assume the value functions are linear in the remaining capacity. This assumption reduces time complexity but also brings error to the estimation of the value functions. When C/T is large, the error caused by this linear assumption exceeds the effect of ignoring the dynamic programming structure. One reason the RELAX method performs extremely bad when C/T is large might be that as C/T increases, the domain of p_{ij} will also become larger, which can be easily observed in (17.14). As a result, the upper bound obtained from the relax method is too loose. As for the MSLAA method, though it generally performs not as well as the inventory balancing methods MSEIB and AEIB, the difference between them is small. This can be partially explained by Theorem 2.

Theorem 2 Denote the linear approximation value at the initial state as $\widehat{V_0}(\boldsymbol{c}_0)$, and the optimal value at the initial state in Eq. (17.5) as $V_0(\boldsymbol{c}_0)$. If the reward for any service is proportional to its capacity consumption, then $V_0(\boldsymbol{c}_0) \leq 2\hat{\mathrm{V}}_0(\boldsymbol{c}_0)$.

Since it has a theoretical guarantee, MSLAA performs more robustly than any other methods.

Our second observation is that inventory balancing methods perform not as well when C/T is small. One reason is that when resources are scarce, we will need a more delicate allocation policy to make full use of the capacity. Inventory balancing methods totally ignore the dynamic programming structure and only use heuristic penalty functions. The error caused by this exceeds the error caused by the linear assumption in the approximation methods. Another possible explanation is that the computed rewards of the inventory balancing methods are always non-negative, so the platform will always display the top L physicians. However, approximation methods might return negative rewards for some physicians, so that they are not displayed at all. As a result, even when a physician still has remaining capacity, patients with low pairing rewards might not see him in the list. When C/T is small, meaning that resources are scarce, approximation methods can better save the capacity for future patients with higher priorities.

To further verify our analysis, we adjust the parameter Λ, which represents the average number of physicians the patients viewed, and obtain Table 17.2. As we can see, the performance of the approximation methods MSLAA and RELAX increases with Λ, while the performance of the inventory balancing method MSEIB decreases with Λ. Also, the maximum difference in performance between these two types of methods increases with Λ. Since when Λ is small, only the first few physicians are likely to be seen, so whether showing those physicians with low pairing rewards or not makes little difference. However, as the average number of physicians viewed grows, even physicians with low pairing rewards are likely to be seen, so whether to display them or not will make a difference.

Table 17.2 Total pairing reward of different Λ

Λ	C/T = 2/3					C/T = 1/2				
	N	MSEIB	MSLAA	RELAX	MAXDIFF	N	MSEIB	MSLAA	RELAX	MAXDIFF
0.1	30	1901.21	1995.78	2067.33	166.12	30	1905.7	2035.36	2118.1	212.4
1	30	1893.64	2023.83	2099.41	205.77	30	1893.1	2056.18	2137.17	244.07
10	30	1853.05	2090.1	2129.93	276.88	30	1856.59	2101.4	2161.62	305.03
0.1	50	5217	5751.65	5706.17	534.65	50	5234.02	5865.14	5792.15	631.12
1	50	5197.41	5809.55	5749.65	612.14	50	5198.39	5904.81	5816.93	706.42
10	50	5104.29	5924.839	5794.75	820.549	50	5090.71	5961.79	5851.82	871.08

Conclusion

Online healthcare platforms have attracted more and more patients recently, and how to assign physicians to different needs to provide better services deserves further study. Motivated by this observation, our model captures most of the critical features of this problem, such as patients' click behaviors, limited physician resources, multiple service types with different capacity consumption, and heterogeneous pairing rewards.

In order to provide a better ranking policy, we first formulate a dynamic program for this problem, then we propose two types of methods, MSEIB and MSLAA to solve the problem. Through numerical experiments, we find that MSEIB performs better than other existing methods when the resources are sufficient, while MSLAA performs better than other existing methods when resources are scarce. We also provide explanations and insights for our findings. Our method is an index based heuristic method and is computationally efficient and easy to implement.

We do not include online learning in this work and assume that the pairing rewards and the parameters for patients' choice behaviors are known. Future directions include relaxing this assumption and updating the parameters dynamically via online learning.

References

1. Agarwal, A., Hosanagar, K., & Smith, M. D. (2011). Location, location, location: An analysis of profitability of position in online advertising markets. *Journal of Marketing Research, 48*(6), 1057–1073.
2. Ryzin, G. V., & Mahajan, S. (1999). On the relationship between inventory costs and variety benefits in retail assortments. *Management Science, 45*(11), 1496–1509.
3. Talluri, K., & Van Ryzin, G. (2004). Revenue management under a general discrete choice model of consumer behavior. *Management Science, 50*(1), 15–33.
4. Bront, J. J. M., Mendez-D´ıaz, I., & Vulcano, G. (2009). A column generation algorithm for choice-based network revenue management. *Operations Research, 57*(3), 769–784.
5. Davis, J. M., Gallego, G., & Topaloglu, H. (2014). Assortment optimization under variants of the nested logit model. *Operations Research, 62*(2), 250–273.

6. Joachims, T., Granka, L., Pan, B., Hembrooke, H., & Gay, G. (2017). Accurately interpreting clickthrough data as implicit feedback. In Acm Sigir Forum, vol. 51, pp. 4–11.
7. Craswell, N., Zoeter, O., Taylor, M., & Ramsey, B. (2008). An experimental comparison of click position-bias models. In *Proceedings of the 2008 international conference on web search and data mining*, pp. 87–94.
8. Guo, F., Liu, C., Kannan, A., Minka, T., Taylor, M., Wang, Y.-M., & Faloutsos, C. (2009). Click chain model in web search. In *Proceedings of the 18th international conference on World wide web*, pp. 11–20.
9. Mehta, A., Saberi, A., Vazirani, U., & Vazirani, V. (2007). Adwords and generalized online matching. *Journal of ACM, 54*, 22–es.
10. Golrezaei, N., Nazerzadeh, H., & Rusmevichientong, P. (2014). Real-time optimization of personalized assortments. *Management Science, 60*(6), 1532–1551.
11. Wen, H., Song, J., & Pan, X. (2020). Physician recommendation on healthcare appointment platforms considering patient choice. *IEEE Transactions on Automation Science and Engineering, 17*(2), 886–899.
12. Bernstein, F., Kok, A. G., & Xie, L. (2015). Dynamic assortment customization with limited inventories. *Manufacturing & Service Operations Management, 17*(4), 538–553.
13. Gallego, G., Li, A., Truong, V.-A., & Wang, X. (2016). Online personalized resource allocation with customer choice. Working Paper.
14. Gallego, G., Ratliff, R., & Shebalov, S. (2015). A general attraction model and sales-based linear program for network revenue management under customer choice. *Operations Research, 63*(1), 212–232.
15. Pan, X., Wen, H., Wang, Z., Song, J., & Feng, X. L. (2021). Physician ranking optimization based on patients' browse behaviors and resource capacities. Internet Research.
16. Wen, H., Pan, X., & Song, J. (2020). Online ranking of physicians with perishable resources. In *2020 IEEE 16th International Conference on Automation Science and Engineering (CASE)*, pp. 140–145. IEEE.
17. Zhang, D., & Adelman, D. (2009). An approximate dynamic programming approach to network revenue management with customer choice. *Transportation Science, 43*(3), 381–394.
18. Rusmevichientong, P., Sumida, M., & Topaloglu, H. (2020). Dynamic assortment optimization for reusable products with random usage durations. *Management Science, 66*(7), 2820–2844.
19. Gallego, G., Iyengar, G. N., Phillips, R. L., & Dubey, A. (2004). Managing flexible products on a network. *PROD: Analytical (Product) (Topic).*
20. Gallego, G., Li, A., Truong, V.-A., & Wang, X. (2016). Online personalized resource allocation with customer choice. Working Paper, Tech. Rep. http://arxiv.org/abs/1511.01837v1

Chapter 18
Analysis on Technological Innovation Efficiency in Equipment Manufacturing Industry

Min Liu and Sifeng Liu

Abstract Based on the panel data of ten subsectors in equipment manufacturing industry, this paper utilizes the DEA-Malmquist index method to analyse the static and dynamic technological innovation efficiency of equipment manufacturing industry in China from 2015 to 2020, and afterwards, analyse the influencing of input–output indexes on comprehensive efficiency value via the grey relational analysis (GRA) model. The static result reveals that most industries fail to achieve DEA effective, where the main reason is that resources have been put into redundancy. Meanwhile, the dynamic result shows that the development of equipment manufacturing industry is slowly rising and experiences some volatility during the empirical research period, in which the trend is mainly contributed by technological efficiency. And the main reason that restricts the improvement of technological innovation efficiency is due to the slowdown in technological progress. Furthermore, the input–output indicators have different effects on innovation efficiency in various industries, where R&D personnel and sales revenue of new products are the input and output indexes having the greatest correlation with technological innovation efficiency respectively. Based on the empirical analysis, relevant suggestions are proposed for the future innovation development of equipment manufacturing industry.

Keywords Equipment manufacturing industry · Technological innovation efficiency · DEA-Malmquist · Grey relational analysis

Introduction

As the core manufacturing industry, equipment manufacturing industry is the pillar industry of the national economy, which development level has an important impact

M. Liu (✉) · S. Liu
College of Economics and Management, Nanjing University of Aeronautics and Astronautics, Nanjing, China
e-mail: student_liumin@163.com

S. Liu
e-mail: sfliu@nuaa.edu.cn

R. Qiu et al. (eds.), *City, Society, and Digital Transformation*, Lecture Notes in Operations Research, https://doi.org/10.1007/978-3-031-15644-1_18

on China's industrialization and industrial upgrading. Compared with developed manufacturing powers, there is a huge gap in China's equipment manufacturing, which is mainly reflected in the lack of original innovation, imperfect equipment service system and weak product competitiveness [1]. While the competitiveness of equipment manufacturing industry is mainly reflected in the technological innovation ability and efficiency [2]. The technological innovation efficiency is the core index to measure the innovation-drive level of the equipment manufacturing industry. Analysing technological innovation efficiency and its influencing factors would help to allocate resources properly and improve the practical problems of input redundancy and output insufficiency [3].

The concept of technological innovation efficiency was first proposed by Afriat in 1972 who hold that the ratio of input and output of R&D innovation activities is significantly correlated with the production boundary which refers to the maximum output under a certain input. At present, scholars at home and abroad have made some fruitful researches on the technological innovation of equipment manufacturing industry, which mainly focuses on the measurement of innovation efficiency and influencing factors. Varum et al. expounded the importance of technological innovation and pointed out that improving the technological innovation efficiency would promote innovative development of equipment manufacturing industry in R&D, structural reform and productivity [4]. Karahan analyzed the technological innovation efficiency of equipment manufacturing industry in some European countries and hold that increasing R&D investment would effectively promote the technological innovation efficiency, especially the manufacturing industry representing high technology and high growth [5]. Lee applied DEA-Malmquist index method to evaluate the development of technological innovation efficiency in the equipment manufacturing industry of several Asian countries [6]. Peng et al. used the two-stage correlative DEA model to evaluate the efficiency of technological innovation in the western region [7]. Zeng comprehensively applied the four-stage DEA model and Bootstrap model to study the technological innovation efficiency of China's high-end equipment manufacturing industry [8]. Wang et al. verified that government R&D subsidies can significantly promote the improvement of innovation efficiency with Tobit model [9]. Duan et al. established the evaluation index system of technological innovation capability of equipment manufacturing industry considering four aspects: technological innovation guarantee capability, innovation resource input capability, technological innovation transformation and absorption capability and innovation resource output capability, and made an empirical analysis on the technological innovation capability of equipment manufacturing industry by using factor analysis method [10]. According to the complex system theory, using the composite system synergy model and based on the panel data of the equipment manufacturing industry, Si et al. evaluated the synergy of the technology collaborative innovation mechanism of China's equipment manufacturing industry [11]. Xiao et al. utilized the Two-stage DEA model to analyse the efficiency based on the panel data of 31 provinces in China and analysed the influencing factors of their comprehensive efficiency value via grey comprehensive correlation degree [12].

At present, relevant researches on technological innovation efficiency of equipment manufacturing industry mainly focus on a certain province or region and pay attention to the whole industry, while the comparative analysis of the technological innovation efficiency in its subindustries is relatively few. Therefore, based on the panel data of ten representative subindustries of equipment manufacturing industry in China from 2015 to 2020, this paper utilizes the DEA-Malmquist index method to analyse the static and dynamic technological innovation efficiency. Besides, most literatures consider the influence of external factors on technological innovation efficiency, few study the impact degree of input–output indicators on technological innovation efficiency. Therefore, this paper analyses the influencing of input–output indexes on comprehensive efficiency value via the grey relational analysis (GRA) model. Through the analysis, this paper puts forward relevant suggestions for the development of equipment manufacturing industry.

Research Methods

Data Envelopment Analysis

Stochastic frontier Analysis (SFA) and data Envelopment analysis (DEA) are mainstream methods to measure technological innovation efficiency. Compared with SFA, DEA method has the advantages of calculating multi-input and multi-output problems without considering the specific form of production function and estimating parameters. Besides, DEA method is completely based on input–output index data and determines the weight through the optimization process, so as to make the DMU evaluation more objective. Therefore, DEA method is selected to study the problem in this paper.

Data envelopment analysis (DEA) is a relative efficiency evaluation method proposed by Charnes and Cooper, which basic principle is to utilize linear programming model to evaluate the relative effectiveness of decision-making unit (DMU) with multiple inputs and outputs, and it is the most commonly used nonparametric frontier efficiency analysis method. This method is based on the degree of deviation of the projected DMUs from the production frontier to show whether they are relatively effective, and it is particularly suitable for analysing object that have multiple inputs and outputs. At present, the basic models of DEA mainly include DEA-CCR [13], DEA-BCC [14].

There will be increasing or decreasing returns to scale in the innovation activities of equipment manufacturing industry, so this paper utilizes the DEA-BCC model proposed by Banker et al. in 1984, which assumes that there are k DMUs, and each DMU has L types of inputs and M types of outputs, which the DEA model of the nth$(n = 1, 2, \ldots, k)$ unit is:

$$\min\left(\theta - \varepsilon\left(\mathrm{e}_1^T s^- + \mathrm{e}_2^T s^+\right)\right)$$

$$\text{s.t.}\begin{cases} \sum_{j=1}^{k} x_{jl}\lambda_j + s^- = \theta x_l^n \quad l = 1, 2, \ldots, L \\ \sum_{j=1}^{k} y_{jm}\lambda_j - s^+ = y_m^n \quad m = 1, 2, \ldots, M \\ \lambda_j \geq 0, j = 1, 2, \ldots, n \\ s^- \geq 0, s^+ \geq 0 \end{cases} \tag{18.1}$$

where $\theta(0 < \theta \leq 1)$ is the comprehensive technical efficiency value of decision-making unit, ε is a nonarchimedean infinitesimal quantity, s^- is a slack variable, s^+ is a residual variable, $e_1^T = (1, 1, \ldots, 1) \in E_m$ is the m-dimensional unit vector space, λ_j is the weight variable, x_{jl} is the input amount of the lth resource of the jth production unit, and y_{jm} is the mth type of the jth production unit output.

Malmquist Productivity Index

The Malmquist productivity index (MPI) was first proposed by Malmquist in 1953. Since then, Caves, Charnes and others have widely applied it to the measurement of total factor productivity [14]· After modification, the MPI from period t to $t + 1$ was constructed, as shown in Eq. (18.2). It can comprehensively analyze multi-input and multi-output indicators and observe the dynamic changes of technological innovation efficiency of DMU, so as to carry out targeted improvement on ineffective DEA units.

$$M(x_{t+1}, y_{t+1}, x_t, y_t) = \left[\frac{d^t(x_{t+1}, y_{t+1})}{d^t(x_t, y_t)} \times \frac{d^{t+1}(x_{t+1}, y_{t+1})}{d^{t+1}(x_t, y_t)} \right]^{\frac{1}{2}} \tag{18.2}$$

where x_t and y_t are the input and output of period t respectively;$d^t(x_t, y_t)$ and $d^t(x_{t+1}, y_{t+1})$ represent the respective distance functions of the DMUs in periods t and $t + 1$ when the data in period t are used as the reference set;$d^{t+1}(x_t, y_t)$ and $d^{t+1}(x_{t+1}, y_{t+1})$ have similar meanings. When $M > 1, = 1, or < 1$, it means that the productivity level is increasing, remains unchanged, or is decreasing.

Under the assumption of constant return to scale (CRS), according to the research of Fare et al. [15], the MPI can be decomposed into two parts: technical efficiency change (TEC) and technical change (TC). Under the assumption of variable return to scale (VRS), TEC can be further decomposed into pure technical efficiency change (PTC) and scale efficiency change (SEC). Therefore, Eq. (18.2) can be further expressed as follows:

$$M(x_t, y_t, x_{t+1}, y_{t+1}) = \frac{d^{t+1}(x_{t+1}, y_{t+1}/VRS)}{d^t(x_t, y_t/VRS)}$$

$$\times \left[\frac{d^t(x_t, y_t/VRS)}{d^t(x_t, y_t/CRS)} \Big/ \frac{d^{t+1}(x_{t+1}, y_{t+1}/VRS)}{d^{t+1}(x_{t+1}, y_{t+1}/CRS)} \right]$$
$$\times \left[\frac{d^t(x_{t+1}, y_{t+1}/CRS)}{d^{t+1}(x_{t+1}, y_{t+1}/CRS)} \times \frac{d^t(x_t, y_t/CRS)}{d^{t+1}(x_t, y_t/CRS)} \right]^{\frac{1}{2}}$$
$$= PTC \times SEC \times TC \tag{18.3}$$

According to Eq. (18.3), TC represents the degree of transition of the technological production boundary from period t to period $t+1$, that is, the TC index, also known as the "frontier movement effect" [16]. When TC > 1, which indicates technological progress, and vice versa. Meanwhile, TEC represents the degree of change in relative technical efficiency from period t to period $t+1$, that is, the change index of technical efficiency, also known as the "catch-up effect." When TEC > 1, it means that the relative efficiency of the DMU is improved in period $t+1$ compared to period t, and vice versa. When PTC > 1, it means that an improvement in management has improved the efficiency, and vice versa. When SEC > 1, it means that the DMU is approaching the optimal scale in the long run, and vice versa.

Grey Relation Model

Most relevant literatures use regression method to measure the correlation between factors, however which needs enough data to gain better results. Grey relation analysis is suitable for small sample analysis and focus on time sequences, reflect the dynamic development process. Grey relational model has been widely used in efficiency analysis. Wang measured production and marketing efficiencies in the printed circuit board industry using grey relation analysis (GRA) and data envelopment analysis (DEA) [17]. In this paper, considering the timeliness and availability of the data, based on five years of data in equipment manufacturing industry, which has the characteristics of small samples in time. Therefore, this paper utilizes grey correlation model to measure the impact of input–output indicators on technological innovation efficiency.

Grey relation analysis measures the relations between elements based on the degree of similarity or difference of development trends among these elements. More precisely, during the process of system development, if the trend of change between two elements is consistent, then it enjoys a higher grade of synchronized change and can be considered as having a greater grade of relation. Grey relation analysis can be applied in the selection of representative indicators, the specific steps are as follows:

Step 1: Let $X_i = [x_i(1), x_i(2), \cdots x_i(n)], (i = 1, 2, \cdots, m)$ represents the comparative sequence and $X_0 = [x_0(1), x_0(2), \cdots x_0(n)]$ be the referential sequence;

Step 2: Data standardization

In order to ensure the equivalence and homogeneity of each factor, the original sequence should be removed dimensionless during the grey correlation degree analysis. As for relatively stable sequences of economic and social systems, initial valuation operators are generally selected for dimensionless transformation.

Let D_1 be the initial valuation operators, then $X_i D_1 = [x_i(1)d_1, x_i(2)d_1, \ldots x_i(n)d_1]$, where $x_i(k)d_1 = \frac{x_i(k)}{x_i(1)}$ is the initial value image and $x_i(k)d_1 = \frac{x_i(k)}{x_i(1)}$ is the dimensionless data sequence.

Step 3: Calculate grey correlation coefficient

$\gamma(x_0(k), x_i(k))$ is said to be the grey relational coefficient of the same at point k. The mathematical equation of grey correlation coefficient is as follows:

$$\gamma(x_0(k), x_i(k)) = \frac{\min\limits_i \min\limits_k |x_0(k) - x_i(k)| + \xi \max\limits_i \max\limits_k |x_0(k) - x_i(k)|}{|x_0(k) - x_i(k)| + \rho \max\limits_i \max\limits_k |x_0(k) - x_i(k)|} \tag{18.4}$$

where $\xi \in (0, 1)$ is the distinguished coefficient, and the value generally takes 0.5.

Step 4: Calculate Deng's grey relational degree

$\gamma(X_0, X_i)$ is designated as the grade of grey relation in x_i corresponding to x_0, According to the Deng's grey relational degree, the relation value can be defined as:

$$\gamma(X_0, X_i) = \frac{1}{n} \sum_{k=1}^{n} \gamma(x_0(k), x_i(k)) \tag{18.5}$$

Index Selection and Data Sources

Indicators Selection

The process of technological innovation is a process with multiple inputs and outputs, which is inseparable from the input of technological personnel and research funds, and the corresponding knowledge achievements and economic benefits are produced in the innovation process. Based on the existing research results [18], considering the principles of comprehensiveness, completeness and availability, the technical innovation evaluation indicators of equipment manufacturing industry selected in this paper are shown in Table 18.1.

Table 18.1 Evaluation index of technological innovation efficiency of equipment manufacturing industry

Category	Primary index	Secondary index	Notion
Input index	Science and technology funds	Internal expenditure on R&D	I_1
		Expenditure on new products development	I_2
	Human resources	Full-time equivalent of R&D	I_3
Output index	Knowledge achievement	Number of inventions in force	O_1
	Economic benefits	Sales revenue of new products	O_2

Data Sources

Equipment manufacturing industry refers to the industry that produces advanced industrial facilities and equipment with high technology and high added value. At present, there is no explicit statistical classification standards in equipment manufacturing industry. Therefore, according to the China Statistical Yearbook on Science and Technology and the development focus of strategic emerging industries, based on the availability, timeliness, scientificalness and integrity of index data, the scope of this research covers ten industries including transportation equipment manufacturing industry, electronic and communication equipment manufacturing industry, electrical machinery and equipment manufacturing, general equipment manufacturing and special equipment manufacturing industry.

The data of this paper is collected from China Statistical Yearbook and China Statistical Yearbook on Science and Technology. Each industry is regarded as a basic decision-making unit when analysing the technological innovation efficiency of equipment manufacturing industry. Generally, in the process of innovation activities, there is a certain time lag in the transformation of innovation achievements, therefore, this paper sets the lag period as one year. That is, the input–output interval is 2015–2019 and 2016–2020 respectively. According to relevant research, the number of decision-making units in efficiency measurement satisfy at least twice the total number of input–output indicators.

Empirical Research

Static Efficiency Measurement

This paper utilizes the input-oriented BCC model to process and analyse the data, that is, reduce the input as much as possible when the output is equivalent. Using

Table 18.2 Static efficiency value of technological innovation in equipment manufacturing industry

		A1	A2	A3	A4	A5	A6	A7	A8	A9	A10
2016	TE	1	0.648	0.728	1	0.872	0.646	0.84	0.641	0.408	0.383
	PTE	1	0.753	1	1	0.93	0.669	1	0.726	0.43	0.385
	SE	1	0.861	0.728	1	0.937	0.966	0.84	0.882	0.949	0.994
2017	TE	1	1	0.329	1	0.638	0.72	0.834	0.625	0.722	0.788
	PTE	1	1	1	1	0.646	0.726	1	0.658	0.749	0.873
	SE	1	1	0.329	1	0.988	0.992	0.834	0.949	0.964	0.902
2018	TE	1	0.38	0.401	0.584	1	0.613	0.633	0.458	1	0.847
	PTE	1	0.621	1	0.677	1	0.643	0.705	0.477	1	0.981
	SE	1	0.613	0.401	0.863	1	0.954	0.899	0.961	1	0.864
2019	TE	1	0.926	0.745	1	1	0.887	0.973	0.93	0.957	0.998
	PTE	1	1	1	1	1	0.891	1	0.944	0.964	1
	SE	1	0.926	0.745	1	1	0.995	0.973	0.986	0.992	0.998
2020	TE	1	0.998	0.571	1	1	0.882	0.944	0.791	0.912	0.982
	PTE	1	1	1	1	1	0.882	1	0.813	0.914	1
	SE	1	0.998	0.571	1	1	1	0.944	0.974	0.998	0.982

DEAP2.1 software, the comprehensive technical efficiency (TE) and its decomposition efficiency of 2016–2020 are obtained by calculating the sample data as shown in Table 18.2.

Comprehensive technical efficiency (TE) reflects the comprehensive evaluation of DMU's resource utilization efficiency and resource allocation ability. Pure technical efficiency (PTE) refers to the production efficiency affected by factors produced by management system and technology. Scale efficiency (SE) reflects the efficiency gap between actual scale and optimal scale. Pure technical efficiency and scale efficiency are subdivisions of comprehensive technical efficiency.

Industries with better overall performance were manufacture of communication equipment industry (A1), manufacture of audio and video equipment industry (A4), manufacture of medical equipment and appliances industry (A5), which achieved DEA effective in most years (TE = 1), suggesting that these industries realized the efficient utilization of resources. Compared with other equipment manufacturing industries, the value of comprehensive efficiency in radar and its fittings manufacture industry (A3) is the lowest in most years, which is mainly caused by low scale efficiency (SE), indicating that the investment of innovation resources is redundant and the resource allocation needs to be optimized. Moreover, from the perspective of equipment manufacturing industry as a whole, the value of innovation efficiency in most industries is between 0.7 and 0.9, but fail to achieve DEA effective. Besides, take the value of technological innovation efficiency in 2020 as an example, as is shown in Fig. 18.1, there is obvious gap in technological innovation efficiency between industries.

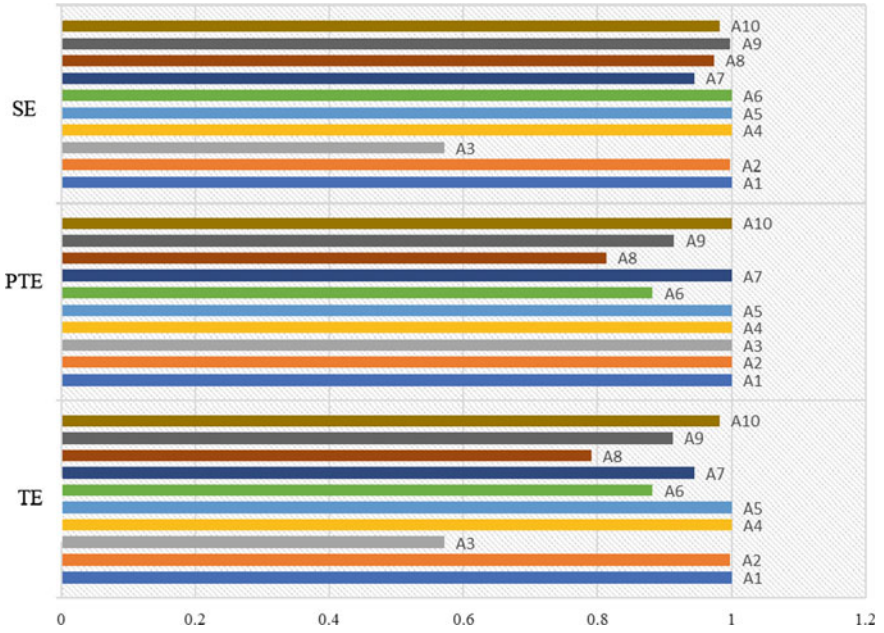

Fig. 18.1 The value of technological innovation efficiency in 2020

Dynamic Efficiency Analysis

However, it is difficult to assess the change degree of efficiency value in different periods with DEA model. In order to accurately reflect the change trend of the technological innovation efficiency of equipment manufacture, this part use the MPI model to further empirically analyse the panel data, which can dynamically reflect the changes in the efficiency values of the sample data in different time series, so as to further identify the factors affecting changes in efficiency. The results are shown in Table 18.3.

The mean value of the MPI from 2016 to 2020 is 1.058, which is more than 1, indicating that the overall technological innovation efficiency is in a growing trend,

Table 18.3 Estimated results of the MPI of equipment manufacturing industry

YEAR	TEC	TC	PEC	SEC	MPI
2016–2017	1.072	1.072	1.136	0.944	1.149
2017–2018	0.886	1.178	0.921	0.962	1.044
2018–2019	1.444	0.660	1.247	1.158	0.953
2019–2020	0.956	1.146	0.979	0.976	1.095
Mean	1.070	0.989	1.063	1.006	1.058

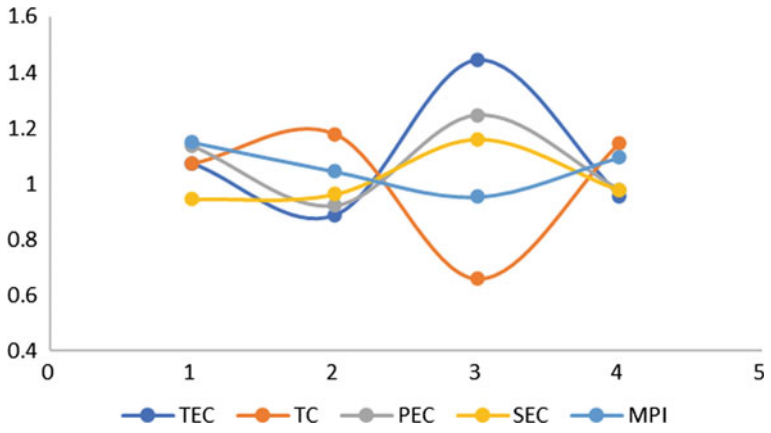

Fig. 18.2 Change curves of each efficiency index

with an average annual growth rate of 5.8%. From the perspective of decomposition indicators, which is the joint promotion of pure technical efficiency (PEC) and scale efficiency (SEC), while technological progress (TC) is decline. Further, during the empirical period, total factor productivity (MPI) is in a state of fluctuating growth, with negative growth from 2018 to 2019, which mainly due to the slowdown of technological progress (TC), and hinders the overall development of equipment manufacturing industry. The change curves of each efficiency index are shown in the Fig. 18.2.

Table 18.4 shows the development of technological innovation efficiency of various industries in the equipment manufacturing industry from 2016 to 2020. The mean value of the technological progress (TC) index is less than 1, which indicates that the overall technological level of the sample object is backward. Although large-scale innovation resources are invested, the technological improvement is not obvious due to the relatively long transformation cycle of innovation achievements. From the perspective of industry, except that the total factor productivity in manufacture of radar and its fittings industry is in a downward trend, other industries show a growth trend, meanwhile the total factor productivity in manufacture of special purpose machinery (A10) experienced the largest increase, which is mainly the contribution of the improvement in pure technical efficiency (PEC). The decline of total factor productivity in radar equipment manufacturing industry (A3) is mainly caused by the decline of scale efficiency (SEC), indicating that there is redundancy in the resource allocation of the industry and fail to reach the optimization state. Moreover, from the decomposition of total factor productivity, most industries show the characteristics that the technical efficiency index (TEC) is greater than the technical progress index (TC) and greater than 1, indicating that the level of technical progress is still a restrictive factor for the development of equipment manufacturing industry.

Table 18.4 Estimated results of the MPI from industry perspective

Industry	TC	TEC	PEC	SEC	MPI
(A1) Manufacture of communication equipment	1.010	1.000	1.000	1.000	1.010
(A2) Manufacture of broadcasting and TV equipment	0.957	1.114	1.074	1.038	1.066
(A3) Manufacture of radar and its fittings	1.006	0.941	1.000	0.941	0.947
(A4) Manufacture of audio and video equipment	1.033	1.000	1.000	1.000	1.033
(A5) Manufacture of medical equipment and appliances	1.034	1.035	1.018	1.016	1.070
(A6) Manufacture of measuring instrument and meter	0.967	1.081	1.072	1.009	1.045
(A7) Manufacture of electrical machinery and apparatus	0.983	1.030	1.000	1.030	1.013
(A8) Manufacture of transport equipments	0.988	1.054	1.028	1.025	1.042
(A9) Manufacture of general purpose machinery	0.944	1.223	1.207	1.013	1.155
(A10) Manufacture of special purpose machinery	0.968	1.265	1.269	0.997	1.225
Mean	0.989	1.070	1.063	1.006	1.058

Analysis of Influencing Factors Based on GRA

In order to further reveal the impact of input–output factors of technological innovation on the innovation efficiency of equipment manufacturing industry, refer to relevant research idea [11], based on the static efficiency measurement, this paper introduces the grey relation analyse method to illustrate the impact of input and output indicators on technological innovation efficiency. In this paper, the comprehensive efficiency value from 2016 to 2020 is taken as the referential sequence, while the input and output indicators are taken as the influence sequence. The results are shown in Table 18.5.

It can be seen from Table 18.5 that the impact of input–output indicators on each industry is different. The communication equipment manufacturing industry (A1), audio-visual equipment manufacturing industry (A4), medical instrument and equipment manufacturing industry (A5), electrical machinery and equipment manufacturing industry (A7) have the highest correlation with the full-time equivalent of R&D index (I_3), suggesting that personnel investment is more important than other indexes to improve the comprehensive efficiency value of these industries; Radar and its fittings equipment manufacturing industry (A3), general equipment manufacturing industry (A9) and special equipment manufacturing industry (A10) have the strongest correlation with number of inventions in force (O_1), while comprehensive efficiency of broadcasting and TV equipment manufacturing industry (A2) and transportation equipment manufacturing industry (A8) are the most affected by the sales revenue of new products (O_2), indicating that the economic benefits of these industry are more significant.

Table 18.5 Correlation between input–output indicators and comprehensive efficiency

	Internal expenditure on R&D (I_1)	Expenditure on new products development (I_2)	Full-time equivalent of R&D (I_3)	Number of inventions in force (O_1)	Sales revenue of new products (O_2)
A1	0.675	0.594	0.848	0.721	0.740
A2	0.608	0.604	0.620	0.655	0.714
A3	0.684	0.610	0.699	0.798	0.753
A4	0.838	0.765	0.853	0.642	0.777
A5	0.790	0.727	0.820	0.677	0.679
A6	0.631	0.726	0.646	0.676	0.723
A7	0.730	0.641	0.854	0.542	0.747
A8	0.694	0.738	0.699	0.554	0.772
A9	0.802	0.801	0.810	0.904	0.771
A10	0.548	0.486	0.566	0.691	0.660
Mean	0.700	0.669	0.741	0.686	0.734

The investment of new product development funds (I_2) shows the greatest impact on technical efficiency of the instrument and meter manufacturing industry (A6). Overall, full-time equivalent of R&D (I_3) and sales revenue of new products (O_2) are the input and output indicators that have the greatest impact on technical efficiency respectively. The impact of R&D expenditure (I_1) on comprehensive efficiency of various industries is not the most significant, which shows that in current stage of industrial development, substantial investment does not necessarily yield high efficiency, and the coordinated development of multiple resources should be realized, which is consistent with the conclusions of related studies. The results show that to improve the efficiency of technological innovation, the proportion of researchers should be increased first, followed by innovation capital investment.

Summary and Thinking

The main content of this paper is to measure the technological innovation efficiency of ten subindustries of equipment manufacturing industry statically and dynamically, and analyse the impact of input–output indicators on technological innovation efficiency by using grey correlation model. Through the empirical analyse, the following conclusions are obtained:

The overall technological innovation efficiency of the sample industries in recent years shows a fluctuating growth trend, where the main reason restricting the improvement of technological innovation efficiency is due to the low level of technological progress. Most industries are in DEA invalid state, and there is redundancy in resource

allocation. Besides, input–output indicators have different effects on the technological innovation efficiency of various industries. Full-time equivalent of R&D and sales revenue of new products are the input and output indicators having the greatest correlation on technological efficiency respectively.

Because of the current development situation in technological innovation efficiency of equipment manufacturing industry, this paper will give relevant suggestions from the following aspects:

1. Strengthen industry collaboration and promote knowledge exchange

   In recent years, with the support of government policies, Chinese enterprises have continuously strengthened technological innovation and transformation. As a result, the overall technological innovation efficiency has been continuously improved. However, the core competitiveness in some high-end equipment manufacturing industries is not strong, the innovation ability fails to reach the expected level. Based on the empirical results of this paper, the level of technological progress in most industries is on a downward trend. Therefore, it is necessary to improve the innovation environment by promoting the improvement of innovative industrial clusters in the equipment manufacturing industry, strengthen knowledge exchange and resource sharing on the basis of professional division of labor. At the same time, more capital, technology, and cooperation platform support should be provided for the technology research and development of cluster enterprises to promote the overall high-quality development.
2. Increase investment in scientific research talents and optimize the innovation mechanisms

   The results of this paper reveal that R&D personnel investment and sales revenue of new products have the greatest impact on the technological innovation efficiency of the sample industries. Besides, the output of innovative knowledge is also an important indicator to measure the technological innovation capability of equipment manufacturing industries. The government should promote the innovation income of enterprises by means of tax incentives, financial support and market mechanism optimization. Meanwhile, the key to efficiency improvement lies in the quality of R&D personnel, enterprises should increase investment in talents and knowledge, promote personnel creativity and technological output ability, gradually establish a long-term mechanism for the cultivation of technical capabilities in equipment manufacturing industry.
3. Strengthen industry innovation management and optimize the configure of innovation resources

   In this paper, the static analysis results of technological innovation efficiency show that most equipment manufacturing industries have not achieved DEA effectiveness, and the grey correlation results also indicate that the impact of each input-output index on the comprehensive efficiency of technological innovation is also different. Therefore, it is necessary to pay attention to the rational allocation of resources, optimize the scale of the industrial structure, strengthen the resource input of important indicators in key industries, reduce investment

redundancy. At the same time, strengthen the management of innovation activities, search the development bottleneck of inefficient industries, promote the efficient transformation of resources, improve technological innovation efficiency and innovation income, and realize the optimal allocation of resources in the whole industry.

References

1. Wu, L. (2015). Study on evaluation of innovation performance in high-end equipment manufacturing industry. *Science and Technology Management Research, 15*, 51–56.
2. Zhao, K. (2020). empirical test of technology innovation efficiency in equipment manufacturing industry based on SFA. *Statistics and Decision, 36*(20), 72–75.
3. Fan, D., & Du, M. (2018). Research on technological innovation resource allocation efficiency and its influencing factors in high-end equipment manufacturing industries—Based on the empirical analysis of the two-stage StoNED-Tobit model. *Chinese Journal of Management Science, 26*(01), 13–24.
4. Varum, C. A., Cibrão, B., Morgado, A., & Costa, J. (2009). R & D, structural change and productivity: The role of high and medium-high technology industries. *Economia Aplicada, 13*(4), 399–424.
5. Karahan, Ö. (2015). Intensity of business enterprise R&D expenditure and high-tech specification in European manufacturing sector. *Procedia-Social and Behavioral Sciences, 195*, 806–813.
6. Lee, H., & Parka, Y. (2009). Comparative evaluation of performance of national R&D programs with heterogeneous objectives: A DEA approach. *European Journal of Operational Research, 196*(3), 847–855.
7. Peng, Y., Chen, S. Y., Sheng, W. W., & Pu, Y.(2013). Efficiency based on the two-stage correlative DEA Malmquist index on western regional technical innovation. *Operations Research and Management Science*
8. Zeng, G., & Geng, C. X. (2021). Measurement and optimization of technological innovation efficiency in high-end equipment manufacturing industry. *Techno economics & Management Research, 3*, 17–22.
9. Wang, L., & Tang, S. (2020). Research on the effect and determinants of government R&D subsidy Policy: From the perspective of innovation efficiency. *Scientific Management Research, 06*, 75–88.
10. Duan, J., & Liu, Y. (2011). Study on the evaluation of technology innovation ability of equipment manufacturing in china based on factor analysis. *Science & Technology Progress and Policy, 28*(20), 122–126.
11. Si, L., & Meng, W. (2017). Evaluation on the synergy degree of technology synergy innovation mechanism of equipment manufacturing industry—An empirical analysis based on the SIM model. *Techno economics & Management Research, 2*, 104–109.
12. Xiao, M., Zhang, W., & Tian, Z. (2020). Evaluation of technical innovation efficiency in 31 provinces based on two-stage DEA and grey relation. *China Science & Technology Resources Review, 52*(5), 78–88.
13. Banker, R. D., Charnes, A., & Cooper, W. W. (1984). Some models for estimating technical and scale inefficiencies in data envelopment analysis. *Management Science, 30*(9), 1078–1092.
14. Charnes, A., Cooper, W. W., & Rhodes, E. (1978). Measuring the efficiency of decision making units. *European Journal of Operational Research, 2*(6), 429–444.
15. Färe, R., Grosskopf, S., & Norris, M. (1994). Productivity growth, technical progress, and efficiency change in industrialized countries. *American Economic Association, 84*(1), 66–83.

16. Jamaluddin, M. Y., & David, H. (1997). The efficiency of the National Electricity Board in Malaysia: An intercountry comparison using DEA. *Energy Econ, 19*, 255–269.
17. Wang, R. T., Ho, C. T. B., & Oh, K. (2010). Measuring production and marketing efficiency using grey relation analysis and data envelopment analysis. *International Journal of Production Research, 48*(1), 183–199.
18. Liu, H., Liu, Y.F., & Qiao, H. (2015). Research on technological innovation efficiency of strategic emerging industries in China. *Systems Engineering—Theory & Practice, 35*(9), 2296–2303

Chapter 19
Bikes Detention Game in Free-Float Bike Sharing Systems

Shichen Zhao, Wenjuan Hou, Ziyao Wang, and Qiaochu He

Abstract Governments are trying to address the illegal parking problems in Free-Float Bicycle Sharing Systems (FFBSS) by quantitatively controlling the parking zone via geo-fencing technologies. Traffic enforcement department may punish the illegally parked bicycle by detaining them to undisclosed locations, which is difficult for the FFBSS enterprise to retrieve and incur surging operational costs. FFBSS enterprise is embracing data science to proactively reposition haphazardly parked bicycles to avoid unexpected detention. We start with a two players' game-theoretical model to capture the main idea, wherein a government makes detention decisions for illegal parking areas while the FFBSS enterprise makes proactive repositioning decisions. We operationalize the game-theoretical model by extending such conflicts to a network, which is then solved via mixed-integer optimization to validate the robustness of our main results.

Keywords Bikes detention game · Free-float bicycle sharing systems · Game theory

Introduction

The Free-Float Bicycle Sharing Systems (FFBSS) is becoming increasingly popular all over the world and this convenient and eco-friendly transport can efficiently solve the first and last-mile problem. However, except for these benefits, the FFBSS bring

S. Zhao (✉) · W. Hou · Z. Wang · Q. He
1088 Xueyuan Avenue, Shenzhen 518055, People's Republic of China
e-mail: 12032750@mail.sustech.edu.cn

W. Hou
e-mail: 11930745@mail.sustech.edu.cn

Z. Wang
e-mail: 11910115@mail.sustech.edu.cn

Q. He
e-mail: heqc@sustech.edu.cn

R. Qiu et al. (eds.), *City, Society, and Digital Transformation*, Lecture Notes in Operations Research, https://doi.org/10.1007/978-3-031-15644-1_19

several operational challenges, especially the illegal parking problem. During the morning rush hour, large-scale shared bikes are parked and accumulated illegally on the roads to subway stations or office buildings, which seriously hinders people's travel and destroys the image of the city. Although traffic enforcement government has imposed restrictions on the quantity of bikes for each parking area via geo-fencing technology (a new technology that allows the company to control the parking area for bicycles by setting virtual boundaries), the phenomenon of illegal parking still exists in the practice. Thus, traffic enforcement department may further punish the illegally parked bicycle by detaining them to undisclosed locations. Once bikes are detained, the enterprise has to make an effort to retrieve bikes, including finding locations where bikes are detained and paying the required fines, which definitely incurs surging operational costs. To avoid such unexpected detention, the bike-sharing enterprise is embracing data science to proactively reposition haphazardly parked bicycles by assigning operation trucks to clear these parking areas before the government makes detention decisions, such as moving bikes from crowded parking areas to underserved parking areas. Either FFBSS enterprise or the government is constrained by their limited resources so they must selectively target some valuable parking areas.

To support their target decisions, we start with a two players' game-theoretical model to capture the main idea, wherein a government makes detention decisions for illegal parking areas while the FFBSS enterprise makes proactive repositioning decisions. From the perspective of the enterprise, we identify that enterprise's efficient management is critical to improving its payoff. For example, they can model the importance of the targets and prioritize those targets with higher returns. From the perspective of the government, firstly, it is important to plan the capacities of parking areas reasonably because parking areas in hot areas of cities are always very crowded. In addition, it's necessary for them to supervise and they can efficiently promote the FFBSS enterprise's management by setting a high detention fine. Next, we operationalize the game-theoretical model by extending such conflicts to a network, which is then solved via mixed-integer optimization to validate the robustness of our main results.

There are two main streams of relevant literature, bike-sharing systems and security games. In the recent bike sharing research, the repositioning problem receives attention because of its natural connection to inventory control. For example, [8] consider the optimization of a ride-sharing match using incomplete information, which is an operational level problem. Some well-known papers also consider both operational and strategic decisions. For instance, [3] construct a structural demand model and estimate the impact of the stations' accessibility and the bicycles' availability. He et al. [2] estimate a structured demanding model for station networks and emphasize the importance of network effect. The bikes detention game in this paper is also closely related to security game studies [4, 5, 7]. Recently, a lot of related research focus on using machine learning and deep learning methods to solve security games. Davis et al. [1] use neural virtual self-play to solve large-scale network security games. Milani et al. [6] study the application of deception in the Stackelberg security game that is based on attack graph. In this dissertation, we study a bikes detention game between the bike-sharing enterprises and the government department.

Table 19.1 The payoff matrix of the sub-game model of the enterprise and the government

Enterprise government	Supervision (q)	No supervision (1-q)
Management (x)	$(R^d - C^d, -C^a)$	$(R^d - C^d, 0)$
No management (1-x)	$(-L^d - P^d, P^d - C^a)$	$(0, -S)$

Model Setup

In the two players' game-theoretical model, both the government department and the FFBSS enterprise have a two-dimensional strategy space. The former chooses to supervise (attack) or not, while the latter chooses to manage (defend) or not. The payoff matrix of two players is showed in Table 19.1. If the FFBSS enterprise manages bikes, it receives a net payoff of $R^d - C^d$ no matter whether the government manages or not, where R^d is the payoff of removed bikes drawing from serving other areas and C^d represents the bike transfer cost. If the FFBSS enterprise does not manage bikes, its payoff depends on the action of the government. In other words, when the government supervises, the FFBSS enterprise gets a net payoff $-L^d - P^d$, where L^d is the economic loss and P^d is the fine for retrieving detained bikes; When the government does not supervise, its net payoff is zero. The government department suffers a supervision cost C^a as long as it surprises the area no matter whether the FFBSS enterprise manages or not. However, if the FFBSS enterprise does not manage, the government department further receives a fine for illegally parked bikes (P^d) when supervising, and further bears a social negative effect ($-S$) when not supervising (Table 19.2).

Analysis

In this Section, we will conduct a complete analysis of the model with a single target (area).

Proposition 1 *The solutions to the model with a single area are as follows:*

When the reward from the management is always less than that under no management ($R^d - C^d < -L^d - P^d$), no management is a dominant strategy for the FFBSS enterprise. Then from the perspective of the government, it chooses supervision (Case 1) only if the payoff from the supervision is higher ($P^d - C^a > -S$), and no supervision (Case 2), otherwise ($P^d - C^a < -S$). When the FFBSS enterprise receives a higher payoff by managing bikes ($R^d - C^d > 0$), management (Case 3) is a dominant strategy for the FFBSS enterprise. At this time, the government will adopt the strategy of no supervision, because the supervision will cost in vain ($-C^a < 0$). When no supervision is a dominant strategy for the government ($P^d - C^a < -S$ and

Table 19.2 Strategy combination

Case	Condition	Strategy combination	Strategy type
1	$R^d - C^d < -L^d - P^d$,$P^d - C^a > -S$	(No management, supervision)	Pure
2	$R^d - C^d < -L^d - P^d$, $P^d - C^a < -S$	(No management, no supervision)	Pure
3	$R^d - C^d > 0$	(Management, no supervision)	pure
4	$0 > R^d - C^d < -L^d - P^d$, $P^d - C^a < -S$	(No management, no supervision)	Pure
5	$0 < R^d - C^d > -L^d - P^d$, $P^d - C^a > -S$	$(1 - \frac{C^a}{P^d+S}, \frac{C^d-R^d}{L^d+P^d})$	Mixed

$-C^a < 0$), and no management is a better strategy for the enterprise ($0 > R^d - C^d$), they will form a strategy combination of (no management, no supervision), which corresponds to Case 4.

In Case 5, neither the FFBSS enterprise nor the government has a dominant strategy. Specifically, if the enterprise chooses management (no management), the government would like to choose no supervision (supervision) because of $-C^a < 0$ ($P^d - C^a > -S$). However, the reverse is not true. If the government chooses supervision (no supervision), the enterprise would like to choose management (no management) because $R^d - C^d > -L^d - P^d$ ($0 > R^d - C^d$). Therefore, not a pure but a mixed strategy exists for Case 5. According to the existence theorem of Nash equilibrium, there is at least one Nash equilibrium for any finite game (pure strategy solution or mixed strategy solution). In the following, we will focus on finding the mixed strategy. A mixed strategy refers to that FFBSS enterprise and the government will adopt a pure strategy with a certain probability. Denote x be the probability that the FFBSS enterprise will manage the target and q be the probability that the government department will supervise the target. Then we have the FFBSS enterprise's expected utility function:

$$\begin{aligned} U^d =& xq(R^d - C^d) + x(1-q)(R^d - C^d) - q(1-x)(L^d + P^d) \\ =& x(R^d - C^d) - q(1-x)(L^d + P^d), \end{aligned} \tag{1}$$

and the government department's expected utility function:

$$U^a = -xqC^a + q(1-x)(P^d - C^a) - (1-x)(1-q)S. \tag{2}$$

We first take a derivation of U^d with respect to x and a derivation of U^a with respect to q, and then let derivations equal to zero. Hence, we can calculate the mixed strategy Nash equilibrium of enterprises and government as:

$$\left\{1 - \frac{C^a}{P^d + S}, \frac{C^d - R^d}{L^d + P^d}\right\} \tag{3}$$

By analyzing the solutions of Nash equilibrium, we can get the following propositions. The proof is in the Appendix.

Proposition 2 *The probability of the FFBSS enterprise choosing management increases with the fine P^d and society negative effects S, but decreases with the government cost C^a. Specifically, $\frac{\partial}{\partial P^d}x^* \geq 0$, $\frac{\partial}{\partial S}x^* \geq 0$, $\frac{\partial}{\partial C^a}x^* \leq 0$.*

The FFBSS enterprise's decision closely depends on those parameters which determine the payoff of the government. The underlying reason is that as P^d and S increase, or C^a decreases, the government prefers to supervise. To defend the government's supervision, the enterprise becomes more likely to manage. Therefore, to enhance the enterprise's management, government should actively supervise by reducing the cost of supervision C^a and increasing the detention fine P^d.

Proposition 3 *The probability of the government choosing supervision increase with the enterprise's management cost C^d, but decreases with the enterprise's fine P^d, the enterprise's loss L^d and the enterprise's management return R^d. Specifically, $\frac{\partial}{\partial C^d}q^* \geq 0$, $\frac{\partial}{\partial P^d}q^* \leq 0$, $\frac{\partial}{\partial L^d}q^* \leq 0$, $\frac{\partial}{\partial R^d}q^* \leq 0$.*

The underlying reason is as follows. As P^d, L^d and R^d increase, or C^d decreases, the FFBSS enterprise prefers to manage to pursue higher payoff. Now that the enterprise has managed bikes, in this case, there is no need for the government to supervise.

Observation 1 *We provide two applicable suggestions for the FFBSS enterprise and the government respectively:*

- *The FFBSS enterprise's efficient management is critical to improving its payoff.*
- *The government's punishment P^d plays a pivotal role in promoting the enterprise to manage.*

Based on the analysis of pure strategy Nash equilibrium, there are three pure-strategy Nash equilibrium solutions: (no management, supervision), (no management, no supervision) and (management, no supervision). In these three equilibrium solutions, (management, no supervision) is the most ideal case because it is optimal for the whole society. From the previous results, the condition for achieving this equilibrium is: $R^d > C^d$. Thus, the FFBSS enterprise should improve management efficiency (such as modeling the importance of the targets and prioritizing those targets with higher returns) to reduce management costs and increase management return. The government can not directly control the social loss or easily adjust the supervision cost, however, the fines for detained bikes can be modified. Therefore, the government can efficiently promote the FFBSS enterprise's management by setting a high fine.

The Network Model of Bikes Detention Game

We then extend the two players' game-theoretical model into a network across N parking areas. Let f_i and C_i denote the number of bikes and the capacity of the target i, respectively. In the two players' game-theoretical model, the enterprise only decides to manage bikes or not. However, in the network model, the enterprise instead decides how to transfer bikes across multiple areas. We use g_{ij} to denote the number of transition bikes from area i to area j. Without loss of generality, we set $g_{ji} = -g_{ij}$. We use λ_i to denote the number of bikes in the target i after the management, which can be calculated as follows:

$$\lambda_i = f_i + \sum_{j \neq i}^{N} g_{ji}. \tag{4}$$

The transfer cost to transfer one bike from target i to transition point j is c_{ij}. Hence, the aggregated transition cost for transporting bikes from area i is:

$$C_i^d = \sum_{j \neq i}^{N} c_{ij} \times g_{ij}^{+}. \tag{5}$$

It is difficult to capture the aggregated management return by transferring bikes from target i to other targets because outsourced bikes may bring either payoff or penalty. Instead, we turn to capture the the aggregated management return of those bikes transferred to target i, which is denoted as R_i^d:

$$R_i^d = r_i \times (\lambda_i - f_i) = r_i \sum_{j \neq i}^{N} g_{ji}, \tag{6}$$

where r_i is the unit economic payoff of one bike within target i. If the government chooses to supervise target i and it has not been managed by the enterprise, the bikes beyond the capacity C_i will be detained. We use l_i, p_i, s_i to denote the unit economic loss, the unit fine, and the unit social loss of the detained bike, respectively. Then, we can calculate the aggregated economic costs L_i^d, the aggregated fines P_i^d, and the aggregated social loss S_i:

$$L_i^d = l_i \times (\lambda_i - C_i)^+, \tag{7}$$

$$P_i^d = p_i \times (\lambda_i - C_i)^+, \tag{8}$$

$$S_i = s_i \times (\lambda_i - C_i)^+. \tag{9}$$

After making bike transferring decisions, the FFBSS enterprise gets the payoff of $(R_i^d - C_i^d)$. If the government supervises target i, the FFBSS enterprise suffers

economic loss L_i^d and fines P_i^d. Thus, the FFBSS enterprise's total expected utility is:

$$\begin{aligned} U^d &= \sum_{i=1}^{N} \left\{ (R_i^d - C_i^d) - q_i (L_i^d + P_i^d) \right\} \\ &= \sum_{i=1}^{N} \left\{ (r_i \sum_{j \neq i}^{N} g_{ji} - \sum_{j \neq i}^{N} c_{ij} \times g_{ij}^{+}) - q_i \left[(l_i + p_i) \times (\lambda_i - C_i)^{+} \right] \right\}. \end{aligned} \tag{10}$$

If the government supervises target i, it receives payoff $P_i^d - C_i^d$, and otherwise, it suffers a social loss S_i. Hence, the government's total expected utility is:

$$\begin{aligned} U^a &= \sum_{i=1}^{N} \left\{ q_i (P_i^d - C_i^a) - (1 - q_i) S_i \right\} \\ &= \sum_{i=1}^{N} \left\{ q_i \left[p_i \times (\lambda_i - C_i)^{+} - C_i^a \right] - (1 - q_i) \left[s_i \times (\lambda_i - C_i)^{+} \right] \right\}. \end{aligned} \tag{11}$$

The profit maximization problem of the enterprise can be summarized as follows:

$$\max_{g_{ij}} \quad U^d \tag{12a}$$

$$s.t. \sum_{i=1}^{N} C_i^d \leq B^d, \tag{12b}$$

$$\lambda_i \geq 0, \forall i. \tag{12c}$$

The constraint (12b) considers the enterprise's limited budget (B^d) for management. The constraint (12c) restricts a nonnegative number of bikes in each target after management action. **The profit maximization problem the government department** can be summarized as:

$$\max_{q_i \in [0,1]} \quad U^a \tag{13a}$$

$$s.t. \sum_{i=1}^{N} q_i C_i^a \leq B^a, \tag{13b}$$

$$q_i \in [0, 1], \forall i. \tag{13c}$$

The constraint (13b) considers the government department's limited budget (B^a) for supervision.

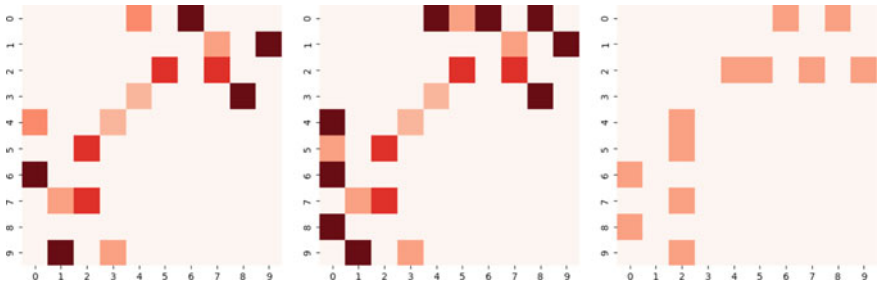

(a) $f_1 = 41$, $C_i = 20$ (b) $f_1 = 100$, $C_i = 20$ (c) $f_1 = 41$, $C_i = 10$

Fig. 19.1 The heat map of bikes transfer matrix (g_{ij}) for different f_1 and C_i

Numerical Experiments

By transferring the profit maximization problem of the FFBSS enterprise into KKT conditions, we can solve the network model via mixed-integer optimization. For numerical experiments, we randomly sample ten different parking areas. To avoid the trivial case that the enterprise never manages bikes, we make the return of transferring less than the loss from detention ($r_i < p_i + l_i$). Consistent with the practice, the transfer cost c_{ij} depends on the distance between target i and target j. C_i is uniformly set to 20 in experiments. Moreover, we suppose that the FFBSS enterprise and the traffic enforcement government have sufficient budgets.

Observation 2 *As the number of the bikes (f_i) within some regions, the fine p_i and the economic loss l_i increase, the FFBSS enterprises would like to transfer more bikes; As the capacity of all parking areas C_i increases, the FFBSS enterprises would like to transfer more bikes.*

The impact of the number of bikes (f_i) and the capacity C_i is showed in Fig. 19.1. As the number of bikes (f_i) increases, more bikes are out of capacity. Therefore, the FFBSS enterprise will transfer more bikes to reduce the fines for detained bikes.Given a higher capacity, the FFBSS enterprise transfers bikes more actively. In practice, parking areas in hot areas of cities are very crowded, so planning the number of bikes put on the market and the capacities of parking areas are very important. The impact of fines p_i and the economic l_i are showed in Fig. 19.2. Facing higher fines and higher economic loss, the FFBSS enterprise prefers to proactively manage bikes. The impacts of p_i and l_i are consistent with the single area.

Conclusion

To solve the conflicts in illegal parking problems, we build a game-theoretical model between the Free-Float Bicycle Sharing System (FFBSS) enterprise and the gov-

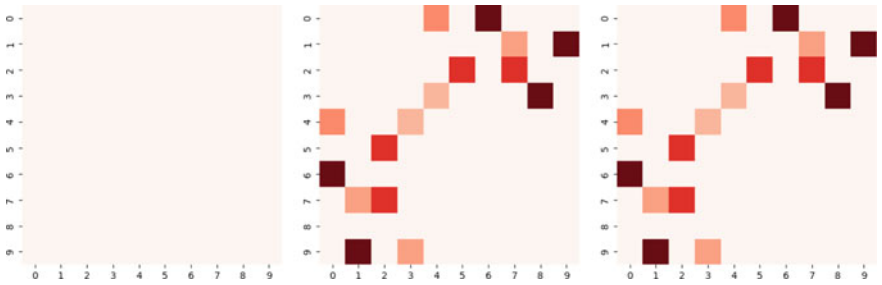

(a) $p_i = 2, l_i = 2$ (b) $p_i = 150, l_i = 2$ (c) $p_i = 2, l_i = 50$

Fig. 19.2 The heat map of bikes transfer matrix (g_{ij}) for different p_i and l_i

ernment. We start with a two players model to capture the main idea, wherein a government makes detention decisions for illegal parking areas while the FFBSS enterprise makes proactive repositioning decisions. Next, we extend the two players model into a network, which is then solved via mixed-integer optimization to validate the robustness of our main results. We find some valuable managerial insights. From the perspective of the FFBSS enterprise, we identify that the enterprise's efficient management is critical to improving its payoff. For example, they can model the importance of the targets and prioritize those targets with higher returns. From the perspective of the government, firstly, it is important to plan the capacities of parking areas and the quantity of shared bikes put on the market reasonably. Secondly, it's necessary for them to supervise by increasing fines P^d.

Appendix.Proof

Proof of Proposition 1 and 2

Proof According to the definition of mixed strategy Nash Equilibrium, the enterprise's response function can be obtained by taking the derivative of expected utility (1) with respect to the probability x of management.

$$\frac{\partial U^d}{\partial x} = (R^d - C^d) + q(L^d + P^d) \tag{14}$$

let $\frac{\partial U^d}{\partial x} = 0$, we can get the optimal management probability:

$$q^* = \frac{C^d - R^d}{L^d + P^d} \tag{15}$$

Similarly, the response function for government is :

$$\frac{\partial U^a}{\partial q} = -xC^a + (1-x)(P^d - C^a) + (1-x)S \tag{16}$$

let $\frac{\partial U^a}{\partial q} = 0$, we can get the optimal supervision probability:

$$x^* = \frac{P^d + S - C^a}{P^d + S} = 1 - \frac{C^a}{P^d + S} \tag{17}$$

Since $C^d > R^d, C^d - R^d < L^d + P^d$ and $P^d + S > C^a$, the mixed strategy Nash equilibrium of enterprises and government is:

$$\left\{1 - \frac{C^a}{P^d + S}, \frac{C^d - R^d}{L^d + P^d}\right\} \tag{18}$$

Therefore, it's easy to get the results of Proposition 1 and 2, i.e., $\frac{\partial}{\partial P^d}x^* > 0$, $\frac{\partial}{\partial S}x^* > 0$, $\frac{\partial}{\partial C^a}x^* < 0$, $\frac{\partial}{\partial C^d}q^* > 0$, $\frac{\partial}{\partial P^d}q^* < 0$, $\frac{\partial}{\partial L^d}q^* < 0$, $\frac{\partial}{\partial R^d}q^* < 0$.

The conclusion is consistent with the results of the pure strategy (Proposition1).

1. With P^d or L^d increment, if $P^d - C^a > -S$, situation will be changed from case 2 to case 4. Otherwise, situation will be changed from case 1 to case 5. The optimal strategy of the enterprise and government changes from (no management, supervision) to mixed strategy.
2. With R^d (C^d) increment (decrement), the pure strategy will tend to Case 3. In this case, the optimal strategy of the enterprise changes from no management to management.
3. With S (C^a) increment (decrement), if $R^d - C^d < -L^d - P^d$, situation will be changed from case 2 to case 1. Otherwise, the situation will be changed from case 4 to case 5. The optimal strategy of the enterprise and government changes from (no management, no supervision) to mixed strategy.

References

1. Davis, T., Waugh, K., & Bowling, M. (2019). Solving large extensive-form games with strategy constraints. *Proceedings of the AAAI Conference on Artificial Intelligence, 33,* 1861–1868.
2. He, P., Zheng, F., Belavina, E., & Girotra, K. (2020). Customer preference and station network in the London bike-share system. *Management Science*.
3. Kabra, A., Belavina, E., & Girotra, K. (2019). Bike-share systems: Accessibility and availability. *Management Science*.
4. Letchford, J., & Vorobeychik, Y. (2011). Computing randomized security strategies in networked domains. In *Applied adversarial reasoning and risk modeling, papers from the 2011 AAAI workshop, San Francisco, California, USA, August 7, 2011*.
5. Mckelvey, R. D., & Palfrey, T. R. (1995). Quantal response equilibria for normal form games. *Games and Economic Behavior, 10*.

6. Milani, S., Shen, W., Chan, K. S., Venkatesan, S., & Fang, F. (2020). Harnessing the power of deception in attack graph-based security games. *Decision and Game Theory for Security*.
7. Nguyen, T. H., Yang, R., Azaria, A., Kraus, S., & Tambe, M. (2013). *Analyzing the effectiveness of adversary modeling in security games*. AAAI Press.
8. Wang, X., Agatz, N., & Erera, A. (2018). Stable matching for dynamic ride-sharing systems. *Transportation Science, 52*(4), 850–867.

Chapter 20
On the Value of Orderly Charging in Improving Power Grid Resilience

Yuqiu Deng, Zihao Jiao, Mengqi Li, and Lun Ran

Abstract The increase of Electric Vehicle (EVs) adoptions has achieved a double harvest of environmental and economic benefits and brings an extra burden on the urban power grid. To this end, efforts have been made to optimize chargers' location and power scheduling to mitigate the adverse impacts of increasing EVs. However, the long duration and high cost of chargers installation curbs further EVs adoption, which also triggers less charging accessibility for urban EV travel. In practice, the low utilization rate of charging piles leads to high idle rates, which motivates charging aggregators to incorporate demand response (i.e., orderly charging in our context) into traditional charging services. In such a context, we attempt to uncover economic and environmental benefits created by orderly charging in the scenario of private charging piles for self-use. The results reference the operation management of personal chargers in the community and the orderly charging scheduling of EVs.

Keywords Demand response · Orderly charging · Multi-objective optimization · Charging sharing

Y. Deng · Z. Jiao (✉)
School of International Economics and Management, Beijing Technology and Business University, Beijing 100089, China
e-mail: jiaozihao@btbu.edu.cn

Y. Deng
e-mail: dengyuqiu1005@163.com

M. Li
Agricultural Development Bank of China, Beijing, China
e-mail: lmq18101357082@163.com

L. Ran
School of Management and Economics, Beijing Institute of Technology, Beijing, China
e-mail: ranlun@bit.edu.cn

R. Qiu et al. (eds.), *City, Society, and Digital Transformation*, Lecture Notes in Operations Research, https://doi.org/10.1007/978-3-031-15644-1_20

Introduction

EVs with good environmental and economic benefits have been rapidly developed and utilized worldwide. Governments of various countries have formulated plans to develop new energy vehicles and introduced support and incentive policies on the supply side. On the demand side, residents gradually adopt EVs. The global sales and proportion of new energy vehicles are increasing yearly.

However, as private EV ownership increases, so does the need for charging. The global EV sales bucked the trend against the backdrop of the new crown epidemic causing total car sales to fall by one-fifth in 2020, 43%, reaching over 3 million [1]. The charging conduct of EVs is random. This random and disordered charging method will affect the operation and maintenance of the power grid system to a certain extent. The report issued by the State Council pointed out that it is necessary to coordinate the charging and discharging of new energy vehicles, and power dispatching needs. Then comprehensively use policies such as peak and valley electricity prices to achieve efficient interaction between EVs and grid energy [2].

Due to the lack of daily operation management of private charging piles, there is an imbalance between the supply and demand of personal charging piles. The possession rate of pure private EVs is only 55% [3], and the existing private charging piles are used less frequently, an idle rate of about 75% [4]. Therefore, it is essential to design a community personal charging pile operation model for the orderly charging of EVs. It can meet the needs of multiple stakeholders, such as community grids, charging service providers, and EV users. The orderly charging operation mode dynamically adjusts the time and place of charging demand based on the total load of the power grid and the unit's operational data in different periods. It is capable of power grid peak shaving and valley filling.

This paper aims to promote the orderly charging of EVs, balance supply and demand, and conduct research on EV charging demand scheduling. The specific contributions of this paper are summarized as follows. Firstly, we explore the impacts of *Orderly charging service* on two sides. For community grids, it can reduce load fluctuation and improve power grid operation safety. For users, it can decrease the charging cost and enhance the charging economy of users. Secondly, A multi-objective optimization model is developed to solve the orderly scheduling problem of EVs. The goal of the model is to minimize grid load fluctuation and user charging costs. Furthermore, an efficient computation technique includes operational research theories and methods such as statistical modeling, nonlinear programming, multi-objective optimization, and linear weighting, providing a reference for other scholars and related research on modeling and solving strategies.

The remainder of this paper is organized as follows: Section "References" reviews the related literature on EV's demand response strategies and orderly charging scheduling, Section "Problem Description and Formulation" prepares the data, Section "Orderly Charging Scheduling Model" explains the algorithm for solving this problem, and Sections "Numerical Study" and "Conclusions and Future Work" are the result and conclusion.

References

Our work contributes to strengthening the literature on sustainable operations management to improve the orderly charging scheduling of EVs. Therefore, two related literature streams are discussed: demand response strategies for EVs and orderly charge scheduling.

Regarding the electricity price of EVs, Monfared et al. [5] proposed that an EV's charging choice is made in reaction to information such as charging location, charging time, and charging price, i.e., modifying its charging behavior to promote charging satisfaction based on the charging information. At present, many scholars discuss the issue of EV charging scheduling below the time-of-use pricing mechanism. In the orderly charge scheduling problem, Choi et al. [6] raised that the pricing incentive model is frequently used to plan the charging requirements of EVs, and it comprises charging subsidies, time-of-use electricity prices, and real-time electricity prices. Lin et al. [7] optimized the schedule to shift energy demand from peak to valley. Gong et al. [8] used the price elasticity coefficient to create a demand-price response model for EV charging loads. Limmer and Rodemann [9] introduced a dynamic time-sharing pricing optimization framework that considers consumer choice uncertainty.

Regarding EV charging scheduling, Daryabari et al. [10] put forward that an EV's charging load is essentially a dispatchable and movable power demand; the charging power can be changed during the charging start and end periods. The economic benefits for many parties, such as the power grid and EV users, can be achieved by systematically managing EVs' charging behavior. As for the orderly charging optimization model, the objectives usually include minimizing the power loss of the grid, the peak-to-valley difference, the charging cost of the user, and maximizing the security of the distribution network. Tao et al. [11] developed a model intending to minimize grid load fluctuations, maximize user charging capacity, and solved it using a linear weighting method. To describe grid pricing uncertainty, AhmadiNezamabad et al. [12] proposed an interval optimization method and solved a dual-objective model with ϵ constraints to obtain the Pareto solution.

Different charging circumstances usually result in some contrasts in the charging characteristics of EVs, with community charging being the most common. Kapustin and Grushevenko [13] pointed out that when the community grid is connected to EVs on a large scale, the peak value of the EV charging load will overlap with the peak value of the conventional electricity load. Gong et al. [14] developed a genetic algorithm to solve a nonlinear programming model for the orderly charging of community EVs based on a dynamic peak pricing mechanism.

In addition to considering a single subject objective, some studies also consider the interests of the grid, users, or aggregators. Wang et al. [15] developed an orderly charging and discharging model for EVs in urban residential areas to minimize total power load variance and lowering power grid costs. Nimalsiri et al. [16] built a quadratic programming model that considered user economics and distribution network security restrictions.

Although there are numerous research results on the orderly charging scheduling of EVs, the optimal charging strategy is still worthy of further discussions, such as considering different application scenarios, the charging frequency of EVs, and the scheduling time. Therefore, this paper will fully consider the price incentive effect of time-of-use electricity prices and specifically study EVs' orderly charging in community scenarios.

Problem Description and Formulation

There are two major problems in the operation and management of charging piles: the disordered charging mode seriously impacts the power grid; the other is that the low level of process and control leads to an imbalance between supply and demand.

Therefore, we build the time-of-use electricity price mechanism for EV charging. The peak-valley electricity price difference is used to guide EVs to charge when the electricity consumption is low to stabilize the load fluctuation of the community power grid.

Model Assumptions

(1) We assume the start of charging is returning to the community that day, and the end is leaving the community the next day. According to the US national household travel survey (NHTS) on domestic cars in 2001, Taylor et al. [17] concluded that the home time of private EVs approximately satisfies the normal distribution. The EV charging start time is t, the expected value $\mu_s = 17.47$, and the standard variance $\sigma_s = 3.41$. The probability density function when the EV starts to charge is:

$$f_s(t) = \begin{cases} \frac{1}{\sqrt{2\pi}\sigma_s}\exp\left[-\frac{(t+24-\mu_s)^2}{2\sigma_s^2}\right], & 0 < t \le \mu_s - 12 \\ \frac{1}{\sqrt{2\pi}\sigma_s}\exp\left[-\frac{(t-\mu_s)^2}{2\sigma_s^2}\right], & \mu_s - 12 < t \le 24 \end{cases}. \tag{20.1}$$

Similarly, the end of charging time of the EV also conforms to the normal distribution, the expected value $\mu_e = 7.92$, the standard variance $\sigma_e = 3.24$, and the probability density function is:

$$f_e(t) = \begin{cases} \frac{1}{\sqrt{2\pi}\sigma_e}\exp\left[-\frac{(t-\mu_e)^2}{2\sigma_e^2}\right], & 0 < t \le \mu_e + 12 \\ \frac{1}{\sqrt{2\pi}\sigma_e}\exp\left[-\frac{(t-24-\mu_e)^2}{2\sigma_e^2}\right], & \mu_e + 12 < t \le 24 \end{cases} \tag{20.2}$$

EV charging power is related to mileage, battery capacity, and charging frequency. The user travel mileage conforms to the log-normal distribution [17]. The daily mileage of an EV is d, the expected daily mileage is μ_D, the standard variance is σ_D, and the probability density function is:

$$f_D(d) = \frac{1}{\sqrt{2\pi}\sigma_D d}\exp\left[-\frac{(\ln D-\mu_d)^2}{2\sigma_d^2}\right]. \tag{20.3}$$

(2) This article is based on the average mileage of 10,912 EVs in Beijing on weekdays in 2019. The expected value of its probability density function is $\mu_D = 2.77$, and the standard variance is $\sigma_D = 0.77$. Assuming that the charging frequency is once a day, d_i represents the daily mileage of EV i, and W_i is the power consumption per 100 kms of the EV:

$$D_i = \frac{d_i W_i}{100} \tag{20.4}$$

Table 20.1 The division results of the peak-to-valley period based on the K-means clustering algorithm

Time	Time-division (No EV, EV penetration rate 20%)	Time-division (EV penetration 30, 40%
peak	17:00–22:00	15:00–22:00
flat	8:00–16:00; 23:00–1:00	8:00–14:00; 23:00–1:00
valley	1:00–7:00	1:00–7:00

Table 20.2 Optimal time-of-use electricity price mechanism under different penetration rate

Time	Penetration—electricity price		
peak	20%–0.25	30%–0.25	40%–0.25
flat	20%–0.5615	30%–0.6010	40%–0.6233
valley	20%–0.7228	30%–0.7520	40%–0.7966

(3) EV charging data from Monte Carlo simulations are applied in our case study. We assume a community of 400 households, each with one private car. This paper sets the EV penetration rate at 40% and lets both ω_1 and ω_2 be 0.5. For ease of calculation, we set $S_i^{\min}$ to a constant value of 10%, at which point there are 26 EVs available for orderly charging. However, EV users have individual differences in the lower limit of acceptable SOC.

(4) We believe that the community charging period can be divided into three segments. Then, we use the K-means clustering algorithm to divide the peak, flat and valley periods. The clustering results are shown in Table 20.1:

We assume that the model adopts the time-of-use pricing mechanism. Through simulation, we obtained the optimal time-of-use electricity price mechanism in each period of the community under different EV penetration rates. The results are shown in Table 20.2:

Parameter

The notations applied in our model are listed in Table 20.3.

Orderly Charging Scheduling Model

Model Formulation

For the community power grid system, we want to minimize grid load variance for community grid systems. It is related to the charging power e_{it} of each EV, as shown

Table 20.3 List of notations

Indices and sets	
$i \in I$	Set of EV with private piles in the community
$i \in I_o$	Set of EV with orderly charging on the day
$i \in I_d$	Set of EV with out-of-order charging on the day
$i \in I_u$	Set of EV not charging for the day
$t \in T$	Set of all time, t is the start time, Δt is the length of the period
$t \in T_i$	Set of time when the EV i connects to the charging pile,$T_i = [t_i^a, t_i^d)$
Parameters	
$e^{\max}$	Maximum charging power of the EV. Maximum output power of the charging pile
$S^{\max}$	SOC upper limit
B_i	Battery capacity of the EV i
W_i	Electricity consumption per 100 km of the EV i
$S_i^{\min}$	SOC lower limit of the EV i
$S_i^{\exp}$	Expected SOC at the end of charge of the EV i
S_i^{ini}	SOC status when leaving the community on the day of EV i
t_i^{arr}	Time to start charging of EV i
t_i^{dep}	Time to end charging of EV i
d_i^1	Estimated mileage of EV i on the day
d_i^2	Estimated mileage of EV i on the following day
L^{limit}	Community transformer power limits
z_t^B	Conventional charging load of the community at time t
$z_t^{EV_d}$	Charging load of the disorderly charging EV set at time t
p_t	Electricity price at te t
Intermediate variables	
$z_t^{EV_o}$	Charging load of orderly charging EV set at time t
z_t	Total charging load in the community at time t
$\overline{z}$	Average daily charging load in the community
Decision variables	
e_{it}	EV charging power of i at time t

in the formula (20.5):

$$f_1 = \min_e \frac{1}{\mathrm{T}} \sum_{t \in T} (z_t(e) - \overline{z}(e))^2 \tag{20.5}$$

The grid load includes the regular electricity load of the community z_t^B, the disordered charging $z_t^{EV_d}$, and the ordered charging $z_t^{EV_o}$, as shown in the formula (20.7), the daily average load $\overline{z}(e)$ is determined by e in (20.8):

$$z_t^{EV_o}(e) = \sum_{i \in I} e_{it}, \quad \forall t \in T \tag{20.6}$$

$$z_t(e) = z_t^B + z_t^{EV_d} + z_t^{EV_o}(e), \quad \forall t \in T \tag{20.7}$$

$$\overline{z}(e) = \frac{1}{\mathrm{T}} \sum_{t \in T} z_t(e), \quad \forall t \in T \tag{20.8}$$

For EV users, we hope to transfer the charging time and power to the low electricity price. The objective function is to minimize the total charging cost of the user, such as formula (20.9):

$$f_2 = \min_e \sum_{i \in I} \sum_{t \in T_i} e_{it} p_t \Delta t \tag{20.9}$$

The charge EV return to the community is $S_i^{arr} = S_i^{ini} - \frac{d_i^1 W_i}{100 B_i}$, and charge capacity is $\frac{\sum_{t \in T_i} e_{it} \Delta t}{B_i}$. Their sum should be greater than the expected EV charge and smaller than the upper limit of the state of charge of the EV, as shown in constraint (20.10). Constraint (20.11) denotes the community transformer power limits. The sum of the daily electricity and charging load is kept within the power limit of the community grid transformer L^{limit}. Constraint (20.12) indicates that the charging power should be greater than 0 and not exceed the upper limit. It is not charged if it equals 0. We assume that if the car owner does not return to the community, the charging power is 0, as shown in the formula (20.13):

$$S_i^{exp} \le S_i^{arr} + \frac{\sum_{t \in T_i} e_{it} \Delta t}{B_i} \le S^{\max}, \quad \forall i \in I \tag{20.10}$$

$$z_t(e) \le L^{limit}, \quad \forall t \in T \tag{20.11}$$

$$0 \le e_{it} \le e^{\max}, \quad \forall i \in I, \forall t \in T_i \tag{20.12}$$

$$e_{it} = 0, \quad \forall i \in I, \forall t \notin T_i \tag{20.13}$$

Therefore, the orderly charging scheduling model for community EVs is as follows:

$$f_1 = \min_e \frac{1}{\mathrm{T}} \sum_{t \in T} (z_t(e) - \overline{z}(e))^2$$

$$f_2 = \min_e \sum_{i \in I} \sum_{t \in T_i} e_{it} p_t \Delta t$$

$$s.t., (10) - (13).$$

Solution Approach

We solve the multi-objective optimization problem using a linear weighted summation method. First, normalize the two objective functions. Then, assign the weighting coefficients to the optimization objective ($\omega_1 + \omega_2 = 1$). The final single-objective minimization problem is obtained as (20.14):

$$\min f = \omega_1 \frac{f_1}{f_1^{\max}} + \omega_2 \frac{f_2}{f_2^{\max}} \tag{20.14}$$

$$s.t., (10) - (13).$$

Numerical Study

Data Descriptions: Monte Carlo Simulation

We use the Monte Carlo simulation method to simulate the total load curve of the community power grid under disordered charging. We use 20, 30, 40% penetration rates of EVs and 100% deployment rate at private charging piles for simulation. According to Eqs. (20.1), (20.2), and (20.3), the charging start time t_i^{arr}, end charging time t_i^{dep}, and daily mileage d_i of the EV are randomly generated. At the same time, based on Eq. (20.4), the vehicle battery capacity B_i and the power consumption W_i per 100 km are randomly set to calculate the daily charging demand D_i of the EV. In order to prevent the rapid aging of EV batteries, Han et al. (2020) proposed that the EV's state of charge should not be less than 10% and exceed 95% of the rated capacity [18]. The acceptable lower limit of SOC $S_i^{\min}$ is set to 10%, and the expected state of charge S_i^{exp} of the EV after each charge is set to 95%. The SOC upper limit $S^{\max}$ for EVs is 100%. As it leaves the community, the daily EV state S_i^{ini} will be randomly generated between $\left[S_i^{ini} + \frac{d_i^1 W_i}{100 B_i}, 95\%\right]$.

After that, we delete unreasonable data records. In addition, the study in this chapter divides a day into 24 time periods T, and the time length Δt is taken as 1. The maximum output power $e^{\max}$ of each charging pile is set to 7 kWh. According to Wang and Yang (2009), the maximum output power of the community distribution transformer L^{limit} is set to 1020 kW, and the daily load z_t^B of the conventional electricity consumption in the community adopts the typical daily load data [19]. We generate community EV charging needs randomly and run 100 simulations. According to simulation results shown in Fig. 20.1, When EVs' penetration rate increases, the peak-to-valley difference between grid load and the total load peak also increases.

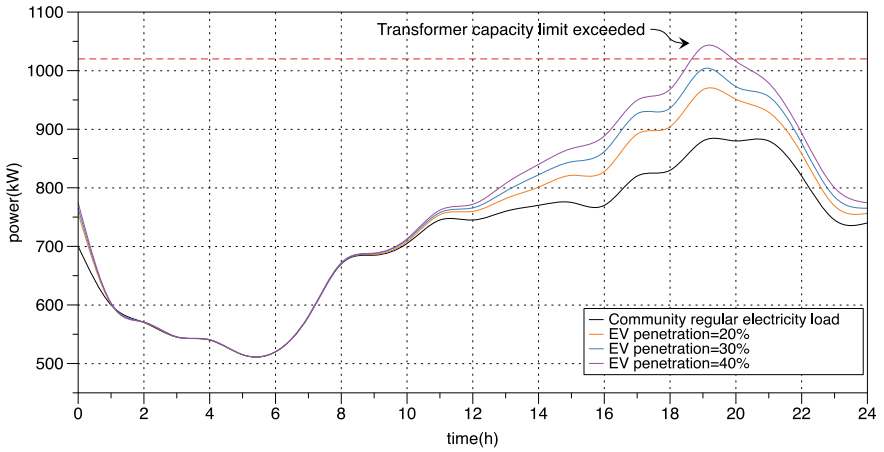

Fig. 20.1 The total load of the community grid under the disordered charging

Orderly Charging Scheduling Policy Performance

Observation

The results showed that the total charging cost of EVs was reduced from 641.37¥ to 364.67¥. The reason is that ordered charging achieves the peak-to-valley transfer. In Fig. 20.2, the charging time and the total charging power of EVs in disordered and ordered charging modes are shown. Based on this, we can conclude that the orderly charging strategy of EVs can reduce the charging costs of users.

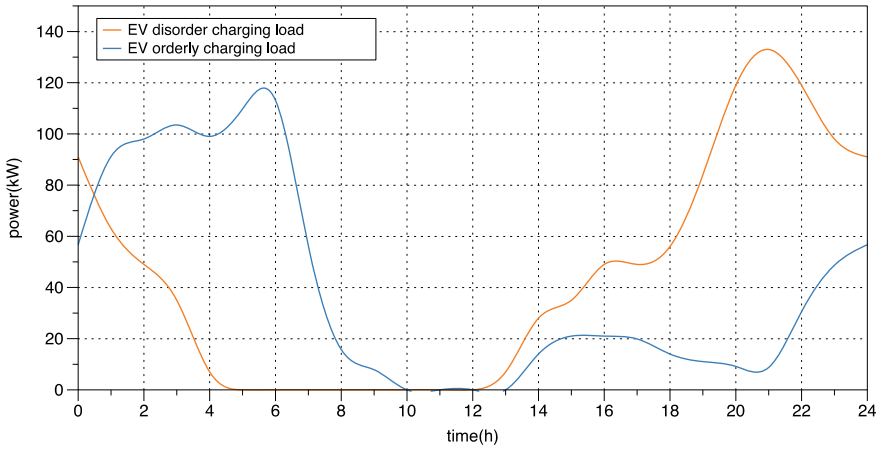

Fig. 20.2 Comparison of orderly charging and disorderly charging loads of EVs

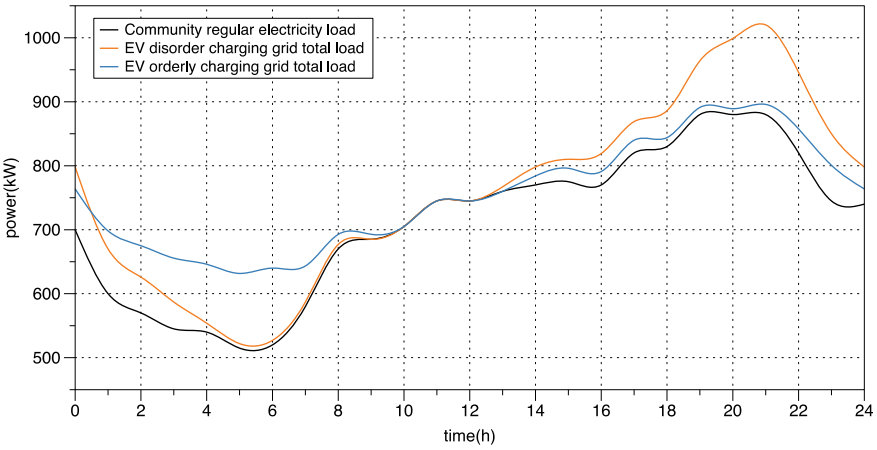

Fig. 20.3 Comparison of orderly charging and disorderly charging total loads of EVs

Observation

The community power grid's total load is calculated, as shown in Fig. 20.3. According to the findings, the orderly charging strategy reduces the grid's peak load by 12.65%, increases the valley load by 21.02%, reduces the peak-valley difference by 47.93%, and reduces the load variance 65.92% to the disordered charging mode of EVs. It is worth noting that, when compared to conventional energy load, the grid load's peak-to-valley difference is decreased by 28.96%, and the load variation is reduced by 49.54% once the orderly charging approach is adopted. It can be seen that the orderly charging mode of EVs can cut peaks and fill valleys, stabilizing load fluctuations. In addition, although the direct benefit to the grid is reduced, the peak load is reduced by 128.98 kW. The total benefit increases. We conclude that the orderly charging strategy of EVs can effectively realize the peak shaving and valley filling of the community power grid and improve the economic benefits of power grid operation.

Influence of Objective Function Coefficients

This section explores the influence of different objective weight coefficients on the results. We assign different weight coefficients to the two objective functions and plot the results in Fig. 20.4. It can be seen that with the increase of the weight coefficient ω_1 for minimizing the power grid load variance, the power grid load variance shows a decreasing trend, the value range is between 7700–7750 kW^2, and the user charging cost is increasing from 362¥ to 374¥. However, the overall degree of change in both is not significant.

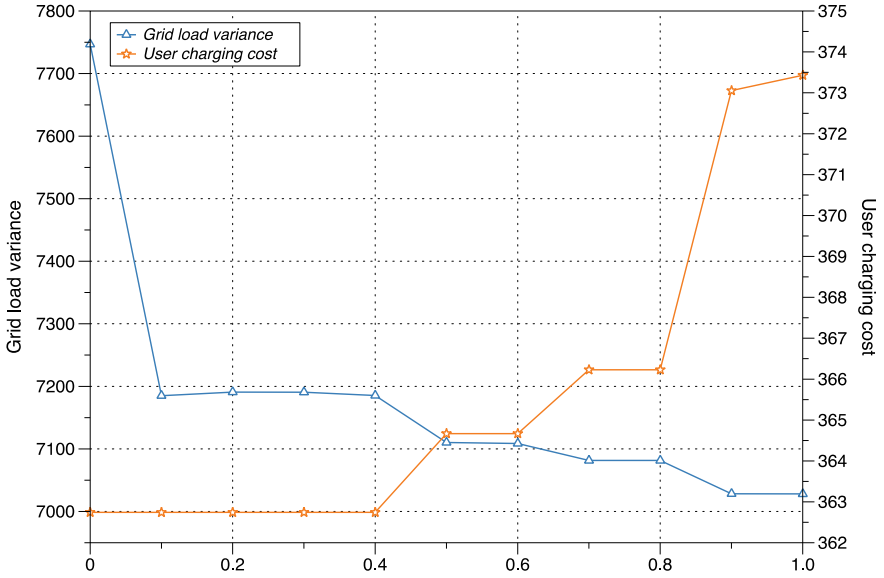

Fig. 20.4 Influence of different target weights on grid load variance and user charging cost

When $\omega_1 = 0$, the grid load variance is not considered. It is observed that the grid load variance (7746.88 kW^2) has been dramatically reduced compared with disordered charging (14091.12 kW^2). In the same way, when $\omega_1 = 1$, the user charging cost is not considered, the user charging cost (373.43¥) is also significantly reduced compared with the disordered charging (641.37¥).

Then, as ω_1 increases from 0 to 0.1, the grid load variance decreases from 7746.88 to 7185.06 kW^2. Then, when the value of ω_1 is in the range of 0.1–0.4, grid load variance and user charging cost variation are not apparent. When $\omega_1 = 0.5$, that is, when the weights of the two objective functions are the same, the grid load variance decreases to 7110.30 kW^2, and the user charging cost increases to 364.67¥. Subsequently, when the value of ω_1 changed from 0.8 to 0.9, the user charging cost increased the most, reaching 373.05¥.

We conclude that a single-objective optimization model that only considers f_1 or uses f_2 can reduce grid load variance and user charging costs. However, taking the two as the objective function and setting reasonable weight can better realize the trade-off between the power grid operation security and the user's charging economy.

Conclusions and Future Work

As EVs grows, the demand for charging rises year after year. The random and disorderly EV charging mode will harm the grid system's operation. Meanwhile, the

lack of routine operation and management of private charging piles in the community results in charging pile idleness and a supply–demand mismatch. Therefore, this paper addresses the above problems by proposing an orderly EV charging scheduling strategy based on relevant research. The specific research results of this paper are as follows:

(1) In the design of the community's private charging piles' operation mode, this paper first uses the Monte Carlo simulation method to predict the disordered charging process of EVs and demonstrate the impact of disordered charging on the community power grid. Second, the K-means clustering algorithm separates the orderly charging period of EVs into peaks, flats, and valleys. Then the time-of-use pricing strategy is calculated for diverse EV penetration rates.
(2) We develop a multi-objective nonlinear programming approach to reduce EV charging costs and grid load changes. Then, it is transformed into a single-objective optimization model using a linear weighting method. The findings suggest that our orderly charging technique can reduce power grid load volatility and user charging costs. If the target weight is set reasonably, the trade-off between the safety of power grid operation and the economic demand for users' charging can be better achieved.

Furthermore, our method can also be applied to other electrically-powered industrial operations. Many aspects of EV scheduling and robustness optimization require more exploration in the future:

(1) The data source for the model provided in this paper is typical electricity grid load data from a single community. The community's actual conventional power grid load statistics can be employed for further investigation. Moreover, the time-of-use tariff strategy is usually implemented on a city basis. In the future, the research can be applied to a larger area.
(2) This paper uses the linear weighting method to obtain relevant management inspiration when solving the multi-objective optimization model. In the future, when dealing with more realistic scenarios, we can try combining methods, constraint methods, and genetic algorithms.

Acknowledgements This paper is supported by the National Science Foundation of China [Grants 72101133, 72101008], China Postdoctoral Science Foundation [Grants 2021M701856], NSFC-FRQSC Research Program on Smart Cities and Big Data [Grants 7191101302].

References

1. EV Volumes. (2020). *The electric vehicle world sales database*. Technical Report, EV Volumes.
2. Office of the State Council. (2020). *Notice on printing and distributing the new energy vehicle industry development plan (2021–2035) (guobanfa [2020] no. 39)*. http://www.gov.cn/zhengce/content/2020-11/02/content_5556716.htm

3. The National Big Data Alliance of New Energy Vehicle. (2020). *China's small pure electric passenger car travel data report*. Technical Report, The National Big Data Alliance of New Energy Vehicle
4. xinhuanet. (2020). *Innovation and development of new energy vehicle infrastructure are critical areas*. http://www.xinhuanet.com/auto/2020-12/25/c_1126906982.htm
5. Monfared, H. J., Ghasemi, A., Loni, A., & Marzband, M. (2019). A hybrid pricebased demand response program for the residential microgrid. *Energy, 185*, 274–285.
6. Choi, D., Lim, M., Murali, K., & Thomas, V. M. (2019) Why have voluntary TimeofUse tariffs fallen short in the residential sector. *SSRN Electronic Journal*.
7. Lin, B., Ghaddar, B., & Nathwani, J. (2021) Electric vehicle routing with charging/discharging under time-variant electricity prices. *Transportation Research Part C: Emerging Technologies, 130*, 9
8. Gong, L., Cao, W., Liu, K., Yu, Y., & Zhao, J. (2020). Demand responsive charging strategy of electric vehicles to mitigate the volatility of renewable energy sources. *Renewable Energy, 156*, 665–676.
9. Limmer, S., & Rodemann, T. (2019). Peak load reduction through dynamic pricing for electric vehicle charging. *International Journal of Electrical Power & Energy Systems, 113*, 117–128.
10. Daryabari, M. K., Keypour, R., & Golmohamadi, H. (2020). Stochastic energy management of responsive plugin electric vehicles characterizing parking lot aggregators. *Applied Energy, 279*, 115751.
11. Tao, Y., Huang, M., Chen, Y., & Yang, L. (2020). Orderly charging strategy of battery electric vehicle driven by real world driving data. *Energy, 193*, 116806.
12. AhmadiNezamabad, H., Zand, M., Alizadeh, A., Vosoogh, M., & Nojavan, S. (2019). Multiobjective optimization based robust scheduling of electric vehicles aggregator. *Sustainable Cities and Society, 47*, 101494.
13. Kapustin, N. O., & Grushevenko, D. A. (2020). Longterm electric vehicles outlook and their potential impact on electric grid. *Energy Policy, 137*, 111103.
14. Gong, L., Cao, W., Liu, K., & Zhao, J. (2020). Optimal charging strategy for electric vehicles in residential charging station under dynamic spike pricing policy. *Sustainable Cities and Society, 63*, 102474.
15. Wang, N., Li, B., Duan, Y., & Jias, S. (2021). A multienergy scheduling strategy for orderly charging and discharging of electric vehicles based on multiobjective particle swarm optimization. *Sustainable Energy Technologies and Assessments, 44*, 101037.
16. Nimalsiri, N. I., Ratnam, E. L., Mediwaththe, C. P., Smith, D. B., & Halgamuge, S. K. (2021). Coordinated charging and discharging control of electric vehicles to manage supply voltages in distribution networks: Assessing the customer benefit. *Applied Energy, 291*, 116857.
17. Taylor, J., Maitra, A., Alexander, M., Brooks, D., & Duvall, M. (2009). Evaluation of the impact of plug-in electric vehicle loading on distribution system operations. In *2009 IEEE Power Energy Society General Meeting* (pp. 1–6), July 2009.
18. Han, X., Wei, Z., Hong, Z., & Zhao, S. (2020). Ordered charge control considering the uncertainty of charging load of electric vehicles based on Markov chain. *Renewable Energy, 161*, 419–434.
19. Shuning, W., & Shaobing, Y. (2016). An orderly control strategy of the electric vehicle charging load in residential areas. *Automation of Electric Power Systems, 40*(4), 7.

Chapter 21
Mixed-Integer Linear Programming Formulations for the Inbound Container Remarshaling Problem in an Automated Container Terminal

Bo Jin, Zhishan Yu, and Mingzhu Yu

Abstract In this paper, we study the inbound container remarshaling problem in an automated container terminal, which jointly optimizes the allocation of inbound containers and the scheduling of an automated stacking crane. The randomness of the future retrieval order of inbound containers and the time limit of the remarshaling process are both considered, and the goal is to minimize the expected time to retrieve all containers in the future. Two mixed-integer linear programming formulations, named the move-based and allocation-based models, are proposed. The move-based model encodes a feasible solution to the problem into a sequence of moves. The allocation-based model decomposes the problem into a master problem that focuses only on the final allocation of containers and a subproblem of scheduling the automated stacking crane. We prove that the subproblem can be solved in linear time by transforming it into a Eulerian graph, and then use its analytical solution to simplify the time constraint in the master problem. Numerical experiments show the outperformance of the proposed models over the existing mixed-integer programming model in the literature.

Keywords Automated container terminal · Inbound containers · Remarshaling · Mixed-integer linear programming · Eulerian graph

Introduction

Maritime transport is the main mode of transportation for the distribution of products in international trade. Due to the high operational efficiency of containerized ocean transport, most cargo in the maritime logistics is transported in containers. However, the increase in container throughput is creating more and more challenges to container terminals. To address these challenges, optimization techniques to improve terminal

B. Jin · M. Yu (✉)
College of Management, Shenzhen University, Shenzhen, China
e-mail: mzyu@szu.edu.cn

Z. Yu
College of Civil and Transportation Engineering, Shenzhen University, Shenzhen, China

R. Qiu et al. (eds.), *City, Society, and Digital Transformation*, Lecture Notes in Operations Research, https://doi.org/10.1007/978-3-031-15644-1_21

yard operations have attracted a great deal of attention from terminal operators in recent years.

There are three main types of containers handled in a container terminal: outbound containers, inbound containers, and transshipment containers. Upon arrival at the terminal, containers are transported to certain storage space in the yard and temporarily stored until being loaded onto the vessels or external trucks. Different from outbound and transshipment containers, the retrieval information (e.g., retrieval order) for inbound containers is usually unknown until an external truck arrives to pick up a container. Therefore, it is necessary to consider the stochastic nature of the future retrieval sequence when making decisions about the relevant terminal yard operations for inbound containers.

All arriving containers will be stored in certain storage space in the yard. An appropriate storage space allocation scheme benefits the future retrieval process by reducing container rehandles, which are required when the target container is buried under other containers during the retrieval process. In addition, yard cranes can reposition the containers in the yard during idle time to accelerate the future container retrieval process. Such rearrangement activity of yard cranes is commonly referred to as *remarshaling*.

Automated container terminals (ACTs) equipped with automated quay cranes (AQCs), automated stacking cranes (ASCs), and automated guided vehicles (AGVs) are safer, more efficient, and more reliable than conventional container terminals, and can significantly reduce the operational costs associated with labor and equipment [1]. Unlike conventional container terminals where external/internal trucks are required to temporarily park beside the block for the yard crane to perform handling activities (i.e., side-loading), the interfaces to external trucks and internal AGVs are restricted at the two ends of each block in an ACT (i.e., end-loading). Therefore, the storage locations of containers in an end-loading block affect not only the future rehandle costs, but also the horizontal movement time for the ASC to retrieve the containers.

In this paper, we consider an integrated optimization problem of container allocation and ASC scheduling during the remarshaling process for inbound containers in an ACT with the aim of minimizing the total expected container retrieval time. The randomness of the future retrieval order of containers and a maximum available remarshaling time are both considered. Two mixed-integer linear programming formulations, which we call the move-based and allocation-based models, are proposed to solve the integrated optimization problem. Numerical experiments are conducted to justify the outperformance of the proposed models over the existing model in the literature.

Literature Review

The relevant container remarshaling research can be divided into three categories: those targeting outbound containers, those targeting inbound containers, and those involving all types of containers.

The remarshaling problem for outbound containers is first studied by Kim and Bae [2]. The authors assume that the current yard map and the desirable layout of containers are both provided. They present a two-stage approach to minimizing the completion time of the remarshaling process. Kang et al. [3] and Choe et al. [4] solve a new remarshaling problem for outbound containers, considering the specific storage slots of containers in the bays before the remarshaling process and allowing arbitrary rehandle-free layouts of containers after the remarshaling process. Kim et al. [5] analyze the dwell time distribution of outbound containers and the impact of storage space utilization on the ship-loading efficiency.

Yu and Qi [6] introduce the remarshaling problem for inbound containers, assuming that the containers will be retrieved in a completely random order, i.e., the probability of being picked up by the next external truck is equal for all containers. The authors present a conceptual formulation for this problem and prove its NP-hardness by reduction from the fixed-size subset sum problem. For the same problem, Qin et al. [7] propose a mathematical programming formulation based on the precedence relationship between the repositioning movements of containers. Due to the NP-hardness of the problem, they develop a two-stage tabu search to solve it.

Choe et al. [8] study the opportunistic remarshaling problem, assuming that the time allowed for remarshaling might be too short so that remarshaling jobs have to be scheduled together with other container handling jobs for all types of containers. Covic [9] also considers a remarshaling problem involving all types of containers, who introduces an online rule-based solution method for the problem and analyzes the influences of the truck appointment system on the remarshaling behavior.

In the existing literature, inbound containers are less studied than outbound containers due to the lack of retrieval information. It makes the stacking and remarshaling operations for inbound containers more challenging. In this paper, we revisit the inbound container remarshaling problem in an ACT, which jointly optimizes the allocation of inbound containers and the scheduling of an ASC, following the previous works [6] and [7]. The problem considers not only the randomness of the future retrieval order of inbound containers, but also the time limit of the remarshaling process. We provide two new mixed-integer linear programming models for this problem and conduct numerical experiments to demonstrate their efficiency.

Problem Definition

In this section, we present a formal definition for the inbound container remarshaling problem in an automated container terminal. Due to the independence among different blocks in the yard, we focus on the remarshaling process for a single block whose results can be applied to other blocks. While studying this problem, we make the following assumptions.

Assumption 1 A single automated stacking crane is used to carry out the remarshaling operation, which starts from the landside interface and must return to the landside interface after finishing the remarshaling process.

Assumption 2 All containers stored in the block are inbound containers and assumed to have a completely random retrieval order, i.e., they are homogeneous in the remarshaling and retrieval processes.

Assumption 3 The remarshaling operation can only be performed when the crane is idle, and therefore the remarshaling process is limited to a given amount of available time.

Assumption 4 There is no container that enters or leaves the block, and therefore the total number of containers in the block is constant throughout the remarshaling process.

The following notation is defined to describe the parameters of the inbound container remarshaling problem. Let m denote the number of bays in the block, which are indexed from 1 to m from landside to seaside, as shown in Fig. 21.1. For the ease of presentation, the landside interface is referred to as bay 0. Let H denote the maximum number of containers that can be stored in each bay. The initial layout of containers in the block (i.e., initial allocation) is denoted by $\boldsymbol{h} = (h_1, \ldots, h_m)$, where $h_i \in \{0, \ldots, H\}$ represents the number of containers initially allocated to bay $i = 1, \ldots, m$, and the total number of containers is denoted by $N = \sum_{i=1}^{m} h_i$. Let t^C denote the time for the crane to lift or drop a container, t^E the time for an empty drive between two adjacent bays, and t^L the time for a loaded drive between two adjacent bays. Naturally, we assume $t^E \leq t^L$. Finally, let T denote the maximum available time for the remarshaling process.

The objective of the problem is to minimize the expected time to retrieve all containers in the block in the future. The future retrieval time consists of three parts: the necessary handling time for lifting and dropping containers, the additional time for performing rehandles, and the horizontal movement time of the crane. Assume

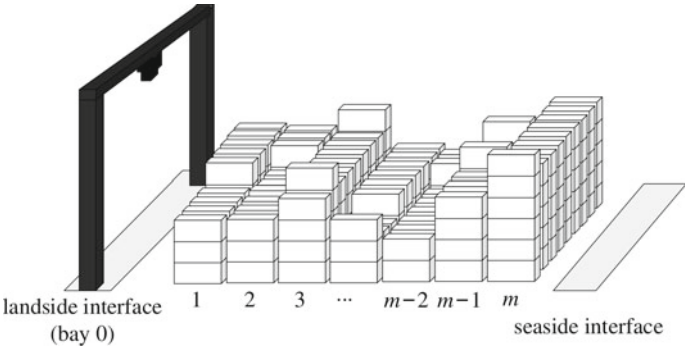

Fig. 21.1 Illustration of bay indices in the block

that the final layout of containers in the block (i.e., final allocation) is denoted by $\boldsymbol{x} = (x_1, \ldots, x_m)$ such that $\sum_{i=1}^{m} x_i = N$, where $x_i \in \{0, \ldots, H\}$ represents the number of containers finally allocated to bay $i = 1, \ldots, m$. We formulate the objective function by summing up the above three parts as

$$F(\boldsymbol{x}) = 2Nt^C + 2t^C \sum_{i=1}^{m} R(x_i) + \left(t^E + t^L\right) \sum_{i=1}^{m} i x_i. \tag{21.1}$$

To estimate the number of rehandles in the retrieval process of inbound containers, Kim [10] conducts a regression analysis and devises a quadratic function

$$R(x) = \left(\tfrac{1}{4s} + \tfrac{1}{16s^2}\right)x^2 + \left(\tfrac{1}{8s} - \tfrac{1}{4}\right)x, \tag{21.2}$$

where x is the number of inbound containers and s is the number of stacks in a bay. An issue with using it directly in the objective function is that it yields negative values for $0 < x < s$. Later, Yu and Qi [6] propose an improved piecewise function that is non-negative and proved to be accurate for $0 \le x < 2s$:

$$R(x) = \begin{cases} 0, if 0 \le x \le s; \\ \frac{s+2}{2s+2}x - \frac{s(s+2)}{2s+2}, if s < x < 2s; \\ \left(\frac{1}{4s} + \frac{1}{16s^2}\right)x^2 + \left(\frac{1}{8s} - \frac{1}{4}\right)x, if 2s \le x \le H. \end{cases} \tag{21.3}$$

However, the estimation error increases as x increases, so Qin et al. [7] propose a simulation module to estimate the number of rehandles. For the purpose of better extensibility, our mixed-integer linear programming formulations proposed in this study are general, which can accept any specific form of the rehandle estimation function.

To transform the initial allocation to a final allocation, the crane needs to carry out a sequence of moves that reposition containers from some origin bays to some destination bays. Given any sequence of moves (o_1, d_1), …, (o_n, d_n), where move (o_j, d_j) means the action of repositioning a container from the origin bay o_j to the destination bay d_j, the resulting allocation of containers is computed as $x_i = h_i - \sum_{j=1}^{n} 1_{o_j=i} + \sum_{j=1}^{n} 1_{d_j=i}$ for $i = 1, \ldots, m$. The associated crane working time is computed as $2t^C n + t^E(o_1 + d_n + \sum_{j=1}^{n-1} |d_j - o_{j+1}|) + t^L \sum_{j=1}^{n} |o_j - d_j|$, where the first term is the total time for lifting and dropping containers, the second term is the total time for empty drives, and the last term is the total time for loaded drives. Note that the crane working time is constrained by the given remarshaling time limit T.

To reduce the solution space, we only search for feasible solutions (o_1, d_1), …,(o_n, d_n) such that no bay is used as origin and destination simultaneously, i.e., $\{o_1, \ldots, o_n\} \cap \{d_1, \ldots, d_n\} = \varnothing$, according to the following property.

Property 1. *In the remarshaling operation, it is not optimal that there are containers being moved into and out of a bay in the same remarshaling period.*

Proof See [6]. □

To summarize, the inbound container remarshaling problem can be formally defined as follows. Given an initial allocation $\boldsymbol{h}$, the goal is to find an optimal sequence of moves (o_1, d_1), …,(o_n, d_n) that can be finished within the time limit T and result in a final allocation $\boldsymbol{x}$ such that the future expected retrieval time $F(\boldsymbol{x})$ is minimized.

Mixed-Integer Linear Programming Formulations

In this section, we propose two new mixed-integer linear programming formulations for the inbound container remarshaling problem. One is the move-based model, which formulates the problem from the perspective of a sequence of moves. The other is the allocation-based model, which focuses only on the final allocation of containers, while the optimal solution to the subproblem of crane scheduling is shown to have an analytical solution.

Move-Based Model

The move-based model directly encodes a feasible solution into a sequence of moves, as the way the problem is defined in section "Problem Definition". More specifically, the move-based model decides the optimal values for the decision variables n, o_1, d_1, …, o_n, d_n.

A critical issue that needs to be addressed is that the rehandle estimation function R is directly embedded in the objective function $F(\boldsymbol{x})$. To linearize the objective function, we treat $x_i \in \{0, \ldots, H\}$ as a categorical variable and use a one-hot vector $(w_{i,0}, \ldots, w_{i,H})$ to encode its value, and thus, the term $R(x_i)$ is linearized as $\sum_{j=0}^{H} R(j) w_{i,j}$ in the objective function for each $i = 1, \ldots, m$. Note that $R(j)$ is constant for all $j = 0, \ldots, H$, which can be pre-computed by any means of estimation.

Another critical issue is that the number of moves needed (i.e., n) is also a decision variable. To this end, we define *real move* as an actual action that repositions a container from one bay to another, and *fake move* as a dummy action expressed by $(0, 0)$ indicating that the crane has returned to the landside interface. The move-based model is aimed at finding the optimal move sequence with exactly N moves, including both real and fake moves. Note that N is a valid upper bound on the number of moves among all feasible solutions, since each container can be moved at most once according to Property 1. The advantage of such representation is that the crane working time can be expressed as $2t^C \sum_{j=1}^{N} r_j + t^E (o_1 + d_N + \sum_{j=1}^{N-1} |d_j - o_{j+1}|) + t^L \sum_{j=1}^{N} |o_j - d_j|$, where binary variable $r_j = 1$ if and only if the j th move is real for $j = 1, \ldots, N$.

A complete list of decision variables used in the move-based model is given as follows:

- Integer variable $x_i \in \{0, \ldots, H\}$ is the final number of containers allocated to bay i, for $i = 1, \ldots, m$;
- Binary variable $w_{i,j} = 1$ if and only if the final number of containers allocated to bay i (i.e., x_i) is equal to j, for $i = 1, \ldots, m$ and $j = 0, \ldots, H$;
- Binary variable $y_{i,j} = 1$ if and only if bay i is the origin of the j th move, for $i = 1, \ldots, m$ and $j = 1, \ldots, N$;
- Binary variable $z_{i,j} = 1$ if and only if bay i is the destination of the j th move, for $i = 1, \ldots, m$ and $j = 1, \ldots, N$;
- Binary variable $a_i = 1$ if bay i acts as origin, for $i = 1, \ldots, m$;
- Binary variable $b_i = 1$ if bay i acts as destination, for $i = 1, \ldots, m$;
- Binary variable $r_j = 1$ if and only if the j th move is real, for $j = 1, \ldots, N$;
- Integer variable $o_j \in \{0, \ldots, m\}$ is the origin of the j th move, for $j = 1, \ldots, N$. Specially, $o_j = 0$ means that the j-th move is fake;
- Integer variable $d_j \in \{0, \ldots, m\}$ is the destination of the j th move, for $j = 1, \ldots, N$. Specially, $d_j = 0$ means that the j th move is fake;
- Integer variable $e_j \in \{0, \ldots, m\}$ is (at least) the distance of empty drive between the destination of the j-th move (i.e., d_j) and the origin of the $(j + 1)$ th move (i.e., o_{j+1}), for $j = 1, \ldots, N - 1$;
- Integer variable $l_j \in \{0, \ldots, m\}$ is (at least) the distance of loaded drive between the origin of the j-th move (i.e., o_j) and the destination of the j th move (i.e., d_j), for $j = 1, \ldots, N$.

The move-based model is formulated as follows:

$$\min\ 2Nt^C + 2t^C \sum_{i=1}^{m} \sum_{j=0}^{H} R(j) w_{i,j} + \left(t^E + t^L\right) \sum_{i=1}^{m} i x_i \tag{21.4}$$

$$\text{s.t. } 2t^C \sum_{j=1}^{N} r_j + t^E \left(o_1 + d_N + \sum_{j=1}^{N-1} e_j \right) + t^L \sum_{j=1}^{N} l_j \le T; \tag{21.5}$$

$$x_i = h_i - \sum_{j=1}^{N} y_{i,j} + \sum_{j=1}^{N} z_{i,j}, \forall i = 1, \ldots, m; \tag{21.6}$$

$$\sum_{j=0}^{H} w_{i,j} = 1, \forall i = 1, \ldots, m; \tag{21.7}$$

$$\sum_{j=0}^{H} j w_{i,j} = x_i, \forall i = 1, \ldots, m; \tag{21.8}$$

$$\sum_{j=1}^{N} y_{i,j} \leq Ha_i, \forall i = 1, \ldots, m; \tag{21.9}$$

$$\sum_{j=1}^{N} z_{i,j} \leq Hb_i, \forall i = 1, \ldots, m; \tag{21.10}$$

$$a_i + b_i \leq 1, \forall i = 1, \ldots, m; \tag{21.11}$$

$$r_j = \sum_{i=1}^{m} y_{i,j} = \sum_{i=1}^{m} z_{i,j}, \forall j = 1, \ldots, N; \tag{21.12}$$

$$r_j \geq r_{j+1}, \forall j = 1, \ldots, N-1; \tag{21.13}$$

$$o_j = \sum_{i=1}^{m} i y_{i,j}, \forall j = 1, \ldots, N; \tag{21.14}$$

$$d_j = \sum_{i=1}^{m} i z_{i,j}, \forall j = 1, \ldots, N; \tag{21.15}$$

$$e_j \geq d_j - o_{j+1}, \forall j = 1, \ldots, N-1; \tag{21.16}$$

$$e_j \geq o_{j+1} - d_j, \forall j = 1, \ldots, N-1; \tag{21.17}$$

$$l_j \geq o_j - d_j, \forall j = 1, \ldots, N; \tag{21.18}$$

$$l_j \geq d_j - o_j, \forall j = 1, \ldots, N; \tag{21.19}$$

$$a_i \in \{0, 1\}, \forall i = 1, \ldots, m; \tag{21.20}$$

$$b_i \in \{0, 1\}, \forall i = 1, \ldots, m; \tag{21.21}$$

$$r_j \in \{0, 1\}, \forall j = 1, \ldots, N; \tag{21.22}$$

$$o_j \in \{0, \ldots, m\}, \forall j = 1, \ldots, N; \tag{21.23}$$

$$d_j \in \{0, \ldots, m\}, \forall j = 1, \ldots, N; \tag{21.24}$$

$$e_j \in \{0, \ldots, m\}, \forall j = 1, \ldots, N-1; \tag{21.25}$$

$$l_j \in \{0, \ldots, m\}, \forall j = 1, \ldots, N; \tag{21.26}$$

$$w_{i,j} \in \{0, 1\}, \forall i = 1, \ldots, m, \; j = 0, \ldots, H; \tag{21.27}$$

$$x_i \in \{0, \ldots, H\}, \forall i = 1, \ldots, m; \tag{21.28}$$

$$y_{i,j} \in \{0, 1\}, \forall i = 1, \ldots, m, \; j = 1, \ldots, N; \tag{21.29}$$

$$z_{i,j} \in \{0, 1\}, \forall i = 1, \ldots, m, \; j = 1, \ldots, N. \tag{21.30}$$

Objective (21.4) minimizes the expected retrieval time for all containers in the block. Constraint (21.5) ensures that the remarshaling time limit is not exceeded. Constraint (21.6) computes the final number of containers in each bay. Constraints (21.7) and (21.8) establish the relation between $(w_{i,0}, \ldots, w_{i,H})$ and x_i for all $i = 1, \ldots, m$. Constraints (21.9) and (21.10) define the role of each bay (i.e., origin or destination), and Constraint (21.11) ensures that no bay acts as origin and destination at the same time. Constraint (21.12) determines whether a move is real or fake, and Constraint (21.13) is an effective cut that forces the real moves to come before all fake moves. Constraints (21.14) and (21.15) compute the origin and destination bays of each move, respectively. Constraints (21.16) and (21.17) together compute the distance of empty drive between two adjacent moves. Constraints (21.18) and (21.19) together compute the distance of loaded drive in a move. Lastly, Constraints (21.20)–(21.30) stipulate the domains of the decision variables.

Allocation-Based Model

The allocation-based model decomposes the addressed problem into a master problem and a subproblem. The master problem focuses only on finding the optimal final allocation $\boldsymbol{x}$ to minimize the objective function $F(\boldsymbol{x})$, while the subproblem, denoted by $G(\boldsymbol{x})$, aims to construct an optimal sequence of moves for the crane to transform the initial allocation $\boldsymbol{h}$ into the given final allocation $\boldsymbol{x}$ such that the crane working time is minimized.

Subproblem of Crane Scheduling

The subproblem is characterized by the remarshaling task of transforming the initial allocation $\boldsymbol{h} = (h_1, \ldots, h_m)$ into the final allocation $\boldsymbol{x} = (x_1, \ldots, x_m)$. Define $\delta_i = h_i - x_i$ for $i = 1, \ldots, m$, which implies that a net number of δ_i containers will be moved out of bay i. Then, define $\lambda_i = \sum_{i'=1}^{i-1} \delta_{i'}$ for $i = 1, \ldots, m$, which implies

that a net number of λ_i containers will be transferred from bay set $\{1, \ldots, i-1\}$ to bay set $\{i, \ldots, m\}$. Lastly, define $\overline{m} = \max\{i = 1, \ldots, m\delta_i \neq 0\}$, which implies that the crane will never travel beyond bay $\overline{m}$ in an optimal solution to the subproblem.

Next, we construct a directed graph to describe the state transitions of the crane, in which the vertices can be divided into two parts. The upper part contains m vertices labeled $v_1^L, \ldots, v_m^L$, where v_i^L represents the state of the crane when it passes by bay i while carrying a container for $i = 1, \ldots, m$. The lower part contains $m+1$ vertices labeled $v_0^E, v_1^E, \ldots, v_m^E$, where v_i^E represents the state of the crane when it passes by bay i without carrying a container for $i = 0, 1, \ldots, m$. The arcs are added in three steps:

Step 1 Based on the sign of δ_i for $i = 1, \ldots, \overline{m}$, we add the following arcs, each of which has a cost of t^C, to link the upper and lower parts: if $\delta_i > 0$, add δ_i parallel arcs from v_i^E to v_i^L; if $\delta_i < 0$, add $-\delta_i$ parallel arcs from v_i^L to v_i^E. The arcs added in this step represent the mandatory operations for the crane to lift or drop containers at each bay;

Step 2 Based on the sign of λ_i for $i = 1, \ldots, \overline{m}$, we add the following arcs, each of which has a cost of t^L, in the upper part: if $\lambda_i > 0$, add λ_i parallel arcs from v_{i-1}^L to v_i^L; if $\lambda_i < 0$, add $-\lambda_i$ parallel arcs from v_i^L to v_{i-1}^L. The arcs added in this step represent the lower bound on the number of loaded drives between adjacent bays for the crane to balance the flow of container transfer between bays;

Step 3 Based on the sign of λ_i for $i = 1, \ldots, \overline{m}$, we add the following arcs, each of which has a cost of t^E, in the lower part: if $\lambda_i > 0$, add λ_i parallel arcs from v_i^E to v_{i-1}^E; if $\lambda_i < 0$, add $-\lambda_i$ parallel arcs from v_{i-1}^E to v_i^E; if $\lambda_i = 0$, add two arcs between v_{i-1}^E and v_i^E in the opposite directions. The arcs added in this step represent the lower bound on the number of empty drives between adjacent bays to balance the flow of crane movement and ensure the connectivity of the crane's trajectory.

We use an example to demonstrate the construction of the state transition graph. Suppose that the remarshaling task is given by $\boldsymbol{h} = (8, 13, 7, 9, 4, 7, 4, 4)$ and $\boldsymbol{x} = (10, 10, 8, 8, 6, 6, 4, 4)$. Here, $m = 8$ and $\overline{m} = 6$. Figure 21.2 depicts the corresponding state transition graph for the considered example.

The obtained graph is Eulerian since it is connected and every vertex has even in-degree and out-degree. Any Eulerian cycle in this graph corresponds to a feasible

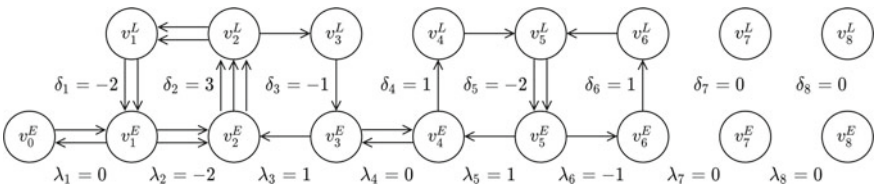

Fig. 21.2 State transition graph

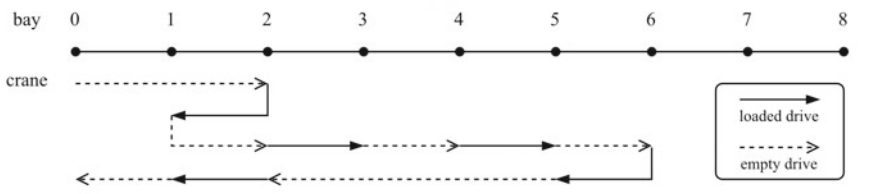

Fig. 21.3 An optimal crane scheduling plan

crane scheduling plan for the subproblem, which is optimal because the total cost of the arcs represents a lower bound on the total crane working time required. For example, Fig. 21.3 shows an optimal crane scheduling plan for the remarshaling task above. Hence, the optimal objective value for the subproblem can be computed in linear time by the following closed-form expression:

$$\begin{aligned} G(\boldsymbol{x}) &= t^C \sum_{i=1}^{\overline{m}} |\delta_i| + t^E \sum_{i=1}^{\overline{m}} \big(|\lambda_i| + 21_{\lambda_i=0}\big) + t^L \sum_{i=1}^{m} |\lambda_i| \\ &= t^C \sum_{i=1}^{\overline{m}} |\delta_i| + \sum_{i=1}^{\overline{m}} \big(\big(t^E + t^L\big)|\lambda_i| + 2t^E 1_{\lambda_i=0}\big) \\ &= t^C \sum_{i=1}^{\overline{m}} |\delta_i| + \sum_{i=1}^{\overline{m}} \max\big\{\big(t^E + t^L\big)|\lambda_i|, 2t^E\big\} \\ &= t^C \sum_{i=1}^{m} |\delta_i| = \sum_{i=1}^{m} \max\big\{\big(t^E + t^L\big)|\lambda_i|, 2t^E 1_{i\le\overline{m}}\big\}. \end{aligned} \tag{21.31}$$

The Formulation

To formulate the allocation-based model into a mixed-integer linear program, the following decision variables are defined:

- Integer variable $x_i \in \{0, \ldots, H\}$ is the final number of containers allocated to bay i, for $i = 1, \ldots, m$;
- Binary variable $w_{i,j} = 1$ if and only if the final number of containers allocated to bay i (i.e., x_i) is equal to j, for $i = 1, \ldots, m$ and $j = 0, \ldots, H$;
- Integer variable $y_i \in \{0, \ldots, H\}$ is (at least) the absolute difference between h_i and x_i (i.e., $|\delta_i|$), for $i = 1, \ldots, m$;
- Binary variable $z_i = 1$ if the crane visits bay i (i.e., $i \le \overline{m}$), for $i = 1, \ldots, m$;
- Integer variable $u_i \in \{0, \ldots, N\}$ is (at least) the absolute net number of containers transferred between bay $i - 1$ and bay i (i.e., $|\lambda_i|$), for $i = 1, \ldots, m$;

- Numeric variable $v_i \geq 0$ is (at least) the total travel time spent between bay $i-1$ and bay i (i.e., $\max\left\{\left(t^E + t^L\right)|\lambda_i|, 2t^E 1_{i \leq \overline{m}}\right\}$), for $i = 1, \ldots, m$.

  The formulation for the allocation-based model is presented as follows:

$$\min 2Nt^C + 2t^C \sum_{i=1}^{m} \sum_{j=0}^{H} R(j) w_{i,j} + \left(t^E + t^L\right) \sum_{i=1}^{m} i x_i \tag{21.32}$$

$$\text{s.t.} t^C \sum_{i=1}^{m} y_i + \sum_{i=1}^{m} v_i \leq T; \tag{21.33}$$

$$\sum_{i=1}^{m} x_i = N; \tag{21.34}$$

$$\sum_{j=0}^{H} w_{i,j} = 1, \forall i = 1, \ldots, m; \tag{21.35}$$

$$\sum_{j=0}^{H} j w_{i,j} = x_i, \forall i = 1, \ldots, m; \tag{21.36}$$

$$y_i \geq h_i - x_i, \forall i = 1, \ldots, m; \tag{21.37}$$

$$y_i \geq x_i - h_i, \forall i = 1, \ldots, m; \tag{21.38}$$

$$y_i \leq H z_i, \forall i = 1, \ldots, m; \tag{21.39}$$

$$z_i \geq z_{i+1}, \forall i = 1, \ldots, m-1; \tag{21.40}$$

$$u_i \geq \sum_{i'=1}^{i-1} (h_{i'} - x_{i'}), \forall i = 1, \ldots, m; \tag{21.41}$$

$$u_i \geq \sum_{i'=1}^{i-1} (x_{i'} - h_{i'}), \forall i = 1, \ldots, m; \tag{21.42}$$

$$v_i \geq \left(t^E + t^L\right) u_i, \forall i = 1, \ldots, m; \tag{21.43}$$

$$v_i \geq 2t^E z_i, \forall i = 1, \ldots, m; \tag{21.44}$$

$$u_i \in \{0, \ldots, N\}, \forall i = 1, \ldots, m; \tag{21.45}$$

$$v_i \geq 0, \forall i = 1, \ldots, m; \tag{21.46}$$

$$w_{i,j} \in \{0, 1\}, \forall i = 1, \ldots, m, \; j = 0, \ldots, H; \tag{21.47}$$

$$x_i \in \{0, \ldots, H\}, \forall i = 1, \ldots, m; \tag{21.48}$$

$$y_i \in \{0, \ldots, H\}, \forall i = 1, \ldots, m; \tag{21.49}$$

$$z_i \in \{0, 1\}, \forall i = 1, \ldots, m. \tag{21.50}$$

Objective (21.32) is the objective function as in the move-based model. Constraint (21.33) computes the total crane working time based on Eq. (21.31), and ensures it within the remarshaling time limit. Constraint (21.34) is the definitional constraint for a feasible allocation $\boldsymbol{x}$. Constraints (21.35) and (21.36) establish the relation between $(w_{i,0}, \ldots, w_{i,H})$ and x_i for all $i = 1, \ldots, m$. Constraints (21.37) and (21.38) together define the absolute difference between $\boldsymbol{h}$ and $\boldsymbol{x}$. Constraints (21.39) and (21.40) together determine the number of bays that will be visited. Constraints (21.41) and (21.42) together define the absolute net number of containers transferred between adjacent bays. Constraints (21.43) and (21.44) together define the total travel time spent between adjacent bays. Lastly, Constraints (21.45)–(21.50) stipulate the domains of the decision variables.

Numerical Experiments

In this section, we conduct numerical experiments to validate the efficiency of the proposed mixed-integer linear programming models, compared to the existing mixed-integer quadratic programming model in [7]. We use the quadratic rehandle estimation function in Eq. (21.2) in the existing model due to its own limitation, while using the piecewise rehandle estimation function in Eq. (21.3) in our models. A total of 18 problem instances with different scales are tested on, where instances #1–#6 are small-scale, instances #7–#12 are medium-scale, and instances #13–#18 are large-scale. A computational time limit of one hour is imposed for each model in solving every instance. All the models are coded in Java and solved by IBM ILOG CPLEX 12.9. The experiments are carried out on a personal computer with an Intel Core i5-6200U 2.8 GHz CPU and 4 GB of RAM.

Table 21.1 demonstrates the computational time of the three models. The meanings of the first seven columns are as follows: # is the instance number, m is the number of bays in the block, s is the number of stacks in each bay, H is the maximum number of containers that can be stored in each bay, N is the total number of containers in the block, T is the remarshaling time limit, and $F(\boldsymbol{x}^*)$ is the true optimal objective value

(i.e., minimum expected retrieval time) for each instance. The parameters of the crane are set to $t^C = 5$ and $t^E = t^L = 20$ to keep in line with [7]. The numbers under the name of each model represent the computational time in seconds for each model to optimally solve each instance, while a short dash means that the model cannot even find a feasible solution (except for the initial allocation) within one hour. Note that the move-based model does not finish its computation for instance #18 in one hour, but the best feasible solution obtained is found to be optimal after a manual check. The results show that the existing model can only solve the small-scale instances. The move-based model is able to solve all the small-, medium-, and large-scale instances within the time limit, significantly outperforming the existing model. Surprisingly, the allocation-based model is able to solve all instances to optimality in less than one second.

Granted the high efficiency of the allocation-based model, we repeatedly solve it with an iteratively increasing remarshaling time limit to investigate the impact of the remarshaling time limit T on the minimum expected retrieval time $F(\boldsymbol{x}^*)$. Figure 21.4 shows the results for small-scale instance #1, medium-scale instance #7, and large-scale instance #13. There is a similar trend that the minimum expected retrieval time decreases as the available remarshaling time increases until a threshold

Table 21.1 Computational time of the mixed-integer programming models

#	m	s	H	N	T	$F(\boldsymbol{x}^*)$	Existing model [7]	Move-based model	Allocation-based model
1	4	3	18	30	10^3	2480.6[a]	2.0	0.1	0.0
2	4	3	18	40	10^3	3677.2	4.2	0.1	0.0
3	4	3	18	30	10^3	2480.6[a]	0.7	0.1	0.0
4	4	3	18	40	10^3	3677.2	3.4	0.0	0.0
5	4	3	18	40	10^3	3677.2	2.6	0.1	0.0
6	4	3	18	40	10^3	3677.2	2.2	0.1	0.0
7	20	5	30	320	10^4	48,539.5	–	43.4	0.0
8	20	5	30	380	10^4	60,893.5	–	12.8	0.1
9	20	5	30	400	10^4	64,984.9	–	36.1	0.1
10	20	5	30	440	10^4	74,526.6	–	8.1	0.1
11	20	5	30	460	10^4	79,305.2	–	34.2	0.1
12	20	5	30	472	10^4	82,129.2	–	21.5	0.1
13	50	7	42	1200	10^5	304,061.9	–	1371.1	0.2
14	50	7	42	1300	10^5	337,990.7	–	3341.8	0.1
15	50	7	42	1400	10^5	380,250.4	–	2229.1	0.2
16	50	7	42	1500	10^5	420,333.2	–	1137.3	0.1
17	50	7	42	1550	10^5	439,540.1	–	2963.5	0.1
18	50	7	42	1594	10^5	457,270.1	–	3600.1	0.1

[a]The value is 2479.4 for the existing model due to the different rehandle estimation function being used

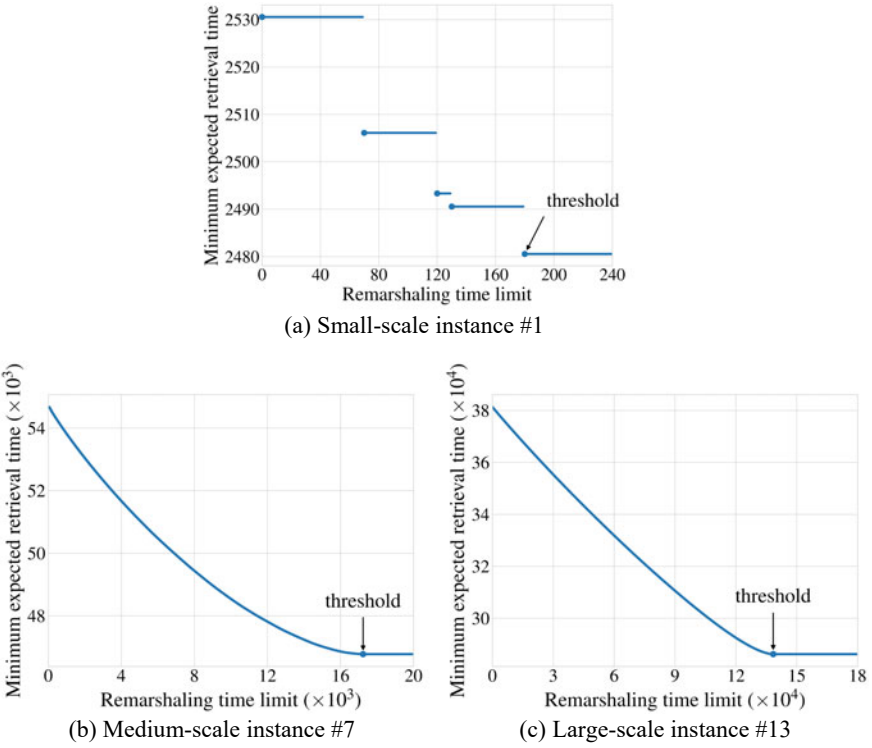

(a) Small-scale instance #1

(b) Medium-scale instance #7

(c) Large-scale instance #13

Fig. 21.4 Impact of the remarshaling time limit on the minimum expected retrieval time

is reached. After that, the minimum expected retrieval time remains the same even if more available remarshaling time is given. These results, from a practical application point of view, can provide a clear basis for terminal operators to make decisions on how much time should be allocated to the remarshaling process.

Conclusion

In this paper, we study the remarshaling problem for inbound containers in an automated container terminal. The randomness of the future retrieval order of inbound containers and the time limit of the remarshaling process are both considered. Two mixed-integer linear programming models are proposed to minimize the expected time in the future retrieval process. The move-based model aims at finding the best move sequence for the crane, and the allocation-based model is built upon the idea of problem decomposition. The latter model is shown to have a surprisingly excellent solution efficiency, which is able to solve all instances with practical sizes in less than one second, although the addressed problem has been proved to be NP-hard.

Such outstanding performance is due to the optimality property of the subproblem, which is shown to be solvable in linear time and can be computed by a closed-form expression.

Acknowledgements This research is supported by the National Natural Science Foundation of China (No. 72101160, No. 72171153, and No. 71771154), the Stable Support Plan Program of Shenzhen Natural Science Fund (No. 20200810160835003), and the Guangdong Basic and Applied Basic Research Foundation (No. 2020A1515011272).

References

1. Hu, H., Chen, X., Wang, T., & Zhang, Y. (2019). A three-stage decomposition method for the joint vehicle dispatching and storage allocation problem in automated container terminals. *Computers and Industrial Engineering, 129*, 90–101.
2. Kim, K. H., & Bae, J. W. (1998). Re-marshaling export containers in port container terminals. *Computers and Industrial Engineering, 35*(3), 655–658.
3. Kang, J., Oh, M.-S., Ahn, E. Y., Ryu, K. R., & Kim, K. H. (2006). Planning for intra-block remarshalling in a container terminal. In M. Ali & R. Dapoigny (Eds.), *Advances in applied artificial intelligence* (pp. 1211–1220). Springer.
4. Choe, R., Park, T., Oh, M.-S., Kang, J., & Ryu, K. R. (2011). Generating a rehandling-free intra-block remarshaling plan for an automated container yard. *Journal of Intelligent Manufacturing, 22*(2), 201–217.
5. Kim, K. H., Woo, Y. J., & Kim, J. G. (2021). Space reservation and remarshalling operations for outbound containers in marine terminals. *Maritime Economics and Logistics, 23*(1), 154–178.
6. Yu, M., & Qi, X. (2013). Storage space allocation models for inbound containers in an automatic container terminal. *European Journal of Operational Research, 226*(1), 32–45.
7. Qin, H., Su, X., Li, G., Jin, X., & Yu, M. (in press). A simulation based meta-heuristic approach for the inbound container housekeeping problem in the automated container terminals. *Maritime Policy and Management*.
8. Choe, R., Kim, T. S., Kim, T., & Ryu, K. R. (2015). Crane scheduling for opportunistic remarshaling of containers in an automated stacking yard. *Flexible Services and Manufacturing Journal, 27*(2), 331–349.
9. Covic, F. (2017). Re-marshalling in automated container yards with terminal appointment systems. *Flexible Services and Manufacturing Journal, 29*(3), 433–503.
10. Kim, K. H. (1997). Evaluation of the number of rehandles in container yards. *Computers and Industrial Engineering, 32*(4), 701–711.

Chapter 22
Products and Services Bundling Under Horizontal Market Competitions

Yimo Yu, Zhitong Liao, Qiaochu He, and Weiling Ke

Abstract This paper investigates the impact of products and services bundling from the perspective of providers and customers by comparing the profit and consumer surplus under two scenarios where providers apply "fully compete" and "no bundle" strategies respectively. The result shows that higher customer value and congestion cost can benefit the providers under the "bundle ban" policy, while the service price greatly influences the profit distribution between products and services providers. Contrarily, the low customer value and congestion cost can benefit customers to some extent. Our study gives managerial insight to policymakers on how products and services bundling can achieve better social welfare under certain circumstances and help providers to execute proper strategies in a competitive market.

Keywords Products and services bundling · Horizontal market · Market competition

Introduction

In many industries, it is a common phenomenon that a customer demands both products and services. For example, a customer who purchases a home appliance will require installation service in the meantime. In the beauty industry, a customer may ask for make-up or skincare service after buying cosmetics. Also in the healthcare context, a patient needs both drugs and diagnosis sometimes. Interestingly, companies

Y. Yu (✉) · Z. Liao · Q. He · W. Ke
Department of Information Systems and Management Engineering, Southern University of Science and Technology, Shenzhen 518000, Guangdong, China
e-mail: yuym2020@mail.sustech.edu.cn

Z. Liao
e-mail: 12131292@mail.sustech.edu.cn

Q. He
e-mail: heqc@sustech.edu.cn

W. Ke
e-mail: kewl@sustech.edu.cn

R. Qiu et al. (eds.), *City, Society, and Digital Transformation*, Lecture Notes in Operations Research, https://doi.org/10.1007/978-3-031-15644-1_22

in different industries apply different strategies in terms of products and services. An appliance company would like to bundle the installation service with the product while a beauty shop accepts customers bringing skincare product themselves and charge for the care service only. More than that, governments can have various attitudes toward the bundling of products and services. For instance, some countries allow health institutions to provide both products and services. Consider a patient's choice under a minor ailment: she can either visit a hospital and pay for prescriptions therein or visit a pharmacist directly who sometimes also provides diagnosis service. Whereas in other countries, the bundle of products and services is prohibited in the healthcare industry, such as the separation of prescribing and dispensing (SPD) policy in the United States.

Many studies have shown that the bundle of products is more profitable [1, 2]. However, the research on bundling of products and services is relatively rare. Wang et al. hold whether firms should offer bundles or products alone depends on the cost structure of the service and customers' sensitivity to service [3]. Moreover, it is not always beneficial to bundle products and services. In healthcare industries, the bundle of prescribing and dispensing may lead to the overuse of drugs and increase drug dispense [4]. On the other hand, the implementation of SPD can create monopoly situations where the price of products and services will be higher for customers.

Based on the above observations and the findings of the previous study, we forward the following research question: What influence will the bundling of products and services bring to providers and customers? What factors and how can they affect the welfare of providers and consumers? What strategy should providers apply in the different market environments? To investigate these questions, we provide a cost and benefit analysis for both bundling and separating strategies for providers, customers as well as social welfare in a competitive market. We consider a market consisting of two horizontally competing providers A and B, who are capable of providing both products and services. When facing competition from B, provider A can choose to apply either a "fully compete" strategy or a "no bundle" strategy. Under the first strategy, A competes in both products and services market and receives revenue therein. Under the second strategy, two providers specialize in either product or service delivery to avoid competition in both markets. We construct an analytical model to study providers' decisions under the two strategies and A's optimal bundling strategy. We also explore how the customer surplus and social welfare are affected by the bundling strategy.

The result shows that a low service price reduces A's profit under the bundle policy while a high service price benefits B under such policy. In a market with expensive labor costs, it is possible to achieve a win–win situation between A and B when customer valuation is high enough. On the other hand, customer surplus is higher under the "no bundle" strategy when the customer cares more about service quality than the product. Furthermore, we identify a situation where the government can prohibit the bundling strategy to redistribute social welfare and benefit customers by cutting the profit of providers.

The rest of this paper proceeds as follows. The second chapter reviews the current literature. Next chapter we introduce the model setup and conduct an equilibrium

analysis. The fourth chapter is a comparison and discussion of the model. The last chapter summarizes the results.

Literature Review

Our study is mainly relevant to the literature on bundling. Adams and Yellen find bundling can be more profitable than simple monopoly pricing by extracting consumer surplus [1]. Venkatesh and Mahajan investigate different strategies (i.e., pure components, pure bundling, and mixed bundling) in performance ticket selling and obtain the result that mixed bundling is most profitable [2]. In a duopoly market, three equilibriums can be achieved, namely differentiated duopoly, monopoly, and perfect competition, depending on whether the firms choose to bundle or not [5]. The bundling strategy can be applied to various industries and conditions. Kameshwaran et al. state a manufacturing firm that intends to bundle its service with the product [6]. In terms of virtual goods, bundling very large numbers of unrelated information goods can be surprisingly profitable [7]. However, it is not always wise to apply bundle strategy. Whether firms should offer bundles or products alone depends on the cost structure of the service and customers' sensitivity to service [3].

Our work departs from the previous literature in two ways. First, we discuss products and services bundling in a horizontal market, where no asymmetry information occurs and all suppliers have the same capability to provide products and services. Second, we take into account the congestion cost in service, which is crucial in our model and generally overlooked in previous bundling literature.

Model Setup and Equilibrium Analysis

Consider a competitive market consisting of two providers A and B who can both sell products and provide services. We refer to a situation when the market is under a "bundle ban" policy if products and services bundling is prohibited. We use Scenario 1 to represent the case where bundling is not prohibited and the providers execute the "fully compete" strategy. In Scenario 2, two providers specialize in products and services respectively under the "bundle ban" policy, i.e. A sells products and B provides services.

We use ϕ to capture the probability of a customer in the requirement of the service. $u(\phi) = \phi(S + c\lambda)$ captures the dis-utility of receiving the service, where S is the service price, c is the congestion coefficient and λ is the equilibrium population who require the service. The market size is normalized to 1. A consumer is located at $x \in [0, 1]$, while provider A is located at $x_A = 0$ and B is located at $x_B = 1$. V, P, β captures the value, retail price, and unit transportation cost of the product respectively. All variables are exogenous except P. A consumer purchases the product if and only if her/his utility is non-negative, i.e., $U(x) \geq 0$.

Scenario 1: A Bundling and B Bundling

In this scenario, the bundle-ban policy does not exist and two providers can compete in both products and services. A consumer is flexible in buying products and receiving services from either A or B. Here we assume the capacity of providers A and B can fully cover the market demand. We use subscript i to denote company $i, i \in \{A, B\}$. A consumer will choose A's service if $u_A(\phi) \leq u_B(\phi)$, and B's otherwise.

The sequence of events is as follows:

1. A and B decide the price of product P_A and P_B simultaneously.
2. Profits are collected.

A consumer's utility of purchasing the product from A or B is

$$U_A(x) = V - P_A - \beta x - u_i(\phi) \tag{22.1}$$

$$U_B(x) = V - P_B - \beta(1 - x) - u_i(\phi) \tag{22.2}$$

Let D_i be the number of customers who purchase the product from provider i. The production cost, selling cost, and service cost is normalized to zero. Then the profit of A and B is

$$\Pi_A^1 = P_A D_A + S_A \lambda_A \tag{22.3}$$

$$\Pi_B^1 = P_B D_B + S_B \lambda_B \tag{22.4}$$

The consumer surplus is

$$CS^1 = \int_{\substack{U_A(x) \geq U_B(x) \\ U_A(x) \geq 0}} U_A(x)dx + \int_{\substack{U_B(x) \geq U_A(x) \\ U_B(x) \geq 0}} U_B(x)dx \tag{22.5}$$

The results of the model are shown in the proposition below.

Proposition 1 There exists a unique equilibrium for the model in Scenario 1 where:

$$P_A = P_B = \beta, D_A = D_B = \frac{1}{2}$$
$$\Pi_A = \Pi_B = \frac{\beta + \phi S}{2}, CS^1 = V - \frac{5}{4}\beta - \phi S - \frac{1}{2}c\phi^2$$

The equilibrium shows that two providers share products and services market equally. The equilibrium price is irrelevant to customer value because of competition. Also, note that an increase in service price and transportation cost will lead to an increase in the provider's profit but a decrease in consumer surplus.

Scenario 2: A Product and B Service

Suppose a bundle-ban policy is implemented, which means a company can choose to provide either product or service but not both. Let's assume A sells the product only while B provides the service and a single provider cannot cover the whole market demand.

The sequence of events is as follows:

1. Provider A decides the price of the final product P.
2. Profits are collected.

A consumer's utility of consuming the product is

$$U(x) = V - P - \beta x - u(\phi) \tag{22.6}$$

The profit of providers A and B is

$$\Pi_A^2 = PD \tag{22.7}$$

$$\Pi_B^2 = S\lambda \tag{22.8}$$

The consumer surplus is

$$CS^2 = \int_{U(x)\geq 0} \mathrm{U}(x)dx \tag{22.9}$$

The results of the model are shown in the proposition below.

Proposition 2 There exist an optimal result for the model in Scenario 1 where:

$$P = \frac{V - \phi S}{2}, D = \frac{V - \phi S}{2\left(\beta + c\phi^2\right)}$$
$$\Pi_A^2 = \frac{(V - \phi S)^2}{4\left(\beta + c\phi^2\right)}, \Pi_B^2 = \frac{\phi S(V - \phi S)}{2\left(\beta + c\phi^2\right)}, CS^2 = \frac{\beta(V - \phi S)^2}{8\left(\beta + c\phi^2\right)^2}$$

Proposition 2 shows the optimal price for provider A is determined by customer value and service price. A higher customer value and lower service price can increase provider A's profit and customer surplus but may be detrimental to B's benefit.

Comparison and Discussion

In this section, we compare the results of two scenarios from the perspective of A's profit, B's profit, aggregate profit, and consumer surplus.

Lemma 1 The comparison result can be divided into six cases in terms of profit (Table 22.1):

$$\begin{aligned}
&(\text{i})\,\Pi_A^1\langle\Pi_A^2,\Pi_B^1\rangle\Pi_B^2,\Pi^1<\Pi^2 if and only if V_5<V<\min\{V_2,V_4\};\\
&(\text{ii})\,\Pi_A^1<\Pi_A^2,\Pi_B^1<\Pi_B^2,\Pi^1<\Pi^2 if and only if \max\{V_3,V_4\}<V<V_2;\\
&(\text{iii})\,\Pi_A^1>\Pi_A^2,\Pi_B^1<\Pi_B^2,\Pi^1<\Pi^2 if and only if V_5<V<\min\{V_2,V_3\};\\
&(\text{iv})\,\Pi_A^1\langle\Pi_A^2,\Pi_B^1\rangle\Pi_B^2,\Pi^1>\Pi^2 if and only if \max\{V_1,V_3\}<V<V_5;\\
&(\text{v})\,\Pi_A^1>\Pi_A^2,\Pi_B^1>\Pi_B^2,\Pi^1>\Pi^2 if and only if V_1<V<\min\{V_3,V_4\};\\
&(\text{vi})\,\Pi_A^1>\Pi_A^2,\Pi_B^1\langle\Pi_B^2,\Pi^1\rangle\Pi^2 if and only if \max\{V_1,V_4\}<V<V_5.
\end{aligned}$$

Lemma 1 shows that for high V(i.e., $V > V_5$), the aggregate profit of A and B is higher under the bundle prohibited scenario. Notice in Scenario 2, the optimal retail price and demand of the product are both positively correlated with customer demand and negatively correlated with service price. A larger customer value implies more purchase intention of products, and providers can take the opportunity to realize a higher profit by sufficient customer demand and high product price. Meanwhile, the service price will influence the allocation of profit between A and B. Specifically, provider A which sells the product benefits from the bundle ban policy only when S is not too large, while B benefits from the policy only when S is large enough. When the service price is small, provider B's profit is decreased while A's is increased. This is intuitive as a lower service price indicates a smaller profit margin for the service provider. Hence B will gain less profit from providing the service in Scenario 2. However, the market demand and product price will increase as the service price goes down. As a result, the profit of A will increase. When S is large, A has to reduce the product price in order to guarantee the product is still attractive enough for customers to purchase. Hence, A will obtain less profit from selling the product in Scenario 2 than providing both products and services in Scenario 1, while B can earn a higher proportion of profit on the contrary. Therefore, the prohibition of bundling will harm the profit of either A or B when the service price is too high or too low. A win–win result is generated only when customer value is high enough

Table 22.1 Thresholds in section "Comparison and Discussion"

Symbol	Terms	Descriptions
V_1	$\phi S+\frac{3}{2}\beta+\frac{1}{2}c\phi^2$	$D\le 1$
V_2	$\phi S+2\beta+2c\phi^2$	$D_A+D_B=1$
V_3	$\phi S+\sqrt{2\beta^2+2\beta\phi S+2\beta c\phi^2+2c\phi^3 S}$	$\Pi_A^1=\Pi_A^2$
V_4	$\phi S+\beta+c\phi^2+\frac{\beta^2}{S\phi}+\frac{\beta c\phi}{S}$	$\Pi_B^1=\Pi_B^2$
V_5	$\sqrt{4\beta^2+4\beta\phi S+\phi^2S^2+4\beta c\phi^2+4c\phi^3 S}$	$\Pi^1=\Pi^2$
V_6	$\phi S+4\beta+8c\phi^2+\frac{4c^2\phi^4-\sqrt{6\beta^4+40\beta^3c\phi^2+78\beta^2c^2\phi^4+60\beta c^3\phi^6+16c^4\phi^8}}{\beta}$	$CS^1=CS^2$

and service price is intermediate, implying a market with sufficient demand and reasonable service price.

Things are quite different for low V(i.e., $V < V_5$). Although the tendency for providers A and B to benefit from the bundle ban policy stays the same, i.e., A benefits when S is small while B benefits when S is large, A requires a smaller S while B requires a larger S to benefit from the bundle ban policy when V is low. The main reason for this intuition is the aggregate profit of A and B is smaller compared with that in the bundling case. As the only decision-maker in Scenario 2, A maximizes the profit itself ignoring the profit of the service market. Hence, he has no incentive to reduce the product price even if this may enlarge the market demand and help B to gain a higher profit. As a result, the aggregate profit is constrained by A's "selfish" strategy. Therefore, the bundle ban policy can hurt both providers in a market with low demand and intermediate service prices (Fig. 22.1).

From the perspective of consumer surplus, we have the following lemma.

Lemma 2 $CS^1 < CS^2$ *if and only if* $c\phi^2 < \frac{\beta}{5+4\sqrt{2}}$ *and* $V_1 < V < V_6$.

Lemma 2 indicates that in most cases, customers take more benefit when bundling is allowed and competition exists between two providers. The customer surplus is higher in Scenario 2 only when customer value and service congestion cost are both small. The reason behind this is that as the customer value goes up, the product price in Scenario 1 remains the same, giving more benefit to customers. However, the product price in Scenario 2 will increase as the customer value increase because of the monopoly. As a result, provider A takes part of the welfare and the customer surplus has less increment compared with that in Scenario 1. In terms of the congestion, a small coefficient suggests relatively more cost is wasted on transportation, which cut down the customer surplus in Scenario 1.

Combining the comparison above, we can identify that the bundle ban policy exerts a different impact on providers' profit and consumer surplus. When customer value is high, the bundle ban policy tends to benefit the provider and when customer value is low, the bundle ban policy can benefit the customer in some cases. Specifically, we find the following proposition.

Proposition 3 $\Pi_A^1 > \Pi_A^2, \Pi_B^1 > \Pi_B^2, CS^1 < CS^2$ *if and only if* $c\phi^2 < \frac{\beta}{5+4\sqrt{2}}$ *and* $V_1 < V < \min\{V_3, V_4, V_6\}$;

Proposition 3 shows that when customer value and congestion cost are both small, the aggregate profit in Scenario 2 is always smaller while the customer can have more surplus. The case is represented as the shadowed area in Fig. 22.2b. This indicates when customers care more about the service quality, the government can apply the "bundle ban" policy to redistribute social welfare by cutting down the profit of providers and increasing the consumer surplus.

In our basic model, we assume a congestion cost will occur when the company processes the service request, which is closer to reality. Next, we will analyze the equilibrium result when c = 0, corresponding to the condition when the service capacity is much larger than the demand or the congestion cost of waiting for the service is zero.

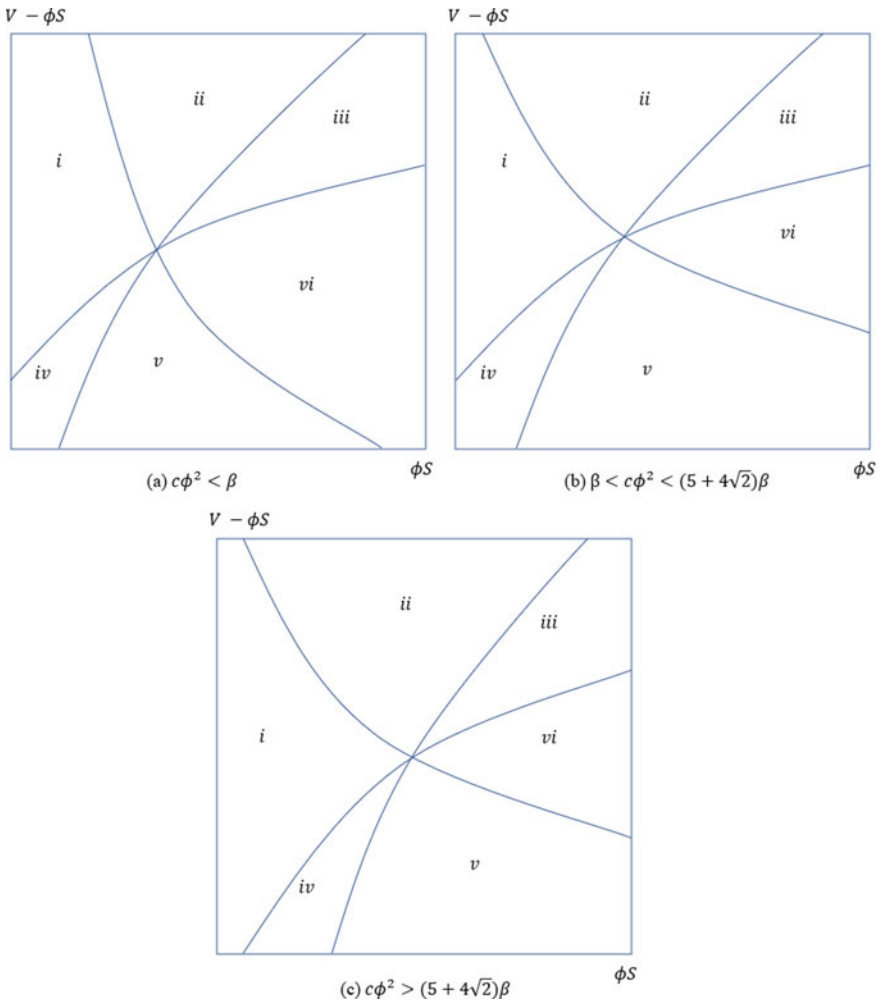

Fig. 22.1 Comparison of provider profits under different conditions

Proposition 4 The aggregate profit is always higher under the bundling strategy when there is no congestion cost.

This result may be counter-intuitive. The profit in Scenario 2 seems to increase at first sight while that in Scenario 1 remains the same when the congestion cost decrease to zero. However, remember the customer value V is also restricted to c, i.e., the V will become smaller when c decrease. As a result, the aggregate profit in Scenario 2 is positively correlated to c. A possible explanation can be that a company tends to lower the price when facing encroachment in a competitive market. This will attract more customers to purchase the product and may lead to a higher profit. However, the demand for the service will also increase and consequently generate

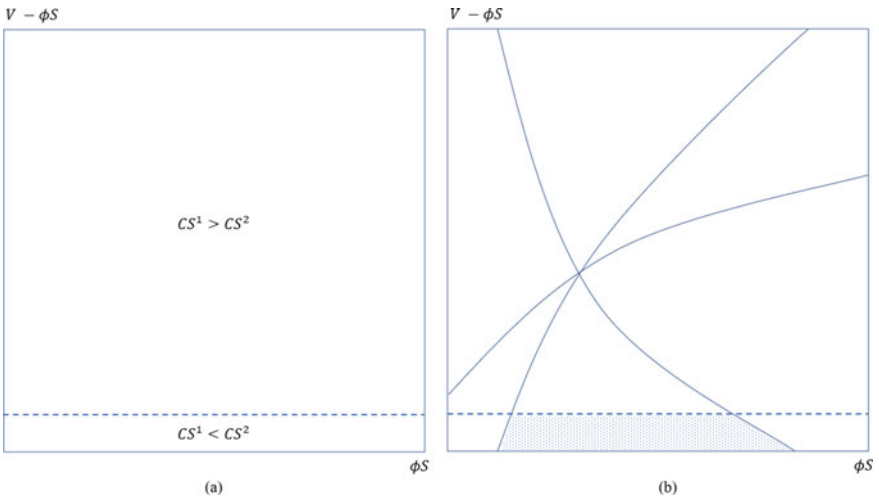

Fig. 22.2 Comparison of consumer surplus

a higher congestion cost. The bundle-ban policy can help providers to gain higher profit because of less congestion loss. Whereas when congestion cost is equal to zero, these cases disappear. The analysis in this section also indicates that the assumption of congestion cost is fundamental in our model and cannot be ignored (Fig. 22.3).

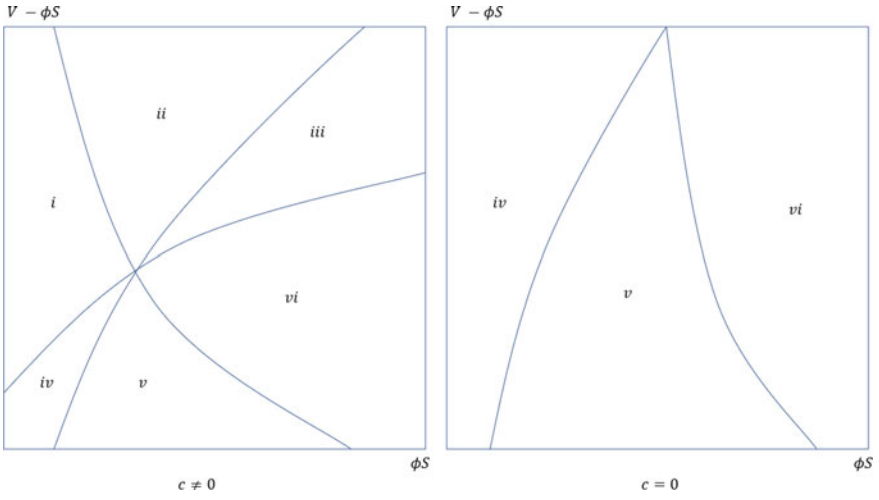

Fig. 22.3 Comparison under different congestion coefficients

Conclusion

Customers' demand for both products and services is a regular occurrence in many cases. The purpose of this research is to investigate the impact of products and services bundling in a competitive horizontal market. We compare the profit and consumer surplus under two scenarios where providers use "completely compete" and "no bundle" strategies respectively. Our findings reveal that under a bundle ban policy, increased customer value and congestion costs benefit providers, whereas service pricing has a significant impact on profit allocation between products and services providers. The low customer value and congestion cost, on the other hand, may benefit customers to some extent.

The above findings provide guidelines for providers to be more competitive by applying proper strategy with regard to different market policies and customer preferences among products and services. We also generate managerial insights which help policy-makers to decide whether products and services bundling should be allowed in such a competitive environment. In particular, products and services bundling achieves better social welfare generally while the separation may redistribute the social welfare under certain conditions.

Our research also has certain limitations. For instance, we investigate the basic horizontal competition model, and more complicated cases, such as corporations between providers, are not considered. In terms of parameters, we assume only the product price as endogenous while the relaxation of the assumption is not discussed. Further research might focus on these topics to analyze the bundling of products and services.

References

1. Adams, W. J., & Yellen, J. L. (1976). Commodity bundling and the burden of monopoly. *The Quarterly Journal of Economics, 90*(3), 475–498.
2. Venkatesh, R., & Mahajan, V. (1993). A probabilistic approach to pricing a bundle of products or services. *Journal of Marketing Research, 30*(4), 494.
3. Wang, Y., Sun, L. Y., Qu, R., Li, G. (2015). Price and service competition with maintenance service bundling. *Journal of Systems Science and Systems Engineering, 24*(2), 168–189.
4. Kwon, S. (2003). Pharmaceutical reform and physician strikes in Korea: Separation of drug prescribing and dispensing. *Social Science & Medicine, 57*(3), 529–538.
5. Araz, K., Guillaume, R., & Uday, S. K. (2019). Competitive Bundling in a Bertrand Duopoly (Unpublished).
6. Kameshwaran, S., Viswanadham, N., & Desai, V. (2007). On bundling and pricing of the service with the product. In *2007 IEEE International Conference on Automation Science and Engineering* (Vol. 1(3), pp. 102–107).
7. Bakos, Y., & Brynjolfsson, E. (1999). Bundling information goods: Pricing, profits, and efficiency. *Management Science, 45*(12), 1613–1630.

Chapter 23
Robust Facility Location Selection Under Facility Failure in Close-Loop Supply Chain

Jianzhi Leng, Lun Ran, and Zihao Jiao

Abstract Public health emergencies, along with worldwide disasters, have been weakening the supply chain's upstream and downstream connections, further threatening the effective operation of facilities. In the closed-loop supply chain of the new energy industry, the failure of intermediate facilities will not only triggers a jump in holding costs, but also affect the supply of raw materials for the following productions. To this end, we develop a two-stage distributed robust optimization model to optimize the location of intermediate facilities in the closed-loop supply chain, and provides an optimal solution for the decision-making of raw material recycling and remanufacturing and the investment ratio of recycling process. We also conduct a case study in Shandong Province, China, and collects relevant data about local impacts of Covid-19 to conduct facility failure simulations. Numerical results show that the model has a more sensitive response to the combination setting of different parameters, and gives the best decision-making scheme considering the worst risk level.

Keywords Facility failure · Close-loop supply chain · Robust optimization · Public emergencies

Introduction

The closed-loop supply chain (CLSC) is a particular case in the supply chain system. After the product has completed its service life, the product user becomes the original

J. Leng · L. Ran (✉)
School of Management and Economics, Beijing Institute of Technology, Beijing 100081, China
e-mail: ranlun@bit.edu.cn

J. Leng
e-mail: lengjianzhi@bit.edu.cn

Z. Jiao
School of International Economics and Management, Beijing Technology and Business University, Beijing 100089, China
e-mail: jiaozihao@btbu.edu.cn

R. Qiu et al. (eds.), *City, Society, and Digital Transformation*, Lecture Notes in Operations Research, https://doi.org/10.1007/978-3-031-15644-1_23

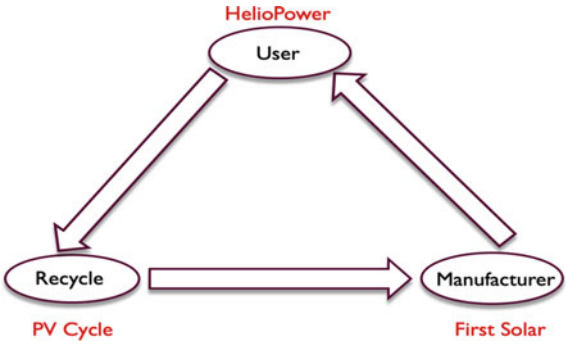

Fig. 23.1 CLSC Structure Schematic in the photovoltaic industry

material supplier of the upstream producer. Through reverse logistics, waste products are recycled and processed to extract valuable raw materials for manufacturers to carry out the next stage of production. Take the waste photovoltaic panels in the photovoltaic industry as an example (Fig. 23.1). The First Solar is a photovoltaic panel (PV panel) manufacturer and its product is offered to *HelioPower* to use until the end of its life. Then PV Cycle will collect and dismantle the waste PV panels to obtain the original materials. Finally, PV Cycle will sell the materials back to First Solar for the next manufacturing stage. These companies construct a mature industry cycle which is a typical CLSC structure. The waste PV panels have a recyclability rate of up to 95%, containing various rare metals such as cadmium and nickel, silicon, and harmful metals such as mercury. Effective recycling and remanufacturing of waste photovoltaic panels can significantly reduce manufacturers' operating costs and is conducive to environmental protection. Another clear example is the lithium battery used in new energy vehicles. The performance of the lithium battery will decline significantly after repeated use. Continuous use will cause energy loss and a negative user experience. Effective recycling and remanufacturing Will refresh the battery. Effective recycling reduces the production costs of new energy vehicle manufacturers and battery suppliers and facilitates the efficient use of energy.

Since the coronavirus outbreak, it has had a significant impact on the supply chain of the global production industry. As of March 22, 14 multinational vehicles More than 100 factories have been shut down or planned to be shut down by enterprise groups. Frequent outbreaks of the epidemic endanger the lives and health of employees in the production industry and cause countries and regions to control the risk of the epidemic, resulting in various degrees of interruption and failure of supply chain facilities. Razat Gaurav, CEO of *LLamasoft*, which focuses on supply chain analysis and optimized design solutions, believes that based on the analysis of data from different industries, the new crown pneumonia epidemic has impacted various industries, reflecting three significant risks in the supply chain. The first point depends on the number of production facilities in the epidemic area, including the situation of supply and demand; the second point is whether the relevant enterprises have some other options, whether there are other suppliers or alternative parts; the

third point is The issue is whether there are enough buffered production material reserves in the company's inventory.

In this paper, by establishing a robust optimization model, considering the uncertainty factors that cause the random failure of manufacturers' facilities due to the epidemic's impact, the paper decides the optimal facility location and process investment ratio of recycling units in the closed-loop supply chain. The proportion of recycled material is determined for different reasons by the facility. The optimal location of the facility and the appropriate recycling ratio can effectively reduce the operating cost of the producer. This is because the model assumes that the price of recycled raw materials is always lower than the price of new materials purchased in the market, but. Still, excessive recycling accumulation will face the failure of facilities and the risk of higher inventory co in To effectively deal with the epidemic's impact on the closed-loop supply chain.

The innovations of this paper are:

(a) In the context of the epidemic, a innovative plan for optimal facility location in the closed-loop supply chain is proposed, which can effectively mitigate the negative impacts caused by the risk of facility failure and reduce operating costs;
(b) Given the unique attributes of the closed-loop supply chain, on the premise of ensuring normal production, make decisions on the proportion of recycling and repurchasing new materials to reduce production costs as much as possible and contribute to environmental protection;
(c) According to different types of recyclable products (for example, photovoltaic panels have different types of cadmium dysprosium, monocrystalline silicon, etc.), other processes and different raw material costs, decide the proportion of process investment in different facilities, and improve the efficiency of recycling as much as possible;

Reference

Our work is to consider the impact of facility failure on the closed-loop supply chain under the epidemic's impact. Before this, many scholars have conducted in-depth research on the problem of facility failure.

In the problem of facility failure, Atamtürk and Zhang [1] established a two-stage robust optimization method to solve the design problem of facility network flows with uncertain demands. The recourse action of this method allows for less conservative than single-stage s solution. Chen et al. [2] studied the joint facility inventory problem, optimized the facility location and inventory management scheme when considering the terminal risk of facility fabrics, and reduced the high cost of service failure. Cui et al. [3] proposed a compact Mixed Integer Programming (MIP) model to study the no-capacity fixed charging location siting problem, which aims to minimize operating and transportation costs under normal and fault conditions. Cheng et al. [4] study a fixed-fee siting problem that considers the risk of interference. A two-stage robust optimization approach is used to make facility location decisions and recourse decisions to reassign customers after uncertainty information about facility availability is determined. Berman et al. [5] studied a type of facility location model, considering that the facility is not completely reliable and

the faults are correlated. The research goal is to determine how the probability of failure and correlation affect the selection of the best location, and verify it through numerical experiments. Lu et al. [6] proposed a model that allows for facility disruptions to be correlated and jointly distributed, using a distributed robust optimization method to minimize expected costs under a worst-case distribution of terminal probabilities.

In the closed-loop supply chain problem, the closed-loop supply chain problem can be traced back to the related research of Fleischmann et al. [7], which has attracted extensive attention. Dai and Zheng [8] used fuzzy programming and chance-constrained programming methods to solve uncertainty, established a multi-period, multi-product closed-loop supply chain network design model, and combined Monte Carlo simulation and genetic algorithm to solve the problem. Govindan and Soleimani [9] made a comprehensive summary of the related research content of closed-loop supply chain. In recent years, many scholars have carried out research on closed-loop supply chain network design. Cui et al. [10] introduced a genetic artificial bee algorithm for the closed-loop supply chain network design composed of multiple manufacturers, remanufacturers and recycling centers. The problem is solved by a swarm algorithm, and the model covers the uncertainty of demand and the number of returns. Shahbazbegian et al. [11] proposed a dual-objective model to design and optimize a thin-film photovoltaic power plant supply chain network with integrated reverse logistics to determine the appropriate supply chain disposal center location and employ a fuzzy robust programming approach to deal with uncertain parameters. Li et al. [12] established a robust optimized recycling network model for the uncertainty of the price of recyclable raw materials in thin-film photovoltaic power generation panels, so as to obtain the maximum recycling benefits under uncertain factors.

Problem Description and Formulation

The model established in this paper is a two-stage robust optimization model. In the first stage, a decision is made on the potential facility construction location and the investment ratio of the recycling process for different facilities, whether to build a facility there and the total number of facilities to be constructed, and a certain investment ratio is allocated to an individual facility to establish its recycling process assembly line. The second stage of the model is to decide on the quantity of recycling and the distribution schedule plan. The concern is which recyclables from which place are sent to which facility for processing. The primary considerations are operating costs, including inventory costs (Ref. EOQ model), the purchase cost of raw materials to maintain average production by giving up recycling, and the road transportation cost incurred in recycling.

Parameter

The notations applied in our model are listed in Table 23.1.

Table 23.1 List of notations

Indices and sets	
$I = \{1, 2, \ldots, i\}$	Set of manufacturers containing waste products
$J = \{1, 2, \ldots, j\}$	Set of ready-to-use recycling center
$M = \{1, 2, \ldots, m\}$	Set of different types of waste products
$P = \{1, 2, \ldots, p\}$	Set of different types of recycling and processing technologies
Parameters	
f_j	Fixed cost of building the facility at j
s_{jp}	The cost of investing in technology p at facility j
h_j	The unit holding cost of facility j
α	Unit road transport cost
d_{ij}	The distance between manufacturer i and recycling center j
ϕ_m	The purchase cost of raw materials for new products of m category
b_{mp}	It is 0 or 1, indicating whether the m-type products can be processed by the p technology
Q_{im}	The quantity of recyclable products of type m from manufacturer i
Fc_j	Maximum capacity limit of a single facility
Decision variables	
o_j	Whether to open the facility j
λ_{jp}	The proportion of investment in technology p in facility j
$x_{imjp} \in N^*$	Quantity of recyclable products of type m received (recycled material) from i to technology p for processing at j
$u_{imjp} \in N^*$	Quantity of recyclable products of type m rejected (purchased new materials) from i to j for processing at technology p
c_{mjp}	Capacity at technology p at facility j for waste product of type m
Stochastic variables	
ξ_{mjp}	The random failure rate of the facility with the mean $= \mu$, variance $= \sigma^2$ and second-order moment matrix Σ_{mjp}

Two Stage Robust Optimization Model

Model Formulation

$$\min_{o,\lambda,x,u} \sum_{J} \sum_{p} \left[f_j o_j + s_{jp} \lambda_{jp} \right] + supE\left(g\left(\xi_{jp}\right)\right) \tag{23.1}$$

$$\lambda_{jp} \leq o_j, \ \forall j, p \tag{23.2}$$

$$\sum_{J} \sum_{p} \lambda_{jp} = 1 \tag{23.3}$$

$$c_{mjp} = \sum_{i} \sum_{m} Q_{im} * \lambda_{jp}, \ \forall m, j, p \tag{23.4}$$

$$c_{mjp} \leq Fc_j, \ \forall m, j, p \tag{23.5}$$

$$supE\left(g\left(\xi_{jp}\right)\right) = \sum_{i,m,j,p} \left\{ \frac{h_j(x_{imjp})^2}{c_{mjp}\xi_{mjp}} + \phi_m u_{imjp} \right\} + \sum_{i,m,j,p} \alpha \cdot d_{ij} x_{imjp} \tag{23.6}$$

$$\sum_j \sum_p x_{imjp} + u_{imjp} = Q_{im}, \forall i, m \tag{23.7}$$

$$\sum_i \sum_m x_{imjp} \leq \sum_m c_{mjp} \cdot \boldsymbol{\xi_{mjp}}, \ \forall j, p \tag{23.8}$$

$$x_{imjp} \leq M \cdot b_{mp}, \ \forall i, m, j, p \tag{23.9}$$

$$x_{imjp}, u_{imjp} \in N^*, \lambda_{jp} \in [0, 1]; o_j = \{0, 1\} \tag{23.10}$$

(1) It is the objective function, aiming to minimize the cost, including whether to open the factory, the investment ratio of the process and the operating cost; (2) It is the investment constraint, which requires that the facility must be built before the investment ratio can be allocated; (3) For all facilities and technics, the sum of the investment ratio is required to be 100%; (4) the facility processing capacity is equal to the investment ratio multiplied by the total amount that can be processed under the total investment; (5) the facility processing capacity is required not to exceed the maximum capacity limit of a single facility; (6) The sum of the accepted quantity of recyclables and the quantity rejected (repurchase of raw materials) is the quantity provided by each factory; (7) For each recycling facility, the accepted quantity does not exceed the facility's processing capacity; (8) The corresponding accepted product must meet the process constraints; (9) Variable description.

Robust Model Transformation

For constraint (23.8), create a chance constraint:

$$\begin{aligned} &\inf_{\mathbb{P}\in\mathcal{P}} \mathbb{P}\left\{ \sum_{\mathrm{i}} \sum_{\mathrm{m}} \mathrm{x_{imjp}} \leq \sum_{\mathrm{m}} \mathrm{c_{mjp}} \cdot \boldsymbol{\xi_{mjp}} \right\} \geq \epsilon, \ \forall \mathrm{j}, \mathrm{p} \\ &x_{imjp} \in \mathcal{X} \end{aligned} \tag{23.11}$$

Among them, $\mathcal{X}$ is the feasible set, which is expressed as:

$$X = \left\{ x \in R^{i*m*j*P} : \inf_{\mathbb{P}\in\mathcal{P}} P\left\{ \sum_i \sum_m x_{imjp} \leq \sum_m c_{mjp} \cdot \boldsymbol{\xi_{mjp}} \right\} \geq \epsilon, \ \forall i, m, j, p \right\} \tag{23.12}$$

Considering the chance constraint of random variable ξ_{mjp} in the worst distribution case is (23.13):

$$\min P\left(\sum_i \sum_m x_{imjp} \le \sum_m c_{mjp} \cdot \boldsymbol{\xi_{mjp}}\right) \ge \epsilon,\ \forall j,\ p \tag{23.13}$$

Equivalent to:

$$\max P\left(\sum_i \sum_m x_{imjp} \ge \sum_m c_{mjp} \cdot \boldsymbol{\xi_{mjp}}\right) \le 1 - \epsilon,\ \forall j,\ p \tag{23.14}$$

For any jp, define an indicative function

$$I\left(\xi_{mjp}\right) = \begin{cases} 1, & \text{if } \sum_i \sum_m x_{imjp} \ge \sum_m c_{mjp} \cdot \boldsymbol{\xi_{mjp}},\ \forall j,\ p \\ 0, & \text{otherwise} \end{cases} \tag{23.15}$$

Then $\max \mathbb{P}\left(\sum_{\mathrm{i}} \sum_{\mathrm{m}} \mathrm{x}_{\mathrm{imjp}} \le \mathrm{c}_{\mathrm{mjp}} \cdot \xi_{\mathrm{mjp}}\right)$ equivalent to:

$$\begin{aligned} &\max \int \mathbb{I}\left(\xi_{\mathrm{mjp}}\right) \mathrm{d}\boldsymbol{P} \\ &\text{s.t.} \\ &\int \begin{bmatrix} \boldsymbol{\xi_{mjp}} \\ 1 \end{bmatrix} \begin{bmatrix} \boldsymbol{\xi_{mjp}} \\ 1 \end{bmatrix}^T d\boldsymbol{P} = \Sigma_{jp} \end{aligned} \tag{23.16}$$

$$\begin{aligned} L\left(p, M_{jp}\right) &= \int \mathbb{I}\left(\boldsymbol{mjp}\right) \mathrm{d}\boldsymbol{P} + M_{jp}, \Sigma_{jp} - \int \begin{bmatrix} \boldsymbol{\xi_{mjp}} \\ 1 \end{bmatrix} \begin{bmatrix} \boldsymbol{\xi_{mjp}} \\ 1 \end{bmatrix}^T d\boldsymbol{P} \\ &= \left\langle M_{jp}, \Sigma_{jp} \right\rangle + \int \mathbb{I}\left(\xi_{\mathrm{mjp}}\right) - \left(\begin{bmatrix} \boldsymbol{\xi_{mjp}} \\ 1 \end{bmatrix}^{\mathrm{T}} \mathrm{M_{jp}} \begin{bmatrix} \boldsymbol{\xi_{mjp}} \\ 1 \end{bmatrix} \right) \mathrm{d}\boldsymbol{P} \end{aligned} \tag{23.17}$$

Make $f\left(\xi_{mjp}\right) = \begin{bmatrix} \boldsymbol{\xi_{mjp}} \\ 1 \end{bmatrix}^T M_{jp} \begin{bmatrix} \boldsymbol{\xi_{mjp}} \\ 1 \end{bmatrix} d\boldsymbol{P}$, then (23.14) equivalent to:

$$g(x) = \min_{M_{jp} = M_{jp}^T} \max_{P \in \mathcal{P}} M_{jp}, \Sigma_{jp} + \int I\left(\xi_{mjp}\right) - f\left(\xi_{mjp}\right) dP, \tag{23.18}$$

$$\begin{aligned} &\max_{P \in \mathcal{P}} \left\langle M_{jp}, \Sigma_{jp} \right\rangle + \int \mathbb{I}\left(\xi_{\mathrm{mjp}}\right) - \mathrm{f}\left(\xi_{\mathrm{mjp}}\right) \mathrm{d}\boldsymbol{P} \\ &= \begin{cases} \left\langle M_{jp}, \Sigma_{jp} \right\rangle, & \text{if } \mathbb{I}\left(\xi_{\mathrm{mjp}}\right) - \mathrm{f}\left(\xi_{\mathrm{mjp}}\right) \le 0 \\ +\infty, & \text{otherwise} \end{cases} \end{aligned} \tag{23.19}$$

Then $g(x)$ is finite if and only if $\mathbb{I}(\xi_{\text{mjp}}) - \text{f}(\xi_{\text{mjp}}) \leq 0$,which can be divided into two cases:

- $f(\xi_{mjp}) \geq 0$, for all $\xi_{mjp} \in R$, equivalent to $M_{jp} \geq 0$;
- $f(\xi_{mjp}) \geq 1$, for all $\xi_{mjp} \in R$, have $\sum_i \sum_m x_{imjp} \geq \sum_m c_{mjp} \cdot \boldsymbol{\xi_{mjp}}$, The above formula holds if and only if there exists λ_{jp},such that: $f(\xi_{mjp}) \geq 1 - 2\lambda_{jp}(\sum_m c_{mjp} \cdot \xi_{mjp} - \sum_i \sum_m x_{imjp})$, which is $M_{jp} + \begin{bmatrix} 0 & \lambda_{jp} \\ \lambda_{jp} & -2\lambda_{jp} \sum_i \sum_m x_{imjp} - 1 \end{bmatrix} \succcurlyeq 0$;

So the problem (23.16) is equivalent to:

$$\begin{aligned} &\min \langle M_{jp}, \Sigma_{jp} \rangle \\ &s.t. \\ &\lambda_{jp} \geq 0, \\ &M_{jp} \succcurlyeq 0, \\ &M_{jp} + \begin{bmatrix} 0 & -\lambda_{jp} \\ -\lambda_{jp} & -2\lambda_{jp} \sum_i \sum_m x_{imjp} - 1 \end{bmatrix} \succcurlyeq 0 \end{aligned} \tag{23.20}$$

In problem (23.18), the optimal value is obtained when $\lambda_{jp} > 0$, Therefore, after combining problems (23.14) and (23.20), λ_{jp} is used on both sides of the equation, and M_{jp} instead of M_{jp}/λ_{jp}, λ_{jp} instead of $1/\lambda_{jp}$, there are

$$\begin{aligned} &\max \langle M_{jp}, \Sigma_{jp} \rangle \leq \lambda_{jp}(1-\epsilon) \\ &s.t. \\ &\lambda_{jp} \geq 0, \\ &M_{jp} \succcurlyeq 0, \\ &M_{jp} + \begin{bmatrix} 0 & -1 \\ -1 & -2 \sum_i \sum_m x_{imjp} - \lambda_{jp} \end{bmatrix} \succcurlyeq 0 \end{aligned} \tag{23.21}$$

Since the following two properties are equivalent.

$$\sqrt{\frac{1-\varepsilon}{\varepsilon}} \sqrt{x^{\mathrm{T}} \Gamma_i x} - \mu^{\mathrm{T}} x \leq \gamma$$

- There exists a symmetric matrix M and $\tau \in R^+$, such that:

$$\begin{aligned} &\langle M, \Sigma \rangle \leq \tau\varepsilon \\ &M \succcurlyeq 0 \\ &M + \begin{bmatrix} 0 & x \\ x & -\tau + 2\gamma \end{bmatrix} \succcurlyeq 0 \\ &\tau \geq 0 \end{aligned} \tag{23.22}$$

The readily available distributed robust chance constraint (23.11) is equivalent to:

$$\sum_{m} c_{mjp} * \left\{ \mu_{mjp} - \sqrt{\frac{1-\epsilon}{\epsilon}} \sqrt{\sigma_{mjp}^2} \right\} \geq \sum_{i} \sum_{m} x_{imjp}, \ \forall j, p \tag{23.23}$$

In particular, for the nonlinear terms $\sum_{i,m,j,p} \frac{h_j x_{imjp}^2}{c_{mjp} \xi_{mjp}}$, the auxiliary variable S_{imjp} is introduced for the following processing:

$$S_{imjp} * c_{mjp} \boldsymbol{\xi_{mjp}} \geq h_j x_{imjp}^2, \ \forall i, m, j, p \tag{23.24}$$

Similar to the transformation of (23.8), the robust optimization form of (23.24) is obtained as:

$$S_{imjp} * c_{mjp} * \left\{ \mu_{mjp} - \sqrt{\tfrac{1-\epsilon}{\epsilon}} \sqrt{\sigma_{mjp}^2} \right\} \geq h_j x_{imjp}^2, \ \forall i, m, j, p \tag{23.25}$$

The original problem then turns into:

$$\min_{\mathrm{o},\lambda,\mathrm{x},\mathrm{u}} \sum_{J} \sum_{p} \left[f_j o_j + s_{jp} \lambda_{jp} \right] + supE\left(g\left(\xi_{jp}\right)\right) \tag{23.26}$$

$$\lambda_{jp} \leq o_j, \ \forall j, p \tag{23.27}$$

$$\sum_{j} \sum_{P} \lambda_{jp} = 1 \tag{23.28}$$

$$c_{mjp} = \sum_{i} \sum_{m} Q_{im} * \lambda_{jp}, \ \forall m, j, p \tag{23.29}$$

$$c_{mjp} \leq F c_j, \ \forall m, j, p \tag{23.30}$$

$$supE\left(g\left(\xi_{jp}\right)\right) = \sum_{i,m,j,p} \left\{ S_{imjp} + \phi_m u_{imjp} \right\} + \sum_{i,m,j,p} \alpha \cdot d_{ij} x_{imjp} \tag{23.31}$$

$$\sum_{j} \sum_{p} x_{imjp} + u_{imjp} = Q_{im}, \ \forall i, m \tag{23.32}$$

$$\sum_{m} c_{mjp} * \left\{ \mu_{mjp} - \sqrt{\frac{1-\epsilon}{\epsilon}} \sqrt{\sigma_{mjp}^2} \right\} \geq \sum_{i} \sum_{m} x_{imjp}, \ \forall j, p \tag{23.33}$$

$$S_{imjp} * c_{mjp} * \left\{ \mu_{mjp} - \sqrt{\frac{1-\epsilon}{\epsilon}} \sqrt{\sigma_{mjp}^2} \right\} \geq h_j x_{imjp}^2, \ \forall i, m, j, p \tag{23.34}$$

$$x_{imjp} \leq M \cdot b_{mp}, \ \forall i, m, j, p \tag{23.35}$$

$$x_{imjp}, u_{imjp} \in N^*, \lambda_{jp} \in [0, 1]; o_j = \{0, 1\} \tag{23.36}$$

Numerical Study

The supply chain structure of the photovoltaic industry is a typical closed-loop supply chain. Upstream photovoltaic panel manufacturers obtain glass, silicon wafers, cadmium, silver, and other raw materials from the raw material market and manufacture different photovoltaic panels to supply downstream photovoltaic power stations. China has a sizeable photovoltaic industry market. With the gradual development of photovoltaic poverty alleviation work, photovoltaic industries have been deployed in eligible districts and counties under various provinces, prefectures, and cities in China. Taking Shandong Province as an example, there are 15 prefecture-level city units in Shandong Province. Among its subordinate districts and counties, 99 districts and counties contain the photovoltaic power generation industry and have been integrated into the power grid. Their number and scale are relatively considerable.

In this section, we take Shandong Province in China as an example for numerical calculation. We use C-Si, CdTe, CIGS, the three most commonly used and widely used photovoltaic panels for different types of photovoltaic panels and corresponding recycling processes. Take the board as an example; its characteristic properties are as in Table 23.2.

Based on the data obtained from the Internet, government reports, and official information data, we have preliminarily set the parameters to be determined in the

Table 23.2 Material recovery rate for different types PV panels

Material	C-Si solar panel (%)	CIGS solar panel (%)	CdTe solar panel (%)	Recovery rate (%)
Glass	74.0	88	96	90
Si	4.0	0	0	90
Al	12.8	7	0	90
Copper	0.1	0.1	3.4	95
Silver	0.1	0	0.04	95

From: FutureBridge Analysis—The Future of Solar Panel Recycling: A Circular Economy Insight

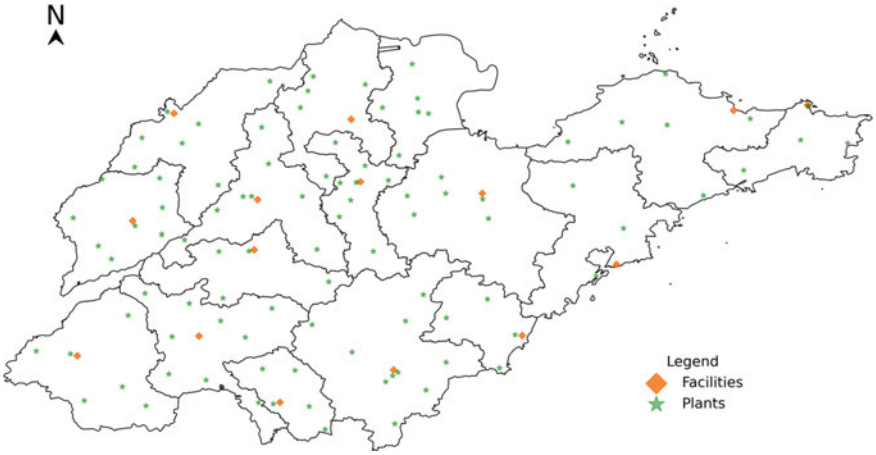

Fig. 23.2 Distribution map of available locations of photovoltaic power plants and facilities in prefecture-level cities in Shandong Province

model. Among them, the most important is that (1) The distance between the factory and the facility is calculated using the latitude and longitude coordinate information, (2) The mean and variance information of the random variable of the facility failure rate is collected from Shandong Province since January 31, 2020. To calculate the epidemic data until March 29, 2022, (3) The number of various types of photovoltaic panels that each site can provide is generated from a set of random integers ranging from 600 to 1000. The number of photovoltaic panels contained is about this number, and there is uncertainty in the scrap rate. (4) The investment cost of the process and the purchase cost of raw materials are obtained from the Internet and are in line with the actual market price ratio. (5) The essential construction cost of facilities at each location is replaced by the official commercial housing price.

This numerical experiment is solved by Gurobi (9.5.1), and the distribution diagram is drawn as follows (Fig. 23.2):

From the comparison between Figs. 23.3 and 23.4, it can be seen that when the facilities affected by the epidemic fail, the selection of open facilities is different. Further comparison is shown in Table 23.3.

Conclusions and Future Work

This paper considers the impact of facility failures on the closed-loop supply chain under uncontrollable factors such as the epidemic. A two-stage robust optimization model is constructed with the goal of minimizing facility construction costs, investment decision options, recovery costs, and recyclable processing projects (including

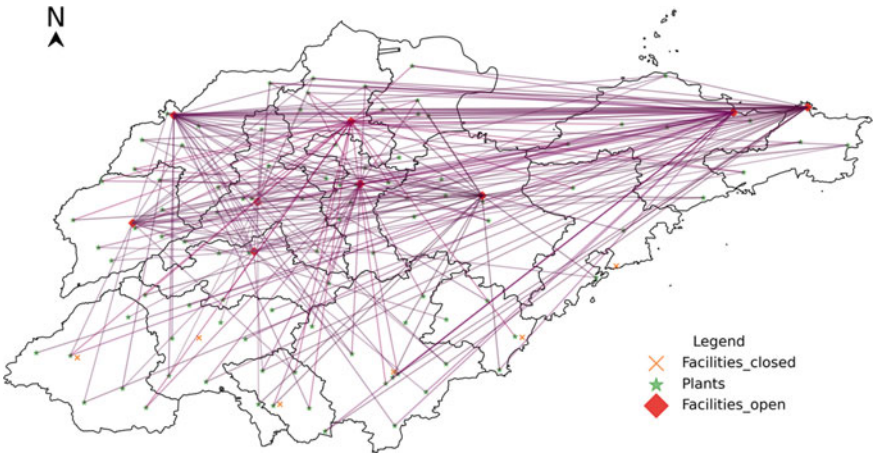

Fig. 23.3 Distribution of PV panel recycling network regardless of facility failure

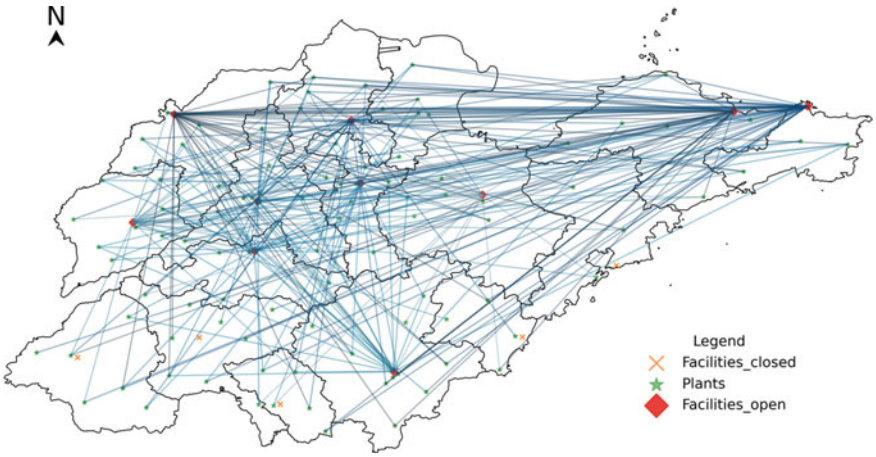

Fig. 23.4 Consideration of PV panel recycling network distribution in case of facility failure

repurchase costs of unrecovered raw materials). In the numerical experiments, Shandong Province, China is selected as a case for analysis.

There are 99 photovoltaic power stations connected to the grid in Shandong Province. In this paper, 15 prefecture-level cities are used as available recycling centers to establish recycling network optimization. Through numerical analysis, our proposed model is sensitive and effective for parameter combinations of random failures of different facilities. When other parameters remain unchanged, when only considering whether the facility faces the risk of failure, the cost is calculated by the scheme given by the model, and the difference is 3.16%. We believe that the model has a good optimization effect on the recycling network of closed-loop supply chains

Table 23.3 Contrastive analysis of failure and normal operation of facilities

Facilities	Opening		Investment	
	Normal	Failure	Normal (%)	Failure (%)
1	0	0		
2	0	1		3.61
3	0	0		
4	0	0		
5	0	0		
6	0	0		
7	1	1	9.39	8.84
8	1	1	10.79	10.43
9	1	1	9.95	9.79
10	1	1	9.76	9.23
11	1	1	12.24	10.94
12	1	1	12.41	12.59
13	1	1	11.45	11.09
14	1	1	11.66	11.05
15	1	1	12.35	12.43
Total cost	611,323,264.4744	630,671,038.4138	GAP = 3.16%	

facing random failures of facilities. At the same time, it can be seen from Table 23.3 that when faced with random failures, the model chooses to open more facilities and diversifies the investment ratio to reduce the risk of cost surge caused by facility failures, rather than choosing to close more facilities and purchase new raw materials. This is a reasonable result due to the existence of the risk sharing effect and the high purchase price of raw materials, which is in line with the economic benefits of production operations and the concept of environmental protection.

In the next stage of work, our primary goal is to further improve the parameter settings of the model to make it more in line with the reality and market operation laws, and replace the case data set of the numerical experiments to obtain better numerical experimental results.

Acknowledgements This paper is supported by the National Science Foundation of China [Grants 72101133, 72101008]; China Postdoctoral Science Foundation [Grants 2021M701856]; NSFC-FRQSC Research Program on Smart Cities and Big Data [Grants 7191101302].

Bibliography

1. Atamtürk, A., & Zhang, M. (2007). Two-stage robust network flow and design under demand uncertainty. *Operations Research, 55*(4), 662–673.
2. Chen, Q., Li, X., & Ouyang, Y. (2011). Joint inventory-location problem under the risk of probabilistic facility disruptions. *Transportation Research Part B: Methodological, 7*(45), 991–1003.
3. Cui, T., Ouyang, Y., & Max Shen, Z.-J. (2010). Reliable facility location design under the risk of disruptions. *Operations Research, 58*(4-part-1), 998–1011.
4. Cheng, C., Adulyasak, Y., & Rousseau, L.-M. (2021). Robust facility location under disruptions. *INFORMS Journal on Optimization, 3*(3), 298–314.
5. Berman, O., Krass, D., & Menezes, M. B. C. (2013). Location and reliability problems on a line: Impact of objectives and correlated failures on optimal location patterns. *Omega, 4*(41), 766–779.
6. Lu, M., Ran, L., & Max Shen, Z.-J. (2015). Reliable facility location design under uncertain correlated disruptions. *Manufacturing & Service Operations Management, 17*(4), 445–455.
7. Fleischmann, M., Bloemhof-Ruwaard, J. M., Dekker, R., van der Laan, E., van Nunen, J. A., & van Wassenhove, L. N. (1997). Quantitative models for reverse logistics: A review. *European Journal of Operational Research, 103*, 1–17.
8. Dai, Z., & Zheng, X. (2015). Design of close-loop supply chain network under uncertainty using hybrid genetic algorithm: A fuzzy and chance-constrained programming model. *Computers & Industrial Engineering, 88*, 444–457.
9. Govindan, K., & Soleimani, H. (2017). A review of reverse logistics and closed-loop supply chains: A journal of cleaner production focus. *Journal of Cleaner Production, 142*, 371–384.
10. Cui, Y. Y., Guan, Z., Saif, U., Zhang, L., Zhang, F., & Mirza, J. (2017). Close loop supply chain network problem with uncertainty in demand and returned products: Genetic artificial bee colony algorithm approach. *Journal of Cleaner Production, 162*, 717–742.
11. Shahbazbegian, V., Hosseini-Motlagh, S.-M., & Haeri, A. (2020). Integrated forward/reverse logistics thin-film photovoltaic power plant supply chain network design with uncertain data. *Applied Energy, 277*, 115538.
12. Li, Q., Liu, K., & Zhang, Z.-H. (2019). Robust design of a strategic network planning for photovoltaic module recycling considering reclaimed resource price uncertainty. *IISE Transactions, 51*(7), 691–708.

Chapter 24
Analysis of Factors Influencing the Selection of Billing Model for Whole-Process Engineering Consulting Services Based on DEMATEL-ISM

Ronghui Sun and Yanfeng Chu

Abstract Whole-process engineering consulting services (WECS) is an emerging consulting service model in China, and the study of the factors influencing the selection of its billing model and the relationship among them can help develop the service. 31 influencing factors of billing model selection are analyzed and summarized. On this basis, the analysis was conducted using the DEMATEL-ISM method. This study simplifies the system of influencing factors and visualizes the relationships and paths between the influencing factors. The results of the study are intended to provide a basis for the selection of WECS. The research results are intended to provide a reference basis for the selection and development of the billing mode of WECS.

Keywords Whole-process engineering consulting service · Billing model selection · DEMATEL · ISM · Factor analysis

Introduction

With the gradual expansion of China's infrastructure scale and the emergence of a large number of large-scale, clustered and complex construction projects with high requirements for efficiency, the traditional project management model can no longer meet the needs of these types of projects. Whole-process engineering consulting services (WECS) is a mature management mode in the international arena, which can provide whole life cycle engineering consulting services to meet the needs of owners. Through the reference of this management mode, China's WECS was born in time.

R. Sun · Y. Chu (✉)
Department of Economics and Management, Nanjing University of Aeronautics and Astronautics, Nanjing 211100, Jiangsu, China
e-mail: yanfengc@nuaa.edu.cn

R. Sun
e-mail: sunronghui@nuaa.edu.cn

R. Qiu et al. (eds.), *City, Society, and Digital Transformation*, Lecture Notes in Operations Research, https://doi.org/10.1007/978-3-031-15644-1_24

As the promotion of WECS mode in China is in the initial stage, there is a lack of legal and regulatory system and specification, and the charging system has not formed a standard. At present, enterprises mainly adopt several billing modes, such as single charge summary, lump-sum rate, labor hours and "1 + N" superposition charge [1], and each mode has certain advantages and disadvantages. On the issue of billing mode selection, unified norms and standards have not yet been formed, and there is a lack of reference basis, which makes the application of enterprises resistant. Therefore, the key influencing factors affecting the selection of billing mode of WECS are studied in the new era of engineering consulting. This can help enterprises grasp more deeply what mode they are more suitable for, and is of great significance for future development strategies to meet the requirements of the new era.

Literature Review

Engineering consulting industry in the academia started earlier, and has entered a mature stage after a long period of development, and the management system has been more perfect. At present, most of the engineering consulting services in China are fragmentary mode, and the engineering consulting services abroad are generally whole-process mode. Due to the different legal system and market environment of each country, the organization mode of foreign WECS is mainly divided into two modes, mainly the U.S. mode and the German mode [2]. The engineering consulting service of American mode is generally one-stop WECS contract signed between owners and large engineering consulting companies, entrusting them to undertake planning and design type and project management type services, and signing one-stop WECS contract with them [3]. German mode engineering consulting is two companies jointly providing WECS, entrusting two different units to provide engineering project planning and design type services and engineering project control and management services respectively [4].

In China, many scholars have devoted themselves to studying the basis of fees or pricing of consulting services. On the one hand, scholars have explored the pricing of different industries and single business charges. Li Ma et al. have analyzed 14 factors affecting the pricing of comprehensive pipe corridor PPP project charges from the stakeholder perspective using Grey-DEMATEL and conducted causality analysis [5]. Xingyu Pan et al. analyzed the current situation and problems of engineering cost consulting service fees in view of the actual situation, and elaborated the development problems and countermeasures of engineering cost consulting service with the future development trend of the industry [6]. On the other hand, scholars explored how to develop about the billing mode of WECS. Yilin Yin et al. summarized the organization mode and charging standard of WECS construction at home and abroad, started research with the entry point of WECS work elements, and proposed

the charging mechanism of WECS [7]. Honghai Wang et al. explored three solution methods, namely superposition method, cost method and value method, for the charge of WECS [8].

At this stage, the four billing models introduced in Sect. 24.1 are most widely used in China. The choice of billing model is an important issue in the process from commissioning to implementation of WECS projects. For different projects, the choice of billing model should not be generalized and rigidly applied to past experience, but should be tailored to local conditions and selected flexibly. The final model is determined as a result of a combination of factors such as policy environment and actual project situation. Therefore, scholars are also thinking about what factors need to be considered in the selection of WECS billing methods. According to Lei Wang et al.'s study, only a small number of principals will let consulting units intervene in the investment consulting stage, and consulting units are not throughout the project. At the same time, many consulting units lack whole-process consulting talents and have insufficient experience in undertaking WECS projects, so it may be more convenient to adopt the single cost aggregation method for practical operation at this time [9].

Framework and Critical Factors for the Selection of Billing Model for Whole- Process Engineering Consulting Services

In a general sense, the WECS mainly includes 6 service contents of pre-planning, survey and design, bidding agent, cost consulting, engineering supervision and project management. For the WECS billing, although the scholars who are currently conducting research on the fees of WECS do not directly mention the influencing factors, the factors that may be associated can be analyzed from their research.

In this paper, we consider four dimensions: external environment, project itself, stakeholders, and billing mode. From the perspective of external environment, we consider geographical factors and industry environment factors. From the perspective of the project itself, the project nature, the project commissioning situation, and the project organization are considered. From the perspective of stakeholders, the factors of commissioner and contractor are considered. Finally, the characteristics and impacts of the billing model are considered from the characteristics of the billing model itself. We summarize 8 aspects that will have influence on the billing mode of WECS, and designs a total of 31 influencing factors for each aspect. The influencing factors for the selection of the billing mode of WECS are finally derived and shown in Table 24.1.

Table 24.1 Factors influencing the billing of whole-process engineering consulting service

Levels	Factors
Geographical factors	Local policy preferences X_1 [10], local price level X_2, local government measures X_3 [11]
Industry Environment	There has been practical experience of WECS projects X_4, the degree of perfection of existing whole process tariff X_5 [12]
Project commissioning situation	bidding mode X_6 [13], organization mode of consulting enterprises X_7 [1], outsourcing consulting business combination mode X_8 [14]
Project nature	Project investment amount X_9 [15], project cycle length X_{10}, project complexity X_{11} [16], project risk level X_{12} [16], project industry X_{13} [13], project informatization level X_{14}
Project Organization	Department establishment mode X_{15}, leadership mode X_{16}, management mode X_{17} [15], workflow arrangement X_{18}, clear division of labor X_{19}, independence of project life cycle stages X_{20}, performance evaluation mode X_{21}
Entrusted party	WECS project experience X_{22}, billing model preference X_{23} [11], liability risk X_{24} preference [17]
Contractor situation	Experience in WECS projects X_{25}, billing model preference X_{26}, personnel qualification X_{27} [13], scope of business that can be undertaken X_{28} [13]
Characteristics and impact of the billing model itself	Social effects generated by the model X_{29} [18], difficulty of implementing the model X_{30}, incentive effect of the model on personnel X_{31}

Factor Analysis and Results

DEMATEL-ISM

The two methods DEMATEL and ISM, as the system analysis methods of commonly used complex system element association relationships, have been applied by scholars in numerous fields. The DEMATEL method is based on the matrix of influence relationships between the factors in the system, and uses indicators such as influence degree, influenced degree, centrality degree and cause degree to determine the cause and effect factors and the degree of influence of each factor on the complex system. The ISM method is based on the accessibility matrix, which reflects the influence relationship between factors in the system. The combination of the two methods can not only identify the critical factors for billing model selection, but also clarify the direct and indirect factors influencing billing model selection through

the hierarchical structure. Therefore, this study adopts the method to conduct the influence factor research 2.3. Numbering and Attributing.

Factor Attribute Analysis Based on DEMATEL

Step 1: Determine the Set of Influence Factors X and Calculate the Direct Influence Matrix O

Determine the set of influence factors $X = \{X_1, X_2, \ldots, X_{31}\}$ for the WECS billing mode selection, and ask a total of 10 experts to evaluate the strength of the relationship between each influence factor, assign values according to five semantic scales of 0, 1, 2, 3 and 4, and process the expert evaluation results by the averaging method to obtain the direct influence matrix $O = [o_{ij}]_{31\times31}$, as shown in Fig. 24.1.

Direct Influence Matrix O

	X1	X2	X3	X4	X5	X6	X7	X8	X9	X10	X11	X12	X13	X14	X15	X16	X17	X18	X19	X20	X21	X22	X23	X24	X25	X26	X27	X28	X29	X30	X31
X1	0	1.4	3.9	0.2	2.2	0.3	0	0	1.7	0	0	0	0	0	0	0	0	0	0	0	2.6	0	3.4	1.2	3	0	0	0.8	2.9	0	2.1
X2	0.9	0	3.6	0.3	0.2	0.7	0.3	0.6	3.2	0	0	0	0	0	0	0	0	0	0	0	3.1	0	3.7	0.7	3.5	0	1.8	0	0	0.8	0
X3	1	0.4	0	0	2.7	1.1	1.5	0.1	0.9	0	0	0	0	0	0	0	0.8	0.1	0.5	0	0.6	0	3	0.6	2.8	0	2.1	0.7	0	2.3	2.7
X4	2.3	2.5	2.2	0	1.6	1	0	0.9	3.4	0	0.2	0	0	1.7	0.9	0.3	1	3.2	2	0	0.6	0	3.1	1	3.2	0.7	1.7	0	1.9	0.3	0.5
X5	2.7	0.1	1.4	0.6	0	0	0	0	0	0	0	0.3	0	0	0	0	0	0	0	0	1.2	0	3.6	2.9	3.7	0	0.3	0	1.2	3.8	3.4
X6	0.7	0	0	0.2	0	0	0	0	2.6	0	0	0	0	0	0	0	0	0	0	0	0	0	1	0.8	1.3	0	0	0.1	0	0	0
X7	0	0	0	0	0	0.3	0	3.8	0	0.3	0	0	0	0	0	0	1.6	0	0.2	0	1.1	0	0	0	2.9	0	0.8	0.5	0	0	0
X8	0	0	0	0	0	0.6	2.5	0	0.2	0.2	0.7	0.8	0	0	0	0	1.4	0.9	0	0	1.3	0	2.7	2.5	3.6	0	0	0	0.2	0	0.3
X9	0	0	0	0	0	1.4	0.2	0.3	0	0.7	0.2	0.1	0	0.3	0	0.2	0.9	1	1.6	0.1	3	0	2.4	2.7	2.4	0	0	0	0	0	0
X10	0	0	0	0	0	0.2	0.4	0.7	3.7	0	0.3	2.9	0	0	0.6	0.3	1.8	1.9	2.1	0	3.1	0	2	1.6	2.8	0	0	0	0	0	0
X11	0	0	0	0	0	0.1	1.7	1.3	3.2	2.1	0	3.3	0	0	1	0.5	2.7	2.2	2.5	0.1	2.8	0	1.9	2	2.3	0	0	0	0	0	0
X12	0	0	0	0	0	0.1	0.6	0.8	2.7	1.6	2.9	0	0	0	0	1	1.3	1.5	1.3	0.3	2.3	0	1.7	2.2	1.7	0	0	0	0	0	0
X13	0	0	0	0	0	0	0.1	0.3	2.6	1.4	3.4	1.7	0	0.2	1.6	0.1	0.6	0.5	0.4	1.3	3.1	0	0.4	0	0.4	0	0	0	0	0	0
X14	0	0	0	0	0	0.2	0.2	0.6	3	1.9	3.1	1.4	0	0	2	1.2	3.4	3.6	1.8	0	3.4	0	1.3	1.1	1.9	0	0	0	0	0	0
X15	0	0	0	0	0	0	0.6	0.9	1.4	0.5	0.4	1.1	0	0	0	1.5	1.4	3.1	2	0	1.4	0	0.1	0.1	0	0	0	0	0	0	0
X16	0	0	0	0	0	0.3	1.2	0.4	1.7	0.8	0.9	1	0	0	3	0	3.2	3	1.1	0	2.4	0	0.5	1	0.1	0	0	0	0	0	0
X17	0	0	0	0	0	0.3	0.1	1.2	1.2	0.3	2.6	0.8	0	0	3.7	2.8	0	2.1	2.5	0	1	0	1.1	0.4	0.4	0	0	0	0	0	0
X18	0	0	0	0	0	0.7	0.3	1.8	0.9	1.1	2.2	1.6	0	0	3.6	2.3	1.6	0	2.7	0	0.9	0	1.3	0	1.1	0	0	0	0	0	0
X19	0	0	0	0	0	0	1	0.7	1.1	1.4	0.8	2.2	0	0	2.9	0.8	0.3	2.3	0	0	2.8	0	1.6	0	0.2	0	0	0	0	0	0
X20	0	0	0	0	0	1.7	0.9	0.2	0.7	1.9	1.4	2.3	0	0	2.9	2.7	2.9	1.6	2.1	0	1	0	2.2	2.1	0.9	0	0	0	0	0	0
X21	0	0.4	0.1	0	0.1	0	0.1	0.1	0.9	1.2	0	1	0	0	0.8	0.3	1.6	0.1	0.7	0	0	0	2.5	0.6	1.4	0	0	0	0	0	0
X22	0.9	0.2	1.1	1.3	0.6	0.1	0.1	1.3	0.9	0.1	0	0.2	0	0.7	0	0.1	1.4	1.2	0.9	0	2.6	0	3.3	3.2	1.3	0	0	0	0	0	0
X23	0.1	1.4	0.5	0	0.1	0	0	0.6	2.4	0	0	0.1	0	0	0	0	0	0	0.2	0	3.4	0.2	0	2.4	3.6	0	0	0	0	0	0
X24	0	0.2	0	0	0	1.5	0.2	1.3	2	0.4	0	0	0	0	0	0	0	0	0.1	0	2	0.5	2.7	0	3.2	0	0	0	0	0	0
X25	0	0.5	0	0	0.3	0	1.1	0.2	3.1	0	0	0.1	0	0	0	0	0	0.2	0	0	1.9	0	0.2	0	0	0.3	0	0	0	0	0
X26	1.5	1.3	0	1.7	1.4	0	3	0.2	2.8	2.3	0	1.5	0	0	0	0	0	1.1	1	0	0.3	0	0.5	0	3.5	0	1	1.2	0.1	0	0
X27	1.9	3	2.7	1.2	0.3	0.2	3.3	1.7	3.5	2.4	0	3.7	0	0	0	0	0	1.8	2.2	0	1.9	0	0.7	1.8	2.9	2.6	0	3.5	0	0	0
X28	0.8	0	1.2	0.4	0.1	0.3	3.6	2.7	3.3	0.3	0	0.9	0	0	0	0	0	1.4	1.5	0	0	0	0.6	1.3	2.7	2.5	0	0	0	0	0
X29	2.1	0	3.3	0	0.7	0	0	0.1	0.5	0	0	0	0	0	0	0	0	0	0.1	0	1.1	0	2.4	0.4	1.5	0	0	0	0	0	1.7
X30	2.4	1.7	3.5	1.8	0.8	0	0	0	3.6	0	0	0	0	0	0	0	0	0	0	0	1.7	0	3.3	0	3.4	0	0	0	0	0	0.1
X31	3.4	0.9	3.7	0.9	0.2	0	0.1	0.1	1.2	0	0	0	0	0	0	0	0	0	1.1	0	2.6	0	1.8	0.9	1	0	0	1.9	2.7	0	0

Fig. 24.1 Direct influence matrix O

Step 2: Calculate the Normalized Direct Influence Matrix G and Total Influence Matrix T

The normalized direct influence matrix G is obtained by Formula (24.1):

$$G = \left[g_{ij}\right]_{31\times 31} = \frac{1}{\max\limits_{1\le i\le 31}\sum_{j=1}^{31} o_{ij}} O \tag{24.1}$$

Based on matrix G, the total influence matrix T is calculated by Formula (24.2), in which I represents the identity matrix. To make the layout of this manuscript more concise, the main context only presents the calculation formula and processes.

$$T = \lim_{n\to\infty}\left(G + G^2 + G^3 + \cdots + G^n\right) = G(I - G)^{-1} \tag{24.2}$$

Step 3: Calculate Four Weights of Factors

$$D_i = \sum_{j=1}^{n} t_{ij} (i = 1, 2, \ldots, 31) \tag{24.3}$$

$$C_i = \sum_{j=1}^{n} t_{ji} (i = 1, 2, \ldots, 31) \tag{24.4}$$

$$M_i = D_i + C_i \tag{24.5}$$

$$R_i = D_i - C_i \tag{24.6}$$

According to Eqs. (24.3)–(24.6), the influence degree D_i, the influenced degree C_i, the central degree M_i and the cause degree R_i are calculated for each influencing factor. With the central degree as the horizontal coordinate and the cause degree as the vertical coordinate, the diagram of the cause results of the influencing factors for the selection of the WECS billing model is drawn, as in Fig. 24.2.

Factors with $R_i > 0$ are causal factors and factors with $R_i < 0$ are consequential factors, $|R_i|$ the larger the factor, the higher the degree of influence of its corresponding factor on other factors (by other factors).

Step 4: Step 4: Screening out factors with low impact.

Taking $\alpha = \beta = 0.85$, the influencing factors are simplified according to Eq. (24.7).

$$M_i < \alpha\frac{\sum_{i=1}^{31} M_i}{31} \quad \text{and} \quad R_i < \beta\frac{\sum_{i=1}^{31} R_i}{31} \tag{24.7}$$

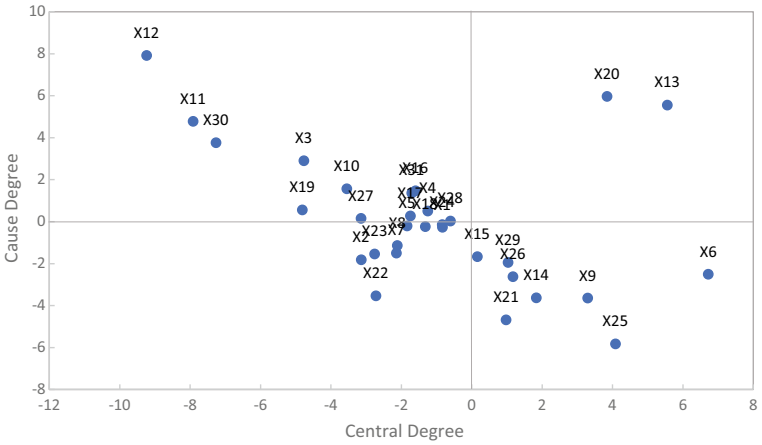

Fig. 24.2 Cause-effect diagram of the factors of the billing of whole-process engineering consulting service

According to the calculation results sieve out X_2, X_5, X_7, X_8, X_{18}, X_{22}, X_{23}.

This is more similar to the results of Sun et al.'s study [14], that is, the influence of business combination on the choice of billing model is not prominent and obvious. Due to the different qualification ability of different consultants and the local price level, it is impossible to determine a uniform standard, and the consulting services with high professionalism are only properly considered. The project experience of the client and the process arrangement of the project have no significant influence on the final settlement of the billing amount, and the client is more interested in whether the consulting company's bid is low enough than the choice of billing model, so the above influencing factors are screened out in the subsequent study.

Hierarchy of Factors Using ISM

Step 1: Calculate the Holistic Influence Matrix B and Reachability Matrix Z

Calculate the relationship matrix A according to Eq. (24.8).

$$\begin{cases} a_{ij} = 1, t_{ij}^{'} \geq \lambda \\ a_{ij} = 0, t_{ij}^{'} < \lambda \end{cases} \tag{24.8}$$

The mean $\overline{x} = 0.6743$ and the standard deviation $\sigma = 1.0373$ for each factor of matrix $T^{'}$. Therefore, $\lambda = \overline{x} + \sigma = 1.7116$.

The relationship matrix A and the unit matrix are summed to calculate the holistic influence matrix B. The holistic influence matrix B is concatenated and multiplied to obtain the reachability matrix Z.

Table 24.2 Hierarchy of factors within the billing of whole-process engineering consulting service

Hierarchy	Factors
L_1	X_{21}
L_2	X_9, X_{24}, X_{25}
L_3	$X_6, X_{10}, X_{11}, X_{12}, X_{15}, X_{16}, X_{17}, X_{19}$
L_4	$X_{13}, X_{14}, X_{20}, X_{26}$
L_5	X_{28}
L_6	$X_1, X_3, X_4, X_{27}, X_{29}, X_{30}, X_{31}$

$$Z = B^{k+1} = B^k \neq B^{k-1} \tag{24.9}$$

Step 2: Hierarchy division based on matrix.Z

Based on the matrix Z, the reachable set $Q(X_i)$, the prior set $D(X_i)$ and the common set $C(X_i)$ are calculated according to Eqs. (24.10)–(24.12).

$$Q(X_i) = \left\{X_j | X_j \in X, r_{ij} = 1\right\} (i = 1, 2, \ldots, 24) \tag{24.10}$$

$$D(X_i) = \left\{X_j | X_j \in X, r_{ji} = 1\right\} (i = 1, 2, \ldots, 24) \tag{24.11}$$

$$C(X_i) = \left\{X_j | X_j \in X, Q(X_i) \cap D(X_i) = Q(X_i)\right\} (i = 1, 2, \ldots, 24) \tag{24.12}$$

The elements in the set C belong to the same stratum, and the rows and columns where the elements of this stratum are located are crossed out in the matrix Z, respectively.

In order to obtain the set of factors satisfying the above requirements for stratification, a total of 6 strata are obtained, and the final division results are shown in Table 24.2.

DEMATEL-ISM Model of Factors in the Billing of Whole-Process Engineering Consulting Service

The circular boxes in Fig. 24.3 are the causal factors and the square boxes are the outcome factors. The numbered corner markers next to the factors indicate the centrality ranking after screening out the factors. The directed arrows between the factors in the figure indicate that there is a causal relationship between the factors; if the arrow is bidirectional, the connection is a loop, which is a strong connection, indicating that the group of factors are causally related to each other.

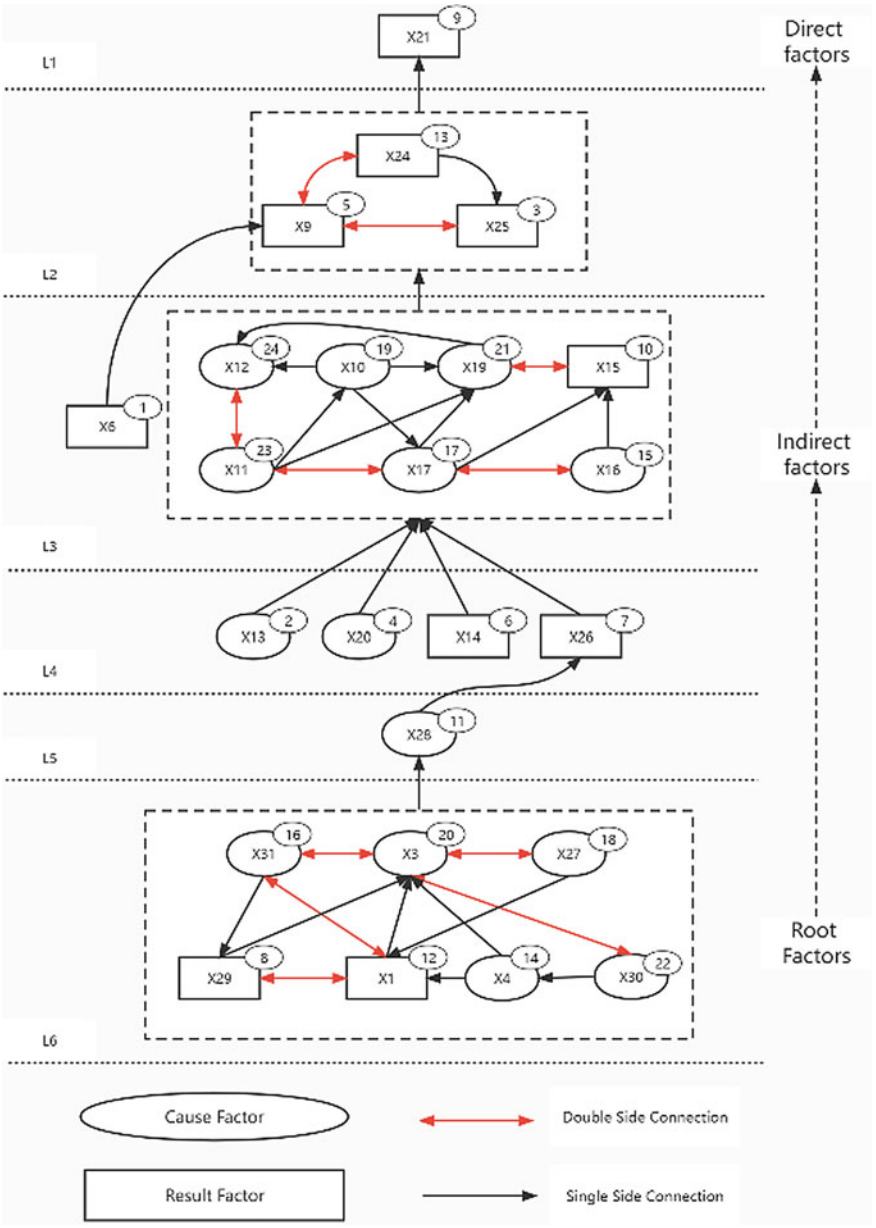

Fig. 24.3 DEMATEL-ISM modle of factors in the billing of whole-process engineering consulting service

Comprehensive Analysis

The factors X_n influencing the billing model of WECS appearing in this section are detailed in Table 24.1.

Hierarchical Analysis

As shown in Fig. 24.3, the system of factors influencing the selection of the WECS billing model is a hierarchical structure of 6 levels and 3 orders from top to bottom in a directional progression. The system is divided into 3 levels: the factor The lower level indicates a stronger degree of influence, and the upper level indicates a stronger degree of being influenced.

(1) Root Factors

It contains $\{X_1, X_3, X_4, X_{27}, X_{29}, X_{30}, X_{31}\}$. The root factors send only directed lines upward and do not receive directed lines, indicating that they only influence other factors and are not influenced by other factors in the system. Therefore, the above root factors are the most fundamental reasons affecting the choice of billing mode for WECS, and should be paid more attention and considered when making the choice of billing mode.

(2) Direct Factors

It contains $\{X_{21}\}$. The direct factor only receives the directed line and does not send down the directed line, indicating that it is influenced by other factors in the system without affecting other factors. Therefore, if the government wants to guide the selection of the WECS billing model effectively, you can start from the direct factor. However, direct factors are more likely to be influenced by other factors, and attention should also be paid to the control of their antecedent factors or reduce the linkage with weakly related factors when making targeted solutions.

(3) Indirect Factors

It is the remaining factors in the hierarchy chart excluding the root and direct factors. Indirect factors send and receive directional lines, indicating that they influence and are influenced by other factors. Indirect factors assume the role of transmitting influence relationships in the influence factor system, and they can also act as sources of influence on other factors. Therefore, it is necessary to consider indirect factors, especially for factors with high centrality, such as $\{X_6, X_{13}, X_{25}, X_{20}, X_9\}$. In addition, in most cases, it is difficult or even impossible for consulting firms to control some of the root factors, such as $\{X_1, X_3, X_4, X_{30}\}$. It can be regulated by controllable factors of indirect factors, such as $\{X_{28}, X_{25}\}$, so as to be more favorable for consulting enterprises to develop WECS.

Cause and Effect Analysis

(1) Loop Analysis

As shown in Fig. 24.3, there are 3 groups of loops in the system of factors influencing the selection of WECS billing mode: $\{X_9, X_{24}, X_{25}\}$, $\{X_{10}, X_{11}, X_{12}, X_{15}, X_{16}, X_{17}, X_{19}\}$, $\{X_1, X_3, X_4, X_{27}, X_{29}, X_{30}, X_{31}\}$. This indicates that the 3 groups of factors are closely connected and causal in themselves. Therefore, when choosing the billing mode for WECS, the above three groups of loop factors should be taken as an integrated and integrated decision to make a reasonable billing mode selection.

(2) Critical Factors

The top five influencing factors in the ranking of centrality can be found in Fig. 24.3 as $\{X_6$ (6.724), X_{13} (5.56), X_{25} (4.086), X_{20} (3.844), X_9 (3.301)$\}$. It shows that these factors are the main influencing factors on the selection of billing mode for WECS, and must be used as critical elements for decision making when making billing mode selection.

(3) Causal Factors

The top five factors in the order of reason degree are $\{X_{12}$ (7.918), X_{20} (5.965), X_{13} (5.56), X_{11} (4.784), X_{30} (3.762)$\}$, which will have a greater influence on the remaining factors. In Fig. 24.3, X_{12} and X_{11} are located at L_3, X_{20} and X_{13} are located at L_4, which are indirect factors affecting the selection of billing model for WECS; X_{30} is located at L_6, which is the root factor affecting the selection. From the above analysis, it is clear that, from the perspective, guiding the billing mode selection of WECS needs to improve the way of billing mode landing, the project itself clarifies the business of each stage, standardizes the billing method for different industries, and then provides risk guarantee as well as technical support to the project, and maximally assists the development of billing method of WECS.

(4) Resulting Factors

The top five factors ranked after the absolute value of the reason degree are $\{X_{25}$ (5.823), X_{21} (4.674), X_9 (3.641), X_{14} (3.625), X_{26} (2.621)$\}$, which are more likely to be influenced by the reason factors in the influence factor system. In Fig. 24.3, X_{25} and X_9 are located in L_2, X_{14} and X_{26} are located in L_4 are indirect factors affecting the selection of billing model for WECS; X_{21} is located in L_1, which is a direct factor affecting the selection. It can be seen in Fig. 24.3 that these factors are influenced by various factors in the lower layer, and the degree of project informationization and the preference of billing mode of the contractor have influence on the experience of WECS project and the size of project investment, and finally these influential relationships act on how to evaluate the performance of the project. Therefore, in the short term, it seems that consulting enterprises focus on taking measures to consider these factors, which have a more significant effect on making choices.

Conclusions

(1) Hierarchical and causal analysis reveals that the project commissioning situation, project nature and project organization are the main influencing factors affecting the choice of WECS billing mode. The second is the situation of the undertaking party. Geographical factors, industry conditions and the characteristics of different billing modes themselves are the root factors affecting the choice of billing mode. The situation of the commissioning party indirectly affects the choice of billing mode.

(2) According to the characteristics of mutual influence between influencing factors of WECS billing mode selection, the causal relationship between each influencing factor and its degree of effect on choices are studied by combining DEMATEL and ISM. It is found that the bidding method and the industry to which the project belongs are important causal factors, and the experience of the WECS project and the performance evaluation method are important result factors, which are of high importance in the system of influencing factors and should be focused on when making the billing mode selection.

(3) A multi-layer recursive structure model of 6 levels and 3 orders of factors influencing the selection of billing mode of WECS is constructed. The hierarchical relationship between factors influencing the selection of WECS billing mode is analyzed. The project performance evaluation mode is a direct factor in the selection of billing mode. Local policy preference, local government measures, practical experience of WECS projects, qualification of personnel of the undertaking party, social effect of the mode, difficulty of implementing the mode, and incentive effect of the mode on personnel are the most fundamental reasons influencing the choice of billing mode for WECS.

References

1. Sun, N., Cao, Z. F., Zhang, N., & Ning, Y. (2020). Research on the organization model and fee collection model of whole process engineering consulting. *Construction Economy* (03), 5–10. https://doi.org/10.14181/j.cnki.1002-851x.202003005
2. Yang, Z. M. (2018). Research on abroad whole process engineering consulting service mode. *Project Management* (07), 9–11+27. https://doi.org/10.15968/j.cnki.jsjl.2018.07.003
3. Huang, X. W. (2022). International experience and enlightenment of whole process engineering consulting. *Chinese Engineering Consultants* (06), 51–55.
4. Ding, S. Z. (2019). Promote whole-process engineering consultation with an international perspective. *China Engineering Consulting* (05), 32–37.
5. Ma, L., & Liu, J. F. (2018). Research on the influence factors of charge for utility tunnel PPP project. *Construction Economy* (05), 73–77. https://doi.org/10.14181/j.cnki.1002–851x.201805073
6. Pan, X. Y., & Peng, C. X. (2019). Discussion on the status and countermeasures of engineering cost consulting service charge. *Engineering Economy* (04), 45–48. https://doi.org/10.19298/j.cnki.1672-2442.201904045

7. Yin, Y. Y., Xie, W. W., Yang, X. H., & Li, M. Y. (2019). Whole process engineering consultation fee machanism in construction projcet. *Project Management Technology* (11), 7–11.
8. Wang, H. H., Miao, Y. P., & Liu, D. (2019). Discussion on charges for whole process engineering consulting services. *China Engineering Consulting* (11), 62–67.
9. Wang, L. (2020). Problems existed in the implementation of whole process engineering consulting and its ponderations. *Project Management* (07), 1–3+15. https://doi.org/10.15968/j.cnki.jsjl.2020.07.001
10. Yu, H. L., Li, Y. J., & Xiao, Y. L. (2018). Research and application of service charge standard of life cycle engineering consulting. *Construction Economy* (12), 10–14. https://doi.org/10.14181/j.cnki.1002-851x.201812010
11. Zhao, Z. Y., & Gao, L. (2019). Problems and countermeasures to implement the life cycle engineering consulting. *Construction Economy* (12), 10–14. https://doi.org/10.14181/j.cnki.1002-851x.201912005
12. Chen, L., Wang, L., Mo, Y. L., & Huang, W. H. (2021). Analysis of the whole process consulting of water conservancy project based on the SWOT-SLEPT model. *Construction Economy* (05), 67–71. https://doi.org/10.14181/j.cnki.1002-851x.202105067
13. Liu, J. W., Yang, X., & Wang, P. (2021). Research on bidding mode and fee collection of whole process engineering consulting projects in Shandong province. *Chinese Engineering Consultants* (07), 77–83.
14. Sun, N., Cao, Z. F., Zhang, N., & Ning, Y. (2020). Selection of the whole process consulting organization mode and fee collection mode under different business combination modes. *Journal of Engineering Management* (06), 1–6. https://doi.org/10.13991/j.cnki.jem.2020.06.001
15. Dong, R., Yin, Y.L., Wang, X., & Ren, Y.R. (2019). Whole-process engineering consulting management compensation model based on work factor weight. *Project Management Technology* (07), 52–58.
16. Cao, M. M. (2020). Implementation analysis of whole process engineering consulting. *City & House* (04), 152–153.
17. Yin, M., Chen, F. L., Shen, S., & Li, Y. (2020). A brief analysis on the problems and countermeasures of the whole process engineering consulting in the implementation of power grid projects. *Project Management Technology* (04), 84–88.
18. Zhu, X. H., Yin, M., & Liu, C. L. (2020). Suggestions on the cost of engineering consulting services in the whole process of power grid projects. *China Power Enterprise Management* (12), 74–75.

Chapter 25
Research on Critical Chain Project Buffer Management Considering Activity Risk

Meng Xiao and Yanfeng Chu

Abstract Critical chain project management is a widely used project schedule management method, the core of which is buffer management. We firstly determine the buffer based on the elasticity of project activities, consider the activity risk when allocating the buffer, then set the buffer monitoring warning points, and give the implementation scheme of dynamic buffer monitoring. Finally, a case simulation demonstrates the effectiveness of the proposed buffer management method in the project schedule monitoring process.

Keywords Critical chain · Buffer sizing · Activity risk · Buffer monitoring

Introduction

In 1997, Israeli physicist Goldratt wrote and published his book Critical Chain on project management. Goldratt introduced the Theory of Constraints (TOC) into the field of project management. The Critical Chain Project Method (CCPM) was proposed to replace the Critical Path Method [1]. The core of CCPM is to extract the safe time of project activities and form a buffer zone at the end of the project to absorb the delay of the activity duration caused by uncertain factors and improve the probability of the project being completed on time.

CCPM mainly includes three kinds of buffer: project buffer, feeding buffer and resource buffer. Critical Chain/Buffer Management (CC/BM) mainly includes two contents: buffer sizing and buffer monitoring.

Buffer sizing is how the buffer size is calculated, and Goldratt uses a Cut-and-Paste Method (C&PM). The cut-and-paste method uses half of the duration of all activities in the critical chain as the safety time and half of the sum of the safety time

This paper is supported by "the Fundamental Research Funds for the Central Universities, NO. 56XAB21015".

M. Xiao · Y. Chu (✉)
School of Economics and Management, Nanjing University of Aeronautics and Astronautics, Nanjing 211106, Jiangsu, China
e-mail: yanfengc@nuaa.edu.cn

R. Qiu et al. (eds.), *City, Society, and Digital Transformation*, Lecture Notes in Operations Research, https://doi.org/10.1007/978-3-031-15644-1_25

of all activities as the project buffer placed at the end of the project to absorb project risks. This buffer sizing method is simple and easy to implement, but the buffer size increases linearly with the length of the critical chain, which may lead to a waste of resources due to an oversized project buffer and does not serve well to shorten the project duration. In 1998, Newbold proposed the Root Square Error Method (RSEM) based on the Cut-and-Paste Method while considering the probability of project completion. That is, the root variance of half of the safe time is calculated and placed at the end of the project as the project buffer [2].

Buffer monitoring is the process of monitoring buffer consumption during project execution to determine whether measures need to be taken to avoid project delay. The Static Buffer Monitoring Method proposed by Goldratt divides the buffer into three equal parts, namely the green zone, the yellow zone and the red zone. The cut-off point of green zone and yellow zone is warning point 1, and the cut-off point of yellow zone and red zone is warning point 2. During the process of the project, if buffer consumption is in the green zone, no action shall be taken; when buffer consumption reaches the yellow zone, the project manager shall pay attention and prepare for action; when buffer consumption reaches the red zone, the project manager shall take immediate action to prevent the delay of the whole project due to the delay of the activity. However, this Static Buffer Monitoring Method does not consider the relationship between buffer consumption ratio and chain completion ratio. In the initial stage of a project, even if an activity consumes a lot of buffer, as long as the buffer consumption is still in the green zone, the project manager does not need to take any action. In the later stage of the project, as long as the buffer consumption reaches the red zone, even if the single activity does not consume much buffer, but the accumulated buffer consumption is already in the red zone, the project manager should take measures to rush work, which obviously does not conform to the actual implementation of the project. Firstly, static buffer monitoring does not consider the dynamic change of the buffer consuming. Secondly, as the activities are implemented, the project will face a decreasing level of uncertainty, and the static monitoring mechanism may give wrong early warning, causing unnecessary rush behavior decisions. To address the shortcomings of the Static Buffer Monitoring Method, Leach proposed the Relative Buffer Monitoring Method, which considers a linear relationship between the chain completion and buffer consumption by setting relative monitoring warning points[3]. However, Leach did not give a specific method to set the linear relationship.

On this basis, subsequent researchers have conducted a large number of studies in the field of buffer management, from Cut-and-Paste Method to Root Square Error Method, to various buffering determination methods based on project activity properties [4–8]; from Static Buffer Monitoring Method to Relative Buffer Monitoring Method, and then to Dynamic Buffer Monitoring Method considering project execution [9–12]. Fewer existing studies have considered both cost and activity risk in buffer management. In this paper, activity cost is considered based on project activity elasticity when buffer is determined, and activity risk is considered in buffer allocation process, then by setting buffer consumption warning point, a project buffer

management method considering activity risk is proposed, which can reduce project cost and improve project management efficiency while ensuring timely completion.

Buffer Sizing Based on Project Activity Properties

Project activity property refers to the multiple properties of each activity, which are used to expand the description of the activity. In critical chain project management, the existing studies have considered the following project activity properties: resource density (including physical resources and information resources), network complexity, overlapping relationship between activities, project complexity, activity flexibility, activity location weight, activity start flexibility, resource sustainability, resource flexibility, activity cost, activity dependency, etc.

In the process of buffer setting, this paper mainly considers two kinds of project activity properties, one is activity elasticity, the other is activity risk.

Buffer Determination Based on Elasticity of Activity

In this paper, activity elasticity is defined as the ratio of the difference between the normal duration of the activity to the minimum emergency duration that can be compressed by a series of measures such as adding resources to the normal duration. In actual projects, some activities cannot be compressed by adding resources and other measures, the activity elasticity of this type of activity is zero.

Additional resources and other measures will inevitably increase the activity cost of the project, we can not blindly pursue the minimum duration of the project regardless of the project cost. Therefore, on the basis of activity elasticity, this paper comprehensively considers the impact of activity cost and determines the buffer size suitable for each activity to be extracted. This approach avoids the huge increase in project cost caused by simply taking all the safe time of the activity out as a project buffer, and ensures the cost effectiveness of the project while ensuring the project duration.

Elastic Coefficient of Project Activity

The activity safe time is defined as the difference between normal duration and emergency duration, and the activity safe time is the maximum buffer time that can be extracted from the activity [11]. Each activity will generate corresponding cost from normal construction duration to emergency construction duration, and the formula of compressed unit time cost is shown in Formula (25.1).

$$AR_i = \frac{Cc_i - Cn_i}{Tn_i - Tc_i} \tag{25.1}$$

where, AR_i is the cost per unit time of activity i; Cc_i is the emergency cost of activity i; Cn_i is the normal cost of activity i; Tn_i is the normal duration of activity i; Tc_i is the emergency duration of activity i.

According to the difference between the unit time cost of the compressed duration and the reward for early completion of the project, the strength suitable for each activity to be compressed, namely the activity elastic coefficient, can be calculated. RP is the reward per unit of time for early completion of the project.

If $\mathrm{AR_i} - \mathrm{RP} \leq 0$, it means that the unit time cost of the activity's compressed duration is less than or equal to the reward for the early completion, it means that the activity can extract all the safe time as a buffer. At this point, the elastic coefficient of the project is the ratio of the difference between the normal duration and the emergency duration of the activity and the normal duration of the activity, as shown in Formula (25.2).

$$K_i = \frac{Tn_i - Tc_i}{Tn_i} \tag{25.2}$$

where, K_i is the activity elastic coefficient of activity i; $(Tn_i - Tc_i)$ is the maximum reasonable buffer time that the activity safe time can be extracted.

If $\mathrm{AR_i} - \mathrm{RP} > 0$, it means that the unit time cost of the activity's compressed construction duration is bigger than the reward of the project's early completion, it means that the activity cannot extract all the safe time. When the difference between the compression cost per unit time and the reward for early completion is larger, it indicates that the activity is less suitable to extract too much safe time as a buffer. In this case, an appropriate cost correction coefficient should be multiplied when calculating the activity elastic coefficient, and the difference between the maximum cost per unit time of the compressed duration in all activities and the early completion reward is used as a comparison parameter. The activity elastic coefficient is shown in Formula (25.3).

$$K_i = \frac{Tn_i - Tc_i}{Tn_i}\left(1 - \frac{AR_i - RP}{AR_{\max} - RP}\right) \tag{25.3}$$

where, K_i is the activity elastic coefficient of activity i; $AR_{\max}$ is the maximum unit time cost of the compressed duration in all activities; $(Tn_i - Tc_i)$ is the activity safe time, that is, the maximum reasonable buffer time; $[1 - (AR_i - RP)/(AR_{\max} - RP)]$ is the cost correction coefficient.

Project Buffer Sizing

According to the elastic coefficient of project activity determined by Formula (25.2) and (25.3), the extracted buffer of activity i is shown in Formula (25.4).

$$PB_i = Tn_i \times K_i \tag{25.4}$$

where, PB_i is the buffer size that activity i is extracted.

According to the activity buffer formula, the project buffer of the critical chain is shown in Formula (25.5).

$$PB = \sum_{i=1}^{n} PB_i \tag{25.5}$$

where, PB is the project buffer size.

The project buffer can be determined according to the activity elasticity. Placing the project buffer at the end of the critical chain can realize the risk sharing of the project. The feeding buffer calculation method is similar to the project buffer calculation method. This paper mainly studies the buffer sizing and monitoring on the critical chain, so the feeding buffer calculation on the non-critical chain will not be described too much.

Buffer Allocation Based on Activity Risk

Activity risk refers to the risk events faced by activities in the project (in this paper, activity resource constraint risk and duration risk are comprehensively defined as activity risk), including the probability of risk occurrence and the degree of impact on activities. Each activity faces different types and quantities of risks, and the uncertainty brought by risks to activities is also different. Therefore, activity risk can be used as an important indicator to measure the uncertainty of activities.

After determining the appropriate buffer size for each activity to be extracted, we choose to allocate buffer to individual project activities. The traditional method is to set all buffer together in a fixed position in the project chain. Generally, the project buffer is set at the end of the critical chain and the feeding buffer is inserted at the intersection of the critical chain and non-critical chain. This centralized setting of buffer is conducive to the overall project response to the impact of uncertain factors, and has a higher completion probability, but centralized settings are the overall protection of the project, the buffer protection for individual activities is not enough, which easily affects the stability of the entire project plan. When the buffer is inserted into each activity, a relatively robust scheduling plan can be generated.

There are various risks and uncertainties in modern engineering projects, so we incorporate the activity risk into the calculation of the buffer allocation weight. The influence of the level of certainty enables activities with high uncertainty to be allocated more buffer time, and activities with low uncertainty to be allocated less buffer time. Such buffer allocation is more reasonable in actual projects.

Activity Risk Impact Coefficient

Assume that the set of risks affecting the project schedule is RS = {R1, R2, R3…, Rj} “, where each risk event is denoted as “R (risk) = {P, I}”, where P represents the probability of risk occurrence; I represents the impact of the risk on the activity duration. Suppose the project has n activities, each of which has m risk events. The influence coefficient of activity risk is calculated based on the above assumptions.

Risk exposure is the product of risk occurrence probability and the loss caused by risk, which can be used to measure the importance of risk. It is denoted as RE, and its formula is shown in Formula (25.6).

$$\mathrm{RE} = \mathrm{P} \times \mathrm{I} \tag{25.6}$$

where, RE is the risk exposure; P is the probability of risk occurrence; I is the degree of impact of risk occurrence on the activity duration.

For activity i, the calculation of risk impact coefficient should take full account of the impact of all risk events in the execution of the activity. The risk exposure of all risk events should be multiplied by 1 respectively, which is the risk impact coefficient of the activity, as shown in Formula (25.7).

$$RI_i = \prod_{j=1}^{m} \left(I_j \times P_j + 1\right) \tag{25.7}$$

where, RI_i is the impact of the risk event of activity i on its duration; m is the number of risk events of activity i; I_j is the impact to the duration of activity i when risk j occurs, and P_j is the probability of risk j occurring.

Buffer Allocation Considering Activity Risk

A. The initial buffer allocation weights

When the impact of activity risk is not considered, the weight of buffer allocation is only related to the duration of the activity after the extraction, and the larger the duration after the extraction, the larger the buffer allocated to the activity, and vice versa. The initial buffer allocation weight is calculated as shown in Formula (25.8) [11].

$$\omega_i = \frac{Tn_i - PB_i}{T - PB} \tag{25.8}$$

where, ω_i is the initial buffer allocation weight; Tn_i is the normal duration of activity i; PB_i is the buffer extracted for activity i; T is the normal duration of the project; PB is the project buffer.

B. Revised buffer allocation weights

Based on the weight of initial buffer allocation, the activity risk impact is considered. For activity i, multiply its initial buffer allocation weight with its risk impact factor to obtain its combined weight impact coefficient. compare the combined weight impact coefficient of activity i with the value obtained by accumulating the combined weight impact coefficients of all activities on the chain, which is the revised buffer allocation weight of activity i. and its calculation is shown in Formula (25.9).

$$\omega_i^R = \frac{\omega_i \times RI_i}{\sum_{i=1}^{n}(\omega_i \times RI_i)} \tag{25.9}$$

where, ω_i^R is the revised buffer allocation weight; n is the total number of activities on the chain. The sum of the revised buffer allocation weights of all activities on the chain is 1.

Therefore, the buffer size allocated to each activity while considering the impact of activity risk is shown in Formula (25.10).

$$PB_i' = PB \times \omega_i^R \tag{25.10}$$

where, PB_i' is the buffer size allocated to activity i; PB is the project buffer; ω_i^R is the revised buffer allocation weight.

Dynamic Monitoring of Project Schedule

Buffer Monitoring Warning Point Setting

Two warning points will be set for each activity buffer, the purpose of which is to determine whether the activity will exceed the planned time and whether the crush measures are required.

In this paper, the setting of warning points also adopts the trisection method, that is, the buffer zone is divided into three equal parts, and the warning points are set at 33% and 66% respectively. PB_i is the buffer extracted from activity i, PB_i' is the buffer allocated for activity i. When $PB_i \geq PB_i'$, the early warning points a and b were respectively a $= 33\% \times PB_i'$, b $= 66\% \times PB_i'$; when $PB_i < PB_i'$ the early warning points a and b were respectively a $= 33\% \times PB_i$, b $= 66\% \times PB_i$. The above formula takes the smaller one between the buffer to which the activity i is extracted and the buffer to which it is allocated as the parameter for setting the warning point. When $PB_i \geq PB_i'$, that is, the extracted buffer of the activity is bigger than or equal to the allocated buffer, indicating that the compression cost of this activity is small, and the faster the completion is, the better; when $PB_i < PB_i'$, the compression cost of this activity is relatively large, and more buffer need to be allocated, but the early warning point setting is based on the extracted buffer, in order

to consume as little buffer as possible during the project execution process, so as to avoid the more allocated buffer being wasted as safe time.

Dynamic Monitoring

Each activity execution process is regarded as a buffer monitoring cycle, that is, a rolling period, and activity i is the monitoring point i. In this paper, the redistribution of buffer is mainly carried out according to the accumulative consumption of buffer in the rolling period of the project so as to improve the ability of replanning in the process of buffer monitoring. During the implementation of activities, some activities may consume much buffer, while others may consume less. In order to allocate the residual buffer of activities with less buffer consumption to the subsequent activities or the buffer used to offset the excessive consumption of some activities, literature [11] put forward the concept of accumulative project buffer (APB) and used accumulative buffer to control the project. When activity i ends, the cumulative buffer of this activity is shown in Formula (25.11).

$$APB_i = PB_i' - PBA_i \tag{25.11}$$

where, APB_i is the accumulated buffer of activity i, and PBA_i is the buffer consumed during the actual execution of activity i.

Project cumulative buffer APB is shown in Formula (25.12).

$$APB = \sum_{i=1}^{n} APB_i = \sum_{i=1}^{n} (PB_i' - PBA_i) \tag{25.12}$$

The project is dynamically monitored by setting a rolling period for the project. Whether to change the allocation buffer of each activity in the next rolling period is determined according to the accumulated buffer of the project, there are mainly the following two possible situations:

(1) $APB \geq 0$, that is, the completion of activities is good, and the project buffer plan does not need to be changed due to the change of the cumulative project buffer;
(2) $APB < 0$, in other words, if the activity is not well completed and delayed, the project buffer plan of the next rolling period shall be changed to share the negative value of the accumulated buffer of the project.

Dynamic Monitoring Steps

The dynamic buffer monitoring steps of this paper are as follows:

Step 1: Determine the critical chain of the project before the project implementation;
Step 2: Calculate the elastic coefficient of project activities;
Step 3: Calculate the buffer that each activity is suitable for being extracted through the elastic coefficient, and accumulate it to get the project buffer;
Step 4: Consider the impact of risk events to calculate the risk impact coefficient of each activity;
Step 5: Based on the influence coefficient of activity risk, the buffer allocation weight is revised, and the buffer monitoring amount of each activity is obtained according to the revised weight.
Step 6: Track the project and monitor it at the monitoring point i (activity i);
Step 7: Check the buffer consumption:

(1) If buffer consumption is below the warning point A, no action is required;
(2) If buffer consumption is between warning point A and B, monitoring should be strengthened and plans should be made to deal with possible problems;
(3) If buffer consumption is above the warning point B, check whether the project has been completed. If it has been completed, no action is required; if not, timely measures should be taken to prevent the project from being delayed;

Step 8: Extract the remaining buffer at the monitoring point;
Step 9: Incorporate the remaining buffer into the subsequent activity buffer (reduce if it is negative, add if it is positive);
Step 10: Monitor the buffer consumption at the next monitoring point and repeat steps 6 to 9 until the project is completed.

Simulation Study

In order to verify the effectiveness of the proposed method in this paper, the buffer monitoring method is compared with the Static Buffer Monitoring Method (SBMM) and the Root Square Error Method (RSEM). The case selected in this paper has 10 activities in the critical chain, with a total planned duration of 168 days and a planned cost of 1,242,000 yuan. The project network diagram is shown in Fig. 25.1, the project activity duration and cost base data are shown in Table 25.1, and the project early completion bonus RP = 6000 yuan/day.

The activity elastic coefficient and activity extracted buffer data calculated according to Formula (25.1)–(25.4) are shown in Table 25.2.

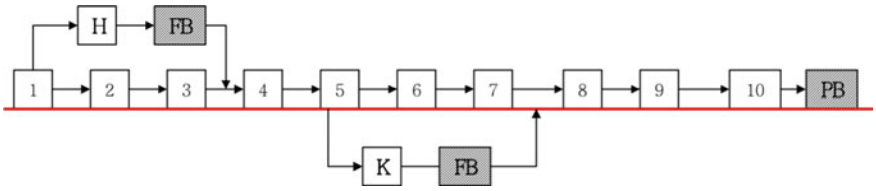

Fig. 25.1 Critical chain project network diagram

According to Table 25.2, we can calculate the planned duration of the project is 168 days, of which the project duration is 124 days and the project buffer is 44 days. And the result calculated according to the RSEM is 30 days for the buffer and 84 days for the duration.

In this project, it is assumed that there are three risks for activity 1 and only one risk for the remaining activities. The identification of the project risk events can be determined and assessed based on historical data or using Delphi Method and Bayesian network method. Since the project has historical data to refer to, the uncertainty of the risk events for each activity of the project is estimated directly by the project staff based on historical data. The risk impact factor for each activity can be calculated from Formula (25.7), as shown in Table 25.3.

The activity buffer allocation data calculated according to Formula (25.7)–(25.9) are shown in Table 25.4.

As can be seen from Table 25.4, the buffer extracted and the buffer allocated are not the same for each activity. It can be calculated that the buffer assigned to the green zone, yellow zone and red zone in the static buffer monitoring method are all 10 days each. While the relative buffer monitoring method divides the buffer into 3 parts as the completion rate changes, the green zone is divided by a straight line determined by (0, 15% $\times$ 30) and (100%, 75% $\times$ 30) points, and the red zone is divided by a straight line determined by (0, 30% $\times$ 30) and (100%, 90% $\times$ 30) points.

After obtaining the above basic data, 1000 simulations of the three buffer monitoring methods were conducted by Matlab, and the corresponding performance of the three buffer monitoring methods in terms of duration and cost were shown in Figs. 25.2 and 25.3.

From Figs. 25.2 and 25.3, it can be seen that the buffer monitoring method proposed in this paper has a greater advantage in terms of both duration and cost. The average duration of the SBMM is 148 days, the average duration of the RBMM is 142 days, and the average duration of the NEW buffer monitoring method is 128 days. The average cost of the SBMM is 1,537,000, the average cost of the RBMM is 1,484,000, and the average cost of the NEW buffer monitoring method is 1,325,000. The buffer management method proposed in this paper has obvious advantages in both duration and cost. The activity cost and early completion reward factors are considered in the buffer determination, and the activity risk factors are considered in the buffer allocation, which make the buffer extraction and allocation more reasonable. Combined with the setting of rolling period, the accumulative

Table 25.1 Basic data of critical chain project

Activity number	1	2	3	4	5	6	7	8	9	10
Normal duration (days)	8	8	12	24	36	28	20	8	16	8
Normal cost (yuan)	36,000	24,000	120,000	144,000	270,000	224,000	200,000	40,000	128,000	56,000
Compressed duration (days)	3	4	8	20	16	12	12	3	6	4
Compressed cost (yuan)	96,000	48,000	152,000	216,000	460,000	408,000	320,000	90,000	268,000	96,000

Table 25.2 Activity elastic coefficient and extracted buffer

Activity number	1	2	3	4	5	6	7	8	9	10
Elastic coefficient	0.31	0.5	0.28	0	0.39	0.31	0.1	0.42	0.21	0.33
Extracted buffer (days)	3	4	3	0	14	9	2	3	3	3
Duration (days)	5	4	9	24	22	19	18	5	13	5

Table 25.3 Activity risk impact factor

Activity number	Risk events	Probability	Impact	Risk impact
1	A	0.4	0.6	0.54
	B	0.6	0.3	
	C	0.5	0.1	
2	D	0.6	0.3	0.18
3	E	0.5	0.6	0.3
4	F	0.5	0.8	0.4
5	G	0.5	0.7	0.35
6	H	0.1	0.3	0.03
7	I	0.4	0.3	0.12
8	J	0.3	0.8	0.24
9	K	0.2	0.6	0.12
10	L	0.2	0.7	0.14

Table 25.4 Activity buffer allocation data

Activity number	1	2	3	4	5	6	7	8	9	10
Duration (days)	5	4	9	24	22	19	18	5	13	5
Extracted buffer (days)	3	4	3	0	14	9	2	3	3	3
Allocated buffer (days)	2.2	1.4	3.4	9.6	8.5	5.6	5.8	1.8	4.2	1.6

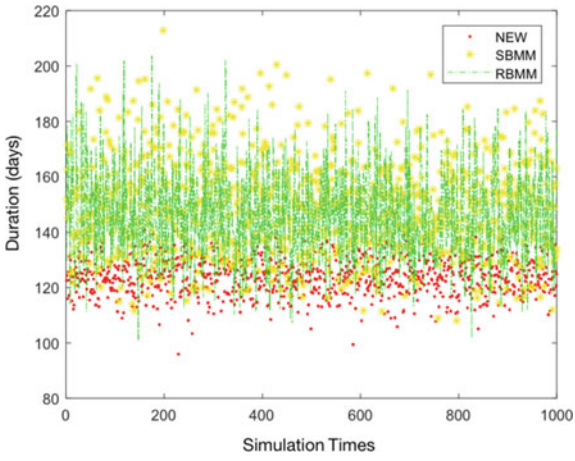

Fig. 25.2 Contrast of duration

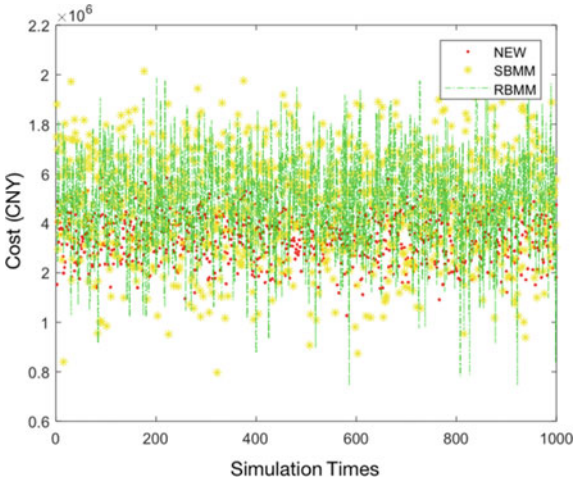

Fig. 25.3 Contrast of cost

buffer can be reallocated in time, which effectively reduces the project duration and cost.

Conclusion

Based on the idea of critical chain, we propose an implementation plan for dynamic monitoring of project schedule considering activity risks. When extracting the project buffer, because the compression of activity duration will lead to the increase of activity cost, not all activities are suitable to be compressed to the shortest duration, the activity cost is compared with the reward of early completion, and the elastic coefficient of activity is calculated to determine the buffer size suitable for extraction of each activity. Due to the high risk and uncertainty of modern projects, we introduce activity risk into buffer allocation, comprehensively considers the compressed activity duration and activity risk coefficient, calculate the weight of comprehensive buffer allocation, and obtains the buffer size allocated for each activity. Dynamic monitoring is adopted in the process of buffer monitoring, which not only ensures the overall schedule of the project but also protects the execution of individual activities. The final simulation shows that the buffer management scheme not only reduces the project duration but also reduces the project cost, which proves the effectiveness of the buffer management scheme for project schedule monitoring.

In this paper, the buffer management method of critical chain project considering activity risk provides a more scientific and reasonable solution to the actual project schedule management problem. Although the proposed method has made some improvements on the existing buffer management method, the monitoring method in this paper still only focuses on the current buffer consumption at the monitoring point to make behavioral decisions, and does not analyze the subsequent

buffer consumption trend. The future research will introduce the buffer prediction method to conduct comprehensive buffer monitoring.

References

1. Goldratt, E. M. (1997). *Critical chain.* North River Press.
2. Newbold, R. C. (1998). *Project Management in the fast lane: Applying the theory of constraints.* CRC Press.
3. Leach, L. P. (2005). Critical chain project management. Artech House.
4. Chen, C., & Wei, W. (2003). Critical chain management based on PERT/CPM. *China Management Science, 11*(6), 35–39.
5. Tukel, O. I., Rom, W. O., & Eksioglu, S. D. (2006). An Investigation of buffer sizing techniques in critical chain scheduling. *European Journal of Operational Research, 172*(2), 401–416.
6. Zhang, J., Song, X., & Díaz, E. (2014). Buffer sizing of critical chain based on attribute optimization. *Concurrent Engineering: Research and Applications, 22*(3), 253–264.
7. Zhang, J., Song, X., & Díaz, E. (2016). Project buffer sizing of a critical chain based on comprehensive resource tightness. *European Journal of Operational Research, 248*(1), 174–182.
8. Bie, L., Cui, N., & Zhang, X. (2012). Buffer sizing approach with dependence assumption between activities in critical chain scheduling. *International Journal of Production Research, 50*(24), 7343–7356.
9. Bie, L., & Cui, N. (2010). Research on the monitoring method of critical chain dynamic buffer. *China Management Science, 18*(6), 97–103.
10. Zhang, J., Jia, S., & Estrella, D. (2018). Dynamic monitoring and control of a critical chain project based on phase buffer allocation. *Journal of the Operational Research Society, 69*(12), 1966–1977.
11. Zhang, J., & Ji, F. (2020). Research on the buffer management method of critical chain projects based on activity elasticity. *Journal of Management, 17*(6), 924–930.
12. Hu, X., Cui, N., et al. (2017). Improved critical chain buffer management framework considering resource costs and schedule stability. *Flexible Services and Manufacturing Journal, 29*(2), 159–183.

Chapter 26
Complex Task Assignment of Aviation Emergency Rescue Based on Multiagent Reinforcement Learning

Che Shen and Xianbing Wang

Abstract Emergency rescue is a powerful countermeasure to disasters, among which Aviation Emergency Rescue (AER) is irreplaceable thanks to its unique aviation attribute. However, traditional optimization methods are not capable of the dynamic task allocation of AER. This study performs a Multiagent Reinforcement Learning (MARL) model to handle the complex task assignment problem faced in AER, carries out a detailed analysis of the problem, and do comparative experiments with the Nearby policy and Best-fit policy. The result shows that the MARL model outperforms other simple models in AER.

Keywords Aviation emergency rescue · Multiagent reinforcement learning · Complex task assignment

Introduction

China has always been a country facing a serious threat from natural disasters. According to the Basic Situation of Natural Disasters in 2021 posted by the Ministry of Emergency Management, China's natural disaster situation is complex and severe, and extreme weather and climate events are frequent. Natural disasters are mainly floods, hail, droughts, typhoons, earthquakes, geological disasters, cryogenic freezing, and snow disasters, while sand and dust storms, forest and grassland fires, and marine disasters also occurred to varying degrees. Natural disasters affected 107 million people, left 867 dead or missing, 5.738 million relocated, and caused a direct economic loss of 334.02 billion yuan.

To reduce the damage caused by disasters, the emergency rescue has become a powerful countermeasure. In all kinds of emergency rescue, Aviation Emergency

C. Shen (✉)
Department of Data Science and Technology, The Hong Kong University of Science and Technology, Hong Kong SAR 999077, China
e-mail: cshenae@connect.ust.hk

X. Wang
College of Economics and Management, Nanjing University of Aeronautics and Astronautics, Nanjing 211106, Jiangsu, China

R. Qiu et al. (eds.), *City, Society, and Digital Transformation*, Lecture Notes in Operations Research, https://doi.org/10.1007/978-3-031-15644-1_26

Rescue (AER), with its unique aviation attribute, is competent for many tasks that ground rescue cannot complete, which makes it irreplaceable in emergency rescue.

When it comes to AER, task assignment is one of the most important parts. Tasks in AER vary from one to another, with different release times, required resources, and urgency. A reasonable task assignment is indispensable for efficient AER.

However, thanks to the complexity of the task assignment of AER, traditional methods face great difficulty in finding a reasonable assignment in time. Given this, this study intends to adopt the modeling method of Multiagent Reinforcement Learning (MARL) to establish a dynamic task allocation model.

Related Works

Related Works of Complex Task Assignment

Complex task assignment has always been a valued area of study. It has been intensively and extensively studied and applied in many fields. In the agriculture production area, Haibo Wang presents a heuristic algorithm using k-Opt as a diversification strategy embedded within the Tabu search [1]. In the transportation field, Di Wang and Hongbin Deng use their proposed algorithm, named TFDueling, to solve task allocation and path planning problems and let the robot reach the target position without collision [2]. In the cloud computing area, Hamza Baniata, Ahmad Anaqreh, and Attila Kertesz propose a model PF-BTS which enables fog components to perform cloud tasks at the edge of the network [3]. Generally, various algorithms have been developed for complex task assignments and fruitful results are gained.

Related Works of MARL

Compared with complex task assignment, MARL is an emerging field developed based on reinforcement learning. Some researchers focus on the improvement of the algorithm of MARL. For instance, Jacopo Castellini quantifies how well various approaches can represent the requisite value functions and identify the reasons that can impede good performance [4]. At the same time, Mudhafar Al-Saadi focuses on control strategies based on multiagent communication and reinforcement learning [5]. Others put this emerging technology into practice. Wei Qin proposes a dynamic task assignment method for vehicles in urban transportation systems based on MARL [6]. Salman Sadiq Shuvo models the sea-level rise socioeconomic system as a Markov decision process and simulated it using MARL [7]. To sum up, though still an emerging algorithm, MARL has gradually attracted the attention of researchers.

Current Status of AER in China

China is a disaster-prone country. The high frequency of natural disasters and the heavy losses lead to the contradiction between China's existing emergency rescue capacity and the requirement for disaster rescue. AER is one of the most common emergency measures to deal with natural disasters and various emergency events, while China's aviation emergency rescue system still needs continuous improvement.

Some researchers have focused on resource allocation and task assignment aspects in AER, using methods with practicality to optimize the allocation. Some scholars build a multi-intelligent body system, MAS, to optimize task assignment to accomplish different kinds of rescue tasks [8], others build a multi-subject scheduling system to optimize aircraft search task assignment and change dynamically with the changing state of the disaster area [9]. In general, researchers in China have been aware of the importance of ARE, and many studies on this have emerged.

Comments on Related Works

From the research shown above, algorithms for complex task assignments have been fully studied, and increasing efforts are put into the study of MARL. But only finite research combines these two fields, among which few use them to deal with emergency rescue. The vigorous development of related technologies and the urgent need for algorithms for AER have formed a serious imbalance. As a result, this study focuses on using MARL algorithms to handle complex task assignment issues faced in AER.

Task Modeling

Task Description

When using AER to respond to sudden natural disasters, different kinds of tasks occur on different occasions from time to time. However, helicopters ready for the AER are always limited, and one helicopter can only perform some of these kinds of tasks. Traditional optimization algorithms, such as generic programming, output a task allocation based on complete task information, so they are not as suitable as reinforcement learning which outputs a strategy set when dealing with dynamic task assignments in AER.

When evaluating a task assignment in AER, timeliness of task completion is always the top priority, while the economic cost of helicopter flight is not a consideration. However, due to the limitation of the number of helicopters reachable and the frequency of tasks occurring, an assignment can hardly complete all tasks on time.

Therefore, the preferred assignment is the one that leads to the highest overall time satisfaction.

Basic Assumptions

In a realistic AER environment, the terrain conditions are very complicated, causing great difficulties to the algorithm design. To simplify the problem, the rescue positions are assumed to be points on an *n-by-n* grid.

Meanwhile, rescue tasks occur continuously on the time scale, while MARL can only deal with task assignments at a discrete-time point. To fit the model to MARL, time is divided into short periods, and MARL is used in each period.

What's more, the benefit of completing the task does not decrease uniformly with the increase of time, and the relationship between the benefit of the task and time varies at different stages, so a step function is introduced, through which the task response time is transformed into the time satisfaction of the task. The step function is shown as follows:

$$f_i^{t^*} = \begin{cases} 1 & t^* \le t_1 \\ (1-r_0)\left(\frac{t_2-t^*}{t_2-t_1}\right)^2 + r_0 & t_1 < t^* \le t_2 \\ r_0\left(\frac{t^*-t_2}{t_{\max}-t_2}\right)^2 + r_0 & t_2 < t^* \le t_{\max} \\ 0 & t^* > t_{\max} \end{cases}$$

where t_1 represents the optimal task allocation time, during which the task benefit is the best as long as the task is completed. After t_1 time, task benefit continuously decreases with time satisfaction, until t_2 time satisfaction drops to r_0, during which task completion is still effective although the benefit is reduced. If the task is still not complete at t_2, the time satisfaction drops sharply, and the benefit of completing the task shrinks in this stage until $t = t_{\max}$, when the task failure time is reached, the time satisfaction becomes 0 and the task fails. Even if the task is completed, there is no benefit (Fig. 26.1).

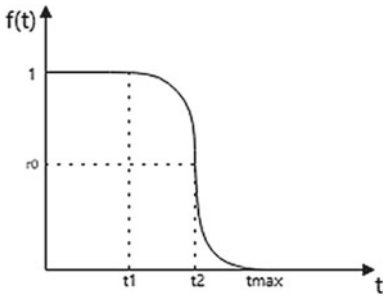

Fig. 26.1 The graph of the step function

Further, as rescue missions are frequent and helicopters are scarce, one helicopter is not supposed to be unoccupied for a long time, so the algorithm will not consider the action of staying still or moving to a position without a rescue mission.

Finally, for simplification, the difference of importance between different kinds of tasks and the difference in time cost between tasks will not be considered at this moment.

Decision Variable

The set of possible positions for rescue missions is defined as

$$Positions = \{0, 1, \ldots, n^2 - 1\}$$

where position $n(p-1)+q-1$ represents the point (p, q) in the grid.

The decision variable is defined as

$$D_j^i \in \{0, 1, \ldots, n^2 - 1\}$$

where D_j^i represents the position of *helicopter i* during *period j*.

Constraints

In AER, tasks can be separated into different categories, and one helicopter is only able to complete part of all kinds. So, the constraint of the model is the limitation of tasks that a helicopter can do.

MARL Model Building

Environment

The environment of the MARL is mainly made up of *helicopter*, *position*, and *task*.

helicopter is defined by

$$helicopter = [number, type, postion, capacity]$$

where *number*, *type,* and *position* represent the serial number, type, and position of the helicopter, and *capacity* shows which types of tasks the helicopter is capable of.

position is defined by

$$position = [number, x, y]$$

where *number* represents the serial number of the position and x, y are the x and y coordinates of the position.

task is defined by

$$task = [number, time, position, type]$$

where *number*, *type,* and *position* represent the serial number, type, and position of the task, and *time* represents the post time of the task.

Agents

The agents of MARL are chosen to be the helicopters in this case.

Observation of the Agent

In MARL, the actions of one agent are based on the observation of this agent, so the design of the observation is crucial to the final result of the model.

In this task, the observation of the agent consists of two parts, the local observation from a specific helicopter, and the global observation from the overall situation. The separation of local and global observations encourages each agent to finish its own job as well as cooperate with each other for the whole task.

The global observation is the task to be done at that moment and the number of types of tasks that can be completed by unoccupied helicopters.

The local observation of a helicopter is the shortest distance it from the nearest capable task and the fitness of the task which is fittest to this helicopter. Manhattan Distance is used to calculate the distance, i.e.

$$Distance = |x_1 - x_2| + |y_1 - y_2|$$

where (x_1, y_1), (x_2, y_2) are the coordinates of two points on the grid.

To describe the fitness of a task, not only the capacity of this agent but also the capacity of other helicopters is considered. For example, if a task can only be done by this helicopter, then the fitness of the task to this helicopter will be relatively high.

Table 26.1 Capacity of helicopters

		Task type			
		1	2	3	4
Helicopter	AW139	1	1	1	1
	AW199Kx	0	1	0	1
	BELL412	1	0	1	0
	H125	1	0	0	0
	AC311A	0	1	0	0

Table 26.2 Unfitness for tasks for helicopters

		Task type			
		1	2	3	4
Helicopter	AW139	3	3	3	3
	AW199Kx	5776	1	5776	1
	BELL412	1	5776	1	5776
	H125	0	5776	5776	5776
	AC311A	5776	0	5776	5776

Tables 26.1 and 26.2 shows the *capacity* and *unfitness* (the reverse of *fitness*) for tasks for each helicopter. For a helicopter, if its *capacity* for a task is 0, then its *unfitness* for this task is a big value (here chosen to be 5776). If its *capacity* for a task is 1, then its *unfitness* for this task is the number of tasks it is capable of besides this task. For example, *helicopter AW139* is capable of *task 1*, together with *task 2, 3* and *4*, so its *unfitness* for *task 1* is 3.

Actions

One agent has three actions to choose from: staying at the current position, flying to the nearest capable task, and flying to the fittest task. The agents will choose from these actions based on their observations.

Reward

To design the reward of the action of an agent, both local reward and global reward are considered. If a helicopter completes its task, it will get a fixed local reward. Meanwhile, a global reward will be given to every agent due to the overall time

Table 26.3 Information of helicopters

Number	Type	Position (initial)	Capacity
0	AW139	0	[1,1,1,1]
1	AW119Kx	0	[1,1,0,0]
2	BeLL412	0	[1,0,1,0]
3	H125	0	[1,0,0,0]
4	AC311A	0	[0,1,0,0]

where [1,0,1,0] represents this helicopter is capable of task types 1 and 3.

satisfaction, which is the sum of the time satisfaction of all tasks. Also, to encourage cooperation between agents, a heavier weight will be given to the global reward.

Processing

In a period, each agent acts individually, but the reward will be given after this round. The process will terminate after all tasks are done and no tasks occur anymore.

Experiment

This study uses the following developing environment:

Programming language: Python 3.8
MARL environment: Pettingzoo [10], Stable Baselines 3
RL training algorithm: PPO (Proximal Policy Optimization).

Data Simulation

helicopter: See Table 26.3.
position: let n be 8 to form an 8-by-8 grid.
task: See Table 26.4.

Result and Analysis

The results of the experiment are inspiring. For instance, an illustration of the running process which highlights the fruitfulness of the algorithm is shown as follows (Fig. 26.2):

Table 26.4 Information of tasks

Number	Time	Position	Type
0	1	1	1
1	1	7	2
2	1	4	1
3	1	8	3
4	2	11	4
5	2	16	4
6	2	2	1
7	2	24	3
8	3	0	1
9	3	38	4
10	3	51	3
11	4	7	4
12	4	14	2
13	4	48	1
14	4	51	3
15	5	60	1
16	5	27	1
17	5	34	2
18	6	40	3
19	6	18	2

From this illustration, though *helicopter* AW139 is at *position* (1,0) at *Clock 2*, it does not go to the nearest task at *position* (2,0), but instead goes to a farther task at *position* (3,1), and lets *helicopter* H125 complete the task at *position* (2,0) at *Clock 3*. This shows that the helicopters have a sense of cooperation during training.

The result of the MARL model is shown below. For comparison, the result of the Nearby model (a helicopter always goes to the nearest capable task) and the Best-fit model (a helicopter always goes to the task with the highest fitness) is shown as well (Table 26.5).

From the result above, the MARL model outperforms simple models like the Nearby model and Best-fit model.

Conclusion

This study performs a MARL model to handle the complex task assignment problem faced in AER. Firstly, the problem is modeled, and assumptions and constraints are made to modify the decision variable. Secondly, the MARL model is built based on the processed model. Lastly, the experiment results of the MARL model show that

```
Clock:2-----------------
Position_0(0,0):   Tasks=[]; Helicopters=['H125[1, 0, 0, 0]']
Position_1(1,0):   Tasks=[-1]; Helicopters=['AW139[1, 1, 1, 1]']
Position_2(2,0):   Tasks=[1]; Helicopters=[]
Position_4(4,0):   Tasks=[-1]; Helicopters=['AW119Kx[1, 1, 0, 0]/busy']
Position_7(7,0):   Tasks=[-2]; Helicopters=['AC311A[0, 1, 0, 0]/busy']
Position_8(0,1):   Tasks=[-3]; Helicopters=['BeLL412[1, 0, 1, 0]']
Position_11(3,1):   Tasks=[4]; Helicopters=[]
Position_16(0,2):   Tasks=[4]; Helicopters=[]
Position_24(0,3):   Tasks=[3]; Helicopters=[]
total rewards: 130.0 {'AW139': 30.0, 'AW119Kx': 30.0, 'BeLL412': 30.0, 'H125': 10.0, 'AC311A': 30.0}
Clock:3-----------------
Position_0(0,0):   Tasks=[1]; Helicopters=[]
Position_2(2,0):   Tasks=[-1]; Helicopters=['H125[1, 0, 0, 0]']
Position_4(4,0):   Tasks=[]; Helicopters=['AW119Kx[1, 1, 0, 0]']
Position_7(7,0):   Tasks=[]; Helicopters=['AC311A[0, 1, 0, 0]/busy']
Position_11(3,1):   Tasks=[-4]; Helicopters=['AW139[1, 1, 1, 1]/busy']
Position_16(0,2):   Tasks=[4]; Helicopters=[]
Position_24(0,3):   Tasks=[-3]; Helicopters=['BeLL412[1, 0, 1, 0]']
Position_38(6,4):   Tasks=[4]; Helicopters=[]
Position_51(3,6):   Tasks=[3]; Helicopters=[]
total rewards: 240.0 {'AW139': 60.0, 'AW119Kx': 40.0, 'BeLL412': 60.0, 'H125': 40.0, 'AC311A': 40.0}
```

Fig. 26.2 An illustration of the running process

Table 26.5 Results of different models

	Total rewards	Average task completion time	Standard deviation
MARL model	595	1.9	1.37
Nearby model	300	2.1	1.76
Best-fit model	260	2.6	2.46

it outperforms other simple models, which means the proposed method provides a fruitful application of MARL on AER.

Traditional task allocations in AER are mainly based on experience, which is neither accurate nor reliable. This study provides a scientific complex task assignment

method for dynamic and emergency AER, which is critical to timely and effective emergency rescue.

There are still some important challenges not addressed in this study and will be considered in the future work. One direction for future work is to modify some assumptions and constraints in this study, so the model would become closer to reality. For instance, instead of using an *n-by-n* grid to represent the rescue site, a detailed map may be given to provide more information about the ARE. Another direction is to summarize the rules through the training data of MARL, so not only the task assignment itself but also principles of task assignment can be obtained.

Acknowledgements This research is supported by the National Key Research and Development Program of China (Grant No.2016YFC0802603).

References

1. Wang, H., et al. (2021). The multi skilled multi period workforce as signment problem. *International Journal of Production Research, 59*(18), 5477–5494.
2. Wang, D., & Deng, H. (2021). Multirobot coordination with deep reinforcement learning in complex environments. *Expert Systems with Applications, 180*, 115–128.
3. Baniata, H., Anaqreh, A., & Kertesz, A. (2021). PF BTS: A privacy aware fog enhanced blockchain assisted task scheduling. *Information Processing & Management, 58*(1), 102–393.
4. Castellini, J., et al. (2021). Analysing factorizations of action value networks for cooperative multi agent reinforcement learning. *Autonomous Agents and Multi Agent Systems, 35*(2).
5. Al Saadi, M., Al Greer, M, & Short, M. (2021). Strategies for controlling microgrid networks with energy storage systems: A review. *Energies, 14*(21).
6. Qin, W., et al. (2021). Multi agent reinforcement learning based dynamic task assignment for vehicles in urban transportation system. *International Journal of Production Economics, 240*, 108–251.
7. Shuvo, S. S., et al. Modeling and simulating adaptation strategies against sea level rise using multiagent deep reinforcement learning. *IEEE Transactions on Computational Social Systems*.
8. Wu, Q., et al. (2013). The research of multi agent system task allocation based on auction. In Proceedings of the International Conference on Computer, Networks and Communication Engineering (ICCNCE 2013), 2013 (Vol. 30, pp. 214–217).
9. Wang, Y., Pan, W., & Liu, K. Multi agent aviation search task allocation method. In 2019 3rd International Conference on Artificial Intelligence Applications and Technologies (AIAAT 2019), 2019 (p. 646).
10. https://www.pettingzoo.ml

Chapter 27
Online Portfolio Management: A Survey of Data-Driven Approaches

Rudraksh Mishra, Abhay Chamu Haridas, Nikhitha Khunduru, Ambika Chundru, Shahed Mahbub, and Dusan Ramljak

Abstract During these unprecedented times, online portfolio management equipped with the right set of tools and guided financial service is a way to financial stability. Wealth management and personalized investments rely solely on the investor's decisions. Most of these decisions are a product of the state of the financial market, and the ability of the investor to perceive and manage risks that come as a part of investing in the market. The increasing complexity of the investment environment has created a need for better quality financial advice. It is essential to assess the client's risk tolerance to cater to the latter's needs based on this assessment. This work uses a systematic mapping methodology to encompass 21,400 works related to personalized investments, the factors that decide the financial risk tolerance (FRT) and risk-taking behaviour (FRB), and the role machine learning can play to carve out the picture of the state of the art. This review revealed that 4 survey papers and 11 articles can help us identify areas of research to build personalized online portfolio management tools with clients' risk tolerance assessments. The results indicate that financial institutions are investing heavily in data-driven approaches to risk management and customer behaviour prediction, but middle and lower-income households have largely been left out of this process.

Keywords Personalized investments · Asset management · Machine learning · Data-driven decision-making · FRT · FRB · Risk assessment

Introduction

Financial instability, one of the dire consequences of the global pandemic, underlines the necessity for planning. Thus, the wealth management scope is rising with a potential to incorporate data-driven approaches to achieve a dynamic portfolio. Wealth management, the financial planning services highest level, covers a large area of financial services processes and products, and includes comprehensive investment

R. Mishra · A. C. Haridas · N. Khunduru · A. Chundru · S. Mahbub · D. Ramljak (✉)
School of Professional Graduate Studies, The Pennsylvania State University, Malvern, PA 19355, USA
e-mail: dusan@psu.edu

R. Qiu et al. (eds.), *City, Society, and Digital Transformation*, Lecture Notes in Operations Research, https://doi.org/10.1007/978-3-031-15644-1_27

management alongside financial advice, tax guidance, estate planning, and even legal assistance [1]. Advisers working with clients in this discipline provide tailored investment strategies and manage their clients' assets. Rotzetter [2] suggests that paradigm should be stated as there is no clear definition of what it really encompasses. For an individual or a set of individuals who want an advisor to suggest actions to take and in which products to invest—in view of the risk appetite of the client and their investment goals, we accept wealth management as the end-to-end process of managing their personal wealth. It would encompass every activity from client acquisition to the closure of the account with that financial service institution (FSI). This paradigm includes providing advice to the client, understanding their investment goals, risk tolerance, financial standing and lifestyles.

Traditionally, wealth managers have aimed their services at the highly affluent [1] and facilitated investments that would minimize the tax exposure of the wealthy. The exclusion of the majority class in wealth management has been exacerbated by market turbulences due to the financial crisis of 2008 and the recent shocks from the Covid-19 pandemic. In fact, according to a recent survey conducted by GOBankingRates,[1] 55% of Americans believe they do not have the money to invest. This is where we believe data-driven approaches in Artificial Intelligence (AI) and Machine Learning (ML) can play a pivotal role. Data and AI are great democratizing forces in financial services. Their synergy fuels progress toward the goal of digital transformation that many FSIs have today [3]. AI is already playing a transformative role in these institutions in creating new revenue streams, empowering risk management, automating processes and enhancing customer retention. According to a survey conducted by the Apache foundation, while currently, only 16% of FSIs have AI integration in all four functions, 64% of those that were surveyed stated that they anticipate employing AI in all categories within the next two years [3]. Concurrently, the growth in big data has far outpaced firms' ability to analyze them leading to rapid developments in AI, Natural Language Processing (NLP), and computer vision algorithms that can provide businesses with the tools needed for real-time analytics and data-driven decision making.

Given the wide paradigm of technologies covered by the terms AI and ML, we drill down their significance in the context of this research. We focus on supervised or unsupervised ML algorithms. Within unsupervised learning there can be clustering, self-organized maps, principal component analysis (PCA), recommender systems/matrix factorization, and deep neural networks [2]. Within supervised learning, there are traditional methods such as linear and polynomial regressions, classifiers such as decision trees, logistic regression, support vector machines, and more complex systems such as random forests, deep neural networks, and autoencoders. Within this paper, we explore in detail the application of these and many other innovative techniques within the financial sector and their implications on personalized wealth investment for most Americans who, potentially have been side-lined from achieving financial security.

[1] https://www.gobankingrates.com/investing/strategy/this-is-why-55-of-americans-arent-investing/

The scope of AI/ML in wealth management can be explored by leveraging a template (that encompasses the key touchpoints) developed in [2]. The following paragraphs illustrate the different stages a client will potentially go through in wealth management and how AI/ML can intertwine at each stage.

Prospecting, conversion, onboarding, and screening of new clients stage has lead generation, customer segmentation, predicting churn, sentiment analysis, and profiling personality traits as key activities that have seen the application of AI/ML in recent years. For example, unsupervised clustering techniques have been employed in banks to categorize their customers and obtain insights into their consumer behavior. Product recommendation and onboarding stage has AI/ML applications for understanding personality traits (PT), risk appetites, and risk perception and are critical to ensuring customer satisfaction and maximizing client investments within a FSI. AI can play a critical role in 'pairing' the right product portfolio based on empirical data and PT leveraging neural networks or ensemble algorithms such as Random forests. In advisory process stage AI/ML can integrate a wide range of inputs from the market and the client to provide advisory services. It can assess the client's sentiments through NLP and pair it against historical data on what has worked and what has not and create a new investment path that will maximize the target return function. In investment research and trading stage AI/ML can leverage Recurrent Neural Networks (RNN) and Long short-term memory (LSTM) networks to predict the prices of bonds and provide recommendations to wealth managers on what position to take. AI/ML can also evaluate new feeds to determine if there is positive or negative news being generated by that company. These models can easily monitor key economic indicators such as Interest rates and take position in the market significantly faster than their human counterparts. Client servicing and support stage sees the needs of the clients within FSI's follow a pattern throughout their lifecycle. AI/ML models can analyze large swathes of customer data and anticipate when a customer might churn, or their requirements change. It can also automate dispensary of basic informational and support services through chatbots and NLP. Predicting customer churn or when a customer might default is the key stage for any FSI. In recent years, clear evidence has emerged that indicates that AI/ML techniques are able to process much more complex patterns with better forecasting power compared to traditional linear regression [4]. Furthermore, by employing AI/ML to create a better synergy between the goals of the customer with the products they are investing in, it can enhance client satisfaction and retention.

Savings and wealth management also has a catalyzing effect on a country's economic growth. There is evidence to suggest that AI driven financial advisors (also referred to as Robo-advisors) can raise the savings—consumption ratio in a country [5]. Concurrently the focus of this paper has been to identify the focus of this paper has been to identify:

- What are the dominant approaches to financial risk management in personal wealth management?
- To what extent is ML/AI driven a more accurate alternative to already established methods?

- What are the key challenges impeding the adoption of AI/ML driven wealth management?
- To what extent does PT impact individual investment patterns?
- How does FRT affect the client's financial asset management?

After performing a systematic search for papers clearly focusing on key topics and stages identified above, we present their findings. This review revealed that most papers are focusing on AI/ML for solving risk management and price prediction problems. While there have been many studies on consumer behaviour and risk appetite, there is a relative dearth of papers on robo-advisors and the application of Deep Learning based AI in providing automated investment advice to end consumers, however middle and lower income households have largely been left out of this process.

The remainder of the text is organized as follows. Related work is reviewed in Section "Related Works". Section "Research Methodology" details the research method used in literature review. The data-driven techniques research into two main topics of interest is described in Section "Results" along with potential improvements of the existing techniques, and suggestions for new methodology that may resolve the considered portfolio management issues. Section "Conclusions" concludes the paper.

Related Works

Based on an initial screening of abstracts, 4 survey papers whose subject matters were deemed to be relevant to our research goals, were chosen to be analyzed. Four reviews and surveys address application of data-driven decision-making with ML and AI in personal investments and risk management. Summaries of these papers have been included in this section along with a comparison of the questions and key topics addressed in those papers.

AI/ML applied on market risks: Leo et al. [6] discuss the need for evaluating the role of ML in managing various forms of risk to banks such as credit risk, market risk, operational and liquidity risks that would identify areas for further research. The authors stated that ML can enable the building of more accurate risk models by identifying complex, nonlinear patterns within large datasets. The survey focused specifically on the various risk management tools and algorithms used within FSIs. The paper connected their findings to potential implications for institutions but did not delve into how these risk mitigation strategies could specifically be tailored to individual investors.

AI/ML applied on market risks and risk tolerance: Arsić [7] through systematic surveys, tackled the question "to what extent AI/ML techniques can be applied to

FRM". Based on data preparation, modelling risk, stress testing, and model validation Arsić underscored how AI largely improved market risk and credit risk management, stating that market risk models can be validated to generate quantifiable and acceptable market risk levels. Clustering mechanisms and Deep neural networks are also being applied to model complex patterns that can predict market risks, book risk management of banks, trading risk prediction etc. Arsić sees the further development of AI implementation in behavioral models, scenario generation, and behavioral and segmentation integration in asset pricing and portfolio optimization. This observation coincides with our research goals, but it was made again for potential implications for institutions, while we are looking for strategies that could be specifically tailored to individual investors.

Market risks, personalized wealth management and risk tolerance: Satish Kumar and Nisha Goyal [8] investigate the impact of cognitive biases on portfolio selection, market returns and volatility in trading behavior. The paper covers a considerable period of time (1980–2013) and highlights the major gaps in existing research on behavioural biases and backs up the need for study on individual investment decisions. However, authors don't focus on data-driven decision-making with AI and ML techniques to assist with eliminating cognitive biases.

AI/ML on personalized wealth management: Shanmuganathan [9] focuses on the actual and potential implications of AI based applications and technical issues that are related to behavioral finance, its performances in a theoretical setting. There is a need for successful execution on customer's financial portfolios and the importance of behavioral financial decisions for the success. However, author doesn't cover the Market risks research (Table 27.1).

Although several studies focus on addressing the issues with portfolio management, there is no comprehensive survey on all identified perspectives. To fill this gap, we conduct a comprehensive survey on the two critical issues faced while building portfolio management tools which is connected to data-driven techniques.

Research Methodology

This paper uses a systematic mapping study approach to conduct a literature evaluation of research works that investigated the personalization of portfolio management, including data-driven techniques and dealing with, processing overhead, scaling, consistency, security, and privacy concerns. Also, discuss how data-driven techniques can be used to address issues like security and inefficient resource utilization. The systematic mapping used the following procedures, which were based on the instructions offered by Pinciroli et al. [10] and successfully applied in another domain by Aranda et al. [11]. Research questions; research methodology; results screening criteria.

Table 27.1 Comparison of related works

Reference	Clear problem statement	Core topics	AI/ML	Market risks	Personalized wealth management	Risk tolerance	AI based products
[7]	Yes	Improve market risk and credit risk through AI	Yes	Yes	No	Partial	Partial
[9]	No	Implications of AI based applications on behavioral finance	Yes	No	Yes	Partial	Yes
[6]	Yes	Evaluation of ML Techniques in Banking, credit scoring and fraud detection	Yes	Yes	No	No	Yes
[8]	Yes	Impact of cognitive biases on trading behaviour, volatility, and portfolio selection	No	Yes	Yes	Partial	No

Research Questions

This paper seeks to provide greater clarity regarding ML in financial risk management and personalized portfolio for wealth management. Therefore, we define one General Question (GQ), four Focused Questions (FQ), and two Statistical Questions (SQ). Table 27.2 presents the questions.

The GQ addresses the information regarding the existing techniques for financial risk management. FQs dwell deeper into the details of selected papers that address the reach of ML/AI, challenges regarding the implementation of ML, and the influence of FRTs and PTs in personal wealth management systems. Finally, SQs aim to verify the chronology and type of publications.

Table 27.2 Research questions

Reference	Questions
General questions	
GQ1	What are the dominant approaches to financial risk management in personal wealth management?
Focused questions	
FQ1	To what extent is ML/AI driven a more accurate alternative to already established methods?
FQ2	What are the key challenges impeding the adoption of AI/ML driven wealth management?
FQ3	To what extent does PT impact individual investment patterns
FQ4	How does FRT affect the client's financial asset management?
Statistical questions	
SQ1	How many publications occurred per year?
SQ2	What is the number of publications per type?

Research Process

The study defined three steps for the research process: specify the search string, select databases, and find the results. The first step identified the main terms and their most relevant synonyms. The chosen search string: ((((machine learning) OR (artificial intelligence)) AND ((personalized investment) OR (wealth management) OR (asset management) OR (financial planning) OR (risk tolerance) OR (personality traits) OR (risk apetite) OR (stock prediction) OR (risk assessment) OR (financial service institution) OR (financial risk management)) ALL) + survey + Fintech.

After defining the search string, the search process encompassed six digital libraries: IEEE Xplore, Science Direct, Google scholar, Springer Link, ACM Digital Library and Penn State Digital Libraries. The researchers focused on identifying the key technologies and ideas behind data-driven with machine learning and AI investments while creating a comparative framework against traditional institution-driven approaches. Based on the works of various authors, the paper then amalgamated the various challenges facing this emerging platform and what steps could potentially ameliorate some of these issues.

Research in ACM and IEEE Xplore, and Science Direct required the use of an advanced search feature. Google Scholar and Penn State Digital Libraries search required a combination of the summary and title fields in the advanced search option. Finally, in Springer Link removing documents categorized as "preview only" and select the search filter titled 'computer science' to obtain relevant results.

Table 27.3 Paper screening process

Portal	Initial search	Keywords	Topic screening	Abstracts	Reviewed	Selected
Google Scholar	19,600	ML/AI Financial risk Management Wealth Management	980	120	14	4
PSU Digital	1576		79	25	8	2
Science Direct	733		22	16	8	2
IEEE	189		19	12	6	2
ACM	3353		101	15	4	1
Total	25,451		1,200	188	40	11

Results Screening Criteria

The approach to selecting papers for the survey, a structured filtering approach was adopted. Each paper was tested using a set of binary questions before being either selected or discarded. For finally identified 40 papers we have focused on screening criteria (b) to make a final selection.

a. Are problem statements clearly defined by the authors?
b. Does the paper provide clear examples of ML/AI being applied to the field of Finance/personal asset management/personal wealth management/financial risk management/investment predictions/customer profiling in terms of risk appetite and PT.
c. The paper was published in between January 2010 and April 2022 (Table 27.3).

Results

The filtering process resulted in 11 papers. At this stage, the selected papers were analyzed according to their objectives and categorized by their potential to answer our research questions. Figure 27.1 provides a graphical representation of the various taxonomies of the literature and the arrows indicate that area that has the arrow pointed to is or could be applied in the source area. Table 27.4 illustrates the findings and what each of the literature surveyed cover. We then move to leverage the concepts of each paper to shed light on the research questions outlined in 3.1.

GQ 1: What are the dominant approaches to financial risk management in personal wealth management?

Kobets et al. [5] presented a detailed implementation of robo-advisor for financial investments consisting of three modules. The first module utilizes LSTM networks to forecast the prices of cryptocurrencies. The second module constructs a plan for

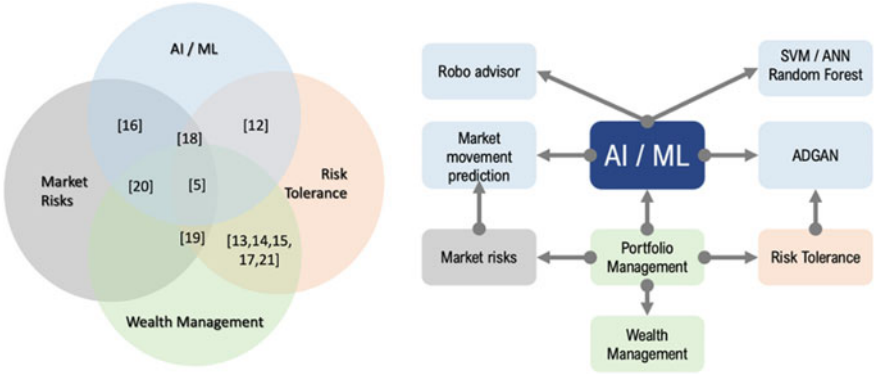

Fig. 27.1 Taxonomy of portfolio management categories

the investor based on different risk tolerance decisions. The third part is ETL for the LSTM model. This approach helps the investor invest based on their risk tolerance with the least amount of fear of losing money. Though they have listed current and previous trends in the price of bitcoin, the past and forecasted trading volume, difficulty in mining coins, general public perceptions, and the total number of coins mined, criteria responsible for accounting to the majority of variability in the price of cryptocurrencies, their LSTM module forecasts the prices by taking only the first two criteria into consideration. Another aspect that the solution covers is constant check and removal of dead coins from the input database by checking if any cryptocurrency was involved in financial fraud and if it is reliable. This is done by extracting the list of banned and unreliable cryptocurrencies from DeadCoins services and removing the obtained list from the current database. Though this proposed implementation provides an end-to-end architecture it lacks in several aspects like lack of security modules, a lack of reasoning of how a particular investor will be categorized as either a risk-taker, neutral or risk-averse investor. Current and previous trends in the price of bitcoin. The past and forecasted trading volume Difficulty in mining coins are measured on how tough it is to find a hash below a specific difficulty value. Perceptions from general public, which also includes new laws and regulations enforced by the government.

Jiang et al. [16] presented a multi-period machine learning integrated mean-risk portfolio rebalancing approach with risk-aversion adjustment. When rebalancing the portfolio, a series of technical indicators is input into machine learning classification models to anticipate market movement likelihood, and investors can modify the risk-aversion coefficient accordingly in the mean-risk optimization to produce portfolio weights. The Gini's Mean Difference was used as the risk metric portfolio optimization model and logistic regression and XGBoost using 14 common technical indicators obtained from a market index (S&P 500). They used a rolling-horizon technique to run a series of empirical experiments to examine the prediction outcomes and the out-of-sample performance of the generated portfolios. They concluded that

Table 27.4 Areas that reviewed papers cover

ID	Year	Reference	Clear problem statement	Core topics	AI/ML	Market risks	Personalized wealth management	Risk tolerance	AI based products
[5]	2018	Kobets et al.	Yes	AI generated financial advice for different risk tolerance levels	Yes	Partial	Yes	Yes	Yes
[12]	2020	Liu et al.	Yes	Measurement of customer risk tolerance levels	Yes	No	No	Yes	Partial
[13]	2017	Onsomu et al.	Yes	Influence of demographics on Investor biases	No	No	Partial	Yes	No
[14]	2018	Martin et al.	Yes	Effects on present assets on the financial risk tolerance perception of customers	No	No	Partial	Yes	No
[15]	2021	Rai et al.	Yes	The effect of PTs on FRTs	No	No	Partial	Yes	No
[16]	2020	Jiang et al.	Yes	The use of ML and technical indicators to predict market movement	Yes	Yes	No	No	Yes
[17]	2005	Yao et al.	Yes	The effect of gender on FRTs	No	No	Partial	Yes	No

(continued)

Table 27.4 (continued)

ID	Year	Reference	Clear problem statement	Core topics	AI/ML	Market risks	Personalized wealth management	Risk tolerance	AI based products
[18]	2020	Mashrur et al.	Yes	Role of ML in overcoming challenges in FRM	Yes	Yes	No	Yes	No
[19]	2021	Pospíšil et al.	Yes	The effect of economic situations on personal financial decisions	No	Partial	No	Partial	No
[20]	2020	Chia-Cheng et al.	No	Predicting stock price movement and evaluate performance	Yes	Yes	Yes	No	No
[21]	2015	Kanndahasan	Yes	Factors affecting the capacity of FRTs in individuals	No	No	Partial	Yes	No

the XGBoost model has better performance. In comparison to the three other benchmarks, the LR and XGBoost portfolios built by their proposed framework perform very well in terms of average return, cumulative return, and annualized return.

Liu et al. [12] talks about measurements and right way to measure the risk tolerance of customers, how the computation of financial risk tolerance (FRT) requires domain specific models. It discusses how consumers' surveys alone aren't a reliable source of FRT score calculator as they are biased, inauthentic and can misrepresent information, for example customers with similar survey answers might not have the same FRT. One of the best sources to estimate a customer's FRT score is through their spending patterns or online shopping history (includes click ratio, purchasing items added to the cart, offer grabbers, etc.). To overcome this problem, the paper proposes an approach to leverage both customer feedback and transaction activities as a measure of FRT score. This model is developed with the use of Asymmetric cross-domain Generative Adversarial Network (ADGAN), i.e. GAN used for cross-domain alignment. As the model is based on GANs it takes care of the imbalanced cross-domain data. ADGAN structure comprises of structural view embedding for domain feature extraction, followed by generator to fill the missing survey data by creating samples, and finally, the discriminator which is used to distinguish generated sample from true sample and also predict customer FRT category.

FQ 1: To what extent is ML/AI driven a more accurate alternative to established methods?

To provide an answer and show the promise of data driven methods we identified the following article. Chia-Cheng et al. [20] state that the Random Forest algorithm followed by SVM, and ANN surpass the benchmark index in the investment i.e., generate the higher mean return. If daily average return is considered, SVM and random forest generate 2 times higher returns than benchmark with ANN being 1.5 times. This is analyzed on the data from the Yahoo finance of 1,258 S&P 500 samples over the period of 2014 to 2018 to predict the stock price movement, evaluate investment performance and risk management.

FQ 2: What are the key challenges impeding the adoption of ML driven wealth management?

Mashrur, Luo et al. [18] addressed financial risk management by discussing financial risk manager (FRM) connection with different machine learning methods. They identified the biggest challenges that are being faced with respect to FRM and provided the future directions that emerge from the research that is happening. Risk management and risk mitigation is important along with return forecasting, risk modelling and portfolio construction. Various machine learning algorithms like Supervised, Unsupervised, Deep Learning methods along with reinforcement learning should be used improving the accuracy of the traditional methods like EWMA, ARCH, Lee-Carter Model, chain-ladder methods. In terms of challenges, there is a sparsity of fitted datasets. Data this is available is burdened with noise, imbalance, and non-stationarity. The explanatory power of models is an important aspect for every domain as this helps to take risk-related decisions in light of external biases with

respect to credit or insurance models. Sequential learning algorithms are gaining popularity in this area. However, their slow training rate is an area of concern. To conclude, research to build federated leaning systems along with explainability and fairness will train the sensitive financial information with accurate results.

FQ 3: To what extent does PT impact individual investment patterns.

The idea of behavioral finance and the cognitive life-cycle assumption are tested for their capacity to explain consumers' financial risk tolerance. Reference [14] The main theoretical framework that governs financial risk tolerance is Consumers' perceptions of their present assets, such as the balances of their checking and savings accounts. More current assets assist customers in mentally mitigating some of the dangers associated with more volatile investments. This shows that just increasing the amounts in customers' checking and savings accounts might enhance their financial risk tolerance. Three key theoretical implications emerge: It is the first study to show that more fundamental financial needs, such as the demand for present assets, may require at least limited fulfillment before the higher-level desire for future income is triggered. Consumers appear to be more conservative in their investing decisions until the need for future income is awakened, even for investment goals such as retirement that may be years away. Their findings contribute to the growing body of evidence that subjective financial knowledge has an influence on consumer investment choices. When paired with increased present assets and a future-oriented mindset, higher degrees of self-determined financial literacy correlates to higher financial risk tolerance. Furthermore, this research has four very important consequences for employers, marketers, the investing sector, and politicians. First, this study reveals that when consumers believe their present assets, such as checking and savings account balances, are acceptable, they are more willing to take on financial risk in their investments, which financial planners consider to be a good thing. Second, when consumers think they are informed about financial matters, the favorable effect of current assets on financial risk tolerance is strengthened, which has a direct influence on financial risk tolerance. Third, both financial service providers and customers can gain from the former by developing financial training programs that are expressly targeted at future-oriented clients. Finally, financial institutions should be cognizant of the psychological benefits of future income growth on consumers' views of their existing financial capabilities, which leads to increased financial risk tolerance.

Jiri et al. [19] state that there is a relationship between the economic situation and the values which influence human financial decisions. The statement is presented after considering the responses from the 3768 individuals from Czech Republic considering financial responsibility, financial well-being and financial knowledge as well as the 36 value parameters based on the Rokeach's value itineraries which is tested on the χ 2 test of independence. The volatility of the economic situation that prevails would directly affect human decisions which calls for designing a robust value based FRM model which would help the people with their choices and recommendations.

Yao [17] explains the impact of gender and marital status on financial risk tolerance. Earlier research compared single men to single women, but this study

also distinguishes married men from married women. The research proposes three hypotheses to compare risk tolerance: (1) There are no variations in risk tolerance between married men and married women (assuming that the responder for couple households reply based on both spouses' preferences.) (2) Unmarried women are more risk-tolerant than unmarried men. (3) Married people are more risk-tolerant than unmarried people.

For most of the levels of risk tolerance examined in the cumulative logits, hypotheses 1, 2, and 3 were rejected. According to Hypotheses 1 and 3, married females had lower risk tolerance for some risk and elevated risk; were as likely as unmarried females to take a considerable risk, contrary to Hypothesis 3; and were less likely than unmarried men to take a substantial risk, contrary to Hypothesis 2. Contrary to Hypothesis 1, married females exhibited lower risk tolerance than married males at all three levels of the cumulative logit. Some of the variations were not significant unless there was a high danger. In general, the findings contradicted the hypothesis as single men had the highest risk tolerance, followed by married men, unmarried women, and married women.

FQ 4: How does FRT affect the client's financial asset management?

Onsomu et al. [13] examine how risk tolerance varies by investor demographics (age, gender, education, and experience), as well as the link between risk tolerance and portfolio results using ANOVA and regression analysis. Female investors, experienced investors, those with little academic degrees, and older investors were shown to be more risk-tolerant, according to the research. As a result, they invested in high-risk equities portfolios. Without taking demographics into account, regression analyses showed that risk is positively associated with portfolio performance. When the link between risk and portfolio returns is moderated by demography, however, the relationship becomes inconsequential. The study shows that the link between risk and portfolio performance is not moderated by age, gender, experience, or education. These findings are significant for stock market investors because they provide insight into how individual differences influence risk tolerance levels and the impact on portfolio outcomes. Investment advisers will benefit as well, because they will be able to provide personalized advice to individual investors based on their demographics.

The Big Five dimensions of personality characteristics (PT) are defined using a standardized prior scale [15]. If all dimensions pass the validity and reliability tests for evaluating PT, their impact on investors' FRT should be examined. First, the relationship/direct influence of Big Five PT on investors' FRT. Second, whether the model can be improved by using second-order confirmatory factor analysis (CFA), which shows that PT leads to investors' FRT. The Big Five PTs are substantially connected with an individual's risk tolerance level, according to correlation studies. The data showed that PTs are necessary for active financial management and increased risk tolerance. However, when the direct effect of the different personality traits as defined by the Big Five model of personality on the level of FRT was examined, it was discovered that individuals with personality traits such as agreeableness, conscientiousness, and openness had a significant relationship with the extent of financial risk tolerance, whereas PTs such as extroversion and neuroticism had no such relationship.

The above-mentioned divergence might be the consequence of overlapping variance across the model's numerous dimensions, known as the Big Five PTs, according to this study, which also identified the PT as a second-order element of FRT. When PT was modelled as a second-order component, the findings revealed that PT predicted 23% of FRT. The findings, however, do not negate the role of extroversion and neuroticism in personality types; rather, they give evidence that these characteristics are crucial in explaining PT, which has a strong positive influence on FRT. Furthermore, these variables were shown to have a significant moderate connection with FRT. The findings suggested that PT, as a second-order component, causes FRT.

Kanndahasan [21] identified the factors that affect the capacity of a person to tolerate risks are different from person to person. This paper examines the factors such as gender, age, marital status, income category, occupation, and education to differentiate among investors in terms of financial risk tolerance (FRT) and Risk-taking behaviors (FRB). 6 among the mentioned factors 4 are significant (Gender, Age, Occupation, and Income). This information can be procured from the customer's data and can be used as a preliminary measure for the FRT. The findings of this paper could encourage the creation of a dataset using which ML/AI algorithms can train to gauge the capacity of a customer to tolerate risks. Demographic factors cannot be considered alone and there is a need for research on the socio-economic factors of customers to s to adequately and more accurately gauge their FRTs.

SQ 1: How many publications occurred per year? SQ 2: What is the number of publications per type?

We identified that computer science venues do not provide an adequate picture of wealth management. More relevant articles were found in financial venues and that indicates a potential and the need for AI/ML techniques. However, our systematic literature review was limited by our attempt to identify where data-driven techniques would be applied. That might have introduced a confirmation bias that leads to the tendency to choose source data or model results that align with currently held beliefs or hypotheses. Our research questions and resulting taxonomy show that we have taken all the matters of precaution to address this bias (Fig. 27.2).

Conclusions

While there is a rising interest from financial service institutions in implementing data-driven techniques to improve risk management and price predictions, the role that the latter can play in creating personalized investment portfolios is yet to achieve its full potential. While some pioneer institutions have invested in robo-advisors, integration of machine learning with customer and application of personality traits can allow institutions to create more compelling investment products to attract middle- and lower-income households who have largely been left out of this process.

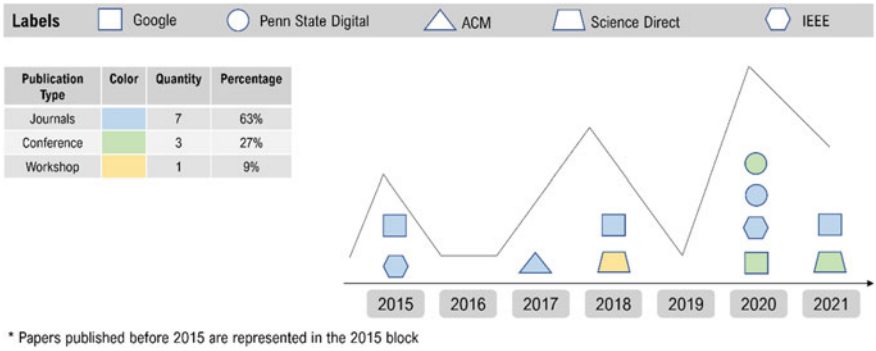

Fig. 27.2 Papers reviewed by year and source

Acknowledgements Robert Merkle from Beacon networking for life, Ira Laefsky, from Ira M Laefsky & Associates, Pammi Bhullar from Edelman Financial Engines, Hardware directors Aleksandar Zoranovic and Bratislav Veljkovic at Advanced Brain Monitoring. Jesse Gardner, Professors Raghu Sangwan, Mohamad Kassab, Satish Srinivasan, and Big Data Lab Penn State Great Valley.

References

1. Coombes, & Benson, A. (2021, December 8) *Nerdwallet* [Online]. Available: https://www.nerdwallet.com/article/investing/what-is-wealth-management. Accessed April 21, 2022.
2. Rotzetter, P. (2020). Machine learning in digital wealth management. In *The AI book.* Wiley
3. Databricks. (2020). Driving innovation in financial services with an unified approach to data + AI. Databricks.
4. Jurczenko, E. (2020). *Machine learning for asset management*. Wiley.
5. Vitaliy, K., Yatsenko, V., Mazur, A., & Zubrii, M. (2018). Data analysis of private investment decision making. In *ICTERI Workshops*, 2018.
6. Leo, M., Sharma, S., & Maddulety, K. (2019). Machine learning in banking risk management. *Risks*, 7–29.
7. Arsić, V. B. (2021). Challenges of financial risk management: AI application. *Journal of Sustainable Business and Management Solutions in Emerging Economies*, 26–33.
8. Satish Kumar, N. G. (2018). Behavioural biases in investment decision making—a systematic literature review. *Qualitative Research in Financial Markets*, 88–108.
9. Shanmuganathan, M. (2020). Behavioural finance in an era of artificial intelligence: Longitudinal case study of robo-advisors in investment decisions. *Journal of Behavioral and Experimental Finance*, 1–9.
10. Pinciroli, F., Justo, J. L., & Forradellasc, R. (2020). Systematic mapping study: On the coverage of aspect-oriented methodologies for the early phases of the software development life cycle. *Science Direct*.
11. Aranda, J. A. S., dos Santos Costa, R., de Vargas, V. W., da Silva Pereira, P., Barbosa, J., Vianna, M. (2022). Context-aware edge computing and internet of things in smart grids: A systematic mapping study. *Computers & Electrical Engineering.*
12. Liu, Z., Yao, L., Wang, X., Bai, L., & An, J. (2020). Are you a risk taker? Adversarial learning of asymmetric cross-domain alignment for risk tolerance prediction. In *2020 International Joint Conference on Neural Networks (IJCNN)* (pp. 1–8).

13. Onsomu, Z. N., Kaijage, E., Aduda, J., & Iraya, C. (2017). Risk tolerance, demographics and portfolio performance. *Journal of Business & Economic Policy*, 69–74.
14. Martin, W. C., & Davari, A. (2018). Examining financial risk tolerance via mental accounting and the behavioral life-cycle hypothesis. *Academy of Marketing Studies Journal*, 1–13.
15. Rai, K., Gupta, A., & Tyagi, A. (2021). Personality traits leads to investor's financial risk tolerance: A structural equation modelling approach. *Management and Labour Studies*, 422–437.
16. Jiang, Z., Ji, R., & Chang, K.-C. (2020). A machine learning integrated portfolio rebalance framework with risk-aversion adjustment. *Journal of Risk and Financial Management*, 155.
17. Yao, R., & Hanna, S. D. (2005). The effect of gender and marital status on financial risk tolerance. *Journal of Personal Finance*, 66–85.
18. Mashrur, Luo, W., Zaidi, A., & Robles-Kelly, A. (2020). Machine learning for financial risk management: A survey. *IEEE Access, 8*, 203–223.
19. Pospíšil, J., Matulayová, N., Macháčková, P., Jurníčková, P., Olecká, I., & Pospíšilová, H. (2021). Value-based financial risk prediction model. *Risk 9, 11*, 205.
20. Chen, C.-C., Chen, C.-H., & Liu, T.-Y. (2020). Investment performance of machine learning: Analysis of S&P 500 index. *International Journal of Economics and Financial Issues, 10*, 59–66.
21. Kannadhasan, M. (2015). Retail investors' financial risk tolerance and their risk-taking behaviour: The role of demographics as differentiating and classifying factors. *IIMB Management Review*, 175–184.

Chapter 28
Comparing Twitter Data for Topic Modling, Clustering, and Predictive Analysis Using LSTM Model

Md. Shamaun Islam and Sadat Bin Shahid

Abstract Extraction topics to find the difference between the two datasets of information, as a rule, seems unused. Machine learning and the calculation of Natural language Process correction are used to analyze the ever-changing statistics of Twitter accessible online, including modelling processes for a longer time. Two datasets of content information were selected to evaluate comparisons based on specific statistical tests, such as quality and response, accuracy, and statistical tests for particular measurements, such as Portion F and Title. Twitter has become amongst the most often used online network site because anyone can easily publish information about their thoughts on a specific issue via a public message called a tweet. Twitter play an essential part in the prioritization of public life. It is necessary to know about the topic and domain on social media sites. This research work performs a topic modelling on Twitter data related to covid19. Two different data sets are discussed, and tweets are clustered through the k-mean clustering algorithm. Topics are also found in each cluster using the LDA technique. The clustered data sets are predictively analyzed through the LSTM model. The results show that the model achieves 96% accuracy.

Keywords Deep convolutional neural networks · Transfer learning · K-means clustering · LDA · Topic modelling · Research trend

Introduction

The World Health Organization (WHO) had an important role during the start of the covid19 period. During the covid-19 start time, they used social media to raise public awareness. Users can interact and exchange information on a number of online social networking platforms and services, such as Facebook, Twitter, LinkedIn, YouTube,

Md. Shamaun Islam
School of Businesses and Economics, Chongqing University of PT, Nan'an, Chongqing 400065, China
e-mail: l202020022@stu.cqupt.edu.cn

S. B. Shahid (✉)
School of Computer Science, Hubei University of Technology, Wuhan, China
e-mail: Sadatshahid18@gmail.com

R. Qiu et al. (eds.), *City, Society, and Digital Transformation*, Lecture Notes in Operations Research, https://doi.org/10.1007/978-3-031-15644-1_28

and Instagram. People all across the world utilize the internet to share their opinions and general thoughts regarding this global issue. In a short amount of time, social media outlets such as Twitter saw an exponential increase in tweets about the sickness. People are using the online social media network Twitter to express their opinions, ideas, emotions, and thoughts regarding the worldwide pandemic during the pandemic [1, 2]. It swiftly spread over the planet due to an increase in the frequency of corona events in a short period of time. On January 30, 2020, the WHO proclaimed COVID-19 a pandemic. Millions of tweets regarding Covid19 are retweeted by the WHO. In early February 2022, the WHO tweeted with the hashtag NoCovid-19 from its account, which received a large number of retweets. Two months later, the WHO tweeted with the hashtag Covid-19 to ensure that all information reached the public and to raise awareness about the pandemic situation. From January 9, 2020, to April 15, 2020, this study focused on tweet analysis and discovered two separate datasets of The WHO with hashtag NoCovid-19 and hashtag with Covid-19. As a result, we applied topic modeling on the two WHO datasets. The purpose of topic modeling is to extract a particular number of themes from a batch of text documents using statistical approaches. This is an unsupervised assignment that requires no prior knowledge of the book. Topic modeling and clustering are both unsupervised learning methods that need a specific number of categories ahead of time but do not require labels to work. Topic modeling offers various advantages in the context of our inquiry; it may be used for both feature reduction and feature selection. To begin, we use topic modeling techniques to reduce and then articulate the vector space model (VSM). This is a feasible answer to the well-known problem of data and text mining's high dimensionality. Second, the proposed technique in this study uses topic modeling as a feature selector by disclosing semantic variables in text texts. This study examines a news dataset [3] composed of two different datasets from The WHO, one with the hashtag NoCovid-19 and the other with the hashtag Covid-19. External metrics such as purity, F-measure, entropy, accuracy, and others are utilized in this study to evaluate the generated clusters. The data is also preprocessed and divided into numerous clusters using the k-mean clustering approach. The elbow technique is used to compute the difference between two datasets of data groups. The data set is then utilized to predict the clusters based on Convolutional Neural Network models. In the circumstances, the tweet's text is represented as the independent variable X. Contemporaneously, the output class label of the data is, i.e., a cluster of the tweet is defined as dependent variable Y.

This paper aims to Compare twitter data for topic modeling of the two datasets of the WHO with semantic analysis after that, applying the k-mean machine learning technique for clustering the data and finding the optimal number of clusters with the LSTM model of convolutional neural network for predicting the cluster.

The rest of the document is organized as follows: Section "Materials and Methods" discusses the materials and methods, Section "Pipeline of the Procedure" discusses the Pipeline of the procedure, Section "Evaluation Matrix" evaluation matrix and approach method are used in this study, Section "Decision Fusion" illustrates experiments and results, and Section "Results and discussion" includes discuss on results

and discussion and Sections "Related Work" and "Conclusion and Future Work" discusses the Related work and concludes the paper.

Materials and Methods

Dataset

Two data sets are obtained from Twitter, an online social media platform. Both the data sets belonged to the official Twitter account of WHO. The data sets contained more than three months, from January 09, 2020, to April 15, 2020. The data set1 contains tweets with no covid19 related hashtags, while the data set2 contains hashtags of covid19. The data set1 has a total of 1706 tweets data. 322,673 people retweeted these 1706 tweets, with an average of 189 retweets per tweet and 44,331 replies with 25 responses per tweet.

The data set2 has 2164 tweets data with real retweets of 948,923 with an average of 439 retweets per tweet, which is three times more than data set1 retweets. A total of 150,536 replies with an average of 70 responses per tweet happens to data set2 tweets, three times more than data set1 replies.

Data Preparation

The data gathered from Twitter sites contain many unwanted and irrelevant materials. Before applying any machine learning model, preparing the data and making it pipelined is essential [4]. The preprocessing includes converting the text to the lower case, removing the stop words, removing the special characters, removing the hyperlinks, removing the words other than the English language, removing the phrase having lengths less than or equal to 3, and converting each dish to its root form. The preprocessing techniques are applied to both the data sets, and the new data sets are prepared. Figures 28.1 and 28.2 are the graphs of the data sets. It has two columns; one column is the original text, and the other has cleaned the preprocessed text.

Pipeline of the Procedure

Preprocessing the Raw Text

Pre-processing of the text data of both the data sets involves the following steps:

Tokenization: First, the text of each data set is broken down into sentences. Each sentence is further split into single words.

	text	cleaned
0	"We are committed to serving the world鈥 peopl...	committed serving world people accountability ...
1	"Neither do we. This is a time for all of us t...	neither time united common struggle common thr...
2	"#COVID19 does not discriminate between rich n...	covid discriminate rich nations poor large nat...
3	WHO is reviewing the impact on our work of any...	reviewing impact work withdrawal funding work ...
4	"WHO is not only fighting #COVID19. We鈥檙e also...	fighting covid also working address polio meas...
...	...	...
2158	Protect yourself & reduce risk from #coronavir...	protect reduce risk coronavirus infection hand...
2159	As surveillance improves around the world, mor...	surveillance improves around world coronavirus...
2160	Novel coronaviruses emerge periodically, as we...	novel coronaviruses emerge periodically seen s...
2161	A novel #coronavirus is a new strain of the vi...	novel coronavirus new strain virus previously ...
2162	Some coronaviruses cause less-severe disease, ...	coronaviruses cause less severe disease severe...

Fig. 28.1 The image of data set 1

	text	cleaned
0	"Our commitment to public health, science and ...	commitment public health science serving peopl...
1	We also work with countries to strengthen heal...	also work countries strengthen health systems ...
2	"With support from the people and government o...	support people government works improve health...
3	"That creed remains our vision today. The has ...	creed remains vision today longstanding genero...
4	"They expressed that desire in the @WHO consti...	expressed desire constitution says enjoyment h...
...	...	...
1703	The lack of visible smog is no indication that...	lack visible smog indication air healthy acros...
1704	#AirPollution is hard to escape, no matter how...	airpollution hard escape matter rich area live...
1705	More than 90% of the world鈥 children breathe ...	world children breathe toxic air every day est...
1706	#CervicalCancer control needs good data http:/...	cervicalcancer control needs good data cervica...
1707	Every 40 seconds someone dies by #suicide. WHO...	every seconds someone dies suicide calls fillm...

Fig. 28.2 The image of data set 2

- The words are converted into lowercase.
- **Lemmatization**: Each verb, adverbs, etc., in the data set is converted into its base form. Like a word, ‘planting’ is converted to ‘plant’. The past and future tense verbs are also converted into present form.
- Special characters and mathematical signs are removed from the data sets.
- Hyperlinks are also removed from the data sets.
- Words having a length of fewer than three characters are removed
- A Dictionary of words is defined as having more than 200 words. All the words are dropped from the data sets as those words have no influence. The comments are them, those, left etc.

Converting Text to Bag of Words

After preprocessing and converting each word of the data set to its root form, a dictionary is created with each word's count. The list is sorted in descending order, i.e., the top word of the list is the most repeating word in the whole data set. The second word is a less repeating word than the first one, and so on.

Latent Dirichlet Allocation (LDA) Analysis

LDA perform the text classification about a specific topic in the documents. It combines multiple words on the base of a topic and various topics at the bottom of documents. The LDA analysis is performed on both data sets. The model split each data set into ten topics. The words in each topic are relevant words to each other. The model also gives a value to each word in each topic based on their importance and sorts them into descending order. The model shows the top ten words in each topic of the data set. It is not necessary that each topic must have unique words, and a word may appear in more than one topic.

Running NMP

TF-IDF Feature Extraction

It uses a bare but burly Bag of Word (BoW) method to convert each tweet into its corresponding feature vector. The BoW presentation was assembled using three phases: token creation, calculation and general practice. First, create a token for each word in a given tweet. Second, measure each word in the token using the inverse document frequency TF IDF the word frequency, as described in subsequent calculations.

$$\mathrm{TF} - \mathrm{IDF}(\mathrm{t}, \mathrm{d}) = \mathrm{TF}(\mathrm{t}, \mathrm{d}) \times \mathrm{IDF}(\mathrm{t}), \tag{28.1}$$

where TF(t, d) is the term frequency of token (t) in the document (d), and IDF is defined as

$$\mathrm{IDF}(\mathrm{t}) = \log 1 + \mathrm{n}1 + \mathrm{DF}(\mathrm{t}) + 1, \tag{28.2}$$

where DF(t) represents the number of tweets containing the term t on the dataset. Last, the TF-IDF vector (V) for each tweet document is normalized using L2-norm as defined in the following

$$V = V/\sqrt{V_{21} + V_{22} + \cdots V_{2n}}. \tag{28.3}$$

Feature Fusion

Likewise, the role of the contents and elements of the context is submitted more accurately to the forum, which is more accurately integrated with the preliminary information and the role of the context. The TFIDF method captures the syntax details of the token, and the FASTTextBased method records context information. Given the effectiveness of two types of information to reflect all the tweets, it is assumed that the authors are compiled to the proposed to increase productivity as shown in (28.4). In addition, the choice of features may help reduce the function's size and increase the class's productivity, as suggested in [5]. However, because our functionality has already been pretty small to train the machine education model, we have not used it.

$$H_{ij} = k = 1 \text{ to } n \sum V_{ik} W_{jk} \tag{28.4}$$

where H_{ij} is the last part of the matrix, V_{kj} is the TF IDF tweet matrix ($M \times N$), and W_{ik} is the name of the FastText based matrix ($N \times 300$). M and N represent the number of tweets and the number of tokens, respectively. The computational complexity of our hybrid element is based primarily on the functional fusion process, which is determined by the cost of iterating over two matrices (V_{kj} size $M \times N$ and W_{ik} size $N \times 300$). So the total time cost to integrate the components is O ($M \times N \times 300$).

Evaluation Metrics

We pose the performance metrics that were used in our study. To test performance, we use well-known metrics such as Precision (an Eq. 28.5), Recall (an Eq. 28.6), F1-score (an Eq. 28.7), and Accuracy (an Eq. 28.8)

$$P = TP/TP + FP \tag{28.5}$$

$$R = TP/TP + FN \tag{28.6}$$

$$F = 2 \times P \times R/P + R \tag{28.7}$$

$$A = TP + TN/TP + TN + FP + FN \tag{28.8}$$

where TP, TN, FP, and FN stand for true positive, true negative, false positive, and false negative, respectively. Similarly, P, R, F, and A stand for Precision, Recall, F1-score, and Accuracy. A confusion matrix was also used to evaluate the machine learning models. The confusion matrix is also made up of TP, TN, FP, and FN.

Proposed Approach

The proposed approach compares two text-related data sets obtained from the Twitter platform. Both data sets belonged to the WHO twitter handle. One data set is crawled using the hashtag covid19, while the other data set contain data not related to covid19. The aim is to compare the two data sets with different data types and determine the difference between their topics. The data sets are preprocessed, and tweets are clustered using a machine learning clustering algorithm. The neural network technique and the K fold method are applied for training the model. Ten topics are generated for each data set, with the top 10 keywords in each topic. Figure 28.3 shows the methodology of the proposed work.

The topic modelling is performed with two methods on both data sets. First, the LDA method is applied, and then the NMF technique is used. The LDA topic modelling is applied after the preprocessing and before the clustering on both data sets, while the NMF topic modelling is applied after the clustering. The NMF topic modelling is based on clusters. For each data set, ten topics are identified for each group. After the topic modelling, both predictive models are evaluated through evaluation metrics (Figs. 28.4 and 28.5).

Along the way, we follow the various steps of emotional separation of COVID-19-related tweets, namely, "vector embedding and representation", "CNN's **==> Long Short-Term Memory (LSTM)** design and training," and "decision-making."

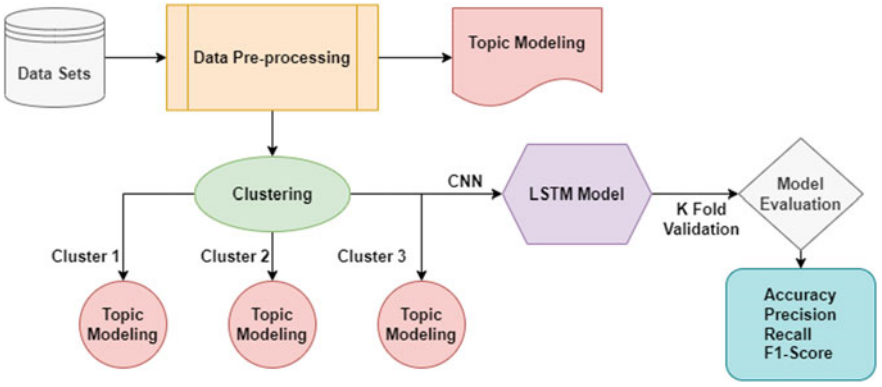

Fig. 28.3 Methodology

Fig. 28.4 Image of data set 1

	cleaned	cluster
0	commitment public health science serving peopl...	0
1	also work countries strengthen health systems ...	0
2	support people government works improve health...	0
3	creed remains vision today longstanding genero...	1
4	expressed desire constitution says enjoyment h...	0

Fig. 28.5 Image of data set 2

	cleaned	cluster
0	committed serving world people accountability ...	0
1	neither time united common struggle common thr...	0
2	covid discriminate rich nations poor large nat...	0
3	reviewing impact work withdrawal funding work ...	0
4	fighting covid also working address polio meas...	0

Vector Extraction and Representation

Before removing the embedding vector for each word in the tweet, run the following code on each green token (or name): To begin, make a token and remove all alphanumeric characters from each tweet. Second, the legal suspension period is removed. Finally, we use Stemmer to determine each token's root name. We use the same processing method as in our previous work [3]. To extract the embedding vectors for each pure token, we prepare three types of vector embeddings (fast text embeddings, backgrounds). As suggested in [6] feature selection is critical in developing features to remove discriminatory features. Nonetheless, we do not do this in our work because our combined features already have a low level of discrimination, making it difficult to differentiate them.

First, we use the built-in vector-based fastText(ft) [1] pre-trained on a multilingual dataset. This creates a context element based on the key metrics associated with each token. The object vector size is 300D. So, we represent each tweet as an N $\times$ 300 matrices and do the job of assembling the scale. Second, we use the 2nd dataset set [3], a multi- part site, for rate-independent vector embeddings (da). This help to gather domain information (non-COVID-19 documents) associated with each token. In this case, each section starts sorting a list of tickets, also known as filter banks. It then computes the probability of each receipt in each list as a feature value.

For example, if you have 17 sections and each token will have an element size of 17D. The second dataset contains 17 segments in our work and we give a 17D feature vector for each ticket. The result is an N $\times$ 17 matrix for each tweet, resulting in a 17D vector after the measure function. Third, we use the possible (ds) method to extract the embedding vector for each token, as suggested by Sitaula et al. [3].

Decision Fusion

We erased the top 3 layers in each well-designed CNN and inserted a weight-determining layer to create the result. The cut of the CNN cluster links appears in Fig. 28.6.

Topics Explored by Researchers

Excluded keywords may not fully represent publisher sites with research sites as they occur less frequently on the website. So, we decided to proceed by modelling the title and extracting the keywords.

Class-Wise Study of Classifiers' Performance on Hybrid Features

To fathom the performance of component assemblies at a deep level, we perform intelligent class analysis for each stage of machine learning. A Smart box structural analysis on performance metrics more than ten times the results used in this study to get the best combination (SVM + IDF + KMeans Tweet group) of components (Figs. 28.7 and 28.8).

Implementation

We use the popular machine learning framework, Sklearn [7], used in Python [8], to implement the proposed methods. We report average performance figures for each model across all given data records to avoid possible bias due to unequal sample numbers. To use the two-machine learning algorithms in our curriculum, we fit the foremost parameters as follows:

(a) ETC: \{n_estimators: (10 to 250), read_date: (0, 2 to 1,2) \}) and

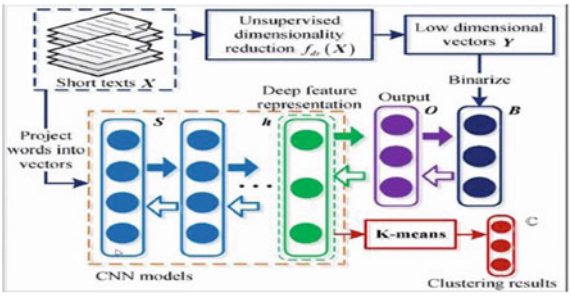

Fig. 28.6 CNN model

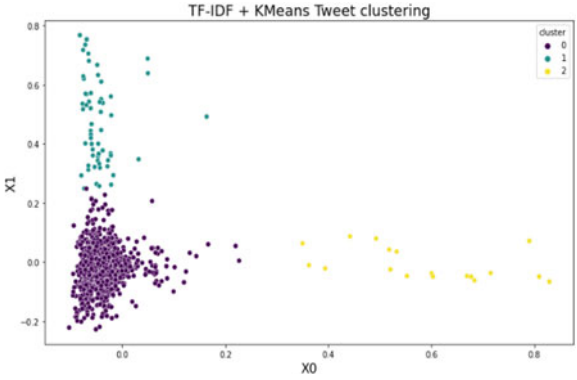

Fig. 28.7 Clustering of data set1

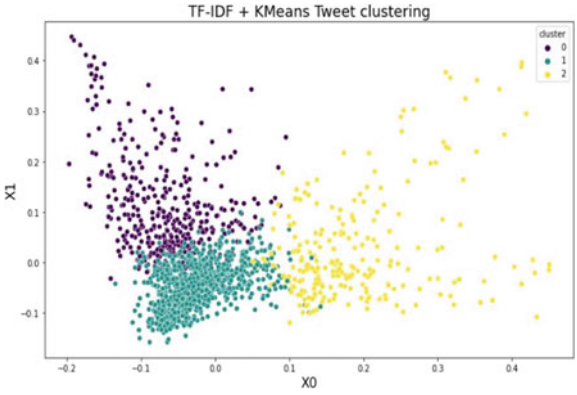

Fig. 28.8 Clustering of data set2

(b) AdaBoost: \ {n_estimators: (10 to 250), level_learning: (0.2 to 1,2)) \}.

Similarly, excellent hyperparameters for the remaining categories were selected from the previous work [9]. All hyperparameter changes were performed using grid search [10]. The Elbow Method determines the optimal number of clusters (k). Figures 28.9 and 28.10 shows the graph of the elbow method.

Results and Discussion

The results section discusses the modelling and performance of machine learning predictive models on both data sets. Table 28.1 shows the top words and their values for each topic of the data set1 after applying LDA modelling.

Table 28.2 shows the top words of each topic of the LDA modelling on the data set2. There is a clear difference between the topics of data sets. Table 28.1 is about covid19 related tweets, with most topics related to covid and health, while Table 28.2 has general topics.

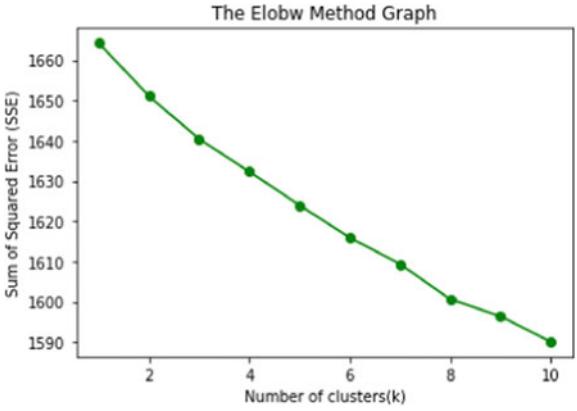

Fig. 28.9 Graph of elbow method

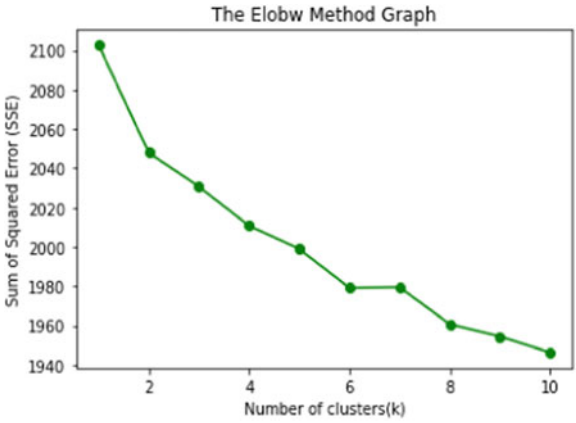

Fig. 28.10 Graph of elbow method

Table 28.1 Top words of LDA on data set1

Topic	Value
Food	7.371961
Amp	6.164435
Tobacco	7.633007
immunization	4.755443
Health	16.388775
People	11.992282
Drtedros	17.180788
Physical	7.298936
Amp	12.592761
Film	16.204960

Table 28.2 Top words of LDA on data set2

Topic	Value
Covid	17.430578
Covid	19.712764
World	5.149754
Briefing	56.140489
China	15.583328
Drtedros	25.057414
Coronavirus	10.576480
Equipment	8.820869
Emergency	18.763865
Coronavirus	10.756779

After the clustering is performed on both the data sets, each data set is split into 3 clusters. After that topic is found for each group. Tables 28.3, 28.4 and 28.5 show the top topic words for the data set1.

Tables 28.6, 28.7 and 28.8 show the topic words for each cluster of data set2.

Tables 28.1, 28.2, 28.3, 28.4, 28.5, 28.6, 28.7 and 28.8 show the topic values of the two data sets. There is a clear difference between the topics of both data sets.

To predict the clusters in both data sets, two neural network models are created. Each model is trained using the k fold cross-validation technique. Long Short Term Memory (LSTM) neural network models have four layers. The first layer is the input layer, and the activation function is the relu function. The hidden layers have the same relu as the activation function. As there are three clusters in each data set, the fourth layer is used as the output layer, with the softmax function as the activation function and three output class labels. Figure 28.11 depicts the LSTM model's k fold evaluation metrics on the data set1. The model's average accuracy is 96%, and its precision is.

Table 28.3 Top words of cluster 1

Topic	Value
Health	1.744777
Film	1.312178
Nurses	1.182157
World	0.881974
Coverage	0.809457
Right	0.907109
Care	0.557890
Health for al	1.464548
Year	0.684092
Supportnursesandmidwives	0.727517

Table 28.4 Top words of cluster 2

Topic	Value
Cancer	1.332049
Healthy	1.308509
Amp	1.404904
Depression	0.972865
Children	0.849636
Tobacco	1.009721
Food	1.219954
Countries	1.132516
People	0.863714
Let	0.944521

Table 28.5 Top words of cluster 3

Topic	Value
Ncov	2.463818
Emergency	0.869713
China	0.923979
Briefing	1.361026
Outbreak	0.716221
Full	1.287731
Committee	0.735832
Situation	0.810617
Research	0.847140
Spread	0.743905

Table 28.6 Top words of cluster 1

Topic	Value
Ncov	2.463818
Emergency	0.869713
China	0.923979
Briefing	1.361026
Outbreak	0.716221
Full	1.287731
Committee	0.735832
Situation	0.810617
Research	0.847140

Table 28.7 Top words of cluster 2

Topic	Value
Regulations	1.434729
Provided	0.736049
Concern	0.656095
Members	1.143086
Outside	0.386735
Statement	0.914186
Meeting	0.587886
reconvene	0.733883
Committee	0.710073
declared	0.506046

Table 28.8 Top words of cluster 3

Topic	Value
Media	1.983065
Full	1.680201
Photos	1.113571
Daily	2.179259
Live	1.122162
Full	0.829757
Issues	0.552410
Coronavirus	1.284739
Africa	0.647788
Ladygaga	0.746465

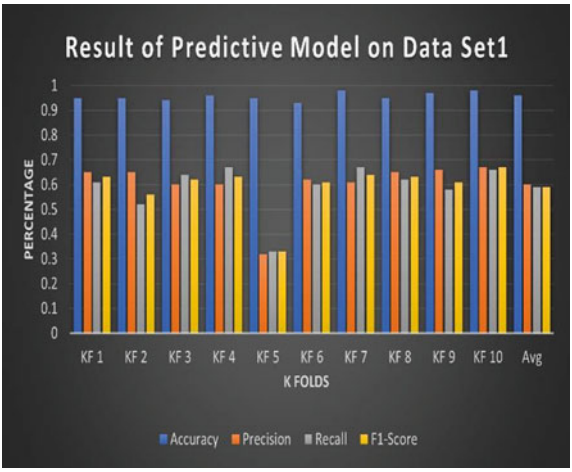

Fig. 28.11 Evaluation metrics of data set1

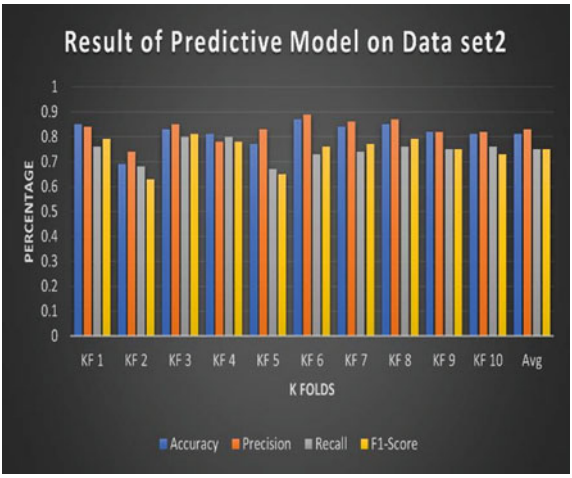

Fig. 28.12 Evaluation metrics of data set2

Figure 28.12 shows the evaluation metrics values of the cross-validation technique on the data set2. However, the average accuracy of the predictive model is 81%, precision is 83%, recall is 75%, and the f1-score is also 75%.

Related Work

Twitter has recently gotten a lot of attention in the scientific community, for example [11, 12]. Our research differs from previous pioneering studies on Twitter in that we attempt to evaluate the material contrasts between Twitter and alternative news outlets. In terms of topic modeling, our model is based on [13], although it samples a single subject for an entire phrase. Reference [14] recently implemented labeled-LDA to Twitter, although the devices that support on hashtags on Twitter, which may not cover all subjects. Reference [15] performed an empirical analysis of several ways for aggregating tweets based on current models. Our suggested Twitter-LDA varies again from models examined in [15] in that, we model two tweet with two subject label, which is comparable to [16–31] but for different applications. Another similar subject

Conclusion and Future Work

We have been a controversy about COVID19 during the ongoing outbreak of COVID19 and presented a study on the general subject of the use of uniform words. We concluded that it is transferred to the use of Covid19 RELED as a substracting instead of identifying the local origin of the virus. Emotions and the use of these

words do not match any term used. First, the LDA model was used to extract articles from the subjects published on the contradictions and data from Twitter was used to compare two sets of data properly. We have been closely related to China in some cases. It is removed before the analysis related to "Chinese Virus", and discussions on unbounded pages are related to the struggle for the US epidemic. The CD includes many CDs with powerful keywords such as "false" and "racist", and "government", such as "government", "government", "work", and "propaganda", including intelligent discussions. Other CDs are included. And "consistency". Conversely, since the knight has many ND spaces, almost all themes are related to "real" conversations, such as theme 5 (emergency) and Article 7 (death) and many keywords. CD Tweets focus on the past and present behaviour of others, whereas ND Tweets focus on the future behaviour of the perpetrator. It appears in CD tweets and moving lyrics to express ideas and opinions. This weakness of ND tweets is like headlines from newspapers like New York. ND's tweets show a strong desire for success. ND users tend to focus more on work and financial matters regarding personal matters. Our conclusion can be based on the recent resurgence of the controversial use of public names. President Trump has mentioned China more than 20 times in his last 14 Republican speeches to Congress. He often uses the term "Chinese virus" to convey anti-Chinese sentiments to his supporters, grandfather. Our research shows that when contrasting words are used, they elicit various emotions in society and how these words can quickly spread strong emotions on social media. Future studies on the use of contradictions related to Covid19 can explore temporary changes in communications concerning the current flash of Covid19. The Development of the US and other significant events (renaming administrators). Some social-political and scientific research studies may be given using integrated data such as nationalism and racial relationships, and the latter is the use of 19 pieces of controversy. In addition, since a trusted classification is achieved with an extensive data set, future research can instruct the use of a separator when monitoring the representation of the representation on social networks. A more advanced relationship and advanced strategy, such as education, reduce education costs and reduces adaptation to rapid changes. Social change. Conversation. In the future, we will investigate systematic methods for summarizing and visualizing Twitter material. Our way of categorizing and categorizing tweets may also aid in the display of Twitter content.

Acknowledgements I would like to thank my supervisor. He showed me how to do research and write quality papers. I am also thankful to my family for their support.

References

1. Bojanowski, P., Grave, E., Joulin, A., & Mikolov, T. (2017). Enriching word vectors with subword information. *Transactions of the Association for Computational Linguistics, 5*, 135–146. https://doi.org/10.1162/tacl_a_00051

2. Cristianini, N., & Shawe-Taylor, J. (2000). *An introduction to support vector machines and other kernel-based learning methods*. Cambridge University Press.
3. Sitaula, C., Basnet, A., & Aryal, S. (2021). Vector representation based on a supervised codebook for Nepali documents classification. *PeerJ Computer Science, 7*. https://doi.org/10.7717/peerj-cs.412.e41
4. Sitaula,C., Xiang, Y., Aryal, S., & Lu, X. (2021) Scene image representation by foreground, background, and hybrid features. *Expert Systems with Applications, 182*. https://doi.org/10.1016/j.eswa.2021.115285.115285
5. Onan, A., & Toçoğlu, M. A. (2020). Weighted word embeddings and clustering-based identification of question topics in MOOC discussion forum posts. *Computer Applications in Engineering Education., 29*(4), 675–689. https://doi.org/10.1002/cae.22252
6. Naseem, U., Razzak, I., Khushi, M., Eklund, P. W., & Kim, J. (2021). COVIDsenti: A large-scale benchmark twitter data set for COVID-19 sentiment analysis. *IEEE Transactions on Computational Social Systems, 8*
7. Pedregosa, F., Varoquaux, G., Gramfort, A., et al. (2011). Scikit-learn machine learning in python. *Journal of Machine Learning Research., 12*(85), 2825–2830.
8. Rossum, G. (1995). *Python reference manual.* Nampa, Idaho: CWI
9. Sitaula, C., Basnet, A., Mainali, A., & Shahi, T. B. (2021). Deep learning-based methods for sentiment analysis on Nepali covid-19—related tweets. *Computational Intelligence and Neuroscience., 2021*, 11. https://doi.org/10.1155/2021/2158184.2158184
10. Zhang, H., Chen, L., Qu, Y., Guo, Z., & Guo, Z. (2014). Support vector regression based on grid-search method for short-term wind power forecasting. *Journal of Applied Mathematics., 2014*, 11. https://doi.org/10.1155/2014/835791.835791
11. Weng, J., Lim, E.P., Jiang, J., & He, Q. (2010). TwitterRank: Finding topic-sensitive influential twitters. In: *Proceedings of the Third ACM WSDM*.
12. Kwak, H., Lee, C., Park, H., & Moon, S. (2010). What is Twitter, a social network or a news media? In: *Proceedings of the 19th WWW.*
13. Steyvers, M., Smyth, P., Rosen-Zvi, M., & Griffiths, T. (2004). Probabilistic author-topic models for information discovery. In: *SIGKDD*.
14. Rose, S., Engel, D., Cramer, N., & Cowley, W. (2010). Automatic keyword extraction from individual documents. In M. W. Berry, & J. Kogan (Eds.), *Text mining: Applications and theory* (1st ed., pp. 1–20). Wiley
15. Hong, L., & Davison, B. D. (2010). Empirical study of topic modeling in Twitter. In: *Proceedings of the SIGKDD Workshop on SMA.*
16. Titov, I., & McDonald, R. (2008). Modeling online reviews with multi-grain topic models. In: *Proceeding of the 17th WWW*.
17. Li, P., Jiang, J., & Wang, Y. (2010). Generating templates of entity summaries with an entity-aspect model and pattern mining. In: *Proceedings of the 48th ACL.*
18. Pedregosa, F., Varoquaux, G., & Gramfort, A. (2011). Scikit-learn machine learning in python. *Journal of Machine Learning Research., 12*, 2825–2830.
19. Almuhaideb, S., & Menai, M. E. B. (2016). Impact of preprocessing on medical data classification. *Frontiers of Computer Science, 10*(6), 1082–1102. https://doi.org/10.1007/s11704-016-5203-5
20. Bougouin, A., Boudin, F., & Daille, B. (2013). TopicRank: Graph-based topic ranking for keyphrase extraction. In *Proceedings of the Sixth International Joint Conference on Natural Language Processing* (pp. 543–551). Nagoya, Japan: Asian Federation of Natural Language Processing.
21. Martinc, M., Škrlj, B., & Pollak, S. (2020). *TNT-KID: Transformer-based neural tagger for keyword identification.* arXiv:2003.09166 [Preprint]. https://arxiv.org/abs/2003.09166
22. Campos, R., Mangaravite, V., Pasquali, A., Jorge, A., Nunes, C., & Jatowt, A. (2020). YAKE! Keyword extraction from single documents using multiple local features. *Information Sciences, 509*, 257–289.
23. Chatzakou, D., & Vakali, A. (2015). Harvesting opinions and emotions from social media textual resources. *IEEE Internet Computing, 19*(4), 46–50.

24. Chen, L., Lu, X., Yuan, J., Luo, J., Luo, J., Xie, Z., & Li, D. (2020). A social media study on the associations of flavored electronic cigarettes with health symptoms: Observational study. *Journal of Medical Internet Research, 22*(6), e17496.s
25. Devlin, J., Chang, M.-W., Lee, K., & Toutanova, K. (2018). *Bert: Pre-training of deep bidirectional transformers for language understanding*. arXiv preprint arXiv:1810.04805.
26. Gagliardone, I., Gal, D., Alves, T., & Martinez, G. (2015). *Countering online hate speech*. Unesco Publishing.
27. Gunsch, M. A., Brownlow, S., Haynes, S. E., & Mabe, Z. (2000). Differential forms linguistic content of various of political advertising. *Journal of Broadcasting and Electronic Media, 44*(1), 27–42.
28. Huang, Q., Singh, V. K., & Atrey, P. K. (2014). Cyber bullying detection using social and textual analysis. In *Proceedings of the 3rd International Workshop on Socially-Aware Multimedia* (pp. 3–6).
29. Kim, E.H.-J., Jeong, Y. K., Kim, Y., Kang, K. Y., & Song, M. (2016). Topic-based content and sentiment analysis of Ebola virus on Twitter and in the news. *Journal of Information Science, 42*(6), 763–781.
30. Loper, E., & Bird, S. (2002). *NLTK: The natural language toolkit*. arXiv preprint cs/0205028.
31. Ramage, D., Dumais, S., & Liebling, D. Characterizing micorblogs with topic models. In *Proceedings of AAAI on Weblogs and Social Media.*

Chapter 29
A Constructive Heuristic Algorithm for 3D Bin Packing of Irregular Shaped Items

Qiruyi Zuo, Xinglu Liu, and Wai Kin Victor Chan

Abstract The three-dimensional bin packing problem (3D-BPP) plays an important role in city logistics and manufacturing environments, due to its direct relevance to operational cost. Most existing literature have investigated the conventional 3D-BPP, in which the shape of items are typically considered as regular shapes, e.g., rectangular-shaped rigid boxes or cylindrical-shaped containers. However, 3D-BPP for non-rectangular shaped items are quite common in varies delivery schemes, especially in fresh food delivery, and few published studies focusing on these issues. In this paper, we address a novel 3D-BPP variant in which the shape changing factor of non-rectangular and deformable items is incorporated to further enhance the loading efficiency and reduce the operational cost of related companies. Motivated by the compression process of item-loading, we propose a constructive heuristic (i.e., an improved dynamic-volume-based packing algorithm) to solve the studied problem. Experimental results over a set of randomly generated instances reveal that considering shape changing factor is indeed able to achieve higher space utilization than that of conventional schemes, thereby has potential to save packaging and delivering cost, as well as enhance operation efficiency.

Keywords Bin packing · Irregular shaped item · Heuristic algorithm · Volume change

Introduction

Three-dimensional bin packing problem(3D-BPP) is critical for those supply chain and logistics companies with massive delivery services due to its direct relevance with operational cost [1], e.g., JD.com, CAINIAO, SF Express, Amazon, etc. According to a news released by a Chinese media,[1] CAINIAO applies a packing algorithm to create packaging materials saving by 15%, achieving a reduction of 290 million in express

Q. Zuo · X. Liu · W. K. V. Chan (✉)
Intelligent Transportation and Logistics Systems Laboratory, Tsinghua-Berkeley Shenzhen Institute, TsinghuaUniversity, Shenzhen 518055, China
e-mail: chanw@sz.tsinghua.edu.cn

[1] VIPUTRANS, https://www.viputrans.com/cainiao-network-exploring-new-models-of-green.

R. Qiu et al. (eds.), *City, Society, and Digital Transformation*, Lecture Notes in Operations Research, https://doi.org/10.1007/978-3-031-15644-1_29

(a) To-be-packed irregular shaped items[1] (b) Packing environments[2] (c) Packing results[3]

Fig. 29.1 Packing irregular shaped items into bins. **a** To-be-packed irregular shaped items.[8] **b** Packing environments.[9] **c** Packing results[10]

parcel amount. This successful application demonstrates that efficient packing solutions have huge potential to achieve considerable operational cost savings for companies in real operations. Moreover, 3D-BPP attracts numerous research efforts from scholars, e.g., Martello et al. [2], Lodi et al. [3], Gzara et al. [4] and Jiang et al. [5].

Although the published literature focusing on optimizing packing solutions is extensive, most of which consider the items are regular-shaped (e.g., rectangular-shaped or cylindrical-shaped). However, irregular-shaped item packing is ubiquitous in delivery and storage environments, especially for fresh food picking and packing (e.g., Amazon fresh,[2] Food For Free,[3] fruitrunner[4] and grocery industry (e.g., Misfits Market,[5] Goteso,[6] Delish[7]). Figure 29.1a–c provides an actual example of packing irregular-shaped items. These full packed boxes will be delivered to the customers (end customer or downstream retailers) after packing procedure.

Solving the conventional 3D-BPP is already extremely challenging due to its NP-hardness nature. Therefore, the problem is even harder to handle after incorporating the characteristic of irregular shape. Currently, the aforementioned irregular-shaped item packing tasks in real schemes are typically performed by workers without providing any reference packing solutions for them in advance (as Fig. 29.1b shows), i.e., these packing operations have not yet well optimized. This inevitably leads to huge container space waste, low packing efficiency, as well as high packaging cost and labor cost.

To cope with these issues, in this work, we first consider the dynamic volume change of irregular-shaped items in 3D-BPP, and propose a constructive heuristic

[2] https://www.amazon.com/

[3] https://foodforfree.org/

[4] https://www.fruitrunner.co.uk/

[5] https://www.misfitsmarket.com/

[6] https://www.goteso.com/

[7] https://www.delish.com/

[8] Misfits Market Review and Latest Coupons - Trial and Eater.

[9] Going the extra miles: Food For Free's Just Eats grocery boxes head to the North Shore - FoodForFree.org.

[10] Fruit and Veg Box - fruitrunner.

algorithm (i.e., dynamic-volume-based packing algorithm) to solve it. We then conduct a series of preliminary numerical experiments to investigate the benefits of volume changing factor. Furthermore, we offer workers with visualized packing sequence to help them accomplish the optimized packing solutions more easily. Results on the tested instances indicates that considering shape changing issue can create significant space utilization improvement compared with the problem under conventional constant volume and shape assumptions. Consequently, developing more realistic approaches for irregular item packing is propose to further save packaging and delivering cost, as well as enhance operation efficiency.

Related Work

The 3D-BPP is NP-hard and thus is extremely hard to solve. Existing literature on this problem mainly focus on various problem variants and solution approaches. From the perspective of problem characteristics, research issues on this topic can be categorized into two groups: (i) regular-shaped item packing; (ii) irregular-shaped item packing.

Regular-shape-focused literature typically aim to load rectangular and cylinder items into bins. They either design exact [6–11] or heuristic [5, 12–16] algorithms to yield high quality solutions. In addition, several papers attempt to apply reinforcement learning techniques to handle 3D BPP, e.g., Jiang et al. [17].

Although the previously mentioned studies are able to enhance the loading efficiency, some realistic features are failed to be contained yet, for example, irregular factor, rotations. Irregular factor refers to item shape and volume. Several published studies have addressed the packing under irregular shape consideration, e.g., Martinez-Sykora et al. [18], Abeysooriya et al. [19]. However, each item is assumed to be rigid and its volume and shape are constant over the entire packing process. This assumption is reasonable for well-packaged express parcels or those hard objects, but it is too ideal for soft items, e.g., fresh food. In fact, the item's actual volume usually changes dynamically as the loading process proceeds, e.g., packing vegetables or groceries into bins. More specifically, the occupied space of an item will reduce if there is pressure from other objects. Ignoring volume changing factor will cause possible space and packaging materials waste to some extent. Therefore, making volume change assumption is propose to create benefits on cost reduction. Nevertheless, to the best of our knowledge, no existing research address this problem. This work maybe the first attempt to consider dynamic volume change in the context of 3D-BPP and develop corresponding solving algorithm.

	product_name	sku_unit_name	stock_out_price	stock_out_count	stock_out_amount	creation_time	completed_time
92226	黄丫头	公斤	39.60	1.32	52.27	2020-10-19 17:25:53	2020-10-20 06:41:15
92227	草鱼	公斤	15.80	2.10	33.18	2020-10-19 17:25:53	2020-10-20 06:41:15
92228	鲫鱼	公斤	31.60	2.08	65.73	2020-10-19 17:25:53	2020-10-20 06:41:15
92599	蜜桔	筐	6.67	23.80	158.75	2020-10-19 12:14:07	2020-10-20 06:41:18
92621	海南香蕉	件	55.00	1.00	55.00	2020-10-19 12:10:47	2020-10-20 06:41:18
92622	娃娃菜3个	包	2.99	2.00	5.98	2020-10-19 12:10:17	2020-10-20 06:41:18
92623	黄豆芽	袋	2.61	2.52	6.57	2020-10-19 12:10:17	2020-10-20 06:41:18
92624	大青菜	公斤	1.00	2.88	2.88	2020-10-19 12:10:17	2020-10-20 06:41:18
92625	洋葱	公斤	1.20	2.10	2.52	2020-10-19 12:10:17	2020-10-20 06:41:18
92626	中青菜	公斤	3.15	2.10	6.62	2020-10-19 12:10:17	2020-10-20 06:41:18
92627	苦瓜	公斤	8.40	1.26	10.58	2020-10-19 12:10:17	2020-10-20 06:41:18

Fig. 29.2 A customer order of fresh wholesalers containing some vegetables and fruits

Problem Description and Formulation

Preliminaries

Before detailing the mathematical descriptions, we first begin with a real scheme. Consider a fresh food wholesale delivery company aims to pack a batch of different kinds of fresh food into a number of rectangular bins and then deliver these bins to the customers. Figure 29.2 shows a particle order received from some customer (e.g., restaurants, supermarkets). The company receives numerous orders from various customers every day. To accomplish these orders, the company first purchases foods and then arrange works to picking and packing foods into bins. Then a fleet of vehicles are dispatched to deliver the packed bins to the customers.

To improve the delivery efficiency, we make the following assumptions according to practical requirements:

1. Fresh food for different customers cannot be packed in the same bin.
2. The same kind of fresh food will be placed in the same bin first.

In addition, to save container (basket) rental cost, companies usually aim to minimize the number of needed bins. In this work, we focus on a simple reduced version of this problem, i.e., we only attempt to maximize the initial volume of all the items of each single bin, which also typically results in greater space utilization.

Mathematical Descriptions

At present, numerous published papers investigate the bin packing problem of two-dimensional irregular shapes. The main methods of solving these problems are approximation and heuristic, e.g., envelope method [20], graph theory method [21], etc. To be more specific, the main idea of rectangle envelope method is to approximate the combination of single or multiple parts with the minimum envelope rectangle,

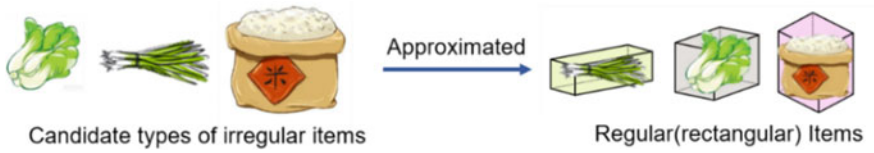

Fig. 29.3 The irregular item is approximated by a regular item which is the corresponding smallest envelope cube

and then convert it into a rectangular-shaped item packing problem. Such approach is simple and easy to implement for real cases.

Motivated by the rectangular envelope method in two-dimensional bin packing problem, we approximate three-dimensional irregular-shaped item as the smallest envelope cube, as shown in Fig. 29.3. This approximation method is simple and easy to implement, but usually suffers from large errors and cannot accurately describe the size of the item. With this in mind, we introduce the process of item compression. Through this method, we take into account the possible compression characteristics of some special objects in real life (such as most of the vegetables and fruits in fresh food), and reduce the volume error after approximation in the meantime. In our work, we consider the irregular-shaped items are deformable and their height will be compressed during the packing process. Therefore, the actual occupied volume of packed items changes dynamically while executing the packing process. But the volume change must lie in reasonable range. If not, the items (foods, vegetables) will be crushed and cannot be used anymore. To avoid this issue, we need to restrict that the actual compressed height ratio is smaller than a maximum compression ratio. Based on the above interpretations, we can first approximate the to-be-packed items with rectangles, and then transfer the 3D irregular-shaped item packing problem into a 3D regular-shaped item packing problem with volume change consideration.

Now let us present a formal mathematical description of 3D-BPP for irregular-shaped items. Consider there are a given set of n three-dimensional, rectangular and deformable items, $I = \{I_1, I_2, \ldots, I_n\}$. Each item in the set I is characterized by its depth d_i, width w_i, initial height h_i, weight m_i, compressibility c_i and maximum compression ratio r_i, $\forall I = \{1, 2, \ldots, n\}$. Compressibility indicates the proportion of deformation of an item due to the total weight of the items above it. The maximum compression ratio indicates the maximum ratio value by which the height of the item can be reduced. This parameter is to avoid over-squeezing and ensure the item can still be utilized. During the process of bin packing, there are also some properties of current item that need to be recorded, including true height after being packed h_i^*, true compression ratio c_i^* and the total weight u_i of all items placed on top of current item. The relations among the characteristics and properties mentioned above satisfy following equations:

$$h_i^* = h_i(1 - c_i^*), \quad \forall i = \{1, 2, \ldots, n\} \tag{29.1}$$

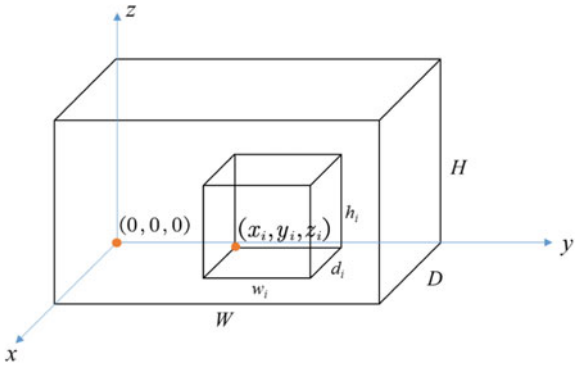

Fig. 29.4 The representations of an item and a bin in the three-dimensional coordinate system

$$c_i^* = \min\left\{r_i, \frac{c_i u_i}{m_i}\right\}, \quad \forall i = \{1, 2, \ldots, n\} \tag{29.2}$$

The items are packed into a number of rectangular bins in k different sizes with dimensions of depth D_j, width W_j and height H_j. The upper face of each bin is opened and it is located in a three-dimensional coordinate system with the back-left-bottom corner in the coordinate origin, i.e. $O(0, 0, 0)$. Each item is represented by its position of back-left-bottom corner coordinate (x_i, y_i, z_i) and dimensions of depth d_i, width w_i and true height h_i^* as shown in Fig. 29.4.

Our objective is to maximize the initial volume of all the items IV packed into each bin, which can be expressed by the following formulas:

$$\max IV = \sum_i d_i w_i h_i x_i, \quad \forall i = \{1, 2, \ldots, n\} \tag{29.3}$$

where x_i is the decision variable. When item i is to be packed in to the bin, $x_i = 1$, otherwise,, $x_i = 0$.

A feasible packing solution in this paper must satisfy the following constraints:

1. *Weight limit*: The total weight of loaded items in the bin cannot exceed the maximum weight limit of the bin.
2. *Space limit*: Items can only be placed inside but not outside the container, that is, the three dimensions width, depth and height of the loaded item cannot exceed those of the bin.
3. *Orthogonality*: Each item must be loaded orthogonally into the bin, that is, the faces of the loaded item are parallel to the walls of the bin.
4. *No overlapping*: Items should not be loaded with overlapping.
5. *Stability*: The loaded items cannot be suspended in the air. Their bottom faces must touch either the top faces of other items or the floor of the bin underneath.
6. *Orientation*: Each item has 6 rectangular facets, but there are only 3 distinct facets because "opposite" facets are identical. Each of the three facets can be rotated orthogonally to obtain a new dimension of the item. Thus, each item can have 6

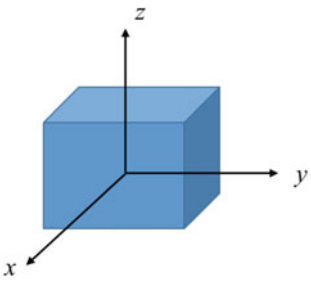

Fig. 29.5 Objects can be rotated about the three axes of symmetry

Table 29.1 Six different rotation types obtained by rotating about different axis

Rotation type	First axis to rotate about	Second axis to rotate about
0	–	–
1	Z	–
2	X	Y
3	Y	–
4	X	Z
5	X	–

different rotation types, which can be obtained by rotating about the x, y and/or z axis as shown in Fig. 29.5 and Table 29.1.

Proposed Algorithm

The Proposed Dynamic-Volume-Based Packing Algorithm

In this paper, we propose a new method for implementing a bottom-left-fill packing strategy, which considers height change due to compression during the packing progress of items and prevents items from hanging in the air. Only one bin will be opened at a time and the algorithms use a series of *pivot points* where to pack the item. Pivot point is an (x, y, z) coordinate which represents a point in a particular three-dimensional bin where an attempt to pack an item will be made. The back-left-bottom corner of the item will be placed at the pivot point. The first and the only one pivot point in an empty bin is always $O(0, 0, 0)$. When item i is placed with its back-left-bottom corner in the pivot point (x, y, z), for example, $O(0, 0, 0)$, it will generate a series of potential pivot points for the items that have not been packed, which includes $pX(x + d_i, y, z)$, $pY(x, y + w_i, z)$ and $pZ(x, y, z + h_i)$ as shown in Fig. 29.6.

To prevent items from hanging in the air after being packed, each pivot point will be considered whether it is feasible. A pivot point is invalid if it's dangling, so we

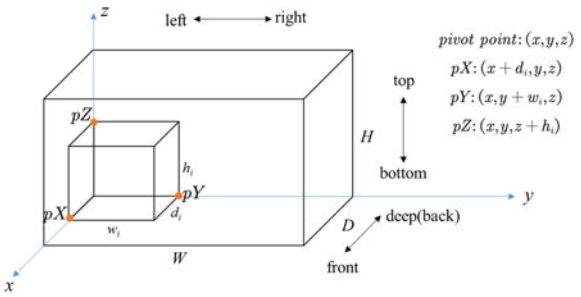

Fig. 29.6 Bottom-left-fill packing strategy: when item i is placed with its back-left-bottom corner in the pivot point (x, y, z), it will generate a series of potential pivot points for the items that have not been packed

need to select a new valid pivot point. The new valid pivot point is generated by looking from top to bottom and take the mapping point on the top surface of the first item below pivot point $pX(pY)$, as shown by the orange dots in Fig. 29.7. What should be particular noted is that the pivot point to the left of new valid pivot point, as shown by the blue dots in Fig. 29.7, will still be given priority. In this case, the item will not be able to be hanging in the air. All the new pivot points will be appended to the list of pivots. The pivot points in list of pivots are sorted in the bottom-left-deepest order, that is, the pivot points are scanned according to lowest z values, breaking ties by lowest y and then by lowest x values.

For each item, the facet with the largest area of the item is defined as the bottom facet, which helps to ensure the stability of the item to a certain extent. The items to be packed into the bin will be first sorted according to the bottom facet area from large to small, and for items with the same bottom facet area they will be sorted according to their compressibility. This sorting approach is more in line with our actual experience, that is to give priority to items with larger bottom facet area and compressibility packed at the bottom of the bin, which will make it easier to load more items. When packing each item, we prioritize the bottom-down rotation type and then traverse the list of pivots until the item can be packed at a pivot point, otherwise item is rotated and re-traverse the list of pivots until we have tried all 6

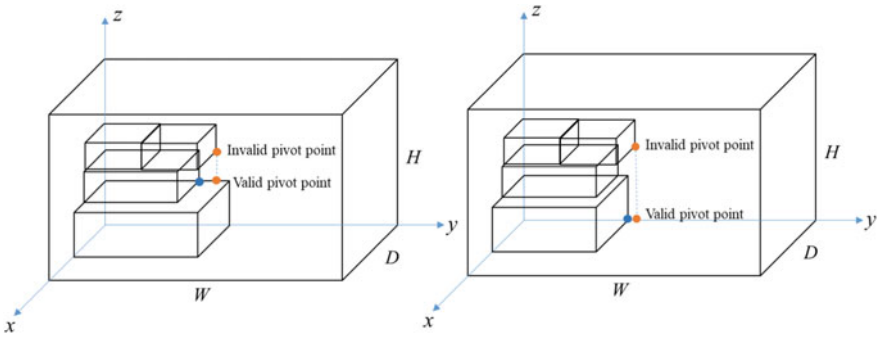

Fig. 29.7 The orange dots represent the mapping of invalid points to valid points. The blue dots are given priority to be considered

possible rotation types. If the item still cannot be packed at the pivot point after being rotated, then we move on to packing the next item and add the unpacked item to a list of items that cannot be packed in to the bin. Algorithm 1 gives the pseudo-code of the proposed dynamic-volume-based loading algorithm, where the list of pivots stores a series of tuples each of which used to store the pivot point and the item under the corresponding point, for example, ((0,0,0), None) for the origin.

Algorithm 1 The proposed dynamic-volume-based loading algorithm.

Algorithm 1 Dynamic-volume-based packing algorithm

1: Initialize pivot point $p \leftarrow [0, 0, 0]$, the item under current pivot point $a \leftarrow \emptyset$, the Pivot_list $P \leftarrow \{(p, a)\}$
2: Three new pivot points pX, pY, pZ generated after packing an item in pivot point p
3: Sort the Items I according to maximum floor area S and compressibility c: sort(I, key $= S, c$)
4: for each item $i \in I$ do
5: for each rotation_type do
6: for each $(p, a) \in P$ do
7: if put_item(i, p, rotation) == True: then
8: $P \leftarrow P/\{(p, a)\}$
9: if pX or pY goes beyond the surface of the item below then
10: $height, a \leftarrow (height, a)$ of the upper surface of the first object found straight down from pX or pY
12: $P \leftarrow P \cup \{([pX(pY)[0], pX(pY)[1], height], a)\}$
13: else
14: $P \leftarrow P/\{pX, a\}$
15: $P \leftarrow P/\{pY, a\}$
16: $P \leftarrow P/\{pY, a\}$
17: sort(P, key $= p[2], p[1], p[0]$)
18: end if
19: end if
20: end for
21: end for
22: end for

Model of 3D-BPP of Deformable Items with Dynamic Volume Change

We establish the 3D-BPP model of irregular deformable items with dynamic volume change that simulates the compression process of items and estimate whether the item can be packed into the bin. The model provides a general framework for handling the 3D-BPP of deformable items and can be used to evaluate the performance of different heuristic algorithms.

For item i with a certain rotation type and a pivot point, the pivot point and the sizes of item are regarded as the position and the dimension of the item respectively. When

trying to put current item i in the top of some other items in the bin, it's necessary to calculate whether the total true height will exceed that of bin. The position, the total weights of items placed on the current item i, true compressibility and true height of each item under item i considering should be updated after being compressed. If item i cannot be packed into the bin even after the process of compression, it means that it will totally not fit in this bin. Algorithm 2 gives the pseudo-code of the model of how to estimate whether current item can fit into the bin.

Algorithm 2 The model of how to estimate whether current item can fit into the bin.

Algorithm 2 Estimate if the item can fit into the bin

```
Function: Put_item(I,(p, a), rotation_type)
Initialize the item under i is n_i ← a, the item on i is m_i ← ∅ the total weight of all the items on current item c is u_c ← 0
if i is wide or deep beyond the edge of the bin then
    return False
end if
if there is no item under p in the bin then
    if (i is high beyond the top of the bin) or (intersect with items in the bin) then
        return False
    end if
end if
while n_i != None do
    n_i ← n_ni
    u_{n_i} ← u_{n_i} + w_{n_i}
end while
item_list L ← [n_i]
while L is not NULL do
    current item c ← L[0]
    calculate and update the actual position, compressibility and true height of current item
    L ← L ∪ {m_c}
    L ← L/{c}
end while
if (the new height beyond the top of the bin) or (intersect with items in the bin) then
    return False
else
    return True
end if
```

Experiments

In this section, we summarize the experimental results. The proposed algorithm and model are implemented in Python3. All the computational experiments are carried out on a laptop with 2.80 GHz CPU and RAM 16 GB.

Experimental Settings

Due to the lack of shared test data for these kinds of studies, we test our algorithm and model using data generated randomly, which includes different sizes of bins (as Table 29.2 shows) and 4 types of items (as Table 29.3 shows). Items are divided into four categories: green vegetables (Type 0), rice (Type 1), melons and fruits (Type 2), and other categories (Type 3), corresponding to different compressibility and maximum compression ratio. Table 29.4 shows the examples of items used in experiment, where only one single bin will be considered at each time.

Table 29.2 Four different types of bins

Bin type	Depth (cm)	Width (cm)	Height (cm)	Max weight (kg)	Quantity
Small bin	40	40	35	55	1
Medium bin	50	45	40	65	1
Large bin	60	50	45	80	1
Larger bin	70	65	60	100	1

Table 29.3 Four different types of items

Item type	Compressibility	Maximum compression ratio
0 (Green vegetables)	0.1	0.3
1 (Rice)	0.03	0.2
2 (Melons and fruits)	0.01	0.1
3 (Other categories)	0	0

Table 29.4 All the candidate items

Item name	Depth (cm)	Width (cm)	Height (cm)	Weight (kg)	Quantity	Type
Chinese cabbage	25	12	12	1.2	50	0
Little cabbage	18	8	8	0.8	50	0
Rice	45	40	8	5	5	1
Millet	35	30	8	2.5	5	1
Bebe pumpkin	10	10	7	0.3	50	2
Potato	12	5	5	0.1	50	2
Eggs	30	20	20	1.6	5	3

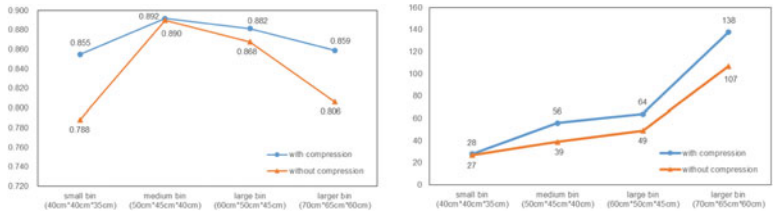

(a) Comparison of space utilization (b) Comparison of the number of items packed in the bin

Fig. 29.8 Comparison of the results with and without compression under different sizes of bins

Table 29.5 Packing situation of each bin

Bin type	Initial volume of total items in the bin	True volume of total items in the bin	The number of items packed into the bin	Space utilization
Small bin	51,412.00	47,881.35	28	0.855
Medium bin	85,200.00	80,259.48	56	0.892
Large bin	155,132.00	143,729.04	64	0.882
Larger bin	264,376.00	234,505.64	138	0.859

Experimental Results

To verify the performance of the new approach, our method is tested on the data set comparing the initial volume and number of all the packed items and space utilization for each bin with and without compression. As shown in Fig. 8a, the space utilization with compression under bins of different sizes is higher than that without compression. Figure 8b demonstrates that the bin can hold more items when taking compression into consideration. Table 29.5 reports the results of the initial volume and true volume (after being compressed) of total items in the bin, the number of packed items and space utilization for different sizes of bins by the proposed method, which shows good behaviour of improving initial volume of total items.

Visualization Bin Packing

In order to show the results more intuitively, we use python for visualization. Figure 29.9 visualizes the effect of different sizes of bins and dynamic loading animation is uploaded on the website https://github.com/3D-irregular-bin-packing/Video/tree/main. It can be seen that our visualization can conveniently give the staff suitable solutions in real time in practice.

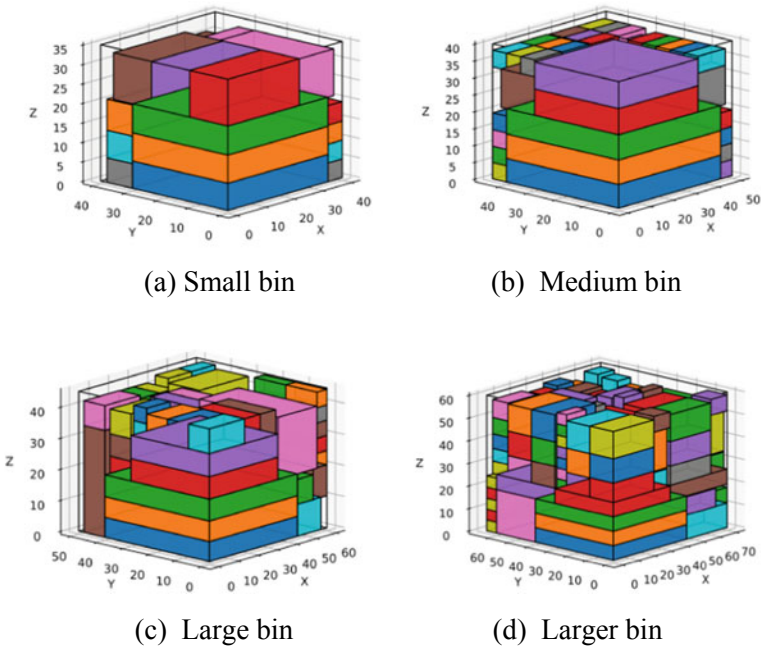

(a) Small bin (b) Medium bin

(c) Large bin (d) Larger bin

Fig. 29.9 Visualization of items with compression

Conclusion

We investigate the 3D BPP for irregular-shaped items. In the context of fresh food delivery in this work, instead of assuming the items are rigid and no deformation will occur during the packing procedure, we consider that the volume of the items changes dynamically while packing due to extrusion. We propose a dynamic-volume-based heuristic to solve the studied problem. Computational results reveal that the space utilization is improved after incorporating the volume change issues.

Future work may focus on proposing the mixed integer programming model to obtain the optimal solution and serve as benchmarks to estimate the solution quality of heuristic solutions yielded in this work.

Acknowledgements This research was partially supported by the Shenzhen Science and Technology Innovation Commission (JCYJ20210324135011030, WDZC20200818121348001), Guangdong Pearl River Plan (2019QN01X890), and National Natural Science Foundation of China (Grant No. 71971127), and Shenzhen Yue Hou Technology Co., Ltd.

References

1. Kaabi, J., Harrath, Y., Bououdina, H. E., & Qasim, A. T. (2018). Toward smart logistics: A new algorithm for a multi-objective 3D bin packing problem. Smart Cities Symposium 2018
2. Martello, S., Pisinger, D., & Vigo, D. (2000). The three-dimensional bin packing problem. *Operations Research, 48*, 256–267.
3. Lodi, A., Martello, S., & Vigo, D. (2002). Heuristic algorithms for the three-dimensional bin packing problem. *European Journal of Operational Research, 141*(2), 410–420.
4. Gzara, F., Elhedhli, S., & Yildiz, B. C. (2020). The pallet loading problem: Three-dimensional bin packing with practical constraints. *European Journal of Operational Research, 287*, 1062–1074.
5. Jiang, J, Cao, L. (2012). A hybrid simulated annealing algorithm for three-dimensional multi-bin packing problems, IEEE.
6. Elhedhli, S., Gzara, F., & Yildiz, B. (2019). Three-dimensional bin packing and mixed-case palletization. *INFORMS Journal on Optimization, 1*(4), 323–352. https://doi.org/10.1287/ijoo.2019.0013
7. Martello, S., Pisinger, D., Vigo, D., et al. (2007). Algorithm 864: General and robot-packable variants of the three-dimensional bin packing problem. *Acm Transactions on Mathematical Software, 33*(1), 7.
8. Fekete, S. P., Schepers, J., & Veen, J. (2006). An exact algorithm for higher-dimensional orthogonal packing. *Operations Research, 55*(3), 569–587.
9. Hifi, M., Kacem, I., Nègre, S., et al. (2010). A linear programming approach for the three-dimensional bin-packing problem. *Electronic Notes in Discrete Mathematics, 36*, 993–1000.
10. Junqueira, L., Morabito, R., & Yamashita, D. S. (2012). Three-dimensional container loading models with cargo stability and load bearing constraints. *Computers and Operations Research, 39*(1), 74–85.
11. Schyns, M., Limbourg, S., et al. (2016). A mixed integer programming formulation for the three-dimensional bin packing problem deriving from an air cargo application. *International Transactions in Operational Research: A Journal of the International Federation of Operational Research Societies, 23*(1/2), 187–213.
12. George, J. A., & Robinson, D. F. (1980). A heuristic for packing boxes into a container. *Computers and Operations Research, 7*(3), 147–156.
13. Scheithauer, G. (1991). A three-dimensional bin packing algorithm. *Elektronische Informationsverarbeitung und Kybernetik, 27*, 263–271.
14. Bischoff, E. E., & Ratcliff, M. (1995). Issues in the development of approaches to container loading. *Omega, 23*(4), 377–390.
15. Eley, M. (2002). Solving container loading problems by block arrangement. *European Journal of Operational Research, 141*(2), 393–409.
16. Crainic, T. G., Perboli, G., & Tadei, R. (2009). TS2PACK: A two-level tabu search for the three-dimensional bin packing problem. *European Journal of Operational Research, 195*(3), 744–760.
17. Jiang, Y., Cao, Z., & Zhang, J. (2021). Solving 3D bin packing problem via multimodal deep reinforcement learning. AAMAS.
18. Martinez-Sykora, A., Alvarez-Valdes, R., Bennell, J., et al. (2017). Matheuristics for the irregular bin packing problem with free rotations. *European Journal of Operational Research, 2017*, S0377221716307950.
19. Abeysooriya, R. P., Bennell, J. A., & Martinez-Sykora, A. (2017). Jostle heuristics for the 2D-irregular shapes bin packing problems with free rotation. *International Journal of Production Economics, 195*, 12–26.
20. Agrawal, P. K. (1993). Minimising trim loss in cutting rectangular blanks of a single size from a rectangular sheet using orthogonal guillotine cuts. *European Journal of Operational Research, 64*(3), 410–422.
21. Kim, J. Y., & Kim, Y. D. (1995). Graph theoretic heuristics for unequal-sized facility layout problems. *Omega, 23*(4), 391–401.

Chapter 30
Implications of Worker Classification in On-Demand Economy

Zhoupeng Jack Zhang, Ming Hu, and Jianfu Wang

Abstract How should workers in the on-demand economy be classified? We study this policy question focusing primarily on the welfare of long-term (LT) workers, who depend on gig jobs as primary income sources. We develop a queueing model with a service platform and two types of workers: LT workers who base their joining decisions on the *long-run earning rate*, while ad hoc (AH) workers who participate according to *real-time payoffs*. We identify two issues with uniform classifications: when all workers previously treated as contractors are reclassified as employees, the profit-maximizing company may *undercut* workers, and LT workers' average welfare can decrease; when all are reclassified as "contractors^{+}", an intermediate status that provides incomplete employee benefits but allows workers to self-join, workers can *overjoin* such that LT workers' utilization rate will remain low and their welfare may not be enhanced. We then consider a discriminatory scheme that classifies LT workers as employees but leaves AH workers as contractors. This hybrid mode suffers from undercutting but curbs overjoining. More importantly, it can do less harm to consumers and the platform operator. We also study a discriminatory dispatch policy that prioritizes LT workers over AH workers. This operational approach can simultaneously counteract undercutting and overjoining. Finally, we empirically calibrate the model and apply our insights to the ride-hailing market in California.

Keywords Worker classification · On-demand economy · Queueing games

Z. J. Zhang (✉) · M. Hu
Rotman School of Management, University of Toronto, Toronto, ON M5S 3E6, Canada
e-mail: zhoupeng.zhang@rotman.utoronto.ca

M. Hu
e-mail: ming.hu@rotman.utoronto.ca

J. Wang
College of Business, City University of Hong Kong, Kowloon 999077, Hong Kong
e-mail: jf.wang@cityu.edu.hk

R. Qiu et al. (eds.), *City, Society, and Digital Transformation*, Lecture Notes in Operations Research, https://doi.org/10.1007/978-3-031-15644-1_30

Introduction

Gig companies like Uber and Lyft have long treated their workers as *independent contractors* (contractors for short) instead of *employees* since these workers have great flexibility in their work schedule [23]. Despite the merits of flexible jobs [9], contractors are not entitled to employee benefits such as the minimum wage and unemployment insurance [31]. To enhance gig workers' welfare, regulators around the globe have attempted to reclassify them as employees. For example, according to the California Assembly Bill No. 5 (AB5), gig workers must be provided with complete employee benefits [24]; importantly, they must be compensated both when working and when waiting for new "gigs".[1] Alternatively, the UK Supreme Court ruled that Uber drivers shall be treated as contractors$^+$, an intermediate status between contractors and employees. The ruling requires less workers' compensation: the company only needs to provide gig workers with some benefits and may not compensate them for their idle times [33]. We term the employee mode (EM) and contractors$^+$ mode (C$^+$M) uniform classifications because current regulations target all gig workers on such platforms.

However, gig workers differ a lot in their backgrounds and needs. Ad hoc (AH) workers do gigs mostly to supplement the income from their full-time jobs elsewhere. For them, the flexibility is more important than the employee benefit [27]. Yet there are also *long-term* (LT) workers who have worked as much as full-time employees and take gig jobs as a primary income source [18]. It has been reported that without the employee benefits, LT Uber drivers in 2018 earned even lower than "the lowest-paid major occupation" [38]. Evidence also shows that gig companies depend on LT workers for a critical portion of their businesses [30]. Therefore, the welfare of LT workers shall be the focus in policy evaluation.

In this research, we will closely examine the implications of uniform classifications for LT workers. In the EM, though workers will be provided with complete benefits, companies will also significantly limit their flexibility to avoid unnecessarily paying for workers' idle time. But then AH workers, who treasure the flexibility, will mostly leave the market. Yet how are market outcomes affected by the presence of AH workers? Can LT workers as a whole be better off with complete benefits on the one hand but companies' strict control on the other? And will they be better off in the C$^+$M, where companies will pay less benefits but also impose less control? We will analyse a game-theoretic queueing model to answer these questions. We will show that uniform classifications may not always help LT workers, while discriminatory schemes that can serve as promising alternatives.

[1] Because workers are "engaged to wait." See https://www.dol.gov/agencies/whd/fact-sheets/22-flsa-hours-worked.

Literature Review

Our work contributes to the burgeoning discussion on how to enhance the welfare of disadvantaged workers in the gig economy. Research in this stream has studied the implications of minimum wage regulations [2] and the labor pool size regulation [3, 37], the gender-related operational issue [35], and workers' welfare on competing platforms [4, 29, 34]. Little research has yet formally looked at the worker classification issue. The work closest to ours is [17]. The authors consider the interaction between a gig company and a single worker. We instead consider a random inflow of heterogeneous workers, and we focus on the welfare implications for those disadvantaged LT workers.

Our work also relates to the literature on platform operations. Researchers have studied capacity management [1, 16], pricing strategies [6, 36], demand and supply matching [10, 15], as well as synergies [25] and competition [5] among companies. In particular, recently there has been an *employees-versus-contractors* debate in this stream. References [12] and [26] study when it is optimal for a company to hire only employees, only contractors, or both types of workers. References [7] and [21] examine how a company shall ration market demand between employees and contractors. These papers have taken the worker classification as given and focus on company's operations. We instead study how gig workers shall be classified, with a primary interest in the welfare of LT workers. In particular, our work differs fundamentally from [26] regarding the role of AH workers. In their model, AH workers help the company hedge the risks of different demand distributions *before* the exact market demand realizes, whereas in our paper AH workers enable the company to operate more efficiently *as* the demand realizes. More importantly, AH workers can encourage the company to raise the piece-rate wage and benefit LT workers. We thus complement [26] by showing that AH workers can be valuable also to their LT co-workers.

Finally, this paper is related to the literature on queueing games (see [19] for a comprehensive survey). References [28] and [13] pioneered the literature by studying monopoly pricing in an observable and unobservable queue respectively. Recent papers have studied queueing systems under more general informational assumptions [11, 20, 22] and analyzed omnichannel service systems (see the discussion in [14]). In our model, LT workers behave similarly to those partly informed customers in [22] while AH workers are analogous to those fully informed ones. We thus contribute to the literature by studying the monopoly pricing with heterogeneously informed customers.

Model and Equilibrium

Consider a service platform operated by a gig company (e.g., Uber). Workers and consumers randomly come to the platform. We model the matching and service

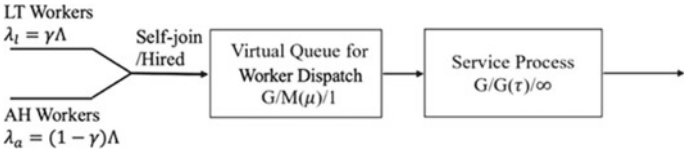

Fig. 30.1 Platform as an open queueing network

processes using a simple two-station Jackson network, which is illustrated in Fig. 30.1. There are two types of workers, long-term (LT) and ad hoc (AH), and they arrive at the platform independently in Poisson processes with rate $\lambda_l \equiv \gamma\Lambda$ and $\lambda_a \equiv (1-\gamma)\Lambda$, respectively. Workers may or may not join the platform upon arrival, and their decisions will be detailed below. Workers who decide to do a gig first enter and wait in the virtual queue for consumer requests. The time between any two consecutive requests is exponentially distributed with mean $1/\mu$. Requests will be assigned to workers in a FCFS manner and lost if there is no worker available. Each worker starts service immediately after getting a request, and service times are i.i.d. with mean $1/\tau$. For each service, the platform charges the consumer a service price $p > 0$. To be parsimonious, we assume away the demand-side pricing. Next we discuss the status quo of CM and two uniform classifications in detail.

Contractor Mode: The Status Quo

In the contractor mode (CM), the company will pay workers a piece-rate wage $w \in [0, p]$ after completing a service, without guaranteeing that workers can receive any employee benefit over time.

AH workers do not depend on gig jobs for a living and thus will not always join the platform. Upon arrival at time t and observing Q_t workers waiting in the virtual queue, an AH worker expects to wait $(Q_t + 1)/\mu$ units of time to get a service request and then take $1/\tau$ units of time to fulfill it. Denote by c_a AH workers' time value. The expected time cost for a gig is thus $c_a((Q_t + 1)/\mu + 1/\tau)$, and AH workers will participate if and only if the real-time labor supply $Q_t < n \equiv \lfloor \mu(w/c_a - 1/\tau) \rfloor$, where $\lfloor x \rfloor$ denotes the largest integer that is less than or equal to x.

LT workers decide whether to commit to working by comparing the long-run earning rate on the platform r with their outside option c_l, which is assumed as the social minimum wage. Their strategy is characterized by the probability $q \in [0, 1]$ of always joining the platform upon arrival. We study the symmetric equilibrium among LT workers, and thus q can also be interpreted as the fraction of committed LT workers. We define r as the ratio of the piece-rate wage w to the average time it takes to earn such a wage in the long run, i.e., $r = w/(W_n(q) + 1/\tau)$, where $W_n(q)$ is the average wait time to be dispatched given the joining probability q and AH workers' participation threshold n.

Define the company's profit as $\Pi \equiv (p - w)\lambda$, where λ is the transaction volume, i.e., the expected number of requests that can be fulfilled by LT and AH workers in any time unit. The company's problem is thus $\max_w \Pi \equiv (p - w)\lambda$. Denote by w^* the piece-rate wage that maximizes Π. Also denote by q^* LT workers' joining probability and by n^* AH workers' participation threshold when the company chooses w^*. Denote by R^* the average earning rate for all LT workers; given that in every time unit LT workers who join the platform will earn r and those who choose the outside option will earn c_l, we have $R^* = q^* w^*/(W_{n^*}(q^*) + 1/\tau) + (1 - q^*)c_l$. Further denote by λ^* the transaction volume and by Π^* the company's profit in equilibrium. We characterize the CM equilibrium as follows.

Lemma 2 (LT-only CM equilibrium). *If* $c_a \geq p/(1/\mu + 1/\tau)$, *we have* $R^* = c_l$, $\lambda^* = \overline{\lambda} \equiv \min\{\lambda_l, \mu - \sqrt{\mu\tau c_l/(p\tau - c_l)}\}$, *and* $\Pi^* = \overline{\Pi} \equiv \left(p - c_l\left(1/\left(\mu - \overline{\lambda}\right) + 1/\tau\right)\right)\overline{\lambda}$.

Proposition 1 (CM Equilibrium). *If* $c_a < p/(1/\mu + 1/\tau)$, *we have*:

(i) *For LT workers,* $R^* \geq c_l$. *There exist* $\overline{\gamma}$, $\underline{c}$ *and* $\overline{c}$ *such that if* $c_a \in \left(\underline{c}, \overline{c}\right)$ *and* $\gamma \leq \overline{\gamma}$, $R^* > c_l$.

(ii) *For consumers, there exist* $\underline{\gamma}$, $\overline{\gamma}'$, $\underline{c}'$ *and such that if* $c_a \geq \overline{c}'$, $\lambda^* \geq \overline{\lambda}$; *if* $c_a < \underline{c}'$ *and* $\gamma \in \left[\underline{\gamma}, \overline{\gamma}'\right]$, $\lambda^* \leq \overline{\lambda}$.

(iii) *For the company,* $\Pi^* \geq \overline{\Pi}$.

It is worthwhile to highlight the result for LT workers. Comparing Proposition 1(i) with Lemma 2, one can see that thanks to AH workers' participation, LT workers can earn strictly more than they would from their outside option. The intuition is that, AH workers participate contingent on the real-time labor supply; when the labor supply is sufficient, to persuade AH workers to keep participating in case the request volume quickly goes up, the company must pay a relatively high piece-rate wage. If AH workers' time value is moderately high [i.e., $c_a \in \left(\underline{c}, \overline{c}\right)$], such a high wage will eventually translate into a high average earning rate for LT workers. This result complements the literature [3, 29], with a fresh insight into the relationship between the labor pool size and average labor welfare. Unlike previous research, our model incorporates the widely observed heterogeneity in gig workers' participation patterns [18], and we show that those who participate regularly (i.e., LT workers) will be better off if those who participate contingently (i.e., AH workers) join the market (i.e., labor pool expansion).

Note also that the company makes more profit in the presence of AH workers [i.e., $\Pi^* \geq \overline{\Pi}$ in Proposition 1(iii)]. We attribute this result again to AH workers' contingent joining behavior: unlike LT workers who join the platform with a predetermined probability, AH workers participate exactly when the labor supply is running low (so that the platform will be quickly "reloaded") and walk away when the supply is abundant (so that the platform will never become overcrowded and some LT workers can commit to working). As such, the presence of AH workers enables the company to fulfill service requests more efficiently and thus make more profit.

Employee Mode

Company's operations in the EM will change in the following ways. First, for every time unit, whether a worker is waiting for a service request or fulfilling one, the company will pay (i) an hourly wage $w' \geq c_l$ and (ii) a lump-sum employee benefit $B \geq 0$. Second, as the employer, the company now will perform admission control of workers, which follows the high-level assumption that gig companies in the EM will impose strict workplace rules rather than give workers the same flexibility as in the CM. The purpose is to keep the utilization rate of workers at a reasonable level and avoid paying for workers' unprofitable activities. Finally, we assume that AH workers will quit the market while LT workers will still come to work. This last assumption follows the fact that most AH workers treasure the flexibility to earn supplemental incomes outside their full-time jobs [9].

Since all LT workers would like to be hired for any $w' \geq c_l$, it is optimal for the company to set $w'* = c_l$. The company then only needs to decide the optimal joining rate of LT workers. Denote by $\lambda_E \in [0, \lambda_l]$ the joining rate of LT workers controlled by the company. Because now only LT workers will come to the platform, the virtual queue becomes an M/M/1 queue and the average wait time for a request is $1/(\mu - \lambda_E)$. Since a hired worker must receive $c_l + B$ for every time unit on the platform, the expected labor cost for each service is $(c_l+B)(1/(\mu-\lambda_E)+1/\tau)$, which is bounded below by $(c_l + B)(1/\mu + 1/\tau)$. Define $B_{max} \equiv p/(1/\mu + 1/\tau) - c_l$.

The platform's profit maximization problem in the EM is $\max_{\lambda_E} \Pi_{\mathrm{E}} \equiv \lambda_E(p - (c_l + B)(1/(\mu - \lambda_E) + 1/\tau))$. Denote by R_E^* LT workers' average earning rate, λ_E^* the transaction volume, and Π_E^* the company's profit in the EM equilibrium. We characterize the EM equilibrium as follows.

Proposition 2 (EM equilibrium). *For $B \in [0, B_{max}]$, we have*:

(i) *For LT workers, $R_E^* = c_l + \left(\lambda_E^*/\lambda_l\right)B$. There exists $B_E < B_{max}$ such that r_E^* is increasing in B on $[0, B_E]$ but decreasing in B on $[B_E, B_{max}]$.*

(ii) *For consumers, $\lambda_E^* = min\{\lambda_l, \mu - \sqrt{\mu\tau(c_l + B)/(p\tau - (c_l + B))}\}$ and is decreasing in B.*

(iii) *For the company, $\Pi_E^* = \left(p - (c_l + B)\left(1/\left(\mu - \lambda_E^*\right) + 1/\tau\right)\right)\lambda_E^*$ and is decreasing in B.*

Proposition 2 says LT workers' average earning rate R_E^* in the EM will first increase and then decrease in the lump-sum benefit B, while both the transaction volume and the company's profit will decrease in B. The properties of λ_E^* and Π_E^* are intuitive: as B increases, the company's labor cost increases so that fewer LT workers will be hired to fulfill requests and less profit can be made by the company. For LT workers, as B increases, some of them will be laid off and lose B, while those who are still employed will be provided with a higher benefit. When B is low, the company hires a large number of LT workers, and the fraction of layoffs is relatively low. Therefore, as B marginally increases, the loss of the layoffs is less than the gain of the hires, and LT workers' average earning rate increases. When B is sufficiently

high, not many LT workers will still be employed by the company, and the fraction of the layoffs becomes relatively large. As a result, the loss of the layoffs dominates the gain of the hires, and LT workers' average earning rate decreases in B.

Contractor$^+$ Mode

The C$^+$M is an intermediate classification between CM and EM. In UK, Uber guarantees that drivers earn the minimum wage and holiday pay, but only for the time they are fulfilling service requests; drivers can still set their own work schedules [33]. Such flexibility implies that AH workers may again participate in the market. As such, the C$^+$M will operate in the same manner as the CM, except that there will be a wage floor $(c_l + B)/\tau$ for the piece-rate wage w. This is to ensure that workers receive prorated employee benefits at least for the time they are providing services. The company's problem thus becomes $\max_{w \geq (c_l+B)/\tau} \Pi = (p - w)\lambda$. For succinctness, we will focus on LT workers' average earning rate R_+^* in equilibrium. We will compare R_+^* with R^* in the next section.

Implications of Uniform Classifications

We first examine whether LT workers will be better off as employees rather than as contractors.

Theorem 1 (EM vs. CM for LT Workers). *Comparing LT workers' average earning rate R_E^* in the EM and R^* in the CM, we have:*

(i) *When $R^* = c_l$, $R_E^* \geq R^*$. In particular, $R_E^* > R^*$ if and only if $B \in (0, B_{max})$.*
(ii) *When $R^* > c_l$, there exist $\underline{B}, \overline{B} \in (0, B_{max})$ such that $R_E^* \leq R^*$ if and only if $B \leq \underline{B}$ or $B \geq \overline{B}$.*

Theorem 1(i) shows that, when LT workers' average earning rate in CM equals their outside option, LT workers will indeed be better off as employees than as contractors. However, if LT workers in the CM already earn strictly more than their outside option, Theorem 1(ii) warns that they will be worse off as employees if the lump-sum benefit is either relatively low or high.

We term the issue in the EM shown by Theorem 1(ii) *undercutting*. To understand this issue, recall that in the CM, all workers can self-join the platform and will be compensated on a per-piece basis. We have shown in the discussion of Proposition 1 that AH workers' contingent participation can encourage the company to pay a relatively high piece-rate wage, which may translate into a high average earning rate R^* for LT workers.

On the contrary, in the EM, the profit-maximizing company will strictly control workers' compensation and the workforce size. First, instead of paying a piece-rate

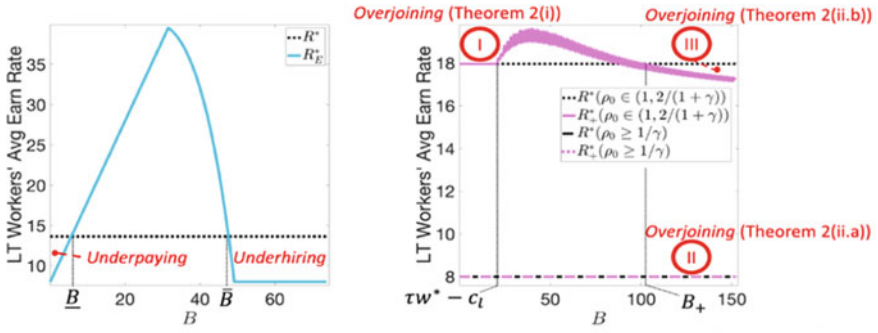

(a) *Undercutting* in EM (b) *Overjoining* in C$^+$M

Fig. 30.2 Uniform classifications ($\gamma = 0.25$, $\tau = 4$, $c_l = 8$, $c_a = 16$; EM: $\Lambda = 15$, $\mu = 10$, $p = 20$; C$^+$M: $\Lambda = 45$, $\mu = 40$, $p = 40$)

wage that depends on market primitives, the company pays each hired LT worker a flat sum of $c_l + B$ for every time unit; if the lump-sum benefit B is too low, LT workers will be underpaid and not necessarily better off than in the CM where they can receive a high wage thanks to AH workers' contingent participation. Second, when B is sufficiently high, only a small number of LT workers will be hired (i.e., underhiring); the rest will have to resort to their outside option and earn the minimum wage c_l. Hence, employee benefits earned by those hired and the lower earnings of those turned away will average out. We illustrate the negative impacts of underpaying and underhiring in Fig. 2a.

Note that [3] show that gig workers will always be better off if regulators impose a wage floor for the average earning rate. Their finding, however, hinges on the assumption that workers are still allowed to freely join the platform. Our work instead stresses that the company can strictly control workers after regulators reclassify them as employees, and LT workers can be undercut by this fundamental change in the company's operations.

Hagiu and Wright [17] find a similar issue in the EM. However, their work and ours differ on why a gig worker may earn more as a contractor. In [17], the company delegates the operation to and shares the final revenue with a contractor. In some cases the contractor will choose the action that not only maximizes the company's profit but also leaves himself a surplus. We show instead that an LT contractor can have a surplus because there can be a high wage thanks to AH contractors' contingent participation. In fact, as we show in the Lemma 2, without AH contractors an LT contractor will never earn more than the outside option, even if the company has delegated to him the pivotal decisions of whether and when to join the platform.

Our results suggest that regulators should exercise caution when attempting to reclassify gig workers as employees, because whether LT workers will be better off hinges on their income levels as contractors. Researchers have not settled on how much gig workers earn in a free market. Using data from Uber, [18] find that in a big U.S. city such as San Francisco, even after adjusting for expenses, an Uber

driver's hourly income is higher than that of an employee taxi driver. In contrast, based on an online survey of 1,121 Uber and Lyft drivers in the U.S., [38] find that 74% of drivers earn less than the minimum wage, and some of them even lose money after accounting for vehicle expenses. As such, it is imperative for regulators to first accurately measure LT workers' incomes as contractors.

We now turn to the implications of C$^+$M. Define $\rho_0 \equiv \Lambda/\mu$ as the company's workload of dispatching workers when all workers join the platform upon arrival. We have the following results.

Theorem 2 (C$^+$M vs. CM for LT Workers). *Comparing the average earning rate R_+^* in the C$^+$M and R^* in the CM, we have: (i) If $B \le \tau w^* - c_l$, $R_+^* = R^*$. (ii) If $B \ge \tau w^* - c_l$, then:*

(a) *If $\rho_0 \ge 1/\gamma$, or equivalently $\lambda_l \ge \mu$, $R_+^* = R^* = c_l$.*
(b) *If $\rho_0 \in (1, 2/(1+\gamma))$ and $R^* > c_l$, there exists B_+ such that if $B \ge B_+$, $R_+^* < R^*$.*
(c) *If $\rho_0 < 1$ or $\rho_0 \in \left[2/(1+\gamma), 1/\gamma\right)$ and $R^* > c_l$, there exists B'_+ such that if $B \ge B'_+$, $R_+^* > R^*$.*

Recall that the C$^+$M attempts to enhance workers' welfare by implementing a wage floor $(c_l + B)/\tau$ on the company's piece-rate wage w. Theorem 2 parts (i), (ii.a) and (ii.b) imply that the wage floor is not enough to make LT workers always better off. We term the issue here workers' *overjoining*.

To understand this issue, first, Theorem 2(i) relates to workers' overjoining in the CM: the more workers joining, the longer the wait times and thus the higher the piece-rate wage w^* in the CM to incentivize workers. As such, unless the lump-sum benefit B is sufficiently high, the wage floor will be too low to make the company raise the piece-rate wage and improve LT workers' welfare, as Fig. 2b area I illustrates. This result complements [3] who study a similar problem but assume that the wage floor will always raise the piece-rate wage.

Theorem 2(ii) parts (a) and (b) are driven by workers' overjoining in the C$^+$M. For Theorem 2(ii.a), because LT workers' arrival rate is higher than the request rate (i.e., $\lambda_l \ge \mu$), the average wait time for a request will be infinitely long if all LT workers join the platform. Hence, not all LT workers will join, and the average earning rate in the CM must equal their outside option. In the C$^+$M, as the wage floor raises the piece-rate wage, LT workers on the outside will be attracted to the platform, ignoring that their participation will increase the average wait time and thus lower the utilization rate of workers already on the platform. In fact, new LT workers will keep joining until the long-run earning rate on the platform falls to their outside option. Therefore, as Fig. 2b area II shows, for any B, LT workers' average earning rate will always equal their outside option.

Finally, for Theorem 2(ii.b), given that in the CM the average earning rate exceeds LT workers' outside option (i.e., $R^* > c_l$), all LT workers have committed to working. Yet as the wage floor in the C$^+$M raises the piece-rate wage, AH workers' real-time payoffs for doing a gig increase, and thus more will join the platform, again ignoring the fact that their participation will reduce the utilization rate of LT workers. Note that

the condition $\rho_0 \in (1, 2/(1+\gamma))$ is equivalent to having AH workers account for a large fraction in the labor pool (i.e., $1-\gamma > (2\rho_0 - 2)/\rho_0$), which implies that LT workers' utilization rate will decrease significantly as more AH workers participate. When the benefit is sufficiently high ($B > B'_+$), the decrease in utilization due to new AH workers is so significant that LT workers will become worse off than in the CM, as Fig. 2b area III illustrates.

Implications of Discriminatory Schemes

In light of the issues with uniform classifications, in this section we will study two discriminatory schemes and examine whether it is indeed more efficient to treat LT and AH workers differently.

Hybrid Mode: A Discriminatory Worker Classification

In the hybrid mode (HM), the company will treat AH workers as contractors but LT workers as employees. This innovative classification that we propose is not without practical foundation. For instance, Uber gives workers bonuses if they participate consistently over time [8].

To set up, think of the HM as an upgrade from the EM. For LT workers, the company will hire at least as many of them as it would do in the EM and will pay those who are hired $c_l + B$ for every time unit on the platform. Define $q_E^* \equiv \lambda_E^*/\lambda_l$ as the fraction of LT workers hired in the EM. Now the company can also enroll AH workers as contractors, i.e., allow them to self-join and will pay them a piece-rate wage w for each service. The discussion in section "Contractor Mode: The Status Quo" implies that it suffices to set the piece-rate wage w at $c_a(n/\mu + 1/\tau)$ to incentivize AH workers to participate up to some threshold $n \geq 0$ in the virtual queue for dispatch. Denote by F_n the probability that the real-time labor supply $Q_t < n$, i.e., the probability that an AH worker will join the platform upon arrival. Therefore, the company's problem in the HM can be written as

$$\max_{q \geq q_E^*, n \geq 0} (p - (c_l + B)(W_n(q) + 1/\tau))q\lambda_l + (p - c_a(n/\mu + 1/\tau))F_n\lambda_a.$$

Theorem 3 (HM vs. EM). *We have* $R_H^* = R_E^*$, $\lambda_H^* \geq \lambda_E^*$ *and* $\Pi_H^* \geq \Pi_E^*$.

Theorem 3 conveys a positive message: to classify gig workers discriminatorily will produce a Pareto improvement over reclassifying all of them as employees, because LT workers will earn as much as in the EM while consumers and the company will both be better off, not to mention that AH workers may participate again and be better off as well.

The equivalence of average earning rates (i.e., $R_H^* = R_E^*$) implies that the HM inherits the undercutting issue in the EM, but curbs the overjoining issue found in the C$^+$M. That is, while LT workers in the HM may still suffer from the company's strict control over their compensation and joining rate, they can be sheltered from their own and their AH counterpart's overjoining. In particular, in the discussion of Theorem 2(ii.b), we show that LT workers will be worse off in the C$^+$M than in the CM as more AH workers join, but here in the HM, their average earning rate $R_H^* = R_E^*$ and will no longer be adversely affected by AH workers' self-interested participation. Moreover, Theorem 2(ii.a) details a case in which given any B, LT workers in the C$^+$M end up earning only the social minimum wage c_l due to their own overjoining; Theorem 2(i) specifies a case in which LT workers only earn c_l because workers have already overjoined in the CM and thus the wage floor in the C$^+$M will not be pushed up by a relatively low B. In stark contrast, Theorem 1(i) implies that LT workers' average earning rate R_H^* in the HM will always exceed c_l for any $B \in (0, B_{max})$.

More importantly, for consumers and the company, if the company enrolls no AH workers at all, clearly both the transaction volume and the company's profit in the HM will be the same as in the EM. Given the ability to treat AH workers as contractors, the company will realize a higher transaction volume and make more profit in the HM than in the EM. In fact, both measures in the HM can even be higher than in the CM. Proposition 3 formalizes this result.

Proposition 3 (HM vs. CM for consumers and the company). *Suppose $q_E^* = 1$ when $B = 0$. There exists a $\overline{B}_H \in [0, B_{max}]$ such that if $B \leq \overline{B}_H$, we have $\lambda_H^* \geq \lambda^*$ and $\Pi_H^* \geq \Pi^*$.*

The intuition for Proposition 3 is as follows. Because workers are now classified discriminatorily, the company can use different wages to incentivize LT and AH workers. As such, the company is generally able to serve as many consumers as before but at a lower total labor cost.

Combined with Theorem 1, Proposition 3 implies that the HM can also Pareto improve over the CM. Figure 30.3 numerically corroborates this positive result.

Corollary 1 (HM vs. CM). *Suppose $q_E^* = 1$ when $B = 0$. For $\underline{\underline{B}}$ defined in Theorem 1 and $\overline{B}_H$ defined in Proposition 1, if $\underline{\underline{B}} \leq \overline{B}_H$, we have $R_H^* \geq R^*$, $\lambda_H^* \geq \lambda^*$ and $\Pi_H^* \geq \Pi^*$ iff $B \in \left[\underline{\underline{B}}, \overline{B}_H\right]$.*

LT Workers' Priority: A Discriminatory Operational Policy

As a companion to the *legal* scheme of worker classification, here we study an *operational* scheme in the CM: when assigning requests, the company prioritizes LT workers over AH workers. Denote this scenario by CM′. Note that in practice gig

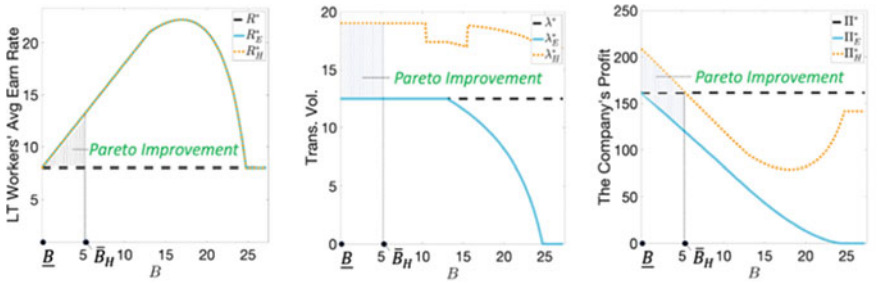

(a) For LT workers (b) For Consumers (c) For the Company

Fig. 30.3 Implications of the priority dispatch ($\gamma = 0.25,\ \Lambda = 50,\ \mu = 20,\ \tau = 2,\ p = 18,\ c_l = 8,\ c_a = 16$)

companies are experimenting with similar approaches. For example, DiDi selects drivers with consistently strong service records to provide premier rides.[2]

One may already notice that this operational scheme can simultaneously counteract both undercutting and overjoining. On the one hand, unlike in the EM, LT workers can self-join the platform and will be paid on a piece-rate basis; thanks to AH workers' contingent participation, again there can be high piece-rate wages that translate into a high average earning rate. On the other hand, unlike in the C$^+$M, LT workers' utilization rate and hence the average earning rate will no longer be adversely affected by AH workers' overjoining, though LT workers themselves may still overjoin the platform. In the proposition below, we formalize the potential to counteract overjoining.

Proposition 4 (CM′ vs. CM for LT workers). *When $n_P^* \geq n^*$, we have $R_P^* \geq R^*$; in particular, if $R^* > c_l$, we have $R_P^* > R^*$.*

Proposition 4 says that if AH workers' participation threshold is higher when LT workers are prioritized than when requests are assigned FCFS (i.e., in the CM), LT workers' average earning rate will always be higher thanks to the priority. This result is in stark contrast to Theorem 2(ii.b), which implies that LT workers in the C$^+$M can be worse off because more AH workers participate.

Proposition 5 below implies that the CM′ could also make both consumers and the company better off than in the CM, and the numerical example in Fig. 30.4 shows that the discriminatory dispatch policy can also Pareto improve over the status quo of CM. The intuition is similar as before. Because LT and AH workers are now treated discriminatorily, the wages to incentivize these two types of workers also change. As such, it is possible for the company to serve as many consumers as before but at a lower total labor cost.

Proposition 5 (CM′ vs. CM for consumers and the company). *Suppose $q_P^* = q^* = 1$ and $n_P^* = n^* > 0$. We have $\lambda_P^* = \lambda^*$, and there exists $\overline{c}''$ such that $\Pi_P^* \geq \Pi^*$ iff $c_a \leq \overline{c}''$.*

[2] See https://www.chinadaily.com.cn/business/2017-05/22/content_29448895.htm.

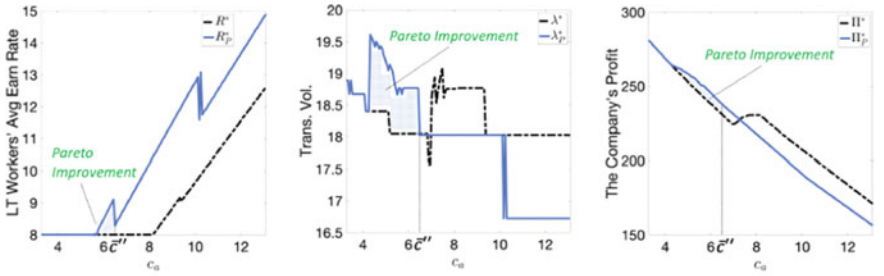

(a) For LT workers (b) For Consumers (c) For the Company

Fig. 30.4 Implications of the priority dispatch ($\gamma = 0.25,\ \Lambda = 30, \mu = 20, \tau = 2, p = 18, c_l = 8$)

Numerical Study

In this section, we calibrate the parameters in our model using real-world data and numerically review our insights. Our motivation is the California Assembly Bill No. 5. The bill was signed into law in 2019, attempting to reclassify gig workers as employees, yet Uber and other gig companies successfully sought exemption from the law in 2020.

For succinctness, we omit the details on parameter calibration. One can refer to Table 30.2 in the appendix for data sources. Table 30.1 provides the summary statistics of parameter calibration at the city level. Figures 30.5, 30.6 and 30.7 display our model's predictions. In each figure, sub-figures (a) and (b) show the implications of two uniform classifications, while sub-figures (c) and (d) demonstrate the implications of two discriminatory schemes. We quantify the implications as the percentage change in certain variables relative to the benchmark of the CM. We color an area green if a change is positive, red if it is negative, and gray if the change is not very significant in scale.

Table 30.1 Summary statistics of calibrated parameters

	Mean	SD	Median	Min	Max
γ	0.080	0.018	0.083	0.050	0.105
Event rate parameters (#/hour)					
Λ	4.089	8.086	2.025	0.809	66.320
μ	4.457	8.814	2.208	0.881	72.289
τ	3.602	1.245	3.613	0.858	6.727
Pecuniary parameters (2019 USD)					
p	15.408	6.174	13.618	8.941	46.044
c_l	12.344	0.854	12.000	12.000	15.000
c_a	22.817	4.398	22.963	14.733	34.546
B	6.383	0	6.383	6.383	6.383

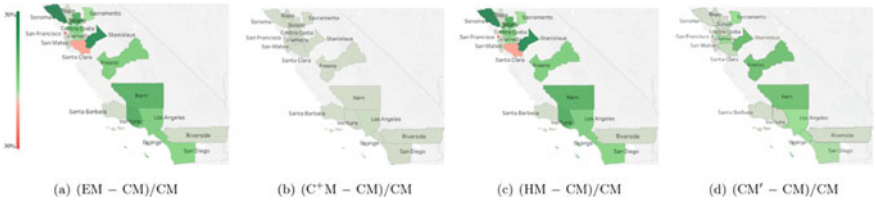

Fig. 30.5 Implications for LT workers

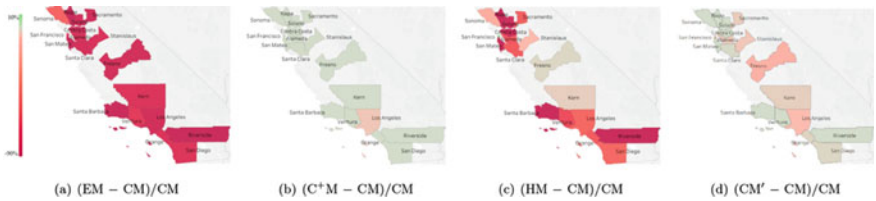

Fig. 30.6 Implications for consumers

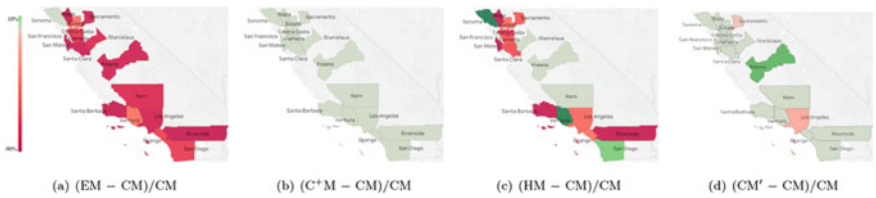

Fig. 30.7 Implications for the company

Sub-figures (a) in three figures together show that the EM can generally improve LT workers' welfare, but at a high cost of other stakeholders in the economy; sub-figures (b) imply that the $C^{+}M$ may not have any significant impact. And by making pairwise comparison between results in sub-figures (c) and (d) with sub-figures (a) and (b), one can see that discriminatory schemes can generally Pareto improve over uniform classifications.

Concluding Remarks

This paper speaks to the recent policy debate over worker classification in the on-demand economy. We highlight the difference between AH and LT workers and focus on the welfare of the latter, who have served effectively as full-time employees yet have not been provided with the employee benefits that they need and deserve. We show that overlooking the heterogeneity among gig workers and reclassifying all workers in the same way will cause problems both with workers being undercut

and with workers overjoining. In light of such limitations, we propose schemes that discriminate both in classification and from an operational perspective and demonstrate the potential of these schemes to Pareto improve over uniform classifications; that is, it is possible to enhance the welfare of the disadvantaged LT workers without hurting other stakeholders in the economy, or at least causing less damage.

Our theoretical framework serves as a basis for better understanding the worker classification issue. An interesting extension would be to endogenize the service price p through the company's demand-side pricing. Another promising avenue is to consider the setting with competing platforms. We expect that our results will continue to provide insights in these general settings, and we leave the investigations to future research.

Appendix

Table 30.2 Data sources for parameter calibration

Parameter	Source
γ	https://www.census.gov/quickfacts/fact/table/CA/HEA775220
$\Lambda\&\mu$	https://www.sfcta.org/sites/default/files/2019-06/trip_stats_taz_0.csv, Population by city on https://www2.census.gov/
τ	[32], Land area by city on https://www.census.gov/
p	https://www.ridesharingdriver.com/how-much-does-uber-cost-uber-fare-estimator/, Land area by city
c_l	https://www.dir.ca.gov/dlse/faq_minimumwage.htm, https://laborcenter.berkeley.edu/inventory-of-us-city-and-county-minimum-wage-ordinances/
c_a	https://www.census.gov/quickfacts/fact/table/CA,US/INC110220, https://www.bls.gov/opub/mlr/cwc/work-schedules-in-the-national-compensation-survey.pdf, https://www.census.gov/quickfacts/fact/table/CA/HSD310220, https://www.census.gov/quickfacts/fact/table/CA/LFE041220
B	Table 9 in https://www.bls.gov/web/ecec/ececqrtn.pdf

References

1. Afeche, P., Liu, Z., & Maglaras, C. (2018). Ride-hailing networks with strategic drivers: The impact of platform control capabilities on performance. SSRN 3120544.
2. Asadpour, A., Lobel, I., & van Ryzin, G. (2020). Minimum earnings regulation and the stability of marketplaces. SSRN 3502607.
3. Benjaafar, S., Ding, J. Y., Kong, G., & Taylor, T. A. (2022). Labor welfare in on-demand service platforms. *Manufacturing Service Operations Management, 24*(1), 110–124.
4. Benjaafar, S., Xiao, S., & Yang, X. (2020). Do workers and customers benefit from competition between on-demand service platforms? SSRN 3645882.

5. Bernstein, F., DeCroix, G. A., & Keskin, N. B. (2021). Competition between two-sided platforms under demand and supply congestion effects. *Manufacturing Service Operations Management, 23*(5), 1043–1061.
6. Cachon, G. P., Dizdarer, T., & Tsoukalas, G. (2021). Pricing in service platforms: Who should set the prices.
7. Chakravarty, A. K. (2021). Blending capacity on a rideshare platform: Independent and dedicated drivers. *Production and Operations Management, 30*(8), 2522–2546.
8. Chen, L., Cui, Y., Liu, J., & Liu, X. (2020). Bonus competition in the gig economy. SSRN 3392700.
9. Chen, M. K., Chevalier, J. A., Rossi, P. E., & Oehlsen, E. (2019). The value of flexible work: Evidence from Uber drivers. *Journal of Political Economy, 127*(6), 2735–2794.
10. Chu, L. Y., Wan, Z., & Zhan, D. (2018). Harnessing the double-edged sword via routing: Information provision on ride-hailing platforms. SSRN 3266250.
11. Debo, L., & Veeraraghavan, S. (2014). Equilibrium in queues under unknown service times and service value. *Operations Research, 62*(1), 38–57.
12. Dong, J., & Ibrahim, R. (2020). Managing supply in the on-demand economy: Flexible workers, full-time employees, or both? *Operations Research, 68*(4), 1238–1264.
13. Edelson, N. M., & Hilderbrand, D. K. (1975). Congestion tolls for Poisson queuing processes. *Econometrica, 43*(1), 81–92.
14. Feldman, P., Frazelle, A. E., Swinney, R. (2022). Managing relationships between restaurants and food delivery platforms: Conflict, contracts, and coordination. *Management Science*, Forthcoming.
15. Feng, G., Kong, G., & Wang, Z. (2021). We are on the way: Analysis of on-demand ride-hailing systems. *Manufacturing Service Operations Management, 23*(5), 1237–1256.
16. Gurvich, I., Lariviere, M., Moreno, A. (2019). Operations in the on-demand economy: Staffing services with self-scheduling capacity. In *Sharing economy* (pp. 249–278). Springer.
17. Hagiu, A., & Wright, J. (2019). The status of workers and platforms in the sharing economy. *Journal of Economics and Management Strategy, 28*(1), 97–108.
18. Hall, J. V., & Krueger, A. B. (2018). An analysis of the labor market for Uber's driver-partners in the United States. *ILR Review, 71*(3), 705–732.
19. Hassin, R., Haviv, M. (2003). To queue or not to queue: Equilibrium behavior in queueing systems. In *International series in operations research and management science*. Springer.
20. Hassin, R., & Roet-Green, R. (2017). The impact of inspection cost on equilibrium, revenue, and social welfare in a single-server queue. *Operatios Research, 65*(3), 804–820.
21. He, E. J., Goh, J. (2021). Profit or growth? Dynamic order allocation in a hybrid workforce. *Management Science*, Forthcoming.
22. Hu, M., Li, Y., & Wang, J. (2018). Efficient ignorance: Information heterogeneity in a queue. *Management Science, 64*(6), 2650–2671.
23. Katz, V. (2015). Regulating the sharing economy. *Berkeley Technology Law Journal*, *34*(4).
24. Lazo, A. (2019). California enacts law to classify some gig workers as employees. WSJ.
25. Lian, Z., Martin, S., & van Ryzin, G. (2021). Labor cost free-riding in the gig economy. SSRN 3775888.
26. Lobel, I., Martin, S., & Song, H. (2021). Employees, contractors, or hybrid: An operational perspective. SSRN 3878215.
27. Mishel, L. (2018). Uber and the labor market. Economic Policy Institute.
28. Naor, P. (1969). The regulation of queue size by levying tolls. *Econometrica, 37*(1), 15–24.
29. Nikzad, A. (2020). Thickness and competition in ride-sharing markets. SSRN 3065672.
30. Parrott, J. A., Reich, M. (2020). A minimum compensation standard for Seattle TNC drivers.
31. Radia, R. (2019). California ride share contracting legislation is a solution in search of a problem. Competitive Enterprise Institute.
32. Rayle, L., Dai, D., Chan, N., Cervero, R., & Shaheen, S. (2016). Just a better taxi? A survey-based comparison of taxis, transit, and ridesourcing services in San Francisco. *Transport Policy, 45*, 168–178.

33. Schechner, S., Olson, P. (2021). Uber grants vacation pay, pensions to U.K. drivers in change of job status. WSJ.
34. Siddiq, A., Taylor, T. A. (2021). Ride-hailing platforms: Competition and autonomous vehicles. *Manufacturing Service Operations Management*, Forthcoming.
35. Tang, Y., Guo, P., Tang, C. S., Wang, Y. (2021). Gender-related operational issues arising from on-demand ride-hailing platforms: Safety concerns and system configuration. *Production and Operations Management*, Forthcoming.
36. Taylor, T. A. (2018). On-demand service platforms. *Manufacturing Service Operations Management, 20*(4), 704–720.
37. Yu, J. J., Tang, C. S., Shen, Z. J. M., & Chen, X. M. (2020). A balancing act of regulating on-demand ride services. *Management Science, 66*(7), 2975–2992.
38. Zoepf, S., Chen, S., Adu, P., Pozo, G. (2018). The economics of ride hailing: Driver expenses, income and taxes.

Chapter 31
Prediction of New COVID-19 Cases Considering Mitigation Policies and Weather Data for European Countries

Mohammad Fili, Kris De Brabanter, Luning Bi, and Guiping Hu

Abstract Since the emergence of the severe acute respiratory syndrome coronavirus 2 (SARS-CoV-2), more than 510 million people have been infected, and more than 6 million deaths have been recorded globally. Accurate estimations for the number of new cases are a crucial step toward controlling and ending the pandemic. The accurate prediction helps decision-makers to prepare for future resource allocation and set the mitigation policies accordingly. The goal of this study is to develop a predictive model that can capture the patterns using the set of past policies, weather conditions, and the historic number of COVID-19 cases to predict future cases. To achieve this goal, we developed a predictive model based on long short-term memory (LSTM) and trained it using a combination of the policies implemented and the weather data to predict the number of new COVID-19 cases in European countries. The results show that the model is capable of capturing the pattern successfully and can predict future new cases. LSTM model outperformed the baseline models, including ridge regression, least absolute shrinkage selection operator (lasso), and multi-layer perceptron (MLP). The results of this study will be used as critical inputs for developing a framework that prescribes policies for the future such that it can reduce the number of new cases while keeping the implementation or post-effect costs as low as possible.

M. Fili · K. De Brabanter · L. Bi · G. Hu (✉)
Industrial and Manufacturing Systems Engineering, Iowa State University, Ames, IA 50011, USA
e-mail: ghgis@rit.edu

M. Fili
e-mail: mfili@iastate.edu

K. De Brabanter
e-mail: kbrabant@iastate.edu

L. Bi
e-mail: luningbi@iastate.edu

G. Hu
Department of Sustainability, Golisano Institute for Sustainability, Rochester Institute of Technology, Rochester, NY, USA

K. De Brabanter
Department of Statistics, Iowa State University, Ames, IA 50011, USA

R. Qiu et al. (eds.), *City, Society, and Digital Transformation*, Lecture Notes in Operations Research, https://doi.org/10.1007/978-3-031-15644-1_31

Keywords COVID-19 · Europe · New case prediction · Long short-term memory (LSTM) · Mitigation policy

Introduction

According to World Health Organization (WHO), as of May 2022, more than 510 million individuals have been infected with COVID-19, and more than 6 million people have died globally [1]. These numbers alone can reflect the necessity of having some mitigation strategies. At the beginning of the pandemic and before vaccine development, using the appropriate set of policies can be a key to keeping situations under control and not letting the virus spread amongst the population. While applying policies in a minimalistic way can result in catastrophe, rigorous mitigation strategies may also be detrimental. For instance, a policy such as "stay at home" is found to reduce the infection's growth rate by 8.6% after two weeks [2]. But applying such policies very stringently imposes a significant financial burden on the economy and impacts people's physical and mental health. Studies showed that the pandemic reduced global economic growth in 2020 by 3.2% and reduced global trade in 2020 by 5.3% [3]. This requires a comprehensive decision-making framework that helps set the right policies while considering the impact in the long term. This ensures that the decision-makers find the best set of policies to reduce the number of new cases while considering applicability, resource constraints, and policies' long-term effects.

One of the important aspects of any decision-making framework is to understand the progression of future events. In order to make effective decisions, one needs to know how the number of new cases changes with time. There are mainly two approaches to integrate future information into the decision-making process. One way is to focus on the wave peaks information about the number of new cases. This enables the decision-maker to prepare for the worst situations and plan accordingly. Amar et al. aimed to predict the peak of the pandemic by using regression models [4]. They found that the exponential, fourth-degree, fifth-degree, and sixth-degree polynomial regression models are good choices to predict the peak of one single wave of the pandemic. They successfully predicted the peak of the first wave in Egypt. In another study predicting the pandemic peak, Wang et al. applied FbProphet, an algorithm from Facebook, to predict the peak time [5].

Another approach is to understand the behavior of changes in the number of new cases throughout the time so that one can plan based on future predictions and plan accordingly. There are studies focusing on predicting new cases or deaths. Different machine learning models have been utilized to do this task, such as logistic regression [5], deep learning models [6], time series generalized linear model [7], Autoregressive Integrated Moving Average (ARIMA) model [8], and Recurrent Neural Network (RNN) models [9–12].

In this study, we developed an LSTM-based model to predict the number of new cases in European countries. This model will be used as a starting point for

prescribing the best set of policies for a given country in future studies. The rest of the paper is organized as follows: Sect. 31.2 discusses the materials and methods. We first describe the datasets used in this study and then explain the details of the model training procedure. In Sect. 31.3, we show the numerical results pertinent to the model performance. Section 31.4 concludes with a summary of the findings and also future plans.

Materials and Methods

In this section, we describe the datasets used in this study along with the set of features in each dataset separately. Then we explain the preprocessing steps taken to prepare the data for training. Finally, we explain the details of the model used for predicting and the procedure for training the models.

Covid-19 Dataset

In this study, we used the Oxford Covid-19 Government Response Tracker (OxCGRT) data [13], which contains daily policies applied in different countries worldwide to control the spread of the SarsCov-2 virus. The dataset in our study has two sets of policies, including closure and healthcare-related policies. Each group has specific policies recorded on a daily basis for different countries. Each policy in a group is an ordinal variable indicating how stringent the policy was implemented at a particular time. The stringency level starts from 0 (no actions) and goes to a maximum level (as shown in Tables 31.1 and 31.2) that shows the strictest level of that policy. In addition to the policy information, we have the daily number of confirmed cases for each country.

The first set of policies is closure and containment. This group establishes restrictions on the gatherings or requires a partial or complete closure of certain places. There are eight policies in this group, denoted as C_1–C_8. Table 31.1 summarizes the policies and their description and the number of stringency levels. An explanation of each stringency level can be seen at (https://github.com/OxCGRT/covid-policy-tracker/blob/master/documentation/codebook.md).

The second set of policies is healthcare which has four policies in it, including public information campaigns (H_1), testing policy (H_2), contact tracing (H_3), and facial coverings (H_4). Table 31.2 summarizes the healthcare policies with the number of levels associated with each policy.

Table 31.1 Summary of policies in closure and containment group

Notation	Description	# of stringency levels
C_1	School closure	4
C_2	Workplace closure	4
C_3	Public events cancellation	3
C_4	Gathering restriction	5
C_5	Public transportation closure	3
C_6	Stay at home requirements	4
C_7	Internal movement restrictions	3
C_8	International travel controls	5

Table 31.2 Summary of policies in healthcare group

Notation	Description	# of stringency levels
H_1	Public information campaigns	3
H_2	Testing policies	4
H_3	Contact tracing	3
H_4	Facial coverings	5

Weather Dataset

To add weather information, we used world weather online's API [14] and extracted the variables of interest for each country. In this dataset, we have average temperatures (°C), heat index (°C), and humidity. One of the essential features of weather data is the average temperature. Figure 31.1 shows the relation between the number of new cases and the average temperature. We used a local polynomial regression of order 3 (green line) to model the relationship. The green shaded area in Fig. 31.1 shows the 95% pointwise confidence interval. To find the optimal bandwidth, h^{opt}, first, we used the rule of thumb for bandwidth selection [15]. Then, we searched around the candidate bandwidth using the cross-validation bandwidth selection method to find the best bandwidth.

In the next step, we inspected whether the up and downs of the local polynomial regression model are statistically significant or not. For this purpose, we used Significant Zero crossings of the derivative (SiZer) map [16], as shown in Fig. 31.2. Each SiZer plot has four colors: blue for significantly increasing slopes, red for significantly decreasing slopes, purple for possibly zero slopes, and the grey region shows insufficient data. The white dashed line in each subplot shows the h^{opt}. We used SiZer package for this analysis [17].

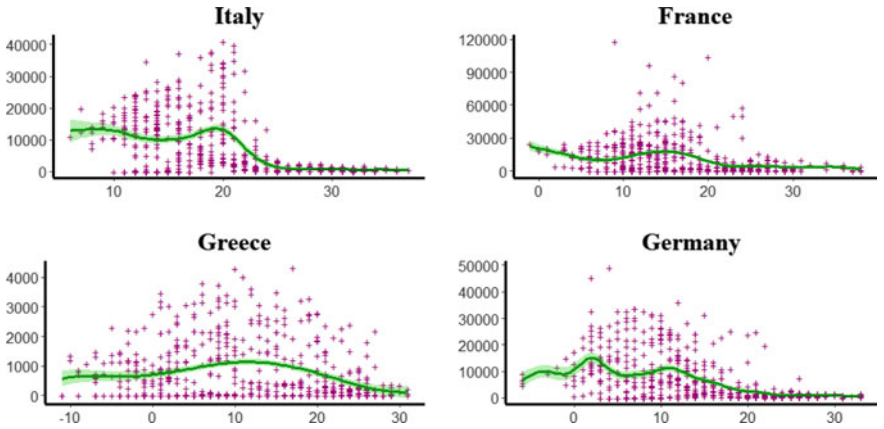

Fig. 31.1 Local polynomial regression fit for the number of new cases (y-axis) against average temperature (°C) (x-axis). The green shaded area shows the 95% pointwise confidence interval. (h^{opt} : 1.9872 for Italy, 3.2819 for France, 2.4239 for Greece, and 1.7887 for Germany)

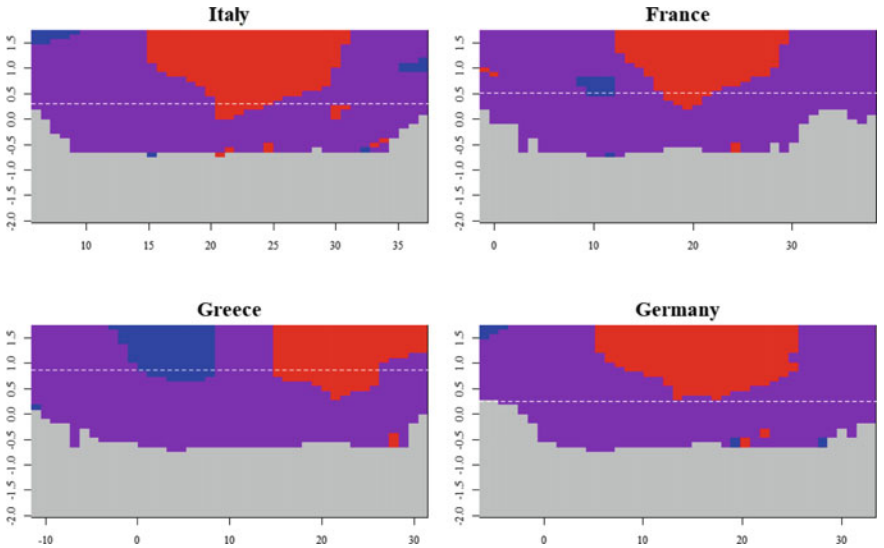

Fig. 31.2 SiZer maps for average temperature (°C) [x-axis is the average temperature, and the y-axis is the $\log_{10}(h)$]

For Italy, we see a significant decrease in the number of new cases, around 20 °C, and it is almost flat elsewhere. In the subplots of France and Greece, a peak can be seen in the middle of the average temperature range. Interestingly, we can observe that for Germany, although the model shows a non-linear relation, the up and downs are non-significant, possibly due to noise in data or outliers.

It might be informative to add time to this analysis and see how temperature and the number of new cases were related throughout the pandemic. Figure 31.3 shows the number of new cases along with the heat index (°C) throughout the time. We can observe that the peak number of the new cases occurred mainly in colder weather conditions for these four countries.

One of the other important weather-related variables is humidity. Figure 31.4 shows the relation between the number of new cases and humidity. As before, we used a local polynomial regression model of order 3 (green line) and a 95% pointwise confidence interval (green area). We also explored the slope significance using SiZer maps for the humidity, as shown in Fig. 31.5. From the set of subplots, we can observe that there exists a significant increase for Italy and Germany, a significant decrease for Greece, and no significant change in the number of new cases for France.

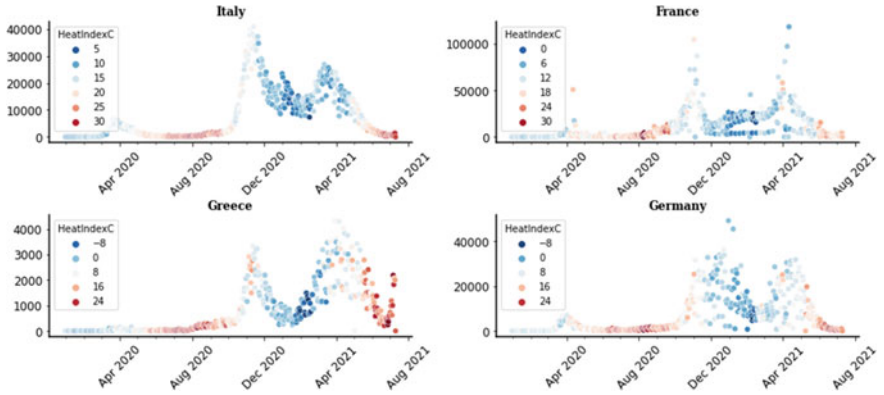

Fig. 31.3 Relation between the number of new cases (y-axis) and heat index (°C) throughout the time

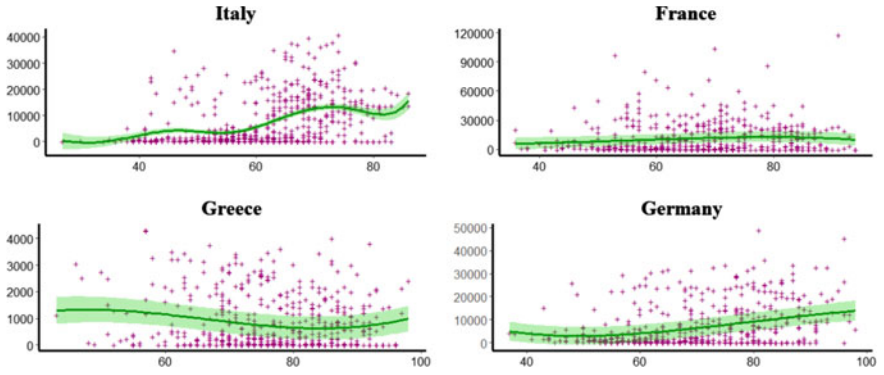

Fig. 31.4 Local polynomial regression fit for the number of new cases (y-axis) against humidity (x-axis). The green shaded area shows the 95% pointwise confidence interval. (h^{opt}: 6.182 for Italy, 35.2275 for France, 36.8827 for Greece, and 43.4066 for Germany)

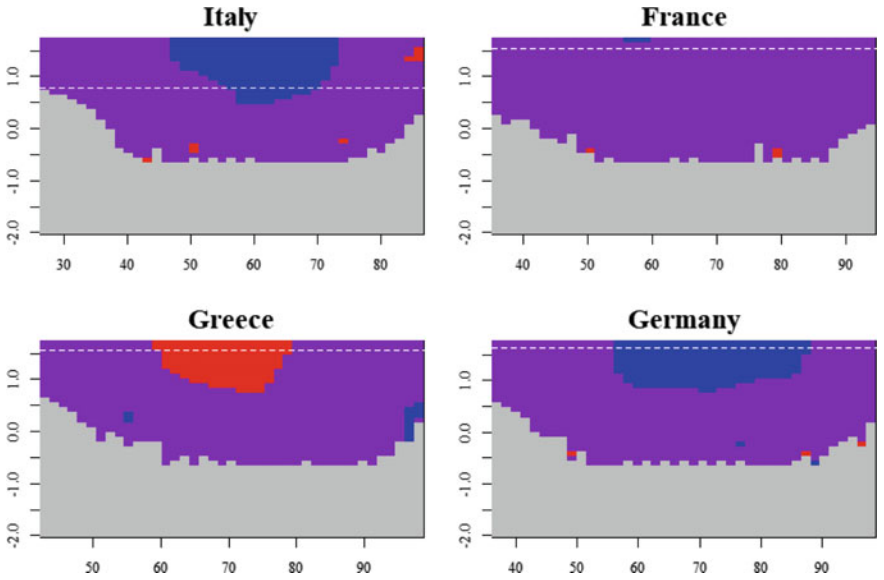

Fig. 31.5 SiZer maps for humidity [x-axis is the humidity, and the y-axis is the $\log_{10}(h)$]

We explored the weather variables using the SiZer maps for different countries using different time lags and the analyses led to using only the average temperature as it showed significant relation with the response variable.

Data Preprocessing

We have done several preprocessing steps, as implemented in [12], to make the data prepared for the modeling phase. In this section, we explain these steps. The OXCGRT data contains data for all countries around the world. In this study, we focused on the European countries.

One of the most important variables in this study is the cumulative number of cases at each time point t and in region r, denoted as C_r^t. We used linear interpolation to impute the missing values for days that the past and previous values were known and used forward fill for days with missing values after it. We then replaced any remaining missing values with zero.

To impute the missing values for the policies, we assumed that the policy is not changed from one day to the next for a specific country; therefore, we used the forward-fill approach. Any remaining missing values for policies are replaced with zeros, meaning no action was taken that day.

We introduced a new feature, denoted as y_r^t, representing the number of new cases at time point t and region r. This variable can be obtained by sequential differencing

of the cumulative cases as shown in Eq. (31.1):

$$y_r^t = \max\left\{C_r^t - C_r^{(t-1)}, 0\right\} \quad t \geq 2, \tag{31.1}$$

We replaced any negative values of y_r^t with 0 since this variable should be non-negative. To remove the noise from the data, we smoothed the number of new cases using rolling mean with weekly windows, as shown in Eq. (31.2):

$$\tilde{y}_r^t = \frac{\sum_{j=t-6}^{t} y_r^j}{7}, \quad t \geq 7 \tag{31.2}$$

where, $\tilde{y}_a^t$ is the smoothed number of new cases at time point t and region r. The initial missing values are replaced with zeros. We then defined the relative change in the smoothed number of new cases. This variable is denoted as R_r^t and is defined as Eq. (31.3):

$$R_r^t = \frac{\tilde{y}_r^t}{\tilde{y}_r^{t-1}}, \quad t \geq 2 \tag{31.3}$$

The number of infected people in a more populated country is expected to be different than in a country with a small population. To take this into account, we defined a new variable, denoted as p_r^t, describing the proportion of people infected by COVID-19 in region r at time point t, using the population of that region. The variable is defined in Eq. (31.4):

$$p_r^t = \frac{C_r^t}{N_r} \tag{31.4}$$

where, N_r is the population of region r. Utilizing Eqs. (31.3) and (31.4), we introduced a new response variable as the ratio of the relative change in the smooth number of new cases over the proportion of the population not being infected until time point t. This new dependent variable, named prediction ratio, is represented in Eq. (31.5).

$$\psi_r^t = \frac{R_r^t}{1 - p_r^t} \tag{31.5}$$

Predictive Models

In this study, we developed an LSTM-based model to predict the number of new cases. We then compared the performance of the model with three baseline models, including lasso, ridge regression, and MLP model. In this section, we explain the predictive models used and the setup corresponding to each model.

- **LSTM**

LSTM is a recurrent neural network (RNN) model which is capable of learning long-term dependencies. The main components of the LSTM model are the memory blocks which avoid the vanishing gradient problem by memorizing the parameters for longer horizons [18]. LSTM model has two states, calculated at each step, called hidden state (h_t) and cell state (c_t) with three gates: forget gate (f_t), input gate (i_t), and the output gate (o_t), where:

$$f_t = \sigma\left(W_{xf}^T X_t + W_{hf}^T h_{t-1} + b_f\right) \tag{31.6}$$

$$i_t = \sigma\left(W_{xi}^T X_t + W_{hi}^T h_{t-1} + b_i\right) \tag{31.7}$$

$$o_t = \sigma\left(W_{xo}^T X_t + W_{ho}^T h_{t-1} + b_o\right) \tag{31.8}$$

where, W is the weights and b is the bias. The values of the hidden state and cell state then can be updated using the following equations:

$$c_t = f_t * c_{t-1} + i_t * \phi\left(W_{xc}^T X_t + W_{hc}^T h_{t-1} + b_c\right) \tag{31.9}$$

$$h_t = o_t * \phi(c_t) \tag{31.10}$$

where, ϕ is the activation function of interest (usually tanh). In this study, we used the Softplus activation function as shown in Eq. 31.11:

$$\phi(x) = \ln(1 + \exp(x)) \tag{31.11}$$

We stacked two layers of LSTM with 32 and 8 units for the cells in each layer, respectively. The structure of the predictive model is plotted in Fig. 31.6. The green rectangles are the LSTM cells which is then fed into a dense layer with 14 nodes to predict the future outcomes.

- **Ridge Regression**

One of the baseline models used in this study is ridge regression. Despite the simplicity, this model is helpful in reducing multicollinearity between the variables by shrinking their effect. The coefficients of the ridge model minimize a penalized residual sum of squares as in Eq. (31.12):

$$Q = \left\|y - X\beta^{ridge}\right\|_2^2 + \lambda\left\|\beta^{ridge}\right\|_2^2 \tag{31.12}$$

where, $\lambda \geq 0$ is the regularization parameter that helps to shrink the coefficients. For the ridge regression model, and when $X^\top X = I$ we can prove that:

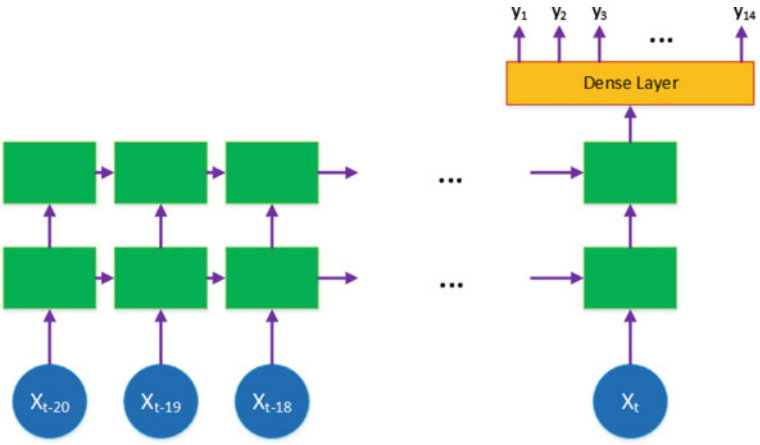

Fig. 31.6 Structure of the proposed predictive model

$$\hat{\beta}^{ridge} = \frac{\hat{\beta}^{OLS}}{1+\lambda} \tag{31.13}$$

which shows that ridge regression shrinks the ordinary least square (OLS) coefficients by a factor of $\frac{1}{1+\lambda}$.

- **Lasso Regression**

One of the other models used as a baseline is lasso which is similar to the ridge regression as they are both shrinkage methods. The coefficients of the lasso regression minimize a penalized residual sum of squares as in Eq. (31.14):

$$Q = \left\| y - X\beta^{lasso} \right\|_2^2 + \lambda \left\| \beta^{lasso} \right\|_1 \tag{31.14}$$

- **MLP**

MLP is a model in the class of artificial neural network (ANN) in which the nodes in a layer are fully connected to the nodes of the next layer. In this study, we used a four-layer model (two hidden layers) with 64 nodes in the first and 32 nodes in the second hidden layer. The activation functions utilized are sigmoid and linear functions for the two hidden layers and rectified linear unit (ReLU) for the output layer.

Table 31.3 Time horizons for the two experiments

	Date range	Testing horizon
Exp. I	01/01/2020–10/14/2020	October 2020 (14 days)
Exp. II	01/01/2020–11/14/2020	November 2020 (14 days)

Procedure

Based on the exploratory data analysis, we incorporated only the average temperature from the weather dataset along with the policies described earlier and the historic prediction ratio into the model for the past three weeks as the input and predicted the prediction ratio for the next two weeks. In this study, we defined two experiments which are summarized in Table 31.3. The first experiment uses data from January 2020 to the end of September for training and the first 14 days in October as the test set. In the second experiment, we utilized the data from January 2020 to the end of October as the training set and the first 14 days of November as the test set.

We fitted the LSTM model to the dataset of all European countries and converted the prediction ratios back to the new cases at the end. We used lasso regression, ridge regression, and MLP as the baseline models to compare against the LSTM model. To tune the lasso and ridge regression models, we used a grid search approach and applied a tenfold cross-validation procedure.

For this analysis, mean absolute error (MAE) is used as the performance metric, which is the objective to minimize in the model training process. We also monitored the mean absolute percentage error (MAPE). It is worth mentioning that, to calculate MAPE, we didn't consider time points with no new cases.

Numerical Results

The prediction results for the developed model and the baseline models are summarized in Table 31.4. We can see that LSTM outperformed the baseline models.

To visualize the prediction results, we used a few countries, as shown in Fig. 31.7. It can be observed that the model captured the future patterns well.

Table 31.4 Performance evaluation of the predictive models

	Experiment I		Experiment II	
	MAE	MAPE (%)	MAE	MAPE (%)
Lasso	600.96	42.6	1719.85	47.7
Ridge	588.05	42.4	1891.08	49.8
MLP	1015.59	55.9	1739.90	42.5
LSTM	**561.04**	**39.4**	**1596.39**	**40.7**

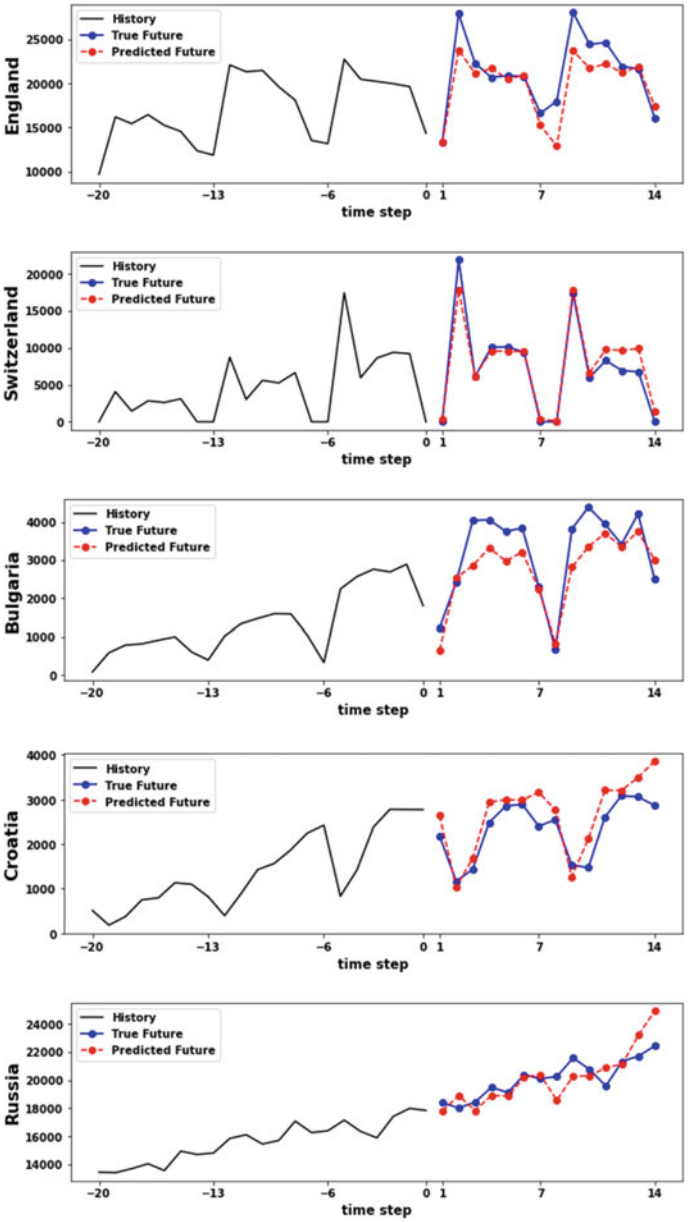

Fig. 31.7 Predicted number of new cases (red dashed line) for England, Switzerland, Bulgaria, Croatia, and Russia (experiment II)

Conclusion and Future Direction

COVID-19 has been a great menace since its emergence. Over 510 million people have been infected, and more than 6 million individuals died as of May 2022. It is crucial to have a predictive model that can predict the number of new cases in subsequent days or weeks so that decision-makers can utilize it for planning future policies. In this study, we incorporated two sets of policies: healthcare and closure. We utilized the policies and the weather data to predict the number of new cases. For this purpose, we developed an LSTM-based model and applied it to the European countries. For a given time point, we used data from the past three weeks as the input to the model and evaluated the model for the next 14 days. We designed two experiments for the validation of the model and compared the performance of the developed model against the lasso regression, ridge regression, and MLP for each of the two experiments separately. The results show that the LSTM model outperforms the baseline models and predicts the future number of new cases well.

The goal of this study has been to develop a starting point for a prescriptive decision-making framework by which the best set of policies for a future period can be found such that it reduces not only the number of new cases but also the cost pertinent to the implementation or long-term effect associated with each policy. This study creates a foundation for such a decision-making framework by providing a predictive model in its first stage.

Acknowledgements In the context of the pandemic response challenge, some of the codes were provided by XPRIZE for data wrangling. We thank XPRIZE for sharing the ideas and codes.

References

1. WHO Coronavirus (COVID-19) Dashboard. (2022). https://covid19.who.int/. Accessed 14 April 2022.
2. Fowler, J. H., Hill, S., Levin, R., & Obradovich, N. (2020). The effect of stay-at-home orders on COVID-19 infections in the United States. *SSRN Electronic Journal*. https://doi.org/10.2139/ssrn.3576826
3. Jackson, J. K., Weiss, M. A., Schwarzenberg, A. B., Nelson, R. M., Sutter, K. M., & Sutherland, M. D. (2021). Global economic effects of COVID-19. *The Effects of COVID-19 on the Global and Domestic Economy*.
4. Amar, L. A., Taha, A. A., & Mohamed, M. Y. (2020). Prediction of the final size for COVID-19 epidemic using machine learning: A case study of Egypt. *Infectious Disease Modelling, 5*, 622–634. https://doi.org/10.1016/j.idm.2020.08.008
5. Wang, P., Zheng, X., Li, J., & Zhu, B. (2020). Prediction of epidemic trends in COVID-19 with logistic model and machine learning technics. *Chaos, Solitons and Fractals, 139*, 110058. https://doi.org/10.1016/j.chaos.2020.110058
6. Said A. B., Erradi, A., Aly, H., & Mohamed, A. (2020). A deep-learning model for evaluating and predicting the impact of lockdown policies on COVID-19 cases. December 2019, pp. 1–17.
7. Iddrisu, W. A., Appiahene, P., & Kessie, J. A. (2020) Effects of weather and policy intervention on COVID-19 infection in Ghana.

8. Senthil Prakash, P. N., Hariharan, B., Kaliraj, S., Siva, R., & Vivek, D. (2021) The impact of various policy factors implemented for controlling the spread of COVID-19. *Materials Today: Proceedings.* https://doi.org/10.1016/j.matpr.2021.01.524
9. Shahid, F., Zameer, A., & Muneeb, M. (2020). Predictions for COVID-19 with deep learning models of LSTM, GRU and Bi-LSTM. *Chaos, Solitons and Fractals*. https://doi.org/10.1016/j.chaos.2020.110212
10. Gautam, Y. (2021). Transfer learning for COVID-19 cases and deaths forecast using LSTM network. *ISA Transactions*. https://doi.org/10.1016/j.isatra.2020.12.057
11. ArunKumar, K. E., Kalaga, D. V., Kumar, C. M. S., Kawaji, M., & Brenza, T. M. (2021). Forecasting of COVID-19 using deep layer recurrent neural networks (RNNs) with gated recurrent units (GRUs) and long short-term memory (LSTM) cells. *Chaos, Solitons and Fractals*. https://doi.org/10.1016/j.chaos.2021.110861
12. Bi, L., Fili, M., & Hu, G. (2022). COVID-19 forecasting and intervention planning using gated recurrent unit and evolutionary algorithm. *Neural Computing and Applications*. https://doi.org/10.1007/s00521-022-07394-z
13. Hale, T., Angrist, N., Goldszmidt, R., Kira, B., Petherick, A., Phillips, T., Webster, S., Cameron-Blake, E., Hallas, L., Majumdar, S., & Tatlow, H. (2021). A global panel database of pandemic policies (Oxford COVID-19 government response tracker). *Nature Human Behaviour*. https://doi.org/10.1038/s41562-021-01079-8
14. World Weather Online. https://www.worldweatheronline.com/developer/api/
15. Fan, J., & Gijbels, I. (1994). *Local polynomial modelling and its applications*. Springer. https://doi.org/10.1007/978-1-4899-3150-4
16. Chaudhuri, P., & Marron, J. S. (1999). SiZer for exploration of structures in curves. *Journal of American Statistical Association.* https://doi.org/10.1080/01621459.1999.10474186
17. Sonderegger, D. (2020) SiZer: Significant zero crossings. https://cran.r-project.org/package=SiZer
18. Chimmula, V. K. R., & Zhang, L. (2020). Time series forecasting of COVID-19 transmission in Canada using LSTM networks. *Chaos, Solitons and Fractals.* https://doi.org/10.1016/j.chaos.2020.109864

Chapter 32
Optimal Unit Locations in Emergency Service Systems with Bayesian Optimization

Wenqian Xing and Cheng Hua

Abstract We model the facility location problem in an emergency service system as an optimization problem in which the objective is to minimize the system-wide mean response time, which requires exponential complexity to solve. We show that this problem is NP-hard and develop lower and upper bounds for the optimal solution from a special case of the classical p-median problem. We propose a Bayesian optimization solution to this problem that includes searching within feasible trust regions and adaptive swapping strategies. We show that our algorithm always converges to a globally optimal solution with a regret bound guarantee. Our algorithm consistently outperforms the p-median solution in numerical experiments and quickly converges to the optimal solution. We also apply our method to solve the optimal ambulance location problem in St. Paul, Minnesota, using one year of real data. We show that our method converges to the optimal solution very quickly. Our method can be applied to solve the optimal unit locations in the emergency service systems of the largest cities.

Keywords Facility location · Bayesian optimization · Combinatorial optimization · Emergency service system

Introduction

In most emergency service systems, system-wide mean response time is a crucial system performance indicator. The response time for a call in an emergency system begins when the system receives this call and ends when the responder arrives at the service location, defined as the sum of the turnout and travel times. By reducing response times, both patients and healthcare providers can benefit. For the patient,

W. Xing (✉)
IEOR Department Columbia University, New York 10027, USA
e-mail: wx2261@columbia.edu

C. Hua
Antai College Shanghai Jiao Tong University, 200030 Shanghai, China
e-mail: cheng.hua@sjtu.edu.cn

R. Qiu et al. (eds.), *City, Society, and Digital Transformation*, Lecture Notes in Operations Research, https://doi.org/10.1007/978-3-031-15644-1_32

shorter response times improve the chances of survival in an emergency and the quality of the subsequent medical care. For service providers, shorter response times save service time and make the system more efficient. However, as we will show in the paper, solving the exact mean response time given a specific configuration requires solving a linear system whose size grows exponentially with the number of units, which is proven to be NP-hard, let alone solving for the best configuration. Therefore, this problem is usually studied in a p-median setting by ignoring the state transitions and assuming all units are always free whenever calls are received in the system, which greatly simplifies the problem.

This study models the facility location problem in an emergency service system to minimize the average response time as a combinatorial optimization problem that is NP-hard. We show that the value of the optimal solution in a particular p-median problem [5] is a lower bound of our problem, and we also obtain an upper bound from this particular p-median problem. We propose a Bayesian optimization scheme for this problem, which includes using feasible trust regions and adaptive swapping to solve for the optimal solution. We show that our algorithm always converges to the global optimum with a regret bound guarantee. We show that our algorithm always beats the p-median solution and converges to the optimal solution very quickly in numerical experiments. We also apply our method to solve the optimal unit location in St. Paul, Minnesota, using one year of real data. We found our method converges to the optimal solution quickly.

Literature Review

Facility location problems in healthcare are widely studied. Ahmadi-Javid et al. [1] provides a comprehensive review of facility location problems in healthcare systems. Li et al. [9] reviews the literature on coverage models and optimization techniques for emergency facility locations. Daskin [3] provides a comprehensive review of discrete location problems and classifies them into three main categories: coverage-based problems, median-based problems, and other problems.

The p-median location problem is one of the most famous problems in facility location. The p-median problem was first proposed by Hakimi [5]. It was shown to be NP-hard even with a simple structure by Kariv and Hakimi [6]. Much of the work in the literature models the location problem of emergency medical facilities as a p-median problem. Rajagopalan and Saydam [10], minimizes the expected response distance of the entire system while satisfying the coverage requirement, by a heuristic tabu search approach. However, their solution has no performance guarantee and is slow to converge.

The p-median problem simplifies the computation of response times, while the exact average response time can be solved by the spatial hypercube model, that was developed by Larson [7]. The hypercube model is used to analyze a system consisting of spatially distributed service units, such as ambulances or fire trucks. This hypercube model and its extensions have been showed to be significant in evaluating

performance of emergency service systems. For instance, it has been implemented in the maximal expected covering location problem Batta et al. [2]. This model entails solving 2^p simultaneous equations for an p-server system, where each server is either busy or available. Larson [8] developed an approximation for larger systems, that reduces the number of equations to p. We will use this approximation algorithm as an approximation to the response time.

Bayesian optimization is a method for optimizing an objective function that requires a relatively long time to evaluate. It also tolerates random noise in function evaluation, such as approximation algorithms or simulations [4]. It creates a surrogate function for the objective, uses Bayesian techniques to quantify the uncertainty of that surrogate function, and then uses the acquisition function defined from that surrogate function to determine the next point to evaluate. The surrogate function is then updated upon evaluation of the evaluated point to form a better belief of the actual function.

Model

This section develops a model for solving the minimum average response time for unit locations in emergency service systems. We show that this problem is NP-hard and develop lower and upper bounds for this problem.

Problem Definition

Our goal in this study is to select the best p unit locations in an emergency service system with N candidate locations to minimize the average response time of all calls. We let I be the set of all candidate locations and $N = |I|$ be the cardinality of I, the total number of candidate locations. The entire region is divided into $|J|$ subregions, where J is the set of all subregions. Calls are generated from each subregion, and the call arrival rate for subregion j is assumed to follow a Poisson distribution with rate λ_j. The region can be divided as finely as desired without increasing the complexity of the problem. We let μ be the average service rate of all units. Calls are assigned to each unit according to a fixed assignment rule (which can be any general assignment policy) that considers the availability of each unit. If all units are busy when the call arrives, we assume it is handled by a unit outside the system, either a private emergency service unit or a unit from an adjacent jurisdiction, which is a common mutual aid policy in emergency service systems. As mentioned in the Introduction, the response time is the sum of the unit turnout time from the base location and the travel time to the scene. We let t_{ij} be the average travel time from location i to call location j and let τ_o be the average turnout time.

Let x_i be the binary variable indicating whether location i is selected or not, where $x_i = 1$ means location i is occupied by a unit, and $x_i = 0$ indicates location i is empty. We let $\boldsymbol{x} = \{x_1, \ldots, x_N\}$ be the location decision set. Our goal is to solve for the optimal location decision set $\boldsymbol{x}^*$ that minimizes the mean response time of the system. The optimal set $\boldsymbol{x}^*$ can be obtained by solving the following integer programming, which we denote as *p-MRT*.

$$\boldsymbol{x}^* = \arg\min_{\boldsymbol{x}} \sum_{i \in I} \sum_{j \in J} t_{ij} q_{ij}(\boldsymbol{x}) \qquad (\textbf{\textit{p-MRT}}) \tag{1}$$

$$\text{s.t.} \sum_{i \in I} x_i = p, \tag{2}$$

$$q_{ij}(\boldsymbol{x}) = \frac{\sum_{\boldsymbol{b} \in S_{ij}(\boldsymbol{x})} \lambda_j P(\boldsymbol{b})}{\sum_{j \in J} \lambda_j (1 - \Pi)}, \forall i \in I, \forall j \in J, \tag{3}$$

$$x_i \in \{0, 1\}, \forall i \in I, \tag{4}$$

where $q_{ij}(\boldsymbol{x})$ is the fraction of all calls in subregion j that are responded to by the unit at location i given unit locations $\boldsymbol{x}$. The objective is to minimize the system-wide mean response time. The first constraint indicates that there are a total of p units to be located, and the second constraint shows the expression for obtaining $q_{ij}(\boldsymbol{x})$ from the spatial hypercube model. The state $\boldsymbol{b} = \{b_1, \ldots, b_p\}$ denotes the state of all p units, where $b_k = 0$ means that unit k is free and $b_k = 1$ means that unit k is busy with a service call. $P(\boldsymbol{b})$ is the probability of being in state $\boldsymbol{b}$, and Π is the probability that all units are busy, also known as the blocking probability. $S_{ij}(\boldsymbol{x})$ is the set of states in which the unit at location i is assigned to calls from subregion j, which is fixed under the assignment policy. Note that the exact values of $q_{ij}(\boldsymbol{x})$ requires knowing $P(\boldsymbol{b})$ and Π, which require solving the following balance equation of the spatial hypercube model. We have, for all $\boldsymbol{b} \in \{0, 1\}^p$,

$$P(\boldsymbol{b}) \left[\sum_{j \in J} \lambda_j + \sum_{k=1}^{p} b_k \mu \right] = \sum_{\boldsymbol{b}': d(\boldsymbol{b}, \boldsymbol{b}') = 1} P(\boldsymbol{b}') r(\boldsymbol{b}, \boldsymbol{b}') + \sum_{\boldsymbol{b}': d(\boldsymbol{b}', \boldsymbol{b}) = 1} P(\boldsymbol{b}') \mu, \tag{5}$$

where $r(\boldsymbol{b}, \boldsymbol{b}')$ is the transition rate from state $\boldsymbol{b}$ to state $\boldsymbol{b}'$ in the spatial hypercube model, and $d(\boldsymbol{b}, \boldsymbol{b}')$ is the Hamming distance from $\boldsymbol{b}$ to $\boldsymbol{b}'$. The spatial hypercube model was originally developed by Larson [7], which contains 2^p simultaneous equations as described in Eq. (5).

The following theorem shows that the *p-MRT* problem is NP-hard, and the proof is in the full version of the paper.

Theorem 1 *The p-MRT problem is NP-hard.*

Performance Bounds

In this section, we develop lower and upper bounds for the optimal solution of the *p-MRT* problem by relating it to the classical p-median problem. The p-median problem, proposed by Hakimi [5], solves the minimum total demand-weighted response time in a simplified setting that ignores the stochasticity of the system.

We first develop the lower bound. In the p-median problem, $x_j \in \{0, 1\}$ is a binary variable indicating the unit location as in the *p-MRT* problem, and $y_{ij} \in \{0, 1\}$ is a binary variable indicating whether calls from subregion j are assigned to the unit at location i. We let $(\tilde{\boldsymbol{x}}^*, \tilde{\boldsymbol{y}}^*)$ denote the optimal solution to the p-median problem. The goal of the p-median problem is to minimize the total demand-weighted response time.

$$(\tilde{\boldsymbol{x}}^*, \tilde{\boldsymbol{y}}^*) = \arg\min_{\boldsymbol{x},\boldsymbol{y}} \sum_{i\in I}\sum_{j\in J} w_j t_{ij} y_{ij} \qquad (\textbf{\textit{p-median}}) \tag{6}$$

$$\text{s.t.} \sum_{i\in I} y_{ij} = 1, \forall j \in J, \tag{7}$$

$$\sum_{i\in I} x_i = p, \tag{8}$$

$$y_{ij} \le x_i, \forall i \in I, \forall j \in J, \tag{9}$$

$$y_{ij} \in \{0, 1\}, \forall i \in I, \forall j \in J, \tag{10}$$

$$x_i \in \{0, 1\}, \forall i \in I, \tag{11}$$

The first constraint indicates that each subregion will be assigned to a unit, and the third constraint indicates that calls in subregion j can only be assigned to a location with a unit. Note that the p-median problem does not include the service rate μ because its underlying assumption ignores state transitions and assumes that all units are always available, which is equivalent to assuming that each unit has a service rate of $\mu \to \infty$, and all units become immediately available for the next call after being assigned to one call.

In the following theorem, we show that the optimal value of the *p-MRT* problem is lower bounded by the optimal value of a special case of the p-median problem. The detailed proof of the theorem is in the full paper.

Theorem 2 *When setting $w_j = \lambda_j / \sum_{j\in J} \lambda_j$, the optimal value to the p-median problem is a lower bound on the optimal value of the p-MRT problem.*

Next, we develop a feasible upper bound from the same p-median problem as in Theorem 2. It can be shown that the optimal unit locations $\tilde{\boldsymbol{x}}^*$ from the above p-median problem is always a feasible solution to the *p-MRT* problem, because it satisfies the constraint $\sum_{i\in I} x_i = p$ of the *p-MRT* problem. Since the *p-MRT* problem is a minimization problem, every feasible solution provides an upper bound

on its optimal value. Therefore, when setting $w_j = \lambda_j / \sum_{j \in J} \lambda_j$, the optimal location $\tilde{\boldsymbol{x}}^*$, obtained from the p-median problem, provides an upper bound on the optimal value to the *p-MRT* problem.

Bayesian Optimization Solution Approach

Bayesian optimization is an optimization method for objective functions that require a relatively long time to evaluate or lack special structure. It also tolerates random noise in function evaluation, such as complex objective functions that can be evaluated only using approximation algorithms or simulations. It generally consists of a surrogate model and an acquisition function based on the surrogate model. This section presents a Bayesian optimization solution for the *p-MRT* problem. We also show the convergence and regret bounds of our method.

Surrogate Model

We let $f(\boldsymbol{x}) = \sum_{i \in I} \sum_{j \in J} t_{ij} q_{ij}(\boldsymbol{x})$ be the exact mean response time obtained from the spatial hypercube model, as shown in Section "Model", and solving it requires extensive computation. To handle this problem, we can use simulation or approximation algorithms to obtain an estimate of $f(\boldsymbol{x})$, and we will discuss the approximation algorithm in detail in Section "Spatial Hypercube Approximation". We let $y = f(\boldsymbol{x}) + \epsilon$ be the estimated mean response time, where $\epsilon \sim \mathcal{N}\left(0, \sigma^2\right)$ is the estimation error and is assumed to follow a Gaussian distribution.

We use the Gaussian process as the surrogate model. We use $\boldsymbol{X}$ to denote the set containing of all evaluated points (each point represents the locations of a set of p units), and $\boldsymbol{y}$ is the set of the corresponding objective values (realized mean response time) of these points. A Gaussian process $GP\left(m(\boldsymbol{X}), k\left(\boldsymbol{X}, \boldsymbol{X}'\right)\right)$ is specified by its mean function $m(\boldsymbol{X}) = E[f(\boldsymbol{X})]$ and the covariance (or kernel) function $k\left(\boldsymbol{X}, \boldsymbol{X}'\right) = E\left[(f(\boldsymbol{X}) - m(\boldsymbol{X}))(f(\boldsymbol{X}') - m(\boldsymbol{X}'))\right]$. The distribution of the Gaussian process is the joint distribution of all currently evaluated points, and each finite subset of all these points follows a multivariate normal distribution. Given the existing set of points $\boldsymbol{X}$, for any point of interest $\tilde{\boldsymbol{x}}$, its posterior distribution follows the normal distribution $\mathcal{N}\left(\mu(\tilde{\boldsymbol{x}}), \sigma^2(\tilde{\boldsymbol{x}})\right)$ and $\mu(\tilde{\boldsymbol{x}})$ and $\sigma^2(\tilde{\boldsymbol{x}})$ are the mean and variance, where

$$\mu(\tilde{\boldsymbol{x}}) = m(\tilde{\boldsymbol{x}}) + k(\tilde{\boldsymbol{x}}, \boldsymbol{X})[k(\boldsymbol{X}, \boldsymbol{X}) + \sigma_n^2 I]^{-1}(\boldsymbol{y} - m(\boldsymbol{X})), \tag{12}$$

$$\sigma^2(\tilde{\boldsymbol{x}}) = k(\tilde{\boldsymbol{x}}, \tilde{\boldsymbol{x}}) - k(\tilde{\boldsymbol{x}}, \boldsymbol{X})[k(\boldsymbol{X}, \boldsymbol{X}) + \sigma^2 I]^{-1} k(\boldsymbol{X}, \tilde{\boldsymbol{x}}). \tag{13}$$

We use the transformed overlap kernel $k\left(\boldsymbol{x}, \boldsymbol{x}'\right) = \exp\left(\sum_{i=1}^{N} \ell_i \delta\left(x_i, x_i'\right) / N\right)$, introduced by Wan et al. [12], where ℓ_i is the lengthscale of the kernel.

Acquisition Function

Due to the high cost of evaluating a unit location set, we want to find the best location set with fewer evaluations. Therefore, in Bayesian optimization, data are sequentially acquired and added to the Gaussian Process (GP) model, and the acquisition function is designed to strategically select the next location set to be evaluated. In contrast, obtaining the optimal solution by complete enumeration does not use any known information about the evaluated points.

In our solution framework, we search within the feasible trust region, as introduced in Section "Feasible Trust Region", and move to a new feasible trust region using a restart strategy with a logic similar to the restart algorithm in the non-stationary bandit problem. An acquisition function chooses the center of the new feasible trust region based on the GP model. After each restart, we fit the GP model on $(\boldsymbol{X}_t, \boldsymbol{Y}_t)$, where t denotes the number of restarts and each $\boldsymbol{x} \in \boldsymbol{X}_t$ is the local optimal solution obtained in the feasible trust region in each restart round. We use a Lower Confidence Bound (LCB) acquisition function to select the new center of the trust region at the beginning of each restart.

$$\boldsymbol{x}_{t+1} = \underset{\boldsymbol{x}}{\operatorname{argmin}}\, \mu(\boldsymbol{x}; \boldsymbol{X}_t, \boldsymbol{Y}_t) - \beta_t^{1/2}\sigma(\boldsymbol{x}; \boldsymbol{X}_t, \boldsymbol{Y}_t), \tag{14}$$

where $\mu(\boldsymbol{x}; \boldsymbol{X}_{t-1}, \boldsymbol{Y}_{t-1})$ and $\sigma(\boldsymbol{x}; \boldsymbol{X}_{t-1}, \boldsymbol{Y}_{t-1})$ are the mean and standard deviation of the GP learned from the observed data $(\boldsymbol{X}_{t-1}, \boldsymbol{Y}_{t-1})$.

Feasible Trust Region

Our algorithm defines the feasible trust region by the Hamming distance as shown in (15).

$$\mathrm{TR}_d\left(\boldsymbol{x}^c\right) = \left\{ \boldsymbol{x} \mid \sum_{i=1}^{N} \delta\left(x_i, x_i^c\right) \leq d \text{ and } \sum_{i=1}^{N} x_i = p \right\}, \tag{15}$$

where δ is the Kronecker delta function.

Updating within the feasible trust region ensures that the next candidate solution always satisfies the constraints and is within the trust region. We apply the adaptive swapping search strategy within the feasible region to find the next candidate solution. The adaptive swapping search strategy performs $s(d)$ rounds of random swapping of an empty location and a location with a unit on the point $\boldsymbol{x}$ with the current best acquisition function with in the trust region, where $s(d)$ is a function of the current length of the trust region d.

Given a trust region center $\boldsymbol{x}^c = \{x_1, \ldots, x_N\}$, we swap the value of each binary variable pair $\{x_i, x_j\} \in \boldsymbol{x}^c$ if one of them has value 1 and the other has value 0. By doing so, we ensure that the constraint of the p-MRT problem remains satisfied.

Consider the trust region length to be d, then we can conduct this swapping operation up to $\lfloor d/2 \rfloor$ times to ensure our searching space lies within the trust region. The trust region length d shrinks by a factor of $\alpha_s \geq 1$ if the adaptive swapping search algorithm fails to improve the value of the acquisition function with a consecutive of n_f trials and expands by a factor $\alpha_e \geq 1$ if the total number of successes reaches n_s.

As mentioned earlier, the restart mechanism is designed to prevent the algorithm from getting stuck in a local optimum, as in Wan et al. [12]. In our algorithm, we initiate a restart whenever $\lfloor d \rfloor < 2$. We evaluate the local optimum obtained based on the objective function, add it to the GP model and update the model. The trust region center for the next restart is obtained from the updated GP model.

Theoretical Results

We denote $r_t = f(\boldsymbol{x}_t) - f(\boldsymbol{x}^*)$ as the regret for the t-th evaluation of the objective function, with the total regret up to time T as $R_T = \sum_t^T r_t$.

Theorem 3 *Our algorithm converges to the global optimum of p-MRT in a finite number of iterations.*

Theorem 4 *The regret bound of our algorithm is, for any* $\zeta \in (0, 1)$,

$$\Pr\left\{R_T \leq \sqrt{16NT\beta_T\kappa\gamma_T}\right\} \geq 1 - \zeta, \tag{16}$$

where $\beta_T = \log\left(2T^2\pi^2/6\zeta\right)$ *and* $\kappa = \sigma^{-2}/\log\left(1 + \sigma^{-2}\right)$.

The detailed proofs of the above two theorems are in the full paper. We give here a brief roadmap of these two proofs. Theorem 3 is proved by contradiction. We show that the size of the feasible trust region d will always be reduced to less than two and that the exploration is complete for the trust region. The proof of Theorem 4 follows a logic similar to that of the GP-UCB algorithm, as shown in Srinivas et al. [11]. The γ_T in the above theorem is the maximum information gain of the acquisition function under the proposed kernel function studied in Wan et al. [12].

Spatial Hypercube Approximation

The Bayesian optimization approach requires evaluating the objective function value of a given location set $\boldsymbol{x}$, which is $\sum_{i\in I}\sum_{j\in J} t_{ij}q_{ij}(\boldsymbol{x})$. Obtaining the exact value, however, requires solving the spatial hypercube model developed by Larson [7], which has an exponential complexity. This section briefly describes the approximation algorithm developed by Larson [8] that we use to approximate the mean response time objective function.

Algorithm 1 Bayesian Optimization with Feasible Trust Region

Input: evaluating function $f(x)$; initial sample size I and trust region TR_0; number of iterations K.
$t \leftarrow 1$, $X_0 \leftarrow \varnothing$, $Y_0 \leftarrow \varnothing$.
restart $\leftarrow True$.
while $t < K$ **do**
  if restart **then**
    Randomly select I initial samples $X_I = \{x_1, ..., x_I\}$ within TR_{t-1}.
    Update observed data $X_t \leftarrow X_{t-1} \cup X_I$, $Y_t \leftarrow Y_{t-1} \cup f(X_I)$
    Initialize the surrogate model with current observations $\hat{f} \leftarrow (X_t, Y_t)$.
    restart $\leftarrow False$.
  else
    Construct a trust region TR_t around the best solution found $x_t^* \in X_t$ using Eq. (14).
    Select next candidate z_t within TR_t by the surrogate model $z_t = \underset{x \in TR(x_t^*)}{\operatorname{argmin}} \hat{f}(x)$.
    Evaluate $f(z_t)$ and record the observation y_t.
    Update observed data $X_t \leftarrow X_{t-1} \cup \{z_t\}$, $Y_t \leftarrow Y_{t-1} \cup \{y_t\}$ and the surrogate model $\hat{f} \leftarrow (z_t, y_t)$.
  if $y_t^* = \min(Y_t)$ keeps unchanged for a certain iterations **then**
    restart $\leftarrow True$.
  $t \leftarrow t + 1$.
Output: Best solution found x_t^*.

Define p_{ijk} as the probability that unit i is dispatched as the k-th preferred unit at node j. Unit i will be dispatched only if it is available and all $k-1$ units more preferred are busy. We have

$$p_{ijk} = \Pr\left[W_i^c \cap \left\{ \bigcap_{l=1}^{k-1} W_{\gamma_{jl}} \right\} \right], \tag{17}$$

where W_i is the event that unit i is busy, and W_i^c is the event that unit i is available.

Recall that the rate that a call arrives at node j is λ_j. Then, the rate at which unit i is dispatched to node j as the k-th preferred unit is $\lambda_j p_{ijk}$, and the rate, S_i, at which unit i is dispatched to calls from all demand nodes is

$$S_i = \sum_{j \in G_i^1} \lambda_j p_{ij1} + \sum_{j \in G_i^2} \lambda_j p_{ij2} + \cdots + \sum_{j \in G_i^N} \lambda_j p_{ijN} = \sum_{k=1}^{N} \sum_{j \in G_i^k} \lambda_j p_{ijk}, \tag{18}$$

where G_i^k is defined as the set of nodes for which unit i is the k-th preferred unit for calls. Specifically, $G_i^k = \{j \in \{1, \ldots, J\} : \gamma_{jk} = i\}$. S_i can also be expressed as the product of the utilization of unit i at calls and the service rate of unit i at calls, i.e.,

$$S_i = \rho_i \mu_i. \tag{19}$$

Larson [8] developed an approximation for p_{ijk} by assuming independence of servers and applying a correction factor.

$$p_{ijk} \approx Q(N, \bar{\rho}, k-1) \prod_{l=1}^{k-1} \rho_{\gamma_{jl}} (1 - \rho_i), \tag{20}$$

where $Q(N, \bar{\rho}, \cdot)$ is a correction factor for server dependence and $\bar{\rho}$ is the average utilization of all units. We have

$$\bar{\rho} = \frac{\lambda}{N\mu}(1 - P_b), \tag{21}$$

where P_b is the blocking probability that all units that can serve a call are busy. Define $P(k)$ as the probability that exactly k servers are busy at calls. The correction factor is given by

$$Q(N, \bar{\rho}, r) = \sum_{k=r}^{N-1} \frac{\binom{k}{r}}{\binom{N}{r}} \frac{N-k}{N-r} \frac{P(k)}{\bar{\rho}^r (1 - \bar{\rho})}. \tag{22}$$

The probabilities $P(k)$ and $P_b = P(N)$ are obtained by the Erlang loss formula.

Now, we have all the components needed to estimate ρ_i. Using (18), (19), and (20), we have

$$\rho_i = \frac{S_i}{\mu_i} = \frac{1}{\mu_i} \sum_{k=1}^{N} \sum_{j \in G_i^k} \lambda_j p_{ijk} = \frac{1}{\mu_i} \sum_{k=1}^{N} \sum_{j \in G_i^k} \lambda_j Q(N, \bar{\rho}, k-1) \prod_{l=1}^{k-1} \rho_{\gamma_{jl}} (1 - \rho_i), \tag{23}$$

where we obtain $Q(N, \bar{\rho}, k)$ from (22). Dividing both sides of (23) by $1 - \rho_i$ and collecting terms of ρ_i, the unit utilizations for calls are approximated by the following N non-linear equations,

$$\rho_i = 1 - \left(1 + \frac{1}{\mu_i} \sum_{k=1}^{N} \sum_{j \in G_i^{1,k}} \lambda_j Q(N, \bar{\rho}, k) \prod_{l=1}^{k-1} \rho_{\gamma_{jl}}\right)^{-1}, \qquad i = 1, 2, \ldots, N \tag{24}$$

These N non-linear equations can be solved iteratively to obtain ρ_i. In contrast, the exact solution requires solving a detailed balance equation consisting of 2^N equations. Recall that the objective function is given by $\min_{\boldsymbol{x}} \sum_{i \in I} \sum_{j \in J} t_{ij} q_{ij}(\boldsymbol{x})$. Denote the estimated unit utilization as $\hat{\rho}$. The hypercube approximation algorithm provides an estimate of q_{ij}. We have

$$\hat{q}_{ij} = \begin{cases} \frac{\lambda_j}{\sum_j \lambda_j} \left(1 - \hat{\rho}_i\right), & i = \gamma_{j1}, \\ \frac{\lambda_j}{\sum_j \lambda_j} Q(N, \bar{\rho}, k-1) \left(\prod_{l=1}^{k-1} \hat{\rho}_{\gamma_{jl}}\right) \left(1 - \hat{\rho}_i\right), & i = \gamma_{jk}, \forall k \geq 2. \end{cases} \tag{25}$$

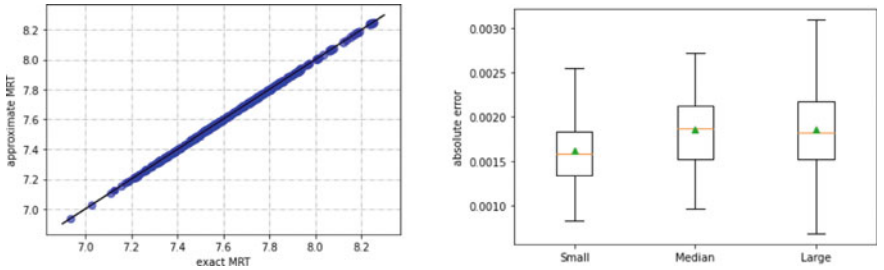

(a) Exact MRT vs. Approximate MRT.

(b) Box-plots of absolute errors.

Fig. 32.1 The accuracy of the spatial hypercube approximation algorithm

We show that the approximate MRT is very close to the exact value in Fig. 32.1, with an mean absolute error of less than 0.002 min, by generating 100 random setups under small, median, and large problems. Such a small difference is assumed to be negligible in solving for the optimal solution.

Numerical Results

In this section, we perform numerical experiments to compare the performance of p-median, our Bayesian optimization approach, and the optimal solution via full enumeration. We constructed a hypothetical region, divided into a 9×9 grid, and randomly place the N candidate locations within the region. The results are displayed in Fig. 32.2.

We show that our algorithm always outperforms the p-median solution and converges very fast in numerical experiments. The average performance of the algorithm in each round and the 95% confidence interval are plotted in the figure. In small-sized problems (Fig. 32.2a, b), we can obtain the global minimum MRT by enumeration. The results show that our method can converge to the optimal solution in very few iterations. In the medium and large problems (Fig. 32.2c, d), we cannot obtain optimal solutions by enumeration, but our method can still surpass the p-median solution quickly. In our large of selecting 50 unit locations from 100 candidate locations, obtaining the optimal solution requires enumerating all 1.01×10^{29} possible solutions. In comparison, our method outperforms the p-median solution in about 90 iterations and converges in about 300 iterations.

Another noteworthy phenomenon is that there is a cusp point at around 20 iterations in all experiments, which means that we always observe a significant drop in MRT after 20 iterations. This is where the algorithm completes the initial exploration sampling phase and enters the Bayesian optimization phase, which means that our algorithm can learn some structure of the problem during the exploration phase, and the following suggested point leverages this learned information.

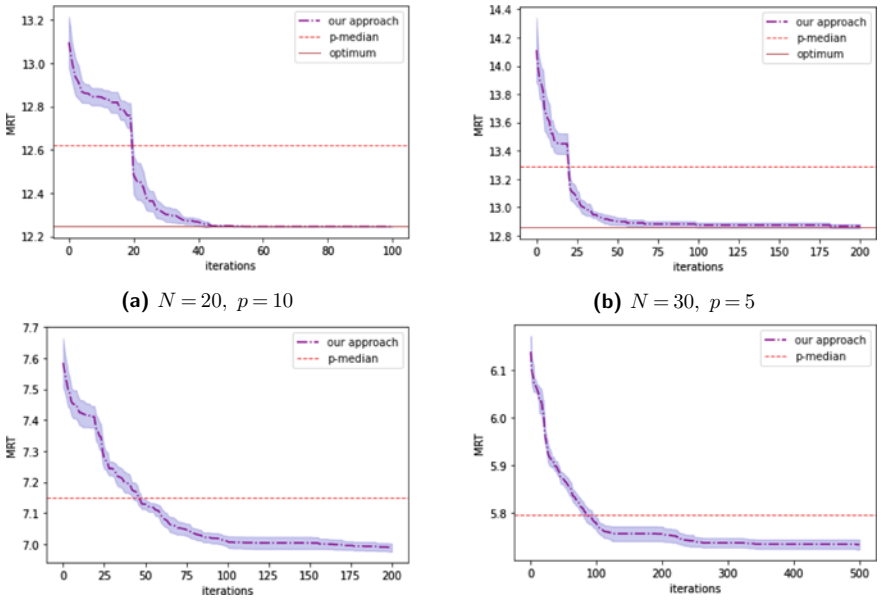

(a) $N = 20,\ p = 10$ **(b)** $N = 30,\ p = 5$

(c) $N = 50,\ p = 20$ **(d)** $N = 100,\ p = 50$

Fig. 32.2 Numerical experiments under different settings

Case Study: St Paul, Minnesota

We collected data on the emergency medical services in St. Paul, Minnesota. According to the most recent census, the population of St. Paul was 285,068 in 2017. We used 2014 Fire Department data for our analysis. In that year, 22,536 medical incidents were reported. This dataset includes the corresponding arrival times of each call, location of the nearest street intersections, and dispatch determinant categories that reveal the priority level of each call. We did not have personally identifiable information about each incident. We divided the map of St. Paul into 71 regions according to census tracts, as displayed in Fig. 32.4. We used Google Maps API to determine the travel time from each tract center to each candidate location, considering one-way streets and other practical issues. In St. Paul, there are 17 existing locations and 11 ambulances. Our goal is to use real data from St. Paul to place these ambulances in candidate locations to reduce the average response time to medical events across the city.

In Fig. 32.3, we plot the results and the best solution for ten runs of our method. Our method converge to the optimal value in the first 50 iterations. The optimal solutions obtained from our method and the p-median are shown in Fig. 32.4. We find that both our method and the p-median give optimal results. This is because St. Paul is a rather small city and the system has relatively little traffic compared to other large cities or cities with limited resources. Our solution can be applied even to the largest cities or countries.

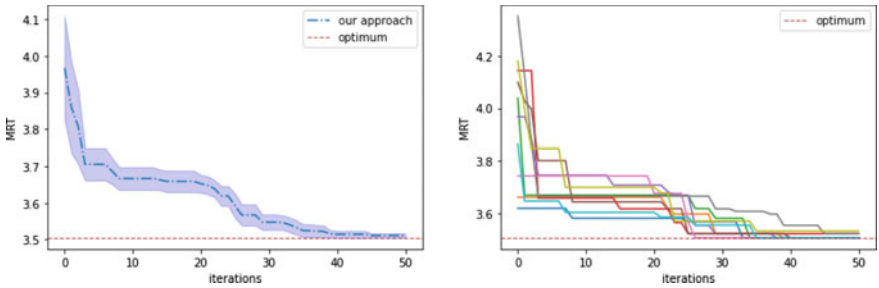

Fig. 32.3 Our solution approach applied to St. Paul, Minnesota

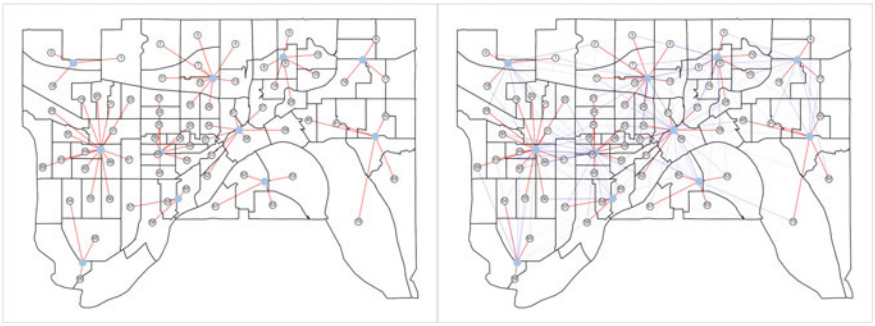

(a) p-median solution **(b)** Our approach

Fig. 32.4 Our approach versus p-median in St. Paul, Minnesota case study. The solid circles indicate unit locations, and the darknesses of the lines indicate the percentage of calls responded by each unit in each subregion. In p-median, there is only one line connected to each subregion, while in p-MRT, there are multiple lines per subregion, indicating that a call may be responded by other units when the closet unit is busy. The fraction of calls in each subregion responded to by the primary unit is marked in red, while the rest are marked in blue

Conclusion

In this paper, we propose a Bayesian optimization scheme to solve the optimal unit locations in emergency service systems that minimizes the system-wide mean response time. We develop both lower and upper bounds from the classical p-median problem. We use feasible trust region and adaptive swapping in searching for a solution and use a spatial hypercube approximation algorithm to obtain an estimate of the objective function. We show that our algorithm always converges to the global optimal solution, with a regret bound guarantee. In numerical experiments, we show that our algorithm always outperforms the p-median solution and converges very fast to the optimal solution. Our approach outperforms the p-median solution in less than 90 evaluations, and converges and yields a better than the p-median solution in less

than 300 evaluations. We also apply our approach in solving the best unit locations in St. Paul, Minnesota, using one-year real data. We show that our approach rapidly converges to the optimal solution.

References

1. Ahmadi-Javid, A., Seyedi, P., & Syam, S. S. (2017). A survey of healthcare facility location. *Computers & Operations Research, 79*, 223–263.
2. Batta, R., Dolan, J. M., & Krishnamurthy, N. N. (1989). The maximal expected covering location problem: Revisited. *Transportation science, 23*(4), 277–287.
3. Daskin, M. S. (2008). What you should know about location modeling. *Naval Research Logistics (NRL), 55*(4), 283–294.
4. Frazier, P. I. (2018). Bayesian optimization. *Recent advances in optimization and modeling of contemporary problems* (pp. 255–278) (Informs).
5. Hakimi, S. L. (1964). Optimum locations of switching centers and the absolute centers and medians of a graph. *Operations research, 12*(3), 450–459.
6. Kariv, O,. & Hakimi, S. L. (1979). An algorithmic approach to network location problems. i: The p-centers. *SIAM Journal on Applied Mathematics, 37*(3), 513–538.
7. Larson, R. C. (1974). A hypercube queuing model for facility location and redistricting in urban emergency services. *Computers & Operations Research, 1*(1), 67–95.
8. Larson, R. C. (1975). Approximating the performance of urban emergency service systems. *Operations Research, 23*(5), 845–868. ISSN 0030364X, 15265463.
9. Li, X., Zhao, Z., Zhu, X., & Wyatt, T. (2011). Covering models and optimization techniques for emergency response facility location and planning: a review. *Mathematical Methods of Operations Research, 74*(3), 281–310.
10. Rajagopalan, H. K., & Saydam, C. (2009). A minimum expected response model: Formulation, heuristic solution, and application. *Socio-Economic Planning Sciences, 43*(4), 253–262.
11. Srinivas, N., Krause, A., Kakade, S.M., & Seeger, M. (2010). Gaussian process optimization in the bandit setting: No regret and experimental design. In *International Conference on Machine Learning (ICML)* .
12. Wan, X., Nguyen, V., Ha, H., Ru, B., Lu, C., & Osborne, M. A. (2021). Think global and act local: Bayesian optimisation over high-dimensional categorical and mixed search spaces. In *International Conference on Machine Learning (ICML)*.

Chapter 33
NLP Integrated Hybrid Model of Semi-Supervised and Supervised Learning for Online Misinformation Classification

Partha Mukherjee, Deeksha Joshi, Youakim Badr, Raghvinder Sangwan, and Satish Srinivasan

Abstract Social media serves as a platform to outsource all kinds of information from politics to entertainment, from health industry to the country's administration. Some of the posts on these platforms are reliable, but most of them have some proportion of misinformation. The diversity of posts, such as the use of different languages, abbreviating words and messages with hidden meanings, make it more complex to identify the authenticity of the published information. This research will focus on identifying a model to find the misinformation in social media using the NLP integrated hybrid framework that uses a combination of semi-supervised and supervised learning. We use hybrid models that consist of two semi-supervised learning algorithms, namely Label Propagation and Label Spreading, with Logistic Regression and Random Forest as the supervised components. Among them we found that the hybrid model combining Label Propagation and Logistic Regression gives better performance in terms of accuracy, precision, recall, F1-score and AUC performance metrics in order to classify the online misinformation.

Keywords Online misinformation · Semi-supervised learning · Label propagation · Label spreading · Supervised learning · Logistic regression · Random forest

Introduction

Social media is the platform where the information explodes every day. Statistics have been collected representing the number of people using social media worldwide, which is forecasted to rise from 3.6 billion (in 2020) to almost 4.41 billion (in 2025) [1]. The quick and widespread use of these technologies is transforming how we meet partners, access news, and demand political change. People cannot wield power without a way of disseminating information. One of the major advantages of social media is the ability to share information with peers, friends, and family. Information

P. Mukherjee (✉) · D. Joshi · Y. Badr · R. Sangwan · S. Srinivasan
Engineering Division, The Pennsylvania State University, Great Valley, Malvern, PA 19355, USA
e-mail: pom5109@psu.edu

R. Qiu et al. (eds.), *City, Society, and Digital Transformation*, Lecture Notes in Operations Research, https://doi.org/10.1007/978-3-031-15644-1_33

can be easily obtained with only a few clicks on social platforms like Facebook, Twitter, Weibo and others.

The anyone, anytime, anywhere aspects of social media have largely expedited the generation and spreading of misinformation, such as rumour, spam, fake news etc. [2]. Misinformation is defined as misleading or erroneous information that is purposefully created and disseminated, whether intentionally or accidentally. However, there are numerous phrases that are quite similar and can easily be mistaken as false information. To define the scope or boundaries of the research or study, a comprehensive understanding of these terminologies is essential. Several recent studies [2, 3] define these various types of misinformation. Fake news is one of the most common forms of misinformation which is created with the goal to deceive or misinform readers but can be proven incorrect by other sources. Serious fabrications (i.e., articles with a malevolent motive), large-scale hoaxes (i.e., reporting of false information masquerading as legitimate news on a huge scale), and humorous fakes news (i.e., satirical pieces masqueraded as real news) are all examples of fake news. Rumours, which are unconfirmed information that can be accurate or untrue, are the second form of misinformation, also termed disinformation. Persistent rumours are those that are flowing around the social media platform for a long time, whereas rumours in breaking news are those that are more recent. There are numerous other types of misinformation, such as clickbait and spam, but the main subject of interest among researchers is fake news and rumours.

Living in a world of misinformation has numerous impacts on our lives, which may be reflected through several statistics. Prior to the United States presidential election in 2016, a huge amount of misinformation was released, and a survey from Stanford University claims that 70% of fake news originated from online social networks [4, 5]. Users' perspectives and decision-making are highly influenced by information supplied through social media. Many people believe that misleading news had a significant effect on the election and the subsequent political subjects [5–9]. Similarly the users became influenced by the misinformation propagated through Twitter related to H1N1 break-out in US-Mexico border in 2009 over time [10–12]. The medium of transmission vector of H1N1 virus (Swine flu) was attributed to eating of pork as the source while there is no evidence in support of it [13]. In separate studies, researchers showed that fabricated news are easily accepted by the users than the real fact based information related to global warming and climate change [14–17]. In recent times QAnon group is formed to promote the false diction to denigrate the mainstream media sources that corroborate the scientific rhetoric [18].

Research on misinformation propagation detection on a broader scale has been facilitated by the increased availability and access to data which has also helped evaluate various interventions to limit the spread of misinformation. Detecting misinformation is difficult for a variety of reasons, including the diversity of posts, such as the use of different languages, and abbreviating words and messages with hidden meanings, which make it more complex to identify the truthfulness of the published information. The issues faced by researchers are that there is no definite benchmark to check the credibility of news. Also, fake news detection studies are mostly either

content-based or context-based approaches, but both have their own limitations and a method that is highly efficient for one has no proof that it will work the same for the other.

Another significant problem in the field of misinformation detection is the scarcity of comprehensive and reliable datasets. As a result of this variation in features of the datasets, researchers use a range of methodologies and metrics to evaluate their findings, making it problematic to compare one approach to another [2, 5]. Also, understanding message stance classification, which identifies whether a social media post bolsters, opposes, or is impartial towards a rumour, is necessary for establishing the trustworthiness of a post [19].

In our research, we intend to address the concerns raised by other studies and develop an NLP integrated hybrid model of semi-supervised and supervised learning that is capable of identifying generic information and misinformation related to COVID-19 pandemic on Twitter. Numerous fake information are circulated in the social media highlighting public health issues and epidemiological factors related to this global pandemic [17]. We performed a pilot study as a first step using a limited number of tweets that involves the online social media content from Twitter. We used the hybrid modes for classification of fake posts and evaluation of the proposed model using probabilistic fact-checkers.

Related Work

Even while misinformation is not a recent concept, advanced technologies have provided a perfect environment for it to spread swiftly in recent years. As a result, it's essential to realize how misinformation is created and circulated via social media, and what impact it has on its users [20]. In addition, we must uncover consistent patterns across multiple domains of belief, time, and socio-political settings in order to comprehend the link between conspiracy theories, beliefs and content consumption [21].

Various studies have discovered a number of strategies for categorizing fake news and detecting its transmission. The research [22] indicates that by utilizing tensor-based embedding and a K-NN graphical approach to propagate labels, an accuracy of 70.92% for recognizing false news can be attained using just 2% of the labelled dataset. A different approach has been taken in [23] where the author advocated utilizing crowdsourcing to place trust labels on websites rather than individual stories by lay people, not specialists, so that a larger number of platform ratings can be easily obtained and sites with broader crowd trust can be quickly discovered. Learning from unlabelled data with a substantial domain shift continues to remain challenging. To address this concern, the MT-tri theory was established, which involved adding a small number of pseudo-labels to each epoch and training one of the three output layers exclusively on these derived pseudo-labels [24]. Analyzing the dynamics of misinformation dissemination in the network, in addition to misinformation categorization, is a significant component of research in this arena [25]. Rumours, according

to scholars, tend to resurface several times compared to real facts [26]. The dissemination process was assumed to be a fixed object in some studies [27–30], whereas misinformation diffusion is believed to be mutable and malleable in others [26].

Several authors have presented various supervised approaches for identifying the reliability of rumours, but few have argued that semi-supervised learning approaches are more successful in terms of classification accuracy, speed, and scalability. Giasemidis et al. [19], for example, developed a graph-based semi-supervised method for message stance categorization and attained an accuracy of 80%. Bondielli et al. [3] gave a detailed review of the performance of available models for fake news identification, as well as an overview of various types of misinformation and feature detection strategies (content vs. context-based). Liang et al. [2] expand on this research by describing the distribution of misinformation in social media and the variables that influence it. Allcott et al. [31] explored how misinformation spreads via social media and its relation with political science. The findings reveal a consistent rise in false news on Facebook and Twitter from early 2015 till the end if US presidential election in 2016. However, post-election, Facebook interactions dropped by more than half, although Twitter views increased.

A study [32] was undertaken to learn more about the characteristics of persons who spread disinformation. The author conducted four studies to investigate the impact of message attributes and viewer characteristics. The finding shows that those who believe the content is accurate and reliable or hold aligned ideas, lead to the spread of disinformation. The research [33] aims to examine the key factors that put-up to the dissemination of the rumors among Nigerians on social media. In comparison to reliance on online information, status-seeking, self-expression, information seeking and sharing, the results reveal that news-finds-me perception and information overload had a stronger impact on fake news sharing behaviour.

One of the most significant aspects of automatic misinformation identification is the ability to process and evaluate large amounts of web material without human intervention. Natural Language Processing (NLP) methods are used to facilitate in achieving this. In [34], the authors cover several NLP techniques, assumptions and significant difficulties encountered when using these methods. The researchers suggest that one should know how to use non-textual data effectively, enhance the verification process to include contents, and whether hand-crafted features can be paired with neural network models. Along with it, emotion detection which is the recognition of emotions in textual data, could potentially be employed for misinformation detection approaches. Various techniques [35] can be used for emotion detection for classifying text into categories of emotions such as happiness, sadness, and anger, which can then be summed up in the dataset's feature matrix.

Dadgar et al. [21] designed Checkovid, a fact-checking website, to identify misinformed and informative statements in the COVID-19 domain from several angles. The COVID-19 associated misinformation dataset from Twitter was used in their study, which included two network-based and content-based methodologies. The categorization models are trained on the content of the tweets and are developed at two levels: paragraph-level and sentence-level. In the content-based procedure, they achieve the greatest performance using the ensemble-learning text categorization

model. A substantial positive statistical association was found between fabrication of social media posts and the circulation of fear related to COVID-19 in research undertaken for the COVID-19 epidemic in Iraqi Kurdistan [36].

Indeed, the previous researches have a strong impact on the foundation of misinformation detection and spreading. However, there is a need of a generalized model, which can detect misinformation in any domain. The goal of this study is to create a generic framework that uses an NLP integrated hybrid model of semi-supervised and supervised learning to determine if the provided information is false. The general architecture for identification of online misinformation for the events of diverse nature facilitates the social media houses on the new policies or moderating the existing policies against content fabrication in the misinformed tweets. This will also help the social media users to disregard the probabilistic misinformed tweets. The research presented here is the first step towards the goal.

Research Objectives and Design

In our research, we have examined the following research question:

- How effective are the semi-supervised algorithms in identifying misinformation in online social media postings?

The objectives for evaluating this research question is:

- To determine how labels can be propagated within a dataset that is largely unlabelled
- To implement hybrid models for classifying whether or not tweets on Twitter include misinformation (true for facts, false for misinformation)
- To evaluate the goodness of manual labelling using probabilistic fact-checkers.

Data Collection

Data scraping tools were used on the Twitter platform, and tweets related to Covid-19 were collected from 03/25/2020 to 10/30/2020. Our dataset consists of 128 data files with a total of 6 million tweets from which we took only 800 tweets from a single day i.e., 10/10/2020 to continue the pilot study. There are 90 features in each tweet.

Data Preprocessing

Data pre-processing is the first and crucial phase in every research project before modelling. It is the process of cleaning, structuring and transforming raw data into a usable format in order to improve the model's performance. Using NLP techniques,

we impute null/NA values and extract relevant characteristics from the textual data of a tweet for our research. To create our final feature matrix, we followed the procedure below:

- Removed from the text data, symbols such as (@), RTs, URLs, special characters, hashtags (#), short words (words having a length less than 2), and unnecessary white spaces.
- Generated new features, labelled 'no_user_mentions', 'no_urls', 'no_hashtags', 'no_chars', 'no_words,' by taking count of mentioned users, URLs, hashtags, characters, and words respectively.
- Applied tokenization, stop word removal, stemming and lemmatization for further structuring the textual data.
- Applied POS tagging using Stanford POS tagger[1] to generate the features such as 'noun_count', 'pronoun_count', 'verb_count', 'adj_count' and 'adverb_count.'
- Extracted and aggregated emotions (anger, disgust, fear, negative, sadness, positive, surprise, anticipation, trust, joy) using the NRC classifier [37], and added them to the feature matrix. Here we identify the total number of each emotional aspect.

Our final matrix had all of the essential properties from the tweets after applying all of the feature extraction methods to its text. As needed for our study, we also performed a few other transformations on other columns to have two more derived attributes such as account_span and ratio_follower_friends. The account_span is calculated as created_at—account_created_at, while the ratio_follower_friends is computed as number of followers divided by the number of friends. The features that are significant for our study were chosen using Random Forest. Table 33.1 displays the attributes that contribute to the final dataset used in the research.

Methodology

This study aims to build a model that can distinguish between misinformation and generic information using data on the Covid-19 pandemic from social media platforms. We will use both qualitative and quantitative methodologies to achieve our objective. The tweets we are experimenting with are completely unlabelled. We manually labelled 20% of the dataset, while the remaining data (80% of the primary dataset) were labelled using our proposed model. Manual labelling was carried out by two human raters who categorized the data by sampling identical random. The human raters agreed on the labelled data using a 90% similarity benchmark. We also used two supervised learning techniques and took their fact-checking agreement (i.e., Cohen's kappa) into account to assess the credibility of the manually assigned labels. The labelled data consists of two classes, label 0 indicating the misinformed tweets and label 1 indicating the authentic tweets. The labelled data was then split into test

[1] https://nlp.stanford.edu/software/tagger.shtml.

Table 33.1 Set of attributes used in the dataset

Name of style	Font size and type
Retweet-count	Total retweets on the tweet
Favorite-count	Total favorite on the tweet
Anger	Total number of tweets represents anger emotion
Anticipation	Total number of tweets represents anticipation emotion
Disgust	Total number of tweets represents disgust emotion
Fear	Total number of tweets represents fear emotion
Joy	Total number of tweets represents joy emotion
Sadness	Total number of tweets represents sadness emotion
Surprise	Total number of tweets represents surprise emotion
Trust	Total number of tweets represents trust emotion
positive	Total number of tweets represents positive sentiment
Negative	Total number of tweets represents Negative sentiment
Characters-account-desc	Total number of characters in the account description of the user
Words-account-desc	Total number of words in the account description of the user
Characters-username	Total number of characters in the username
No-user-mentions	Total number of mentions against a tweet
No-urls	Total number of urls in a tweet
No-hashtags	Total number of hashtags in a tweet
No-chars	Total number of characters in a tweet
No-words	Total number of words in a tweet
Noun-count	Total number of nouns in a tweet
Pronoun-count	Total number of pronouns in a tweet
Adjective-count	Total number of adjectives in a tweet
Verb-count	Total number of verbs in a tweet
Adverb-count	Total number of adverbs in a tweet

(continued)

Table 33.1 (continued)

Name of style	Font size and type
ratio_follower_friends	Number of followers/number of friends of a user
username_len	Total length of screen name of the user
is_quote	Binary value for the post is quoted or not
is_retweet	Binary value for the post is retweeted or not
user_desc_len	Total length of description of the posts
is_verified	Binary value to check the user is verified or not

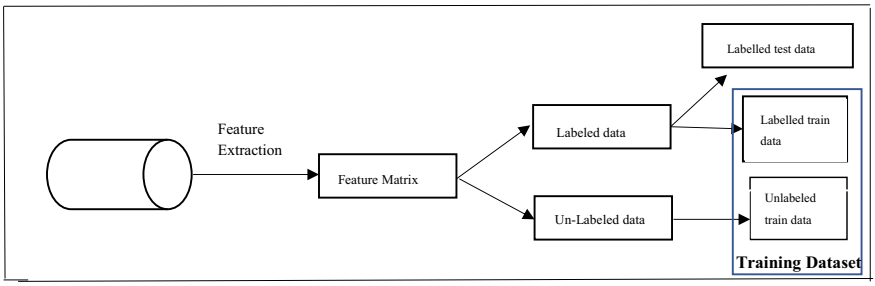

Fig. 33.1 Dataset labeling and splitting representation

and train data. Figure 33.1 depicts the schematic diagram that captures the process we followed.

Baseline Model

We used a self-training method as a baseline model for our research. We divided labelled data instances into train and test sets for the self-training strategy and trained a classification algorithm on the labelled training dataset. We predicted labels for unlabeled data using the trained model. Those with the highest probabilities would be used as 'pseudo-labels.' After integrating the labelled dataset with the newly generated pseudo-labels, we retrained our classifier. This process was repeated until we had a pre-determined number of labelled data and then used the test dataset to evaluate our model's performance. We have used Naïve Bayes classifier as the generative probabilistic and self-trained model.

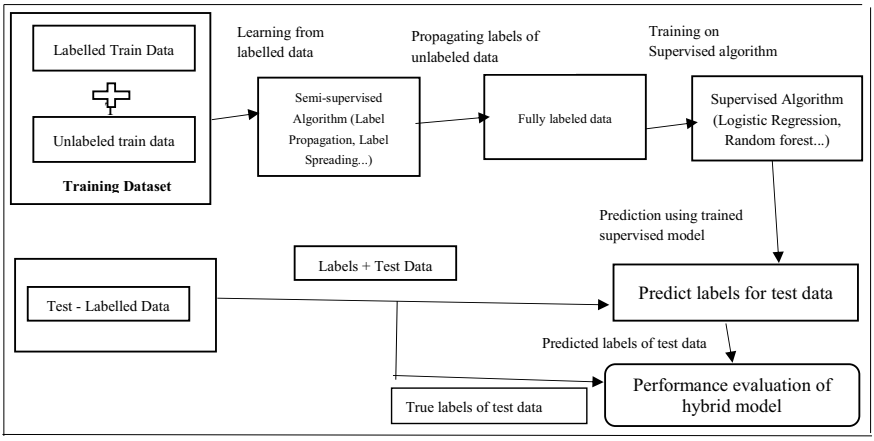

Fig. 33.2 NLP integrated hybrid model of semi-supervised and supervised learning algorithms

Proposed Model

The proposed model is an NLP-integrated hybrid model that combines semi-supervised and supervised learning. For the semi-supervised component of our model, we employed two semi-supervised algorithms: (a) Label Propagation (LP) [38], and (b) Label Spreading (LS) [39]. The labelled train dataset together with unlabeled data was transmitted to the first component after partitioning the labelled dataset into train and test set. Both methods are graph-based semi-supervised machine learning approaches that take input (labelled and unlabeled data) and produce fully labelled data as an output using community network methodology to assign labels to unlabeled data. Our next module, which is based on supervised learning methods, employs Logistic Regression and Random Forest. These supervised classifiers were trained using the output from this semi-supervised learning components. Finally, the performance of this model was evaluated using test data. Figure 33.2 displays our proposed method.

Performance Metrics

For the dataset used, the performance and efficiency of (1) the method for labelling unlabeled data, (2) the method for self-training using Naïve Bayes classifier, and (3) the hybrid model using semi-supervised and supervised learning was evaluated based on five performance metrics namely: accuracy, precision, recall, f1-score, and area under ROC curve (AUC). In our case we need to focus on the misinformation detection and therefore precision and recall are the major statistics that we need to focus on as precision and recall refer to positive predictive value and sensitivity of

analysis respectively. Apart from that we also choose f1-score as it is a function of precision and recall and hence be considered as a better statistic to find a balance between precision and recall particularly when there is class imbalance. AUC identifies the degree of predictive power of the model, which we considered important for our analysis of the results. We also put accuracy in our set of performance metrics, as there is previous research that focused on accuracy [22].

Results

Credibility of Manual Labeling

To check the correctness of our manually labelled dataset, we split the dataset into a 75:25 ratio between train and test sets, respectively. Then, we trained Logistic Regression and Random Forest classifiers using the training set and checked the performance of these classifiers on test data set in terms from accuracy and ROC curve perspectives. From both the classifiers, we get an accuracy of 84.78%, but ROC-AUC score of the random forest was 0.760, and Logistic Regression was 0.777. We considered these two supervised algorithms as the probabilistic fact-checkers (i.e., the raters) of the test set. When two independent raters agree on the same vote for the same experiment, inter-rater agreement score was computed. In our study the inter-rater agreement score or Cohen's kappa involving these two classifiers was computed, and it was 76.36%. This score indicated how accurate the data obtained in the research are for the variables being examined and the agreement score of 0.76 was considered to be satisfactory. We infer that the goodness criterion of the manually labelled data was adequate for carrying out the modelling.

Baseline Model Performance

We used the Naive Bayes classifier to implement the self-training method as a baseline model. We started by splitting the labelled dataset into training and test with the ratio of 75:25 and then again split the training dataset into labelled and unlabelled sets with the ratio of 1:99. We then use the train labelled dataset to train the Naïve Bayes classifier [33] and then use the model repeatedly to predict labels of the unlabelled training set. In each iteration, the generated pseudo-labels are included in the original train labelled dataset, and the model is retrained. Finally, we evaluated the model's performance using test data and achieved an accuracy of 71.74% with a ROC-AUC score of 0.50. The precision and recall for the misinformed tweets in case of Naïve Bayes classifier is low: 0.36 and 0.50 respectively.

Table 33.2 Performance metrics of the hybrid models

Hybrid algorithm	Accuracy	Average precision	Average recall	Average F1 score	AUC value
Label Propagation + Logistic regression	0.824	0.83	0.72	0.75	0.719
Label Propagation + Random Forest	0.784	0.76	0.66	0.68	0.662
Label Spreading + Logistic Regression	0.811	0.81	0.70	0.72	0.695
Label Spreading + Random Forest	0.783	0.76	0.65	0.68	0.662

Performance of the Hybrid Models

For implementing the hybrid model using semi-supervised and supervised learning, we used Label Propagation (LP) and Label Spreading (LS) as the semi-supervised components and Logistic Regression (LR) and Random Forest (RF) as the supervised components. As a result, we developed four (2×2) different combinations of models and compared their performance metrics' scores. Table 33.2 provides an overview of the performance of these models.

From Table 33.2, we observe that all four hybrid models outperformed the baseline model w.r.t. all five performance metrics. It is interesting to observe that the hybrid model combining Label Propagation and Logistic Regression outperformed the remaining three hybrid combinations and was followed by the combination involving Label Spreading and Logistic Regression. The performance of the hybrid model with Label Propagation and Random forest is almost same as those for the combination of Label Spreading and Random Forest. From the results shown in Table 33.2, it is clear that inclusion of Logistic Regression supervised algorithm with any semi-supervised algorithm as hybrid model raises the performance of classifying the online misinformation. On the other hand Label Propagation algorithm works better as the semi-supervised component of the hybrid model to detect the misinformed tweets. We further analysed the precision, recall and F1-score of the best hybrid model i.e., Label Propagation with Logistic regression. Table 33.3 showed its label-wide precision, recall, and F1-score.

Table 33.3 Micro-level analysis of the performance metrics for the best hybrid model

Class labels	Precision	Recall	F1 score
0 (misinformed)	0.83	0.48	0.61
1 (authentic)	0.82	0.96	0.89

From Table3, it was observed that precision to detect the misinformed tweets of the hybrid model with Label Propagation and Logistic regression is 83% while the recall for misinformed tweets is low. This means that it correctly detects 83% of the misinformed tweets while it identifies 96% of the tweets correctly from the whole population of the authentic tweets (recall = 0.96).

Limitations and Future Works

The study presented in the paper has lot of limitations like other research do. In this research, we have conducted a pilot study and current analysis is on a minimal subset of our primary dataset. We intend to extend our research using the primary dataset that contains millions of tweets. We need to check the performance of each model with the tuning of the parameters. This experiment did not include the emotion scores identified by the NRC classification but the total number of tweets that identifies different emotions. Besides the content based features are missing in our experiment. We need to incorporate the content words in out experiment. We need to include the computed emotion scores as the features of our data in future.

We will explore complex algorithms for both the semi-supervised and supervised components of the model. In future, we need to extend our feature set with content based and context based semantic features such as word embedding in terms of word2vec, sentiments and emotions scores in our analysis. The semantic features will lead to use of deep learning algorithm as semi-supervised and supervised components to carry out the label propagation through the unlabeled data. In the present research we did not pay attention to the class imbalance from the perspective of misinformed and authentic tweets, which we will take care in future. We also intend to extend our study to carry out the causality analysis between the online misinformation and peoples' interests on the information searching on the web related to Covid-19. We will test our framework on different dataset related to topics other than Covid-19 in order to test the generality of the framework.

Conclusion

In this research we carried out a pilot study on classifying the online misinformation using a hybrid framework that involved the combinations of semi-supervised and supervised classifiers. Our intention is to build a generic framework to classify the misinformation from the online social media posts irrespective of the topics. Though in this study we particularly used a minimal subset of Covid-19 related unlabelled tweets, we believe that our result is promising to scale the research using large datasets related to different topics which are vulnerable to information fabrication and propagation through online social networks.

Acknowledgements This material is based upon work funded and supported by the 2020 IndustryXchange Multidisciplinary Research Seed Grant from Pennsylvania State University.

References

1. https://www.statista.com/statistics/278414/number-of-worldwide-social-network-users
2. Wu, L., Morstatter, F., Carley, K. M., & Liu, H. (2019). Misinformation in social media: Definition, manipulation, and detection. *ACM SIGKDD Explorations Newsletter, 21*(2), 80–90.
3. Bondielli, A., & Marcelloni, F. (2019). A survey on fake news and rumour detection techniques. *Information Sciences, 497*, 38–55.
4. Allcott, H., & Gentzkow, M. (2017). Social media and fake news in the 2016 election. *Journal of Economic Perspectives, 31*(2), 211–236.
5. Mansouri, R., Naderan-Tahan, M., & Rashti, M. J. (2020). A semi-supervised learning method for fake news detection in social media. In: *Proceedings of the 28th Iranian conference on electrical engineering (ICEE)* (pp. 1–5). Tabritz, Iran.
6. https://www.documentcloud.org/documents/4429952-Fake-News-May-Have-Contributed-to-Trump-s-2016
7. www.theguardian.com/commentisfree/2016/nov/14/fake-news-donald-trump-election-alt-right-social-media-tech-companies/
8. Azzimonti, M., & Fernandes, M. (2018) Social media networks, fake news, and polarization. National Bureau of Economic Research.
9. Spohr, D. (2017). Fake news and ideological polarization: Filter bubbles and selective exposure on social media. *Business Information Review, 34*(3), 150–160.
10. https://www.nielsen.com/us/en/insights/article/2009/swine-flu-news-and-concern-dominates-online-buzz/
11. https://www.npr.org/templates/story/story.php?storyId=103562240
12. Chew, C., & Eysenbach, G. (2010). Pandemics in the age of Twitter: Content analysis of tweets during the 2009 H1N1 outbreak. *PLoS ONE, 5*(11), e14118.
13. Chamberlain, P. R. (2010). Twitter as a vector for disinformation. *Journal of Information Warfare, 9*(1), 11–17.
14. https://www.brandwatch.com/blog/react-climate-change-fake-news/
15. Miller, M. (2019) Fake news: Separating truth from fiction. Minneapolis: Twenty-First Century Books™.
16. Schmid-Petri, H., & Bürger, M. (2022). The effect of misinformation and inoculation: Replication of an experiment on the effect of false experts in the context of climate change communication. *Public Understanding of Science, 31*(2), 152–167.
17. Al-Rawi, A., O'Keefe, D., Kane, O., & Bizimana, A. J. (2021). Twitter's fake news discourses around climate change and global warming. *Frontiers of Communication*, *6*, 1–9.
18. https://www.theatlantic.com/magazine/archive/2020/06/qanon-nothing-can-stop-what-is-coming/610567/
19. Giasemidis, G., Kaplis, N., Agrafiotis, I., & Nurse, J. R. C. (2018). A semi-supervised approach to message stance classification. *IEEE Transactions on Knowledge and Data Engineering, 32*(1), 1–11.
20. Hilary, I. O., & Dumebi, O. O. (2021). Social media as a tool for misinformation and disinformation management. *Linguistics Culture Review, 5*(S1), 496–505.
21. Dadgar, S., & Ghatee, M. (2021). Checkovid: A COVID-19 misinformation detection system on twitter using network and content mining perspectives. arXiv preprint arXiv:09768
22. Guacho, G. B., Abdali, S., Shah, N., & Papalexakis, E. E. (2018) Semi-supervised content-based detection of misinformation via tensor embeddings. In *Proceedings of IEEE/ACM international conference on advances in social networks analysis and mining (ASONAM)* (pp. 322–325). Barcelona, Spain.

23. Pennycook, G., & Rand, D. G. (2019). Fighting misinformation on social media using crowdsourced judgments of news source quality. *Proceedings of the National Academy of Sciences (PNAS), 116*(7), 2521–2526.
24. Ruder, S., & Plank, B. (2018). Strong baselines for neural semi-supervised learning under domain shift. arXiv preprint arXiv:09530
25. Shin, J., Jian, L., Driscoll, K., & Bar, F. (2018). The diffusion of misinformation on social media: Temporal pattern, message, and source. *Computers in Human Behavior, 83*, 278–287.
26. DiFonzo, N., & Bordia, P. (2007). *Rumor psychology: Social and organizational approaches.* American Psychological Association.
27. Bessi, A., Coletto, M., Davidescu, G. A., Scala, A., Caldarelli, G., & Quattrociocchi, W. (2015). Science vs conspiracy: Collective narratives in the age of misinformation. *PLoS ONE, 10*(2), e0118093.
28. Friggeri, A., Adamic, L., Eckles, D., & Cheng, J. (2014). Rumor cascades. In *Proceedings the 8th International AAAI Conference on Web and Social Media (ICWSM)* (pp. 101–110). Ann Arbor.
29. Kwon, S., Cha, M., Jung, K., Chen, W., & Wang, Y. (2013). Prominent features of rumor propagation in online social media. In *Proceedings of IEEE 13th International Conference on Data Mining (ICDM)* (pp. 1103–1108). Dallas, USA.
30. Del Vicario, M., Bessi, A., Zollo, F., Petroni, F., Scala, A., Caldarelli, G., Stanley, H. E., & Quattrociocchi, W. (2016). The spreading of misinformation online. *PLoS ONE, 113*(3), 554–559.
31. Allcott, H., Gentzkow, M., & Yu, C. (2019). Trends in the diffusion of misinformation on social media. *Research Politics, 6*(2), 2053168019848554.
32. Buchanan, T. (2020). Why do people spread false information online? The effects of message and viewer characteristics on self-reported likelihood of sharing social media disinformation. *PLoS ONE, 15*(10), e0239666.
33. Apuke, O. D., & Omar, B. (2021). Social media affordances and information abundance: Enabling fake news sharing during the COVID-19 health crisis. *Health Informatics Journal, 27*(3), 14604582211021470.
34. Oshikawa, R., Qian, J., & Wang, W. Y. (2018). A survey on natural language processing for fake news detection. arXiv preprint arXiv:00770
35. Hasan, M. (2021). *Automatic emotion detection in text messages using supervised learning.* University of Massachusetts, Boston.
36. Ahmad, A. R., & Murad, H. R. (2020). The impact of social media on panic during the COVID-19 pandemic in Iraqi Kurdistan: Online questionnaire study. *Journal of Medical Internet Research, 22*(5), e19556.
37. Mohammad, S. M. (2021). Sentiment analysis: Automatically detecting valence, emotions, and other affectual states from text. In *Emotion measurement* (2nd ed., pp. 323–379). Elsevier.
38. Xiaojin, Z., & Zoubin, G. (2002). Learning from labeled and unlabeled data with label propagation. Carnegie Mellon University.
39. Chen, X., & Wang, T. (2017). Combining active learning and semi-supervised learning by using selective label spreading. In *Proceedings of 17th IEEE international conference on data mining workshops (ICDMW)* (pp. 850–857). Pitscataway, NJ, USA.

Chapter 34
Pattern Language for Designing Distributed AI Systems

Satish Mahadevan Srinivasan, Shahed Mahbub, Raghvinder S. Sangwan, Youakim Badr, and Partha Mukherjee

Abstract Design of Artificial Intelligence (AI) and Machine Learning (ML) applications, hereafter referred to as AI systems, is often based on a typical ML pipeline. One of the reasons for choosing this approach is its simplicity and modularity. While simple, such an approach tends to be rigid with respect to changing needs, technologies, devices, and algorithms. Recent research on design patterns for ML has introduced best practices for engineering AI systems. We examine a set of these patterns, or a pattern language, where individually selected patterns can build on each other to offer a complete design solution for a distributed AI system. We demonstrate the use of this pattern language to design an AI system for emotion classification of social media content. The result is an AI system that is not only easy to change and reuse in a similar context, for instance emotion classification of image data, but one whose architecture has better performance, usability, maintainability, security, and reliability.

Keywords AI engineering · Distributed AI system · Design pattern · Pattern language · Artificial intelligence · Machine learning

S. M. Srinivasan (✉) · S. Mahbub · R. S. Sangwan · Y. Badr · P. Mukherjee
Engineering Department, Penn State Great Valley, Malvern, PA 19355, USA
e-mail: sus64@psu.edu

S. Mahbub
e-mail: sim5783@psu.edu

R. S. Sangwan
e-mail: rsangwan@psu.edu

Y. Badr
e-mail: yzb61@psu.edu

P. Mukherjee
e-mail: pom5109@psu.edu

R. Qiu et al. (eds.), *City, Society, and Digital Transformation*, Lecture Notes in Operations Research, https://doi.org/10.1007/978-3-031-15644-1_34

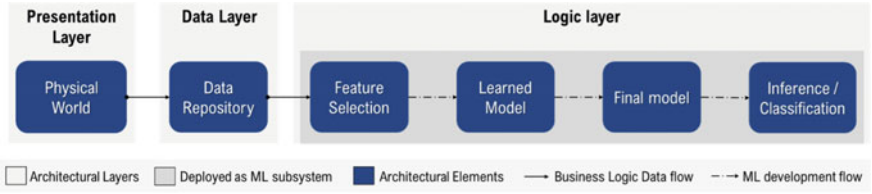

Fig. 34.1 Classic ML pipeline in an AI system

Introduction

Depending upon a business use case, an AI system can use a simple process of collecting data from the physical world and loading it into a data repository. The data collected from diverse sources can be pre-processed and stored in data repositories that can range anywhere from a simple relational database to a complex data warehouse, data lake or a data mart. The pre-processed data can then be channeled through feature-selection algorithms for extracting features relevant to the use case. Training datasets containing instances pertaining to the relevant features identified in the previous step are constructed which can then be fed to appropriate ML algorithms for the model to learn and extract relevant motifs in the data. Finally, the trained or learned ML models are applied on unlabeled instances of the data to determine their association with different motifs (class). This ML pipeline-based architecture used in the development of an AI system is shown in Fig. 34.1.

Designing AI systems using this simple approach makes its architecture rigid and does not directly address challenges associated with heterogeneity of data sources, errors and inconsistencies in these data sources, untimely arrival of data, data localized elsewhere, incorrect data formatting types, and poor quality of the data that can seriously compromise the quality of an AI system [1]. However, recent advances in best practices for architecting AI systems have emerged in the form design patterns that make ingesting, modelling, enhancing, transforming, and delivering data much more flexible while decoupling all of these activities from an AI system. These design patterns can also help architect AI systems with desired performance, usability, maintainability, security, and reliability; we refer to these 'ilities' as quality attributes. In this research, we demonstrate the use of a set of design patterns on an Emotion Classifier AI System that help achieve these quality attributes and yield a system that is much more flexible in adapting to change.

Patterns and Pattern Language

A design pattern is a general, reusable solution to a commonly occurring problem with a given context in system design. They do not represent a finished product that can be directly transformed to production (code, functioning system etc.). Rather

patterns are descriptions or templates that describe how to solve a problem i.e., to address the ever-changing requirements of the system. The design patterns can speed up the development process by providing tested, proven development paradigms. Building effective system designs require considering issues that may not become visible until later in the implementation. Each time a system is designed from scratch without following any template, it can result in hidden subtle issues that take time to be detected, issues that sometimes can cause major problems down the road. Using design patterns can help in preventing such subtle issues and also improve the reusability of these systems. Pattern languages are derived from a combination of different patterns that together provide a solution to complex problems [2]. They are a way of expressing complex solutions that were derived from experience such that others can gain a better understanding of the solution.

Figure 34.2 shows an ML design pattern called *Distinguish Business Logic from ML Model* that aims at improving the operational stability of an AI system [3]. It underscores the importance of decoupling business logic from ML and proposes an alternative to the traditional three-layer architecture. Yokoyama [3] discusses the widespread usage of three-layer architecture in enterprise applications where the data can potentially influence the business logic due to tight coupling with the ML module and identify data dependency as one of the main technical debts in an AI system.

Horizontally, this pattern decouples an AI system in to three layers namely the presentation layer, logic layer and the data layer (see Fig. 34.2). The presentation layer focuses on designing user interfaces that facilitates user interaction and the data collection process. The logic layer entails designing modules that implement the business logic, inference engines and enables data pre-processing. The data layer focuses on designing databases, data marts and data lakes for storing the raw and processed data.

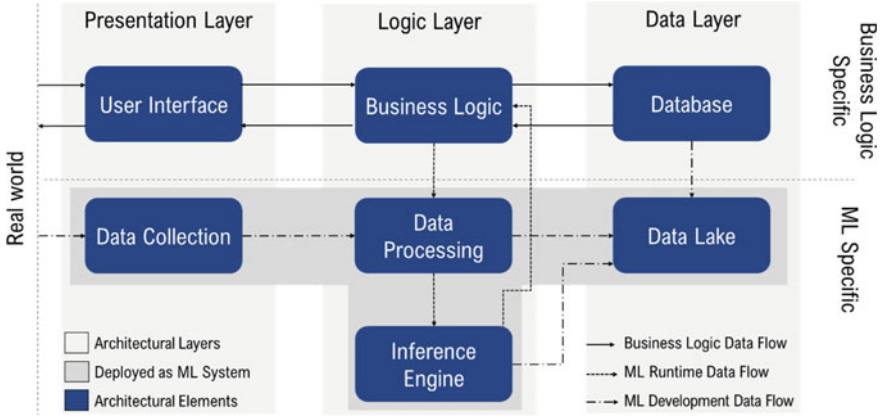

Fig. 34.2 "Distinguish business logic from ML model" pattern (adpated from [3])

Vertically, the pattern decouples the business logic specifics of AI system from its ML specifics (see Fig. 34.2). Business logic in the model encompasses the dashboard elements and rules on how the reports should be interpreted and communicated. The inference engine on the other hand, is only focused on data interpretation and pattern detection. The highlight here is the decoupling of the inference engine from the business logic that allows the ML subsystem to be easily updated and tested. ML algorithms derive their own set of functions, weights and biases based on the data available. This can be an inherent source of instability as the model's efficacy is contingent on the quality and currency of the data being fed to it. Therefore, in a tightly coupled system, instability of the inference engine will destabilize the business logic, which is undesirable from the client's perspective. Furthermore, this complicates the troubleshooting process as it is necessary to check both business logic and inference engine to localize the error. In the medium to long term, other factors can also lower the efficacy of an AI system such as changes in trends, data staleness and lack of data on new items or queries. On the other hand, the proposed decoupling in Fig. 34.2 makes the rollback process significantly easier as architects do not have to modify the business logic. In summary, the proposed pattern segregates business logic from ML hierarchically by introducing four additional elements within the ML subsystem, namely, data collection, data processing, data lake and inference engine.

Another observation of the decoupled architecture that results from this pattern is separating of data collection from data storage. The data collection module continuously collects data from the sources and passes them onto the data processing module. This in-turn stores the cleaned data into the data lake. This ensures that the data collection is separate and independent from the user interface and the database. This decoupled architecture ensures that inference engine can provide inputs to the business logic without being directly influenced by it. Finally, the architecture also proposes that the data lake (which can house various types of data) is separate from the structured database used to query user questions.

The use of *Distinguish Business Logic from ML Model* pattern yields a structure with decoupled elements that can be deployed in a distributed manner. Separation of data collection, processing and storage elements can help address some of the data quality issues mentioned earlier in the paper and can be a good starting point for designing a distributed AI system. The next section provides application of this decoupling to distributed AI system and outlines the concrete benefits this pattern yielded for the project. *Distinguish Business Logic from ML Model* pattern, can be combined with additional design patterns [1–5] to form a pattern language for building distributed AI systems with improved performance, usability, maintainability, security, reliability and portability. We provide a description of these patterns in Table 34.1 along with the layer, and element within that layer, of the *Distinguish Business Logic from ML Model* pattern they refine to achieve the desired quality attribute(s).

In the next section, we use the patterns from Table 34.1 combined with *Distinguish Business Logic from ML Model* pattern to design an AI system for emotion classification of unstructured tweets obtained from Twitter.

Table 34.1 Design patterns for refining *Distinguish Business Logic from ML Model* pattern

Design pattern	Pattern description	Layer and element refined	Quality attribute targeted
Rebalancing [1]	Use different strategies, such as downsample, upsample, or a weighted loss function, to deal with imbalanced datasets	Data processing element within logic layer	Reliability
Reproducibility [1]	Focuses on separating the input data from the features, explicitly capturing and storing the transformations applied to convert the inputs into features to ensure reproducibility	Data processing element within logic layer	Reliability
Checkpoints [1]	Save a snapshot of the model's internal state so that training can be resumed from this state in case a long running training job experiences a machine failure	Inference engine element within logic layer	Reliability
Workflow pipeline [1]	Isolate and containerize individual steps of a ML workflow so they can not only be run independently to ensure fault-tolerance and track performance but also chained together to create a pipeline	Data collection element within presentation, data processing and inference engine elements within logic layer	Maintainability, performance, reliability
Explainable predictions [1]	Explain the model behaviour aiding in diagnosing errors, identifying biases in the model, understanding how and why models make predictions and improve trust	Inference engine element within logic layer	Reliability, usability
Multisource extractor [5]	Ingest multiple data types from multiple data sources handling variability in data velocity, size, frequency, and formats over an unreliable network, mixed network bandwidth, different technologies, and systems	Data collection element within presentation layer	Performance, reliability

(continued)

Table 34.1 (continued)

Design pattern	Pattern description	Layer and element refined	Quality attribute targeted
Multidestination [5]	Publishes the data collected and cleaned by the multisource extractor by broadcasting it to the subscriber destinations	Data processing element within logic layer	Performance, reliability
Just-In-Time [5]	Used in situations where data needs to be stored before transformation and pre-processing can happen independently	Data collection element within presentation layer	Performance
Real-time streaming [5]	Continuous and real-time processing of the unstructured data	Data collection element within presentation layer, data processing and inference engine elements within logic layer	Performance
Façade pattern [5]	Provide a way for business intelligence tools, such as Tableau and Qlik, to access data (raw, processed or inferred)	Database and data lake elements in the data layer	Maintainability
NoSQL [5]	Facilitate rapid access and querying of large volume of data by storing it in a non-relational format	Data collection element within presentation, data processing and inference engine elements within logic layer	Performance
Lightweight stateless [5]	Provide access to ML pipeline through web services (restful API) independent of implementation platform or language	Database and data lake elements in the data layer	Maintainability
Near-real time [5]	Ensure rapid determination and analysis of data (within seconds not minutes)	Data collection element within presentation, data processing and inference engine elements within logic layer	Performance

Application of Design Patterns: A Distributed AI System for Emotion Classification

The connected society we live in today has allowed online users to willingly share opinions on an unprecedented scale. Motivated by the advent of mass opinion sharing, it is then crucial to devise algorithms that efficiently identify the emotions expressed

within the opinionated content. Recently, Twitter has received a lot of interest and attention from a wide range of Internet users across the globe. One of the main reasons for using Twitter is the ease of expressing opinions on diverse topics such as sports and politics. Such ease of use, coupled with the widespread use of connected portable devices, has made Twitter the primary channel for users to voluntarily share opinions, feelings, news, activities, interests, and other types of event-related information happening around them. Consequently, social networks have become some of the richest data repositories online.

Compared to traditional web articles, there is a special characteristic richly embedded in social media data: emotions. Emotion-bearing content has been used to detect opinions, disambiguate situations (earthquake vs. just nervous), infer user interests, and even predict the elections [4]. A data pipeline that can collect real-time transmissions based on directed topics, glean information from it through processing, and provide real-time analytics can be beneficial in detecting trends in any area of interest. For example, it can be used to gauge sentiments of users on economic or health related issues, political changes or even reactions to entertainment or current events.

The distributed AI system for emotion classification was developed with these specific use cases in mind. However, given its modular nature, it also exhibits a degree of flexibility in integrating additional processing pipelines to detect other dimensions of social media (such as detecting fake news, or classifying emotions from images).

As shown in Fig. 34.3, the overall architecture of the system closely resembles the Distinguished Business Logic from ML Model pattern discussed in Sect. 34.2. The system is segregated both vertically and horizontally.

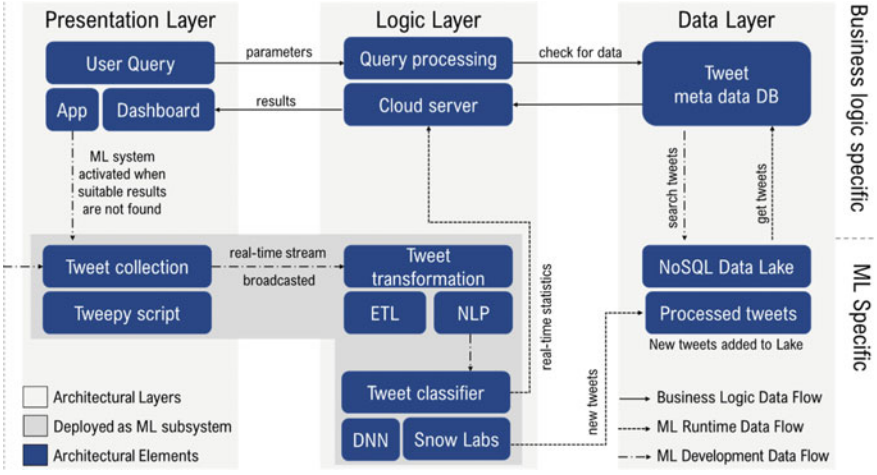

Fig. 34.3 Emotion classifier AI system

The business logic component is highly configurable and contains the reporting rules, granularity and dashboard designs. These can and will change frequently based on the client's requirements. To mine employer reviews from Glassdoor (to gauge emotions and create word clouds), for instance, would entail replacing the 'Tweepy' module with a custom web scraper. The dashboard elements and parameters to be gauged would also be different. The decoupling of the business logic from the inference engine ensures that any changes in the former components does not have a direct impact on the latter. In addition, any errors arising from such changes are easily localized and remedied within the business logic.

A typical workflow for this system would start with a user-initiated query in the presentation layer that may be satisfied using pre-classified tweets or the user can choose the option to retrieve and classify tweets in real time. The user query passes through the logic layer, where the query is checked against business requirements (such as reporting needs, dashboard designs, frequency of data refresh, etc.). The system will also determine at this stage whether the ML subsystem needs to be initiated or to pass the query directly to the Meta Data DB in the data layer. The ML subsystem will only be initiated should the user pick the option for real time processing, or if the configured query did not match the classified tweets stored in the NoSQL Data Lake (checked via the Tweet Meta Data DB). This decoupling allows the resources to be allocated judiciously and only engage the ML subsystem when necessary. For such queries, data is collected, processed and categorized real-time by the ML subsystem which stores both the raw tweets and classified ones in different partitions of the data lake. The DNN Classifier can also provide direct output to the Cloud Server in the logic layer which in turn can help populate a dashboard in the presentation layer. Furthermore, since the ML subsystem is decoupled from the logic layer, each can be configured independently of the other.

Apart from the *Distinguished Business Logic from ML Model*, the Emotion Classifier AI system leverages additional design patterns identified in Table 34.1; we discuss them here:

1. *Workflow Pipeline*: Components within the AI system are containerized and are independently deployable. Each element within the ML subsystem have been segregated to enable independent function (see Fig. 34.3).
2. *Real Time Streaming*: When a user indicates so, the ML subsystem will initiate real time processing that involves collection, transformation, and classification of tweets from Twitter.
3. *Near-Real Time*: The ML subsystem can perform near real-time processing of the unstructured tweets.
4. *Lightweight Stateless*: The ML subsystem is accessible through a web-based API.
5. *NoSQL*: Tweets are stored in non-relational format so that they can be quickly queried based on any of the predefined keys.
6. *Reproducibility*: Tweets are stored in multiple different partitions; one partition that stores all the raw tweets (and potentially other unstructured data such as images, audio and video) acting as a staging area for all raw data and another secondary partition that stores all processed and classified tweets.

7. *Explainable Predictions*: Explanations are provided for how and why the DNN Classifier makes its predictions to both understand the model and improve trust.
8. *Checkpoints:* The steady state of the DNN model is preserved before and after each re-training phase. This ensures the model employs the combination of weights and biases that minimizes the cost function for classification tasks.

While the paper had taken a high-level approach, there are time savings in form of localizing issues quickly (within this modular structure) and quicker updates to only those parts that requires tuning when moving from one project to another. To accurately measure the concrete gains in performance efficiency from application of the discussed design patterns would entail A/B testing. This would require the creation of a secondary pipeline where such design patterns were not implemented. While such a comparative framework was not feasible for the study, there were several works which points to significant efficiency gains from application of design patterns in the fields of data analytics and software development [2–5].

Discussion and Conclusion

The paper identified patterns for designing the architecture of a distributed emotion classification AI system that supports ease of change and reuse. We used as an additional criterion, quality attributes specified in the ISO/IEC 25010:2011 standards [6], to further evaluate the impact these patterns have on the overall quality of the system. A summary of this evaluation is presented in Table 34.2.

We were interested in designing a system that was not only functionally correct but one that would also be dependable. As can be seen, these patterns help promote quality attributes that make an AI system achieve performance efficiencies, reliability, trust, maintainability and portability, and is less burdened with technical debt that stems from tight coupling of the data with the rest of the system.

Table 34.2 Evaluation of the spark pipeline

Quality criteria	Connected patterns	Pattern implications for AI system
Functional suitability	Reproducibility, explainable predictions	Tweets are stored in their raw format so that they can be reprocessed later for verifying functional correctness of a ML subsystem. Explanations also provide insights into the inner workings of the ML subsystem
Performance	Workflow pipeline, real time streaming, near-real time, NoSQL	Data can be queued for ML pipelines, enabling the latter to consume it real-time or when it is ready to do so. Data is stored in a non-relational format for faster querying
Usability	Explainable predictions	Predictions of the ML subsystem can be explained for building trust
Reliability	Reproducibility, explainable predictions, distinguished business logic from ML model, workflow pipeline	Predictions of the ML subsystem can be reproduced anytime using tweets stored in their raw format. Explanations of the inner workings of the ML subsystem provide confidence that the system is working correctly. Independently deployed and executing components can be easily replicated to provide fault-tolerance
Maintainability	Distinguished business logic from ML model, workflow pipeline, lightweight stateless	Components are decoupled from each other making the system more modular. The ML subsystem can be accessed using restful API
Portability	Workflow pipeline, lightweight stateless	Each stage of the pipeline can be deployed via virtualization technology such as docker with key units being hosted in the clous for easier scalability. The pipeline can be accessed via restful API

Acknowledgements This material is based upon work funded and supported by the 2020 IndustryXchange Multidisciplinary Research Seed Grant from Pennsylvania State University. The distributed AI system at present employs an emotional classifier developed at John Snow Labs [7]. We wish to thank our graduate students, Raghava Rao Sunkanapally (raghavarao1997@gmail.com) and Nikhitha Kunduru (kundurunikhitha@gmail.com), for their instrumental contributions in realizing this body of work.

References

1. Lakshmanan, V., Robinson, S., & Munn, M. (2020). Machine learning design patterns. O'Reilly Media, Inc.
2. Buschmann, F., Henney, K., & Schmidt, D. (2007). Pattern oriented software architecture: On patterns and pattern languages (Wiley Software Patterns Series). Wiley.
3. Yokoyama, H. (2019). Machine learning system architectural pattern for improving operational stability. In *IEEE international conference on software architecture companion* (pp. 267–274). https://doi.org/10.1109/ICSA-C.2019.00055
4. Washizaki, H., Khomh, F., Guéhéneuc, Y. G., Takeuchi, H., Natori, N., Doi, T., & Okuda, S. (2022). Software-engineering design patterns for machine learning applications. *Computer, 55*(03), 30–39. https://doi.org/10.1109/MC.2021.3137227
5. Raj, P., Raman, A., Subramanian, H. (2017). Architectural patterns. Packt Publishing Ltd., ISBN 978-1-78728-749-5.
6. International Organization for Standardization. (2011, March). *Systems and software engineering—Systems and software quality requirements and evaluation (SQuaRE)—System and software quality models.* Retrieved 24 April 2022, from iso.org: https://www.iso.org/obp/ui/#iso:std:iso-iec:25010:ed-1:v1:en
7. John Snow Labs Inc. (2021). Emotion detection classifier. https://nlp.johnsnowlabs.com/2021/01/09/classifierdl_use_emotion_en.html